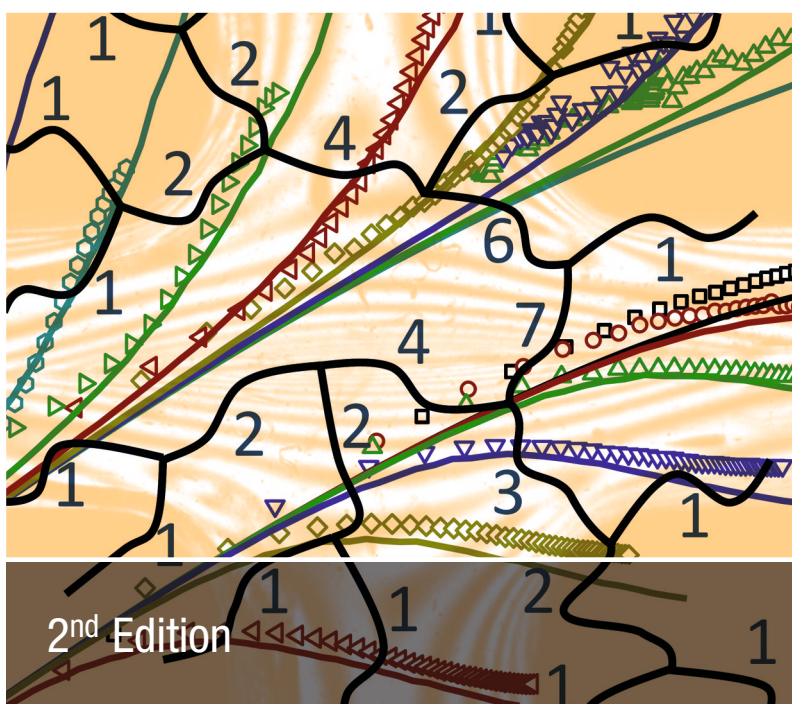


John M. Dealy
Daniel J. Read
Ronald G. Larson

Structure and Rheology of Molten Polymers

From Structure to Flow Behavior and Back Again



HANSER

Dealy / Read / Larson
Structure and Rheology of Molten Polymers

John M. Dealy
Daniel J. Read
Ronald G. Larson

Structure and Rheology of Molten Polymers

From Structure to Flow Behavior
and Back Again

2nd Edition

HANSER

Hanser Publishers, Munich

Hanser Publications, Cincinnati

The Author:

Dr. John M. Dealy, Emeritus Professor, McGill University, Montreal, Canada

Dr. Daniel J. Read, Professor, University of Leeds, UK

Dr. Ronald G. Larson, Professor, University of Michigan, Ann Arbor, USA

Distributed in the Americas by:

Hanser Publications

6915 Valley Avenue, Cincinnati, Ohio 45244-3029, USA

Fax: (513) 527-8801

Phone: (513) 527-8977

www.hanserpublications.com

Distributed in all other countries by:

Carl Hanser Verlag

Postfach 86 04 20, 81631 München, Germany

Fax: +49 (89) 98 48 09

www.hanser-fachbuch.de

The use of general descriptive names, trademarks, etc., in this publication, even if the former are not especially identified, is not to be taken as a sign that such names, as understood by the Trade Marks and Merchandise Marks Act, may accordingly be used freely by anyone. While the advice and information in this book are believed to be true and accurate at the date of going to press, neither the authors nor the editors nor the publisher can accept any legal responsibility for any errors or omissions that may be made. The publisher makes no warranty, express or implied, with respect to the material contained herein.

The final determination of the suitability of any information for the use contemplated for a given application remains the sole responsibility of the user.

Cataloging-in-Publication Data is on file with the Library of Congress

All rights reserved. No part of this book may be reproduced or transmitted in any form or by any means, electronic or mechanical, including photocopying or by any information storage and retrieval system, without permission in writing from the publisher.

© Carl Hanser Verlag, Munich 2018

Editor: Dr. Mark Smith

Production Management: Jörg Strohbach

Coverconcept: Marc Müller-Bremer, www.rebranding.de, München

Coverdesign: Stephan Rönigk

Typesetting: Manuela Treindl, Fürth

Printed and bound by Druckerei Hubert & Co GmbH und Co KG BuchPartner, Göttingen

Printed in Germany

ISBN: 978-1-56990-611-8

E-Book ISBN: 978-1-56990-612-5

Preface to the Second Edition

There have been many important developments in this field since the first edition of the book appeared over 10 years ago, and these are described in some detail in this new edition. Results of recently developed molecular models suggest the possibility of predicting the rheological behavior of a molten polymer when its molecular structure is well-known. Such models also provide the basis of methods for using rheological data to obtain information about the structure of a polymer whose structure is not known in detail. These models and relationships between structure and rheology are presented here from both phenomenological and molecular-theoretical points of view.

This book was designed for several types of reader. For those who have a basic knowledge of rheology but little experience with polymers, we provide in the early chapters sufficient information about polymer physics and chemistry for an understanding of the later chapters on the rheological behavior of melts. For readers who are currently active in polymer rheology and would like to know the state of the art with respect to quantitative relationships between molecular structure and rheology, the later chapters of the book provide this information. Thus, the book provides both an introduction to polymers and rheological concepts as well as an advanced treatment of potential interest both to polymer scientists and plastics engineers.

Until recent years, there existed major barriers to the development of quantitative relationships between the molecular structures of commercial polymers and their rheological behavior. Methods used to produce these materials yielded materials having complex and imprecisely controlled structures. The molecular weight distributions of linear polymers tended to be broad and somewhat irreproducible. And the branching structures of long-chain branched polymers, particularly low-density polyethylene, involve multidimensional distributions that can neither be predicted nor characterized with precision.

However, over the last 10 years, advances in the areas of catalysis and molecular modeling have changed this situation dramatically. Using single-site catalysts, it is possible to produce, on an industrial scale, polymers having structures that are much better defined and reproducible than those produced previously. Furthermore, recent advances in molecular models based on tube or slip-link concepts have made

it possible to predict the behavior of a widening range of molecular structures. While still requiring further work, particularly to deal with broad molecular weight distributions and complex branching structures, the new models are beginning to be used for the prediction of flow behavior of some commercial polymers. The objective of this book is to present these important developments, along with the background necessary to understand them, and to provide industrial and academic researchers with the up-to-date knowledge and expertise required to use them effectively.

It is not feasible to mention here all the people who have helped us in various ways during the several years we spent writing this book, but we would like to mention the following who were helpful in particularly important ways: Stéphane Costeux, Chinmay Das, Jeffrey Giacomin Jörg Läuger, Thomas Schweizer, João Soares, Manfred Wagner, and Manfred Wilhelm. And we must mention the support of our tolerant families and the patient guidance of our Editor, Mark Smith, who were essential for the completion of the project.

August 15, 2017

Montreal, Quebec

Leeds, England

Ann Arbor, Michigan

Preface to the First Edition

Results of recently developed molecular models suggest the possibility of predicting the rheological behavior of a molten polymer when its molecular structure is well-known. Such models also provide the basis of methods for using rheological data to obtain information about the structure of a polymer whose structure is not known in detail. These models and relationships between structure and rheology are presented here from both phenomenological and molecular-theoretical points of view.

This book is intended to be useful to several types of reader. For those who have a basic knowledge of rheology but little experience with polymers, we have provided in the early chapters sufficient information about polymer physics and chemistry for an understanding of the later chapters. For readers who are currently active in polymer rheology and would like to know the state of the art with respect to quantitative relationships between molecular structure and rheology, the later chapters of the book provide this information. Thus, the book provides both an introduction to polymers and rheological concepts as well as an advanced treatment of potential interest both to polymer scientists and plastics engineers.

Until recent years, there existed major barriers to the development of quantitative relationships between the molecular structure of molten polymers and their rheological behavior. First, reaction systems capable of producing polymers on an industrial scale yielded materials with complex and imprecisely controlled structures. Second, the molecular weight distributions of linear polymers tended to be broad and somewhat irreproducible. And, finally, the branching structure of long-chain branched polymers, particularly low-density polyethylene, involves multidimensional distributions that can neither be predicted nor characterized with precision.

However, over the last ten years, advances in the areas of catalysis and molecular modeling have changed this situation dramatically. Using single-site catalysts, it is now possible to produce on an industrial scale polymers having structures that are much better defined and reproducible than those produced previously. Furthermore, new molecular models, particularly those based on the concept of a “molecule in a tube”, have been developed that can predict rheological behavior based on knowledge of molecular structure. While still requiring further work, particularly to deal

with broad molecular weight distributions and complex branching structures, the new models show great promise for the quantitative prediction of flow behavior of polymers of commercial importance. The objective of this book is to present these important developments, along with the background necessary to understand them, and to provide industrial and academic researchers with the up-to-date knowledge and expertise required to use them effectively.

It is not feasible to mention here all the people who have helped us in various ways during the several years we spent writing this book, but we would like to mention the following who were helpful in particularly important ways: Ralph Colby, Stéphane Costeux, Richard Graham, Willem de Groot, Teresa Karjala, David Lohse, Guiseppe Marrucci, Hiroshi Watanabe, and Paula Wood-Adams. And we cannot fail to mention that the support of our tolerant families and the patient guidance of our Hanser editor, Dr. Christine Strohm, were essential to the completion of the project.

September 29, 2005

Montreal, Quebec

Ann Arbor, Michigan

Contents

Preface to the Second Edition	V
Preface to the First Edition	VII
1 Introduction	1
1.1 Melt Structure and Its Effect on Rheology	1
1.2 Overview of This Book	2
1.3 Applications of the Information Presented.....	4
1.4 Supplementary Sources of Information	4
References.....	5
2 Structure of Polymers	7
2.1 Molecular Size.....	7
2.1.1 The Freely-Jointed Chain	7
2.1.2 The Gaussian Size Distribution.....	8
2.1.2.1 Linear Molecules	8
2.1.2.2 Branched Molecules	12
2.1.3 The Dilute Solution and the Theta State.....	14
2.1.4 Polymer Molecules in the Melt	16
2.2 Molecular Weight Distribution	17
2.2.1 Monodisperse Polymers.....	17
2.2.2 Average Molecular Weights and Moments of the Distribution.....	18
2.2.3 Continuous Molecular Weight Distribution	20
2.2.4 Distribution Functions	22
2.2.5 Narrow Distribution Samples	26
2.2.6 Bimodality	27
2.3 Tacticity	28
2.4 Branching.....	29
2.5 Intrinsic Viscosity.....	31
2.5.1 Introduction.....	31
2.5.2 Rigid Sphere Models.....	32

2.5.3	The Free-Draining Molecule.....	34
2.5.4	Non-Theta Conditions and the Mark-Houwink-Sakurada Equation.....	35
2.5.5	Effect of Polydispersity.....	36
2.5.6	Effect of Long-Chain Branching.....	37
2.5.7	Effects of Short-Chain Branching	38
2.5.8	Determination of Intrinsic Viscosity—Extrapolation Methods	40
2.5.9	Effect of Shear Rate.....	41
2.6	Other Structure Characterization Methods	41
2.6.1	Membrane Osmometry.....	41
2.6.2	Light Scattering.....	42
2.6.3	Gel Permeation Chromatography	44
2.6.3.1	MWD of Linear Polymers	44
2.6.3.2	GPC with Branched Polymers.....	47
2.6.3.3	GPC with LDPE.....	48
2.6.3.4	Interactive Chromatography.....	49
2.6.3.5	Field Flow Fractionation	50
2.6.4	Mass Spectrometry (MALDI-TOF)	50
2.6.5	Nuclear Magnetic Resonance.....	51
2.6.6	Separations Based on Crystallizability: TREF, CRYSTAF, and CEF	52
2.6.7	Bivariate (Two-Dimensional) Characterizations	54
2.6.8	Molecular Structure from Rheology	54
2.7	Summary	55
	References.....	57
3	Polymerization Reactions and Processes	65
3.1	Introduction.....	65
3.2	Classifications of Polymers and Polymerization Reactions	67
3.3	Structural Characteristics of Polymers.....	68
3.3.1	Introduction.....	68
3.3.2	Chemical Composition—Role of Backbone Bonds in Chain Flexibility.....	69
3.3.3	Chemical Composition—Copolymers	69
3.3.4	Tacticity	69
3.3.5	Branching.....	70
3.4	Living Polymers Having Prescribed Structures.....	71
3.4.1	Anionic Polymerization	73
3.4.2	Living Free-Radical Polymerization (Reversible Deactivation Radical Polymerization—RDRP).....	75
3.4.3	Model Polyethylenes for Research.....	75

3.5	Industrial Polymerization Processes	76
3.6	Free-Radical Polymerization of Low-Density Polyethylene (LDPE)	78
3.6.1	Shear Modification	79
3.7	Linear Polyethylene via Complex Coordination Catalysts	79
3.7.1	Catalyst Systems	79
3.7.2	Branching in High-Density Polyethylene	80
3.7.3	Ultrahigh Molecular Weight Polyethylene	81
3.8	Linear Low-Density Polyethylene via Ziegler-Natta Catalysts	81
3.9	Single-Site Catalysts	82
3.9.1	Metallocene Catalysts	83
3.9.2	Long-Chain Branching in Metallocene Polyethylenes	84
3.9.3	Post-Metallocene Catalysts	89
3.10	Polypropylene	90
3.11	Reactors for Polyolefins	91
3.12	Polystyrene	93
3.13	Summary	94
	References	95

4	Linear Viscoelasticity—Fundamentals	105
4.1	Stress Relaxation and the Relaxation Modulus	105
4.1.1	The Boltzmann Superposition Principle	105
4.1.2	The Maxwell Model for the Relaxation Modulus	110
4.1.3	The Generalized Maxwell Model and the Discrete Relaxation Spectrum	113
4.1.4	The Continuous Relaxation Spectrum	114
4.2	The Creep Compliance and the Retardation Spectrum	115
4.3	Experimental Characterization of Linear Viscoelastic Behavior	119
4.3.1	Oscillatory Shear	120
4.3.2	Experimental Determination of the Storage and Loss Moduli	123
4.3.3	Creep Measurements	125
4.3.4	Other Methods for Monitoring Relaxation Processes	127
4.4	Calculation of Relaxation Spectra from Experimental Data	127
4.4.1	Discrete Spectra	127
4.4.2	Continuous Spectra	128
4.5	Time-Temperature Superposition	130
4.5.1	Time/Frequency (Horizontal) Shifting	130
4.5.2	The Modulus (Vertical) Shift Factor	131
4.5.3	Validity of Time-Temperature Superposition	135
4.6	Time-Pressure Superposition	136
4.7	Alternative Plots of Linear Viscoelastic Data	137
4.7.1	Van Gurp-Palmen Plot of Loss Angle Versus Complex Modulus .	137

4.7.2	Cole-Cole Plots.....	139
4.8	Summary	141
	References.....	141
5	Linear Viscoelasticity—Behavior of Molten Polymers.....	147
5.1	Introduction.....	147
5.2	Zero-Shear Viscosity of Linear Polymers	147
5.2.1	Effect of Molecular Weight.....	148
5.2.2	Effect of Polydispersity.....	150
5.3	The Relaxation Modulus.....	152
5.3.1	General Features.....	152
5.3.2	How Can a Melt Act like a Rubber?.....	154
5.4	The Storage and Loss Moduli.....	154
5.5	The Creep and Recoverable Compliances.....	158
5.6	The Steady-State Compliance.....	160
5.7	The Plateau Modulus	162
5.7.1	Determination of G_N^0	162
5.7.2	Effects of Short Branches and Tacticity	164
5.8	The Molecular Weight between Entanglements, M_e	165
5.8.1	Definitions of M_e	165
5.8.2	Molecular Weight between Entanglements (M_e) Based on Molecular Theory	167
5.9	Rheological Behavior of Copolymers.....	170
5.10	Effect of Long-Chain Branching on Linear Viscoelastic Behavior	172
5.10.1	Introduction.....	172
5.10.2	Ideal Branched Polymers	173
5.10.2.1	Zero-Shear Viscosity of Ideal Stars and Combs	173
5.10.2.2	Steady-State Compliance of Model Star Polymers	176
5.10.3	Storage and Loss Moduli of Model Branched Systems	178
5.10.4	Randomly Branched Polymers.....	181
5.10.5	Low-Density Polyethylene	184
5.11	Use of Linear Viscoelastic Data to Determine Branching Level	186
5.11.1	Introduction.....	186
5.11.2	Correlations Based on the Zero-Shear Viscosity	187
5.12	Summary	188
	References.....	189
6	Tube Models for Linear Polymers—Fundamentals	197
6.1	Introduction.....	197
6.2	The Rouse-Bueche Model for Unentangled Polymers	199
6.2.1	Introduction.....	199

6.2.2	The Rouse Model for the Viscoelasticity of a Dilute Polymer Solution	200
6.2.3	Bueche's Modification for an Unentangled Melt	203
6.3	Entanglements and the Tube Model	208
6.3.1	The Critical Molecular Weight for Entanglement M_C	209
6.3.2	The Plateau Modulus G_N^0	211
6.3.3	The Molecular Weight Between Entanglements M_e	213
6.3.4	The Tube Diameter a	214
6.3.5	The Equilibration Time τ_e	218
6.3.6	Identification of Entanglements and Tubes in Computer Simulation	218
6.4	Modes of Relaxation	224
6.4.1	Reptation	224
6.4.2	Primitive Path Fluctuations	226
6.4.3	Reptation Combined with Primitive Path Fluctuations	228
6.4.4	Constraint Release—Double Reptation	231
6.4.4.1	Monodisperse Melts	232
6.4.4.2	Bidisperse Melts	233
6.4.4.3	Polydisperse Melts	239
6.4.5	Rouse Relaxation within the Tube	242
6.5	An Alternative Picture for Entangled Polymers: Slip-Links	244
6.6	Summary	249
	References	250
7	Tube Models for Linear Polymers—Advanced Topics	255
7.1	Introduction	255
7.2	Limitations of Double Reptation Theory	256
7.3	Constraint-Release Rouse Relaxation in Bidisperse Melts	259
7.3.1	Non-Self-Entangled Long Chains in a Short-Chain Matrix	259
7.3.2	Self-Entangled Long Chains in a Short-Chain Matrix	263
7.3.3	Thin Tubes, Fat Tubes, and the Viovy Diagram	265
7.4	Polydisperse Melts and “Dynamic Dilution”	272
7.4.1	Polydisperse Chains	272
7.4.2	Tube Dilation or “Dynamic Dilution”	274
7.5	Input Parameters for Tube Models	277
7.6	Summary	287
	References	288
8	Determination of Molecular Weight Distribution Using Rheology	291
8.1	Introduction	291
8.2	Viscosity Methods	291

8.3	Empirical Correlations Based on the Elastic Modulus	293
8.4	Methods Based on Double Reptation.	294
8.5	Generalization of Double Reptation.	298
8.6	Dealing with the Rouse Modes	298
8.7	Models that Account for Additional Relaxation Processes	299
8.8	Determination of Polydispersity Indexes	302
8.9	Summary	303
	References.	303
9	Tube Models for Branched Polymers.	307
9.1	Introduction.	307
9.2	General Effect of LCB on Rheology	309
9.2.1	Qualitative Description of Relaxation Mechanisms in Long-Chain-Branched Polymers	314
9.3	Star Polymers	317
9.3.1	Deep Primitive Path Fluctuations	317
9.3.2	Dynamic Dilution	319
9.3.3	Comparison of Milner-McLeish Theory to Linear Viscoelastic Data	322
9.3.3.1	Monodisperse Stars	322
9.3.3.2	Bidisperse Stars	327
9.3.3.3	Star/Linear Blends.	328
9.4	Multiply Branched Polymers	330
9.4.1	Dynamic Dilution for Polymers with Backbones	330
9.4.2	Branch Point Motion.	332
9.4.3	Backbone Relaxation.	336
9.5	Tube Model Algorithms for Polydisperse Branched Polymers	339
9.5.1	“Hierarchical” and “BoB” Dynamic Dilution Models	340
9.5.2	The “Time-Marching” Algorithm.	344
9.5.3	Data and Predictions for Model Polymers and Randomly Branched Polymers.	345
9.6	Slip-Link Models for Branched Polymers	353
9.6.1	Symmetric Star Polymers and Blends with Linear Polymers	354
9.6.2	Branch Point Hopping in Slip-Link Simulations	358
9.7	Summary	360
	References.	362
10	Nonlinear Viscoelasticity	369
10.1	Introduction.	369
10.2	Nonlinear Phenomena—A Tube Model Interpretation.	369
10.2.1	Large Scale Orientation—The Need for a Finite Strain Tensor	370

10.2.2	Chain Retraction and the Damping Function.....	370
10.2.3	Convective Constraint Release and Shear Thinning	373
10.3	Constitutive Equations	374
10.3.1	Boltzmann Revisited.....	375
10.3.2	Integral Constitutive Equations.....	377
10.3.3	Differential Constitutive Equations.....	381
10.4	Nonlinear Stress Relaxation.....	382
10.4.1	Doi and Edwards Predictions of the Damping Function	383
10.4.2	Estimating the Rouse Time of an Entangled Chain.....	385
10.4.3	Damping Functions of Typical Polymers	386
10.4.4	Normal Stress Relaxation.....	388
10.4.5	Double-Step Strain	391
10.5	Dimensionless Groups Used to Plot Rheological Data.....	392
10.5.1	The Deborah Number	392
10.5.2	The Weissenberg Number	393
10.6	Transient Shear Tests at Finite Rates	393
10.6.1	Stress Growth and Relaxation in Steady Shear	393
10.6.2	Large- and Medium-Amplitude Oscillatory Shear	398
10.7	The Viscometric Functions	402
10.7.1	Dependence of Viscosity on Shear Rate	402
10.7.1.1	Empirical Viscosity Models	403
10.7.1.2	Viscosity Function in Terms of Tube Models	405
10.7.1.3	Effect of Molecular Weight Distribution on Viscosity ..	406
10.7.1.4	Effect of Long-Chain Branching on Viscosity	407
10.7.2	Normal Stress Differences in Steady Simple Shear.....	409
10.8	Experimental Methods for Shear Measurements	413
10.8.1	Rotational Rheometers	413
10.8.1.1	Generating Step Strain	414
10.8.1.2	Flow Irregularities in Cone-Plate Rheometers	415
10.8.1.3	Measurement of the Second Normal Stress Difference ..	416
10.8.2	Sliding Plate Rheometers	417
10.8.3	Optical Methods—Flow Birefringence	418
10.8.4	Capillary and Slit Rheometers	419
10.8.5	The Cox-Merz Rule	421
10.9	Extensional Flow Behavior of Melts and Concentrated Solutions	422
10.9.1	Introduction	422
10.9.2	Solutions versus Melts	429
10.9.3	Linear, Monodisperse Polymers	429
10.9.4	Effect of Polydispersity.....	430
10.9.5	Linear Low-Density Polyethylene	430
10.9.6	Model Branched Systems	431

10.9.7	Long-Chain Branched Metallocene Polyethylenes	433
10.9.8	Randomly Branched Polymers and LDPE	434
10.9.9	Stress Overshoot in Extensional Flow	436
10.10	Experimental Methods for Extensional Flows	437
10.10.1	Introduction	437
10.10.2	Rheometers for Uniaxial Extension	438
10.10.3	Uniaxial Extension—Approximate Methods	442
10.10.4	Rheometers for Biaxial and Planar Extension	443
10.11	Summary	443
	References	446

11	Tube Models for Nonlinear Viscoelasticity of Linear and Branched Polymers	461
11.1	Introduction	461
11.2	Relaxation Processes Unique to the Nonlinear Regime	462
11.2.1	Retraction	462
11.2.2	Convective Constraint Release	464
11.3	Monodisperse Linear Polymers	465
11.3.1	No Chain Stretch: The Doi-Edwards Equation	465
11.3.2	Chain Stretch: The Doi-Edwards-Marrucci-Grizzuti (DEMG) Theory	469
11.3.3	Convective Constraint Release (CCR) and the GLaMM Model	474
11.3.4	Toy Models Containing CCR and Chain Stretch	476
11.3.4.1	“Rolie-Poly” Model for CCR	476
11.3.4.2	Differential Model of Ianniruberto and Marrucci	478
11.3.5	Comparison of Theory with Data for Monodisperse Linear Polymers: Shearing Flows	480
11.3.6	Extensional Flows of Melts and Solutions of Linear Polymers	484
11.3.7	Constitutive Instabilities and Slip	490
11.3.8	Entanglement Stripping and Chain Tumbling	492
11.3.9	Processing Flows	493
11.4	Polydisperse Linear Polymers	494
11.5	Polymers with Long-Chain Branching	497
11.5.1	The Pom-Pom Model	502
11.5.2	Revisions to the Pom-Pom Model	508
11.5.2.1	Drag-Strain Coupling	508
11.5.2.2	Correction for Reversing Flows	509
11.5.2.3	Second Normal Stress Difference and Other Corrections: The Extended Pom-Pom Model	509
11.5.2.4	Stress Overshoots, Accelerated Relaxation, and Entanglement Stripping	510

11.5.3 Empirical Multi-Mode Pom-Pom Equations for Commercial Melts.....	511
11.6 Towards Prediction of Nonlinear Viscoelasticity from Molecular Parameters.....	515
11.6.1 Seniority and Priority.....	515
11.6.2 Computational Prediction of Nonlinear Rheology for Polydisperse Branched Polymers	517
11.7 Summary	522
References.....	525
12 State of the Art and Challenges for the Future.....	535
12.1 State of the Art	535
12.2 Progress and Remaining Challenges.....	539
Appendix A: Structural and Rheological Parameters for Several Polymers...	547
Appendix B: Some Tensors Useful in Rheology.....	549
Nomenclature	555
Author Index	563
Subject Index.....	581

1

Introduction

■ 1.1 Melt Structure and Its Effect on Rheology

Our subject is how molecular structure affects melt flow and how rheological behavior can provide information about structure. Rheology has been used as a semiquantitative tool in polymer science and engineering for many years, for example for quality control, but quantitative relationships between structure and measurable properties were elusive, particularly in the case of commercial polymers. However, catalyst systems and synthesis methods have greatly improved our control of molecular structure. This, together with major advances in the modeling of rheological behavior, has brought us much closer to quantitative correlations between structure and rheology.

The relationship between the structure and the rheology of polymers is of practical interest for two reasons. First, rheological data are both very sensitive to certain aspects of the structure and easier to obtain than those of analytical methods such as gel permeation chromatography. Second, it is the rheological properties that govern the flow behavior of polymers when they are processed in the molten state.

When we speak of the structure of a polymer, we mean the size and shape of the molecules and the distributions of these characteristics among molecules. Thus, quantities of interest include molecular weight and its distribution, tacticity (when the monomer has a pseudochiral center), and branching (types, lengths, and their distributions). For linear homopolymers in which tacticity is not an issue, the molecular weight distribution contains complete information regarding structure. This is not a trivial special case, as it includes linear polyolefins that are used in many applications ranging from blow-molded milk bottles to molded polycarbonate compact disks. And even for such relatively simple materials, rheology provides a valuable tool for polymer characterization. Obviously, the determination of the structure of branched polymers is more complex.

■ 1.2 Overview of This Book

We treat here only systems in which most of the molecules are of a sufficient length to be in a highly entangled state. The basic idea of “entanglement” is that polymer molecules in a melt are embedded in a sea of other very long molecules, and this greatly restricts their motion in response to an imposed deformation or stress. Solutions of polymers in which the concentration and molecular weight are sufficient to generate a strong entanglement effect are also governed by the relationships discussed here and are mentioned from time to time. Immiscible blends are not treated, because their rheological behavior is strongly affected by interfacial tension. Neither do we deal with filled polymer systems; useful treatments of the rheological behavior of these materials are available [1–3].

Most of the data shown are for polyolefins and vinyl polymers, because these are the materials that are most commonly met with in a highly entangled state. They can be easily polymerized at high molecular weights (that is, molecular weights above 10,000), and their entanglement molecular weights are sufficiently low that the products are highly entangled. In addition, polymers in these categories, particularly polyethylene, polypropylene, and polystyrene, are the world’s most important commercial polymers and are generally very highly entangled.

Chapter 2 describes quantitative, nonrheological methods for determining molecular structure. But all characterization methods are limited in what they can tell us about structure in the absence of any information about how a sample was polymerized. Chapter 3 surveys the types of reaction systems used in polymerization and describes the molecular structures that can be produced by each. Anionic and living free-radical polymerizations are used in the laboratory to prepare samples having ideal structures, while processes used in industry produce materials that are more complex in structure. The development of single-site catalysts has led to the commercial production of polymers that, while they do not have the homogeneity of model polymers, do have structures that are reproducible and simply described.

Chapter 4 introduces the subject of linear viscoelasticity for readers new to rheology and also defines a number of terms that are used in the remainder of the book. The relaxation spectrum is introduced as well as methods for its measurement. Also, time-temperature superposition and its application are explained.

Chapter 5 contains a detailed discussion of the linear viscoelastic behavior of polymer melts. The most-often-used linear properties are the zero-shear viscosity and the storage and loss moduli; the effects of molecular weight, molecular weight distribution, and branching on these properties are described. While the approach is primarily phenomenological, melt behavior is interpreted qualitatively in terms of the molecular models that are presented in mathematical detail in later chapters.

Chapter 6 treats mean-field theories of melt behavior. We begin with the Rouse model for molecules in dilute solution and its modification by Bueche to deal with unentangled melts. The longest Rouse relaxation time emerges from this treatment and plays an important role in all molecular models. The tube model is introduced, in which the basic relaxation mechanisms involved in linear viscoelastic behavior are assumed to be “equilibration” among segments of the molecule within in a “tube” formed by surrounding molecules, and “reptation” out of this tube. The large difference between the time scales for these two processes explains the prominent plateau in the relaxation modulus of a monodisperse, entangled melt. In a polydisperse melt, short molecules cause the tube to become less restrictive of lateral motion during the reptation process, and this eliminates the flat plateau in the relaxation modulus. The slip link concept is an alternative to the tube picture, and models based on it are presented.

Chapter 7 describes the physics of the tube model in more detail and presents alternative approaches to dealing with polydispersity.

In Chapter 8, methods for inferring the molecular weight distribution of a linear polymer from rheological data are presented and compared. These range from semiempirical methods based on measurement of the viscosity as a function of shear rate to sophisticated techniques based on the molecular models presented in Chapters 6 and 7.

Chapter 9 presents tube models for linear viscoelasticity in systems with long-chain branching. Reptation of the molecule as a whole is suppressed by branch points, and relaxation takes place primarily by primitive path fluctuation, a relatively slow process.

Chapter 10 deals with nonlinear viscoelasticity primarily from a phenomenological point of view. Nonlinear behavior provides structural information that supplements that available from linear data, particularly in the case of long-chain branched polymers. Stress relaxation after large step strain reveals a new feature that is described in terms of the “damping function,” and it is explained by tube models as the result of retraction following chain stretch. Nonzero normal stress differences are nonlinear phenomena that occur in all large, rapid shearing deformations. In order to explain the effect of shear rate on the viscosity, the concept of “convective constraint release” is introduced into the tube picture. Except for step strain, shearing deformations do not generate significant chain stretch, but uniaxial (simple) extension does, and thereby displays interesting new phenomena such as “strain hardening,” which has been found to be particularly useful in the detection of long-chain branching.

Tube models capable of describing the essential features of nonlinear behavior are described in Chapter 11, which also introduces constitutive equations based on tube models. Such equations are of practical importance, as they aim to predict the way a melt behaves during industrial forming operations.

Chapter 12 briefly summarizes the book and lists remaining challenges.

■ 1.3 Applications of the Information Presented

The recent developments mentioned above open the door to the development of quantitative models relating molecular structure to rheological behavior. The two direct applications of these models are the prediction of rheological behavior when the molecular structure is known and the determination of key aspects of molecular structure by means of rheological measurements. Going beyond the scope of this book, the relationship between melt structure and rheology is one link in a chain of relationships that starts from reaction conditions and ends in the way polymers behave in industrial melt-forming operations. Making use of developments in the modeling of polymerization reactions and of melt forming operations, one can imagine a not very distant future in which it will be possible to do the following steps:

1. Predict the detailed structure of a polymer given the monomer(s) catalyst system and reaction conditions used to prepare it.
2. Given its structure, predict the rheological behavior of a polymer using molecular models.
3. Invert the above process by using rheology to determine polymer structure, or to confirm the predictions of structure that were made based on Step 1 above.
4. Using numerical flow simulations, predict the detailed behavior of a polymer during processing based on predicted rheological properties.

There have been major advances in each item in this list in recent years, and one can imagine a future when it is possible to predict *a priori* the reaction conditions required to produce a polymer having a prescribed melt processing behavior. This book simply summarizes what is known about Step 1 of this chain, but provides a more thorough treatment of Step 2, and to the extent currently possible, Step 3. The book contributes also to Step 4 by describing rheological constitutive equations that might be used in the simulation of flows and stresses in polymer processing operations.

■ 1.4 Supplementary Sources of Information

We mention here some books for readers looking for more information on particular topics. The book by Ferry [4] continues to be a classic source in the area of polymer rheology, in spite of the fact that the third edition is now more than 35 years old. More recent but less encyclopedic books on rheology include those of Macosko [5], Morrison [6], and Münstedt and Schwarzl [7]. Dealy and Wang [8] deal with applica-

tions of rheology in the plastics industry. The structure and rheology of a broad range of complex fluids is the subject of a monograph by Larson [9]. The phenomenology of polymer flow and continuum models are the domain of the book by Bird et al. [10]. Treatments of polymer physics that will be of particular interest to rheologists are those of Rubinstein and Colby [11] and Graessley [12]. There is also a second and closely related book by Graessley on polymer rheology. [13]. The tube theory for melts was first presented in book form by Doi and Edwards [14].

■ References

- [1] Leblanc, J.L., *Filled Polymers: Science and Industrial Applications*, CRC Press, Boca Raton (2010)
- [2] Münstedt, H., *Rheological and Morphological Properties of Dispersed Polymeric Materials*, Hanser Publishers, Munich (2016)
- [3] Mewis, J., Wagner, N.J., *Colloidal Suspension Rheology*, Cambridge Univ. Press (2012)
- [4] Ferry, J.D. *Viscoelastic Properties of Polymers*, 3rd ed., John Wiley & Sons, New York (1980)
- [5] Macosko, C.W., *Rheology: Principles, Measurements and Applications*, VCH Publishers, New York (1994)
- [6] Morrison, F.A., *Understanding Rheology*, Oxford Univ. Press, New York (2001)
- [7] Münstedt, H., Schwarzl, F.R., *Deformation and Flow of Polymeric Materials*, Springer-Verlag, Heidelberg (2014)
- [8] Dealy, J.M., Wang, J., *Melt Rheology and its Applications in the Plastics Industry*, Springer, Dordrecht (2013)
- [9] Larson, R.G., *The Structure and Rheology of Complex Fluids*, Oxford Univ. Press, New York (1999)
- [10] Bird, R.B., Armstrong, R.C., Hassager, O., *Dynamics of Polymeric Liquids, Vol. 1, Fluid Mechanics*, 2nd ed., John Wiley & Sons, New York (1987)
- [11] Rubinstein, M., Colby, R.H., *Polymer Physics*, Oxford Univ. Press, Oxford (2003)
- [12] Graessley, W.W., *Polymer Liquids & Networks: Structure and Properties*, Garland Science, New York (2004)
- [13] Graessley, W.W., *Polymer Liquids & Networks: Dynamics and Rheology*, Garland Science, New York (2005)
- [14] Doi, M., Edwards, S.F., *The Theory of Polymer Dynamics*, Clarendon Press, Oxford (1986)

2

Structure of Polymers

The features that distinguish one polymer molecule from another are the monomer or monomers involved, the molecular size, and the molecular architecture. This chapter presents ways of describing molecular size and architecture and explains how these can be determined using analytical methods. A much more thorough treatment of polymer structure can be found in the monograph of Graessley [1]. The development of many new polymer analysis techniques over the last decade has led to the introduction of a bewildering array of abbreviations, and to help the reader deal with these, they are listed at the end of this chapter.

■ 2.1 Molecular Size

2.1.1 The Freely-Jointed Chain

The reader will encounter here a bewildering array of parameters used to describe the size of a molecule, and it is futile to try to remember all of them after one reading. A suggested approach is to follow the logic in their derivation and return to their definitions when the need arises.

If we know the molecular weight of a linear polymer, it is easy to calculate the hypothetical, stretched-out length of a molecule. However, this dimension is very much larger than the size of a coiled-up molecule in a solution or melt. And it is essential to our purposes to establish a quantitative measure of the size of such a coil. Due to Brownian motion, a polymer molecule is constantly exploring a very large number of possible conformations due to its great length and flexibility. These conformations can only be described in terms of statistical averages, and to define the molecular size parameters required for our purposes we can make use of a much simplified model in which the random coil molecule is replaced by a freely-jointed chain consisting of beads connected together by springs, with the mass of the molecule concentrated in the beads. Of course the segments of the molecule that consist of atoms and chemical bonds do not constitute a freely-jointed chain because of lim-

itations on bond angles and orientations, but the number of beads is much smaller than the number of repeating units in the molecule, and this results in the greatly enhanced degree of freedom of a freely-jointed chain.

In addition to the assumption of a freely-jointed chain, we will ignore restrictions on molecular conformation due to the inability of two segments of a molecule to occupy the same space. A chain for which this is allowed is called a *phantom* or *ghost* chain. Finally, we will assume that the chain is not stretched very much. To summarize, in the following development for the freely-jointed chain we will make use of three assumptions: 1) the molecule is very long; 2) it is a phantom chain; and 3) the chain is not extended by flow or external forces. Assumptions two and three imply that the molecule is in an *unperturbed* state, i.e., that it is free of the effects of external forces resulting from flow or solvation. These assumptions are applicable to a molten polymer and to a very dilute solution when the combination of solvent and temperature is such that the conformation of the polymer molecules is unaffected by polymer-polymer or polymer-solvent interactions; such a solution is said to be in its *theta state*. The theory of the freely-jointed chain is described only in general terms in the following section, and a more detailed discussion can be found in polymer science texts such as that of Boyd and Phillips [2].

2.1.2 The Gaussian Size Distribution

2.1.2.1 Linear Molecules

In order to calculate the coil size of a freely-jointed, phantom chain, we start with the assumptions noted above and consider a chain consisting of N_f freely-jointed segments of length b_f . Since there are no restrictions on the orientation of one segment with respect to its neighbors, the position of one end of the chain relative to the other is given by a three-dimensional random-walk calculation, more correctly called a random-flight calculation since motion occurs in three dimensions. Such calculations can be used to determine the average end-to-end distance, i.e., the root-mean-square end-to-end vector of a molecule, $\sqrt{\langle R^2 \rangle_0}$, where the subscript indicates that this average applies to the unperturbed molecule, i.e., a dilute solution in its theta state (defined in Section 2.1.3) or a melt. For a vinyl polymer with a degree of polymerization of 1000, the root-mean-square end-to-end distance is about 22 nm.

Figure 2.1 shows a freely-jointed chain superposed on the molecule that it represents. Due to Brownian motion, the configuration of a molecule fluctuates very rapidly among all its possible configurations in any significant period of time. Assuming that each configuration is equally probable, random flight calculations show that when N_f is large, the mean-square end-to-end distance is given by Eq. 2.1.

$$\langle R^2 \rangle_0 = b_f^2 N_f \quad (2.1)$$

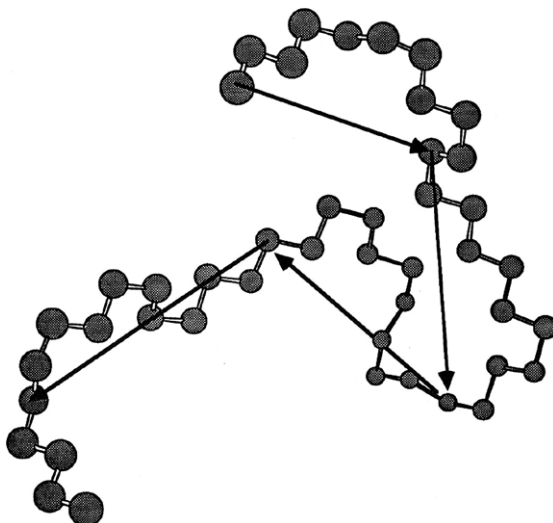


Figure 2.1 Segment of a polyethylene molecule with vectors showing a freely-jointed chain that can be used to simulate its behavior. In the chain shown there is about one segment for every ten bonds, and each segment is about eight times as long as a PE bond. From Boyd and Phillips [2]

Values of this parameter for several polymers are tabulated in Appendix A. The *radius of gyration* R_g of a molecule is the root-mean-square distance of mass elements of the chain from its center of gravity. (It is also the radius of a body having the same angular momentum and mass as the molecule but whose mass is concentrated at the radius, R_g .) Averaged over all possible conformations of the freely-jointed chain, the mean-square radius of gyration is given by Eq. 2.2.

$$\langle R_g^2 \rangle_0 = \frac{1}{6} b_f^2 N_f = \frac{1}{6} \langle R^2 \rangle_0 \quad (2.2)$$

It is also possible to calculate the distribution of end-to end vectors for a random walk, and while the result is rather complex, it is very closely approximated by Eq. 2.3:

$$P(R) = \left[\frac{3}{3 \pi N_f b_f^2} \right]^{3/2} e^{-3R^2/2N_f b_f^2} \quad (2.3)$$

where $P(R) dR$ is the fraction of all possible random flights having end-to-end radii between R and $R + dR$. The function defined in Eq. 2.3 is called a Gaussian distribution, and a molecule in which the end-to-end distance follows this distribution is called a Gaussian chain or a random coil. We note that this probability density only approaches zero at very large values of R , while in reality the maximum extension of the chain is limited to a finite value. This reminds us that the Gaussian (freely-jointed) chain model is not valid for a highly extended molecule.

Note that the mean-square end-to-end distance has no meaning for a branched molecule, while the mean-square radius of gyration is still a meaningful measure of size. We can now use the Gaussian distribution to recalculate the mean-square end-to-end distance:

$$\langle R^2 \rangle_0 = \int R^2 P(R) dR = N_f b_f^2 \quad (2.4)$$

Thus, the approximate distribution function of Eq. 2.3 leads to the correct mean-square value.

The useful results that arise directly from the freely-jointed chain model of a polymer molecule are the relationships between the average size parameters, $\langle R^2 \rangle_0$ and $\langle R_g^2 \rangle_0$, and the Gaussian distribution. Now we want to relate the average size parameters to those describing the chemical bonds making up the backbone of the actual molecule and thus to its molecular weight. At the level of carbon-carbon bonds, the chain is not freely-jointed, as the relative motions of the bonds are limited by the bond angle and rotational energy potentials. One manifestation of this is that the fully-extended length or *contour length* of the molecule is less than $n l$, where n is the number of backbone bonds, and l is the bond length.

$$L = \text{Extended (Contour) Length} = N_f b_f = K_{\text{geom}} n l \quad (2.5)$$

where K_{geom} is the sine of one half the bond angle, which for polyethylene is 109.47° , so that K_{geom} is equal to 0.816. Another manifestation of the limitations on motions in the actual molecule is that the mean-square end-to-end distance $\langle R^2 \rangle_0$, which is equal to $N_f b_f^2$ for the freely-jointed model chain, is considerably greater than $n l^2$. The ratio of $\langle R^2 \rangle_0$ to $n l^2$ is thus a measure of the flexibility of the chain. This quantity, the *characteristic ratio*, C_∞ , can be calculated from the chain valence angles and the distribution of bond rotational energy states, and it is a constant for a given polymer.

$$C_\infty \equiv \frac{\langle R^2 \rangle_0}{n l^2} \quad (2.6)$$

The infinity subscript indicates that this value applies when n is sufficiently large that the ratio is independent of n . For polyethylene C_∞ is equal to 6.8, while for polystyrene, a stiffer molecule, it is 9.85 [3]. Values for several other polymers are tabulated in Appendix A.

We will let N be the *degree of polymerization*, which is M/M_0 , where M is the molecular weight of the polymer, and M_0 is the monomer molecular weight. The number of bonds in the backbone, n , is then $j N$, where j is the number of bonds per monomer unit. For vinyl polymers $j = 2$. Using these symbols, the mean-square end-to-end distance can be written in terms of the molecular weight as shown by Eq. 2.7.

$$\langle R^2 \rangle_0 = C_\infty n l^2 = C_\infty j N l^2 = \left(C_\infty l^2 j / M_0 \right) M \quad (2.7)$$

This shows that $\langle R^2 \rangle_0$ is proportional to the molecular weight and that $\langle R^2 \rangle_0/M$ is a constant for a given polymer. Combined with Eq. 2.2 it shows that the unperturbed mean-square radius of gyration is also proportional to the molecular weight:

$$\langle R_g^2 \rangle_0 = \left(C_\infty l^2 j / 6 M_0 \right) M \quad (2.8)$$

Several additional characteristic lengths will also be used in this book. One is the *effective random-walk step*, b_n , which is defined by use of Eq. 2.1, with the number of freely-jointed segments set equal to the actual number of backbone bonds, n :

$$\langle R^2 \rangle_0 = n b_n^2 \quad (2.9)$$

so that b_n is defined by Eq. 2.10:

$$b_n \equiv \sqrt{\langle R^2 \rangle_0 / n} \quad (2.10)$$

Thus, b_n is the bond length of a hypothetical, freely-jointed molecule of n segments that has the same value of $\langle R^2 \rangle_0$ as the actual molecule.

Another length closely related to b_n is the structural length introduced by Ferry (see ref. [4], p. 185). This is the *statistical segment length* for which we will use the symbol b (Ferry uses the symbol a). This is defined in a similar manner as b_n , but with n replaced by N , the degree of polymerization:

$$b \equiv \sqrt{\langle R^2 \rangle_0 / N} = \sqrt{\langle R^2 \rangle_0 j / n} = l \sqrt{C_\infty j} = b_n \sqrt{j} \quad (2.11)$$

where j is the number of backbone atoms per monomer unit. Note that when the monomer is an alkene with a single double bond or a vinyl monomer, $j = 2$, and $b = b_n \sqrt{2}$.

The *persistence length*, L_p , is the distance along the molecule at which the orientation of one segment loses its correlation with the orientation of another. In other words, a bond located a distance L_p from a second bond experiences negligible effect on its orientation due to the second bond. Quantitatively it is defined as the average projection of the end-to-end vector of an infinitely long chain in the direction of the first segment. Doi and Edwards (see ref. [5], p. 317) show that for a Gaussian chain, this length is related to $\langle R^2 \rangle_0$ and the contour length L as follows:

$$L_p = \frac{\langle R^2 \rangle_0}{2 L} \quad (2.12)$$

Yet another length parameter that will be useful is the Kuhn length, b_K . Kuhn [6] imagined an *equivalent* freely-jointed chain that has the same extended length L as the actual molecule. Thus, if the equivalent chain has N_K segments of length b_K ,

$$N_K b_K^2 = R_0^2 = C_\infty n l^2 \quad (2.13)$$

and,

$$R_{\max} = L = N_K b_K = K_{\text{geom}} n l \quad (2.14)$$

Where K_{geom} is a constant for a given chain structure, as explained below Eq. 2.5. In the remainder of the book, R_{\max} will be referred to simply as L . (l is the bond length.) The Kuhn parameters b_K and N_K can be expressed as follows:

$$\frac{b_K}{l} = \frac{C_\infty}{K_{\text{geom}}} \quad \text{and} \quad \frac{N_K}{n} = \frac{K_{\text{geom}}^2}{C_\infty} \quad (2.15)$$

For polyethylene, using the values mentioned above, $b_K/l \approx 8$, and $N_K/n \approx 1/10$. We also note that the persistence length L_p is just one half the Kuhn length.

2.1.2.2 Branched Molecules

The question of size is considerably more complicated for branched molecules. One measure of the effect of branching on the size of a molecule is the *branching factor* g , also called the chain contraction factor, which reflects the effect of branching on the mean square radius of gyration for a given molecular weight:

$$g \equiv \frac{\langle R_g^2 \rangle_B}{\langle R_g^2 \rangle_L} \quad (2.16)$$

The radii of gyration in this equation refer to a molecule in solution in its unperturbed state, i.e., in its theta state, and as we will see shortly, they also apply to molecules in the melt.

To relate g to parameters describing the branching level, information about the type of branching is required. Such information can be developed from knowledge of the polymerization process. (Note that $\langle R^2 \rangle$ has no meaning for a branched polymer.) Small [7] lists sources of formulas giving g for a number of well-defined branching structures, and we present a few examples here.

For star molecules with f arms of equal length, Zimm and Stockmayer [8] showed that g is given by:

$$g = \frac{3f - 2}{f^2} \quad (2.17)$$

For randomly-branched molecules of uniform molecular weight, each with n branch points having a functionality of f , Zimm and Stockmayer [8] made several simplifying assumptions to arrive at the expressions for $g_f(n)$ shown below as Eqs. 2.18 to 2.20 for one, two, and three branch points per molecule (n) respectively.

$$g_f(1) = \frac{6f}{(f+1)(f+2)} \quad (2.18)$$

$$g_f(2) = \frac{3(5f^2 - 6f + 2)}{f(4f^2 - 1)} \quad (2.19)$$

$$g_f(3) = \frac{3(13f^2 - 20f + 8)}{f(9f^2 - 9f + 2)} \quad (2.20)$$

For heterogeneous polymers with larger, uniform numbers of randomly distributed branch points per molecule with a random distribution of branch lengths, they derived Eqs. 2.21 and 2.22 for tri- and tetra-functional branch points, respectively:

$$\langle g_3 \rangle_w = \frac{6}{n_w} \left(\frac{1}{2} \left(\frac{2+n_w}{n_w} \right)^{1/2} \ln \left[\frac{(2+n_w)^{1/2} + n_w^{1/2}}{(2+n_w)^{1/2} - n_w^{1/2}} \right] - 1 \right) \quad (2.21)$$

$$\langle g_4 \rangle_w = \frac{1}{n_w} \ln(1+n_w) \quad (2.22)$$

In these equations, n_w is the weight average number of branch points per molecule. Lecacheux et al. [9] reported that for n greater than 5, the following approximation is accurate to within 3%.

$$g = \frac{3}{2} \left(\frac{\pi}{n} \right)^{1/2} - \frac{5}{2n} \quad (2.23)$$

Equation 2.21 is often used to interpret GPC data for branched commercial polymers, including LDPE, although this is not a randomly branched polymer. It can also be shown that the average number of branch points per 1000 carbon atoms λ , for molecules having j backbone bonds per monomer unit, is as follows:

$$\lambda(M) = 1000 M_0 n_w / j M_n \quad (2.24)$$

For m randomly distributed branch points in each molecule of a monodisperse sample resulting from fractionation by molecular weight, Zimm and Stockmayer [8] showed that for larger values of m , average values of g can be approximated by Eq. 2.25 for a functionality of 3 and by Eq. 2.26 for a functionality of 4.

$$g_3 = \left[(1+m/7)^{1/2} + (4m/9\pi) \right]^{-1/2} \quad (2.25)$$

$$g_4 = \left[(1+m/6)^{1/2} + (4m/3\pi) \right]^{-1/2} \quad (2.26)$$

Here $m = \sum n w_n$ and w_n is the fraction of chains having n branch points. Hadjichristidis et al. [10] noted that the Zimm and Stockmayer model describes the sizes of lightly branched molecules but that the predicted sizes of more highly branched polymers are too low due to crowding of the branches.

2.1.3 The Dilute Solution and the Theta State

Several important techniques for determining molecular size involve measurements in dilute solution and the use of the Gaussian chain relationships. It is thus important to know when a molecule in a dilute solution can be modeled as a Gaussian chain. To answer this question, we will review the basic assumptions of the chain model that led to the Gaussian size distribution. A key assumption was that of the phantom chain, which says that the chain is free to intersect itself and is thus free of long-range interactions between two portions of the molecule far from each other. But in fact only a fraction of all possible random-flight configurations are completely free of such interactions. As a result, in a neutral or good solvent the size of the molecule is significantly larger than that indicated by the phantom chain model. This volume effect manifests itself in values of molecular size parameters, such as $\langle R^2 \rangle$, that are larger than those for an unperturbed, phantom chain, in this case $\langle R^2 \rangle_0$. This phenomenon was described by Flory [11] in terms of *excluded volume*, and modern treatments of this concept are available [1, 12]. The main conclusion of these analyses for the purposes of the present book is that in a good solvent, $\langle R^2 \rangle$ and $\langle R_g^2 \rangle$ are larger than they would be for an unperturbed chain. One important effect of this phenomenon is in relating intrinsic viscosity to molecular weight, which is explained in Section 2.5. The complex problem of calculating the distribution of molecular sizes in a good solvent, where excluded volume must be taken into account, has been successfully approached by the use of Monte Carlo studies of the self-avoiding random walk (SAW) problem [13] and by renormalization group theories.

To summarize, because of excluded volume the actual molecule expands into more volume than does the unperturbed, Gaussian chain used to model it, but that is not the end of the story. In the words of Paul Flory (see ref. [11], p. 34), this “long-range (or volume) effect depends not only on the volume of the chain unit itself but also on its interaction with the solvent”. This opens the door to the judicious selection of solvent in order to manipulate the excluded volume. In a very poor solvent, segments along the chain will prefer to contact other chain segments rather than the solvent, and the chain will thus coil up on itself more tightly than it would without the solvent. This will cause it to occupy less volume than it would for a random-flight conformation. But as the power of the solvent is increased, the molecule will expand, and for certain combinations of solvent and temperature, the excluded volume can be effectively cancelled out, so that the possible conformations of the molecule will

have a Gaussian distribution. Such combinations are said to put the solution in its *theta state*, and at a given temperature, a solvent that produces this state is called a *theta solvent*. Thus, in the theta state, the energetic effect of self-attraction between segments of the molecule is exactly balanced by the entropic effect of expansion due to the excluded volume. A theta solvent turns out to be a relatively poor solvent, barely keeping a high-molecular-weight polymer in solution.

It is often impractical to make measurements under theta conditions, and it is thus important to know how the use of a good solvent affects the size of a molecule. This effect is sometimes described in terms of an *expansion parameter* α defined by Eq. 2.27. (Doi and Edwards [5] call α the “swelling coefficient.”)

$$\langle R^2 \rangle = \alpha^2 \langle R^2 \rangle_0 = \alpha^2 N b^2 \quad (2.27)$$

At one time, it was thought that this parameter depended only on the solvent and temperature for a given polymer. However, it was later realized that the scaling of the radius with molecular weight is not accounted for correctly by a constant value of α and that this parameter depends on molecular weight. Experimental data indicate that the root-mean-square end-to-end vector is in fact proportional to $M^{0.6}$.

Flory [11], in developing what he called a “mean field theory,” hypothesized that the size of a molecule in a good solvent is the result of a balance between repulsive, excluded volume interactions and elastic interactions that tend to shrink the molecule. This idea leads to the conclusion that:

$$\sqrt{\langle R^2 \rangle} \propto N^{3/5} \quad (2.28)$$

While this result is in accord with observations, other predictions of the model are incorrect (see ref. [5], p. 28).

A “two-parameter” model [14] predicts that α is a universal function of an excluded volume parameter, z , which is a dimensionless excluded volume, and the theory of Edwards and Singh [15] leads to the same conclusion. Their “self-consistent” model is based on the assumption of uniform expansion, i.e., that the expansion of the chain can be represented by an increase in the effective bond length. This affects the size of the molecule and thus the value of α . Edwards and Singh developed the following explicit relationship between α and z for large N :

$$\alpha^5 - \alpha^3 = \frac{4}{3} z \quad (2.29)$$

They represent the expansion parameter z in terms of the excluded volume v as follows:

$$z \equiv \left(\frac{3}{2\pi} \right)^{3/2} \frac{v \sqrt{N}}{b^3} \quad (2.30)$$

For large z , this relationship implies that the root-mean-square end-to-end distance is proportional to $N^{3/5}$, which agrees with observations. As in the case of the Flory concept, implicit in this model is the assumption that the end-to-end distance in a good solvent is Gaussian. However, the Gaussian chain model for a polymer molecule is increasingly inaccurate as the solvent power increases. This is taken into account by a mean field theory proposed to describe the excluded volume effect [16].

Baumann [17] proposed an empirical equation for calculating the unperturbed mean square radius of gyration, $\langle R_g^2 \rangle_0$, based on light scattering measurements made in a good solvent rather than a theta solvent:

$$\left(\frac{\langle R_g^2 \rangle_0}{M} \right)^{3/2} = \left(\frac{\langle R_g^2 \rangle}{M} \right)^{3/2} + B M^{1/2} \quad (2.31)$$

We note that according to Eq. 2.31 for a good solvent at high molecular weight, R_g becomes proportional to $M^{2/3}$, while it is now generally agreed that the exponent on M is very close to $3/5$. Nonetheless, Baumann's equation has been used to estimate small deviations from the theta state. For example, Fetters et al. [18] compiled $\langle R_g^2 \rangle_0$ data for a number of polymers and summarized their results in the form of empirical, power-law equations. For example, for polystyrene in cyclohexane at 34.5 °C, they reported:

$$\langle R_g^2 \rangle_0^{1/2} = 2.25 \cdot 10^{-2} M^{0.512} \quad (2.32)$$

But for an unperturbed random coil, i.e., in the theta state, the root-mean-square radius of gyration should be proportional to the square root of the molecular weight. Thus, Eq. 2.32 indicates that this system deviates slightly from its theta state. Using an extrapolation procedure based on Baumann's equation, Fetters et al. [18] obtained the following expression for the radius of gyration in the theta state:

$$\langle R_g^2 \rangle_0^{1/2} = 2.79 \cdot 10^{-2} M^{0.5} \quad (2.33)$$

While the above discussion involves the size of a molecule mainly under theta conditions, Monte Carlo simulations have been used to predict the shape distributions of linear and star molecules in dilute solution [19].

2.1.4 Polymer Molecules in the Melt

The above discussion of chain dimensions was based on consideration of a single molecule in a dilute solution. We will find the results to be of use in the later sections of this chapter that deal with techniques for measuring the size of polymer molecules. However, our primary interest is in the behavior of molten polymers.

In making use of concepts developed for dilute solutions, we need to know how the conformation of a polymer in its theta state compares with that in a melt. It turns out that the conformation of a molecule in a melt, where it is surrounded by other polymer molecules rather than solvent molecules, is very close to that in a theta solvent. In fact, small-angle neutron scattering (SANS) experiments have revealed that even in the glassy state, the molecules of an amorphous polymer have the same size as in a theta solvent [20]. We can understand this by noting that a segment of a chain is not able to differentiate between surrounding segments that are parts of its own chain and those that are parts of other chains. Therefore, we can use many of the results derived above to describe bulk polymers.

While this helps us to describe the *conformation* of the unperturbed molecule in a melt, the *rheological behavior* of a melt is dramatically different from that of a dilute solution if the molecular weight exceeds a certain critical value. This is the result of an extremely important phenomenon that occurs in a melt and has no counterpart in a dilute solution. Over a certain narrow range of molecular weights the dynamic interaction between polymer molecules starts to have a very marked effect on the rheological behavior of a melt. This strong interaction is traditionally said to be due to *entanglements*, although it is now understood that it is not the result of the looping of one molecule around another but more simply the fact that the displacement of a molecule due to Brownian motion is highly constrained laterally by neighboring molecules that cannot move out of the way as solvent molecules do. Graessley termed this characteristic of long polymer molecules “uncrossability.” This phenomenon does not affect molecular dimensions in an unstressed melt, but it has a very strong effect on the relationship between molecular structure and rheological properties, which is the subject of this book. It is thus important to be able to know the molecular weight at which this effect becomes prominent. Methods of defining and estimating values for several *critical molecular weights for entanglement* are presented in Chapter 5.

■ 2.2 Molecular Weight Distribution

2.2.1 Monodisperse Polymers

For a linear homopolymer of specified tacticity, if relevant (see Section 2.3 for an explanation of tacticity), molecular structure is completely determined by the molecular weight distribution (MWD). The simplest system is one in which all the molecules have exactly the same molecular weight. Then the fraction of molecules $n(M)$ having the molecular weight M is given by the following distribution:

$$n(M) = \begin{cases} 1 & (M = M_1) \\ 0 & (M \neq M_1) \end{cases}$$

Such a polymer is said to be *monodisperse*. It is actually impossible to synthesize a high-molecular-weight sample that is perfectly monodisperse. However, by means of anionic polymerization it is possible to produce a sample having a very narrow molecular weight distribution, i.e., one in which nearly the entire sample consists of molecules whose weights differ from the average by a very small percentage. By fractionation, the distribution can be made even narrower. Clearly, terms such as “nearly the entire sample” and “very small percentage” are not of practical use in polymer science, and we need to establish quantitative measures of the molecular weight distribution.

According to the standard nomenclature of the International Union of Pure and Applied Chemistry (IUPAC) a polymer is *uniform* when all its molecules are uniform with respect to both molecular weight and composition. Thus what is commonly called a monodisperse sample should be referred to as one that is *uniform with respect to molecular weight*. However, the traditional terminology is firmly entrenched, and we will use it here.

2.2.2 Average Molecular Weights and Moments of the Distribution

First, we need to define an average molecular weight, and then we can use higher moments of the distribution to describe the breadth and shape of the distribution. The most basic average is the *number average molecular weight*, \bar{M}_n (or simply M_n). If n_i is the fraction of molecules having the molecular weight, M_i , in a blend of monodisperse species described by the set of numbers $[n_i, M_i]$, then the number average molecular weight is:

$$\bar{M}_n \equiv \frac{\sum n_i M_i}{\sum n_i} \quad (2.34)$$

where the sum is taken over all the species present. Of course it is impossible to count the numbers of molecules having a given mass, although it is useful to think of a sample as consisting of many fractions, in each of which the molecular weight is within a certain small range and is characterized by an average value, M_i . The number-average molecular weight is equal to the monomer molecular weight M_0 times the average degree of polymerization \bar{N} .

Note that the sum in the denominator of Eq. 2.34 should be equal to one, since it is the sum of number fractions. However, there is a reason to show it explicitly.

Suppose we have estimated the fractions n_i , but because our technique for doing this is not perfect, which is always the case, some material will be missed. Then the sum of the values will not be one, and if we scale our values so that they sum to one, the distribution is said to be *normalized*.

We generally prefer to describe the composition of a mixture in terms of weight (actually mass) fractions rather than number fractions of molecules. The weight fraction, w_i , is related to the number fraction as follows.

$$w_i = \frac{n_i M_i}{\sum n_i M_i} \quad (2.35)$$

$$\text{Thus, } n_i = \frac{w_i}{M_i} \sum n_i M_i \quad (2.36)$$

We can then rewrite Eq. 2.34 in terms of weight fractions.

$$M_n = \frac{\sum w_i}{\sum w_i / m_i} \quad (2.37)$$

Another useful average is the *weight average molecular weight*, which is the second moment of the number fraction distribution. In other words, instead of averaging over the numbers of molecules having various weights, we average over their weights. Obviously, this average gives greater importance to the heavier molecules and is therefore larger than M_n .

$$M_w \equiv \frac{\sum w_i M_i}{\sum w_i} = \frac{\sum n_i M_i^2}{\sum n_i M_i} \quad (2.38)$$

The *polydispersity index*, PI , is the ratio of the weight and number averages.

$$PI = M_w / M_n$$

If a sample is perfectly monodisperse, with a molecular weight M , then:

$$M_n = M_w = M \text{ (monodisperse)}$$

and the polydispersity index is one. However, if the sample is not monodisperse then:

$$PI = \frac{\sum w_i M_i \sum w_i / M_i}{(\sum w_i)^2} > 1 \quad (2.39)$$

The polydispersity index is thus a primitive measure of the breadth of the MWD.

Higher moments can also be defined and provide additional information about the shape of the distribution. The next two after M_w are:

$$M_z \equiv \frac{n_i M_i^3}{\sum n_i M_i^2} = \frac{\sum w_i M_i^2}{\sum w_i M_i} \quad (2.40)$$

and

$$M_{z+1} = \frac{\sum n_i M_i^4}{\sum n_i M_i^3} = \frac{\sum w_i M_i^3}{w_i M_i^2} \quad (2.41)$$

In Section 2.5.5 we will make use of a viscosity-average molecular weight M_v , which can be determined by dilute solution viscometry. It is defined as follows:

$$M_v \equiv \left(\sum_i w_i M_i^a \right)^{1/a} \quad (2.42)$$

The constant a is defined and discussed in Sections 2.5.1 and 2.5.3.

Obviously, the higher moments give increasing importance to high-molecular-weight species. To get an idea of how these quantities work, consider a binary blend of two monodisperse polymers containing 95 wt.% A ($M_A = 50,000$) and 5 wt.% B ($M_B = 200,000$). The various molecular weight averages and the polydispersity index for this blend are shown in Table 2.1.

Table 2.1 Molecular Weight Averages for a Bimodal Blend (95% $M = 5 \cdot 10^4$; 5% $M = 2 \cdot 10^5$).

Number average, M_n	$5.19 \cdot 10^4$
Weight average, M_w	$5.75 \cdot 10^4$
Z-average, M_z	$7.61 \cdot 10^4$
Viscosity average, M_v ($\alpha = 0.8$)	$5.64 \cdot 10^4$

2.2.3 Continuous Molecular Weight Distribution

These moments are useful in describing the dependence of rheological properties on the MWD, because different properties vary a greatly in their sensitivity to various portions of the distribution. For example, the zero-shear viscosity depends primarily on M_w and only very weakly on the higher moments of the distribution, whereas the steady-state compliance is a very strong function of the breadth of the distribution.

Because polymers are not mixtures of many monodisperse components, they have practically continuous molecular weight distributions. To accommodate this reality, we define a continuous molecular weight distribution, $w(M)$, such that $w(M) dM$ is the mass fraction of material having molecular weights between M and $M + dM$. Obviously, the integral of $w(M) dM$ over the entire distribution should equal one.

$$\int_0^{\infty} w(M) dM = 1 \quad (2.43)$$

The upper limit is set equal to infinity, because while the largest molecule present is probably very large, we never know exactly what its molecular weight is. Also, it is practically impossible to detect molecules of every size in a sample. Thus, as in the case of the discrete distributions, if we scale experimental data in the form of $w(M)$ so that Eq. 2.43 is obeyed, we say that the distribution has been normalized.

There is, of course, also a continuous number distribution function, $n(M)$. The value of M at the peak in the curve of $w(M)$ is always larger than that at the peak of the $n(M)$ curve, if there is a peak in the latter.

The function $w(M)$ is called the differential molecular weight distribution. We can also define a cumulative distribution, $F(M)$, which is the fraction of all the molecules in the sample that have molecular weights equal to or less than M . This can be represented in terms of $w(M)$ as shown by Eq. 2.44.

$$F(M) = \int_0^M w(M') dM' \quad (2.44)$$

Likewise, the differential distribution can be expressed in terms of the cumulative distribution.

$$w(M) = \left[\frac{dF(M')}{dM'} \right]_{M'=M} \quad (2.45)$$

There is a simple relationship between the weight and number distribution functions, regardless of the form of the distribution. This can be demonstrated as follows:

$$w(M) dM = \frac{M n(M) dM}{\int M n(M) dM} = \frac{M}{M_n} n(M) dM \quad (2.46)$$

Thus:

$$w(M) = \frac{M}{M_n} n(M) \quad (2.47)$$

In terms of the continuous distribution function, $w(M)$, the various averages are:

$$M_n \equiv \frac{\int_0^{\infty} w(M) dM}{\int_0^{\infty} [w(M)/M] dM} \quad (2.48)$$

$$M_w \equiv \frac{\int_0^{\infty} w(M) M dM}{\int_0^{\infty} w(M) dM} \quad (2.49)$$

$$M_z \equiv \frac{\int_0^{\infty} w(M) M^2 dM}{\int_0^{\infty} w(M) M dM} \quad (2.50)$$

Sometimes it is convenient to work with a weight distribution function expressed in terms of the logarithm of M rather than M itself. We represent such a function as $w(\ln M)$, so that $w(\ln M) d\ln M$ is the weight fraction of molecules having $\ln M$ values between $\ln M$ and $(\ln M) + d(\ln M)$. For example, the weight average molecular weight, in terms of this distribution, is:

$$M_w = \int_{-\infty}^{\infty} M w(\ln M) d(\ln M) \quad (2.51)$$

The viscosity average determined by dilute solution viscometry is related to the molecular weight distribution as shown by Eq. 2.52.

$$M_v = \left[\frac{\int w(M) M^\alpha dM}{\int w(M) dM} \right]^{1/\alpha} \quad (2.52)$$

Obviously, when $\alpha = 1$, the viscosity average molecular weight becomes equal to the weight average.

2.2.4 Distribution Functions

A number of functional forms have been proposed to describe the function $w(M)$. Some of these are entirely empirical, while others are predicted by models of polymerization reactions (see Chapter 3). All of these are described and compared in the monograph by Peebles [21].

We present first the one-parameter function derived by Schulz [22] and Flory [23] for the following ideal cases.

1. Linear, addition polymer formed at constant rate of initiation, constant monomer concentration, transfer to solvent but not to monomer and termination by disproportionation.

2. Linear condensation polymer formed with equal reactivity of all chain ends.
3. Linear condensation polymer formed by allowing units to interchange in a random manner.
4. Low molecular weight polymer formed from higher MW linear polymer by random scission.

In terms of the extent of reaction, p , of a condensation polymer the Schultz-Flory, or *most probable distribution*, is given by Eq. 2.53.

$$w(r) = r p^{r-1} (1-p)^2 \quad (2.53)$$

where r is the degree of polymerization, i.e., the ratio M/M_0 (which is elsewhere in this book represented by N). To obtain the distribution in terms of M , r is replaced by M/M_0 , and the expression is divided by M_0 .

$$w(M) = \frac{M}{M_0^2} p^{M/M_0-1} (1-p)^2 \quad (2.54)$$

As the extent of reaction p (fraction of monomer reacting) approaches one, the first three moments of the molecular weight distribution are in the ratios of 1:2:3, so that the polydispersity index approaches two.

For addition polymerization, the number average molecular weight is related to the extent of reaction by Eq. 2.55.

$$M_n = \frac{M_0}{1-p} \quad (2.55)$$

When r is large and p is close to one, the most probable weight distribution function is very closely approximated by Eq. 2.56.

$$w(M) = \frac{M}{M_n^2} \exp\left(-\frac{M}{M_n}\right) \quad (2.56)$$

Inserting this expression into the integrals of Eqs. 2.49 and 2.50, we find that $M_w/M_n = 2.0$, as expected. In describing polymers made using multiple-site catalysts, this distribution is often generalized as a sum of terms, each with a different weighting factor and value of M_n .

Schulz [22] derived another distribution for the case of constant rate of initiation and termination by second-order interaction with the monomer. The Schulz molecular weight distribution is given by Eq. 2.57.

$$w(r) = (-\ln p)^2 r p^r \quad (2.57)$$

This was later generalized by Schulz [23] and Zimm [25] to give the Schulz-Zimm distribution (Eq. 2.58).

$$w(r) = (-\ln p)^{k+1} r^k p^r / \Gamma(k+1) \quad (2.58)$$

where $\Gamma(x)$ is the gamma function, a generalization of the factorial function for the continuous argument, x :

$$\Gamma(x) \equiv \int_0^\infty e^{-t} t^{x-1} dt$$

If $k = 2$ in Eq. 2.58, we obtain the distribution for addition polymerization with constant rate of initiation, constant monomer concentration, no transfer, and termination by coupling with active molecules (see Chapter 3). Noting that $-\ln p \approx (1-p)$ when p is close to one, we can write the Schulz-Zimm distribution in the form shown by Eq. 2.59.

$$w(M) = \left(\frac{1-p}{M_0} \right)^{k+1} M^k \exp \left[-\left(\frac{1-p}{M_0} \right) M \right] / \Gamma(k+1) \quad (2.59)$$

The first three moments of the distribution are:

$$\begin{aligned} M_n &= M_0 k / (1-p) \\ M_w &= M_0 (k+1) / (1-p) \\ M_z &= M_0 (k+2) / (1-p) \end{aligned} \quad (2.60)$$

from which we see that $PI = 1 + 1/k$.

Several empirical distributions have also found wide use in describing commercial polymers. The simplest of these is the normal or Gaussian distribution.

$$w(r) = \frac{\exp \left[-(r - r_n)^2 / 2 \sigma^2 \right]}{\sqrt{2 \pi} \sigma} \frac{r}{r_n} \quad (2.61)$$

For a normal distribution, the polydispersity index is given by Eq. 2.62:

$$PI = 1 + \sigma^2 / M_n^2 \quad (2.62)$$

This distribution gives negative values of M for a polymer with a broad molecular weight distribution. Thus, integrals of the distribution must be taken over the range $-\infty < M < \infty$. The occurrence of negative molecular weights is eliminated by the use of the log-normal distribution, which is described below.

A more general function, which includes several other distributions as special cases, is the generalized exponential (Gex) distribution [26, 27], which has three parameters.

$$w(M) = \frac{m}{\Gamma[(1+k)/m]} \frac{M^k}{M_G^{k+1}} \exp\left[-\left(\frac{M}{M_G}\right)^m\right] \quad (2.63)$$

The average molecular weights, in terms of the parameters of this model are:

$$M_n = M_G \frac{\Gamma[(k+1)/m]}{\Gamma(k/m)} \quad (2.64)$$

$$M_w = M_G \frac{\Gamma\left(\frac{k+2}{m}\right)}{\Gamma\left(\frac{k+1}{m}\right)} \quad (2.65)$$

$$M_z = M_G \frac{\Gamma\left(\frac{k+3}{m}\right)}{\Gamma\left(\frac{k+2}{m}\right)} \quad (2.66)$$

Gloor [28] found that he could not fit data for some polymers using the Gex distribution if he restricted himself to positive values of m and k but that these data could be fitted if these parameters were allowed to have negative values. He noted that this required that k be less than -3. Many distributions can be shown to be special cases of the Gex distribution; $m = 1$: $k > 0$ gives the Schulz-Zimm distribution; $k = 1$ gives the most probable distribution; $k > 1$ gives the Schulz distribution, and $k \gg 1$ gives the Poisson distribution (Eq. 2.72). When $m = k + 1$ and $k > 0$, we obtain the Weibull-Tung distribution [29].

Wesslau [30] found that the MWD of several polyethylenes polymerized using Ziegler catalysts could be described by the two-parameter log-normal distribution:

$$w(\ln r) = \left\{ \frac{1}{\sqrt{2\pi}\sigma} \exp\left[\frac{-(\ln r - \ln r_m)^2}{2\sigma^2} \right] \right\} \quad (2.67)$$

where r_m is the median of the distribution. Several average molecular weights are:

$$\begin{aligned} M_n &= M_m \exp(-\sigma^2/2) \\ M_w &= M_m \exp(\sigma^2/2) \\ M_z &= M_m \exp(3\sigma^2/2) \\ M_v &= M_m \exp(a\sigma^2/2) \end{aligned} \quad (2.68a, b, c, d)$$

From these expressions, it is easily shown that the parameters are related to the first two moments of the distribution as follows.

$$\sigma^2 = \ln(M_w/M_n) \quad (2.69)$$

$$M_m = \sqrt{M_n M_w} \quad (2.70)$$

Finally, because the distribution is symmetric,

$$PI \equiv \frac{M_w}{M_n} = \frac{M_z}{M_w} \quad (2.71)$$

Chiang [31] related the constants of this distribution to the viscosity average molecular weight.

It will be explained in Section 3.4 that an “ideal living polymer” has a very narrow molecular weight distribution that is described by the Poisson distribution:

$$w(r) = \frac{r(r_n - 1)^{r-1}}{r_n(r-1)!} \exp(1 - r_n) \quad (2.72)$$

where r_n is the number-average degree of polymerization, and the polydispersity index is given by:

$$PI = 1 + \frac{M_0}{M_n} - \left(\frac{M_0}{M_n} \right)^2 \quad (2.73)$$

In practice, samples have PI values higher than this, because, as explained in Chapter 3, it is impossible to eliminate all traces of termination agents.

2.2.5 Narrow Distribution Samples

Even so-called *monodisperse* samples have polydispersities that are rarely smaller than 1.01. But even at this low value, the sample contains some high- and low-molecular-weight material. This is illustrated in Fig. 2.2, which shows the distributions calculated using the log-normal distribution (Eq. 2.67) for $M_w = 100,000$ and polydispersity index values of 1.01, 1.03, and 1.1. We see that even the material with the smallest PI has a small amount of polymer with M 20% higher or lower than the mean.

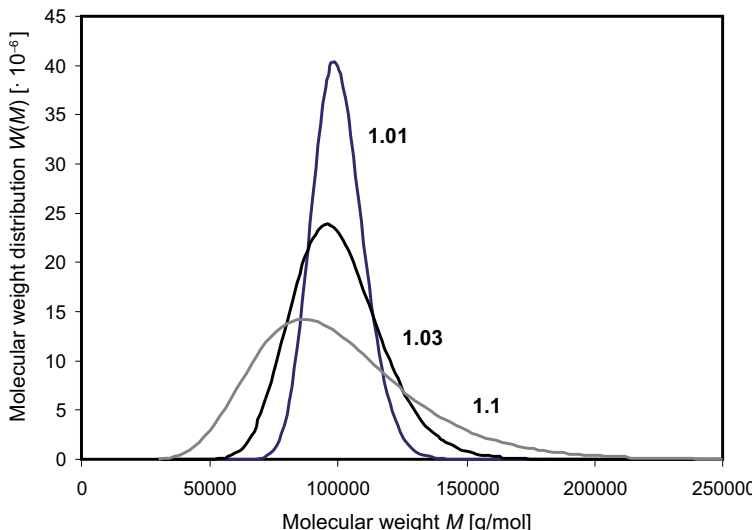


Figure 2.2 Molecular weight distributions calculated using the log-normal distribution function (Eq. 2.67) for $M_w = 100,000$ and $PDI = 1.01, 1.03$, and 1.10 . Although these samples might be described as “nearly monodisperse” in comparison to commercial polymers, there are many molecules that are significantly larger or smaller than average.

2.2.6 Bimodality

A blend of two monodisperse polymers having different molecular weights is said to have a *bimodal* molecular weight distribution. Extending this concept to polydisperse systems, it is also common practice to refer to a system whose $w(M)$ curve has two peaks as “bimodal”. Multi-mode systems are also possible by obvious extension. However, there are pitfalls in the use of this terminology. It is well known that the observed modality of a distribution, as indicated by a graph, can be different depending on whether it is the number fraction or the weight fraction distribution that is plotted [21, 22]. However, even if we restrict ourselves to the weight distribution, Friedman [32] has pointed out that it is possible for a given system to have two peaks in a plot of $[w(\log M)]$, whereas there is only one peak in the plot of $w(M)$. Finally, if high-molecular-weight polymer is gradually added to a sample having a substantially lower weight, at first there will be only a small effect on the MWD, but eventually a shoulder will appear, which will develop into a clear peak as more high MW material is added. At what exact point during this gradual evolution do we say that the distribution is “bi-modal?”

■ 2.3 Tacticity

The presence of any pendant group, even if it is only a methyl group, has an important effect on the crystallinity of a polymer. A polymer that has many such groups has a property called *tacticity*, which describes the distribution of orientations of side-groups along the chain. There are three types of distribution: *isotactic*, *syndiotactic*, and *atactic*. The simplest example is polypropylene, which can be polymerized in forms having all three tacticities. In isotactic polypropylene (i-PP), all the ethyl groups are on the same side of the chain, while the syndiotactic polymer (s-PP) has these groups on alternating sides. These two structures are sketched in Fig. 2.3. Of course, the actual molecule is not planar, so the sketch is, in fact, a projection of the molecule onto a plane. While the carbons in the backbone that are attached to the pendant groups are chiral centers, polypropylene does not have optical activity, because the atoms adjacent to it are also carbons.

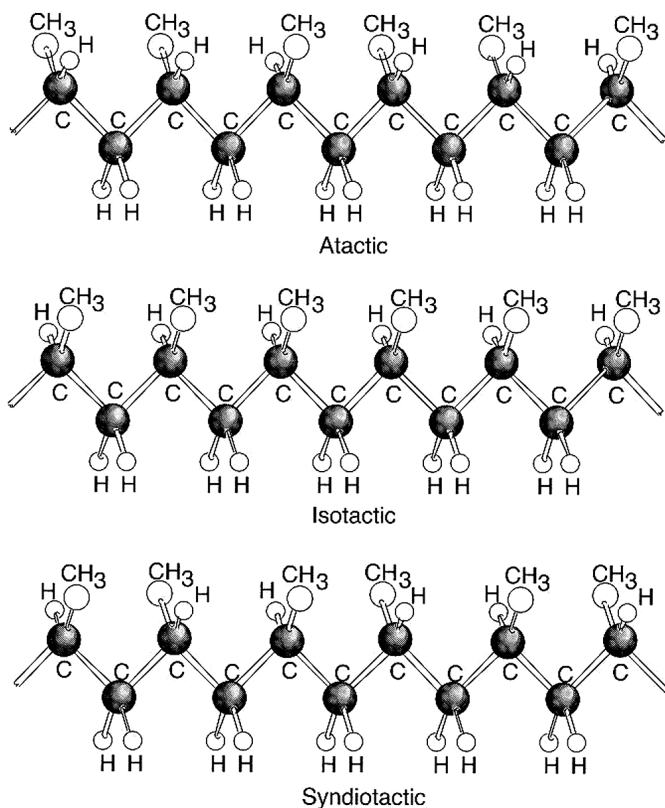


Figure 2.3 Sketch of projections onto the plane of atactic, isotactic and syndiotactic polypropylene molecules. The latter two are crystallizable, whereas the atactic isomer does not crystallize.

In a perfectly random, atactic polymer, the position of pendant groups varies randomly along the chain. Such a random distribution is said to be Bernoullian or a zero-order Markov chain. There are also intermediate structures, such as hemiisotactic and isotactic stereoblock polymers, which have randomly occurring, short runs of isotactic or syndiotactic structures. A detailed explanation of tacticity is given by Koenig [33]. Isotactic and syndiotactic polymers can crystallize, while atactic polymers cannot. Polymers other than polypropylene that have tacticity include polystyrene, poly(vinyl chloride), and poly(methyl methacrylate). Thus there are crystalline and non-crystalline forms of these polymers.

Tacticity can affect important physical properties such as the intrinsic viscosity and thus must be taken into account in characterization methods such as gel permeation chromatography. Jones et al. [34] used small-angle neutron scattering to study the chain dimension of syndiotactic polypropylene and found that the s-PP chain is substantially larger than that of i-PP. This implies that the s-PP molecule is stiffer than that of i-PP, which results in significant differences in the rheological and thermodynamic behavior of the two forms [34, 35]. The effect of tacticity on rheological properties is discussed in Chapter 5.

■ 2.4 Branching

The copolymerization of a higher α -olefin comonomer with polyethylene yields a polymer having short side-branches; for example the use of butene introduces ethyl branches. However, these short branches do not have an important effect on rheological properties such as viscosity. Much longer branches, on the other hand, have dramatic effects on rheological behavior [36]. Adding long-chain branches, while keeping the molecule weight constant, reduces the size of a molecule. As is explained in Section 5.10, this results in a reduction in viscosity at low molecular weight but an increase in viscosity at high MW. This is of great practical importance, as it provides a mechanism for altering the flow behavior of a polymer without affecting its crystallinity. For example, adding long-chain branches to a copolymer such as LLDPE makes it possible to control, independently, the flow behavior and the crystallinity.

There are three general types of fairly well-defined branching structures: stars, combs and randomly branched polymers (see Fig. 2.4). In addition, systems of any degree of complexity can be produced. A hyperbranched polymer (HBP) is randomly branched and has a complex structure in which there are branches on branches. In general, such a system has broad distributions of molecular weight and branching structure. An idealized model for a hyperbranched polymer is the n-Cayley tree. This is a structure in which each branch point, or vertex, has n branches, and this struc-

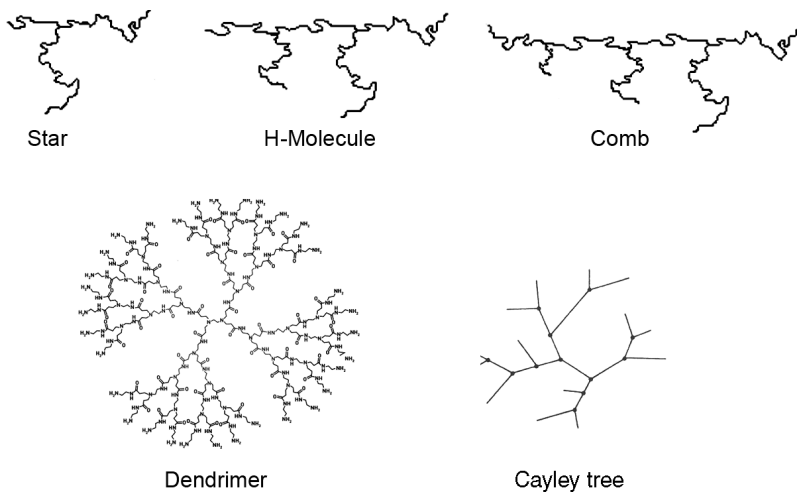


Figure 2.4 Sketches illustrating various branched structures: star, H-polymer, dense comb, Cayley tree, and dendrimer.

ture is propagated through multiple generations. A dendrimer is a highly-branched, monodisperse, symmetrical molecule built up from a multifunctional core by adding monomer layers in a stepwise fashion. The shape of the molecule becomes more and more spherical until steric hindrance prevents further symmetrical growth. Dendrimers must be made under very precisely controlled conditions to ensure the orderly build-up of the molecule. A dendrimer is a special case of a hyperbranched polymer. The branching structures mentioned above are illustrated in Fig. 2.4.

Long-chain branching greatly complicates the characterization and description of molecular structure. It is possible, by painstaking procedures, to prepare samples having reasonably uniform branching structures such as stars and combs [37]. But branched commercial polymers are usually randomly branched and may have complex structures in which there are distributions of backbone lengths, branch lengths, branch point locations and branching complexity. In fact, even the identification of a *backbone* is problematic when there are branches on branches. Low-density polyethylene (LDPE), made by a high-pressure, free-radical process, is an example of an important commercial material with a complex branching structure.

A parameter that describes the level of branching in a mainly linear polymer is the branching frequency λ , which is the average number of branch points per 1000 backbone carbon atoms. This is related to the average number of branch points per molecule β and the number average molecular weight, M_n . For polyethylene this is:

$$\lambda = \frac{\beta(14)(1000)}{M_n} \quad (2.74)$$

■ 2.5 Intrinsic Viscosity

2.5.1 Introduction

The oldest, simplest and most widely used method for obtaining information about molecular weight is based on measurement of the viscosity of a dilute solution. We will see that this quantity is less sensitive to molecular weight than the zero-shear viscosity of the melt. However, the apparatus required is much simpler and can be used in combination with GPC to determine molecular weight distribution. Furthermore, it is often impossible using a commercial rheometer to determine the zero-shear viscosity of a melt. Kulicke and Clasen [38] provide additional information regarding intrinsic viscosity.

Several quantities are used to describe the low-shear-rate limiting viscosity of a solution η in terms of the viscosity of the solvent, η_s , and the concentration of polymer, c . These are defined as follows.

The relative viscosity (viscosity ratio): $\eta_{\text{rel}} \equiv \eta/\eta_s$

The specific viscosity: $\eta_{\text{sp}} \equiv \eta_{\text{rel}} - 1 = \eta/\eta_s - 1 = (\eta - \eta_s)/\eta_s$

The reduced viscosity (viscosity number): $\eta_{\text{red}} \equiv \eta_{\text{sp}}/c$

The inherent viscosity: $\eta_{\text{inh}} \equiv (\ln \eta_{\text{rel}})/c$

The intrinsic viscosity: $[\eta] \equiv \lim_{c \rightarrow 0} \left(\frac{\eta_{\text{sp}}}{c} \right) = \lim_{c \rightarrow 0} (\eta_{\text{red}}) = \lim_{c \rightarrow 0} (\eta_{\text{inh}})$ (2.75)

The units for c (concentration) in all these definitions are g/cm³, and those for $[\eta]$ are thus cm³/g.

Because it is evaluated in the limit of infinite dilution, the intrinsic viscosity provides information about the average size of molecules in a solution in which there is no interaction between molecules. In practice, for a linear, monodisperse polymer, the relationship used to calculate the molecular weight from the intrinsic viscosity is the one proposed by Mark [39], Houwink [40], and Sakurada [41] and given here as Eq. 2.76.

$$[\eta] = K_m M^a \quad (2.76)$$

where the empirical constants K_m and a depend on the polymer, the solvent and the temperature. We will call this the MHS equation and describe its use in detail in Section 2.5.4. However, because the intrinsic viscosity is so widely used, and because this book is concerned primarily with molecular structure, it is important to

examine the physical basis of the MHS equation. This subject has been reviewed in detail by Kamide and Saito [42], and we provide here only a brief review of the most important theories concerning the relationship between $[\eta]$ and molecular weight.

Many readers will have no interest in these theories, and for them, the key results are Eq. 2.86, based on the equivalent sphere model when a theta solvent is used, and the MHS empirical equation, Eq. 2.76 above, when a theta solvent is not used. Since in the use of intrinsic viscosity for polymer characterization, it is not practical to use a theta solvent, many readers will want to cut to the chase and skip ahead to Section 2.5.4.

2.5.2 Rigid Sphere Models

The first approach is based on Einstein's century-old equation for the viscosity of a very dilute suspension of spheres in a Newtonian fluid, which is given by Eq. 2.77.

$$\eta = \eta_s (1 + 2.5 \phi) \quad (2.77)$$

where η_s is the viscosity of the liquid, which we consider to be the solvent, and ϕ is the volume fraction occupied by the spheres. Applying this equation to a very dilute colloid, the specific viscosity is given by Eq. 2.78.

$$\eta_{sp} \equiv \frac{\eta}{\eta_s} - 1 = 2.5 \phi \quad (2.78)$$

If the volume fraction ϕ is replaced by the concentration c (g/cm³) times the specific volume of the solute, v (cm³/g) the intrinsic viscosity is, according to Einstein's theory, given by Eq. 2.79.

$$[\eta] = 2.5 v \quad (2.79)$$

Equation 2.79 works well for rigid particles with roughly spherical shapes, but the intrinsic viscosity of polymer solutions is more than one hundred times the value given by this model.

The large disparity results from the fact that a polymer molecule is not a solid sphere but a randomly coiled chain that pervades a volume much greater than the physical volume occupied by the monomer units. One way to account for this is to introduce an *equivalent sphere radius*, R_e , that can be used in Eq. 2.77 in place of the volume implied by the concentration. Using this quantity, we can calculate the effective volume fraction corresponding to a given polymer concentration, c .

$$\phi = \frac{c N_A}{M} \left(\frac{4 \pi R_e^3}{3} \right) \quad (2.80)$$

where N_A is Avogadro's number, and M is the molecular weight of the polymer. Now inserting this into Eq. 2.77, we obtain:

$$\eta = \eta_s \left[1 + \frac{2.5 c N_A}{M} \left(\frac{4 \pi R_e^3}{3} \right) \right] \quad (2.81)$$

Thus, the reduced viscosity is:

$$\eta_{\text{red}} = \frac{2.5 N_A}{M} \left(\frac{4 \pi R_e^3}{3} \right) = \frac{2.5 N_A}{M} V_h \quad (2.82)$$

And in the limit of infinite dilution, this is equal to the intrinsic viscosity. The quantity in parentheses is called the *hydrodynamic volume* V_h , and it is essential to our objective to relate this empirically defined size parameter to molecular weight.

A measure of molecular size that can be calculated for a random coil is the root-mean-square end-to-end radius, $\sqrt{\langle R^2 \rangle_0}$, and Flory argued that $\langle R^2 \rangle_0^{3/2}$ should be proportional to the hydrodynamic volume V_h of an unperturbed molecule. It was shown earlier in this chapter by Eq. 2.7, repeated below as Eq. 2.83, that the mean square end-to-end distance is proportional to the molecular weight:

$$\langle R^2 \rangle_0 = (C_\infty l^2 j / M_0) M \quad (2.83)$$

We note that this implies that $\langle R^2 \rangle_0 / M$ is a constant for a given polymer. Since this applies to an infinitely dilute solution in its theta state, we can use this fact, together with Eq. 2.82, to obtain the intrinsic viscosity under theta conditions:

$$[\eta]_\theta = \Phi \left(\frac{\langle R^2 \rangle_0}{M} \right)^{3/2} M^{0.5} \quad (2.84)$$

This equation was first proposed by Flory and Fox [43], who proposed that Φ is a universal constant for all flexible polymer molecules. It is now known that this parameter depends to some degree on the solvent (even under theta conditions) and M , but a value established on the basis of many experiments under theta conditions is $2.5 \pm 0.1 \cdot 10^{23} \text{ mol}^{-1}$ when $[\eta]$ is expressed in (cm^3/g) . If the factors involving M in Eq. 2.84 are combined and brought to the left-hand side we have:

$$[\eta]_\theta M = \Phi \langle R^2 \rangle_0^{3/2} \quad (2.85)$$

This indicates that the product $[\eta] M$ is proportional to the hydrodynamic volume for a given polymer and solvent. This relationship is the basis of the universal calibration procedure used to determine molecular weight distribution from a GPC elution curve (see Section 2.6.3).

If $\langle R^2 \rangle_0 / M$ is, indeed, a constant for a given polymer, Eq. 2.84 can be rewritten in terms of a constant, K_θ , so that for a given polymer and solvent, we have, in the theta state:

$$[\eta]_\theta = K_\theta M^{0.5} \quad (2.86)$$

2.5.3 The Free-Draining Molecule

The rigid sphere is not an accurate picture of how a polymer molecule affects the flow of the fluid in which it is dissolved, because the fluid can penetrate within the molecular coil. This recognition led to the development of models in which the molecule is represented as a chain of beads that contain all the mass of the molecule, connected by springs. In the *free-draining* model of Rouse [44], there is no effect of one bead on the flow pattern around other beads. This model starts from Stokes' law, which gives the drag force F_D on a sphere in a Newtonian fluid flowing past it at the velocity U as proportional to the radius a of the sphere. In terms of the coefficient of friction ζ ($\equiv F_D/U$), Stokes law for flow past a sphere is:

$$\zeta = 6 \pi \eta_s a \quad (2.87)$$

This theory predicts an incorrect scaling of the intrinsic viscosity under theta conditions, $[\eta] \propto M$, and it is now known that it is only valid for polymers of very low molecular weight. A measure of molecular size in solution that is used primarily by biochemists is *Stokes' radius*. This is the radius that gives the correct friction coefficient when used in Eq. 2.87 as the value of a .

Zimm [45] and others [42] later addressed the more complex problem in which there is hydrodynamic interaction between the beads and derived a *nonfree-draining* theory that gives the same scaling as the rigid sphere model, i.e., $[\eta] \propto M^{0.5}$. Öttinger [46] analyzed the non-free-draining case in more detail to obtain the velocity profile within the coiled chain, and his results show that there is, indeed, substantial flow through the molecule except near its core. Nevertheless, the equivalent sphere model leads to the correct scaling of intrinsic viscosity with molecular weight.

A method for correcting intrinsic viscosity data for small departures from the theta state to determine K_θ was proposed by Burchard [47] and by Stockmayer and Fixman [48]. While the model on which this method is based is no longer thought to be valid, the equation that results, the BSF equation, has been found useful for dealing with *small deviations* from theta conditions. The BSF equation is shown here as Eq. 2.88:

$$[\eta] = K_\theta M^{1/2} + C M \quad (2.88)$$

This implies that K_θ can be determined as the intercept of a plot of $[\eta] M^{-1/2}$ versus $M^{1/2}$.

2.5.4 Non-Theta Conditions and the Mark-Houwink-Sakurada Equation

For the usual case of a solution not in its theta state, the volume pervaded by a polymer molecule is greater than that assumed in the above discussion, and in place of Eq. 2.86, the empirical Mark-Houwink-Sakurada (MHS) equation is used:

$$[\eta] = K_m M^a \quad (2.89)$$

where K_m and a depend on the polymer, the solvent and the temperature. Experimental data reveal that for a solution not in its theta state the exponent a on the molecular weight in equation Eq. 2.89 is normally greater than 0.5. Flory and Fox [43] argued that this exponent should depend on the temperature and the solvent, varying from 0.5 under theta conditions to 0.8 in a good solvent. Values have been determined for many combinations of these factors and can be found in reference [49]. Some typical values are shown in Table 2.2.

Fetters et al. [18] tabulated data from many sources for five polymers that had been studied using nearly monodisperse samples at theta or near-theta conditions. Four of the polymers, 1,4-polybutadiene, 1,4-polyisoprene, polystyrene, and poly(α -methylstyrene), were prepared by means of anionic polymerization, while the fifth, polyisobutylene, was a nearly monodisperse sample obtained by fractionation. They found that data for twelve samples of 1,4-polybutadiene in dioxane at 26.5 °C could be described by the MHS equation with the factors shown in Eq. 2.90.

$$[\eta] = 1.77 \cdot 10^{-1} M^{0.503} \quad (2.90)$$

The fact that the exponent is very close to one-half implies that this system is very close to its theta state. Using an extrapolation procedure based on the BSF Eq. 2.88 to obtain the value of the constant appropriate for the theta condition yields:

$$[\eta]_\theta = 1.84 \cdot 10^{-1} M^{0.5} \quad (2.91)$$

Table 2.2 Selected Values for Constants in MHS Equation 2.89. From [49].

Polymer	Solvent	Temp (°C)	K_m (cm^3/g) ($\cdot 10^4$)	a	MW range ($\cdot 10^{-4}$)
Polybutadiene	Benzene	30	8.5	0.78	15–50
Polyethylene (HD)	Decalin	135	62	0.7	2–104
Polypropylene (atactic)	Decalin	135	11.0	0.80	2–62
Polyacrylonitrile	Dimethylformamide	20	46.6	0.71	7–170
Poly(methyl methacrylate)	Benzene	25	5.5	0.76	2–740
Polystyrene (atactic)	Butanone	25	39	0.58	1–180
	Cyclohexane	34.5	88	0.50	1–6000
Poly(vinyl chloride)	Cyclohexanone	25	13.8	0.78	1–12

Since both K_m and α depend on the same characteristics of the solution, there have been several attempts to establish a direct relationship between them [42]. Rai and Rosen [50] analyzed the MHS parameters in reference [47] and proposed an empirical correlation valid for polymers having $M > 10,000$, at temperatures between 20 and 135 °C.

$$\log\left(\frac{K}{K_0}\right) = m(a - 0.5) \quad (2.92)$$

where K_0 is the value of K under theta conditions, and m is a constant for a given polymer. However, there is significant scatter around the curve represented by Eq. 2.92, and it is always best to use system-specific parameters if they are available.

2.5.5 Effect of Polydispersity

The above discussion applies to a monodisperse polymer, but it is impossible to produce a sample in which every molecule has exactly the same mass. Even in so-called monodisperse samples, PI is slightly greater than one, and for commercial polymers having the lowest values of PI , those produced using metallocene catalysts, $PI \geq 2$. It is thus important to know how polydispersity affects the intrinsic viscosity. In the limit of infinite dilution, the effect of molecules of different size is additive. This means that the intrinsic viscosity of the whole sample can be represented as a sum of terms, each based on the MHS equation (Eq. 2.88) applied to a component having molecular weight M_i present at weight fraction $w(M_i)$.

$$[\eta] = K_m \sum M_i^\alpha w(M_i) \quad (2.93)$$

This leads to an expression relating the MWD to the *viscosity average molecular weight* M_v that was introduced as Eq. 2.42 and is repeated here as 2.94.

$$M_v = \left[\sum M_i^\alpha w(M_i) \right]^{1/\alpha} \quad (2.94)$$

In terms of this average, the MHS equation for a polydisperse sample is:

$$[\eta] = K_m M_v^\alpha \quad (2.95)$$

We note that M_v depends strongly on α . This parameter varies from 0.5 to 1, which implies that $M_n < M_v \leq M_w$, so that $M_v = M_w$ corresponds to $\alpha = 1$. For theta conditions, $\alpha = 0.5$, but for many common polymer-solvent pairs, α is closer to 0.8, so that the viscosity average molecular weight is usually closer to M_w than to M_n .

The sum in Eq. 2.94 can be replaced by an integral for use with a continuous molecular weight distribution to give:

$$[\eta] = K_m \int_0^{\infty} M^a f(M) dM \quad (2.96)$$

One can then derive relationships between the intrinsic viscosity and various molecular weight averages, if a distribution function is specified. For example, for the Schulz-Zimm distribution function (Eq. 2.59), we obtain the following relationships between $[\eta]$ and the weight and number average molecular weights.

$$[\eta] = K_m M_w^a \frac{\Gamma(h+a+1)}{\left[(h+1)^a \Gamma(h+1)\right]} \quad (2.97)$$

$$[\eta] = K_m M_n^a \frac{\Gamma(h+a+1)}{h^a \Gamma(h+1)} \quad (2.98)$$

2.5.6 Effect of Long-Chain Branching

The intrinsic viscosity depends on the hydrodynamic volume of a molecule and is thus sensitive to the presence of long-chain branching, since the presence of branches causes the molecule to occupy a smaller volume than a linear molecule of the same molecular weight. A measure of this effect is the branching parameter g' , which is the ratio of intrinsic viscosities of branched and linear polymers having the same molecular weight:

$$[\eta]_B / [\eta]_L \equiv g' \quad (\text{same } M) \quad (2.99)$$

Of course, the intrinsic viscosities of the branched and linear polymers must be measured in the same solvent, but a related issue is the effect of the solvent on the value of g' . It is often assumed that changing the solvent will have similar effects on the intrinsic viscosities of both species, in which case the value of g' would not be affected.

Intrinsic viscosity reflects the hydrodynamic volume of a molecule, but a more fundamental parameter describing molecular size is the radius of gyration. And the effect of branching on molecular size is more commonly described in terms of the branching factor, g , which was defined in Eq. 2.16, shown again here as Eq. 2.100, as the ratio of the mean square radii of gyration of branched and linear molecules having the same molecular weight.

$$g \equiv \frac{\langle R_g^2 \rangle_B}{\langle R_g^2 \rangle_L} \quad (\text{same } M) \quad (2.100)$$

Formulas for calculating g for several well-defined branching structures, based on the assumption of a Gaussian chain, were shown in Section 2.1.2, and Small [7] lists sources of formulas for many other structures. If the hydrodynamic volume of the branched molecule, like that of a linear one, is proportional to the cube of the root mean square radius of gyration, then there should be a relationship between the two branching parameters g and g' . Zimm and Kilb [51] derived an equation for this relationship for ideal stars and for a molecule with two long and eight short branches and found that all the results could be described with reasonable accuracy by Eq. 2.101.

$$g' = g^{0.5} \quad (2.101)$$

Tobita and Hamashima [52] used Monte Carlo simulations to show that this relationship is also valid for randomly branched polymers. Wood-Adams et al. [53] found that Eq. 2.101 described the behavior of a series of long-chain branched metallocene copolymers.

Zimm and Kilb [51] suggested that Eq. 2.101 might be used as an approximate, empirical formula for “all branched molecules of whatever shape,” with 0.5 replaced by an empirical constant, as shown by Eq. 2.102.

$$g' = g^\varepsilon \quad (2.102)$$

The quantity ε is sometimes called the “drainage factor”. This form has been widely used, and values of ε ranging from 0.5 and 1.5 have been reported for various materials. However, there is no scientific basis for this generalization, and ε probably depends not only on the type of branching structure but also molecular weight. For stars and some combs, it has been found that $\varepsilon = 0.6$.

For a homogeneous sample one can use light scattering to measure radius of gyration and a viscometer to measure intrinsic viscosity and thus determine the branching factors g and g' . But for mixtures of molecules having various branching structures this yields only average values that reveal nothing about detailed branching structure. For example various values of the constant epsilon in empirical Eq. 2.102 have been reported for whole samples of LDPE [54, 55], but these have little if any fundamental significance.

2.5.7 Effects of Short-Chain Branching

Making simplifying assumptions, Stockmayer [56] derived an equation for the ratio of intrinsic viscosities in short-chain branched and linear polymers of the same molecular weight, which is shown below as Eq. 2.103. The assumptions, which are unrealistic for any real material, are that the polymer is monodisperse and that the short branches are equally spaced.

$$g'_{\text{SCB}} \equiv \frac{[\eta]_{\text{SCB}}}{[\eta]_L} = \left[1/(S+1) \right] \left[1 + S(1 - 2f + 2f^2 - 2f^3) + S^2(-f + 4f^2 - f^3) \right] \quad (2.103)$$

where (in this equation only) S is the number of branches per molecule, and f is the number of carbons in branches divided by the number of carbons in the backbone.

Branches with fewer than six carbon atoms occur often in commercial copolymers of ethylene and alpha-olefins. These are thought to be random copolymers (a special case of a statistical copolymer) in which the probability of finding a structural unit at a given location on the chain is independent of the neighboring units. As in the case of long branches, short branches reduce the size, and thus the intrinsic viscosity, of the molecule as compared to a linear one having the same molecular weight. It follows that a branched molecule having the same size and intrinsic viscosity as a linear one will have a higher molecular weight. Scholte et al. [57] derived the following relationship for the intrinsic viscosity of such an ethylene copolymer.

$$[\eta] = (1 - S)^{e+1} K_{\text{PE}} M^e \quad (2.104)$$

where K_{PE} is a constant for polyethylene copolymers, S is the mass fraction of short branches, which is related to n , the number of carbon atoms in the alpha-olefin comonomer, and W , the mass fraction of comonomer, by Eq. 2.105.

$$1 - S = 1 - (1 - 2/n) W \quad (2.105)$$

Considering the copolymer to be branched polyethylene, the branching index, g' , is given by:

$$g' = (1 - S)^{a+1} \quad (2.106)$$

Scholte et al. [57] found Eqs. 2.104 and 2.106 to be reasonably reliable for polypropylene and ethylene-propylene copolymers.

For a polydisperse polymer in which the fraction of short side chains, i.e., the comonomer fraction, is defined to be f_i for all molecules having the molecular weight M_i , Ambler [58] derived the following equation for the intrinsic viscosity:

$$[\eta] = K_m^{\frac{1}{1+e}} \sum f_i ([\eta]_i M_i)^{\frac{e}{1+e}} \quad (2.107)$$

Aerts [59] modeled the intrinsic viscosity of dendritic and hyperbranched materials.

When a copolymer also contains long-chain branches, one approach [57] is to use separate branching factors for the long and short branches and assume that the overall effect can be described as follows:

$$g' = g'_{\text{LCB}} g'_{\text{SCB}} \quad (2.108)$$

Sun et al. [60] studied the effect of alpha-olefin comonomer content on polyethylene and concluded that models based solely on molecular weight are too simple to describe quantitatively the effect of the short branches. By analogy with Eqs. 2.16 and 2.99, they defined branching factors for short chain branches and found that their data obeyed Eq. 2.109.

$$g'_{\text{SCB}} = g_{\text{SCB}}^{3/2} \quad (2.109)$$

They found that the two branching factors varied linearly with comonomer weight fraction but that the slope depended strongly on the comonomer used.

Information about the distribution of short-chain branches cannot be obtained from intrinsic viscosity measurements but can be investigated using carbon-thirteen NMR and crystallization techniques such as TREF and CRYSTAF, as explained in Section 2.6.6.

2.5.8 Determination of Intrinsic Viscosity—Extrapolation Methods

Determination of the intrinsic viscosity requires the measurement of the viscosities of several dilute solutions of varying concentration. The viscosities are quite low, and the most precise method for their measurement involves the use of glass capillary viscometers. Gravity drives the flow of the solution through a glass tube having a very small diameter, and the resulting flow rate is determined. For Newtonian fluids, there is a simple relationship between the flow time and the viscosity. The in-line intrinsic viscosity detectors that are used in conjunction with gel permeation chromatography (see Section 2.6.3) work on a slightly different principle, as the flow is generated by a pump and the resulting pressure drop is measured.

For precise laboratory measurements, the intrinsic viscosity is determined by the extrapolation to zero concentration of data obtained at several concentrations. This procedure will be subject to large uncertainty if the function plotted is not linear with concentration. Several methods have been proposed for carrying out the extrapolation, but those most commonly used are the Huggins plot, based on Eq. 2.110, and the Kraemer plot, based on Eq. 2.111.

$$\eta_{\text{red}} \equiv \eta_{\text{sp}}/c = [\eta] + k' [\eta]^2 c \quad (2.110)$$

$$\eta_{\text{inh}} \equiv (\ln \eta_r)/c = [\eta] + k'' [\eta]^2 c \quad (2.111)$$

For a solution in its theta state, the Huggins constant, k' , is about 0.5, and $k'' = (k' - 0.5)$. Extrapolation of either the reduced or inherent viscosity to $c = 0$ should give the intrinsic viscosity. Because k'' is less than k' , the slope of a Kraemer plot is lower, which should provide better precision in the extrapolated value, but the Huggins plot is the one most commonly used.

In making the extrapolation on a Huggins plot, the presence of concentration in the denominator of the dependent variable poses a problem in error management. Reilly et al. [61] showed how this problem could be solved and proposed a method for selecting optimal dilutions.

2.5.9 Effect of Shear Rate

The intrinsic viscosity is defined in terms of the viscosity in the limit of zero shear-rate, but the viscosity of a polymer solution depends on the shear-rate. Factors that enhance the shear-rate dependency of $[\eta]$ are high solvent power, large molecular weight and broad molecular weight distribution [62, 63]. To avoid consideration of this parameter, measurements must be made at sufficiently low shear rates that the viscosity is very close to its low-shear rate limiting value.

■ 2.6 Other Structure Characterization Methods

Several non-rheological methods for probing molecular structure are described briefly here, as these often provide important information that complements rheological data or is required to verify or calibrate a rheological method for structure determination.

2.6.1 Membrane Osmometry

Membrane osmometry is one of two osmometry techniques that are used to determine molecular weight. The other is vapor-pressure osmometry. The latter requires calibration using samples of known molecular weight, while membrane osmometry is an absolute technique. Only membrane osmometry is described here. The osmotic pressure of a polymer solution is directly related to the number-average molecular weight of the polymer and is useful when M_n is less than about 500,000. The basic principle is that if a polymer solution and pure solvent are placed on opposite sides of a semi-permeable membrane, i.e., one that allows solvent to pass but not polymer, there will be a tendency for solvent to flow into the solution, where its chemical potential is lower. If the pressure of the solution is raised above that in the solvent, the chemical potential will be balanced, and the flow will stop when the pressure difference reaches the *osmotic pressure*, π . The thermodynamic expression required to determine the molecular weight is the van't Hoff equation:

$$\frac{\pi}{c} = R T \left(\frac{1}{M_n} + A_2 c + A_3 c^2 + \dots \right) \quad (2.112)$$

where A_2 and A_3 are the second and third virial coefficients ($A_1 = 1/M_n$), and c is the concentration of polymer in the solution. The osmotic pressure is measured at several low concentrations, and the curve of π/c versus c is extrapolated to $c = 0$ to find M_n . For theta conditions, the higher virial coefficients are zero, and π/c is independent of c , so an extrapolation is not required. Thus, to minimize the slope of the curve to be extrapolated, it is best to use a relatively poor solvent, i.e., to stay close to the theta state. A useful approximation of Eq. 2.112 that includes the effect of the second virial coefficient is:

$$\left(\frac{\pi}{c} \right)^{1/2} = \left(\frac{\pi}{c} \right)_{c=0}^{1/2} \left(1 + \frac{M_n A_2 c}{2} \right) \quad (2.113)$$

Thus, a plot of $(\pi/c)^{1/2}$ versus c will be more linear than a plot of π/c versus c .

Automatic osmometers are now available that achieve equilibrium very quickly, often within minutes [64].

2.6.2 Light Scattering

The preferred method for determining the weight average molecular weight is light scattering. The basic principle is that light passing through a polymer solution is scattered by the polymer molecules, which are large enough to cause significant scattering but small compared to the wavelength of the light. It is necessary to choose a solvent having a refractive index that is sufficiently different from that of the polymer. The measurement consists of determining the intensity $I(\theta)$ of light scattered at various angles θ . The results are expressed in terms of the Rayleigh ratio, R_θ :

$$R_\theta \equiv \frac{I(\theta)}{I_0} \frac{R^2}{V_s} F(\theta) \quad (2.114)$$

where I_0 is the intensity of the incident light, R is the distance to the light source, V_s is the scattering volume, and $F(\theta)$ is an instrument constant. There are two contributions to the scattering from the polymer, one arising within the molecules and one involving interactions between molecules. These give rise to the two terms on the right hand side of Eq. 2.115.

$$R_\theta = K_s c \left[M P(Q) + V_s N_A c S(Q) \right] \quad (2.115)$$

where c is the concentration of polymer, K_s is a constant that involves the variation of solution refractive index with concentration, and Q is the magnitude of a scattering vector defined by Eq. 2.116.

$$Q \equiv \frac{4\pi n_0}{\lambda_0} \sin \frac{\theta}{2} \quad (2.116)$$

Here, n_0 is the refractive index, λ_0 is the wavelength of light in a vacuum. The first scattering function, $P(Q)$ approaches zero as Q approaches one, and the second function, $S(Q)$ is a second scattering function. We see that the second term, which is the contribution from intermolecular effects, approaches zero as the concentration vanishes. For the special case, $P = 1$ ($\theta \rightarrow 0$) and $c \rightarrow 0$, we have:

$$R_\theta = K_s c M \quad (2.117)$$

It can be shown [65] that for a polydisperse polymer, this equation is still valid with M replaced by M_w . Thus, light scattering provides a measure of the weight-average molecular weight. In order to determine M_w , it is necessary to extrapolate data obtained for various combinations of c and θ to $c = 0$ and $\theta = 0$. This double-extrapolation can be accomplished by means of a Zimm plot, which is a plot of $K_s c / R_\theta$ versus $X c + \sin^2 \theta / 2$ where X is a multiple of 10, often 1000.

The basic light scattering technique involves low-angle laser light scattering (LALLS). However, the sensitivity of the technique to various ranges of molecular weights depends on the angle, and if more than one angle is used, the mean-square radius of gyration can be determined. For this application, multiangle laser light scattering (MALLS) is optimal, while two-angle (TALLS) and right-angle (RALLS) light scattering are simpler techniques for the radius of gyration that provide somewhat less precision.

Great care is necessary in making light scattering measurements, as the presence of minute amounts of contaminant will lead to large errors. However, if sufficient care is taken, the following information can be obtained: M_w from the intercept, A_2 from the limiting slope of the $\theta = 0$ curve, and $\langle R_g^2 \rangle_0$ from the limiting slope of the $c = 0$ curve. We will see in the next section that light scattering can be used to advantage in combination with gel permeation chromatography. In the determination of the radius of gyration, we note that the size of a molecule in solution depends on the solvent and temperature, and the unperturbed value corresponds to behavior under theta conditions.

In summary, low-angle laser light scattering is useful for the absolute determination of molecular weight, while if more than one angle is used, the mean-square radius of gyration and the second virial coefficient can also be determined. It is useful over a wide range of molecular weights but is less sensitive to low-molecular-weight material. Some potential problems are that the solvent must have a different index

of refraction than the solute, contaminants must be avoided, and copolymers are not readily dealt with.

2.6.3 Gel Permeation Chromatography

The most widely used method for determining molecular weight distribution is *gel permeation chromatography* (GPC), also called *size exclusion chromatography* (SEC). A small amount of polymer is dissolved in a solvent and pumped through one or more columns containing porous beads. Because for some polymers, particularly polyolefins, elevated temperatures are required to keep the polymer in solution, the technique may be called high-temperature chromatography. Because the sample is in solution, the technique is also called liquid chromatography (LC). Over the last two decades, for most applications the size of the column used has been reduced, leading to faster analyses and lower solvent consumption. This is called high-performance liquid chromatography (HPLC). Pasch and Trathnigg [66] describe in detail the operation and use of HPLC. While chromatography continues to be used primarily for the determination of molecular weight distribution in linear polymers, recent developments make it possible to analyse samples that are heterogeneous in chain architecture and chemical composition [67], and the newer techniques are described briefly in later sections of this chapter. All fractionation techniques are described in detail in a recent monograph [68].

2.6.3.1 MWD of Linear Polymers

The process of analysis is as follows. A steady stream of pure solvent is fed to the column and at time $t = 0$, a small amount of polymer solution is injected into the stream. As the polymer molecules flow through the bead-packed column, the smaller molecules diffuse into the pores of the beads, while the largest molecules instead flow primarily directly through and out of the column. Thus, the largest molecules exit first, while the small molecules only appear after they have had time to diffuse back into the increasingly pure solvent stream. The concentration of polymer in the solvent leaving the column is measured, usually by means of a differential refractive index (DRI) detector and sometimes by an ultraviolet detector. A DRI detector measures the difference between the refractive index of the solution leaving the column and that of pure solvent. But an infrared (IR) detector for concentration measurement is now more common. The primary data from the analysis are the amount of liquid that has exited the column at time, t , called the retention volume, V_r , and the concentration of polymer in the liquid at that time. While one tries to maintain a precisely constant flow rate through the column, this is impossible to achieve in practice, and the liquid leaving the column is collected, often in batches

of five cubic centimeters, and the times at which the collection of a given batch starts and ends are recorded. The final *elution curve* shows the concentration as a function of retention volume, and may also include vertical lines showing the *count*, the number of the batch being collected during each V_r interval.

The actual separation of molecules in the column is based on molecular size rather than molecular weight. However, for linear molecules we saw in Section 2.1.2 that molecular weight is proportional to molecular size, as measured for example by the mean square radius of gyration $\langle R_g^2 \rangle_0$. Therefore, to interpret the elution curve to obtain the molecular weight distribution, it is necessary to calibrate the column. This is done by injecting a series of solutions of monodisperse samples of the polymer being analyzed and determining the retention volume when the polymer emerges. Ideally, the elution curve is very narrow and square shaped, since all the molecules injected should have the same retention volume, although in reality longitudinal diffusion (axial mixing) causes some dispersion in the elution curve. Chain scission and clogging make it impractical to use GPC for polymers with very high molecular weights. For many purposes in the plastics industry only a DRI detector is used, without calibration, and the data are used for comparison of resins rather than absolute MW determination.

In some cases, monodisperse samples of the polymer of interest are not available. In such a case, the *universal calibration* procedure is used. This involves the measurement of intrinsic viscosity. The quantity actually measured is the difference between the IV of the polymer solution and that of the pure solvent, and the detector is called a differential viscometer (DV). As implied by Eq. 2.85, the product of intrinsic viscosity and molecular weight is proportional to molecular size, i.e., hydrodynamic volume, V_h , which is the actual basis of the separation in a chromatography column.

$$[\eta] M = f(V_h) \quad (2.118)$$

In universal calibration, samples of a monodisperse polymer, often polystyrene, that is different from the polymer to be analyzed, are dissolved in the solvent of interest, and the intrinsic viscosities of the resulting solutions are measured. Then identical samples are injected into the column to be used, and the refractive index of the effluent is measured as a function of retention volume, V_r , which depends on V_h . Then a calibration plot of $[\eta] M$ versus V_r is prepared, and this plot is assumed to be valid also for the polymer to be analyzed. The retention time can also be used as the independent variable, since it is linear in V_r at constant flow rate. It is convenient to fit an equation, for example a third-order polynomial, to the universal calibration curve. Carrying this concept a step further, if an on-line IV detector is used along with the DRI detector, the data from an analysis can be interpreted directly in terms of a molecular size distribution, and from this the MWD can be determined.

An on-line viscosity detector actually detects the pressure drop ΔP resulting from flow at a constant volumetric flow rate, Q through a capillary. The viscosity of the solution is then calculated using the Poiseuille equation:

$$\eta = \frac{\pi R^4 \Delta P}{8 L Q} \quad (2.119)$$

where R and L are the radius and length of the capillary. It is not practical to make measurements at several concentrations, which would permit the extrapolation to zero concentration, and it is assumed that the concentration of the solution leaving the chromatographic column is sufficiently small that the intrinsic viscosity can be estimated as η_{sp}/c . This requires precise determination of the very small difference between the viscosity of the solution and that of the solvent. If light scattering is used in place of intrinsic viscosity, the data from the analysis give the MWD directly, since light scattering is sensitive to molecular weight rather than size, as is shown by Eq. 2.117. However, in this case, molecular weight information comes from the light scattering detector rather than from the cumulative volume of column effluent, which is a smooth function of time, and the light scattering signal inevitably includes noise. When this signal is differentiated the noise is amplified. Also, the properties of the eluent are not monitored continuously but for a series of small batch samples, and the R_g value detected by light scattering is the z-average for a given sample.

Because GPC has become such an important tool in polymer analysis, considerable attention has been directed toward optimizing its reliability. Major issues are the separation power of the column and longitudinal dispersion (axial mixing), which causes the spreading of the elution curve. Thus, liquid entering the detectors in a given elution volume contains material with some polydispersity. Errors resulting from axial diffusion are largest when the MWD of the sample is narrow. Correcting for axial dispersion requires a model of the flow in the column. High-performance columns and short connecting lines are used to minimize dispersion. A correction for axial dispersion may also be used. The effect of dispersion on the output signal depends on the nature of the detector. Since light scattering is sensitive to the weight-average molecular weight of a polydisperse sample, M_w for the whole polymer will be correct, but M_n will be overestimated. Sommer and Müller [69] have explored this issue in detail.

As with all sophisticated analytical techniques, one must always be concerned about the issues of *repeatability* and *reproducibility*. The more fundamental concepts of precision and accuracy are not directly useful. Precision is replaced by *repeatability*, which is defined by ASTM (The American Society for Testing and Materials) as the result of comparing measurements made using the same sample under identical conditions on the same instrument and within short intervals of time. Accuracy is not applicable, because one never knows the true value of the quantity to be deter-

mined. In its place one examines reproducibility, which involves the comparison of measurements made on the same sample under identical conditions using the same method, but in different laboratories using different instruments. D'Agnillo et al. [70] have reported on the results of an extensive round-robin program involving GPC analyses of seven polyethylenes in fifteen laboratories. The results of this valuable testing program revealed large variations among laboratories.

2.6.3.2 GPC with Branched Polymers

The above discussion applies only to linear polymers. Very short branches, such as those resulting from the use of an α -olefin comonomer with ethylene, have only a moderate effect on the size of the molecule and thus on the GPC separation. However, the short branches in these copolymers do affect the intrinsic viscosity and the radius of gyration, so one cannot use a calibration curve for the homopolymer or for a copolymer based on a different comonomer. But universal calibration using a differential viscometer is still appropriate. Methods of determining the distribution of short branches in copolymers are described in Section 2.6.6.

For architectures involving longer branches, the picture is complicated by the fact that the size of a molecule depends on the branching structure as well as the molecular weight. This poses a problem in the interpretation of GPC data, but it also provides a technique for obtaining information about the level of branching in a sample. If both LALLS and DV detectors are used, one obtains the distributions of both the molecular weight and the intrinsic viscosity. This arrangement is called triple-detector GPC or GPC-3D.

If the intrinsic viscosity of the linear analog of each fraction of the branched system has been measured, then one knows $[\eta]$ for a linear sample having the same M_w as each branched fraction, and g' can be calculated. This is useful only if g' can be related to the branching structure. The parameter g , the ratio of radii of gyration of branched and linear molecules, has a more fundamental relationship with molecular structure than $[\eta]$, i.e., the hydrodynamic volume, which is reflected in g' , as shown, for example, by Eqs. 2.17 to 2.26. Thus, one needs to estimate g from g' . The only theoretical relationship between these quantities is the one derived by Zimm and Kilb [51] for ideal stars and given as Eq. 2.101. For other structures, the relationship must be established empirically, and Eq. 2.102 is often assumed the form.

For systems containing species with various branching structures, e.g., mixtures of linear molecules, stars and combs, molecules having the same hydrodynamic volume and thus eluting at the same time can have widely varying molecular weights. In other words, each fraction can have significant polydispersity. Tobita and Saito [71] used a Monte Carlo scheme with random sampling to simulate the GPC separation of polydisperse stars and combs. They simulated two types of operation: universal calibration with differential refractive index (UC-RI) and with light scattering (LS).

For stars, both methods gave satisfactory results, but for the combs, UC-RI significantly underestimated the MWD. Light scattering was much better for the combs but still not exact. Tobita and Hamashima [72] also simulated the separation of randomly branched polymers. It is necessary to know or assume the nature of the reaction that produced the branched system, and he assumed a homogeneous distribution of branch points and a most-probable distribution for the degree of polymerization of the primary chains. However, he noted that such a structure does not arise from polymerization in even an ideal CSTR (continuous stirred tank reactor) because of the broad residence time distribution.

If MALLS is used instead of LALLS, along with a DV detector, it is possible to make a direct determination of the radius of gyration, and thus the value of g , for each fraction coming from the GPC column. This technique has been used to study long-chain branching in isotactic propylene [73]. The final step in establishing the branching structure is to relate g to structure. This requires knowledge of the way the polymer was synthesized. For a number of known structures, theoretical equations have been derived. Equations 2.17 to 2.26 are examples, and Small [7] lists sources for many others. The GPC-MALLS technique is clearly a valuable tool in the study of branched polymers. On the one hand, it can be used to verify polymerization models, and on the other, it produces data that can be used to predict rheological properties using the models presented in Chapters 9 and 11.

The long-chain branched metallocene polyethylenes made using the “constrained geometry” catalysts described in Chapter 3 pose their own special problem, because the level of branching, 0.01 to 0.1 LCB per 1,000 carbon atoms, is too low to be detected by means of GPC-MALLS. For these materials the factor β in Eq. 2.102 has been established to be 0.5 by use of C-13 NMR [53], and this makes it possible to use GPC-LALLS-DV to determine the distribution of radii of gyration and the number of branches per 1000 carbon atoms. Then using the results of Monte Carlo simulations of the polymerization process [74] it was shown that knowledge of this parameter makes it possible to determine the rheologically-significant features of the branching structure.

2.6.3.3 GPC with LDPE

Low-density polyethylene (LDPE) poses special problems, as it contains a broad spectrum of chain architectures. It is not possible to separate a sample according to a given structural feature while avoiding the effects of others. A further complication is that two types of reactor are widely used to manufacture LDPE, namely autoclave and tubular, and each one produces a different mix of structures. These structures are discussed in Section 3.6. But because of its commercial importance, there have been many attempts to characterize its distributions of molecular weight and branching

structure using liquid chromatography [76–80]. Early efforts made use of universal calibration [75], while more recent studies made use of multiple detectors. If, in addition to DRI and DV, a light scattering detector is added (GPC-3D), one obtains both the size and the molecular weight of each slice of eluant. However, the complexity of this polymer makes it very difficult to achieve a reliable characterization. Since chromatographic columns separate according to size, not mass, molecules with inhomogeneous structure and polydispersity elute in the same retention volume.

Equation 5.4 is an empirical relationship between zero-shear viscosity and weight average molecular weight that applies quite well to polydisperse, linear polymers, and there have been attempts to apply it to branched polymers, particularly LDPE. For example, the viscosity calculated from the equation based on M_w of an LDPE is compared with that of linear PE having the same M_w . However, this use of M_w for LDPE is problematic. The temperature dependence of viscosity is different for the two structures, so varying the temperature will affect the relationship between them. And a more serious issue is that various methods for determining M_w lead to quite different numbers. The most commonly used method, which we will call “conventional GPC,” yields a value we will call gpc- M_w , and makes use of an infrared detector and a calibration curve based on linear standards. This is called the “backbone” molecular weight. An alternative is an “absolute value,” abs- M_w , which makes use of a light-scattering detector and responds to the entire molecule. Both the short and long-chain branches in LDPE affect η_0 , and one cannot distinguish between the effects of molecular weight and that of branches. This issue is taken up in more detail in Section 5.10.5

2.6.3.4 Interactive Chromatography

Since SEC (GPC) separates molecules on the basis of size, it is not well-suited to separations based on the chemical composition of copolymers, tacticity and other heterogeneities. To meet this need, interactive chromatographic (IC) techniques have been developed, as they are sensitive to chemical structure. Their separation mechanisms make use of enthalpic interactions to vary the adsorption of molecules on a stationary phase. IC also provides better resolution than SEC for separation by molecular weight, and this is particularly important in dealing with samples having very narrow MWD. The first IC technique was solvent-gradient interactive chromatography (SGIC) in which the composition of the solvent is varied [80, 81]. A major advance was the use of a carbon-substrate in the separation column [82, 83]. Ethylene copolymers have been separated by use of SGIC [83, 84]. A disadvantage of SGIC is that light scattering and viscosity detectors cannot be used to monitor concentration.

A newer development is temperature gradient interactive chromatography (TGIC), which is preferred to SGIC for most purposes, because light scattering and viscosity

detectors can be used to monitor concentration [85, 86]. Cong et al. [86, 87] demonstrated the use of TGIC with a carbon substrate for the analysis of ethylene copolymers. There is a linear relationship between elution time and level of comonomer incorporation, and this is independent of molecular weight when it is greater than 20,000 [88]. TGIC has been used to reveal that model branched polymers made by means of elaborate anionic polymerization contain byproducts and are thus somewhat heterogeneous [89–92]

2.6.3.5 Field Flow Fractionation

Problems in LC associated with column packing, such as the degradation of very large molecules, are avoided in field flow fractionation (FFF). Also filtration is not required, and complex materials containing particles and gels can be analyzed [93]. Pasch and Malik [68] provide a detailed description of several versions of this technique. As in SEC a sample is injected into a carrier fluid (solvent) that flows through a slit where a force field drives polymer molecules toward one wall according to their size. The two most common versions are asymmetric flow field fractionation (AF4) and thermal-flow fractionation (ThF3). Because ThF3 requires a 50 °C temperature difference between the slit walls, it is not suitable for use with polyolefins, and AF4 is used for these polymers. In this technique the driving force for lateral diffusion is provided by a crossflow normal to the sample flow.

2.6.4 Mass Spectrometry (MALDI-TOF)

Matrix-assisted laser desorption/ionization (MALDI) followed by time-of-flight (TOF) mass spectrometry has been applied to the absolute determination of molecular weight for certain polymers [94, 95]. In this technique, the sample is mixed in very small proportion with a solid matrix that is irradiated with laser light. The matrix absorbs the light and transfers energy to the polymer leading to its desorption and ionization. The energy transfer must occur very gently so as not to damage the polymer. The ionized polymer is then separated into its components by use of a mass spectrometer. This technique is directly applicable to polymers having polar, unsaturated or aromatic groups, which can be readily cationized by metals. Since it is a less laborious technique than GPC or NMR, MALDI-TOF has attracted interest as a possible technique for characterizing commercial polymers such as polyethylene. However, polyolefins cannot be analyzed using MALDI-TOF, since they lack a functional group that can be cationized. Bauer et al. [96] proposed a technique for overcoming this problem in the case of polyethylene by the chemical modification of the polymer prior to analysis. Altuntas and Schubert [97] recently reviewed methods of using mass spectrometry to determine polymer structure features, including

molecular weight distribution, monomer units, side-chain substituents, end groups, functionalities and copolymer composition. And Pasch [98] has described the use of mass spectrometry in conjunction with chromatographic separation.

2.6.5 Nuclear Magnetic Resonance

The use of NMR to elucidate the structure of polyolefins was pioneered by Randall [99]. Structural features that can be probed include the identity of the repeat unit and its chirality, copolymer sequence structures and their distributions, identity of end groups, degree of polymerization, and branching. Carbon-13 is a naturally-occurring isotope that represents about one percent of the carbon atoms present in a polymer. In a typical experiment, a sample is excited by a series of radio frequency pulses, which alter local nuclear moments by a certain angle, after which they decay to their undisturbed (equilibrium) state. The decay is monitored by a detector coil, and the output curve shows the frequencies at which resonance occurred. In order to achieve sufficient precision for the applications mentioned above, experiments of quite long duration are required, often many hours, or even several days. Pasch [98] has recently described the use of NMR together with fractionation to reveal the microstructure of each eluate.

Carbon-13 resonances result from the local environment of carbon atoms, and the NMR specialist must interpret these to infer the specific structural features indicated by each one. Wood-Adams et al. [53] described in detail an NMR technique for detecting low levels of branching in polyethylene homopolymers. Weng et al. [100] compared GPC-MALLS with NMR for the determination of long-chain branching in isotactic polypropylene and found that branching levels given by the two techniques were in good agreement. In addition, they found that NMR provided information about the mechanism of branch formation.

NMR resonances are sensitive to structural contributions of carbon atoms up to about four atoms away from a given atom. As a result, this technique is unable to detect, for example, the difference between a short-chain branch resulting from the presence of octene comonomer in polyethylene, and a branch long enough to be entangled. When dealing with a polymer that contains both types of branch, additional techniques are required to elucidate the structure. Striegel and Krejsa [101] showed how NMR and GPC can provide complementary information about both long- and short-chain branching in polyethylene. This technique can, in principle, reveal the degree of randomness in comonomer distributions, but the procedure is rarely used because it is very time-consuming. In general, it is not practical to use NMR to detect branching levels below 0.01 branches per 1000 carbons because of the limited solubility of the polymer and the low concentration of carbon-13 nuclei.

2.6.6 Separations Based on Crystallizability: TREF, CRYSTAF, and CEF

The techniques mentioned in this section are described in detail and compared in an extensive review [88] and in a recent book [68]. Random copolymers, in which the comonomer is randomly distributed along the chain, are of substantial commercial importance, particularly copolymers of ethylene with an α -olefin, e.g., LLDPE (linear low-density polyethylene) and metallocene LLDPE (mLLDPE). The average comonomer content can be determined by FTIR or NMR, but of equal importance is the chemical composition distribution (CCD), which is the distribution of comonomer content among the molecules. The crystallization behavior of a chain is governed by the ethylene sequence distribution (ESD) along its backbone. Differential scanning calorimetry (DSC) yields the degree of crystallinity for a whole sample, which is an average over all the molecules, but not the distribution among the molecules. Solution-DSC, on the other hand is thought to be capable of tracking the crystallization temperature of segments having various lengths and thus the ESD.

However, the crystallization of the entire chain is thought to be governed by the longest ethylene sequence (LES), and temperature rising elution fractionation (TREF), crystallization analysis fractionation (CRYSTAF), and crystallization elution fractionation (CEF) are techniques for fractionating semicrystalline polymers according to their crystallizability from dilute solution. These techniques are widely used for the characterization of polyolefins, particularly polypropylene and copolymers of ethylene and alpha-olefins. The ability of a molecule to crystallize is impeded by the presence of irregularly spaced side groups resulting from the use of a comonomer or the lack of tacticity, and techniques based on crystallizability thus provide information about these aspects of molecular structure. If an appropriate calibration curve is available, the longest ethylene sequence distribution (copolymers) or tacticity distribution (polypropylene) can be established. Long-chain branching is presently thought not to affect elution temperatures, and molecular weight is not a factor as long as it is greater than about 10,000.

Factors contributing to the CCD include catalyst type, polymerization conditions, and reactor inhomogeneity. Ziegler-Natta multiple-site catalysts produce polymers with broad distributions of chemical composition in copolymers and of tacticity in polypropylene, and such distributions are important in plastics applications. For example, low-crystallinity fractions are extractable and render a material unsuitable for food packaging, while high-crystallinity fractions result in haze and low impact strength in plastic films.

The basic principle of TREF is that material with a high degree of crystallizability crystallizes from solution at a higher temperature than material with a lower degree. Thus, crystalline material is produced by slowly cooling a dilute solution. Then the crystalline material, together with a support, is packed into a column through which

solvent is passed. The temperature of the solvent is gradually increased, and the concentration of polymer in the effluent is tracked by an in-line sensor (A-TREF) or by collecting samples for off-line study (P-TREF). A typical TREF result is a plot of the amount of polymer dissolved and eluted as a function of temperature. Because a reliable model of the process is not available, no universal calibration method exists, and a calibration curve is required to determine the distribution of tacticity or chemical composition. Because regio-regularity, stereoregularity, and tacticity all affect crystallizability, it is essential that the microstructure of the polymer used for calibration be the same as that of the material to be analyzed. A typical calibration curve for an olefin polymer is a plot of methyl groups per thousand carbon atoms versus temperature. The result for a given solvent is usually a straight line with a negative slope.

Crystallization analysis fractionation (CRYSTAF) provides the same information as TREF but is much faster, as it uses only the dissolution process to accomplish the separation. The basic principle is that material with a low-level of crystallinity dissolves in a solvent at a lower temperature than material with a higher level. It also avoids the use of a column and thus the peak broadening and requires no support. However, CRYSTAF involves very small quantities of material and is therefore not useful as a preparative technique. The sample is placed in a small sample vial equipped with a stirrer and a sampling line with a filter that prevents crystals from leaving. The vial is placed in an oven whose temperature is gradually increased. Samples are collected at small temperature intervals by nitrogen pressurization, and the polymer concentration is detected by an IR sensor. A cumulative curve of polymer concentration versus temperature of crystallization is obtained. Taking the derivative, a TREF-type curve can be obtained, and for conversion to CCD the calibration procedure is the same as in TREF. Monrabal et al. [103] compared TGIC with TREF for CCD determination of ethylene-octene copolymers and showed that while resolution was a bit better with TREF, there was less co-crystallization with TGIC. And of course crystallizability techniques are not useful for elastomers.

An even faster technique is crystallization elution fractionation (CEF) in which the solution is pumped slowly through a column containing a support [104]. The temperature decreases gradually along the column, and when the crystallization temperature of a fraction is reached, it is deposited on the support. This method provides better separation and minimizes cocrystallization. Monrabal et al. [103] compared CEF with TGIC for the determination of CCD and also discussed the combined use of TGIC and TREF or CEF.

A thorough review of TREF and CRYSTAF is that of Pasch and Malik (see ref [92], Chapter 2).

2.6.7 Bivariate (Two-Dimensional) Characterizations

Polymers that are heterogeneous in more than one way, for example in terms of molecular weight and also of chemical structure or architecture, pose challenging characterization problems. Dealing with such bivariate distributions requires the use of more than one separation technique, and such characterizations are said to be “two dimensional” (2D). Some of these are described by Monrabal [89]. For example, in the case of many polyolefins, one wishes to determine both CCD and MWD. This problem has been attacked by the combination of two or more analytical techniques. An example is TREF-GPC [104].

The combination of SGIC with SEC is another 2D technique (SGIC2D) that reveals mass-composition interdependence. In the SEC stage standard concentration detectors can be used [105]. This technique has been used to characterize ethylene copolymer rubbers [106], which cannot be analyzed by means TREF-GPC, because they do not crystallize.

Baumgaertal and Altuntas [107] describe recent developments in the use of chromatography in combination with advanced characterization tools, including the use of liquid chromatography at critical conditions (LCCC).

2.6.8 Molecular Structure from Rheology

In subsequent chapters we will see that the rheological properties of a melt are very sensitive to molecular structure, although measuring such properties requires significantly larger amounts of sample than the characterization techniques described above. The very strong sensitivity of the viscosity to molecular weight makes the measurement of viscosity a valuable tool for the determination of the weight average molecular weight and even the molecular weight distribution of a polydisperse sample. Moreover, melt rheology data are often more sensitive to high-molecular-weight components than GPC. Chapter 8 explains how such data can be used to infer the molecular weight distribution, and Chapters 10 and 11 mention methods for elucidating branching structure. The use of the zero-shear viscosity to detect long-chain branching is discussed in Chapter 5. In the case of samples with unknown, complex branching structures, each additional characterization technique adds something to one’s understanding of the structure. But no finite set of measurements can reveal all the details of a complex branching situation, because many independent distributions would have to be specified for a complete characterization.

■ 2.7 Summary

The size of a polymer molecule is of central importance in relating molecular structure to measurable quantities. Each possible conformation of the molecule corresponds to a different size, and detailed analysis of all possible conformations is not feasible. The freely-jointed chain model, however, along with random flight calculations, make it possible to derive the Gaussian distribution of sizes along with relationships between the mean square end-to-end distance, the mean square radius of gyration, and the molecular weight. Equations showing the effects of well-defined branching structures on these quantities have also been derived.

Dilute solutions are used to measure quantities related to molecular size and weight, and for the special case of a molecule in its unperturbed state it is possible to derive equations for the relationships of interest. Because of the excluded volume effect, the molecule is not normally in its unperturbed state, but for particular combinations of solvent and temperature, the factors contributing to the departure from the unperturbed state cancel out so that the theoretical equations are valid; at this condition, the molecule is said to be in its theta state.

The molecular weight distribution can be described in terms of moments or by a continuous function, either empirical or based on a model of the polymerization reaction. Other features of molecular structure include tacticity and branching.

Methods for determining an average molecular weight involve measurements of the properties of the dilute solution, including intrinsic viscosity, osmotic pressure, and light scattering. Of these, intrinsic viscosity is the property most often measured, and for linear polymers there is a simple relationship with molecular weight. Molecular weight distribution is determined by means of gel permeation chromatography (GPC) commonly combined with a differential viscometer. But since intrinsic viscosity is related to molecular volume rather than mass, it does not provide the MWD of branched polymers. A light scattering detector is sensitive to molar mass, but if a sample is heterogeneous in structure, it provides no quantitative information about molecular structure.

The use of NMR and mass spectrometry (MALDI-TOF) make it possible to probe details of molecular features not accessible using other techniques. For heterogeneous materials, advanced analytical techniques have been developed in recent years. These include multidetector SEC, interactive chromatography (IC) including SGIC, TGIC, and field flow fractionation (FFF).

TREF, CRYSTAF and crystallization elution fractionation (CEF) are techniques based on crystallizability in solution and are used for the determination of the level and distribution of the short-chain branches in copolymers.

Abbreviations Used in Chapter 2

AF4	Asymmetric flow field fractionation
CCD	Chemical composition distribution
CEF	Crystallization elution fractionation
CRYSTAF	Crystallization analysis fractionation
DI	Differential intrinsic viscosity
DRI	Differential refractive index
FFF	Field flow fractionation
FTIR	Fourier transform infrared
GPC	Gel permeation chromatography (same as SEC)
HPLC	High performance liquid chromatography
HT-TGIC	High-temperature thermal gradient interactive chromatography
IC	Interaction chromatography
IR	Infrared
IV	Intrinsic viscosity
LC	Liquid chromatography
LCB	Long-chain branching
LDPE	Low-density polyethylene
LLDPE	Linear low-density polyethylene
LAS	Low-angle light scattering
LS	Light scattering
MALS	Multi-angle light scattering
RI	Refractive index
SEC	Size exclusion chromatography (Same as GPC)
SGIC	Solvent gradient interaction chromatography
TGIC	Temperature gradient interactive chromatography
ThF3	Thermal field flow fractionation
TREF	Temperature rising elution fractionation

■ References

- [1] Graessley, W.W. *Polymeric Liquids & Networks: Structure and Properties* (2004) Garland Science, New York
- [2] Boyd, R.H., Phillips, P.J. *The Science of Polymer Molecules* (1993) Cambridge Univ. Press, Cambridge
- [3] Brandrup, J., Immergut, E.H. *Polymer Handbook*. 3rd ed. (1989) Wiley, New York
- [4] Ferry, J. *Viscoelastic Properties of Polymers*. 3rd ed. (1980) John Wiley & Sons, New York
- [5] Doi, M., Edwards, S.F. *The Theory of Polymer Dynamics* (1986) Oxford University Press, Oxford
- [6] Kuhn, W. Beziehungen zwischen Molekülgröße, statistischer Molekülgestalt und elastischen Eigenschaften hochpolymerer Stoffe. *Kolloid-Z.* (1936) 76, pp. 258–271
- [7] Small, P.A. Long-chain branching in polymers. *Adv. Polym. Sci.* (1975) 18, pp. 1–64
- [8] Zimm, B H., Stockmayer, W.H. The dimensions of chain molecules containing branches and rings. *J. Chem. Phys.* (1949) 17, pp. 1301–1314
- [9] Lecacheux, D., Lesec, J., Quivoron, C. High-temperature coupling of high-speed GPC with continuous viscosity. I. Long-chain branching in polyethylene. *J. Appl. Polym. Sci.* (1982) 27, pp. 4867–4877
- [10] Hadjichristidis, N., Xenidou, M., Latrou, H., Pitsikalis, M., Poulos, Y., Avgaropoulos, A., Sioula, S., Paraskeva, S., Velis, G., Lohse, D.J., Schulz, D.N., Fetters, L.J., Wright, P.J., Mendelson, R.A., García-Franco, C.A., Sun, T., Ruff, C.J. Well-defined, model long chain branched polyethylene. Synthesis and characterization. *Macromol.* (2000) 33, pp. 2424–2436
- [11] Flory, P.J. *Statistical mechanics of chain molecules* (Reprinted with corrections and remarks) (1989) Hanser Publications, Munich
- [12] Rubinstein, M., Colby, R.H. *Polymer Physics* (2003) Oxford Univ. Press, Oxford
- [13] Sokal, A.D. Monte Carlo methods for self-avoiding walk, Chapt. 2 In *Monte Carlo and Molecular Dynamics Simulations in Polymer Science*, Binder, K. (Ed.) (1995) Oxford Univ. Press, Oxford
- [14] Yamakawa, H. *Modern Theories of Polymer Solutions* (1971) Harper and Row, New York
- [15] Edwards, S.F., Singh, P. Size of a polymer molecule in solution Part 1.—Excluded volume problem. *J. Chem. Soc., Faraday Trans. 2* (1979) 75, pp. 1001–1019
- [16] Edwards, S.F. The Statistical mechanics of polymers with excluded volume. *Proc. Phys. Soc.* (1965) 85, pp. 613–624
- [17] Baumann, H. On the estimation of unperturbed dimensions of long-chain molecules in solution. *J. Polym. Sci., Part B: Polym. Lett.* (1965) 3, pp. 1069–1073
- [18] Fetters, L.J., Hadjichristidis, N., Lindner, J.S., Mays, J.W. Molecular weight dependence of hydrodynamic and thermodynamic properties for well-defined linear polymers in solution, *J. Phys. Chem. Ref. Data* (1994) 23, pp. 619–639

- [19] Zifferer, G. Monte Carlo simulation studies of the size and shape of linear and star-branched polymers embedded in the tetrahedral lattice. *Macromol. Theory Simul.* (1999) 8, pp. 433–462
- [20] Kirste, R.G., Kruse, W.A., Scholten, J. Die Bestimmung des Trägheitsradius von Polymethylmethacrylat im Glaszustand durch Neutronenbeugung. *Die Makromolekulare Chemie* (1973) 162, pp. 299–303
- [21] Peebles, L.H. *Molecular Weight Distributions in Polymers* (1971) Interscience, New York
- [22] Schulz, G.V. Über die Beziehung zwischen Reaktionsgeschwindigkeit und Zusammensetzung des Reaktionsproduktes bei Makropolymerisationsvorgängen. *Z. Phys. Chem. B* (1935) 30, p. 379
- [23] Flory, P.J. *Principles of Polymer Chemistry* (1953) Cornell Univ. Press, Ithaca, New York
- [24] Schulz, G.V. Über die Kinetik der Kettenpolymerisationen. 5th ed. Der Einfluss verschiedener Reaktionsarten auf die Polymolekularität. *Z. Phys. Chem. B* (1939) 43, pp. 25–46
- [25] Zimm, B.H. Apparatus and methods for measurement and interpretation of the angular variation of light scattering. *J. Chem. Phys.* (1948) 16, p. 1099
- [26] Gloor, W.E. A continuum of molecular weight distributions applicable to linear homopolymers. *J. Appl. Polym. Sci.* (1975) 19, pp. 273–279
- [27] Gloor, W.E. The numerical evaluation of parameters in distribution functions of polymers from their molecular weight distributions. *J. Appl. Polym. Sci.* (1978) 22, pp. 1177–1182
- [28] Gloor, W.E. Extending the continuum of molecular weight distributions based on the generalized exponential (GEX) distribution. *J. Appl. Polym. Sci.* (1983) 28, pp. 795–805
- [29] Tung, L.H. Fractionation of polyethylene. *J. Polym. Sci.* (1956) 20, pp. 495–506
- [30] Wesslau, W. Die Molekulargewichtsverteilung einiger Niederdruckpolyäthylen. *Makromol. Chem.* (1956) 20, pp. 11–142
- [31] Chiang, R. Comments on intrinsic viscosity-weight average molecular weight relationships for polyethylene, *J. Polym. Sci.* (1959) 36, pp. 91–103
- [32] Friedman, E.M. Modality of Molecular Weight Distributions. *Polym. Eng. Sci.* (1990) 30, pp. 569–570
- [33] Koenig, J.L. *Chemical Microstructure of Polymer Chains* (1988) John Wiley & Sons, New York
- [34] Jones, T.D., Haraman, E.W., Kim, M.-H., Chaffin, K.A., Bates, F.S., Annis, B.K., Man-Ho, K., Wignall, G.D., Fan, W., Waymouth, R. Effect of tacticity on coil dimensions and thermodynamic properties of polypropylene. *Macromol.* (2002) 35, pp. 5061–5068
- [35] Eckstein, A., Suhm, J., Friedrich, C., Maier, R.-D., Sassmannshausen, J., Bochmann, M., Mulhaupt, R. Determination of plateau moduli and entanglement molecular weights of isotactic, syndiotactic, and atactic polypropylenes synthesized with metallocene catalysts. *Macromol.* (1998) 31, pp. 1355–1340

- [36] Bersted, B.H. Effects of long chain branching on polymer rheology. Chapt. 22 In *Rheology and non-Newtonian flows*, Vol. 7 of *Encyclopedia of Fluid Mechanics*, Cheremisinoff, N.P. (Ed.) (1998) Gulf Publishing Co., Houston
- [37] Pitsikalis, M., Pispas, S., Mays, J.W., Hadjichristidis, N. Nonlinear block copolymer architectures. *Adv. Polym. Sci.* (1998) 135, pp. 1–138
- [38] Kulicke, W.-M., Clasen, C. Viscometry of polymers and polyelectrolytes (2004) Springer-Verlag, Berlin
- [39] Mark, H. *Der Feste Körper*, Hirzel, Leipzig (1983) p. 103
- [40] Houwink, R. Relation between the polymerization degree determined by osmotic and viscometric methods. *J. Prakt. Chem.* (1940) 157, pp. 15–18
- [41] Sakurada, I. *Kasenkouenshyu* (1941) 6, p. 177
- [42] Kamide, K., Saito, M. Viscometric determination of molecular weight. Chapt. 8 In *Determination of Molecular Weight*. Cooper, A.R. (Ed.) (1989) John Wiley & Sons, New York
- [43] Flory P.J., Fox, T.G. Treatment of intrinsic viscosities. *J. Am. Chem. Soc.* (1951) 73, pp. 1904–1908
- [44] Rouse, P.E., Jr. A theory of the linear viscoelastic properties of dilute solutions of coiling molecules. *J. Chem. Phys.* (1953) 21, pp. 1272–1280
- [45] Zimm, B.H. Dynamics of polymer molecules in dilute solution: viscoelasticity, flow birefringence and dielectric loss. *J. Chem. Phys.* (1956) 24, pp. 269–278
- [46] Öttinger, H.C. Velocity field in nondraining polymer chains. *Rheol. Acta* (1996) 35, pp. 134–138
- [47] von Burchard, W. Über den Einfluss der Lösungsmittel auf die Struktur linearer Makromoleküle. I. *Die Makromol. Chem.* (1961) 50, pp. 20–36
- [48] Stockmayer, W.H., Fixman, M. On the estimation of unperturbed dimensions from intrinsic viscosities. *J. Polym. Sci., Part C: Polym. Symp.* (1963) 1, pp. 137–141
- [49] Kurata, M., Tsunashima, Y., Iwama, M., Kamada, K. Chapt. 4 In *Polymer Handbook*. 4th ed., Brandrup, J., Immergut, E.H., Grulke, E.A. (Eds.) (1999) Wiley Interscience, New York
- [50] Rai, P., Rosen, S.L. An empirical relation between the Mark-Houwink-Sakurada constants. *J. Polym. Sci., Part B: Polym. Phys.* (1997) 35, pp. 1985–1987
- [51] Zimm, B.H., Kilb, R.W. Dynamics of branched polymer molecules in dilute solution. *J. Polym. Sci.* (1959) 37, pp. 19–42
- [52] Tobita, H., Hamashima, N. Monte Carlo simulation of size exclusion chromatography for randomly branched and crosslinked polymers. *J. Polym. Sci., Part B: Polym. Phys.* (2000) 38, pp. 2009–2018
- [53] Wood-Adams, P.M., Dealy, J.M., de Groot, A.W., Redwine, O.D. Effect of molecular structure on the linear viscoelastic behavior of polyethylene. *Macromol.* (2000) 33, pp. 7489–7499
- [54] Meira, G.R. Chapt. 2 In *Modern Methods in Polymer Characterization*, Barth, H.G., Mays, J.W. (Eds.) (1991) John Wiley, New York
- [55] Seo, Y., Kwang, U.K. A new model for rapid evaluation of the degree of long-chain branching in polymers. *Polymer* (1994) 19, pp. 4163–4167

- [56] Stockmayer, W.H. Personal communication. As cited by Billmeyer, F.W. The molecular structure of polyethylene. III. Determination of long chain branching. *J. Am. Chem. Soc.* (1953) 75, pp. 6118–6122
- [57] Scholte, G., Meijerink, N.L.J., Schoffeleers, H.M., Brands, A.M.G. Mark-Houwink equation and GPC calibration for linear short-chain branched polyolefins. *J. Appl. Polym. Sci.* (1984) 29, pp. 3763–3787
- [58] Ambler, M.R. Universal calibration in GPC: A new approach for the calculation of molecular weights. *J. Polym. Sci., Polym. Chem. Ed.* (1973) 11, pp. 191–201
- [59] Aerts, J. Prediction of intrinsic viscosities of dendritic, hyperbranched and branched polymers. *Comput. Theor. Polym. Sci.* (1998) 8, pp. 49–54
- [60] Sun, T., Brant, P., Chance, R.R., Graessley, W.W. Effect of short chain branching on the coil dimensions of polyolefins in dilute solution. *Macromol.* (2001) 34, pp. 6812–6820
- [61] Reilly, P.M., van der Hoff, B.M.E., Ziogas, M. Statistical study of the application of the Huggins equation to measure intrinsic viscosity. *J. Appl. Polym. Sci.* (1979) 24, pp. 2087–2100
- [62] Kotaka, T., Suzuki, H., Inagaki, H. Shear-rate dependence of the intrinsic viscosity of flexible linear macromolecules. *J. Chem. Phys.* (1966) 45, pp. 2770–2773
- [63] Suzuki, H., Kotaka, T. Inagaki, H. Shear-rate dependence of the intrinsic viscosity of flexible linear molecules. II. Solvent effect. *J. Chem. Phys.* (1969) 51, pp. 1279–1285
- [64] Hunt, B.J. Chapt. 9 In Vapour pressure osmometry/membrane osmometry/viscometry. *Modern Techniques for Polymer Characterization* Pethrick, R.A., Dawkins, J.V. (Eds.) (1999) John Wiley & Sons, New York
- [65] Berry, G.C., Cotts, P.M. Chapt. 4 In Static and dynamic light scattering. *Modern Techniques for Polymer Characterization*. Pethrick, R.A., Dawkins, J.V. (Eds.) (1999) John Wiley & Sons, New York
- [66] Pasch, H. Trathnigg, B. *HPLC of Polymers* (1998) Springer-Verlag, Berlin.
- [67] Chang, T. Recent advances in liquid chromatography analysis of synthetic polymers. *Adv. Polym. Sci.* (2003) 165, pp. 1–60
- [68] Pasch, H., Malik, M.I. *Advanced Separation Techniques for Polyolefins* (2014) Springer, New York
- [69] Sommer, C., Müller, G. Relationships between separation power and the MW averages in SEC measurements with molecular mass sensitive detectors. *J. Liq. Chromatogr. Relat. Technol.* (2001) 24, pp. 1047–1060
- [70] D'Agnillo, L., Soares, J.B.P., Penlidis, A. Round-robin experiment in high-temperature gel permeation chromatography. *J. Polym. Sci., Part B: Polym. Phys.* (2002) 40, pp. 905–921
- [71] Tobita, H., Saito, S. Size exclusion chromatography of branched polymers: Star and comb polymers. *Macromol. Theory Simul.* (1999) 8, pp. 513–519
- [72] Tobita, H., Hamashima, N. Monte Carlo simulation of size exclusion chromatography for branched polymers formed through free-radical polymerization with chain transfer to polymer. *Macromol. Theory Simul.* (2000) 9, pp. 453–462

- [73] Agarwal, P.K., Somani, R.H., Weng, W., Mehta, A., Yang, L., Ran, S., Liu, L., Hsiao, B.S. Shear-induced crystallization in novel long-chain branched polypropylenes by *in situ* rheo-SAXS and WAXD. *Macromol.* (2003) 36, pp. 5226–5235
- [74] Costeux, S., Wood-Adams, P., Beigzadeh, D. Molecular structure of metallocene-catalyzed polyethylene: Rheologically relevant representations of branching architecture in single catalyst and blended systems. *Macromol.* (2002) 35, pp. 2514–2528
- [75] Drott, E.E., Mendelson, R.A. Determination of polymer branching with gel permeation chromatography. *J. Polym. Sci., Part A-2* (1970) 8, pp. 1361–1385
- [76] Tackx, P., Tacx, J.C.J.F. Chain architecture of LDPE as a function of molar mass using SEC and MALLS. *Polymer* (1989) 30, pp. 3109–3113
- [77] Nordmaier, E., Lanver, U., Lechner, M.D. The molecular structure of low-density polyethylene 1. Long-chain branching and solution properties. *Macromol.* (1990) 23, pp. 1072–1076
- [78] Nordmeier, E., Lanver, U., Lechner, M.D. The molecular structure of low-density polyethylene 2. Particle scattering factors. *Macromol.* (1990) 23, pp. 1077–1084
- [79] Kuhn, R., Krömer, H. Structures and properties of different low density polyethylenes. *Colloid Polym. Sci.* (1982) 260, pp. 1083–1092
- [80] Macko, T., Brüll, R., Zhu, Y., Wang, Y. A review on the development of liquid chromatography systems for polyolefins. *J. Sep. Sci.* (2010) 33, pp. 3446–3454
- [81] Macko, T., Pasch, H., Kazakevich, Y.V., Fadeev, A.Y. Elution behavior of polyethylene in polar mobile phases on a non-polar sorbent. *J. Chromatogr. A* (2003) 988, pp. 69–108
- [82] Macko, T., Pasch, H. Separation of linear polyethylene from isotactic, atactic, and syndiotactic polypropylene by high-temperature adsorption liquid chromatography. *Macromol.* (2009) 42, pp. 6063–6067
- [83] Miller, M.D., de Groot, W., Lyons, J.W., Van Damme, F.A., Winniford, B.L. Separation of polyolefins based on comonomer content using high-temperature gradient adsorption liquid chromatography with a graphitic carbon column. *J. Appl. Polym. Sci.* (2012) 123, pp. 1238–1244
- [84] Macko, T., Brüll, R., Wang, Y., Coto, B., Suarez, I. Characterization of ethylene-propylene copolymers with high-temperature gradient adsorption liquid chromatography and CRYSTAF. *J. Appl. Polym. Sci.* (2011) 122, pp. 3211–3217
- [85] Chang, T., Lee, H.C., Lee, W., Park, S., Ko, C. Polymer characterization by temperature interaction chromatography. *Macromol. Chem. Phys.* (1999) 200, pp. 2188–2204
- [86] Cong, R., de Groot, A.W., Parrott, A., Yau, W., Hazlitt, L., Brown, R., Cheatham, M., Miller, M.D. High-temperature thermal gradient interaction chromatography (HT-TGIC) for microstructure analysis of polyolefins. *Macromol. Symp.* (2012) 312, pp. 108–114
- [87] Cong, R., de Groot, W., Parrott, A., Yau, W., Hazlitt, L., Brown, R., Miller, M., Zhou, Z. A new technique for characterizing comonomer distribution in polyolefins: high-temperature thermal gradient interaction chromatography (HT-TGIC). *Macromol.* (2011) 44, pp. 3062–3072

- [88] Monrabal, B. Polyolefin characterization: Recent advances in separation techniques. *Adv. Polym. Sci.* (2013) 257, pp. 203–252
- [89] Perny, S., Allgaier, J., Cho, D., Lee, W., Chang, T. Synthesis and structural analysis of an H-shaped polybutadiene. *Macromol.* (2001) 34, pp. 5408–5415
- [90] Snijkers, F., van Ruymbeke, E., Kim, P., Lee, H., Nikopoulou, A., Chang, T., Hadjichristidis, N., Pathak, J., Vlassopoulos, D. Architectural dispersity in model branched polymers: Analysis and rheological consequences. *Macromol.* (2011) 44, pp. 8631–8643
- [91] Li, S.W., Park, H.E., Dealy, J.M., Maric, M. Lee, M.H., Im, K., Chopi, H., Chang, T., Rahman, M.S., Mays, J. Detecting Structural Polydispersity in Branched Polybutadienes. *Macromol.* (2011) 44, pp. 208–214
- [92] Van Ruymbeke, E., Chang, H.K., Nikopoulou, A., Hadjichristidis, N., Snijkers, F., Vlassopoulos, D. Molecular rheology of branched polymers: Decoding and exploring the role of architectural dispersity through a synergy of anionic synthesis, interaction chromatography, rheometry and modeling. *Soft Matter* (2014) 10, pp. 4762–4777
- [93] Schimpf, M.E., Caldwell, K., Giddings, J.C. *Field Flow Fractionation Handbook* (2000) John Wiley, Hoboken, NJ
- [94] Scamporrino, E., Vitalini, D. Recent advances in mass spectrometry of polymers. Chapt. 8 in *Modern Techniques for Polymer Characterization*. (Eds.) Pethrick, R.A., Dawkins, J.V. (1999) John Wiley & Sons, New York
- [95] Pasch, H., Schrepp, W. *MALDI-TOF Mass Spectrometry of Synthetic Polymers* (2003) Springer-Verlag, Berlin
- [96] Bauer, B.J., Wallace, W.E., Fanconi, B.M., Guttman, C.M. Covalent cationization method for the analysis of polyethylene by mass spectrometry. *Polymer* (2001) 42, pp. 9949–9953
- [97] Altuntaş, E., Schubert, U.S. Polymeromics: Mass spectrometry based strategies in polymer science toward complete sequencing approaches: A review. *Anal. Chim. Acta* (2014) 808, pp. 56–69
- [98] Pasch, H. Advanced fractionation methods for the microstructural analysis of complex polymers. *Polym. Adv. Technol.* (2015) 26, pp. 771–784
- [99] Randall, J.C. A review of high resolution liquid ^{13}C carbon nuclear magnetic resonance characterizations of ethylene-based polymers. *J. Macromol. Sci., Rev. Macromol. Chem. Phys.* (1989) C29 (2&3), pp. 201–317
- [100] Weng, W., Hu, W., Dedmezian, A.H., Ruff, C.J. Long chain branched isotactic polypropylene. *Macromol.* (2002) 35, pp. 3838–3843
- [101] Striegel, A.M., Krejsa, M.R. Complementarity of universal calibration of SEC and ^{13}C NMR in determining the branching state of polyethylene. *J. Polym. Sci., Part B: Polym. Phys.* (2000) 38, pp. 3120–3135
- [102] Monrabal, B., Mayo, N., Cong, R. Crystallization elution fractionation and thermal gradient interactive chromatography. Technique comparison. *Macromol. Symp.* (2012) 312, pp. 115–129

- [103] Monrabal, B., Sancho-Tello, J., Mayo, N. Romero, L. Crystallization elution fractionation. A new separation process for polyolefin resins. *Macromol. Symp.* (2007) 257, pp. 71–79
- [104] Ortín, A., Monrabal, B., Sancho-Tello, J. Development of an automated cross-fractionation apparatus (TREF-GPC) for full characterization of the bivariate distribution of polyolefins. *Macromol. Symp.* (2007) 257, pp. 13–28
- [105] Roy, A., Miller, M.D., Meunier, D.M., de Groot, A.W., Winniford, W.L., Van Damme, F.A., Pell, R.J., Lyons, J.W. Development of comprehensive two-dimensional high temperature liquid chromatography × gel permeation chromatography for characterization of polyolefins. *Macromol.* (2010) 43, pp. 3710–3720
- [106] Ginsburg, A., Macko, T., Dolle, V., Brüll, R. Characterization of polyolefins by comprehensive high-temperature two-dimensional liquid chromatography. (HT 2D-LC) *Eur. Polym. J.* (2011) 47, pp. 319–329
- [107] Baumgaertl, A., Altuntaş, E. Recent developments in the detailed characterization of polymers by multidimensional chromatography. *J. Chromatogr. A* (2012) 1240, pp. 1–20

3

Polymerization Reactions and Processes

■ 3.1 Introduction

The objective of this chapter is to demonstrate how molecular structure, also called architecture, is governed by the polymer synthesis reaction mechanism and how this, in turn, depends on polymerization conditions. This information is essential for establishing relationships between molecular structure and rheological properties. It is only from knowing the reaction process that we can have *a priori* knowledge of the molecular structure. And in the case of complex structures, it is our only source of such knowledge.

Even for a material known to be a linear homopolymer, so that it is only necessary to establish its molecular weight distribution, it was explained in Chapter 2 that experimental methods for this determination are not perfect and can fail to reveal a small amount of high molecular weight material that can have an important effect on rheological properties. And when a comonomer is involved, or there is the possibility of long-chain branching, the detailed description of a sample becomes much more complicated. In fact, given a sample whose molecular structure is completely unknown, there is no combination of analytical and rheological techniques that can reveal its detailed structure, including all the possible distributions of comonomer content and branching structures among the molecules.

For this reason, if one wishes to study the relationship between molecular structure and rheological behavior, knowledge of the molecular structure must come from modeling the reaction by which a polymer was produced. We will see that there are techniques for preparing, in the laboratory, linear samples having quite narrow molecular weight distributions and well-defined branching structures. Commercial polymers, on the other hand, usually have somewhat ill-defined structures. Ziegler-Natta catalysts and those of a similar nature produce materials with broad molecular weight distributions, due to the variability in the reactivity of reaction sites. Moreover, some of these catalysts may introduce long-chain branching to a degree that is poorly controlled and unknown. The development of metallocene catalysts led to a dramatic improvement in our ability to produce, on an industrial scale,

materials having fairly well-defined structures. But there are still distributions of molecular weight, chemical composition (comonomer incorporation) and long-chain branch content, and knowledge of these can only come from a reliable model of the polymerization reaction.

Methods for modeling polymerization processes are not taught in the present book, but references to work on this subject are provided. In the case of living polymers, which have very well-defined structures and are invaluable in polymer research, the reaction is simply modeled, and the distributions of molecular weight and structure can be fairly narrow. In the case of commercial polymers, however, modeling is required in order to know anything about the molecular weight distribution and branching structure. Analytical predictions of polymer composition are possible when random processes are involved with constant probabilities, as in an ideal continuous, stirred-tank reactor (CSTR). Batch reactors generally require numerical solutions of the kinetics equations. Monte Carlo modeling is useful when a direct solution is not possible and the various reaction mechanisms can be described in terms of a small set of probabilities. In this technique, the experimental distribution of molecular species is represented by a large number of molecules that are “created” on the computer using random numbers and statistical rules. The Monte Carlo method is therefore perhaps more properly referred to as “random sampling.”

This chapter begins with a description of two schemes used to classify a polymer on the basis of either its structure or the type of reaction used to produce it and proceeds to a list of the various features that define molecular structure. This is followed by a description of the processes used to prepare samples with uniform and well-defined structures for research purposes. Finally, we discuss the processes used to make some commercial polymers and the molecular structures that result. An important modern development that comes close to bridging the gap between model polymers made for research and commercial products was the discovery of metallocene and other “single-site” catalysts. The polymers produced using these catalysts have structures that are much more homogeneous and well-defined than earlier commercial polyolefins.

Because the development of polymerization catalysts and the processes for their commercial use are intimately associated with certain individuals, it will be of interest to mention some of these ingenious people in this chapter. Detailed accounts of the history of polymer science can be found in several interesting books [1–3].

■ 3.2 Classifications of Polymers and Polymerization Reactions

Wallace Carothers, DuPont's famous polymer chemist, proposed classifying polymers by reference to the stoichiometry of the polymerization reaction. If the entire monomer molecule ends up in the polymer, he called it an *addition polymer*, whereas if there is a byproduct, often water, the primary product is called a *condensation polymer*. He thus considered vinyl polymers to be addition polymers and polyesters to be condensation polymers. However, it was later found to be possible to make some "addition polymers" by reactions in which there is a byproduct and to make some "condensation polymers" by reactions in which there is no byproduct. Paul Flory, who started his career as the theoretician in Carother's DuPont research group, later proposed that the reaction mechanism be used as the basis for classifying polymers. In this scheme, in a *step polymerization*, any two reactive molecules can combine, so polymerization occurs uniformly throughout the reaction mixture. In *chain growth polymerization*, on the other hand, monomer units are added only to species containing an active center or initiator, which can be a free radical, an ion, or an active catalyst site. Condensation polymers are usually produced by step reactions, and addition polymers are usually made by chain growth. Because of the variety of reactions that can be used to prepare a given polymer, no classification scheme divides polymers neatly into two or more categories. For example, it is possible to produce some addition polymers by means of stepwise reactions and to make some condensation polymers by means of chain growth polymerization. Also, so-called "living polymers" are said by some authors to arise from chain growth but by others to arise from a stepwise reaction.

In chain-growth polymerization, the monomer reacts only with active groups, and there are at least three reactions involved: initiation, propagation, and termination. There may also be transfer and inhibition. In living polymerization, on the other hand, there is only initiation and propagation, and the reaction continues as long as any monomer is present. And by changing the monomer during the reaction, one can produce block copolymers. In stepwise reactions, species of all sizes react with each other, and there is only one type of reaction, between two functional end groups, which are usually, e.g., nylon 6-6, but not always, e.g., nylon 6, different.

The most important chain-growth polymers are polyolefins and vinyl polymers. Examples of the former are polyethylene and polypropylene, and examples of the latter are poly(vinyl chloride), polystyrene, poly(vinyl alcohol), polyacrylonitrile, and poly(methyl acrylates). The most common stepwise reactions are condensation polymerizations. Polyamides, such as nylon 6-6, which is poly(hexamethylene adipamide), and polyesters, such as poly(ethylene terephthalate), are the most important

commercial condensation polymers. These polymers were originally developed for use in fiber manufacture because of their high melting points but are now used also as thermoplastics for a broad range of applications. Polycarbonate is an engineering plastic that is made from bisphenol A and phosgene by a stepwise reaction.

This book deals exclusively with addition polymers made by chain growth. This is because the molecules are usually much more flexible than those of condensation polymers made by stepwise reactions, and this greatly enhances the dependence of rheological properties on molecular structure. In addition, because they do not rely exclusively on van der Waals forces for their strength in the solid state, commercial versions of condensation polymers usually have molecular weights that are below the entanglement level. When reference is made in subsequent chapters to specific systems, these will always be highly-entangled polyolefins or vinyl polymers. We use the term polyolefin here to mean a polymer based on a small monomer that consists entirely of carbon and hydrogen atoms and that is not completely saturated. The principal examples are polyethylene and polypropylene. Vinyl polymers are based on monomers containing the vinyl group ($\text{H}_2\text{C}=\text{CH}-$), where the remainder of the molecule is other than a hydrogen or small hydrocarbon group. Common commercial examples are polystyrene and polyvinyl chloride (PVC). However, a hydrocarbon group, such as a methyl group, is often considered to be a vinyl group, so that polypropylene and polybutadiene are sometimes considered to be vinyl polymers.

Addition polymers are made using one of three processes: free radical, ionic, and complex coordination catalysis. Ionic polymerization can be either anionic or cationic. Except for some elastomers that are made by ionic polymerization, commercial polymers are made by free-radical polymerization or by use of complex coordination catalysts. So-called living polymers are widely used in polymer research, because they can be made with very narrow molecular weight distributions and defined branching structures. These were traditionally made using anionic polymerization, but living polymers can now also be made using a free-radical “living controlled” or cationic process. The latter are more easily carried out but yield less homogeneous products.

■ 3.3 Structural Characteristics of Polymers

3.3.1 Introduction

The features that make one polymer sample behave differently than another include: chemical composition, including comonomer content and distribution along and among molecules, distribution of molecular weights, often described briefly by giving two or more average molecular weights, tacticity, and long-chain branching structure.

3.3.2 Chemical Composition—Role of Backbone Bonds in Chain Flexibility

A single carbon–carbon bond provides maximum flexibility to a chain, as is illustrated by polyethylene and polyisobutylene. The carbon–carbon double bond, as in polybutadiene and polyacetylene, generally increases chain stiffness, although natural rubber is an exception. We will see in later chapters that chain flexibility, in turn, has an important effect on the molecular weight at which entanglement effects become important, which is called the *molecular weight between entanglements*, M_e . Increasing flexibility lowers the molecular weight for entanglement. For example, polyethylene ($M_e \approx 1250$) is more flexible than polystyrene ($M_e = 19,000$). As the molecular weight is increased above this level, entanglement effects become more and more important, eventually dominating rheological behavior.

3.3.3 Chemical Composition—Copolymers

A comonomer is used in commercial polymers to alter the properties of a base polymer, for example to change its glass-transition temperature, degree of crystallinity or swelling behavior, or to make it more compatible with a plasticizer or dye or enhance its stability. An example of the use of a comonomer to reduce crystallinity is linear low-density polyethylene (LLDPE), which is a copolymer of ethylene with an α -olefin that is described in Section 3.8. Because the monomers are usually not equally reactive, the chemical composition of a chain varies during polymerization. Alternating and blocky distributions along a chain represent the two extremes in the spectrum of possible distributions, with random copolymers falling in between. In addition, a complete description of the copolymer includes the distribution of comonomer among chains. These distributions define the chemical composition distributions (CCD) of a polymer. Techniques for modeling the CCD of binary [4] and multicomponent [5] copolymers have been reported. Techniques for determining these distributions (TREF, CRYSTAF, CEF) were described in Chapter 2.

3.3.4 Tacticity

Vinyl monomers, such as styrene, and alkenes with a side group such as propylene, can polymerize in several molecular forms whose crystallization behaviors are quite different from each other. If the side groups are all on one side of the backbone, the structure is called isotactic, and if they are on alternating sides, it is syndiotactic. If they are distributed in a random fashion, the polymer is said to be atactic. The isotactic and syndiotactic forms are crystallizable, often in a helical structure, while the atactic form does not crystallize and solidifies only at its glass transition tem-

perature. Figure 2.3 illustrated the three tacticities for the case of polypropylene. It has been found that polypropylene tacticity can also have an important effect on chain dimensions [6] and rheological behavior [7], as will be explained in Chapter 5.

3.3.5 Branching

Short branches are much shorter than the backbone of the linear molecule to which they are attached and than any “long-chain branches” that may be present. The term “short branches” is most often used for branches that have only a few carbon atoms, such as are produced by copolymerizing ethylene with an α -olefin such as butene or octene. A “long-chain” branch usually has a molecular weight exceeding that required for entanglement, M_e . As is explained in Chapter 5, this is the molecular weight at which entanglement begins to have an effect on rheological behavior. The simplest long-chain branched molecules are stars and combs. These can be produced by carefully-controlled reactions, usually anionic polymerization. A *pom-pom* polymer has a backbone whose ends have many free arms. This idealized structure has been widely used as the basis for rheological constitutive equations derived using the tube model for stress relaxation that is described in Chapter 6. It has also served as the basis for an empirical model of the rheology of low-density polyethylene [7].

While high-density polyethylene (HDPE) is generally considered to be unbranched, branching is known to occur in some HDPEs, as is described in Section 3.7.2. Low-density polyethylene (LDPE) contains both short and long-chain branches and is produced commercially in very large quantities. Its structure is described in Section 3.6.

A hyperbranched polymer (HBP) is randomly branched and has a complex structure in which there are branches on branches. In general, such a system has broad distributions of molecular weight and branching structure. Hyperbranched polyesters can be synthesized by a one-pot polycondensation, and fractions having low polydispersity have been prepared for rheological study [8]. An idealized model for a hyperbranched polymer is the n-Cayley tree. This is a structure in which each branch point, or vertex, has n branches. For example, the simplest 3-Cayley trees are the three-armed star and the H-molecule, which is also the simplest comb molecule. And the simplest 4-Cayley tree is tetra-methyl methane. A dendrimer is a highly-branched, monodisperse, symmetrical molecule built up from a multifunctional core by adding monomer layers in a stepwise fashion. The shape of the molecule becomes more and more spherical until steric hindrance prevents further symmetrical growth. Dendrimers must be made under very precisely controlled conditions to ensure the orderly build-up of the molecule. A dendrimer is a special case of a hyperbranched polymer. The branching structures mentioned above were illustrated in Fig. 2.4.

■ 3.4 Living Polymers Having Prescribed Structures

In order to test molecular dynamics models and empirical correlations, it is necessary to synthesize polymers having precisely controlled molecular structures [9]. Such “model polymers” were for many years *living polymers* made in reactions with negligible termination or chain transfer. Termination halts the growth of a chain, while chain transfer terminates one chain but simultaneously generates a new radical. Thus, active centers are never lost, and polymerization continues until all the monomer is depleted. If more monomer is then added, the reaction continues, and if a different monomer is added, a block copolymer is produced. Such living polymers are made by chain reactions of monomers containing a double bond. A more recently developed technique is free-radical (*living/controlled*) polymerization, which is described in Section 3.4.2. (IUPAC has adopted the term “reversible deactivation radical polymerization” (RDRP) for this process.) This process is much simpler than true living polymerization, but the products are not as homogeneous.

In a living polymer, the number-average molecular weight is simply the grams of monomer present initially per mole of initiator. An ideal living polymer has a molecular weight distribution described by the Poisson distribution (given in Chapter 2). The polydispersity index (M_w/M_n) corresponding to a Poisson molecular weight distribution is given by:

$$PI = 1 + \frac{M_0}{M_n} - \left(\frac{M_0}{M_n} \right)^2 \quad (3.1)$$

where M_0 is the molecular weight of the monomer. For high molecular weights, $M_n \gg M_0$, the polydispersity approaches unity in accord with the following approximation that is valid near the limit of monodispersity:

$$\frac{M_w}{M_n} = 1 + \frac{M_0}{M_n} = 1 + \frac{1}{P_n} \quad (3.2)$$

where P_n is the number-average degree of polymerization. In fact, it is not possible to produce a polymer in which every molecule has exactly the same mass, but if P_n and the ratio of the rate of propagation to the rate of initiation are small, very narrow distributions can be produced. For example, Gold [14] calculated that when this ratio is 0.1, the polydispersity is 1.008, and when it is 10, the polydispersity is still only 1.019.

With the exception of a few commercial polymers such as polyisobutylene, polybutadiene and styrene-butadiene block copolymers, living polymers are prepared in small quantities under stringent conditions. Larger amounts can only be prepared by

repeating the synthesis many times, and this is a costly and time-consuming process. In the case of hydrogenated polybutadiene, used to prepare samples that resemble polyethylene, the need for the secondary hydrogenation step renders the process even more costly. This has so far limited the extent to which it has been possible to use these materials. Gell et al. [15] prepared asymmetric stars with structures similar to ethylene-propylene copolymers by hydrogenation of star-branched polyisoprene. The reactions to produce these materials took up to three weeks, and fractionation was required to remove by-products. While a single linear viscoelastic characterization at one temperature can be completed with a few grams, it is necessary to repeat tests a number of times in order to establish the precision of data. And for studies of nonlinear viscoelastic behavior, even larger samples are needed.

It is important to keep in mind that it is not possible to synthesize samples that are perfectly homogeneous in size and structure. Even for linear molecules, there is always a distribution of molecular weights. For example, Fig. 3.1 shows molecular weight distributions for ideal living polymers calculated using Eq. 2.72. We note that even for these low values of the polydispersity index ($M_w/M_n = 1.005$ and 1.001), there are still significant numbers of molecules having molecular weights much larger and smaller than the mean.

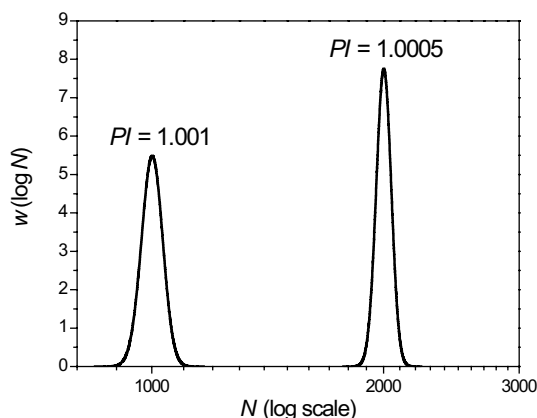


Figure 3.1 Molecular weight distributions in terms of degree of polymerization N according to the Poisson function (Eq. 2.72, in which $r_n = N$) for $M_w/M_n = 1.001$ and 0.005. The number-average degrees of polymerization are 1000 and 2000, respectively. Even these very narrow distributions include many molecules smaller or longer than average.

3.4.1 Anionic Polymerization

Anionic polymerization is a versatile technique widely used in polymer research [10, 11]. The key elements in making a living polymer by anionic polymerization are rapid initiation, so that all chains begin growing nearly simultaneously; elimination of chain transfer by reaction at a low temperature; and suppression of termination by the rigorous exclusion of impurities, particularly water and oxygen. In practice, it is impossible to eliminate all traces of termination agents, but one can achieve polydispersity indexes (M_w/M_n) of less than 1.01.

By means of anionic polymerization, it is also possible to produce polymers having many types of branching such as multi-armed stars and combs. Anionic polymerization has been used, for example, to make polystyrene, polybutadiene, and polyisoprene. An example of the anionic polymerization of a branched polymer is the technique of Roovers and Toporowski [16] for making comb polystyrenes. The model branched polymers that can be produced by means of block copolymerization and coupling chemistries include stars, H-shaped molecules and combs of various types [9]. So-called pom-pom polymers are of special interest, because their rheological behavior has been modeled by McLeish and Larson [17]. These molecules have several arms at each end of a central crossbar, and polybutadienes having this structure have been studied [18, 19].

Substituent groups on the double bond must stabilize the negative charge that develops in the transition state for the monomer addition step. They must also be stable to reactive anionic chain ends. Monomers that can be polymerized anionically include vinyl, diene, and some carbonyl-type and cyclic monomers. We note that because of its lack of any substituent group, polyethylene cannot be polymerized anionically. We describe in a later section how to make living polymers that are similar to polyethylene by hydrogenation of polybutadiene.

Polybutadiene and its branched derivatives have been popular choices for basic studies because of their relatively low entanglement molecular weights and the usefulness of anionic polymerization for their synthesis. However, complications arise, because there are three ways in which the butadiene double bonds can be incorporated into the polymer molecule; cis, trans, and vinyl, and the actual chain structure depends on the catalyst and solvent used. The cis- and trans- forms are optical isomers arising from the rigidity of the double bonds in the backbone. A typical product might contain 45% cis, 48% trans, and 7% vinyl isomers. Because the entanglement molecular weight varies somewhat from one isomer to another, this leads to some inhomogeneity in the degree of entanglement. If the sample is hydrogenated to make a polymer similar to polyethylene, the optical isomerism is lost, but the vinyl groups remain. It is possible to reduce the vinyl content, but this leads to a broadening of the molecular weight distribution [20].

Copolymerization of two monomers, one to form a backbone and the other to form branches, can be used to make a remarkable range of materials. The backbone is first constructed, and the branch monomer is polymerized to form *macromonomers*, i.e., chains with a terminal double bond. Using this technique combs of various types can be made. If the backbone is very short and the grafting density is high, the result is a star. If the backbone is long and the grafting density is high, the resulting comb is called a “bottle brush.”

Anionic polymerization produces linear polymers having the lowest polydispersity achievable by any process. By use of TGIC (Section 2.6.3.4) it has been shown that anionic polymerization can yield samples with polydispersity indexes well below 1.01 and MWD very close to the theoretical Poisson distribution. Anionic polymerization can also produce very high MW polymers having PDI values near unity. It is also the only living polymerization that works well with conjugated dienes like butadiene and isoprene, which are preferred for making model polymers because of their very low values of M_e . It is also the best way to make branched polymers. The truly living nature of the chain ends is advantageous during coupling reactions, and arms are much narrower in PDI, because they are grown by a truly living (termination free) process.

However, it was reported as early as 2002 [21] that carefully synthesized three-arm polystyrene stars can contain residual uncoupled arms, i.e., linear molecules. And more recently the use of TGIC analysis (described in Section 2.6.3.4) has revealed that even the most carefully carried out anionic polymerizations of branched structures produce some reaction byproducts that are larger or smaller than the target molecule. Perny et al. [22] discuss the problem of larger molecules, while Li et al. [23], Snijkers et al. [24], and Van Ruymbeke et al. [25] discuss the issue of fragments. In the latter case, the impurities relax faster than the molecule intended and act as a diluent for the latter, which should lead to acceleration of the relaxation of the target molecules. It has been suggested that this acceleration should not have a major effect if the purity is above 80%. We note, however, that at least one synthesis method designed to make H polymers yielded products that were revealed by TGIC to contain 50% or fewer H molecules, with the rest consisting of smaller, incompletely reacted species [23]. However, using TGIC data to identify the byproducts and their concentrations it was still possible to use tube models to model their rheological behavior [26]. This subject is addressed in Chapter 9.

3.4.2 Living Free-Radical Polymerization (Reversible Deactivation Radical Polymerization—RDRP)

In recent years there has been rapidly growing interest in free-radical reaction schemes in which side reactions are suppressed, leading to *living/controlled* (i.e., nonterminated) free-radical polymerization techniques [27]. These processes are not truly “living,” as there are always irreversible reactions occurring, but they can produce samples having low polydispersites.

Many variants of controlled/living radical polymerization techniques are in use. These include stable free-radical polymerization (SFRP) [28–38], nitroxide mediated polymerization (NMP) [29, 30], atom transfer radical polymerization (ATRP) [31] and degenerate transfer processes (DT), which include radical addition-fragmentation transfer (RAFT) [32] and catalyst chain transfer (CCT). These techniques have been used to polymerize many monomers, including styrene (both linear and star polymers) acrylates, dienes, acrylamides, methacrylates, and ethylene oxide. Research activity in this field is currently expanding rapidly, as is indicated by the many papers published and patents issued.

3.4.3 Model Polyethylenes for Research

Because of its low entanglement molecular weight and great industrial importance, it would be desirable to be able to synthesize polyethylenes having known structures using anionic polymerization. While this is not possible, polybutadiene (PBd) can be made by anionic polymerization and then hydrogenated to eliminate unsaturation [33] to produce a polymer that is very similar to polyethylene. However, Rochefort et al. [20] reported that it is not possible to synthesize polybutadiene having negligible vinyl content and also a very narrow molecular weight distribution. In addition, as mentioned above, double bonds can be incorporated into the polybutadiene molecule in three ways: cis, trans, and vinyl. While the cis-trans isomerism disappears after hydrogenation, the vinyl side groups produced by 1,2 addition, typically found in about seven percent of the monomer units, end up as ethyl branches after hydrogenation.

By use of chlorosilane chemistry, various branched structures can be prepared. For example, star-branched PBd can be prepared [20] and hydrogenated to produce analogs of star-branched polyethylene [34]. Hadjichristidis et al. [35] described the preparation of polyethylene analogs based on butadiene. Using the methods, they describe, a remarkable array of structures can be produced, including stars, H-shaped molecules, super-H molecules (three-armed stars at both ends of a backbone segment), pom-poms (multi-armed stars at the ends of a backbone) and combs of various types. Rheological data have been published for the polymers they described [36].

An analogous procedure for preparing model atactic polypropylene is based on the polymerization of 1,3-dimethyl-1-buteneylene, followed by hydrogenation [37].

Two methods of synthesizing branched polyethylenes without starting from butadiene are chain walking polymerization [38] and acyclic diene metathesis (ADMET). The former process yields hyperbranched polyethylene (HBPE) using Pd–diamine-catalyzed chain walking polymerization. This process produces a broad range of HBPEs having various chain structures, molecular weights, and functionalities. Potential applications include lubricants and nanoencapsulation. Acyclic diene metathesis (ADMET) is a step polycondensation polymerization [39] that has been used to synthesize polyethylenes with side chains of specific lengths, for example 21 carbons [40, 41], at specified locations on the backbone. These side chains are excluded from crystals on cooling.

■ 3.5 Industrial Polymerization Processes

The type of polymerization reactor used and reactor conditions have important effects on the molecular structure of a polymer. Laboratory syntheses used to make samples having well-defined and uniform molecular structures are virtually always done in stirred batch or semi-batch reactors, which allow for very good control of reaction conditions. Semibatch reactors are also used to manufacture condensation polymers, which experience reverse reaction of product back to reactants, so that it is necessary to remove product to force the reaction towards the product. On the other hand, except in the case of specialty polymers, industrial reactors always involve stirred-tank or tubular reactors with a continuous feed of reactants and withdrawal of product. A continuous-flow, stirred-tank reactor (CSTR) can be operated alone or as a series of reactors. A stirred tank operated at high temperature and pressure, such as that used to make low-density polyethylene is called an autoclave. In an ideal CSTR, the mixing is perfect so that the composition everywhere in the reactor is the same as that at the exit. The mixing in large commercial reactors is far from ideal, and this greatly complicates their modeling. One approach to this problem is to consider the reactor to be “segregated” into one or more, smaller, homogeneous reactors. A second type of continuous reactor is the tubular reactor, with or without recycle. For turbulent flow, the velocity profile is nearly flat giving rise to plug flow, and radial gradients are assumed negligible. The modeling of tubular reactors is complicated by axial gradients, and they are simulated either as a large number of CSTRs in series or, assuming plug flow, as a batch reaction with the distance along the reactor proportional to the reaction time. Axial gradients result in a broader distribution of molecular size and composition than are predicted for an ideal reactor.

Polymerization reactions can also be classified in terms of the reaction medium, and the principal types are bulk, solution, slurry, emulsion, and gas-phase. In bulk polymerization, the reactor initially contains only monomer, and the product is a viscous melt. This is the type of system usually used for step (condensation) polymers. In solution polymerization, both the monomer and polymer are soluble, while in emulsion and slurry reactors, the polymer is not soluble in the reaction medium, which is called the diluent. The principal monomers polymerized by means of emulsion polymerization are vinyl acetate, methyl methacrylate, and vinyl chloride. In a gas-phase reactor or slurry reactor, the gaseous or liquid monomer is polymerized on the surface of catalyst particles, which are dispersed either by stirring in a horizontal reactor, or by fluidization in a vertical reactor. Slurry and gas-phase reactors are used primarily to make polyolefins.

Each combination of reactor system, polymerization conditions and initiators or catalysts produces a different molecular structure. In addition, some variation in catalyst activity and operating conditions is inevitable in an industrial setting, so that some variability in product properties from one day to the next is a normal aspect of commercial polymer production.

The commercial polymers produced in the largest quantity are polyethylene and polypropylene. Polyvinyl chloride (PVC) and polystyrene are also produced in very large volumes, but PVC is not discussed in this book. Because of its high melting point, it is not stable in the molten state and is processed below this temperature and always blended with heat stabilizers, lubricants, plasticizers, fillers, and other additives to make processing possible, and all of these influence the flow behavior of the resin. Rigid (unplasticized) PVC has a total additives content below ten percent, while flexible (plasticized) PVC can consist of 50% additives. Thus, this chapter deals exclusively with polyolefins and polystyrene. While the basic chemistry of these latter two types of polymer seems simple, they are produced in hundreds of grades varying greatly in molecular structure and flow behavior.

In the case of polyolefins, because the chain is quite flexible the entanglement molecular weight is relatively low. And since they rely entirely on van der Waals forces for their strength in the solid state, nearly all commercial grades have molecular weights well above the entanglement molecular weight. For example, hundreds of grades of commercial HDPE grades are available having molecular weights ranging from 20,000 to 1,000,000 g/mol. As a result, the rheological properties of the melt are strongly influenced by molecular structure. For these reasons, we will give special attention to polyethylene and polypropylene.

■ 3.6 Free-Radical Polymerization of Low-Density Polyethylene (LDPE)

The first polyolefin to be produced commercially was low-density polyethylene (LDPE) [42]. The high-pressure, free-radical process by which this is produced was discovered serendipitously in the laboratories of Imperial Chemical Industries in 1935. The free radical initiator is oxygen (air), an azo-compound, a peroxide or a peroxyester. Because of the free-radical mechanism of polymerization, LDPE contains both long and short branches, generally from one to five carbons long, by intermolecular hydrogen extraction (“backbiting”). The primary means for controlling molecular weight is the use of a chain-transfer agent, for example propylene, butane, isobutene, etc. The free-radical mechanism used to make LDPE is also effective for the copolymerization of polyethylene with polar comonomers such as vinyl acetate, carbon monoxide, acrylates, and acrylic acid. The polymerization is carried out at high pressure to permit reaction in the bulk using supercritical ethylene.

There is a broad range of branching structures in an LDPE resin, with long and short branches and complex, tree-like molecules. The short-chain branches suppress crystallinity, which explains why the density in the solid phase is relatively low and flexibility is high. Meanwhile, the long-chain branches cause the viscosity to decrease markedly as the shear rate is increased, and this enhances the ease with which this material can be processed in its molten state, i.e., its *processability*. However, the materials made from this polymer are relatively soft and weak. (High-density polyethylene is stronger but less easy to process.)

Molecular structure depends greatly on how the polymer was manufactured. LDPE is made by high-pressure, free-radical polymerization in either a tubular reactor or an autoclave (stirred tank reactor), and autoclave LDPE has a much higher branching level and a more tree-like structure than that produced in a tubular reactor. Because of more effective cooling, the conversion per pass in a tubular reactor is substantially higher than in an autoclave reactor. Kuhn and Krömer [43] studied the branching structures of LDPEs made using a tubular reactor, an autoclave, and two autoclaves in series. They found that neither the short nor the long branches were randomly distributed among the molecules.

The analytical determination of LDPE structure poses major difficulties. Because it contains both short and long-chain branches, the use of carbon-13 NMR is limited, since all branches longer than six carbons give the same response [44]. Axelson et al. [45] concluded from their NMR study that “there is no unique LDPE molecule, since the concentration, type and distribution of subgroups vary widely.” In other words, the variety of branching structures present, each with distributions among and within molecules, makes it impossible to describe in a quantitative way the

molecular structure. Moreover, the variety of reactor types and operating conditions in the plastics industry means that there is great variation from one product to another and even among batches from the same reactor. In spite of these challenges, attempts continue to be made to characterize the structure of LDPE.

There have been many attempts to model the processes that take place in LDPE reactors of both types to predict the structure of the product, especially in recent years [46–59]. However, there is no way to verify the predicted structure because of the limitations of analytical methods. Read et al. [7] used the Tobita 2001 model [46] as the basis of a tube-model simulation of the rheological properties of LDPE. They fitted the model results to the parameters of the pom-pom tube model to accomplish this, as described in Chapter 9.

3.6.1 Shear Modification

It was observed many years ago that when long-chain-branched commercial polymers, such as LDPE and ethylene-vinyl acetate copolymer, have been sheared, the effect on their subsequent behavior, particularly their response to uniaxial extension, is very long-lasting. This phenomenon is called *shear modification*. For example, if such a polymer is extruded and immediately converted to pellets, when these pellets are re-melted, the properties of the melt are different from those of the polymer originally fed to the extruder. However, if the extruded polymer is allowed to stand in the molten state for a sufficiently long time, it regains its original properties [60, 61]. It has been hypothesized that this phenomenon results from the alignment of the long branches along the backbone chain [62]. Yamaguchi and Takahashi [63] carried out a quantitative study of shear modification using a melt strength test and found that autoclave LDPE is more sensitive to shear history than that produced in a tubular reactor.

■ 3.7 Linear Polyethylene via Complex Coordination Catalysts

3.7.1 Catalyst Systems

Around 1950, several groups independently discovered ionic catalysts with transition metal centers that were able to make linear polyethylene, and this led to the development of commercial processes to manufacture high-density polyethylene (HDPE). Compared to LDPE, linear polyethylene has a higher crystallinity in the

solid phase and is thus less flexible and stronger. Such catalysts are called *complex coordination catalysts* (CCC) or simply coordination catalysts.

Since initiation occurs only at active catalyst sites, the polymerization is of the step-reaction type. And because each particle contains multiple reactive sites having different reactivities, these catalysts yield polymers with rather broad molecular weight distributions. CC catalysts are useful mainly with non-polar monomers, particularly olefins and dienes. Phillips Petroleum in 1951 developed the Chromox catalyst, consisting of chromium oxide impregnated into porous silica-alumina, and Amoco patented a molybdenum oxide catalyst at about the same time.

But the development that was to play the central role in the commercial polymerization of linear polyethylene was that of Ziegler who discovered a versatile heterogeneous catalyst system based on a transition metal halide with an aluminum alkyl cocatalyst. Natta later used catalysts of this type to make isotactic propylene, and these are now known as Ziegler-Natta catalysts [64]. The ones widely used for polyethylene manufacture are based on titanium chloride. They yield polymers having significantly narrower molecular weight distributions than those produced using a chromium oxide catalyst [64]. Later modifications of Ziegler-Natta catalysts continue to dominate polyethylene manufacture, although over the last several decades, single-site catalysts have been found advantageous for a number of applications [65].

3.7.2 Branching in High-Density Polyethylene

While HDPE is generally thought of as a linear polymer, there have been reports that materials carrying this label sometimes contain low levels of long-chain branching, particularly in the case of those made using chromium oxide catalysts [66, 67]. The level of LCB in these products is said to range from nearly zero up to levels similar to long-chain branched PEs produced by some single-site catalysts. At the highest level, this branching has a strong effect on the rheological behavior of the melt. Many variables affect branch formation in these polymers [67]. It is not clear whether the branching occurs during polymerization or subsequently, as the molecules are vinyl terminated and can react during melt processing.

Another source of long-chain branches in a nominally linear polyethylene is the cross-linking that can occur whenever it is heated above its melting point, particularly in the presence of air. This is a potential source of uncertainty in laboratory measurements.

Because even a small amount of long-chain branching has an important effect on the flow behavior of polyethylene melt, it has been of interest to study this effect quantitatively. One approach is to use anionic polymerization to produce well-defined branched structures, but this is a laborious procedure, and the product is never a

true model for LDPE. A much easier approach is to treat linear polyethylene with a peroxide [69, 70], although the precise branching structure produced by the peroxide is somewhat uncertain and difficult to quantify. Intentional cross-linking is used commercially to enhance the properties of HDPE or LLDPE for particular applications.

3.7.3 Ultrahigh Molecular Weight Polyethylene

Polyethylenes having average molecular weights of several million are used in applications requiring exceptional toughness and strength, high abrasion-resistance, or low surface friction. Most *ultrahigh molecular weight polyethylene* (UHMWPE) is made in CSTR reactors using conventional, heterogeneous Ziegler-Natta catalysts [72]. This material has a very high viscosity and cannot be processed using standard thermoplastic extrusion techniques. Compression molding and ram-extrusion of reactor particles are used to produce standard shapes which are then machined to form the final product. Phase boundaries between particles tend to remain even in the “molten” state because of the very long time required for chains to move across these boundaries [73]. For optimal processing, it is advantageous to reduce the entanglement density [74]. This can be accomplished by having a high crystallization rate compared to polymerization rate, so that newly created polymer does not have an opportunity to become entangled [75]. This is achieved by carrying out the polymerization at a low temperature or in a hydrocarbon solution. Methods for making branched UHMWPE have been described by Chen et al. [76]. But for preparation of samples for rheological measurements, it is essential not only to eliminate structures present in the solid particles but to produce a melt having an equilibrium state of entanglement, and very long times are required to accomplish this [74].

■ 3.8 Linear Low-Density Polyethylene via Ziegler-Natta Catalysts

For several major applications, it is desirable to have a polymer that has a lower crystallinity than HDPE without the long-chain branches present in LDPE, since the long branches make the polymer weaker, although easier to process. This need led to the development of copolymers of ethylene with an α -olefin, which is usually butene, hexane, or octene. The short branches arising from the olefinic side groups reduce the crystallinity but have little effect on the flow properties. By the addition of a specified amount of comonomer, the crystallinity of the solid polymer can be precisely controlled from zero (elastomer) up to that of HDPE. The degree of comonomer

incorporation is important and can be determined by NMR, IR, or UV techniques. At very low comonomer levels, 1 to 2 mole-percent, the products are “medium density polyethylenes” having densities between 0.926 and 0.940 and crystallinities around 50%. At comonomer levels from 2.5 to 3.5 mole-percent, the product is a “linear low density polyethylene” (LLDPE) having a density between 0.915 and 0.925 and a crystallinity between 45 and 30 percent. Using this material, it is possible to make plastic films that are stronger than those of the same thickness made from LDPE. These materials are produced commercially with molecular weights from 20,000 to over 200,000. The use of α -olefins longer than propylene enhances somewhat the reduction of density at a given mole fraction.

These copolymers are thought to be random copolymers, which means that the comonomer is randomly distributed along the chains [77]. In other words, the probability of finding a structural unit at a given point along the chain is independent of the state of neighboring units. Another important copolymer characteristic is the distribution of comonomer content among chains, which is called the chemical composition distribution (CCD). The CCD varies with the polymerization process. Ziegler-Natta catalysts tend to place more comonomer on shorter chains [78], while metallocene copolymers (mLLDPEs) have a more uniform distribution [79], which is advantageous in controlling crystallinity. The key characteristic for controlling crystallinity is the comonomer sequence length distribution of the whole polymer. Techniques for the determination of CCD are described in Chapter 2.

Most of the catalyst systems used for HDPE can also be used to make LLDPE. These include the original Ziegler-Natta titanium chloride or the later vanadium version, the Phillips chromox system, and the metallocene catalysts described in Section 3.9. Vanadium catalysts yield a substantial fraction of high-molecular weight polymer, while titanium catalysts yield molecular weight distributions ($PI = 3.5-6$) that are narrower than those with vanadium and chromox catalysts. Metallocene catalyst systems produce polymers with PI values approaching two. Much LLDPE is now made in gas-phase reactors with butene or hexene as the comonomer.

■ 3.9 Single-Site Catalysts

Traditional CC (Ziegler-Natta) catalysts, which were used to make almost all linear polyethylenes until the advent of the metallocene catalysts, have multiple active sites and therefore yield polymers having a moderately broad MWD and CCD. Techniques used to control the distribution include blending, use of mixed catalysts or cocatalysts, and the use of staged batch reactors or multiple, cascaded continuous reactors. These techniques complicate the already poorly-defined MWD due to the

heterogeneity of the catalyst, and as a result, the distribution cannot be reliably modeled or described using the equations presented in Chapter 2.

Unlike traditional CC catalysts, single-site catalysts have only one reactive site and thus yield products with a narrower MWD and a homogeneous comonomer distribution [80]. These catalysts are soluble and are used in homogeneous, solution processes. This limits their use to products with quite low crystallinity such as low molecular weight homopolymers, low-density copolymers and elastomers. To avoid this limitation, the catalyst was later fixed on an insoluble carrier to make it heterogeneous [81] so that it could be used in slurry, bulk or gas-phase reactors to make the high-crystallinity, high MW polymers, linear-low-density polyethylene and isotactic polypropylene.

3.9.1 Metallocene Catalysts

The first single-site catalysts were the metallocenes. These had been known since the 1950s, but commercially useful versions were first reported only in 1977, when Kaminsky demonstrated that a metallocene together with methyl aluminoxane (MAO) cocatalyst could polymerize olefins. These catalysts contain a transition metal sandwiched between two cyclopentadienyl ligands. There are also unbridged metallocene complexes with high activity, but their bridged counterparts (also called *ansa*-metallocenes) dominate commercial olefin production [82]. Kaminsky et al. [84] compared the products of solution and gas-phase polymerizations of ethylene using pentalenyl bridged *ansa*-metallocenes. Developments during the first twenty years of metallocene advances were reviewed by Kaminsky [83].

The constraint imposed by the ring structure on the active site of the catalyst makes the reaction more homogeneous, and the activity and stereoselectivity of metallocenes make it possible to produce polymers having relatively narrow molecular weight distributions and uniform comonomer distributions. The MWD is described quite well by the *most probable* (Schultz-Flory) distribution described in Section 2.2.4, which predicts a PDI (M_w/M_n) of 2.0. Metallocene polymers have PDI values very close to this theoretical value, demonstrating that the catalyst sites are indeed nearly equally active.

Metallocenes are homogeneous catalysts and can be used only for solution polymerization. In order to adapt them for use in slurry or gas-phase reactors, they must be immobilized on a support. This is normally carried out in a separate preparatory process, although the catalyst can be reacted with its support *in situ* in the polymerization reactor [85].

Copolymers made using metallocene catalysts, e.g., mLLDPE, have a more uniform distribution of comonomer among the chains than do LLDPEs made using Ziegler-

Natta catalysts, which tend to have more comonomer in the lower molecular weight fractions [79]. The comonomer distribution, i.e., the chemical composition distribution (CCD) is the key to controlling crystallinity, and models for predicting the CCD have been published for binary [4] and multicomponent [5] copolymers. The key factor controlling crystallinity is the distribution of longest ethylene sequences; a more even distribution leads to shorter ethylene sequences, which enhance the reduction in crystallinity for a given fraction of comonomer. Because mLLDPE is more compositionally homogeneous than LLDPE [86] it makes more effective use of the comonomer. For example, a traditional, gas-phase, hexene LLDPE with a density of 0.98 g/cm^3 has about 18 short branches per thousand carbon atoms, while an mLLDPE with the same density made by the same type of reactor requires only about 11 branches per thousand carbon atoms. Metallocenes can also be used to copolymerize ethylene with styrene [87].

Products made with metallocenes have improved mechanical properties but are more difficult to process because of their lower degree of shear thinning, as compared with more polydisperse or long-chain-branched polymers. Products with broader distributions can be made with metallocene catalysts by blending or the use of multiple catalysts. Another approach to improving the processability of these materials is the introduction of long-chain branching, which is discussed in the next section.

3.9.2 Long-Chain Branching in Metallocene Polyethylenes

Long-chain branches can be introduced into any nominally linear polyethylene by crosslinking, which may occur unintentionally when a sample is heated without adequate thermal stabilization. In addition, it is possible that some metallocene catalysts intended for synthesis of linear chains have the ability to generate vinyl macromonomers and incorporate these into the growing chain to produce branches under certain conditions. Thus, samples thought to be linear sometimes show evidence of low levels of long-chain branching that have a significant effect on rheological behavior [66]. These issues complicate the study of the structure and rheology of metallocene polyolefins [88, 89].

The first single-site catalyst used to synthesize polyethylene and its copolymers with alpha-olefins having precisely-controlled levels of long chain branching ranging from 0.01 to 3 branches per 1000 carbon atoms was the *constrained-geometry* (mono-cyclopentadienyl) catalyst (CGC) developed by Dow Chemical [90, 91]. It is a “half-metallocene” catalyst similar to that described by Canich [92]. Other metallocene catalysts such as those used by Piel et al. [93] could in principle be used to produce similar branched structures, as shown by Karimkhani et al [94]. While CGC polyethylenes are sometimes called branched metallocene polyethylenes,

some might not consider CG catalysts to be “true” metallocenes, as their ligands are mono-cyclopentadienyl rather than bis-cyclopentadienyl. They are thus sometimes classified as “post-metallocene” catalysts (see Section 3.9.3).

A broad range of products can be made using this technology [95]. The reaction proceeds in the liquid phase in a continuous, stirred-tank reactor or an equally well-mixed loop reactor. Soares and Hamielec [96] explained why this arrangement is optimal for LCB formation. The branching process starts with the formation of a *macromonomer*, i.e., a dead polymer chain with a terminal double bond, by β -hydride elimination. This unit is incorporated into a growing chain at the active center of the catalyst. The introduction of the LCB has an important effect on the viscosity, substantially increasing the degree of shear thinning. It is thus possible to have the advantages of a controlled, narrow molecular weight distribution, low crystallinity, and good processability.

A significant amount of work has been done on modeling the polymerization process [96–104]. The resulting models are valid for solution reaction in a CSTR in which the reaction medium is homogeneous, and in spite of their structural polydispersity, the distribution of structures produced is completely defined by the molecular weight and one branching parameter. The level of branching is often expressed in terms of λ , the average number of branch points per thousand carbon atoms, which is related to β , the average number of branch points per molecule by Eq. 3.3 for the case of polyethylene.

$$\beta = \frac{M_N \lambda}{14 \cdot 10^3} \quad (3.3)$$

However, this single parameter contains no information about the distributions of branch points per molecule and the molecular weights of the various types of segment. For example, we note that many combinations of M_N and β can give the same value of λ . To determine the detailed structure, it is necessary to make a more detailed analysis of the reaction. Because this reaction system has been analyzed in great detail, it will be of interest to summarize the models used. Soares and Hamielec [96] developed a kinetic model based on the following reactions:

1. Addition of a monomer to increase the chain length
2. β -hydride elimination by the catalyst to give a dead chain with a terminal vinyl unit, i.e., a macromonomer
3. Addition of a macromonomer to form a branch
4. Termination by transfer to a chain transfer agent

If one is interested only in the final structures of the molecules formed rather than the rate of reaction, only two parameters are important [103]: pp , the probability of propagation (processes 1 and 3) relative to that of termination (process 4), and

lp , the probability of adding a monomer (process 1) relative to that of adding a macromonomer (process 3). Given only these two parameters, one can, in principle, calculate all the quantities of interest. A simple example of such a relationship is shown as Eq. 3.4.

$$\lambda = \frac{10^3}{2} pp(1-lp) \quad (3.4)$$

Alternatively, the branching distribution can be described by the molecular weight between entanglements and a branching probability [102].

It had been noted earlier by Read and McLeish [102] that the key feature of the structure from the point of view of rheological behavior is the distribution of segment types among the molecules rather than simply the number of branches. For example, free arms all relax in the same way, regardless of the total number of branches on the same molecule. And a chain segment with branch points at both ends relaxes much more slowly than a free end. We will see in Chapter 10 that a key aspect of extensional flow behavior is directly related to the presence of segments with branch points at both ends. This inspired Costeux et al. [103] to use the results of their Monte Carlo simulations to calculate the branching distributions of a number of polymers that can be formed using a single constrained-geometry catalyst in a single reactor. Each combination of the parameters pp and lp corresponds to a system consisting of particular fractions of linear molecules, free arms and inner backbones. They represented these ternary systems by use of a triangular diagram in which the vertexes correspond to linear molecules, free arms, and inner backbone segments. Ten simulated systems are shown on such a diagram in Fig. 3.2. The point nearest the lower-right-hand vertex corresponds to a system made up mostly of linear molecules with a few three-armed stars. This point corresponds to $lp = 0.99984$ and $pp = 0.999176$. The number of inner backbones increases steadily along the curve, and the point corresponding to the highest branching level corresponds to $lp = 0.99980$ and $pp = 0.99960$. The equation for the curve on which all these points lie was derived analytically and represents the locus of all possible structures that can be achieved with a single CGC.

If one wants to use the methods described in later chapters to simulate the rheological behavior of these polymers, or to calculate the way they are separated in a GPC column, it is necessary to use a Monte Carlo method, so that the additional calculations can make use of the entire ensemble of molecules. The analytical equations of Costeux [104] can be used to dramatically accelerate this calculation.

This procedure was used to calculate the structures of the seven materials whose segment compositions correspond to the points in Fig. 3.3. The values of M_w , λ , and β for these materials are given in Table 3.1, and the rheological behavior of these materials is discussed in Chapters 5 and 10, where it is shown that long-chain branching

strongly influences both the linear and nonlinear behavior of the polymers and can be used to “tune” the rheology to optimize processing performance. Such tuning is a delicate process, however, and a quantitative understanding of the relationship between branching and rheology is required to do it effectively.

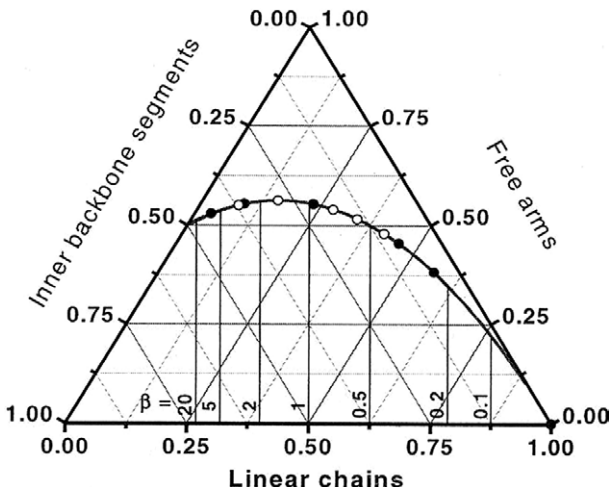


Figure 3.2 Ternary diagram based on Monte Carlo simulations showing all possible combinations of linear molecules, free arms and inner backbones in long-chain branched polyethylenes made using a single, constrained-geometry catalyst in a single reactor; from Costeux et al. [103]

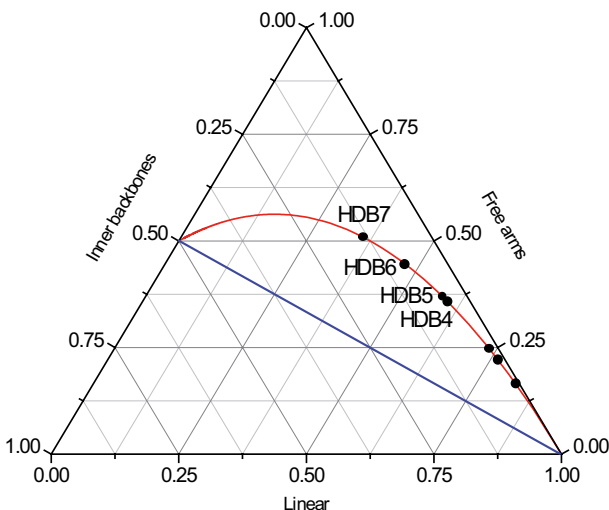


Figure 3.3 Ternary diagram of Fig. 3.2 showing the segment compositions of the seven branched metallocene polyethylenes whose GPC separations were simulated using the method of Costeux et al. [103]. Key parameters for these polymers are given in Table 3.1

Table 3.1 Molecular Weights and Branching Levels of the Polymers Corresponding to the Seven Points in Fig. 3.3

	M_w	λ	β
HDB1	77,000	0.026	0.067
HDB2	82,000	0.037	0.099
HDB3	86,000	0.042	0.116
HDB4	96,000	0.080	0.224
HDB5	79,000	0.090	0.210
HDB6	68,000	0.190	0.343
HDB7	70,000	0.330	0.537

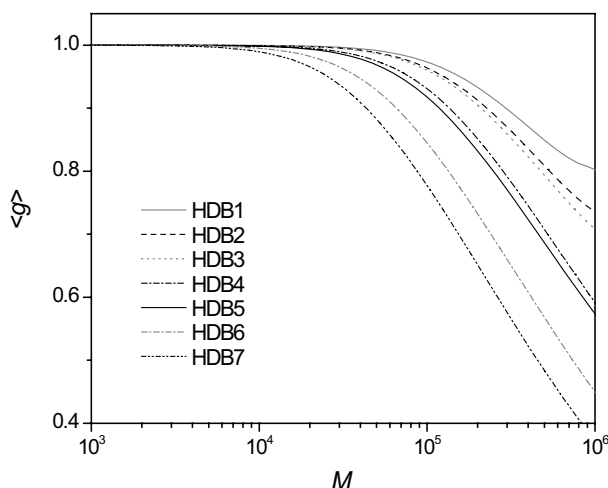


Figure 3.4 Branching factor \hat{g} versus M for portions of simulated elute having weight average molecular weights M for the polyethylenes whose segment compositions fall on the curve in Fig. 3.3. These were computed using the Zimm-Stockmeyer equations and the method of Costeux et al. [103] (calculations carried out by S. Costeux)

Unlike model polymers prepared by anionic polymerization, the broader polydispersity of mPE and dispersity in molecular architecture result from random macromonomer incorporation. Therefore, statistical modeling by averaging all possible conformations provides an accurate representation of the actual synthesis of CGC-catalyzed PE. This cannot be said of anionic polymerization of branched molecules in which side reactions or incomplete reactions produce molecules that can differ markedly from the targeted structure, as was pointed out above. For this reason, branched CGC polymers attracted the interest of polymer scientists, as they do not require an elaborate synthesis process and can be made in substantial quantities; they are also of great commercial importance.

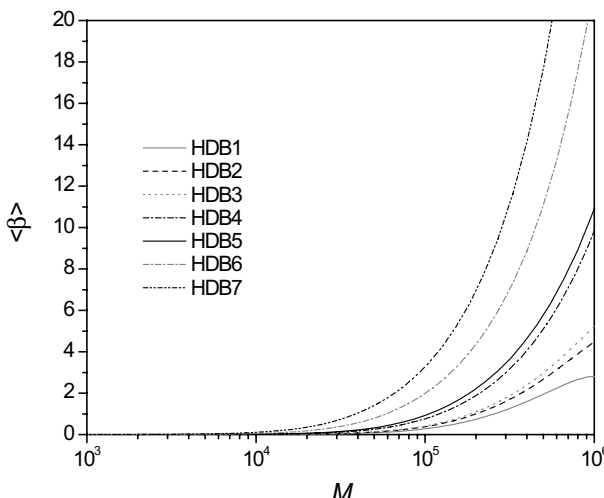


Figure 3.5 Average number of branch points per molecule β versus M for portions of simulated elute having weight average molecular weights of M for the polyethylenes whose segment compositions are shown in Fig. 3.4. These were computed using the method of Costeux et al. [103] and the Zimm-Stockmeyer relationships (calculations carried out by S. Costeux)

Wood-Adams et al. [105] were the first to report the rheological properties of several sets of linear and long-chain branched homo- and copolymers made using these catalysts, and this work has been cited many times. The materials studied were among a set synthesized by Dow Chemical for research purposes. The long-chain branched polymers, HDB 1-7, whose structures are shown in Fig. 3.3 were among those synthesized, and while the 2000 study included only the first four of these, Torres et al. [106] more recently reported a comprehensive rheological study of samples HDB5 to HDB7. The linear and extensional flow rheological behavior of all seven polymers is described in Chapters 5 and 10, and the modeling of their linear viscoelastic behavior is detailed in Chapter 9. Members of the HDB sample set were also the subject of theoretical and experimental studies by Wood-Adams and Costeux [107], Wood-Adams [108], Robertson et al. [109], He et al. [110], Das et al. [111], Takeh et al. [112], Das et al. [13], Torres et al. [106], and Ramachandran et al. [114].

3.9.3 Post-Metallocene Catalysts

The success of metallocenes in the polymerization of olefin polymers and copolymers inspired studies of other systems involving new ligands. Like the metallocenes these *post-metallocenes* require a cocatalyst, such as MAO, and Baier et al. [115] reviewed work on the new systems up to 2014. As mentioned earlier, the CG catalysts can

be considered to fall in this category. Several techniques were later used to make olefin multiblock copolymers that are thermoplastic elastomers, and these are briefly reviewed by Park et al. [116]. An approach reported by Arriola et al. [117] makes use of a “chain shuttling agent” (CSA) that is now used to make a range of commercial products. The CSA switches the growing chain between two catalysts at random intervals. One catalyst suppresses insertion of comonomer, while the other promotes insertion. The final chain contains alternating “hard blocks” consisting essentially of ethylene homopolymer with very low levels of comonomer, and “soft blocks” of ethylene/higher alpha-olefin copolymer. These materials undergo mesophase separation on cooling to form thermoplastic elastomers.

■ 3.10 Polypropylene

Polypropylene can have one of three tacticities: isotactic, syndiotactic, and atactic, although we saw in Chapter 2 that there are intermediate structures in which the distribution of methyl units is neither regular nor perfectly random. Atactic polypropylene is a viscous amorphous liquid with limited industrial applications. Both isotactic and syndiotactic versions are crystallizable, but because of its much faster rate of crystallization isotactic polypropylene is the commercially important type, second only to polyethylene in global level of production. Nearly monodisperse polypropylene for use in research can be prepared by the polymerization of a suitable diene, with subsequent hydrogenation [37].

Commercial polypropylene coming from the reactor has PI values (M_w/M_n) between 5 and 15. For certain applications such as thin-walled injection molding and cast film, grades with narrower molecular weight distributions are required, and until recently these were made by chemical or thermal degradation (visbreaking) of a high molecular weight reactor product. These so-called “controlled rheology” grades of PP are made by reactive extrusion, and this process has been studied experimentally [118] and modeled [119–121]. Good mixing of the peroxide is an essential element of a successful process. Such grades can now be made in the reactor by means special catalyst systems, such as the donor-assisted Ti/Mg system developed by Montell (now part of Basell). Isotactic polypropylene having a prescribed molecular weight can also be made using metallocene catalysts [122].

Linear polypropylene suffers from the same processing limitations as HDPE, and considerable effort has been directed at improving its processability by introducing long-chain branching. The branched product is called “high-melt-strength polypropylene” (HMSPP). The long branches can be introduced *in situ*, for example by use of special catalyst systems [123, 124]. Ye and Zhu [125] reported a binary,

single-site catalyst system for making polypropylene with an isotactic backbone and atactic long-chain branches. However, commercial HMSPP is currently made by post-reactor treatment involving peroxide crosslinker, electron beam irradiation, or macro-monomer grafting. Peroxides and electron beam irradiation cause chain scission to generate free radicals, which can recombine to form branched chains, and this generally broadens the molecular weight distribution. Polyfunctional monomers can be used to enhance the effect of electron beam irradiation [126]. The reaction mechanism of this process has been examined by Rätzch [127]. The effect of long branches, introduced by these methods, on rheological behavior has been reported by several groups [128, 129].

He et al. [130] used a Monte Carlo technique to simulate the post-reactor branching of linear PP precursors made using a Ziegler-Natta catalyst. De Rosa et al. [131] described a method to control the concentration of stereodefects in isotactic polystyrene using metallocene catalysts, and Kissin et al. [132] reported a method to make almost purely atactic polypropylene using a novel ternary catalyst that is claimed to have high activity, low cost, and ease of use.

■ 3.11 Reactors for Polyolefins

Low-density polyethylene is made using both tubular and stirred-tank (autoclave) reactors. Because of more effective cooling, the conversion per pass in a tubular reactor is substantially higher than in an autoclave reactor. Kuhn and Krömer [133] studied the branching structure of LDPEs made using a tubular reactor, an autoclave, and two autoclaves in series, and they found that neither the short nor the long branches were randomly distributed among the molecules. Several LDPEs made by BASF in a tubular reactor were used in important IUPAC-sponsored studies [134, 135]. Samples of these same polymers were also used later in a number of other rheological studies.

Because of the nonuniform temperature and complex flow pattern in the reactors, it is not possible to model the process in order to predict all the distributions required to describe the structure. In addition, it is not possible to characterize the structure of LDPE in any detail using analytical methods because of its complex and irreproducible structure. Finally, different batches of polymer made in the same reactor often vary in their structure. These variations may not be detectable using standard test methods while still affecting processing behavior.

Linear polyolefins were originally produced commercially in single-stage stirred-tank reactors using Ziegler catalysts, and the degree to which molecular structure

could be controlled was quite limited. The later development of new catalysts and reactor technologies vastly expanded the range of molecular structures that could be produced and provided much improved control of structural features such as molecular weight distribution, comonomer distribution, and even the addition of a prescribed degree of long-chain branching.

The slurry reactor was developed by Höchst to make polyethylene using Ziegler catalysts. The reaction medium, i.e., diluent, is a hydrocarbon that is a solvent for the monomer but not for the polymer. The product is thus formed as a suspended powder. Bimodal products, i.e., products that are, in effect, blends of two polymers having distinctly different molecular weight distributions, can be made using a cascade of two reactors in which the reaction conditions are substantially different [136]. Phillips Petroleum later developed a pipe-loop slurry reactor for use with its chromium oxide catalyst, which required moderately high temperatures and pressures to accommodate the isobutane diluent used.

A later development was the “multizone circulating reactor” (MZCR) developed by Basell (“Spherizone” process), in which a given polymer particle flows back and forth between two reaction zones of a loop reactor, in each of which the conditions are different [137]. This makes it possible, for example, to make a very homogeneous blend of polymers having distinctly different molecular weights.

The development of new catalysts spurred the development of new types of polymerization reactor, the most remarkable of which was the fluidized bed process developed at Union Carbide [138]. In this process, ethylene is fed to the reactor along with the catalyst and a chain transfer agent, which is usually hydrogen. The gas is continuously removed, cooled and recycled to remove the heat of reaction. An important advantage of the process is that the high catalyst activity makes it unnecessary to remove the catalyst from the product. Ziegler-Natta titanium catalyst was used initially, but it was later found that gas-phase polymerization could also be carried out using metallocene catalysts [139]. Fasano [140] discussed the modeling of the polymerization reaction that occurs on this form of catalyst in a gas-phase process. The overall process is complex, involving the diffusion of monomer through the layer of polymer already formed. Heat transfer must also be modeled, as the temperature in the catalyst-polymer system is not uniform.

A later advance in gas-phase polymerization was the condenser mode of operation in which the gas is partially condensed before returning to the reactor, thus speeding up the removal of heat and the production rate. Later catalyst developments led to the production of LLDPE having a rather narrow MWD, and a third-generation catalyst made it possible to broaden the MWD. The development of a process for the gas-phase manufacture of polypropylene was later developed in collaboration between Union Carbide and Shell Chemical, and the product is called Unipol PPP.

Polymer chains in the powder that comes directly from gas-phase or slurry reactors are not fully entangled when first melted. This poses problems in making rheological measurements, as the degree of entanglement has a strong effect on rheological properties, and this effect is the basis for the useful relationships between flow properties and molecular structure.

■ 3.12 Polystyrene

Polystyrene is an important commercial thermoplastic that has been described by Priddy [141]. Its entanglement molecular weight is around 18,000, and for both structure-rheology studies and commercial applications, molecular weights much higher than this are of primary interest. Nearly all commercial polystyrene is atactic and thus a brittle, transparent glass at ambient temperatures, because its T_g is 100 °C. New catalyst systems are able to produce isotactic and syndiotactic versions, and at least one commercial SPS is currently in production in Japan. This brittle material has a very high melting point, and commercially grades are glass-fiber reinforced. Styrene polymerizes spontaneously on heating by a free-radical mechanism. Some commercial polystyrene is produced by suspension and emulsion polymerization, but the principal route is solution polymerization. This is carried out in either a tubular or a continuous stirred tank reactor (CSTR).

Random branching occurs to a small extent in commercial, free-radical polymerized polystyrene, either during polymerization by chain transfer or afterward by exposure to radiation. Because of its advantages for certain applications, processes have been developed specifically for the production of branched polystyrene. Peroxide initiators are used to promote hydrogen abstraction, and a small amount of chain-transfer solvent is used to maintain a high level of termination and prevent reactor fouling. Ferri and Lomellini [142] prepared randomly branched polystyrenes by copolymerizing styrene with divinylbenzene and studied their rheological properties. Koppi and Priddy [143] have reviewed the subject of branching in polystyrene. They point out that because of the high M_e of PS, branching is not useful for modifying flow behavior, as very high molecular weights would be required, and the resulting material would have too high a viscosity for use in standard forming processes.

General purpose polystyrene (GPPS), i.e., not rubber toughened, has a molecular weight in the range of 200,000 to 400,000. Its molecular weight decreases by about 10% during melt processing due to thermal degradation, especially if a peroxide initiator is used in the polymerization. Free-radical polymerization is the preferred commercial process, which yields a product with M_w/M_n ranging from 2.1 to 3.0.

While nearly all commercial polystyrene is atactic, it is possible using stereospecific Ziegler-Natta catalysts to produce tactic versions. The isotactic version crystallizes too slowly to be of practical use, but an effort is currently underway in the U.S. and Japan to develop a crystalline, syndiotactic polystyrene for commercial applications. Mineral oil is often added to GPPS to reduce viscosity, although this lowers the heat deflection temperature. In order to overcome the brittleness of PS for many applications rubber particles are added to produce high-impact polystyrene (HIPS). The rubber particles increase the viscosity of the melt, and this effect is described in the article by Priddy [141].

Bubble formation is a common problem in the preparation of polystyrene samples for rheological measurements. The usual solution to this problem is to heat the sample to a temperature a bit above the glass temperature under a vacuum for a period of time.

■ 3.13 Summary

In order to make progress in understanding how molecular structure is related to the physical properties of a polymer, it is necessary to know the structure of the polymer of interest. The structural characteristics whose distributions are of central interest are molecular weight, comonomer content (chemical composition), tacticity, and long-chain branching structure. In Chapter 2 it was shown that it is not possible to resolve the details of molecular structure, especially in branched systems, using only analytical methods. In fact, if no information at all is available concerning the molecular structure of a polymer, unless it is a monodisperse homopolymer, analytical data cannot be interpreted in any meaningful way. It is therefore necessary either to prepare samples having uniform and known structures or to have a reliable model of the polymerization process so that the distributions of molecular weight and structure and structure can be reliably predicted. At the least, one must have some idea of the types of structure present. Model polymers for research are most often prepared by anionic polymerization, although similar results can now be obtained for some polymers using living, free-radical techniques. Materials with very narrow molecular weight distributions and a wide variety of branching structures can be made in this way.

The structure of the polymer coming from an industrial reactor depends on the type of reactor, the reaction medium, reaction conditions, and the choice of catalyst. Commercial polymerization processes are difficult to model because of inevitable variations in process conditions, nonhomogeneous reactor conditions, and the use of multi-site catalysts. The structure of low-density polyethylene, which is produced

by a free-radical process in either autoclaves or tubular reactors, is particularly complex, involving a broad MWD and many types of branching structure. Linear polyolefins made using Ziegler-type catalysts have a fairly broad MWD that cannot be reliably predicted. Polyolefins made using metallocene catalysts have a much more predictable molecular weight distribution, and those made using constrained geometry catalysts have branching structures that can also be reliably predicted. To produce useful polypropylene materials, it is necessary to control the tacticity. This was originally done using Ziegler-Natta catalysts, but newer catalysts have improved our ability to control tacticity, not only in polypropylene but in other polymers including polystyrene. Commercial polystyrene is now made by a thermal, free-radical process that often produces some long-chain branching, and additional branches are often added to improve processing.

■ References

- [1] McMillan, F.M. *The Chain Straighteners* (1979) The Macmillan Press Ltd., London
- [2] Seymour, R.B., Cheng, Tai (Eds.) *History of Polyolefins* (1986) D. Reidel Publ. Co., Dordrecht
- [3] Furukawa, Y. *Inventing Polymer Science* (1998) Univ. of Pennsylvania Press, Philadelphia
- [4] Costeux, S. Anantawaraskul, S. Wood-Adams, P.M., Soares, J.P.B. Distribution of the longest ethylene sequence in ethylene/α-olefin copolymers synthesized with single-site catalysts. *Macromol. Theory Simul.* (2002) 11, pp. 326–347
- [5] Anantawaraskul, S., Soares, J.B.P., Wood-Adams, P.M. Chemical composition distribution of multicomponent copolymers. *Macromol. Theory Simul.* (2003) 12, pp. 229–236
- [6] Jones, T.D., Chaffin, K.A., Bates, F.S., Annis, B.K., Hagaman, E.W., Kim, Man-Ho, Wignall, G.D., Fan, W., Waymouth, R. Effect of tacticity on coil dimensions and thermodynamic properties of propylene. *Macromol.* (2002) 35, pp. 5061–5068
- [7] Read, D.J., Auhl, D., Das, C., den Doelder, J., Kapnistos, M., Vittorias, I., McLeish, T.C. B. Living models of polymerization and dynamics to predict branched polymer structure and flow. *Science* (2011) 333, pp. 1871–1874
- [8] Kunamaneni, S., Buzzia, D.M.A., De Luca, D., Richards, R.W. Rheology of fractionated and unfractionated hyperbranched polyesters. *Macromol.* (2004) 37, pp. 9295–9297
- [9] Hadjichristidis, N., Hirao, A., Tezuka, Y., DuPrez, F. (Eds.) *Complex Macromolecular Architectures: Synthesis, Characterization and Self-Assembly* (2011) John Wiley & Sons (Asia) Pte. Ltd.
- [10] Hadjichristidis, N., Hirao, A. *Anionic Polymerization: Principles, Practices, Strength, Consequences and Applications* (2015) Springer, Tokyo

- [11] Hirao, A., Goseki, R., Ishizone, T. Advances in living anionic polymerization systems, to macromolecular architectures. *Macromol.* (2014) 47, pp. 1883–1905
- [12] Kostjuk, S.V. Recent progress in the Lewis acid co-initiated cationic polymerization of isobutylene and 1,3-dienes. *RSC Adv.* (2015) 5, pp. 13125–13144
- [13] Ouardad, S., Deffieux, A., Peruch, F. Polyisoprene synthesized via cationic polymerization: State of the art. *Pure Appl. Chem.* (2012) 84, pp. 2065–2080
- [14] Gold, L. Statistics of polymer molecular size distribution for an invariant number of propagating chains. *J. Chem. Phys.* (1958) 28, pp. 91–99
- [15] Gell, C.B., Graessley, W.W., Efstratiadis, V., Pitsikalis, M., Hadjichristidis, N. Viscoelasticity and self-diffusion in melts of entangled asymmetric star polymers. *J. Polym Sci., B, Polym Phys.* (1997) 35, pp. 1943–1954
- [16] Roovers, J., Toporowski, P.M. Preparation and chemistry of H-shaped macromolecules. *Macromol.* (1981) 14, pp. 1174–1178
- [17] McLeish, T.C.B., Larson, R.G. Molecular constitutive equations for a class of branched polymers: The pom-pom polymer. *J. Rheol.* (1998) 42, pp. 81–110
- [18] Houli, S., Iatrou, H., Hadjichristidis, N., Vlassopoulos, D. Synthesis and viscoelastic properties of model dumbbell copolymers consisting of a polystyrene connector and two 32-arm star polybutadienes. *Macromol.* (2000) 35, pp. 6592–6597
- [19] Archer, L.A., Varshney, S.K., Synthesis and relaxation dynamics of multiarm polybutadiene melts. *Macromol.* (1998) 31, pp. 6348–6355
- [20] Rochefort, W.E., Smith, G.G., Rachapudy, H., Raju, V.R., Graessley, W.W. Properties of amorphous and crystallizable hydrocarbon polymers. II. Rheology of Linear and Star-Branched Polybutadiene. *J. Polym. Sci., Polym. Phys. Ed.* (1979) 17, pp. 1179–1210
- [21] Kaivez, A., Gallez, X.A., Daoust, D., Devoux, J., Godard, P. Molecular structure coupled with viscometry. *Polymer* (2002) 43, pp. 3181–3190
- [22] Perny, S., Allgaier, J., Cho, D., Lee, W., Chang, T. Synthesis and structural analysis of an H-shaped polybutadiene. *Macromol.* (2001) 34, pp. 5408–5415
- [23] Li, S.W., Park, H.E., Dealy, J.M., Maric, M., Lee, M.H., Im, K., Chopi, H., Chang, T., Rahman, M.S., Mays, J. Detecting structural polydispersity in branched polybutadienes. *Macromol.* (2011) 44, pp. 208–214
- [24] Snijkers, F., van Ruymbeke, E., Kim, P., Lee, H., Nikopoulou, A., Chang, T., Hadjichristidis, N., Pathak, J., Vlassopoulos, D. Architectural dispersity in model branched polymers: Analysis and rheological consequences. *Macromol.* (2011) 44, pp. 8631–8643
- [25] Van Ruymbeke, E., Chang, H.K., Nikopoulou, A., Hadjichristidis, N., Snijkers, F., Vlassopoulos, D. Molecular rheology of branched polymers: Decoding and exploring the role of architectural dispersity through a synergy of anionic synthesis, interaction chromatography, rheometry, and modeling. *Soft Matter* (2014) 10, pp. 4762–4777
- [26] Li, S.W., Dealy J.M. Evaluation of molecular linear viscoelastic models for polydisperse H-polybutadienes. *J. Rheol.* (2011) 55, pp. 1341–1373

- [27] Müller, A.H.E., Matyjaszewski, K. (Eds.) *Controlled and Living Polymerizations: Methods and Materials.* (2009) Wiley-VCH, Weinheim
- [28] Li, J., Zhang, Z., Zhu, X., Zhu, J., Cheng, Z., Xu, W. Stable free radical polymerization of styrene. *Polym. Bull.* (2010) 64, pp. 1–13
- [29] Nicolas, J., Guillaneuf, Y., Lefay, C., Bertin, D., Gigmes, D., Charleux, B. Nitroxide-mediated polymerization. *Prog. Polym. Sci.* (2013) 38, pp. 63–235
- [30] Gigmes, D. (Ed.) *Nitroxide mediated polymerization: From fundamentals to applications in materials science.* (2015) Royal Soc. Chem., London
- [31] Matyjaszewski, K., Tsarevsky, N.V. Molecular engineering by atom-transfer radical polymerization. *J. Am. Chem. Soc.* (2014) 136, pp. 6513–6533
- [32] Keddie, D.J., Moad, G., Rizzardo, E., Thang, S.H. RAFT agent design and synthesis. *Macromol.* (2012) 45, pp. 5321–5342
- [33] Rachapudy, H., Smith, G.G., Raju, V.R. Properties of amorphous and crystallizable hydrocarbon polymers. III. Studies of the Hydrogenation of Polybutadienes. *J. Polym. Sci., Polym. Phys. Ed.* (1979) 17, pp. 1211–1235
- [34] Raju, V.R., Rachapudy, H., Graessley, W.W. Properties of amorphous and crystallizable hydrocarbon polymers. IV. Melt rheology of linear and star-branched hydrogenated polybutadiene. *J. Polym. Sci., Polym. Phys. Ed.* (1979) 17, pp. 1223–1235
- [35] Hadjichristidis, N., Xenidou, M., latrou, H., Pitsikalis, M., Poulos, Y., Avgaropoulos, A., Sioula, S., Paraskeva, S., Velis, G., Lohse, D.J., Schulz, D.N., Fetters, L.J., Wright, P.J., Mendelson, R.A., García-Franco, C.A., Sun, T., Ruff, C.J. Well-defined, model long chain branched polyethylene. 1. Synthesis and characterization. *Macromol.* (2000) 33, pp. 2424–2436
- [36] Lohse, D.J., Milner, S.T., Fetters, L.J., Xenidou, M., Hadjichristidis, N., Mendelson, R.A., Garcia-Franco, C.A., Lyon, M.K. Well-defined, model long chain branched polyethylene. 2. Melt rheological behavior. *Macromol.* (2002) 35, pp. 3066–3075
- [37] Pearson, D.S., Fetters, L.J. Younghouse, L.B., Mays, J.W. Rheological properties of poly(1,3-dimethyl-1-butylene) and model atactic polypropylene. *Macromol.* (1988) 21, pp. 478–484
- [38] Dong, Z., Ye, Z. Hyperbranched polyethylenes by chain walking polymerization: Synthesis, properties, functionalization, and applications. *Polym. Chem.* (2012) 3, pp. 286–301
- [39] Attalah, P., Wagener, K.B., Schulz, M.D. ADMET: The Future Revealed. *Macromol.* (2013) 46, pp. 4735–4741
- [40] Li, H., Rojas, G., Wagener, K.B. Precision Long-Chain Branched Polyethylene via Acyclic Diene Metathesis Polymerization. *ACS Macro Lett.* (2015) 4, pp. 1225–1228
- [41] Li, H., Rojas, G., Wagener, K.B. Precision Long-Chain Branched Polyethylene via Acyclic Diene Metathesis Polymerization. *ACS Macro Lett.* (2015) 4, pp. 1225–1228
- [42] Ballard, D.G.H. The discovery of polyethylene and its effect on the evolution of polymer science In *History of Polyolefins*, Seymour, R.B., Cheng, Tai (Eds.) D. Reidel Publ. Co., Dordrecht (1986) pp. 9–53
- [43] Kuhn, R., Krömer, H., Structures and properties of different low density polyethylenes. *Colloid & Polym Sci.* (1982) 260, pp. 1083–1092

- [44] Usami, T., Takayama, S. Fine-branching structure in high-pressure, low-density polyethylenes by 50.10-MHz ^{13}C NMR analysis. *Macromol.* (1984) 17, pp. 1756–1761
- [45] Axelson, D.E., Levy, G.C., Mandelkern, L. A quantitative analysis of low-density (branched) polyethylene by Carbon-13 Fourier transform nuclear magnetic resonance at 67.9 MHz. *Macromol.* (1979) 12, pp. 41–52
- [46] Tobita, H. Simultaneous long-chain branching and random scission. *J. Polym. Sci. B* (2001) 38, pp. 391–414
- [47] Tobita, H. Free radical polymerization with long-chain branching and scission in a continuous stirred tank reactor. *Macromol. React., Eng.* (2013) 7, pp. 181–192
- [48] Tobita, H. Free-radical polymerization with long-chain branching and scission: Markovian solution of the weight-average molecular weight. *Macromol. Th. Simul.* (2014) 23, pp. 477–489
- [49] Tobita, H., Continuous free radical polymerization with long-chain branching and scission in a tanks-in-series model. *Macromol.* (2014) 23, pp. 182–197
- [50] Tobita, H. Continuous tanks-in-series process for free radical polymerization with long-chain branching and scission: Effect of the order of a large tank. *Macromol. React. Eng.* (2015) 9, pp. 556–569
- [51] Iedema, P.D., Wulkow, M., Hoefsloot, C.J. Modeling molecular weight and degree of branching distribution of low-density polyethylene. *Macromol.* (2000) 33, pp. 7173–7184
- [52] Kim, D.-M., Iedema, P.D. Modeling of branching density and branching distribution in low-density polyethylene polymerization. *Chem. Eng. Sci.* (2008) 63, pp. 2035–2046
- [53] Yaghini, N., Iedema, P.D. Molecular weight/branching distribution modeling of low-density-polyethylene accounting for topological scission and combination termination in continuous stirred tank reactor. *Chem. Eng. Sci.* (2014) 116, pp. 144–160
- [54] Yaghini, N., Iedema, P.D. New models of radical polymerization with branching and scission predicting molecular weight distribution in tubular and series continuous stirred tank reactors allowing for multiradicals and gelation. *Chem. Eng. Sci.* (2015) 130, pp. 301–309
- [55] Yaghini, N., Iedema, P.D. Branching determination from radius of gyration contraction factor in radical polymerization. *Polymer* (2015) 59, pp. 166–179
- [56] Yaghini, N., Iedema, P.D. Predicting molecular weight distribution by deterministic modeling and Monte Carlo simulations of radical polymerization with branching and scission allowing for multiradicals and gelation in various reactor configurations. *Chem. Eng. Sci.* (2015) 130, pp. 310–318
- [57] Yaghini, N., Iedema, P.D. Population balance modeling of full two-dimensional molecular weight and branching distributions for LDPE with topological scission in continuous stirred tank reactor. *Chem. Eng. Sci.* (2015) 137, pp. 556–571
- [58] Krall, A., Kiparissides, C. Mathematical modeling of the bivariate molecular weight-long chain branching distribution of highly branched polymers. A population balance approach. *Chem. Eng. Sci.* (2007) pp. 5304–5322

- [59] Meimargolou, D., Pladis, P., Baltas, A., Kiparissides, C. Prediction of the molecular and polymer solution properties of LDPE in a high-pressure tubular reactor using a novel Monte Carlo technique. *Chem. Eng. Sci.* (2011) 66, pp. 1685–1696
- [60] Hanson, D.E. Shear Modification of Polyethylene. *Polym. Eng. Sci.* (1969) 9, pp. 405–414
- [61] Rodukai, M., Mihara, S., Fujiki, T.J. Influence of shear history on the rheological properties and processability of LDPE. *Macromol.* (1979) 32, pp. 3289–3294
- [62] Leblans, P.J.R., Bastiaansen, C. Shear modification of LDPE. *Macromol.* (1989) 22, pp. 3312–3317
- [63] Yamaguchi, M., Takashi, M. Rheological properties of low-density polyethylenes produced by tubular and vessel processes. *Polymer* (2001) 42, pp. 8663–8670
- [64] Sinn, H. H., Kaminsky, W. Ziegler-Natta Catalysis. *Adv. Organomet. Chem.* (1980) 18, pp. 99–149
- [65] Soares, J. B. P., Pérez, O. Coordination polymerization, Chapt. 5 In Saldívar-Guerra, E., Vivaldo-Lima, E. (Eds.) *Handbook of Polymer Synthesis, Characterization, and Processing*. (2013) John Wiley & Sons, Hoboken, NJ
- [66] Vega, J.F., Santamaria, A. Small-amplitude oscillatory shear flow measurements as a tool to detect very low amounts of long chain branching in polyethylenes. *Macromol.* (1998) 31, pp. 3639–3647
- [67] Benham, E., McDaniel, M., *Ethylene Polymers, HDPE*. In Encyclopedia of Polymer Science and Technology (2002) John Wiley & Sons, New York
- [68] McDaniel, M.P., Rohlffing, D.C., Benham, E.A. Long-chain branching in polyethylene from the Phillips chromium catalyst. *Polym. React. Eng.* (2003) 11, pp. 101–132
- [69] Ghosh, P., Dev, D., Chakrabarti, A. Reactive melt processing of polyethylene: effect of peroxide action on polymer structure, melt rheology and relaxation behavior. *Polymer* (1997) 38, p. 6175
- [70] Lazar, M., Kleinova, A., Fiedlerova, A., Janigova, I., Borsig, E. Role of minority structures and mechanism of peroxide crosslinking of polyethylene *J. Polym. Sci.: A: Polym. Chem.* (2003) 42, pp. 675–688
- [71] Zhou, W., Zhu, S. ESR study of peroxide-induced cross-linking of high density polyethylene. *Macromol.* (1998) 31, pp. 4335–4341
- [72] Padmanabhan, S., Sarma, K.R., Sharma, S., Synthesis of Ultrahigh Molecular Weight Polyethylene Using Traditional Heterogeneous Ziegler-Natta Catalyst. *Systems Ind. Eng. Chem. Res.* (2009) 48, pp. 4866–4871
- [73] Gao, P., Mackley, M.R. The structure and rheology of molten ultra-high-molecular-mass polyethylene. *Polymer* (1994) 35, pp. 5210–5216
- [74] Rastogi, S., Kurelec, L., Cuypers, J., Lippits, D., Wimmer, M., Lemstra, P.J. Disentangled state in polymer melts; a route to ultimate physical and mechanical properties. *Macromol. Mater. Eng.* (2003) 288, pp. 964–970
- [75] Pandey, A., Champouret, Y., Rastogi, S. Heterogeneity in the Distribution of Entanglement Density during Polymerization in Disentangled Ultrahigh Molecular Weight Polyethylene. *Macromol.* (2011) 44, pp. 4952–4960

- [76] Chen, Z., Mesgar, M., White, P.S., Daugulis, O.P., Brookhart, M. Synthesis of Branched Ultrahigh-Molecular-Weight Polyethylene Using Highly Active Neutral, Single-Component Ni(II) Catalysts. *ACS Catal.*, (2015) 5, pp. 631–636
- [77] Utracki, L.A., Schlund, B. Linear low density polyethylenes. Part 1. Molecular characterization. *Polym. Eng. Sci.* (1987) 27, pp. 359–366
- [78] Mirabella, F.M., Ford, E.A. Characterization of low-density polyethylene: Cross fractionation according to copolymer composition and molecular weight. *J. Polym. Sci. B, Polym Phys.* (1987) 25, pp. 777–790
- [79] Zhang, M., Lynch, D.T., Wanke, S.E. Effect of molecular structure distribution on melting and crystallization behavior of 1-butene/ethylene copolymers. *Polymer* (2001) 42, pp. 3067–3075
- [80] Heurtelieu, B., Vaultier, F., Leino, R., Boisson, C., Cramail, H. *Single-Site Catalysts*. In Encyclopedia of Polymer Science and Technology, (2012) John Wiley & Sons, New York
- [81] Hlatky, G.G. Heterogeneous single-site catalysts for olefin polymerization. *Chem. Rev.* (2000) 100, pp. 1347–1376
- [82] Hanson, S. *New Catalysts for Olefin Polymerization* (2010) Masters of Science Thesis, Dept. of Chem., University of Saskatchewan
- [83] Kaminsky, W., Müller, F., Sperber, O. Comparison of olefin polymerization processes with metallocene catalysts. *Macromol. Mater. Eng.* (2005) 290, pp. 347–352
- [84] Kaminsky, W., Olefin polymerization catalyzed by metallocenes. *Adv. Catal.* (2001) 46, pp. 89–159
- [85] Chu, K.-J., Soares, J.B.P. Effect of experimental conditions on ethylene polymerization with in-situ supported metallocene catalysts. *J. Polym. Sci., Polym. Chem.* (2000) 38, pp. 1803–1810
- [86] Simpson, D.M., Vaughan, G.A. *Ethylene Polymers, LLDPE*. In Encyclopedia of Polymer Science and Technology (2002) John Wiley & Sons, New York
- [87] Kaminsky, W., Albers, I., Bathauer, M. New copolymers of olefins and styrene by metallocene catalysts. *Designed monomers and polymers* (2002) 5, pp. 155–162
- [88] Malmberg, A., Gabriel, C., Steffl, T., Münstedt, H., Lofgren, B. Long-chain branching in metallocene-catalyzed polyethylenes investigated by low oscillatory shear and uniaxial rheometry. *Macromol.* (2002) 35, pp. 1038–1048
- [89] Gabriel, C., Kokko, E., Löfgren, B., Seppälä, J., Münstedt, H. Analytical and rheological characterization of long-chain branched metallocene-catalyzed ethylene homopolymers. *Polymer* (2003) 43, pp. 6383–6390
- [90] Stevens, J.C., Neithamer, D.R., Metal complex compounds (1992) US Patent 5,132,380 A
- [91] Braunschweig, H., Breitling, F.M. Constrained geometry complexes—Synthesis and applications. *Coord. Chem. Rev.* (2006) 250, pp. 2691–2720
- [92] Canich, J. M., Process for producing poly- α -olefins with monocyclopentadienyl transition metal catalyst. (1991) US Patent 5,026,798 A

- [93] Piel, C., Stadler, F.J., Kaschta, J., Rulhoff, S., Münstedt, H., Kaminsky, W., Structure-property relationships of linear long-chain branched metallocene high-density polyethylenes characterized by shear rheology and SEC-MALLS. *Macromol. Chem. Phys.* (2006) 207, pp. 6–38
- [94] Karimkhani, V., Afshar-Taromi, F., Pourmahdian, S., Stadler, F.J., Revisiting long-chain branch formation mechanism in metallocene catalyzed polyethylenes. *Polym. Chem.* (2013) 4, pp. 3774–3790
- [95] Chum, P.S., Kao, C.I., Knight, G.W. *Structure, properties and preparation of polyolefins produced by single-site catalyst technology*. Chapt. 12 In Metallocene-based Polyolefins, Vol. 1. Scheirs, J., Kaminsky, W. (Eds.) (1999) John Wiley & Sons, New York
- [96] Soares, J.B.P., Hamielec, A.E. Bivariate chain length and long chain branching distribution for copolymerization of olefins and polyolefin chains containing terminal double-bonds. *Macromol. Theory Simul.* (1996) 5, pp. 547–572
- [97] Soares, J.B.P., Hamielec A.E, The chemical composition component of the distribution of chain length and long chain branching for copolymerization of olefins and polyolefin chains containing terminal double bonds, *Macromol. Theory Simul.* (1997) 6, pp. 591–596
- [98] Beigzadeh, D., Soares J.B.P., Hamielec A.E., Study of long-chain branching in ethylene polymerization, *Polym. React. Eng.* (1997) 5, pp. 141–180
- [99] Beigzedeh, D., Soares J.B.P., Duever, T.A. Combined metallocene catalysts: an efficient technique to manipulate long-chain branching frequency of polyethylene. *Macromol. Rapid Commun.* (1999) 20, pp. 541–545
- [100] Beigzadeh, D., Soares J.B.P., Hamielec, A.E. Recipes for synthesizing polyolefins with tailor-made molecular weight, polydispersity index, long-chain branching frequencies, and chemical composition using combined metallocene catalyst catalyst systems in a CSTR at steady state. *J. Appl. Polym. Sci.* (1999) 71, pp. 1753–1770
- [101] Kolodka, E., Want, W.-J., Charpenier, P.A., Zhu, S., Hamielec, A.E. Long-chain branching in slurry polymerization of ethylene with zirconocene dichloride/modified methylaluminoxane. *Polymer* (2000) 41, pp. 3985–3991
- [102] Read, D.J., McLeish, T.C.B. Molecular rheology and statistics of long chain branched metallocene-catalyzed polyolefins. *Macromol.* (2001) 34, pp. 1928–1945
- [103] Costeux, S., Wood-Adams, P., Beigzadeh, D. Molecular structure of metallocene-catalyzed polyethylene: Rheologically relevant representation of branching architecture in single catalyst and blended systems. *Macromol.* (2002) 35, pp. 2514–2528
- [104] Costeux, S. Statistical modeling of randomly branched polymers produced by combination of several single-site catalysts: Toward optimization of melt properties. *Macromol.* (2003) 36, pp. 4168–4187
- [105] Wood-Adams, P., Dealy, J.M. deGroot, A. W., Redwine, O. D. Effect of molecular structure on the linear viscoelastic behavior of polyethylene, *Macromol.* (2000) 33, pp. 7489–7499
- [106] Torres, E., Si-Wan, L., Costeux, S., Dealy, J.M. Branching structure and strain hardening of branched metallocene polyethylenes. *J. Rheol.* (2015) 59, pp. 1151–1172

- [107] Wood-Adams, P.M., Costeux, S. Thermorheological behavior of polyethylene: Effects of microstructure and long-chain branching, *Macromol.* (2001) 34, pp. 6281–6290
- [108] Wood-Adams, P.M. The effect of long chain branches on the shear flow behavior of polyethylene. *J. Rheol.* (2001) 45, pp. 203–210
- [109] Robertson, C.J., García-Franco, C.A., Srinivas, S., Extent of branching from linear viscoelasticity of long-chain branched polymer, *J. Polym. Sci., Part B: Polym. Phys.* (2004) 42, pp. 1671–1684
- [110] He, C., Costeux, S., Wood-Adams, P.M. A technique to infer structural information for low level long chain branched polyethylenes. *Polymer* (2004) 45, pp. 3747–3754
- [111] Das, C., Inkson, N.J., Read, D.J., Kelmanson, M.A., McLeish, T.C.B. Computational linear rheology of general branch-on-branch polymers, *J. Rheol.* (2006) 50, pp. 207–234
- [112] Takeh, A., Worch, J., Shanbhag, S. Analytical rheology of metallocene-catalyzed polyethylenes. *Macromol.* (2011) 44, pp. 3656–3665
- [113] Das, C., Read, D.J., Auhl, D., Kapnistos, M., den Doelder, J., Vittorias I., McLeish T.C.B. Numerical prediction of nonlinear rheology of branched polymer melts. *J. Rheol.* (2014) 58, pp. 737–757
- [114] Ramachandran, R., Beaucage, G.A., Kulkarni, S., McFaddin, D., Merrick-Mack J., Galiatsatos, V. Branch content of metallocene polyethylene, *Macromol.* (2009) 42, pp. 4746–4750
- [115] Baier, M.C., Zuiderveld, M.A., Mecking, S. Post-metallocenes in the industrial production of polyolefins. *Angew. Chem. Int. Ed.* (2014) 53, pp. 9722–9744
- [116] Park, H.E., Dealy, J.M., Marchand, J.M.G., Wang, J., Register, R.A., Li, S. Rheology and structure of molten, olefin multiblock copolymers. *Macromol.* (2010) 43, pp. 6789–6799
- [117] Arriola, D.J., Carnahan, E.M., Hustad, P.D., Kuhlman, R.L., Wenzel, T.T. *Science* (2006) 312, pp. 714–719; see also supporting online material
- [118] Ebner, K., White, J.L. Peroxide induced and thermal degradation of polypropylene. *Intern. Polym. Proc.* (1994) 9, pp. 233–239
- [119] Pabedinskas, A., Cluett, W.R., Balke, S.T. Modeling of polypropylene degradation during reactive extrusion with implications for process control. *Polym. Eng. Sci.* (1994) 34, pp. 598–612
- [120] Mead, D.W. Evolution of the molecular weight distribution and linear viscoelastic rheological properties during reactive extrusion of polypropylene. *J. Appl. Polym. Sci.* (1995) 57, pp. 151–173
- [121] Vergnes, B., Berzin, F. Peroxide-controlled degradation of polypropylene. *Macromol. Symp.* (2000) 158, pp. 77–90
- [122] Soya, K., Wozumi, Kaji, E. *Synthesis of isotactic polypropylene by metallocene and related catalysts* Chapt. 17 In Metallocene-based polyolefins, Vol. 1, Scheirs J., Kaminsky, W. (Eds.) (1999) John Wiley & Sons, New York
- [123] Weng, W., Hu, W., Dekmezian, A.H., Ruff, C.J. Long chain branched isotactic polypropylene. *Macromol.* (2002) 35, pp. 3838–3843

- [124] Ye, Z., AlObaidi, F., Zhu, S. Synthesis and rheological properties of long-chain-branched isotactic polypropylenes prepared by copolymerization of propylene with nonconjugated dienes. *Ind. Eng. Chem. Res.* (2004) 43, pp. 2860–2870
- [125] Ye, Z., Zhu, S. Synthesis of branched polypropylene with isotactic backbone and atactic side chains. *J. Polym. Sci. A* (2003) pp. 1152–1159
- [126] Yoshii, F., Makuuchi, K., Kikukawa, S., Tanaka, T., Saitoh, J., Koyama, K. High-melt-strength polypropylene with electron beam irradiation in the presence of polyfunctional monomers. *J. Appl. Polym. Sci.* (1996) 60, pp. 617–623
- [127] Rätzsch, M., Reaction mechanism in long chain branched PP. *J. Macromol. Sci., Pure Appl. Chem.* (1999) 36, pp. 1759–1769
- [128] Lagendijk, R.P., Hogt, A.H., Buijtenhuijs, A., Gotsis, A.D. Peroxydicarbonate modification of polypropylene and extensional flow properties. *Polymer* (2001) 42, pp. 10035–10043
- [129] Gotsis, A.D., Zeevenhoven, B.L.F., Tsengoglou, C. Effect of long branches on the rheology of polypropylene. *J. Rheol.* (2004) 48, pp. 895–914
- [130] He, C., Costeux, S., Wood-Adams, P., Dealy, J.M. Molecular structure of high-melt-strength polypropylene and its application to polymer design. *Polymer* (2003) 44, pp. 7181–7188
- [131] De Rosa, C., Auriemma, F., Di Girolamo, R., Ruiz de Ballesteros, O. Crystallization of the mesomorphic form and control of the molecular structure for tailoring the mechanical properties of isotactic polypropylene. *J. Polym. Sci., Part B: Polym. Phys.* (2014) pp. 677–699
- [132] Kissin, Y.V., Rishina, L.A., Lalayan, S.S., Krasheninnikov, V.G. A new route to atactic propylene: The second life of premetallocene homogeneous polymerization catalyst. *J. Polym. Sci.* (2015) 53, pp. 2124–2131
- [133] Kuhn, R., Krömer, H. Structures and properties of different low density polyethylenes. *Colloid Polym Sci.* (1982) 260, pp. 1083–1092
- [134] Meissner, J. Basic parameters, melt rheology, processing and end-use properties of three similar low density polyethylenes. *Pure Appl. Chem.* (1975) 42, pp. 553–612
- [135] Winter, H.H. A collaborative study on the relation between film blowing performance and rheological properties of two low-density and two high-density polyethylene samples. *Pure Appl. Chem.* (1983) 55, pp. 943–976
- [136] Alt, F.P., Böhm, L.L., Endere, H.-F., Berthold, J. Bimodal polyethylene—Interplay of catalyst and process. *Macromol Symp.* (2001) 163, pp. 135–143
- [137] Covezzi, M., Mei, G. The multizone circulating reactor technology. *Chem. Eng. Sci.* (2001) 56, pp. 4059–4067
- [138] Karol, F.J. Catalysis and the UNIPOL process in the 1990s. *Macromol. Symp.* (1995) 89, pp. 563–575
- [139] Karol, F.J. *UNIPOL gas phase copolymer with SSC metallocene technology*, In Metallocene-Catalyzed Polymers: Materials, Properties & Markets, Benedikt, G.M., Goodall, B.L. (Eds.) (1998) Plastics Design Library, Norwich, New York, pp. 35–42

- [140] Fasano, A. *Mathematical models for polymerization processes of Ziegler-Natta type.* Chapt. 1 In Mathematical modeling for polymer processing. Capasso, V. (Ed.) (2000) Springer, Berlin
- [141] Priddy, D. *Styrene polymers.* In Encyclopedia of Polymer Science and Technology (2001) John Wiley & Sons, New York
- [142] Ferri, D., Lomollini, P. Melt rheology of randomly branched polystyrenes. *J. Rheol.* (1999) 43, pp. 1355–1372
- [143] Koppi, K.A., Priddy, D.B. *Branched polystyrene.* Chapt. 24 In Modern styrenic polymers: polystyrenes and styrenic copolymers. Scheirs, J., Priddy, D.B. (Eds.) (2003) John Wiley & Sons, New York

4

Linear Viscoelasticity— Fundamentals

The treatment of linear viscoelasticity presented in this chapter is sufficient for a full understanding of the models described in subsequent chapters. However, readers wishing to delve more deeply into this subject may wish to consult the monographs by Ferry [1] and Tschoegl [2]. Ferry treats the rheological properties of polymers, while Tschoegl's book is a compendium of empirical models and relationships between various linear material functions.

■ 4.1 Stress Relaxation and the Relaxation Modulus

4.1.1 The Boltzmann Superposition Principle

The *raison d'être* of this book is that rheological properties of the melt are very sensitive to the molecular structure of a polymer. Rheological properties describe how stress develops in a sample undergoing a prescribed deformation. They also describe the deformation that is caused by a prescribed stress. The most fundamental rheological experiment for a viscoelastic material is a step-strain test, and for melts this nearly always means a step *shear* strain. In a step shear-strain test, a sample is subjected to a sudden shear strain of magnitude, γ_0 at time $t = 0$. The shear stress is measured as a function of time, and the ratio of the stress to the applied strain defines the relaxation modulus, $G(t)$.

$$G(t) \equiv \sigma(t)/\gamma_0 \quad (4.1)$$

If the experiment is repeated, with the amount of strain doubled to $2\gamma_0$, another result will be obtained. If the resulting stress at any given value of t is exactly twice that measured in the first test at the same value of t , the relaxation modulus determined in the two experiments will be identical to each other. *From an experimental point of view this is a key feature of linear viscoelastic behavior.* The implication is

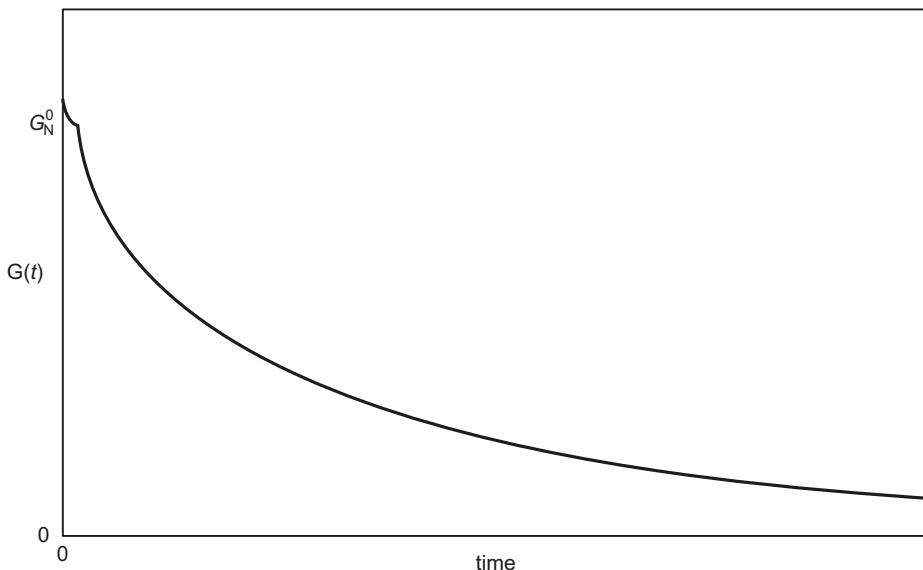


Figure 4.1 Typical stress relaxation curve for a molten polymer using linear scales for both axes. The pattern of the very fast relaxation at short times is not visible using a time scale that is suitable to show the final, long-term stage of the relaxation.

that in both experiments the strain is sufficiently small that the departure of the molecules from their equilibrium state is negligible. Thus, both experiments reveal the behavior of the polymer in its unstrained state. This, in turn, implies that the response to a series of small, step strains will be simply the sum of the responses to each step, where the same relaxation modulus governs each response.

Figure 4.1 shows a typical stress relaxation curve for a **highly entangled**, linear polymer sample in which all the molecules have the same molecular weight, i.e., a monodisperse sample. In this plot using linear scales, important phenomena that occur at very short times and at long times, where the stress is very small, cannot be seen. The same information is replotted in Fig. 4.2 using logarithmic scales for both axes. This has the effect of greatly expanding the behavior at very short times and very low stresses that were not visible using linear scales. The various features of this curve will be discussed in detail in Chapter 5. For the present, we will simply list the various zones in which distinctive relaxation mechanisms occur. At extremely short times there is a glassy zone in which the polymer is very stiff and has a very high “glassy modulus,” G_g . This is followed by a “transition zone” in which additional mechanisms of relaxation come into play, and this leads into a *plateau zone*, in which very little relaxation occurs. Finally, at long times, a new mechanism of relaxation comes into play, and in this “terminal zone,” the stress falls toward zero, which it must finally do in any liquid. The value of $G(t)$ in the zone of constant modulus is called the *plateau modulus*, and has the symbol G_N^0 .

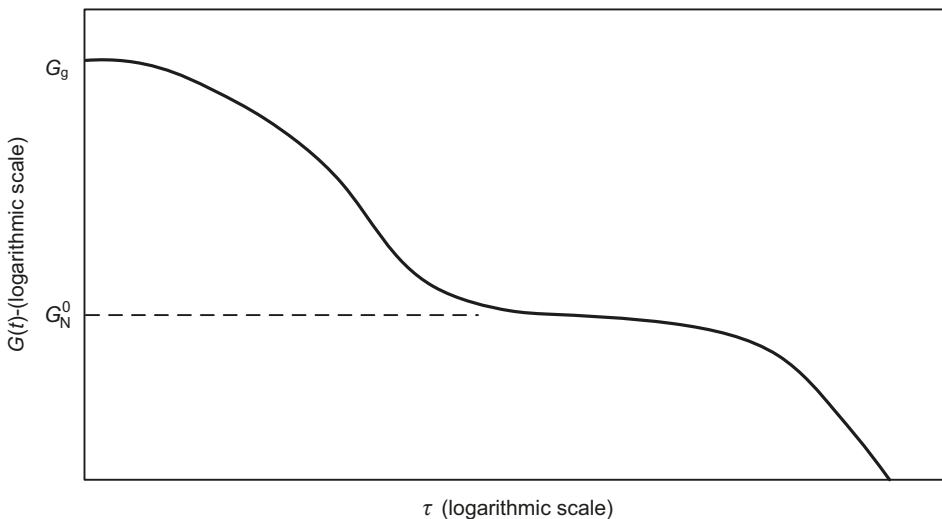


Figure 4.2 Stress relaxation curve for a linear, entangled, monodisperse polymer sample, where logarithmic scales are used for both axes. In this representation, distinct mechanisms of relaxation are apparent in the glassy, transition, plateau and terminal time zones.

Crosslinked elastomers do not flow, and the relaxation modulus of these materials drops to a non-zero constant value, the equilibrium modulus, G_e , which is its final plateau. It is important to note that if one is shown only the transition and plateau regions of the relaxation modulus curve for a monodisperse melt, this curve is virtually indistinguishable from that of a crosslinked material. Thus, in the plateau zone, a melt does an excellent impersonation of a rubber!

The additivity of responses can be expressed quantitatively by Eq. 4.2, which gives the stress as a function of time in response to a sequence of small shearing deformations, $\delta\gamma(t_i)$, occurring at times, t_i ,

$$\sigma(t) = \sum_{i=1}^N G(t-t_i) \delta\gamma(t_i) \quad t > t_N \quad (4.2)$$

Ludwig Boltzmann generalized this to give the response to a continuously varying shear deformation, rather than a series of step strains, by letting $\delta\gamma$ approach zero and writing Eq. 4.2 as an integral.

$$\sigma(t) = \int_{-\infty}^t G(t-t') d\gamma(t') = \int_{-\infty}^t G(t-t') \dot{\gamma}(t') dt' \quad (4.3)$$

Here, $d\gamma(t')$ is the shear strain that occurs between t' and dt' , and $\dot{\gamma}$ is the shear rate during this period. Equation 4.3 is the form of the *Boltzmann superposition principle* for simple shearing deformations.

The Boltzmann superposition principle is valid for very small deformations, but it is also valid for very slow deformations, even if they are large. This is because polymeric liquids have a *fading memory* of past strains, which is reflected in the fact that $G(t)$ decays to zero at long times. As a result, as long as the accumulated strain is small for a time long enough for the memory to fade practically to zero, the response will still be governed by Eq. 4.3. However, it may prove impossible in practice to make a measurement at a sufficiently small shear rate for Eq. 4.3 to be valid, especially if very high molecular weight components or long chain branches are present. The stress generated may be too small to measure, the shear rate may be too small to be generated reliably, or the sample may degrade during the very long time required to reach steady state.

While we have considered only shearing deformations, the superposition principle applies to deformations having any kinematics. To generalize Eq. 4.3 to account for this, we need only replace the shear stress, shear strain, and shear rate by the corresponding tensorial quantities. The tensorial form of the Boltzmann superposition principle can then be used to determine all the components of the stress tensor arising from a deformation having any kinematics. Since we are interested here only in very small deformations, it is possible to use the infinitesimal strain tensor, whose components, $\gamma_{ij}(t, t')$ are related to the displacement vectors of neighboring particles of fluid particle at a time, t' , relative to the “present” time, t , i.e., the time at which the stress is to be determined. The infinitesimal strain tensor and its use are described in detail by Dealy and Wang (ref. [3], p. 121). Using this tensor, we can write the general form of the Boltzmann superposition principle in terms of the components of the infinitesimal stress and rate-of-deformation tensors:

$$\sigma_{ij}(t) = \int_{-\infty}^t G(t-t') \dot{\gamma}_{ij}(t') dt' \quad (4.4)$$

For readers not familiar with this notation, a few words of explanation may be useful. The indices on a typical component of the stress tensor have the following meaning. The second index j indicates that this component of the stress acts in the x_j direction, while the first index indicates that it acts on a surface normal to the x_i axis. A component is positive when it acts on a fluid element in the plus x_j direction on the face of that element having the larger value of x_i . Thus, a tensile stress has a positive value, while a compressive stress is negative. Note that the opposite sign convention is used by some people, notably, R. B. Bird.

An important concept is that in an incompressible (constant density) fluid, an isotropic (i.e., the same in all directions) stress will cause no change in the shape or size of an element of the fluid. Since rheology deals with deformations, some isotropic portion of the total stress on an element is of no rheological significance. One way of recognizing this is to say that the stress tensor shown in Eq. 4.4 is the

extra or viscous stress, i.e., that portion of the total stress that will cause deformation in an incompressible fluid. We generally do not have any information about the isotropic component, and this means that there is uncertainty regarding the absolute value of normal stresses, i.e., those components for which $i = j$. However, this is not a problem, because in describing rheological behavior we will deal only with shear stresses and normal stress *differences*, for which isotropic components will cancel out.

While we will not need the general tensorial form of the superposition principle for the purposes of this book, we will show the result of its use to describe the special case of axisymmetric, uniaxial (tensile) extensional flow:

$$\sigma_{zz} - \sigma_{rr} = \int_{t'=-\infty}^{t'=t} 3G(t-t') d\varepsilon(t') = \int_{-\infty}^t 3G(t-t') \dot{\varepsilon}(t') dt' \quad (4.5)$$

where σ_{zz} is the normal component of the stress tensor acting in the z (axial) direction, σ_{rr} is the normal component of the stress tensor acting in the r (radial) direction, $d\varepsilon(t')$ is the Hencky strain accumulating during the time interval dt' , and $\dot{\varepsilon}(t')$ is the Hencky strain rate at time t' . The Hencky strain, $\varepsilon(t, t')$, that accumulates over the time interval from t' to t for a cylindrical sample of instantaneous length $L(t)$ is defined as:

$$\varepsilon(t, t') = \ln[L(t)/L(t')] \quad (4.6)$$

The response to any deformation that is either very small, or occurs at very low strain rates, is given by Eq. 4.4. For example, the shear stress, $\sigma(t)$ following the sudden imposition at time t_0 of shearing at a steady rate, $\dot{\gamma}$, is given by:

$$\sigma(t) = \dot{\gamma} \int_0^t G(t-t') dt' \quad (4.7)$$

The lower limit on the integral is zero rather than minus infinity, since the sample is known to be in a stress-free state at $t = 0$. The ratio of the stress to the shear rate is called the shear stress growth coefficient and has units of viscosity:

$$\eta^+(t) \equiv \sigma(t)/\dot{\gamma} = \int_0^t G(t-t') dt' = \int_0^t G(s) ds \quad (4.8)$$

where $s \equiv (t-t')$. In the long-time limit, this transient function will approach the (steady-state) viscosity, which is thus given by:

$$\eta_0 = \lim_{t \rightarrow \infty} \eta^+(t) = \int_0^\infty G(s) ds \quad (4.9)$$

The subscript zero indicates that this is the viscosity exhibited in the regime of linear viscoelasticity, i.e., the low-shear-rate limiting viscosity. It is thus defined as shown by Eq. 4.10 and is called the *zero-shear viscosity*.

$$\eta_0 \equiv \lim_{\dot{\gamma} \rightarrow 0} \eta(\dot{\gamma}) \quad (4.10)$$

In discussions involving only this viscosity the subscript is sometimes omitted, but this is not recommended. This material constant is of great importance, as it is very sensitive to molecular weight and branching structure. This structure dependency is described in detail in Chapter 5.

4.1.2 The Maxwell Model for the Relaxation Modulus

In practice it is not possible to establish with perfect precision the relaxation modulus over the entire range of times from zero to infinity. Even if we replace infinity by a time sufficiently long that we are reasonably certain that the material is in its equilibrium, unstressed state, we are still limited by the precision of the apparatus generating the data from which $G(t)$ is inferred. Nevertheless, we assume that such a material function $G(t)$ exists and is a well-defined property of any physically homogeneous, viscoelastic material.

While we do not know the functional form of $G(t)$, we have a good understanding of its general behavior, based on many experimental observations. The detailed shape of the curve is described in the next section of this chapter, but for the present purpose, we need only note, as shown in Figs. 4.1 and 4.2, that the stress starts at a high value and then decays monotonically with time, very rapidly at first, and ultimately approaches a steady value at long times. For a cross-linked elastomer, i.e., a rubber, the long-time, limiting value of G is the equilibrium modulus G_e , while for a melt it is zero [$G(t \rightarrow \infty) = 0$]. A transcendental function that behaves in a general way like $G(t)$ is the exponential:

$$G(t) = G_0 e^{-t/\tau_0} \quad (4.11)$$

where G_0 is the instantaneous modulus $G(0)$ and τ_0 is a *relaxation time*. This function is plotted in Fig. 4.3 in dimensionless form, i.e., (G/G_0) versus (t/τ_0) . We note the very fast initial decay and the long-time, asymptotic approach to zero. In order to reveal details of the short-time behavior without losing the long-time data off the graph on the right, logarithmic scales are almost always used in plotting rheological material functions. For example, the curve shown in Fig. 4.3 is replotted using logarithmic scales in Fig. 4.4. This is a useful technique, but it is very important to realize that the use of nonlinear scales greatly changes the shape of the curve. For example, one gets the impression from Fig. 4.4 that there is a short-time plateau in the behavior, but this is not so at all.

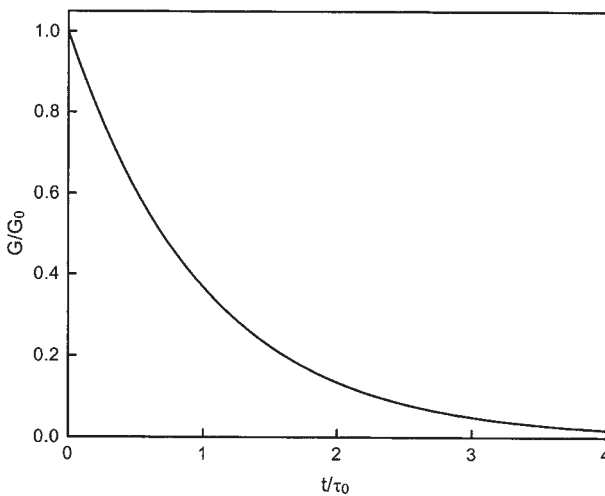


Figure 4.3 Plot of dimensionless relaxation modulus versus dimensionless time as modeled by a single exponential function, Eq. 4.11. On this plot using linear scales the detailed behavior at very short time is obscured.

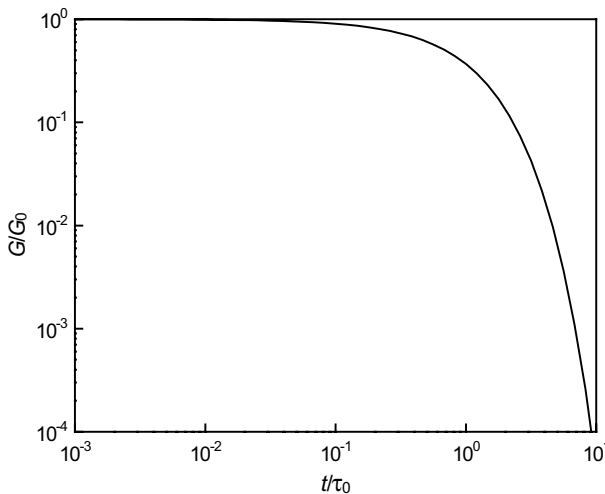


Figure 4.4 Dimensionless relaxation modulus versus dimensionless time according to Eq. 4.11, as in Fig. 4.3, but plotted using logarithmic coordinates. The use of logarithmic scales dramatically changes the shape of a curve and confirms that the characteristic time for the relaxation corresponds to $t/t_0 = 1$, i.e., $t = t_0$.

It is useful as an aid to understanding viscoelastic phenomena to interpret this function in terms of the behavior of a mechanical assembly consisting of a linear (Hookean) spring and a linear *dash-pot*, connected in series as shown in Fig. 4.5. A dash-pot is an element in which the force is proportional to the rate of displacement and is thus analogous to a Newtonian fluid. This assembly was proposed by Maxwell as a model for the behavior of gases, and it is referred to as Maxwell element.

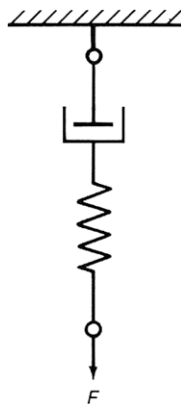


Figure 4.5 Maxwell element consisting of a spring and a dashpot in series. This is the simplest mechanical analog of stress relaxation in a viscoelastic liquid. As in the case of any physical system that involves both energy dissipation and energy storage, there is at least one material parameter having units of time.

If this element is suddenly stretched by an amount X at time $t = 0$, the force will be transmitted through the spring and the dashpot and will thus be the same in both. This force is proportional to the spring extension, X_s , and also to the rate of extension of the dashpot, dX/dt . We can then write a differential equation that describes the relaxation of the force as a function of time, $F(t)$, as follows:

$$F(t) = K_e X_s = K_v \frac{dX_d}{dt} \quad (4.12)$$

The total displacement, X is simply $X_s + X_d$, and for a step-strain experiment is given by a step function. The differential equation can then be solved as follows for $F(t)$:

$$F(t) = X K_e \exp(-t K_e / K_v) \quad (4.13)$$

We note that $X K_e$ is the initial value of the stress, since all of the extension must initially be absorbed by the spring, and that K_v / K_e has units of time and is thus a characteristic time, which we will call τ_M . Now Eq. 4.13 can be written as:

$$F(t) = F_0 \exp(-t/\tau_M) \quad (4.14)$$

It is useful to note that the dynamic behavior of any system that incorporates both energy storage and energy dissipation must have at least one characteristic time. Another example is an electrical circuit that includes both resistance and capacitance. Furthermore, we note that Eq. 4.14 is the same as Eq. 4.11, with F_0 replaced by G_0 and τ_M by τ_0 . The Maxwell element is thus said to be a mechanical analog of the viscoelastic behavior described by Eq. 4.11. It will often prove useful in our discussion of the linear viscoelastic behavior of polymers to refer to the viscoelastic analog of the Maxwell element.

4.1.3 The Generalized Maxwell Model and the Discrete Relaxation Spectrum

While the exponential stress relaxation predicted by the viscoelastic analog of the Maxwell element, i.e., a single exponential, is qualitatively similar to the relaxation of polymeric liquids, it does not describe the response of real materials. If, however, it is generalized by assembling a number of Maxwell elements in parallel, it is possible to fit the behavior of real materials to a level of accuracy limited only by the precision and time-range of the experimental data. This leads to the generalized, or multi-mode, Maxwell model for linear viscoelastic behavior, which is represented mathematically by a sum of exponentials as shown by Eq. 4.15.

$$G(t) = \sum_{i=1}^N g_i e^{-t/\tau_i} \quad (4.15)$$

The g_i parameters are called *relaxation strengths*. If $N = \infty$, Eq. 4.15 is a sum over a Dirichlet series, and it can be shown that it converges as long as:

$$\sum_{i=1}^{\infty} \tau_i = \infty$$

Furthermore, for a given function $G(t)$ and an infinite set of time constants, $\{\tau_i\}$, there is a unique set of moduli, $\{g_i\}$. However, if the sum is over a finite number, N , of terms, then the relaxation strengths depend on N .

As will be shown in Chapter 6 there are molecular theories of polymer behavior that lead to relaxation moduli of the form of Eq. 4.15 with $N = \infty$, where the parameters are precisely specified in terms of a few measurable parameters.

However, even when such a model is not being used, it is often useful to describe the relaxation modulus by use of Eq. 4.1 where the constants are inferred from experimental data by an empirical procedure. The resulting set of constants $\{\tau_i, g_i\}$ constitutes a *discrete relaxation spectrum*. While these empirical parameters have no physical significance, in the limit of large N they should, in principle, approach the underlying function $G(t)$, which is a material property. Methods of determining the constants for a discrete spectrum from experimental data are described in Section 4.4.

The response to any given (small or slow) deformation can be described in terms of a discrete spectrum by substituting Eq. 4.15 into Eq. 4.4 and integrating. For example, Eq. 4.9 can be used to show that the zero-shear viscosity is given by:

$$\eta_0 = \sum_{i=1}^N g_i \tau_i \quad (4.16)$$

A discrete or line spectrum is often used to describe the relaxation modulus of molten polymers. It lends itself to the conversion of one response functional into another and can be inferred from data in such a way that it describes those data with a precision limited only by that of the data themselves. It is important to note that the parameters of a discrete spectrum obtained by fitting data are not related to those of a molecular theory. Methods for inferring a useful discrete spectrum from data are described in Section 4.4.1.

4.1.4 The Continuous Relaxation Spectrum

If the number of elements in the generalized Maxwell model is increased toward infinity, one arrives at the continuous spectrum function, $F(\tau)$, where $F(\tau)d\tau$ is the contribution to $G(t)$ due to Maxwell elements having relaxation times between τ and $\tau + d\tau$. The relaxation modulus is related to the spectrum function as shown by Eq. 4.17.

$$G(t) = \int_0^{\infty} F(\tau) [\exp(-t/\tau)] d\tau \quad (4.17)$$

However, because of the concentration of relaxation information at very short times, it is generally preferable to work with a logarithmic time scale. This leads to a relaxation spectrum function $H(\ln \tau)$ that is a time-weighted spectrum function defined as $F\tau$, so that the relaxation modulus is given by:

$$G(t) = \int_0^{\infty} H[\ln(\tau)] [\exp(-t/\tau)] d(\ln \tau) \quad (4.18)$$

Relationships between the various material functions describing linear behavior are given by Ferry [1] and by Tschoegl [2].

The experimental techniques nearly universally used to characterize the linear viscoelastic behavior of polymers are small-amplitude oscillatory shear and creep, which are described later in this chapter. Most often data are reported as plots of the storage and loss moduli versus frequency, and such plots are used as the basis for discussions of relationships between molecular structure and rheological behavior. However, a continuous spectrum can reveal structure-property relationships that are not apparent in such plots, especially for model polymers synthesized for research. Methods for inferring meaningful continuous spectra from data are presented in Section 4.4.

■ 4.2 The Creep Compliance and the Retardation Spectrum

In a creep experiment, the stress, rather than the strain, is increased suddenly from zero to a constant value σ_0 at time $t = 0$. The resulting data are interpreted in terms of the *creep compliance* $J \equiv \gamma(t)/\sigma_0$,

In order to apply the Boltzmann superposition principle, we write it in a form in which stress is the independent variable rather than the strain. For the most common case of simple shear, this is shown by Eq. 4.19.

$$\gamma(t) = \int_{-\infty}^t J(t-t') d\sigma(t') \quad (4.19)$$

The material function that describes the linear response to a stress history is $J(t)$, the creep compliance. It can, in principle, be determined by suddenly subjecting a sample to a constant stress and monitoring the deformation. The creep compliance is the ratio of the time-dependent shear strain to the applied stress, as shown by Eq. 4.20.

$$J(t) = \gamma(t)/\sigma_0 \quad (4.20)$$

We are interested here only in linear viscoelastic behavior, which means that σ_0 must be sufficiently small that the strain will stay within the linear range until steady-state is reached. At long times, the shear rate approaches a steady value and the creep compliance becomes linear with time. The slope of the linear asymptote is $1/\eta_0$, and the intercept of its extrapolation to zero time is the *steady-state compliance* J_s^0 .

$$J(t) = J_s^0 + t/\eta_0 \quad (\text{long-time steady flow}) \quad (4.21)$$

A crosslinked elastomer does not flow, and instead of a steady-state compliance it has an *equilibrium compliance* J_e . (Although this symbol is sometimes used for the steady-state compliance, the Official Nomenclature of The Society of Rheology and the European Society of Rheology recommends the symbol shown in Eq. 4.21.)

Figure 4.6 is a sketch of the typical shape of the creep compliance curve using linear scales. The limiting long-time slope and its extrapolation to $t = 0$ to obtain the steady-state compliance are shown. Also shown is the creep curve of a crosslinked elastomer. The creep compliance for an entangled, linear, monodisperse polymer sample is shown in Fig. 4.7, this time using logarithmic scales for both axes.

This type of plot magnifies the pre-steady-state behavior and new features become visible, in particular, the plateau compliance J_N^0 , which is the reciprocal of the plateau modulus.

$$J_N^0 = 1/G_N^0 \quad (4.22)$$

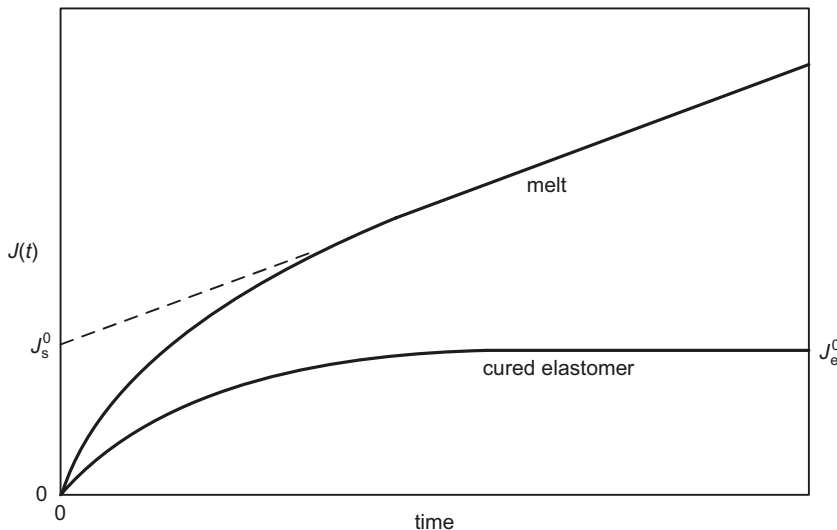


Figure 4.6 Sketch showing general features of creep compliance curves for a viscoelastic melt and a crosslinked elastomer. The strain in the melt approaches a straight line (Eq. 4.21) with a slope of $1/\eta_0$ and an intercept of J_s^0 , while that in the elastomer approaches an equilibrium compliance, J_e^0 .

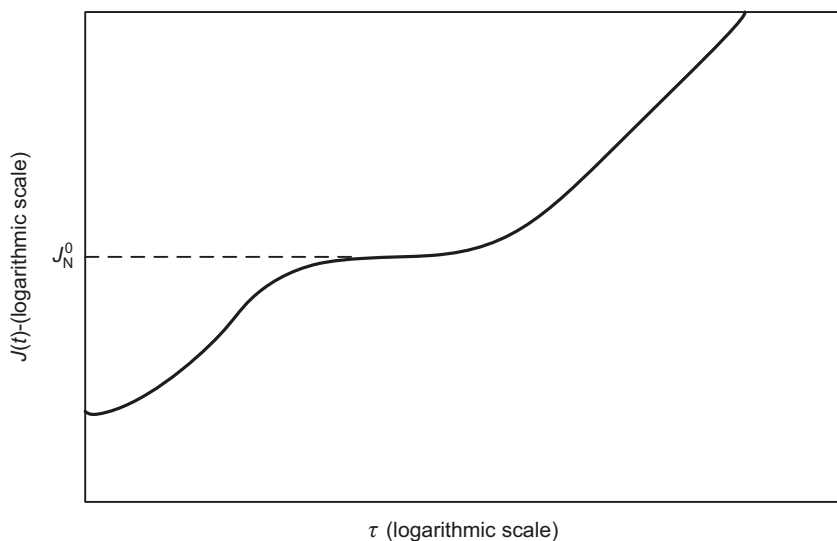


Figure 4.7 Typical creep compliance curve for a linear, entangled, monodisperse polymer, using logarithmic scales for both axes. The distinct characteristics of the creep behavior in several ranges of time are apparent in this representation. We see the glassy, transition, plateau, and terminal zones.

An experiment closely related to creep is creep recovery or constrained recoil. After a creep experiment has proceeded for a time t_0 , the shear stress is suddenly removed, and the recoil or recovered strain is measured as a function of time. It is often found that more precise measurements can be made in this test than in a creep test, especially at long times. The recovered strain, γ_r , is equal to the strain at time t_0 minus the strain at times greater than t_0 , as shown below.

$$\gamma_r(t - t_0, t_0) \equiv \gamma(t_0) - \gamma(t) \quad (t > t_0) \quad (4.23)$$

Note that the strain $\gamma(t)$ at time t is less than that at a smaller time t_0 , because the recoil process removes some of the previously imposed strain from the sample. We see that the recovered strain depends on both the preceding creep time t_0 and the duration of time $(t - t_0)$ since the stress was removed. Figure 4.8 is a sketch showing the strain as a function of time for a creep and recovery experiment.

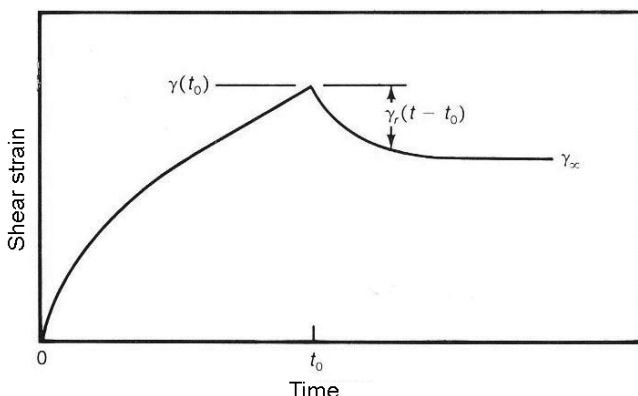


Figure 4.8 Sketch of shear strain versus time for a creep and recovery experiment. At time t_0 into a creep test, the shear stress is released, and there is a time-dependent, constrained recoil.

If, at time, t_0 , the creep experiment has reached a steady-state (constant shear rate) then the recovered strain no longer depends on t_0 , and it is convenient to set t_0 equal to zero, thus “resetting the clock.” This leads to:

$$\gamma_r(t) = \gamma(0) - \gamma(t) \quad (4.24)$$

The recoverable compliance is defined as:

$$J_r(t) \equiv \gamma_r/\sigma_0 \quad (4.25)$$

And the Boltzmann superposition principle can be used to show that:

$$J_r(t) = J(t) - t/\eta_0 \quad (4.26)$$

Thus, creep recovery leads to the same material function as creep (as long as we are in the linear viscoelastic regime). The ultimate recoil or recoverable shear γ_∞ is the recovered shear in the limit of long time when recoil has ended, and this quantity is directly related to the steady-state compliance.

$$\gamma_\infty \equiv \lim_{t \rightarrow \infty} [\gamma_r(t)] = \sigma_0 J_s^0 = \eta_0 \dot{\gamma} J_s^0 \quad (4.27)$$

We see that creep recovery provides an alternative method for determining the steady-state compliance, since $J_r(\infty) = \gamma_\infty / \sigma_0 = J_s^0$. The product $\eta_0 J_s^0$ has units of time and is sometimes used as a characteristic retardation time.

The multi-mode Maxwell model is not useful for modeling creep, and in its place the *generalized Voigt model* is often used. This generalized model consists of a group of Voigt elements (springs and dash pots in parallel) connected in series as shown in Fig. 4.9.

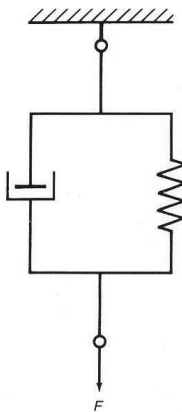


Figure 4.9 Voigt model for the creep and recovery of a cured elastomer, consisting of a spring and a dashpot in parallel (to obtain behavior analogous to that of an elastic liquid, another dashpot must be added in series with a Voigt element).

There must be at least one dashpot that is not in parallel with a spring in order to allow for flow. This picture leads to the following representation of the creep compliance in terms of a discrete spectrum of retardation times $\{J_i, \tau_i\}$.

$$J(t) = \sum_{i=1}^n J_i (1 - e^{-t/\tau_i}) + t/\eta_0 \quad (4.28)$$

A continuous retardation spectrum, $L[\ln(\tau)]$, can also be defined, which is analogous to the continuous relaxation spectrum, $H[\ln(\tau)]$. In terms of this function the creep compliance is given by Eq. 4.29.

$$J(t) = \int_{-\infty}^{\infty} L(\tau) [1 - \exp(-t/\tau)] d \ln \tau + t/\eta_0 \quad (4.29)$$

By comparison with Eq. 4.21, we see that at long times, the sum on the right of Eq. 4.28 and the integral on the right of Eq. 4.29 approach the steady-state compliance. Plazek and Echeverria [4] argue that the retardation spectrum provides more insight into relaxation processes than the relaxation spectrum. An example of a retardation spectrum is shown in Fig. 5.7.

It can be shown that the steady state compliance is related to the relaxation modulus in its continuous and discrete forms, as follows:

$$J_s^0 = \frac{\int_0^\infty G(s) s \, ds}{\left[\int_0^\infty G(s) \, ds \right]^2} = \frac{1}{\eta_0^2} \int_0^\infty G(s) s \, ds \quad (4.30)$$

$$J_s^0 = \frac{\sum G_i \tau_i^2}{(\sum G_i \tau_i)^2} = \frac{\sum G_i \tau_i^2}{\eta_0^2} \quad (4.31)$$

Methods of measuring creep and creep recovery and problems that arise in their use are described in Section 4.3.3.

■ 4.3 Experimental Characterization of Linear Viscoelastic Behavior

If the relaxation modulus is known as a function of time for times from zero to infinity, the viscoelastic behavior of a material in the linear regime is fully specified. However, even if we replace infinity by a time long enough that the sample is practically completely relaxed, this ideal state of knowledge is never achieved with real materials due to instrument limitations or long-time sample stability. Furthermore, the precision of step strain data is limited by difficulties involved in generating a nearly instantaneous deformation, and tracking the very rapid initial decay of stress following the strain and the very small stress at long times. The experiments most often used to characterize the linear behavior of a molten polymer are oscillatory shear and creep. Oscillatory shear is the most popular, because it is easier to measure the storage and loss moduli using oscillatory shear experiments than to generate step strains or stresses and measure the resulting strain or stress. In addition, in an oscillatory experiment with a sine wave strain input, the resultant stress waveform is fitted to a sinusoid at each frequency, and this fitting process acts as a filter that rejects noise that is non-sinusoidal or is at a frequency other than that imposed.

This noise rejection improves with increasing numbers of cycles and averaging. Hence, it is both easier and more precise to study relaxation in the frequency domain than in the time domain. The transformation of oscillatory shear data into discrete and continuous relaxation moduli is discussed in Section 4.4.

4.3.1 Oscillatory Shear

In an oscillatory shear experiment, the sample is subjected to a homogeneous deformation at a sinusoidally varying shear strain or shear stress. In a controlled strain experiment, one generates a strain that is as close as possible to a sine wave.

$$\gamma = \gamma_0 \sin(\omega t) \quad (4.32)$$

If the strain amplitude is sufficiently small that the response is linear, the resulting stress is also sinusoidal and can be written in terms of a stress amplitude, σ_0 , and a phase shift, δ , called the loss angle, as follows:

$$\sigma(t) = \sigma_0 \sin(\omega t + \delta) \quad (4.33)$$

This technique is called *small-amplitude oscillatory shear* (SAOS). As is the case for any linear system in the frequency domain, the results of an oscillatory shear test can be represented in terms of an amplitude ratio $G_d \equiv \sigma_0/\gamma_0$ and a phase shift δ which are functions of frequency. While the loss angle $\delta(\omega)$ is sometimes used to characterize the linear behavior of a melt, SAOS data are usually reported in terms of the storage and loss moduli G' and G'' as functions of frequency. Using trigonometric identities, Eq. 4.33 can be rewritten in terms of these material functions.

$$\sigma(t) = \gamma_0 [G'(\omega) \sin(\omega t) + G''(\omega) \cos(\omega t)] \quad (4.34)$$

where G' and G'' are related to G_d and δ as follows:

$$G' = G_d \cos(\delta) \quad (4.35a)$$

$$G'' = G_d \sin(\delta) \quad (4.35b)$$

It is sometimes useful in deriving equations to consider the storage and loss moduli to be the real and imaginary components of the *complex modulus*, $G^*(\omega)$, which is defined as follows:

$$G^*(\omega) = G'(\omega) + i G''(\omega) \quad (4.36)$$

In this interpretation, we see that the parameter defined above as G_d is the absolute magnitude of the complex modulus $|G^*|$, and the loss angle is the angle between the storage and loss moduli in the complex plane. An alternative representation of dynamic data is in terms of the complex viscosity η^* defined as follows:

$$\eta^* = \eta' - i \eta'' \quad (4.37)$$

where the real and imaginary components, which are functions of frequency, are related to the storage and loss moduli as follows:

$$\begin{aligned} \eta' &= G''/\omega \\ \eta'' &= G'/\omega \end{aligned} \quad (4.38)$$

The absolute magnitude of the complex viscosity $|\eta^*|$ is of interest in connection with the “Cox-Merz rule,” which relates it empirically to the (steady-shear) viscosity, a nonlinear property discussed in Chapter 10.

If the two material functions, $G'(\omega)$ and $G''(\omega)$, were known with sufficient precision over the range of frequencies from zero to a frequency higher than the reciprocal of the shortest relaxation time of interest, one would have a complete characterization of the linear viscoelastic behavior of a material. However, for the purposes of flow modeling, it is useful to have an equation that describes the stress relaxation modulus, $G(t)$. By substituting the expression for strain given by Eq. 4.34 into Eq. 4.3 and integrating, one can show that the storage and loss moduli are integral transforms of the relaxation modulus:

$$G'(\omega) = \omega \int_0^\infty G(s) \sin(\omega s) ds \quad (4.39a)$$

$$G''(\omega) = \omega \int_0^\infty G(s) \cos(\omega s) ds \quad (4.39b)$$

These transforms can, in principle, be inverted to give $G(s)$, given the storage and loss moduli (see ref. [1], p. 68).

SAOS results constitute the discrete data set, $\{G'_k, G''_k, \omega_k\}$, and an equation describing the relaxation modulus can be obtained by representing $G(t)$ as a discrete relaxation spectrum, i.e. as the parameter set $\{g_i, \tau_i\}$. This transformation is based on the discrete form of Eqs. 4.39a, b shown below:

$$G'(\omega) = \sum_{i=1}^N \frac{g_i (\omega \tau_i)^2}{[1 + (\omega \tau_i)^2]} \quad (4.40a)$$

$$G''(\omega) = \sum_{i=1}^N \frac{g_i (\omega \tau_i)}{[1 + (\omega \tau_i)^2]} \quad (4.40b)$$

The inversion of these summations to determine the parameter set $\{g_i, \tau_i\}$ is an ill-posed problem, and methods of dealing with this issue are described in Section 4.4.

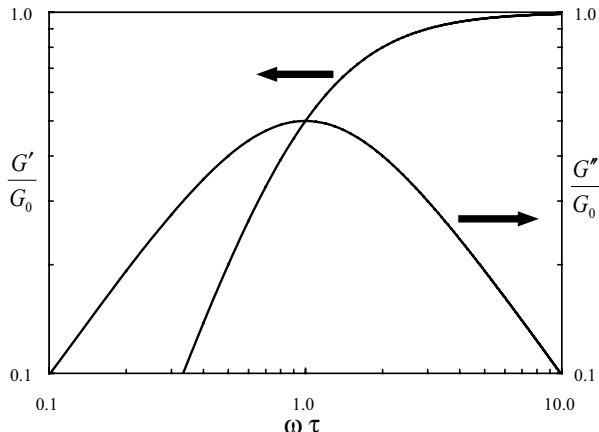


Figure 4.10 Storage and loss moduli divided by G_0 versus $\omega\tau_0$ for a viscoelastic fluid as modeled by a single-Maxwell element. The slopes approach two and unity respectively as the frequency approaches zero on this double-logarithmic plot.

Because the generalized Maxwell model is widely used in the interpretation of linear viscoelastic behavior of polymers, it will be helpful here to plot the storage and loss moduli corresponding to a single Maxwell element. The appropriate models are easily obtained by using a single term in the summations in Eqs. 4.40a and b. The resulting double logarithmic plots of G'/G_0 and G''/G_0 as functions of $\omega\tau$ are shown in Fig. 4.10. We note that at low frequencies on the double logarithmic plot, the loss modulus approaches a line with a slope of one, while the storage modulus approaches a line having a slope of two. At high frequency the storage modulus approaches a constant, G_0 , while the loss modulus goes to zero. Both moduli are equal to $G_0/2$ at $\omega\tau = 1$.

Using Eqs. 4.40a, b, it is possible to derive the following limiting values of the storage and loss moduli and their ratios as the frequency approaches zero.

$$\lim_{\omega \rightarrow 0} G' = \lim_{\omega \rightarrow 0} \eta'' = 0 \quad (4.41)$$

$$\lim_{\omega \rightarrow 0} G'' = 0 \quad (4.42)$$

$$\lim_{\omega \rightarrow 0} \left(\frac{G''}{\omega} \right) = \lim_{\omega \rightarrow 0} \eta' = \eta_0 \quad (4.43)$$

$$\lim_{\omega \rightarrow 0} \left(\frac{G'}{\omega^2} \right) = \int_0^\infty G(s) s \, ds \equiv A_G = J_s^0 \eta_0^2 \quad (4.44)$$

$$\lim_{\omega \rightarrow 0} \left(\frac{G'}{G''^2} \right) = J_s^0 \quad (4.45)$$

Oscillatory shear can also be performed by varying the stress sinusoidally and measuring the resulting strain as a function of time. The results can be interpreted in terms of the real and imaginary components of the complex compliance, $J^* = J' - i J''$. These components, the storage and loss compliances, are simply related to the storage and loss moduli as shown below.

$$J' = G' / G_d^2 \quad (4.46a)$$

$$J'' = G'' / G_d^2 \quad (4.46b)$$

The storage and loss compliances can be used to determine the “retardation spectrum function” $L[\ln(\tau)]$ as follows:

$$J'(\omega) = \int_{-\infty}^{\infty} \left[L(\ln \tau) / (1 + \omega^2 \tau^2) \right] d \ln \tau \quad (4.47a)$$

$$J''(\omega) = \int_{-\infty}^{\infty} \left[L(\ln \tau) \omega \tau / (1 + \omega^2 \tau^2) \right] d \ln \tau + 1 / \omega \eta_0 \quad (4.47b)$$

The storage and loss compliances can also be expressed in terms of a discrete spectrum of retardation times:

$$J'(\omega) = \sum_{i=1}^N \frac{J_i}{(1 + \omega^2 \tau_i^2)} \quad (4.48a)$$

$$J''(\omega) = \sum_{i=1}^N \frac{J_i \omega \tau_i}{(1 + \omega^2 \tau_i^2)} + \frac{1}{\omega \eta_0} \quad (4.48b)$$

4.3.2 Experimental Determination of the Storage and Loss Moduli

In order to obtain an accurate picture of the relaxation behavior of a polymer it is essential to have oscillatory shear data over the broadest possible range of frequencies. Rotational, controlled strain rheometers are usually used for SAOS measurements. Rheometrical methods are described in some detail in several other books [5, 6].

The fixtures in contact with the sample, which constitute the rheometer “geometry,” can be either a cone and a plate or two parallel plates. For linear viscoelasticity measurements, parallel disks are preferred, as the loading of samples and setting of the gap are much simplified. Factors that must be taken into consideration in order to obtain reliable data are:

- Sample preparation—residual stresses
- Trimming of samples after insertion in the rheometer
- Thermo-oxidative degradation—stabilization of samples
- Maximum amplitude for linear behavior
- Repeat measurements to improve precision

Rheological properties depend strongly on temperature so it is essential that the temperature be constant and uniform and that its value be known precisely. A common type of temperature control chamber for rotational rheometers is a forced-convection oven in which heated nitrogen flows through the chamber. Such a system has the advantage that the temperature can be changed rapidly, but it has been noted [7] that the temperature of the sample can differ from the set-point temperature due to gradients within the oven. And gradients within the oven are inevitable, because the upper and lower shafts that support the fixtures act as heat sinks. Other heating systems have been developed to reduce these gradients, for example based on conduction and radiation [7]. While the edge effects that pose a major problem in the measurement of nonlinear behavior do not affect the measurement of linear properties, care must be taken to see that the procedure for loading and trimming samples is always the same [8].

Because of the elevated temperatures necessary to melt most polymers, thermo-oxidative degradation will occur over time. The time during which the sample must be stable includes the *dwell time*, when temperature homogeneity is being established and residual stresses are relaxing, as well as the actual time for measurements. The useful melt-temperature lifetime of a polymer is determined by carrying out a *time sweep* at a fixed frequency and the temperature of measurement. The storage modulus is monitored as a function of time. Crosslinking manifests itself by an increase in the modulus, while chain scission results in a decrease.

Care must be taken to ensure that the moduli determined represent linear behavior. Software provided by rheometer manufacturers calculate and display values of the storage and loss moduli even if the output signal is not a sinusoid, based on the principal harmonic of the output signal. It is therefore necessary to determine the maximum strain for linear behavior over the frequency range of interest. This is done by carrying out an amplitude sweep. The moduli will start to decrease with amplitude when the behavior becomes nonlinear. This amplitude depends on frequency, so amplitude sweeps must be carried out at several frequencies. It is desirable to increase the amplitude at low frequencies, because a very small part of the response comes from G' as compared to G'' .

Because of random error, a statistical approach is required in the evaluation of precision. A set of data that is not accompanied by a statement of statistical significance has limited quantitative scientific value. The use of error bars is a useful

way of providing this information, but the meaning of the bars must be stated (e.g., 95% conf. limit or std. dev.). A number of studies have been made of the variations that arise within and between laboratories. Rides and Allen [9] sent samples of polyethylene and polypropylene to 10 industrial laboratories using controlled strain instruments. They reported that the repeatability within a laboratory ($2.8 \cdot \text{std. dev.} = 95\% \text{ conf. level}$) improved from 9% to 4% as the frequency increased from 1.0 to 100 s^{-1} . The uncertainty is expected to increase at low frequencies, because the torque value is generally smaller here. Rides and Allen [9] found that the variation between laboratories was substantially greater than the repeatability within a lab, ranging from 30 to 20% as frequency increased. Much of the difference between laboratories was attributed to differences in measurement procedure. This reveals the crucial importance of a sound and consistent test protocol and demonstrates that good precision does not imply high accuracy.

Accuracy can only be established by a calibration based on independently verifiable quantities, such as mass and displacement, together with a reliable model to relate these to the rheometrical quantity measured. A model of the effect of fluid inertia [10] can be used to show that for high-viscosity melts, inertia has no effect on oscillatory flow data. Instrument compliance, however, is a concern. In order to minimize the compliance effect, one uses the stiffest possible spring that is consistent with the torque levels anticipated, and this may require the use of more than one transducer to cover a wide range of stress levels. In order to minimize compliance effects and allow measurements over a broad range of shear stress, the force-rebalance transducer was developed. This is a null-meter in which a feedback loop provides an electromotive torque that counteracts that generated by the melt to keep the transducer shaft from rotating.

4.3.3 Creep Measurements

For melts whose longest relaxation time is very large, it is often not possible to probe the terminal zone using SAOS because of the very low frequencies and torques involved. Since long-time (low-frequency) behavior in the terminal zone is closely related to molecular structure, this information is of great interest to us. To deal with this issue, creep and/or creep recovery tests can be used to probe the terminal zone and the data converted to storage and loss moduli values that can be merged with SAOS data.

For very polydisperse materials, particularly those with even small amounts of high-molecular-weight polymer, creep measurements become problematic as a result of the need to measure extremely slow deformations while maintaining the stress at a low, constant value. The low stress is required to ensure that the behavior will

be linear. Also, if, as is usually the case with melts, the measurement is made at an elevated temperature, the thermal stability of the sample is likely to be a problem if the experiment lasts many hours, as may be required at very low stress levels to obtain large enough strain. In addition, the signals from the instrument must be very stable and free of drift.

Creep recovery tests are particularly challenging because of the requirement that the torque be reduced to zero at some point during the test, and air flow in an air bearing generates a small but significant torque. The solution to this problem is to use a magnetic-bearing. Instruments incorporating such a bearing were described by Plazek et al. [11] and by Link and Schwarzl [12], and these have been used to study the creep recovery of linear [13, 14] and branched [15, 16] polyethylenes. Gabriel and Kaschta [17] compared the performance of magnetic-bearing and air-bearing instruments.

One would like to use a high shear stress in order to achieve good precision, but this runs the risk of entering the nonlinear regime at strains large enough to achieve steady state. Kraft et al. [18] proposed a technique for determining the creep compliance up to the steady-state flow region without moving outside the regime of linear behavior and without the use of a super-sensitive creep meter. During a standard creep experiment at a stress σ_0 , they reduce the stress back to zero at a time, t_1 , when the deformation is still within the range of linear behavior, and monitor the resulting recoil. This experiment can be analyzed by use of Eq. 4.19, which is an expression of the Boltzmann superposition principle for an experiment in which the stress, rather than the strain, is the controlled (independent) variable. The unloading that takes place at t_1 represents a second creep experiment commencing at this time and driven by a negative stress of $-\sigma_0$. From Eq. 4.19, the resulting shear deformation, $\gamma(t)$, is related to the creep compliance as follows:

$$\gamma(t) = J(t)\sigma_0 + J(t-t_1)(-\sigma_0) = \sigma_0 [J(t) - J(t-t_1)] \quad (4.49)$$

The creep compliance is only measured directly from $t = 0$ to t_1 . However, solving Eq. 4.49 for $J(t)$, we find that we can use the recovery data to extend $J(t)$ up to $t = 2 t_1$ as follows:

$$J(t) = \gamma(t)/\sigma_0 + J(t-t_1) \quad (t_1 < t < 2t_1) \quad (4.50)$$

Once $J(t)$ has been determined up to $t = 2 t_1$, this information can be used in combination with the next portion of the $\gamma(t)$ curve to determine the compliance at times up to $3 t_1$. This procedure is repeated until the terminal zone is reached, i.e., until $J(t)$ becomes linear with time. Finally, the zero-shear viscosity can be calculated as the reciprocal of the slope of this line.

Since the preferred technique for characterizing linear viscoelastic behavior in the terminal and terminal zones is oscillatory shear, there remains the problem of com-

bining creep data with storage and loss modulus data to obtain a characterization valid over the broadest possible time range. He et al. [19] calculated continuous retardation spectra using both modulus and creep data and plotted these together. The resulting graph showed clearly the zones in which each technique provided reliable data and the zone of overlap.

4.3.4 Other Methods for Monitoring Relaxation Processes

Dielectric properties reflect different averages of chain configuration and motion than viscoelastic properties and can thus be used to track features of chain dynamics that are different from those to which the stresses respond [20]. This technique has been used, for example, to evaluate the tube model dilation concept [21] and determine the contribution of constraint release to relaxation processes [22].

Small angle neutron scattering (SANS) is another technique that can be used to monitor molecular behavior during a rheological experiment. This method reveals how the degree of deformation varies along the chain contour [23, 24]. Nuclear magnetic resonance (NMR) has also been used to track molecular motions during deformation [25].

■ 4.4 Calculation of Relaxation Spectra from Experimental Data

4.4.1 Discrete Spectra

We first address the problem of converting a set of experimental data in the form $\{G'_i, G''_i, \omega_i\}$ into a discrete relaxation spectrum, i.e., the set of parameters $\{g_i, \tau_i\}$. This requires the deconvolution of the summations in Eq. 4.40, repeated here as Eqs. 4.51.

$$G'(\omega) = \sum_{i=1}^N \frac{g_i (\omega \tau_i)^2}{[1 + (\omega \tau_i)^2]} \quad (4.51a)$$

$$G''(\omega) = \sum_{i=1}^N \frac{g_i (\omega \tau_i)}{\left[1 + (\omega \tau_i)^2\right]} \quad (4.51b)$$

It is very important to note that the success of this transformation is limited by the following features of oscillatory shear data.

1. Data are obtained at discrete frequencies.
2. Data are available only between maximum and minimum frequencies that are imposed by the capabilities of the instruments used. This range of frequencies is called the “experimental window.”
3. There is always some level of random error (called scatter or noise) in the data. (There may also be systematic error (bias) in the data, but there is no way of correcting for this if it cannot be modeled accurately.)

The inference of a discrete spectrum from data using Eqs. 4.51a and b is an ill-posed problem, because the result is quite sensitive to random error in the data. There are, in principle, an infinite number of discrete spectra that can be obtained by straightforward curve-fitting, depending on which data are used. In addition, Laun [26] found that the use of linear regression, selecting one relaxation time parameter τ_i per decade, and determining the g_i values corresponding to them on both G' and G'' data yielded parameters that produced a relaxation modulus with spurious waviness. It is also possible using this approach to arrive at a parameter set that includes one or more negative values of g_i . And if the number N of empirical constants fitted exceed the number of data available, one ends up modeling the scatter in the data. This problem can be solved by using a more sophisticated algorithm that avoids fitting the noise. Baumgaertel and Winter [27] use nonlinear regression and an optimization algorithm to calculate a “parsimonious” spectrum,” i.e., one having the fewest possible Maxwell modes consistent with the level of random error in the data, without smoothing or filtering the data. A commercial software package IRIS is based on this method.

4.4.2 Continuous Spectra

The continuous relaxation spectrum defined in Eq. 4.18 provides a graphical representation of relaxation behavior that often reveals more clearly key relaxation mechanisms than plots of the storage and loss moduli, especially for model polymers synthesized for research. The inference of $H(\ln \tau)$ from data requires the inversion of the integrals in Eqs. 4.52 and 4.53.

$$G'(\omega) = \int_{-\infty}^{\infty} H(\ln \tau) \left(\frac{\omega^2 \tau^2}{1 + \omega^2 \tau^2} \right) d(\ln \tau) \quad (4.52)$$

$$G''(\omega) = \int_{-\infty}^{\infty} H(\ln \tau) \left(\frac{\omega \tau}{1 + \omega \tau} \right) d(\ln \tau) \quad (4.53)$$

As in the case of the discrete spectrum, this is an ill-posed problem, and many techniques have been proposed to overcome this difficulty. However, very few of these are used to describe the behavior of polymeric systems, because readily-available, user-friendly versions of the algorithms are not available. The principal exception is the method of Honerkamp and Weese [28]. They assume that the spectrum and its first and second derivatives are continuous and that the second derivative is small. To avoid modeling the noise (random error) in the data, they employ Tikhonov regularization, which requires the selection of a value for the regularization parameter.

Another problem that arises in inferring a continuous spectrum from data is that the magnitudes of the storage and loss moduli and of the relaxation strength vary enormously over the range of frequencies and times of interest. Honerkamp and Weese [28] addressed this problem by the use of nonlinear regression in which it is the base-ten logarithm of $H[\log(\tau)]$ that is calculated rather than the spectrum function itself. The algorithm, NLREG, can be found in the CPC Program Library. A brief description of this method is provided by Ankiewicz et al. [29] along with notes on its use, including mention of an error in the instructions that accompany the code. Takeh and Shanbhag (30) developed a code called ReSpect that is based on NLREG but is easier to use. Ankiewicz et al. [29] report that it is capable of producing an accurate spectrum *if the parameters are properly selected*. It is available online at (<http://www.mathworks.com/matlabcentral/fileexchange/40458-respect>).

It is often assumed that the spectrum inferred from a set of data is valid between values of τ equal to the reciprocal of the maximum and minimum frequencies of the data set. However, Davies and Anderssen [31] showed that this gives an overly optimistic estimate. Their analysis indicates that the range of t over which the relaxation spectrum can be reliably determined is 2.36 decades less than the range of frequencies over which experimental data are available. Stadler [32] argues that under certain circumstances the range of the inferred spectrum can significantly exceed these limits, but it is necessary to know something about the spectrum to identify the reliable range.

If shifted data are used, and time-temperature superposition (see following section) is not precisely obeyed, nonrandom deviations between data obtained at different temperatures can appear in the resulting master curve in frequency ranges where data at two temperatures overlap; this cannot be dealt with by regularization and often leads to waviness in the inferred spectrum. Ankiewicz et al. [29] describe a method for minimizing the effect of this.

■ 4.5 Time-Temperature Superposition

We describe here the application of time-temperature superposition to linear behavior, but it is also applicable to nonlinear data, as is mentioned on Chapter 10. Time-temperature superposition is a technique for substantially increasing the range of times or frequencies over which linear behavior can be obtained.

4.5.1 Time/Frequency (Horizontal) Shifting

Standard oscillatory shear rheometers are effective over a limited range of frequencies, but this limitation can be circumvented by obtaining data at a number of temperatures over this limited range and shifting them to obtain a plot with a much expanded frequency range all valid at a single *reference temperature*. The basic premise is that if all the relaxation phenomena contributing to $G(t)$ (and the storage and loss moduli) have the same temperature dependence, then changing the temperature of a measurement will have the same effect as shifting the data horizontally on the log(time) or log(frequency) axis [1]. Let us say that a change in the temperature from a reference value T_0 to a different temperature T has the following effect on all the relaxation times:

$$\tau_i(T) = a_T(T) \tau_i(T_0) \quad (4.54)$$

The factor a_T is thus a time or frequency (horizontal) shift factor that can be used to shift data taken at a temperature T along the time or frequency axis so that they will equal data taken at the reference temperature, T_0 . This leads to the definition of a reduced time t_r for use in making a temperature-independent *master curve*:

$$t_r \equiv t/a_T \quad (4.55)$$

When oscillatory shear data are being shifted, the frequency shift factor is a_T , and the *reduced frequency* is:

$$\omega_r \equiv \omega a_T \quad (4.56)$$

The $a_T(T)$ relationship required for time shifting is usually obtained by linear regression of the raw data. But this should be done only after stress (vertical) shifting, if any, is applied. Using a statistical method to carry out both shifts is not advised, as the resulting shift factors will just be empirical parameters with no physical significance.

Several empirical expressions have been proposed to describe the dependence of a_T on temperature. The two that are most commonly used are the Arrhenius dependence and the WLF dependence, which are given by Eqs. 4.57 and 4.58, respectively.

$$a_T(T) = \exp\left[\frac{E_a}{R}\left(\frac{1}{T} - \frac{1}{T_0}\right)\right] \quad (4.57)$$

$$\log(a_T) = \frac{-C_1^0(T - T_0)}{[C_2^0 + (T - T_0)]} \quad (4.58)$$

where E_a , C_1^0 and C_2^0 are empirical constants. By analogy with reaction rate theory, E_a is called the *activation energy for flow*. The WLF equation 4.58 can be derived from the empirical Doolittle equation that relates viscosity to fractional free volume together with assumption that the free volume is linearly related to the temperature (see ref. [1], p 287). Equation 4.57 is generally used when the temperature is at least 100 degrees above the glass transition temperature, while the WLF Eq. 4.58 usually provides a better fit of data at temperatures closer to T_g . Both of the above equations are basically empirical, and one should not expect them to be strictly obeyed by any material. An extensive tabulation of WLF parameters for many polymers is available [33].

4.5.2 The Modulus (Vertical) Shift Factor

When bringing together data obtained at several temperatures onto a master curve, the effect of temperature on the modulus must also be dealt with. In the Rouse model of the linear viscoelasticity of unentangled polymer melts [34], which is presented in Section 6.2, the stresses, e.g., $G(t)$ or $G'(\omega)$ and $G''(\omega)$, are proportional to the product of density and temperature. For entangled polymer systems, the molecular models most widely used predict that the magnitude of the relaxation modulus is proportional to the factor ρT that appears in the Rouse prediction multiplied by a factor that depends very weakly on temperature, but data are rarely if ever precise enough to reveal this effect. This implies the following shifting of moduli.

$$G_i(T) = G_i(T_0) T \rho / T_0 \rho_0 \quad (4.59)$$

This leads to the definition of a modulus (vertical) shift factor, b :

$$b_T \equiv T_0 \rho_0 / T \rho \quad (4.60)$$

and a *reduced modulus*, G_r ,

$$G_r \equiv b_T G(T) \quad (4.61)$$

Thus, a master curve of relaxation modulus data is a plot of $b_T G$ versus t/a_T , and for storage modulus versus frequency it is a plot of $b_T G'$ versus ωa_T . (The reader should be aware that an alternative definition of b_T has been used, for example in the

earlier publications of Graessley and his colleagues and in the book by Rubinstein and Colby [35].)

It is sometimes claimed that Eq. 4.60 does not describe the vertical shift required to achieve superposition. This usually arises when the horizontal and vertical shift factors are dealt with as fitting parameters for an entire data set [36]. But if the resulting master plot is examined closely, it is often found that the data do not actually superpose over the entire range of frequency due either to systematic discrepancies between data obtained at different temperatures or to failure of superposition. In any event, one should either use Eq. 4.60 or let $b_T(T)$ be unity. Furthermore, if $b_T(T)$ is allowed to be a fitting parameter, $a_T(T)$ will have no fundamental significance.

We note that the plateau modulus should vary with temperature in accord with b_T , i.e.:

$$G_N^0(T) = b_T G_N^0(t_0) \quad (4.62)$$

If the coefficient of thermal expansion α is constant with temperature, the vertical shift factor is given by:

$$b_T(T) = \frac{T}{T_0} \exp[-\alpha(T - T_0)] \quad (4.63)$$

In practice, the vertical shift factor, b_T , may vary little over the range of temperatures experimentally accessible, particularly in the case of semi-crystalline polymers, since it is approximately proportional to the absolute temperature.

To summarize, data obtained at a temperature T can be “reduced” to superpose on those at a reference temperature, T_0 , if the reduced modulus is plotted as a function of the reduced time, t_r . When data obtained at several temperatures are plotted in this way, the result is called a *master curve*. And a material for which data can be reduced to a master curve in this way is said to be *thermorheologically simple* [37]. Likewise, when the data do not superpose, the material is said to be *thermorheologically complex*. Figure 4.11 shows master curves of the storage and loss moduli of a polybutadiene binary blend [38]. The actual frequency range of the rheometers used was only about three decades, but by making measurements at eight temperatures, the reduced frequency extends over nine decades. At the highest reduced frequency, i.e., the lowest temperature, the superposition is starting to fail, because the frequency shift factor appropriate for the plateau and terminal zones is not appropriate for the Rouse modes that dominate the high-frequency behavior.

It is easy to show that for a thermorheologically simple material, master curves can also be obtained for any material function of linear viscoelasticity. For example to obtain a compliance master curve one plots $J(t, T)/b_T(T)$ versus $t/a_T(T)$. Viscosity, which involves both stress and time, requires the application of both shift factors. For example, a master curve of the absolute value of the complex viscosity is constructed by means of a double-logarithmic plot of

$$\frac{b_T}{a_T} |\eta^*(T)| \text{ versus } \omega a_T$$

And it can be shown that a zero-shear viscosity measured at a temperature T can be transformed to its value at the reference temperature as follows:

$$\eta_0(T_0) = \eta_0(T) \frac{1}{a_T} \left(\frac{T_0 \rho_0}{T \rho} \right) = \eta_0(T) \left(\frac{b_T}{a_T} \right) \quad (4.64)$$

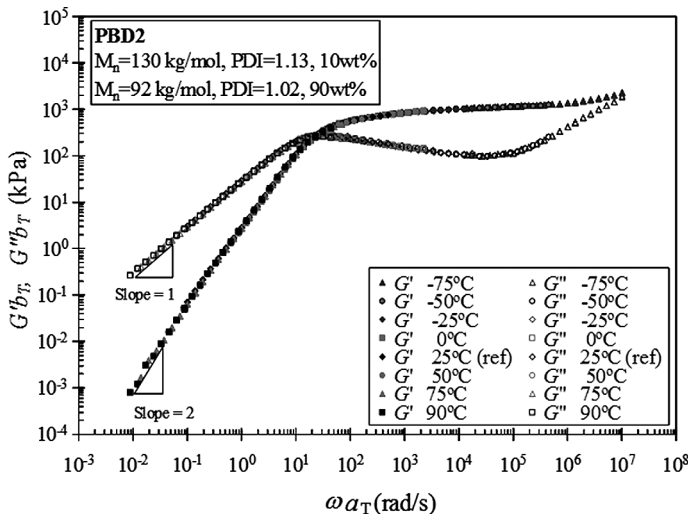


Figure 4.11 Master curves of storage and loss moduli for a blend of two narrow MWD polybutadienes. The reference temperature is 25 °C, and the vertical shift factor was calculated using Eq. 4.60. From Li et al. [38]

Thus if the vertical shift factor is neglected, the time shift factor can be obtained as a function of temperature by measuring the zero-shear viscosity at several temperatures.

$$a_T(T) \equiv \eta_0(T)/\eta_0(T_0) \quad (4.65)$$

And this implies that a temperature-independent master curve can be constructed simply by plotting the storage and moduli as functions of the product of frequency times the zero-shear viscosity.

Figure 4.12 shows the storage and loss modulus mastercurves of Plazek [39] for a poly(vinyl acetate) covering a very broad range of reduced frequency. The moduli are inferred from creep and creep recovery data. The times governing the various relaxation times involved do not have exactly the same temperature dependencies, but Plazek was able to achieve impressive superposition using only two time-shift factors, one for short time behavior and the other for the plateau and terminal zones.

The assignment of the data to one of these zones was somewhat arbitrary, but the result provides a good general picture of the linear response of the material over a very broad range of frequencies. As a result of the different temperature-dependencies of the two shift factors, the width of the plateau zone is a strong function of the choice of reference temperature. Similar behavior has been reported for polystyrenes [40] and polybutadienes [41].

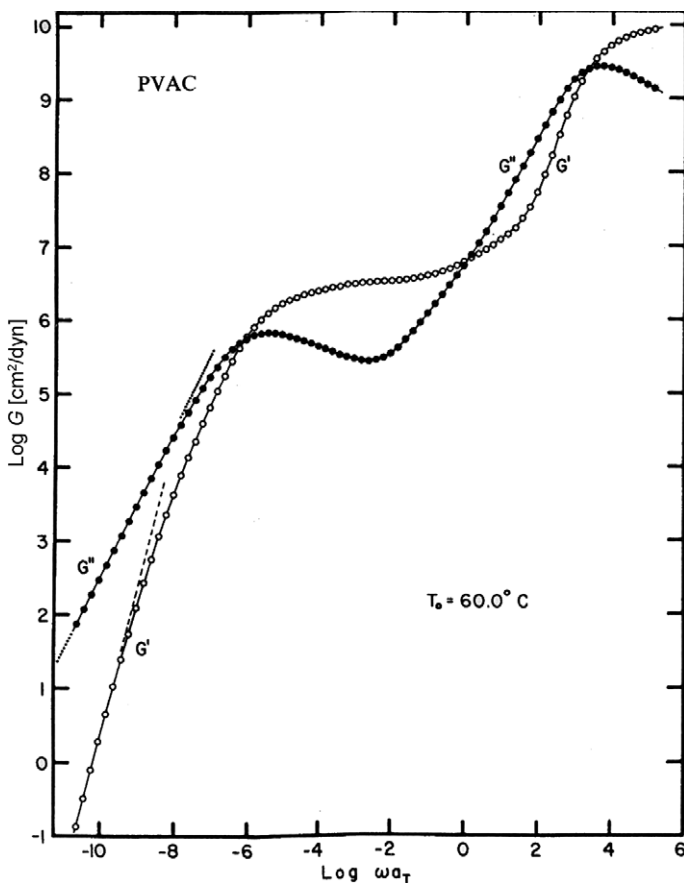


Figure 4.12 Storage and loss moduli versus reduced frequency for poly(vinyl acetate) with a very narrow MWD as calculated from creep data using the retardation spectrum as an intermediary (logarithmic scales). It was not possible to achieve superposition over the entire range of frequencies, and two shift factors were used to deal with data in high and low-frequency zones. The reference temperature is 60 °C. All the relaxation zones are clearly exhibited. From Plazek [39].

4.5.3 Validity of Time-Temperature Superposition

Time or frequency shifting is based on the premise that the characteristic times for all the relaxation mechanisms involved over the range of reduced frequencies or times of concern have the same temperature dependence. One would not expect this to be precisely valid, even for linear monodisperse samples in the transition and plateau/terminal zones, because of the different relaxation mechanisms operating in these zones. However, Ferry believed in 1980 [1] that for homogeneous samples time-temperature superposition had been demonstrated to be a general and experimentally proven technique for homogeneous molten polymers and that the time shift factor would not be affected by long-chain branching in homogeneous melts, because it should depend only on chemical microstructure. Of course superposability will not continue to very high frequencies (or very short times) where glassy behavior comes into play.

However, it has since been recognized that there are many exceptions to this basic principle. In his thorough review of time-temperature superposability, Plazek [42] shows many examples where it fails but also that superposition can still be useful in the identification and separation of relaxation mechanisms.

For chemically heterogeneous samples (blends), there is an overlap of mechanisms between the transition and longer-time regions, and thermorheological complexity is to be anticipated. Also short-time relaxation mechanisms will come into play at longer times as the temperature is lowered. For binary blends superposition works very well when the two monomer times are fairly close together or very far apart.

As for chemically uniform homopolymers, long-chain branching brings into play new relaxation processes whose time dependencies are likely to be different from those for linear chains. And even when data can be superposed for a given branching structure, a modest change in chemistry can render them complex. For example, Graessley [45] reported that while stars of polystyrene, polybutadiene, and polyisoprene obey superposability, hydrogenated polybutadiene stars do not.

In general, we do not expect branched polymers to rigorously obey time-temperature superposition, but in spite of modest departures from superposability, master curves for model branched polymers such as stars and combs are widely used for the identification of relaxation mechanisms. Examples of data for branched polymers that appeared to obey superposition well, based on data plots covering many decades of frequency, are those of Kapnistos et al. [44] for combs, Daniels et al. [45] for H polystyrene, and Nielsen et al. [46] for star polystyrenes. Data for significantly more complex branching structures, however, are generally not superposable. And low-density polyethylene is clearly thermorheologically complex.

One approach to describing temperature-dependency for thermorheologically complex materials is to define a time-dependent activation energy [47]. However,

the resulting activation energy spectrum is sensitive to the data on which it is based, and Wood-Adams and Costeux [48] reported that the storage modulus provided the most accurate estimation of this spectrum. An apparent activation energy that is free of this uncertainty is that based on the zero-shear viscosity, assuming that the data extend into the terminal zone. This apparent activation energy, however, does not describe the temperature dependency of the longest relaxation time but is a weighted average of the energy spectrum [48].

It must be kept in mind that conclusions about the superposability of data are generally based on the inspection of shifted modulus data plotted using log scales, and modest departures from superposability are not revealed by such plots. The use of a linear rather than logarithmic scale for the vertical axis provides a much better basis for evaluating superposability. Wood-Adams and Costeux [48] proposed plotting G^* (linear scale) versus the $\log(\omega a_T)$ to reveal thermorheological complexity, and the van Gurp-Palmen plot (δ versus $\log|G^*|$) that is discussed at the end of Chapter 5 has also been used to detect complexity.

■ 4.6 Time-Pressure Superposition

The effect of pressure on linear viscoelastic properties can also be accounted for in terms of shift factors. One can define an isothermal time-shift factor $a_p(P)$ that accounts for the effect of pressure on the relaxation times at constant temperature, and it has been found that this factor obeys the well-known Barus equation:

$$\ln(a_p) = \beta(P - P_0) \quad (4.66)$$

Ferry (see ref. [1], p. 291) describes several equations that have been proposed to describe the combined effects of temperature and pressure; like the WLF equation, these equations arise from assumptions regarding the dependence of free volume on pressure and temperature. The vertical shift factor b_T can be easily generalized to account for the effect of pressure on density, but this effect is usually negligible.

$$b_T = T_0 \rho(T_0, P_0) / T \rho(T, P) \quad (4.67)$$

■ 4.7 Alternative Plots of Linear Viscoelastic Data

Rather than simply plotting the storage and loss moduli as functions of frequency, several other types of plot have been found useful, particularly in regard to systems with blends and branched structures. These involve plotting one linear property versus another so that time or frequency is not involved.

4.7.1 Van Gurp-Palmen Plot of Loss Angle Versus Complex Modulus

Van Gurp and Palmen [49] proposed plotting of the loss angle δ (linear scale) versus the logarithm of the magnitude of the complex modulus $|G^*|$ to test for the validity of time-temperature superposition. If data obtained at several temperatures all fall on the same curve on such a plot, this indicates that the time-temperature superposition is valid. Van Gurp and Palmen noted that data plotted in the usual manner, i.e., G' and G'' versus frequency, can appear to show that time-temperature superposition is valid, while when the loss angle is plotted versus the log of the complex modulus, there is clearly a failure of time-temperature superposition.

Trinkle and Friedrich [50] used this type of plot to characterize the polydispersity of a linear polymer. Specifically, they found that the value of $|G^*|$ where $\delta = 60^\circ$ correlated approximately with the value of M_w/M_n . Trinkle et al. [51, 52] suggested using this type of plot to reveal the presence of long-chain branching in polyethylene. Lohse et al. [53] found that the use of a Van Gurp-Palmen plot to display data for hydrogenated polybutadienes having well-defined structures was a useful way to bring out the distinctive effects of branching on linear viscoelastic behavior. Figure 4.13 shows such a plot of their data for linear, star, and comb polymers, and we see clearly the distinctive features of the curves that are associated with each branching structure.

Figure 4.14a shows the storage and loss moduli (data for the comb are shifted for comparison), while 4.14b is a van Gurp-Palmen plot of the same data [54]. The moduli do not provide a clear differentiation between the behaviors of the two polymers, while the van Gurp-Palmen is quite revealing. In particular, the latter reveals a second relaxation process for the comb that results from arm retraction.

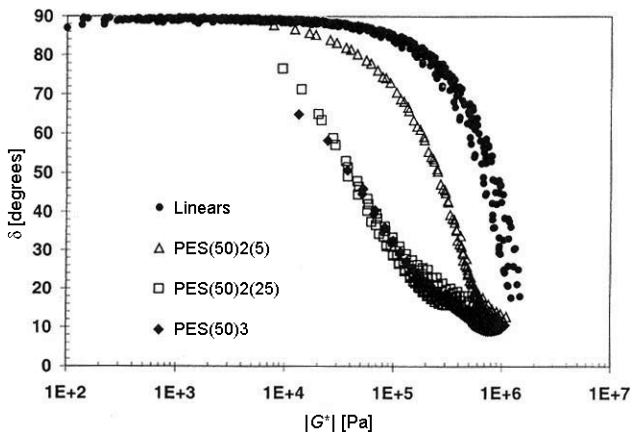


Figure 4.13 Van-Gurp Palmen plot (loss angle versus magnitude of complex modulus) of data for linear (solid line), star-branched (dashed line), and comb (dotted line) polymers prepared by the hydrogenation of anionically polymerized polybutadienes. The branching structure has a distinct effect on the shape of the curve. From Lohse et al. [53].

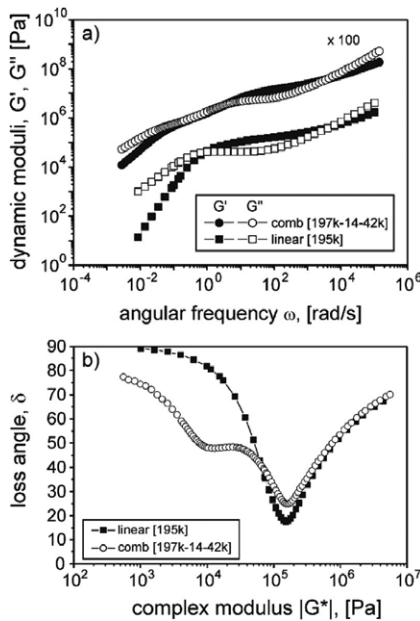


Figure 4.14 Two representations of linear viscoelastic behavior for two poly(*p*-methylstyrene) samples, one linear and the other a comb. The molecular weights of the linear sample and the backbone of the comb are similar. Figure 4.14a shows storage and loss moduli (data for comb are shifted for comparison), while 4.14b is a van Gurp-Palmen plot of the same data. The van Gurp-Palmen plot reveals a second relaxation process for the comb that results from arm retraction. From Kempf et al. [54].

4.7.2 Cole-Cole Plots

A technique that has been used to some extent for the representation of viscoelastic material functions was inspired by a suggestion of Cole and Cole [55] for the plotting of data for complex dielectric constant, $\epsilon^* = \epsilon' - i\epsilon''$. They proposed plotting of ϵ'' versus ϵ' . This plotting technique, together with empirical equations describing the shape of the resulting curve, have been used to verify time-temperature superposition and to reveal structural features of polymers.

According to a theory of Debye for polar gases and dilute solutions, the complex dielectric constant is related to the frequency as shown by Eq. 4.68.

$$\epsilon^* - \epsilon_\infty = \frac{(\epsilon_0 - \epsilon_\infty)}{[1 + (i\omega\tau_0)]} \quad (4.68)$$

where ϵ_0 is the value of the dielectric constant at zero frequency, ϵ_∞ is the limiting value at very high frequency, and τ_0 is the time constant for the relaxation of the dielectric constant. If data obeying this theory are plotted in the form of ϵ'' versus ϵ' , the result is a semicircle with its origin on the real (ϵ') axis having intercepts of ϵ_∞ and ϵ_0 on this axis. While data for polar liquids do not obey the Debye theory, it was noted that a plot of ϵ'' versus ϵ' was a circular arc having its origin below the real axis, as shown in Fig. 4.15. Cole and Cole noted that this arc is described by Eq. 4.69.

$$\epsilon^* - \epsilon_\infty = \frac{(\epsilon_0 - \epsilon_\infty)}{\left[1 + (i\omega\tau_0)^{1-\alpha}\right]} \quad (4.69)$$

The parameter α is related to the angle θ between the radius of the arc at the point ($\epsilon' = \epsilon_\infty; \epsilon'' = 0$) and the real axis by the expression $\theta = \alpha\pi/2$. This is shown in Fig. 4.15.

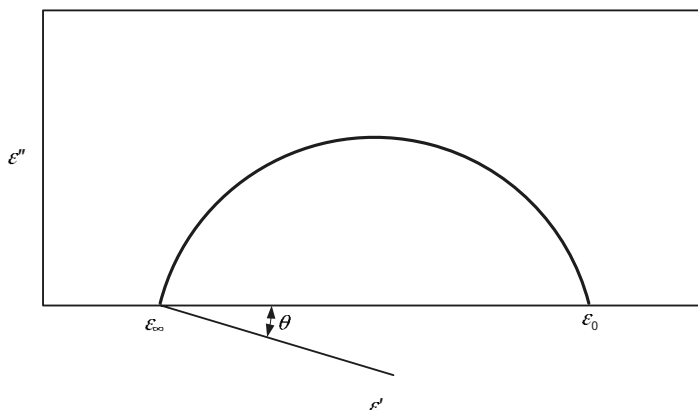


Figure 4.15 The imaginary versus real components of the complex dielectric constant according to the Cole-Cole function (Eq. 4.69) showing the meaning of the angle theta.

Malik and Prud'homme [56] found that the temperature shift factors for the dielectric relaxation of several blends were very close to those for the shift of mechanical linear viscoelastic data, if a slightly different reference temperature was used for the two types of data.

The idea of plotting one material function versus another has been applied to the viscoelastic properties of polymers. (The van Gurp-Palmen plot is an example.) We note that in this type of plot, information concerning time-dependency is lost. Thus, if relaxation data at several temperatures can be superposed onto a master curve, such data will superpose on such a plot without any shifting.

Havriliak and Negami [57, 58] proposed the generalization of the Cole-Cole function shown as Eq. 4.70.

$$\varepsilon^* - \varepsilon_\infty = \frac{(\varepsilon_0 - \varepsilon_\infty)}{\left[1 + (i\omega\tau_0)^{1-\alpha}\right]^\beta} \quad (4.70)$$

Marin and Graessley [59] used Cole-Cole plots, together with the original Cole-Cole function (Eq. 4.70) to interpret data for several polystyrenes prepared by anionic polymerization. They plotted the imaginary versus the real components of the complex retardational compliance, $J_r^*(\omega)$, defined as $J^*(\omega) - 1/(i\omega\eta_0)$. They found that for the sample with a molecular weight of about 37,000, which is near the critical molecular weight for viscosity, M_c , a plot of $J_r''(\omega)$ versus $J_r'(\omega)$ took the form of a circular arc and could thus be fitted to Eq. 4.71, by analogy with Eq. 4.69.

$$J_r^*(\omega) = \frac{J_t}{\left[1 + (i\omega\tau_t)^{1-b}\right]} \quad (4.71)$$

The subscript, t, refers to transition zone behavior, while the glassy compliance is relatively negligible and has been omitted. The time constant τ_t has the same temperature dependence as the viscosity, and b is independent of temperature. For samples with molecular weights well above M_c , a second circular arc appeared at lower frequencies, reflecting the appearance of a plateau in the storage modulus.

Cole-Cole type plots have been used to represent data for narrow-distribution polystyrenes [59], binary blends [60], stars [61], combs [62], and linear [63] and branched [64] polyethylenes.

■ 4.8 Summary

Linear viscoelastic behavior is exhibited by melts in response to deformations that are very small or very slow. The Boltzmann superposition principle is the mathematical embodiment of this type of behavior, and it reveals that if a single material function, the relaxation modulus $G(t)$ is known for a material, the response of that material to any very slow or very small deformation can be calculated. The simplest deformation pattern is a step-strain, which yields the relaxation modulus directly. The relaxation modulus is often represented analytically by a sum of exponentials that is called the generalized Maxwell model. The parameters of this model comprise a set of moduli, g_i and corresponding relaxation times τ_i . Alternatively, a continuous relaxation spectrum can be used to describe the relaxation modulus. In a creep experiment, one measures the deformation resulting from the imposition of a sudden stress. In this way the creep compliance is determined, which can be transformed into a retardation spectrum. In practice, oscillatory shear is the technique usually used to study the viscoelasticity of a molten polymer. Such an experiment yields the storage and loss moduli as functions of frequency, and techniques are available to transform this information into the relaxation modulus and a relaxation spectrum. Time-temperature superposition can sometimes be used to extend the range of frequencies over which the storage and loss moduli can be determined at a single reference temperature. Data for long-chain branched polymers may not exhibit time-temperature superposability and such materials are said to be thermorheologically complex.

■ References

- [1] Ferry, J.D. *Viscoelastic Properties of Polymers*, 3rd edition (1980) John Wiley & Sons, New York
- [2] Tschoegl, N.W. *The Phenomenological Theory of Linear Viscoelastic Behavior*, (1989) Springer, Berlin
- [3] Dealy, J.M., Wang, J. *Melt Rheology and Its Applications In the Plastics Industry* (2013), Springer, New York
- [4] Plazek, D.J., Echeverría, I. Don't cry for me Charlie Brown, or with compliance comes comprehension. *J. Rheol.* (2000) 44, pp. 831–841
- [5] Macosko, C.W. *Rheology: Principles, Measurements, and Applications* (1994) VCH, New York.
- [6] Collyer, T.A., Clegg, D.W. (Eds.) *Rheological Measurement*, 2nd edition (1998) Chapman & Hall, London

- [7] Halley, P.J., Mackay, M.E., van den Brule, B.H.A.A. An oven design for torsional rheometers. *Rheol. Acta* (1992) 31, pp. 208–211
- [8] Kalika, D.S., Nuel, L., Denn, M.M. Gap-dependence of the viscosity. *J. Rheol.* (1989) 33, pp. 1059–1079
- [9] Rides, M., Allen, C.R.G. Round robin for parallel plate oscillatory rheometry using polyethylene and polypropylene melts. Report CMMT(A)11, Centre for Materials Measurement and Technology, Natl. Phys. Laboratory, Teddington, United Kingdom
- [10] Böhme, G., Stenger, M. On the influence of fluid inertia in oscillatory rheometry. *J. Rheol.* (1990) 34, pp. 415–424
- [11] Plazek, D.J. Magnetic bearing torsional creep apparatus, *J. Polym. Sci.* (1968) A2, 6, pp. 621–638
- [12] Link, G., Schwarzl, F.R. Measuring device for precise evaluation of torsional creep and recovery data. *Rheol. Acta* (1985) 24, pp. 211–219
- [13] Plazek, D.J., Raghupathi, N., Kratz, R.F., Miller, W.R. Recoverable compliance behavior of high-density polyethylenes. *J. Appl. Polym. Sci.* (1979) 24, pp. 1305–1320
- [14] Gabriel C., Münstedt, H. Creep recovery behavior of metallocene linear low density polyethylenes. *Rheol. Acta* (1999) 38, pp. 393–403
- [15] Agarwal, P.K., Plazek, D.J. Shear creep recovery behavior of IUPAC low-density polyethylenes. *J. Appl. Polym. Sci.* (1977) 21, pp. 3251–3260
- [16] Gabriel, C., Kaschta, J., Münstedt, H. Influence of molecular structure on rheological properties of polyethylenes, I. Creep recovery measurements in shear. *Rheol. Acta* (1998) 37, pp. 7–20
- [17] Gabriel, C., Kaschta, J. Comparison of different shear rheometers with regard to creep and creep recovery measurements. *Rheol. Acta* (1998) 37, pp. 358–364
- [18] Kraft, M., Meissner, J., Kaschta, J. Linear viscoelastic characterization of polymer melts with long relaxation times. *Macromol.* (1995) 32, pp. 751–757
- [19] He, C., Wood-Adams, P., Dealy, J.M. Broad frequency characterization of molten polymers. *J. Rheol.* (2004) 48, pp. 711–724
- [20] Watanabe, H. Viscoelasticity and dynamics of entangled polymers. *Prog. Polym. Sci.* (1999) 42, pp. 1253–1403
- [21] Watanabe, H., Ishida, S., Matsumiya, Y., Tadashi, I. Viscoelastic and dielectric behavior of entangled blends of linear polyisoprenes having widely separated molecular weights: Test of tube dilations picture. *Macromol.* (2004) 37, pp. 1937–1951
- [22] Matsumiya, Y., Kumazawa, K., Nagao, M., Urakawa, O., Watanabe, H. Dielectric relaxation of monodisperse linear polyisoprene: Contribution of constraint release. *Macromol.* (2013) 46, pp. 6067–6080
- [23] McLeish, T.C.B. et al. Dynamics of entangled H-polymers: Theory, rheology, and neutron scattering. *Macromol.* (1999) 32, pp. 6734–6758
- [24] Bent, J. et al. Neutron-mapping polymer flow: scattering, flow visualization, and molecular theory. *Science* (2003) 301, pp. 1691–1695
- [25] Adams, C.H., Brereton, M.G., Hutchings, L.R., Klein, P.G., McLeish, T.C.B., Richards, R.W., Ries, M.E. A deuterium NMR study of selectively labeled polybutadiene star polymers. *Macromol.* (2000) 33, pp. 7101–7106

- [26] Laun, H.M. Description of the non-linear shear behavior of a low-density polyethylene. *Rheol. Acta* (1978) 17, pp. 1–15
- [27] Baumgaertel, M., Winter, H.H. Determination of discrete relaxation and retardation spectra from dynamic mechanical data. *Rheol. Acta* (1989) 28, pp. 511–519
- [28] Honerkamp, J., Weese, J. A nonlinear regularization method for the calculation of relaxation spectra. *Rheol. Acta* (1993) 32, pp. 65–73
- [29] Ankiewicz, S., Orbey, N., Watanabe, H., Lentzakis, H., Dealy, J.M. On the use of continuous relaxation spectra to characterize model polymers. *J. Rheol.* (2016) 60, pp. 1115–1120
- [30] Takeh, A., Shanbhag, S. A computer program to extract the continuous and discrete relaxation spectra from dynamic viscoelastic measurements. *Appl. Rheol.* (2013) 23 (2), 24628: pp. 1–10
- [31] Davies, A.R., Anderssen, R.S. Sampling localization in determining the relaxation spectrum. *J. Non-Newtonian Fluid Mech.* (1997) 73, pp. 163–179
- [32] Stadler, F.J. Effect of incomplete datasets on the calculation of continuous relaxation spectra from dynamic-mechanical data. *Rheol. Acta* (2010) 49, pp. 1041–1057
- [33] Ngai, K.L., Plazek, D.J. Temperature dependencies of the viscoelastic response of polymer systems. In: Mark, J.E. (Ed.) *Physical Properties of Polymers Handbook* (2007) Springer, New York
- [34] Rouse, P.E., Jr. A theory of the linear viscoelastic properties of dilute solutions of coiling polymers. *J. Chem. Phys.* (1953) 21, pp. 1272–1280
- [35] Rubinstein, M., Colby, R. *Polymer Physics* (2003) Oxford Univ. Press, Oxford
- [36] Honerkamp, J., Weese, J. A note on estimating mastercurves. *Rheol. Acta*, (1993) 32, pp. 2–57
- [37] Schwarzl, F., Staverman, A.J. Time-temperature dependence of linear viscoelastic behavior. *J. Appl. Phys.* (1952) 23, pp. 838–843
- [38] Li, S.W., Park H.E., Dealy, J.M. Evaluation o f molecular linear viscoelastic models for polydisperse H-polybutadienes. *J. Rheol.* (2011) 55, pp. 1341–1373
- [39] Plazek, D.J. The temperature dependence of the viscoelastic behavior of poly(vinyl acetate). *Polym. J.* (1980) 12, pp. 43–53
- [40] Plazek, D.J. Temperature dependence of the viscoelastic behavior of polystyrene. *J. Phys. Chem.* (1965) 69, pp. 3480–3487
- [41] Zorn, R., McKenna, G.B., Willner, L., Richter, D. Rheological investigation of polybutadienes having different microstructures over a large temperature range. *Macromol.* (1995) 28, pp. 8552–8562
- [42] Plazek, D.J. Oh, thermorheological simplicity, wherefore art thou? *J. Rheol.* (1996) 40, pp. 987–1014
- [43] Graessley, W.W. Effect of long branches on the temperature dependence of viscoelastic properties in polymer melts. *Macromol.* (1982) 15, pp. 1164–1167
- [44] Kapnistos, M., Vlassopoulos, D., Roovers J., Leal, L.G. Linear rheology of architecturally complex macromolecules: comb polymers with linear backbones. *Macromol.* (2005) 38, pp. 7852–7862

- [45] Daniels, D. et al. Linear rheology of diluted star and model long chain branched polymer melts. *Rheol. Acta* (2001) 40, pp. 403–415
- [46] Nielsen, J.K. et al. Nonlinear branch-point dynamics of multiarm polystyrene. *Macromol.*, (2006) 39, pp. 8844–8853
- [47] Keßner, U., Kaschta J., Münstedt, H. Determination of method-invariant activation energies of long-chain branched low-density polyethylene. *J. Rheol.* (2009) 53, pp. 1001–1016
- [48] Wood-Adams, P., Costeux, S. Thermorheological behavior of polyethylene: Effects of microstructure and long chain branching. *Macromol.* (2001) 34, pp. 6281–6290
- [49] van Gurp, M., Palmen, J., Time-temperature superposition for polymeric blends. *Rheol. Bull.* (1998) 67(1), pp. 5–8 (Public. of Soc. of Rheol.)
- [50] Trinkle, S., Friedrich, C. Van Gurp-Palmen plot: a way to characterize polydispersity of linear polymers, *Rheol. Acta*, (2001) 40, pp. 322–328
- [51] Walter, P., Trinkle, S., Mülhaupt, R. Influence of zirconocene structure and propene content on melt rheology of polyethene and ethene/propene copolymers. *Polym. Bull.* (2001) 46, pp. 205–213
- [52] Trinkle, S., Walter, P., Friedrich, C. Van Gurp-Palmen plot II—Classification of long chain branched polymers by their topology, *Rheol. Acta*, (2002) 41, pp. 103–113
- [53] Lohse, D.J., Milner, S.T., Fetter, L.J., Xenidou, M., Hadjichristidis, N., Mendelson, R.A., Garcia-Franco, C.A., Lyon, M.K. Well-defined, model long chain branched polyethylene. 2 Melt rheological behavior. *Macromol.* (2002) 35, pp. 3066–3075
- [54] Kempf, M., Ahirwal, D., Cziep, M., Wilhelm, M. Synthesis and linear and nonlinear melt rheology of well-defined comb architectures of PS and PpMS with a low and controlled degree of long-chain branching. *Macromol.* (2013) 46, pp. 4978–4994
- [55] Cole, K.S., Cole, R.H. Dispersion and absorption in dielectrics I. Alternating current characteristics. *J. Chem. Phys.* (1941) 9, pp. 341–353
- [56] Malik, T.M., Prud'homme, R.E. Dielectric properties of Poly (α -methyl- α N-propyl- β -propiolactone)/Poly(vinyl chloride) blends. *Polym. Eng. Sci.* (1984) 24, pp. 144–152
- [57] Havriliak, S., Negami, S. A complex plane representation of dielectric and mechanical relaxation processes in some polymers. *Polymer* (1967) 8, pp. 161–210
- [58] Havriliak, S., Negami, S. On the equivalence of dielectric and mechanical dispersions of some polymers. *Polymer* (1969) 10, pp. 859–871
- [59] Marin, G., Graessley, W.W. Viscoelastic properties of high molecular weight polymers in the molten state. 1. Study of narrow molecular weight distribution samples. *Rheol. Acta* (1977) 16, pp. 527–533
- [60] Montfort, J.P., Marin, G., Arman, J., Monge, Ph. Blending law for binary blends of fractions of linear polystyrene. *Polymer* (1978) 19, pp. 277–284
- [61] Marin, G. Oscillatory rheometry. In *Rheological Measurement*, 2nd ed. A.A. Collyer and D.W. Clegg (Eds.) (1998) Chapman and Hall, London, pp. 3–45
- [62] Marin G., Labaig J.J., Monge, Ph. Dynamic viscoelasticity of entangled polymers. *Polymer* (1975) 16, pp. 223–226

- [63] Garcia-Franco, C.A., Mead, D.W. Rheological and molecular characterization of linear backbone flexible polymers with the Cole-Cole model relaxation spectrum. *Rheol. Acta* (1999) 38, pp. 34–47
- [64] Labaig, J.J., Monge, Ph., Bednarick, J. Steady flow and dynamic viscoelastic properties of branched polyethylene. *Polymer* (1973) 14, pp. 384–386

5

Linear Viscoelasticity— Behavior of Molten Polymers

■ 5.1 Introduction

In this chapter, we review what is known about how molecular structure affects linear viscoelastic properties such as the zero-shear viscosity, the steady-state compliance, and the storage and loss moduli. For linear polymers, linear properties are a rich source of information about molecular structure, rivaling more elaborate techniques such as GPC and NMR. Experiments in the linear regime can also provide information about long-chain branching but are insufficient by themselves and must be supplemented by nonlinear properties, particularly those describing the response to extensional flow. The experimental techniques and material functions of nonlinear viscoelasticity are described in Chapter 10.

■ 5.2 Zero-Shear Viscosity of Linear Polymers

In the theory of linear viscoelasticity, the viscosity is independent of shear rate. We expect molten polymers to approach this behavior at very low shear rates, and the limiting, low-shear-rate value is called the zero-shear viscosity, η_0 . This material constant plays an important role in polymer rheology because of its strong dependence on molecular weight.

The direct measurement of η_0 is sometimes practically impossible, especially for polydisperse samples. This is because standard melt rheometers may be unable to provide reliable data at sufficiently low shear rates to reach the region of Newtonian behavior. While this issue is discussed in Section 10.8, it is important to note that the use of an empirical equation for the viscosity function $\eta(\dot{\gamma})$ to extrapolate data to low shear rates is a very unreliable procedure. Sometimes it is found that within a given family of polymers (same structure and shape of the MWD) a certain equation fits the entire viscosity curve quite well for several members of the family for which η_0 is experimentally accessible. In such a case, there is some basis for using the same equation to extrapolate incomplete data for other members of the same family.

5.2.1 Effect of Molecular Weight

In Section 6.2 it is shown that the Rouse-Bueche model for unentangled melts predicts that the zero-shear viscosity is proportional to the molecular weight, and this has been found to be valid for linear polymers of low molecular weight. However, when the molecular weight exceeds a critical value M_C , the value of η_0 of a monodisperse melt increases with molecular weight much more quickly. In fact it is proportional to M raised to a much higher power that is usually in the neighborhood of 3.4 [1]. Figure 5.1 is a plot of zero-shear viscosity versus molecular weight for several polymers originally compiled by Berry and Fox [2]. We can summarize the behavior described above and shown in Fig. 5.1 as follows:

$$\eta_0 \propto M \quad M < M_C \quad (5.1)$$

$$\eta_0 = K M^\alpha \quad M > M_C \quad (5.2)$$

While the proportionality constant K and the critical molecular weight M_C depend on both the polymer and the temperature, the exponent varies rather little from one polymer to another; values for all linear, flexible molecules that have been studied to date have exponents on M in the range of 3.5 ± 0.2 . Van Meerveld [3] tabulated published values of K and α for a number of polymers. The values of α range from 3.4, for 1,4-polybutadiene and polystyrene, to 3.6 for polyethylene. However, there are large differences between values reported by different groups for the same polymer. For example, values for HDPE range from 3.41 to 3.6, and those reported for atactic polypropylene range from 3.4 to 3.59. It is pointed out below and in Chapter 6 that current molecular theories predict that this exponent is actually the local slope of a curve that approaches a slope of three at very high molecular weights.

The dramatic increase in the exponent around M_C is one of the remarkable effects of entanglement coupling, which takes effect when the molecules become long enough to seriously impede the motions of each other. This is not a sudden change that occurs when M_C is reached, but a gradual change. Kreer et al. [4] carried out Monte Carlo simulations that indicated that the crossover from Rouse (Eq. 5.1) to entangled (Eq. 5.2) behavior occurs over a fairly broad range of molecular weights. Harmandaris et al. [5] examined the crossover from Rouse to entangled behavior for hydrogenated polybutadiene using both molecular dynamic simulations and experiments.

The original Doi-Edwards tube model for polymer relaxation, in which *reptation*, a slow process explained in Chapter 6, is the only relaxation mechanism that operates at long times, predicts that the value of α should be three at sufficiently high molecular weights, i.e., when entanglement effects are overwhelmingly dominant. A useful measure of the relative importance of entanglements is the ratio of M to the *molecular weight between entanglements* M_e . This latter quantity, which is defined in

Section 5.8.1, is based on the value of the plateau modulus together with an analogy with the theory of rubber elasticity. The value of M_e turns out to be significantly smaller than two other characteristic molecular weights M_C and M'_C that are also defined in this chapter. It has been observed that $\alpha = 3.5 \pm 0.2$ for M/M_e up to about 150. In Chapter 6 it is explained that the inclusion of *primitive path fluctuations* (also called *contour length fluctuations* (CLF) or *breathing modes* or *concertina modes*) predicts that α is, indeed, equal to about 3.5 over a broad range of molecular weights but should still approach three when M/M_e is so large that contour length fluctuations make a negligible contribution to relaxation.

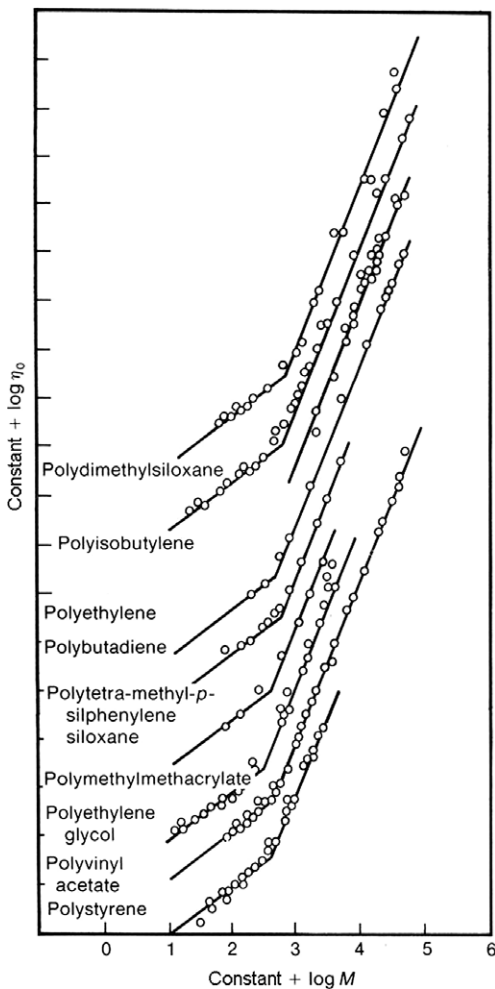


Figure 5.1 Zero-shear viscosity versus molecular weight (logarithmic scales) for several polymers. The axes have been shifted to avoid crowding. The low-MW lines for unentangled samples have slopes of one, while the high-MW lines for entangled samples have slopes of 3.4. From Berry and Fox [2].

Measurements involving polybutadienes with M up to 8,000 were carried out by Colby et al. [6], and they found that α does start to decrease when M/M_e reaches about 200. However, very high molecular weight materials are quite difficult to work with, and the data were of insufficient precision to show clearly the anticipated approach to a value of three at the largest values of M . Fetters et al. [7] summarized what is known about this subject and introduced a parameter, M_r , which is the molecular weight above which the M^3 dependence is obeyed. Based on the packing length model described in Section 5.8.2, they predicted that this molecular weight should be related to M_e and M_C as follows:

$$\frac{M_r}{M_e} = 1.36 \left(\frac{M_C}{M_e} \right)^{6.0} \quad (5.3)$$

Since M_C/M_e is usually in the range of two to three (See Eq. 5.34) M_r/M_e is clearly very large, in the range of 100 to 1000. Vega et al. [8] measured the viscosities of several metallocene polyethylenes having M_w up to $3.6 \cdot 10^6$ and M_w/M_n from 1.8 to 2.9. For $M_w/M_e > 150$ they found that the slope of the $\log(\eta_0)$ versus $\log M_w$ data was very close to three.

Sen et al. [9] used molecular dynamics simulations to investigate why M_C is several times larger than M_e . They concluded that while the Rouse contribution to relaxation, which leads to the viscosity behavior described by Eq. 5.1, stops increasing with chain length N when $N \approx 40$, the contribution of the largest relaxation times, which govern the zero-shear viscosity, increases linearly and only overtakes the Rouse contribution at about $N \approx 80$, where it also begins to increase more rapidly with N . The “packing length” concept introduced in Section 5.8.2, leads to a quantitative relationship between M_C and M_e .

5.2.2 Effect of Polydispersity

It has been found that η_0 is rather insensitive to polydispersity and that for a given polymer, Eq. 5.2 continues to hold with M replaced by M_w , as long as there are not present in the system a significant number of unentangled chains for which $M_w < M_C$ [10].

$$\eta_0 = K M_w^\alpha \quad M_w \geq M_C \quad (5.4)$$

This relationship, usually with $\alpha = 3.5 \pm 0.2$, has come to be widely accepted as fact. The generalization of Eq. 5.2 to Eq. 5.4 to deal with polydisperse polymers is of great importance. For example, in some methods for inferring a molecular weight distribution from rheological data (described in Chapter 8), Eq. 5.4 is assumed to be exactly obeyed. In addition, considerable effort has been made to develop molecular

models for rheological behavior that predict Eq. 5.4 with $\alpha \approx 3.4$. And models that do not predict this are deemed unacceptable. It is thus important to explore the origins of this relationship.

There have been a number of efforts to determine experimentally the precise effect of polydispersity on η_0 , but there is as yet no consensus on this point. There are several major challenges in conducting such a study. First, polydisperse melts, particularly commercial materials, often contain components that are sufficiently high in molecular weight that it is not possible to measure the zero-shear viscosity directly. (And for very broad MWD with low-molecular weight components a well-defined terminal zone may not even exist.) For this reason, extrapolated values of η_0 are usually used, but this is not a reliable procedure, as there is no universally valid technique for doing the extrapolation. This issue is explored in more detail in Section 10.7.1.1. In addition, high molecular weight fractions pose major difficulties in the determination of the MWD using a GPC column. For these reasons, the most definitive tests of Eq. 5.4 have involved blends of nearly monodisperse samples. For example, studies of blends of polystyrene [10] and polybutadiene [11] indicated that Eq. 5.4 is valid.

Wood-Adams et al. [12] found that with $\alpha = 3.6$, Eq. 5.4 described quite accurately their data for six linear metallocene polyethylenes having $M_w/M_n = 2$ and the “most probable” molecular weight distribution defined in Section 2.2.4. Gabriel and Münstedt [13] reported that the presence of a high molecular weight component in a linear metallocene polyethylene had no effect on the relationship between η_0 and M_w . But they also observed a negative deviation from Eq. 5.4 when there were significant numbers of molecules having M less than M_C . Wasserman and Graessley [14], however, suggested that the presence of high molecular weight fractions could require the additional factor shown in Eq. 5.5.

$$\eta_0 = K M_w^\alpha \left(\frac{M_z}{M_w} \right)^b \quad (5.5)$$

For polyethylene, Stadler et al. [15] reported $\alpha = 3.6$ and $b = 0$ for M_z/M_w from 2 to 3.8, while Ansari et al. [16] found $\alpha = 3.6$ and $b = 1$ for M_z/M_w from 2.7 to 4.7. Vega et al. [17] studied several polyethylenes having very large M_z/M_w values ranging from 18.7 to 28.7 and found that the value of α decreased with decreasing M_z/M_w , which corresponded to increasing M_w in their samples. They concluded that the value of α depends on the shape of the molecular weight distribution.

We conclude that at present there is no strong basis for adopting any particular correlation for the effect of polydispersity on η_0 . The only well-documented deviation from Eq. 5.4 occurs when a substantial number of *unentangled* molecules are present. On the other hand, it may be unwise to accept Eq. 5.2 as a fundamental principle of polymer science.

Equation 5.4 leads to a formula for calculating the viscosity of a blend $\eta_{0,b}$. Since the M_w of a blend is simply the weighted average of those of its components, for a binary blend Eq. 5.4 implies that:

$$\eta_{0,b} = K M_w^\alpha = \left(w_1 \eta_{0,1}^{1/\alpha} + w_2 \eta_{0,2}^{1/\alpha} \right)^\alpha \quad (5.6)$$

where w_1 and w_2 are the weight fractions of the two components. This blending rule has been used as the basis for a method for inferring the molecular weight distribution from the curve of viscosity versus shear rate, as is mentioned in Chapter 8. The effects of tacticity, comonomer, and long-chain branching on the zero-shear viscosity are discussed in later sections of this chapter.

■ 5.3 The Relaxation Modulus

5.3.1 General Features

Figure 5.2 shows the general shapes of the relaxation moduli for: A) an unentangled polymer; B) a monodisperse, entangled polymer; and C) a polydisperse polymer with M_w well above M_e . In addition, the relaxation modulus of a typical cross-linked elastomer is shown by curve D. At extremely short times, the only mechanism for relaxation is the stretching and bending of bonds, as there is no time for translational Brownian motion to act. This results in a very large “glassy” modulus, G_g , around 10^9 Pa. However, this parameter is not accessible using a standard melt rheometer, and a special instrument is required to achieve the very high-frequency deformations required. At longer, but still quite short times, short-range molecular motions come into play, and there is a transition zone in which there is a significant relaxation of stress. The behavior of all three types of sample is the same in this region, as entanglements do not interfere with this mechanism of stress relaxation. We will see in Chapter 6 that the longer-time portion of the transition zone can be described by a model developed by Rouse for dilute solutions and modified by Bueche for use with melts. If the molecular weight is below the critical value for entanglement (sample A) the stress continues to fall, entering a flow or terminal zone leading to the total relaxation of the stress.

However, for the entangled, monodisperse sample (B) there is a range of times during which further relaxation of any given molecule is almost completely blocked by the severe topological constraints imposed by the presence of other molecules. These topological constraints are universally referred to as “entanglements.” During this period, further relaxation is strongly suppressed, and there is a plateau in the curve. The value of the relaxation modulus corresponding to this plateau is

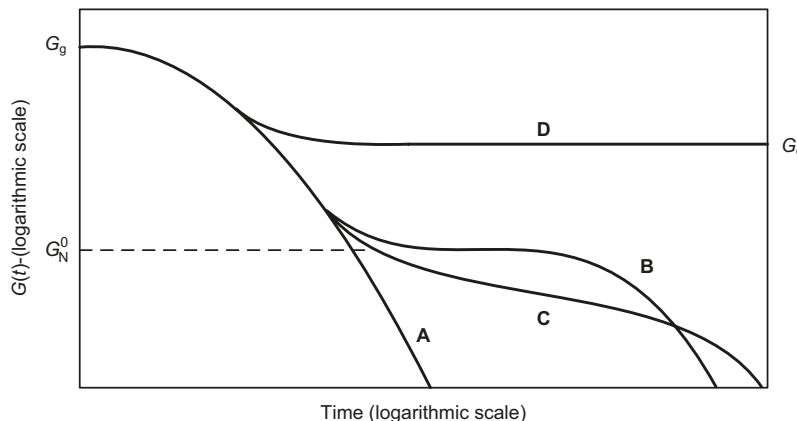


Figure 5.2 Relaxation moduli of three samples of a linear polymer: A) an unentangled molten sample, B) an entangled, monodisperse molten sample, C) an entangled, polydisperse molten sample, and D) a cross-linked sample. At short times, all the samples relax first by a glassy mechanism and then by Rouse relaxation involving only very short segments of the chain (log scales). The unentangled melt then flows in the terminal zone. The entangled, monodisperse melt has a plateau modulus followed by terminal relaxation, while for the polydisperse melt the plateau zone of the longest molecules overlaps with the terminal zones of the shorter molecules.

the *plateau modulus* G_N^0 . Values of this parameter for several polymers are listed in Appendix A. Establishing a reliable value for G_N^0 is not as straightforward as it might first appear to be and several methods for estimating G_N^0 from experimental data are described in Section 5.7. Eventually, a molecule escapes its entanglement constraints by means of the relatively slow process of wriggling along its length. In the “tube model” (Doi-Edwards model) for relaxation presented in Chapter 6, this wriggling motion is called *reptation*. This leads finally to the terminal zone, in which complete relaxation becomes possible.

Finally, sample (C) shows the relaxation modulus for a polydisperse material having a polydispersity index (M_w/M_n) of about four, with $M \gg M_e$. The broadening of the molecular weight distribution results in the loss of a true plateau, because there is now a broad range of times over which relaxation occurs via the slow process of escape from entanglements.

It is important to note that short-time relaxation mechanisms arise from molecular phenomena that are localized along the molecule. They depend only on the local structure of the chain and not its large-scale architecture. They thus provide no information regarding molecular weight, molecular weight distribution or branching. Since our primary concern in this book is how structure affects rheological behavior, we will mainly be interested in the plateau and terminal zones. If the sample of interest were made up of long, linear molecules all having the same molecular

weight, there would be a distinct plateau, and we could easily disregard data in the transition zone. However, we would like to relate rheological behavior to the structure of polydisperse systems, and schemes for dealing with this problem are discussed in several sections of this book.

5.3.2 How Can a Melt Act like a Rubber?

It is of interest to compare the behavior of the monodisperse polymer with $M \gg M_e$ (curve B) with that of the cross-linked elastomer, (rubber) which is illustrated by curve D. At very short times the rubber also shows glassy behavior, and at somewhat longer times, it is able to relax by means of Brownian motion involving short segments of chains. However, it cannot flow because of chemical cross-links, and the relaxation modulus falls only to an *equilibrium modulus*, G_e , at long times. Thus, at times up to the end of the plateau zone, the relaxation modulus of the highly entangled melt is indistinguishable from that of the rubber. This is the reason why a melt can impersonate a rubber in short-time phenomena. For example, “silly-putty” or “bouncing putty” is poly(dimethyl siloxane), which is molten at room temperature. It can be easily shaped by hand, and if left on a table-top, it will flow very slowly into a puddle like any other liquid. However, if rolled into the shape of a ball and dropped on a table, it bounces quite nicely, undergoing no change of shape in the process! This is because the time during which the ball is in contact with the table is much shorter than the time required to reach the end of the plateau zone, and the melt acts exactly like a cross-linked rubber.

The similarity between the behavior of an entangled melt and that of a rubber led to the definition of the *molecular weight between entanglements* M_e , in terms of the plateau modulus G_N^0 by analogy with the equilibrium modulus of a cured elastomer. This important polymer property, M_e , is discussed in detail in Section 5.8.

■ 5.4 The Storage and Loss Moduli

Small-amplitude oscillatory shear is usually used to determine the linear viscoelastic characteristics of molten polymers. Figure 5.3 shows the storage moduli of the samples whose relaxation moduli are shown in Fig. 5.2. Note that logarithmic scales are used for both axes. The same features are present as in a plot of $G(t)$, but the terminal zone is now found at the left end of the curve, while the short-time response corresponds to high-frequency behavior. And here again it is the behavior in the plateau and terminal zones that is sensitive to molecular structure and is thus of primary interest to us.

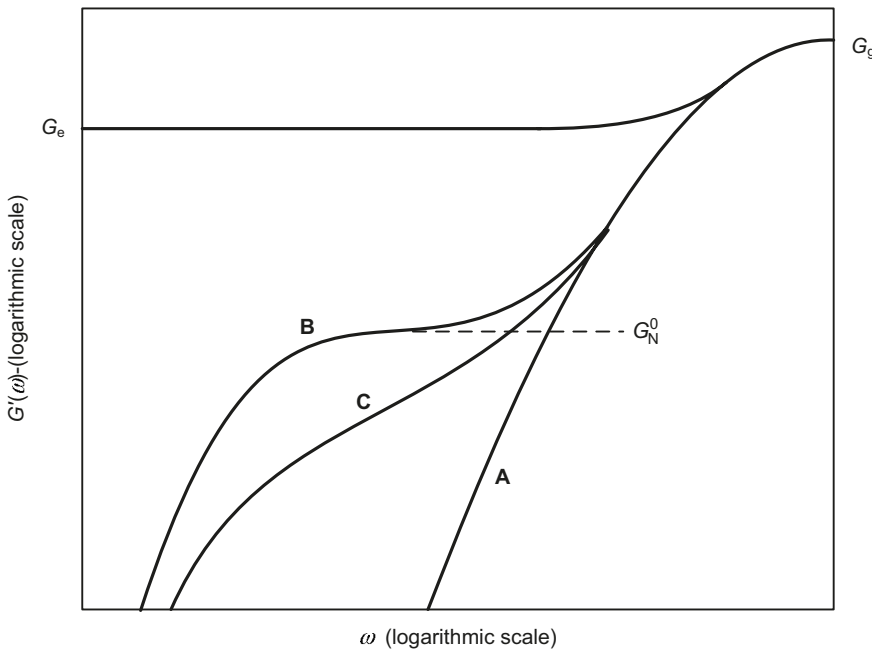


Figure 5.3 Storage moduli of same materials as in Fig. 5.2: A) unentangled polymer, B) entangled, monodisperse melt, C) entangled, polydisperse melt, D) cross-linked polymer (logarithmic scales). The plateau modulus is G_N^0 , G_g is the glassy modulus, and G_e is the equilibrium modulus of the cross-linked material.

Figure 5.4 shows storage and loss modulus mastercurves of Plazek [18] for a poly(vinyl acetate)]. This sample was not perfectly monodisperse, and while the plateau zone can be identified, there is no region in which the storage modulus is truly flat. Relaxation times governing the various relaxation times involved did not have the same temperature dependency, but Plazek achieved reasonable superposition using only two time-shift factors, one for short-time behavior and another for the plateau and terminal zones. There is a minimum in the loss modulus in the plateau zone, reflecting the fact that there is a marked decrease of energy dissipation in this region.

At low-frequencies the slopes on these log-log plots become one for (G'') and two for (G'). We can understand this limiting behavior at very low frequencies by reference to Eqs. 4.40a and 4.40b. The denominators approach unity, and if the longest relaxation time τ_1 is significantly larger than τ_2 the numerator will be dominated at long times by τ_1 , which is called the *terminal relaxation time*. We will see in Chapter 6 that some molecular models predict a discrete spectrum for monodisperse systems in which the longest relaxation time is significantly larger than the next longest one. Thus, in the terminal zone the storage modulus becomes proportional to the square of the frequency, while the loss modulus becomes proportional to the frequency.

This behavior manifests itself in a log-log plot of storage and loss moduli as lines having slopes of two and one, respectively, as shown in Fig. 5.4. For polydisperse polymers, or those with long-chain branching, the discrete relaxation times are closer together, and the approach to the terminal slopes is more gradual. As a result, it is often impossible to carry out experiments at sufficiently low frequencies to reach a terminal zone. This also prevents determination of the zero-shear viscosity.

As we move away from the terminal zone for a monodisperse polymer we come to a range of frequencies over which the storage modulus is essentially constant and the loss modulus has a marked minimum. This is the plateau or rubbery region. Finally, at very high frequencies beyond the range of melt rheometers, Brownian motion is not fast enough to allow any motion except local vibrations, and the polymer behaves like a glass and has a very high modulus.

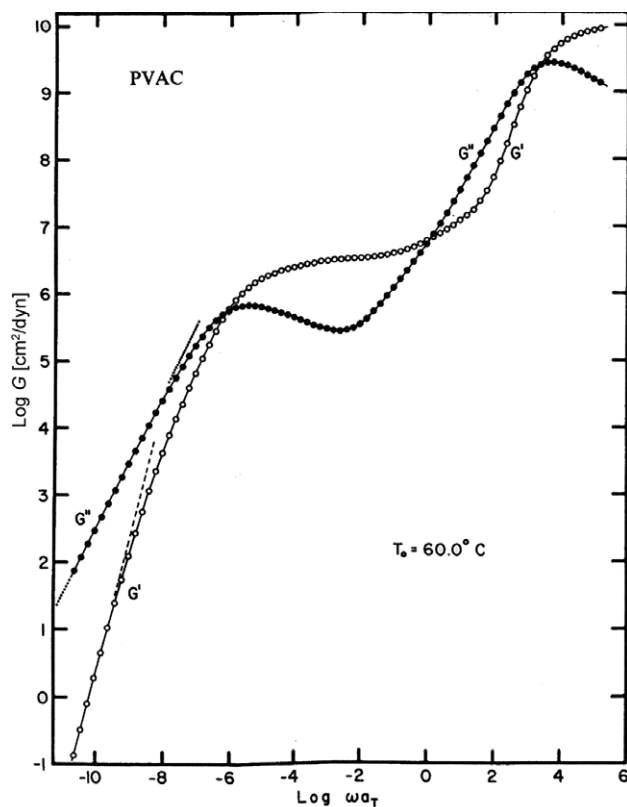


Figure 5.4 Storage and loss moduli versus reduced frequency for poly(vinyl acetate) with a very narrow MWD as calculated from creep data using the retardation spectrum as an intermediary (logarithmic scales). It was not possible to achieve superposition over the entire range of frequencies, and two shift factors were used to deal with data in high and low-frequency zones. The reference temperature is 60 °C. All the relaxation zones are clearly exhibited. From Plazek [18].

Figure 5.5 shows master curves of storage and loss moduli data reported by Wang et al. [19] for four monodisperse polybutadienes having widely varying molecular weights. As the molecular weight increases, the plateau zone grows in length. The longer the molecules, the longer the delay between the frequency where entanglements start to impede relaxation and the frequency where reptation starts to allow relaxation.

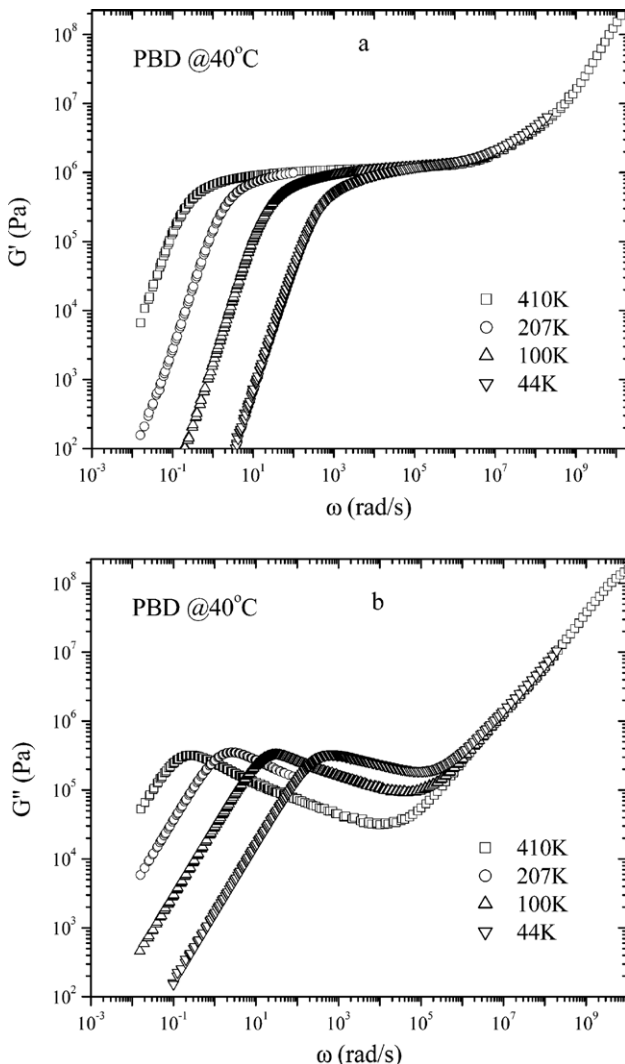


Figure 5.5 Master curves of storage and loss moduli for four monodisperse polybutadienes having widely varying molecular weights. As the molecular weight increases, the plateau zone lengthens. The longer the molecules, the longer the delay between the frequency where entanglements start to impede relaxation and the frequency where reptation starts to allow relaxation. From Wang et al. [19].

■ 5.5 The Creep and Recoverable Compliances

Figure 5.6 shows the creep and recoverable compliances of Gabriel and Münstedt [20] for a metallocene, linear low-density polyethylene at 150 °C. This polymer has a polydispersity index (M_w/M_n) of about two. The data shown start in the transition from the plateau to the terminal zones, and the last few points are in the terminal zone, which corresponds here to steady flow. Note that the experiment had to be continued for about 2.5 hours to reach steady state, where $J(t) = J_s^0 + t/\eta_0$, and $J_r(t) = J_s^0$. J_r is the recoverable compliance defined by Eq. 4.25. It is of interest to compare the creep compliance of an entangled polymer melt with that of a cross-linked elastomer. The latter cannot flow, so at long times $J(t)$ approaches a constant value, the equilibrium compliance, J_e^0 .

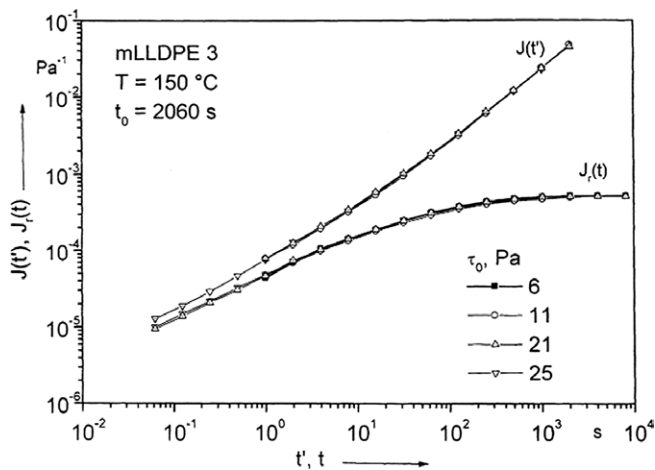


Figure 5.6 Creep and recoverable compliances of a metallocene, linear low density polyethylene (logarithmic scales). The time variable for the recovery starts at the moment the stress is removed. Data at several stresses superposed indicating that all experiments were in the linear regime. From Gabriel and Münstedt [20].

The storage and loss moduli shown in Fig. 5.4 were inferred from the creep data used to calculate the retardation spectrum shown in Fig. 5.7 [18]. Equation 4.29 showed how the creep compliance is related to the retardation spectrum $L(t)$. As in the case of the relaxation spectrum, this function reveals clearly the distinct role played by each relaxation mechanism. We recall that in order to carry out time-temperature superposition for this material, it was necessary to use two shift factors having different temperature dependencies. For this reason, changing the reference temperature shifts the long-time portion of the curve horizontally with respect to the short-time portion. While the data points are based on a reference temperature of 60 °C, the dotted curve shows the master curve for a reference temperature of 35 °C.

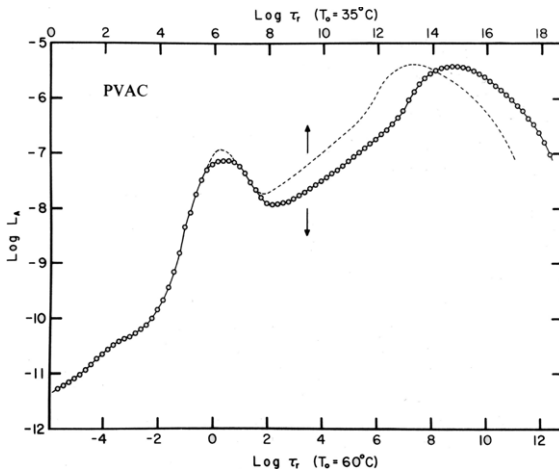


Figure 5.7 Retardation spectrum of the poly(vinyl acetate) of Fig. 5.4 versus reduced time (log scales). The slope is 1/3 in the glassy region suggesting Andrade creep. The plateau zone is between the two peaks, the second of which marks the start of the terminal zone. It was not possible to superpose all the data using a single reference temperature, and different values were used in the short and long-time zones. This is reflected in the difference between the curves obtained using $T_0 = 35^\circ\text{C}$ (dashed line) and with 60°C (points). From Plazek [18].

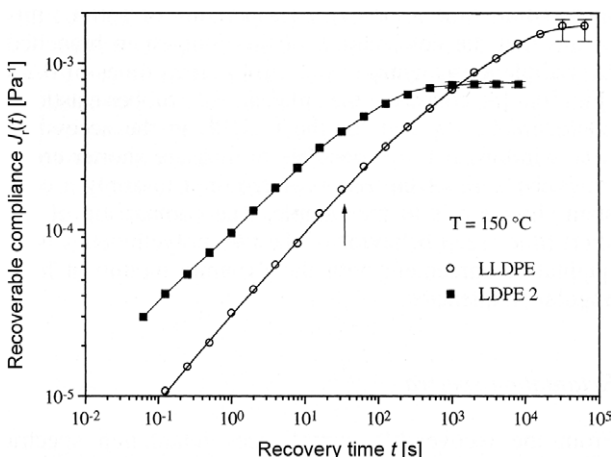


Figure 5.8 Recoverable compliance versus recovery time for an LLDPE and an LDPE at 150°C . At short recovery times the slopes are close to unity, while at long times the curves level out at the steady-state compliance J_s^0 . From Gabriel et al. [21].

Figure 5.8 shows recoverable compliance data for an LLDPE and an LDPE as reported by Gabriel et al. [21]. At early times, the recoverable compliance is linear with time, later approaching the steady-state compliance, as shown by Eqs. 4.25 and 4.27. The marked difference in behavior that involves the crossing of the curves is an effect of the long-chain branching in the LDPE.

■ 5.6 The Steady-State Compliance

The steady-state compliance J_s^0 of a linear, monodisperse polymer increases linearly with M when M is less than a critical value M'_C but becomes independent of M when $M > M'_C$, i.e., when entanglements become important. This behavior is sketched in Fig. 5.9.

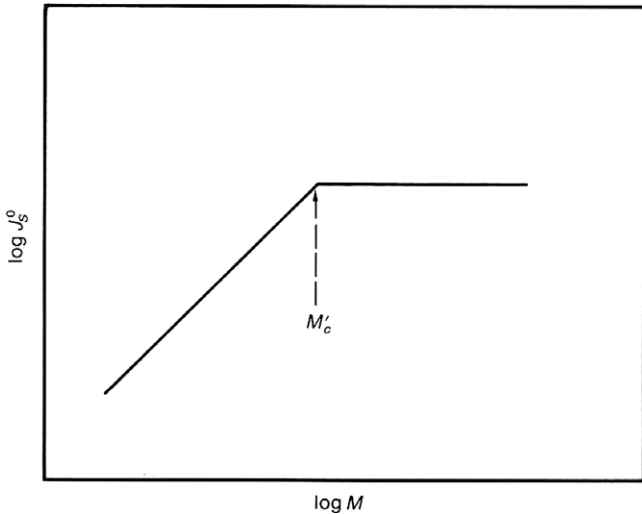


Figure 5.9 Sketch of steady-state compliance versus molecular weight for samples of a monodisperse, linear polymer. Below M'_C the linear increase is in accord with the Rouse-Bueche model (Eq. 5.7), while above this critical molecular weight, a further increase is suppressed by entanglements (Eq. 5.8).

Curiously, M'_C is much larger than M_C , the critical value of M for the effect of entanglements on η_0 , often by a factor of four or five.

An explanation of the dependence of J_s^0 on M when $M < M'_C$ according to the Rouse-Bueche theory of unentangled melts is given in Chapter 6. The equations governing behavior in the two regimes are as follows:

$$J_s^0 = \frac{0.4 M}{\rho R T} \quad M \leq M'_C \quad (5.7)$$

$$J_s^0 = \frac{0.4 M'_C}{\rho R T} \quad M \geq M'_C \quad (5.8)$$

For polydisperse materials the steady-state compliance is very sensitive to molecular weight distribution. This effect shows up even in so-called “monodisperse” samples. Fuchs et al. [22] fitted the following empirical equation to their data for a series of PMMAs having polydispersity indices (M_w/M_n) of less than 1.15.

$$J_s^0 = \frac{0.4 M'_C}{\rho R T} \left[1 - \exp\left(-\frac{M_w}{M'_C}\right) \right] \quad (5.9)$$

For more non-uniform samples the effect is much more dramatic. For example, in a blend of two compatible, linear, monodisperse polymers J_s^0 can be several times larger than the values of J_s^0 of either of the two components. This is illustrated in Fig. 5.10, which shows the steady-state compliances of two, monodisperse, silicone polymers as well as those of various binary blends of these [23]. Several of the many models relating J_s^0 to various moments of the MWD were compared with data for blends of two monodisperse samples by Struglinski and Graessley [11]. They found that the empirical mixing rule of Montfort et al. [24] gave the best fit to their data. However, there is at present no generally accepted method for predicting the steady-state compliance of a polydisperse sample.

Because of its strong dependence on polydispersity even a tiny amount of high molecular weight polymer can increase J_s^0 significantly, and this can cause problems in the experimental determination of this quantity.

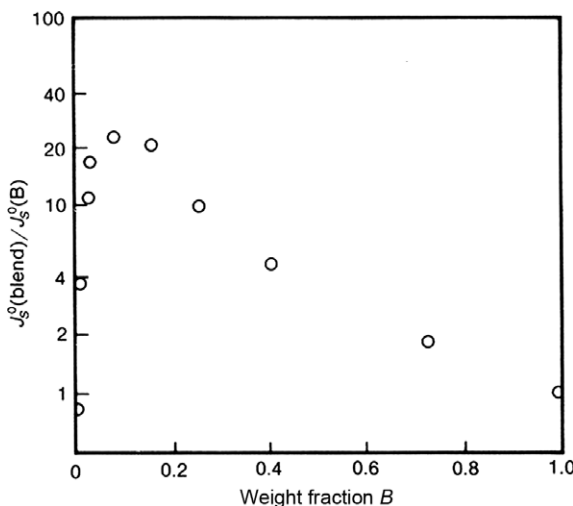


Figure 5.10 Ratio of steady-state compliance for a blend of A and B to that of B versus weight-fraction B for a binary blend of two polydisperse silicones: $M_w)_A = 5.85 \cdot 10^4$; $M_w)_B = 5.98 \cdot 10^5$. The dramatic effect of polydispersity on the compliance is clearly demonstrated by the more than twenty-fold increase in J_s^0 compared to the blend components. From Graessley [23].

■ 5.7 The Plateau Modulus

5.7.1 Determination of G_N^0

For very high molecular weight, essentially monodisperse polymers, the plateau modulus can be determined by inspection of the curve of storage modulus or the compliance, but this is often not feasible, and most reported values rely on approximate methods. In theory it is equal to the integral of the loss modulus in the neighborhood of its peak as shown in the equation below, which is based on the fluctuation-dissipation theorem (see ref. [25], p. 373).

$$G_N^0 = \frac{2}{\pi} \int_{-\omega}^{\infty} G''_{\text{FP}}(\omega) d \ln \omega \quad (5.10)$$

The subscript FP signifies that only contributions from the flow and plateau regions should be taken into account in the integration, as Rouse relaxations that begin in the transition region are not related to entanglements and thus to the plateau modulus.

In the absence of Rouse modes of relaxation, the loss modulus would descend continuously to zero after its maximum, but in reality it goes through a minimum and then increases again. This problem has been addressed by a straight-line extrapolation of the curve from a point past its peak. However, the selection of this point is arbitrary, leading to significant uncertainty in the estimated value of the integral in Eq. 5.10.

Because of uncertainties arising from integrating G'' other approximate methods are used, and a useful review of these is that of Liu et al. [26]. When highly entangled samples with low polydispersities are available, even when there is no true plateau in the storage modulus, if there is a minimum in the loss modulus, the value of the storage modulus at this frequency provides a reliable estimate of the plateau modulus.

$$G_N^0 = G'(\omega)_{G''=\min} \quad (5.11)$$

An example was shown in Fig. 5.5, which showed data for monodisperse, highly entangled polybutadienes [19], where there was a well-defined minimum in the loss modulus.

Figure 5.11 shows data for a somewhat polydisperse polyisobutylene with $M_w = 8 \times 10^4$ and $M_w/M_n \approx 2$ and $M_w/M_e \approx 15$ [26]. There is neither a well-defined plateau in the storage modulus nor a minimum in the loss angle, but there is a clear minimum in $\tan(\delta)$. For monodisperse samples the minimum in $\tan(\delta)$ is generally found to lie at a frequency near the middle of the plateau zone, and Wu [27] proposed using the value of the storage modulus at this frequency as a reasonable estimate of the plateau modulus.

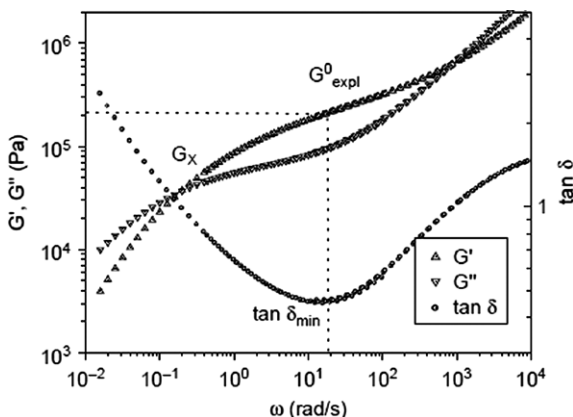


Figure 5.11 Storage and loss moduli and $\tan \delta$ for a somewhat polydisperse polyisobutylene with $M_w = 8 \times 10^4$ and $M_w/M_n \approx 2$ and $M_w/M_e \approx 15$. There is neither a well-defined plateau in the storage modulus nor a minimum in the loss angle, but there is a clear minimum in $\tan(\delta)$. For monodisperse samples the minimum in $\tan(\delta)$ is generally found to lie at a frequency near the middle of the plateau zone, and Wu [27] proposed using the value of the storage modulus at this frequency as the plateau modulus. From Liu et al. [26].

An empirical relationship between the plateau modulus and the local *maximum* in $G''(\omega)$ that is said to be based on the assumption of uniform entanglement spacing is shown below (see ref. [25], p. 376).

$$G_N^0 = 4.83 G_{\max}'' \quad (5.12)$$

This expression is often used when the data do not have features allowing the use of other methods. And when even this fails, the use of the crossover modulus where $G' = G''$ has been proposed [27].

Polyolefins cannot be made by anionic polymerization, and for polyethylene several methods have been used to prepare narrow-distribution samples that are similar to polyethylene. These methods have yielded a wide range of values: 1.58 MPa @ 190 °C [28], 2.6 MPa @ 140 °C [29], and 3.5 MPa @ 25 °C [30]. The hydrogenation of monodisperse polybutadiene produces a polymer very similar to polyethylene, although it has some ethyl side groups. Based on a study of a series of hydrogenated polybutadienes (HPB) having varying vinyl content, with an extrapolation to zero vinyl content (ethyl side groups) to obtain a value for polyethylene, Carrela et al. [31] obtained a value of 2.3 MPa for the plateau modulus. They also reported a weak dependence of the plateau modulus (and M_e) on temperature. Fetters et al. [30] provide an extensive list of plateau moduli and other parameters for many polymers. (Note that they use G_e to represent the plateau modulus rather than G_N^0 .) Appendix A of this book lists values of the plateau modulus and some other parameters for a shorter list of polymers.

5.7.2 Effects of Short Branches and Tacticity

One can look on the work of Carella et al. [31] on hydrogenated polybutadiene (HPB) as a study of the effect of short branches on G_N^0 and M_e . They measured the linear viscoelastic properties of a series of polybutadienes and HPBs in which the fraction of 1,2 addition polymer with ethyl side groups was varied. They found that the effect of the ethyl branches on the plateau modulus of the HPBs could be estimated using Eq. 5.13.

$$G_N^0 \propto \left(\frac{28}{2 - x_{12}} \right)^{-2.3} C_\infty^{1.6} \quad (5.13)$$

where x_{12} is the fraction of HPB with 1,2 addition and C_∞ is the characteristic ratio defined by Eq. 2.6. It is likely that the relative amounts of the *cis*- and *trans*-isomers of 1,4 PB also affect the plateau modulus of this polymer.

The introduction of short-chain branches into polyethylene by use of an alpha-olefin comonomer yields the commercially important polymer linear low-density polyethylene (LLDPE). These short branches would also be expected to affect the entanglement molecular weight. Based on previously published data on poly (α -olefins) [8,29], Fetters et al. [32] developed the following empirical equations for estimating the plateau moduli of polymers of this type, given only the average molecular weight per backbone bond, m_b .

$$G_N^0 = 24820 m_b^{-3.49} \quad (m_b = 14 - 29) \quad (5.14a)$$

$$G_N^0 = 41.84 m_b^{-1.58} \quad (m_b = 35 - 56) \quad (5.14b)$$

Tacticity also has a significant effect on rheological properties. Liu et al. [33] studied three syndiotactic polystyrenes made with a metallocene catalyst having pentad levels around 87%, M_w values between 320 and 440 kg/mol, and polydispersities between 2 and 2.3. They used Eqs. 5.10 and 5.12 and two other methods to estimate values of the plateau modulus. The values based on Eqs. 5.10 and 5.12 were within $\pm 5\%$ with an average value of 0.87 MPa at 190 °C. Huang et al. [34] reported results for nine syndiotactic, four atactic, and one isotactic polystyrenes. The syndiotactic samples had high stereoregularities with heptad levels of racemic units between 90 and 96%, and their zero-shear viscosities followed a 3.64 power law with M_w . It was found that the viscosities of all the samples, including those with all three types of tacticity, could be fitted to a single line with a slope of 3.64 when plotted versus M_w/M_e , where M_e is related the plateau modulus as shown by Eq. 5.20 in Section 5.8.1. Ahmad et al. [35] studied polypropylenes having various degrees of stereoregularity with pentad levels of racemic units from 26 to 93%. They reported that the plateau modulus increased with stereoregularity, increasing especially rapidly at low defect levels and leveling out at defect levels approaching 100%.

■ 5.8 The Molecular Weight between Entanglements, M_e

A property of central importance in polymer rheology is the molecular weight between entanglements, M_e , which is closely related to the plateau modulus. (This quantity is not to be confused with the *critical molecular weights*, M_C and M'_C defined in Chapter 4.) It is desirable to have a reliable value for this parameter, but there are two difficulties in arriving at such a value. First, there is some ambiguity in its definition. On the one hand, it can be defined, more or less empirically, by a relationship with a measurable rheological property, most often the plateau modulus. And it also appears as a parameter in tube models for rheological behavior. And since it is defined in terms of the plateau modulus, its experimental determination is subject to the limitations cited above.

5.8.1 Definitions of M_e

According to the classical theory of rubber elasticity (see ref. [25], p. 234), the equilibrium shear modulus for infinitesimal deformations is:

$$G_e = \nu R T \quad (5.15)$$

where ν is the number of moles of network strand per unit volume. Ferry (see ref. [25], p. 372) suggested that an entangled melt could be considered to be a rubber in which the crosslink network is replaced by entanglements. Thus, the density of network strands is replaced by the density of entanglement network strands, ν_e , and the equilibrium modulus is replaced by the plateau modulus to give Eq. 5.16.

$$G_N^0 = \nu_e R T = \rho R T / M_e \quad (\text{Ferry definition}) \quad (5.16)$$

Or, in terms of the plateau compliance:

$$J_N^0 = M_e / \rho R T \quad (5.17)$$

The molecular weight between entanglements would thus be given by:

$$M_e \equiv \rho / \nu_e \quad (5.18)$$

Equation 5.16 involves the experimentally observed plateau modulus, and this assumes that it reflects all the relaxation that occurs in response to the initial stress, except for the extremely short-time glassy modes. However, relatively fast Rouse modes of relaxation allow re-equilibration of tension along the chain, and as a result, one-fifth of the initial stress relaxes quickly, before the entanglement

network interrupts the process. Thus, the plateau modulus actually observed in an experiment is expected to be about 4/5 of the quantity on the right in Eq. 5.16. Graessley [1] thus proposed that M_e for entangled melts be defined as shown below.

$$G_N^0 = \frac{4}{5} v_e R T = \frac{4}{5} \rho R T / M_e \quad (\text{Graessley-Fetters definition}) \quad (5.19)$$

In order to avoid confusion, in the present book we will reserve the symbol M_e for the entanglement molecular weight defined by Eq. 5.16 and will use M_e^G for the quantity in Eq. 5.19. The two definitions of the molecular weight between entanglements are thus given by Eqs. 5.20 and 5.21:

$$M_e \equiv \frac{\rho R T}{G_N^0} \quad (5.20)$$

$$M_e^G \equiv \frac{4}{5} \frac{\rho R T}{G_N^0} \quad (5.21)$$

(Note that the symbol M_e^F is sometimes used for the Ferry definition given by Eq. 5.20.) Both of these definitions have been used in the literature, represented by the undifferentiated symbol, M_e . This has led to confusion and some errors in later publications. This problem has been discussed by Larson et al. [36].

A few authors have used an “entanglement modulus” G that is defined as 4/5 of the observed plateau modulus. In this way, we have:

$$M_e^G \equiv \frac{\rho R T}{G_e}$$

This G_e is not to be confused with the “equilibrium modulus” of a cross-linked elastomer in Eq. 5.18, although it is defined in such a way as to strengthen the analogy between an entangled melt and a cross-linked elastomer.

The *number of entanglements per molecule Z*, or degree of entanglement, is defined as the ratio of the molecular weight to the molecular weight between entanglements M/M_e . However, we recall that the experimentally observed plateau occurs only after the very fast equilibration relaxation process, so that entanglements actually start influencing relaxation just prior to the experimental plateau. In tube-model theory Z is called “number of tube segments” M/M_e^G , but we will use the Ferry value of M_e in this chapter; the relationship between the two definitions of Z is given by Eq. 5.22.

$$\frac{M}{M_e^G} = \frac{5}{4} \frac{M}{M_e} \quad (5.22)$$

For a polymer to be considered highly entangled, Z should have a value of at least 30–40.

In concentrated polymer solutions, as the concentration of the polymer increases, M_e decreases, and G_N^0 is found to be approximately proportional to c^2 (see ref. [25], p. 502), which is in accord with the scaling proposed by Brochard and deGennes [37] for the theta state. This trend is also followed when an entangled bulk polymer is blended with a low-molecular weight homologue for which $M < M_e$, and this scaling has been used as the basis of a procedure for determining the molecular weight distribution from the loss modulus that is described in Section 8.3. Some studies have indicated an exponent greater than two, and on the basis of a scaling argument, Colby and Rubinstein [38] argued that in the theta state it should be $7/3$. In a good solvent, de Gennes [39] proposed a value of $9/4$.

5.8.2 Molecular Weight between Entanglements (M_e) Based on Molecular Theory

Wolkowicz and Forsman [40] wrote that the idea of a uniquely defined entanglement molecular weight that can be determined directly from rheological data is an oversimplification of the concept of entanglement. Since then, several theories have been proposed to give quantitative meaning to the idea of a molecular weight between entanglements. Heymans [41] compared five such models. Three of these she described as “interactive,” and these predict a decrease in M_e with increasing chain stiffness, based on the idea that a more flexible chain coils more on itself and interacts less with other chains. These models include the packing model of Fetters et al. [29], the “binary contact per chain model” of Edwards [42] and the “binary contacts per pervaded volume” model of Colby et al. [43]. The remaining two models are those of Wu [27] and Wool [44], which predict that M_e decreases with increasing chain flexibility. Richter et al. [45] earlier studied one sample that tended to support the interaction models. After a thorough analysis of many published data, including the extensive tabulation of Fetters et al. [29], Heymans concluded that M_e decreases as chain stiffness increases, i.e., that it varies inversely with the characteristic ratio, C_∞ . She found that the packing model [29] gives the best correlation with M'_C , the critical entanglement molecular weight for compliance, while the model of Colby et al. [43] gives the best correlation with M_C , the critical entanglement molecular weight for viscosity.

The packing model is based on the concept of a *packing length* first introduced by Witten et al. [46]. They found this length parameter to be important in modeling the interfacial tension between two immiscible polymers. Fetters et al. [29] later found it to be useful in correlating rheological properties with the degree of entanglement and then with the size of molecular coils. The packing length, p , reflects the degree to which molecules interpenetrate each other's space. To obtain a quantitative

measure of this effect we first define the average volume, V_c , “occupied” by one molecule as follows:

$$V_c = \frac{M}{\rho N_A} \quad (5.23)$$

where N_A is Avogadro’s number. Now we define the volume “pervaded” by a molecule, V_{sp} , as that of the smallest sphere that can completely contain a molecule; this is difficult to calculate, but if we assume that it is proportional to the cube of the root-mean-square radius of gyration, we obtain:

$$V_{sp} \equiv A \langle R_g^2 \rangle_0^{3/2} \quad (5.24)$$

where A is a universal constant approximately equal to one for flexible polymers. Now our measure of the degree of entanglement will be the number N_{sp} of chains of length M that would completely fill the volume V_{sp} . This is simply the ratio of V_{sp} to V_c :

$$N_{sp} \equiv \frac{V_{sp}}{V_c} = \frac{A \langle R_g^2 \rangle_0^{3/2} \rho N_A}{M} \quad (5.25)$$

If we assume that the mean-square radius of gyration is proportional to the molecular weight, i.e., that $\langle R_g^2 \rangle_0 / M$ is a constant for a given polymer, we can rewrite Eq. 5.25 as follows:

$$N_{sp} = A \left(\frac{\langle R_g^2 \rangle_0}{M} \right)^{3/2} \rho N_A M^{1/2} \quad (5.26)$$

When $N_{sp} = 2$, there are, on average, two chains occupying the space pervaded by each one. Fetters et al. [32] proposed that this be used as a criterion for the onset of entanglement, so that the condition for transition from the unentangled to the entangled state is obtained by setting N_{sp} equal to two in Eq. 5.26. Noting that $\langle R^2 \rangle_0 = 6 \langle R_g^2 \rangle_0$ (Eq. 2.2) this leads to the following expression for the molecular weight at which we expect to observe the transition to the entangled state.

$$M \text{ (threshold of entanglement)} = \left(\frac{\langle R^2 \rangle_0}{M} \right)^{-3} (B \rho N_A)^{-2}$$

where $B \equiv A/[2(6^{3/2})]$. Finally, Fetters et al. [29] proposed that this molecular weight be identified with M_e^G , defined by Eq. 5.21, in terms of the plateau modulus.

$$M_e^G = \left(\frac{\langle R^2 \rangle_0}{M} \right)^{-3} (B \rho N_A)^{-2} \quad (5.27)$$

The packing length p is defined by Eq. 5.28 and is essentially constant for a given polymer.

$$p \equiv \frac{M}{\langle R^2 \rangle_0 \rho N_A} = \frac{V_c}{\langle R^2 \rangle_0} \quad (5.28)$$

Equation 5.27 can now be written in terms of the packing length.

$$M_e^G = p^3 \rho N_A / B^2 \quad (5.29)$$

where $B \equiv A / [2(6^{3/2})]$.

Fetters et al. [7, 31] published an extensive tabulation of packing lengths and values of M_e [7] or M_e^G [31] determined from rheological data. Values of these parameters for several polymers are listed in Appendix A. Fetters et al. [47] proposed the following empirical relationships, which were thought to be independent of temperature and universal for Gaussian chains in the melt state.

$$M_e^G / \rho = 218 p^3 \quad (5.30)$$

$$d_t = 19 p \quad (5.31)$$

In Eq. 5.31, d_t is the tube diameter that will be used extensively in Chapter 6, where it is given the symbol a . Krishnamoorti et al. [48] later represented G_N^0 and M_e (Ferry's definition) in terms of n_t , which is "the number (≈ 21) of entangled strands in a cube with dimensions of the tube diameter" to give the following species-independent relationships:

$$G_N^0 \text{ (MPa)} = \frac{k T}{n_t^2 p^3} \quad (5.32)$$

$$M_e = \rho N_A n_t^2 p^3 \quad (5.33)$$

An earlier approach to this problem by Graessley and Edwards [49] led to the conclusion that $G_N^0/k T$ was a universal function of the "length of uncrossable chain contour per unit volume." The predictions of this theory were reported to give fair agreement with data for polybutadienes by Carella et al. [31].

Fetters et al. [7] also used the packing length concept to develop the following relationship between the critical molecular weight for viscosity M_C and the entanglement molecular weight M_e (Ferry's definition):

$$M_C = 4.24 M_e p^{-0.65} = M_e \left(\frac{p^*}{p} \right)^{0.65} \quad (5.34)$$

where $p^* \equiv 9.2 \text{ \AA}$. This shows how M_C/M_e varies from one polymer to another. For example, Eq. 5.34 indicates that M_C/M_e is 3.04 for polyethylene and 1.72 for

polystyrene. Osaki et al. [50] estimated a value of 1.5 for polystyrene using storage modulus data. Equation 5.34 can be combined with Eq. 5.3 to show the effect of the packing length on M_r , the molecular weight above which the zero-shear viscosity is predicted to reach its M^3 dependency, which is expected when reptation becomes the dominant relaxation mechanism.

$$M_r \approx M_e \left(\frac{p^*}{p} \right)^{3.9} \quad (5.35)$$

The packing length concept can also be used to develop an equation for estimating the entanglement molecular weight M_e^G from intrinsic viscosity data [29]. We start with Eq. 2.86 for the intrinsic viscosity of a polymer in its theta state, repeated here as Eq. 5.36:

$$[\eta]_\theta = K_\theta M^{1/2} = \Phi \left(\frac{\langle R^2 \rangle_0}{M} \right)^{3/2} M^{1/2} \quad (5.36)$$

We recall from Chapter 2 that $\Phi = 2.5 \cdot 10^{23}$. Equation 5.36 can be combined with Eq. 5.27 to give:

$$M_e^G = \left(\frac{\Phi}{B K_\theta \rho N_A} \right)^2 \quad (5.37)$$

Byutner and Smith [51] used these relationships as the basis of a procedure for calculating the plateau modulus using only fundamental molecular parameters that can be determined by numerical simulation.

■ 5.9 Rheological Behavior of Copolymers

An important class of commercial polymers is that of copolymers of ethylene and alpha-olefins, which are commonly referred to as linear low density polyethylenes (LLDPE). The use of a copolymer introduces short-chain side branches onto the polyethylene backbone, and the effect of these short-chain branches on rheological properties depends very much on the method of polymerization. If a heterogeneous, Ziegler catalyst is used, the side-chains tend to be distributed in blocks rather than randomly along the backbone, and Wardhaugh and Williams [52] point out that this can lead to microphase separation in the melt, which could have an important effect on rheological behavior.

Fetters et al. [32] proposed that their empirical equations (Eqs. 5.14a and b above) for calculating the plateau modulus of a poly(α -olefin), given only the average molecular weight per backbone bond, could be used to estimate the plateau moduli of ethylene/ α -olefin copolymers.

If the copolymer is prepared using a single-site (metallocene) catalyst, the short-chain branching distribution is expected to be random. Wood-Adams et al. [53] studied the effect of comonomer content in three ethylene-butene copolymers prepared using such a catalyst in which the butene level ranged from 11 to 21%. While the three materials studied had nearly identical polydispersities, there was a modest variation in average molecular weight, and this was accounted for by dividing the complex viscosity by the zero-shear viscosity. The resulting master curve is shown as Fig. 5.12. The superposition is good but not perfect, but noting that there was no trend in the scatter with regard to butene content, the authors concluded that the variation was probably due to the differences in MWD. Wood-Adams and Costeux [54] found that the copolymers used in this study were each thermorheologically simple, i.e., that they obeyed time-temperature superposition. Curiously, however, they found that the activation energy was insensitive to butene content at levels above 7 wt%.

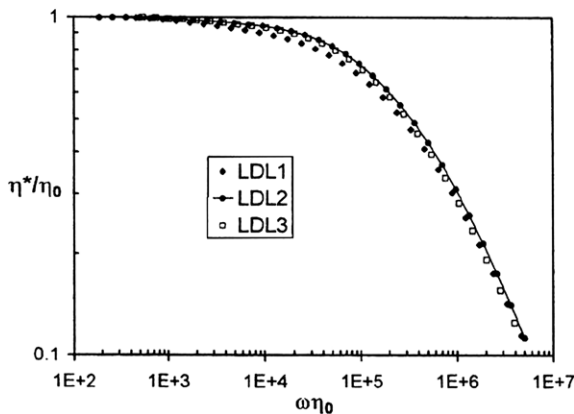


Figure 5.12 Complex viscosity versus reduced frequency for three ethylene-butene copolymers in which the butene level ranged from 11 to 21% at a single temperature (log-log plot). All had nearly identical polydispersities, but there was a modest variation in average molecular weight, which was accounted for by dividing the complex viscosity by the zero-shear viscosity. The data for the three samples do not superpose perfectly, but there is no trend with regard to butene content, and the authors concluded that the variation was probably due to the differences in MWD rather than the presence of the comonomer. From Wood-Adams et al. [53].

■ 5.10 Effect of Long-Chain Branching on Linear Viscoelastic Behavior

5.10.1 Introduction

When is a branch a “short” branch and when is it a “long” one? The answer depends on your point of view. If you are using NMR to probe the structure of a polymer, all side-chains longer than five monomer units give the same response and thus might be classified as “long.” From a phenomenological rheology point of view, the key length parameter is the critical molecular weight M_C , and a “long” molecule is one whose molecular weight is substantially larger than this. As we have seen, this empirically defined quantity is several times larger than the molecular weight between entanglements, M_e , which has a more fundamental definition. Another possible point of view arises in considering the commercially important copolymers of polyethylene and an α -olefin that are called linear, low-density polyethylenes (LLDPE). In this case, a short branch might be considered to be one resulting from the incorporation of the comonomer, and a long branch would then be a longer branch introduced during polymerization or subsequent chemical treatment, for example by a peroxide.

Another complication that arises in dealing with branching is that a very large variety of branching structures are possible, and it is not possible to generalize about their effects. Even with the copolymers mentioned above, the distribution of comonomer along and among the chains may have a subtle effect. In the case of long branches, the structure can become very complicated, and it is impossible to draw any definitive conclusions from rheological data on branched polymers unless something is known about the type of branching structure involved. This information can only come from information about the way the polymer was produced. Without any knowledge of its origin, it is not possible to use any combination of characterization techniques to determine the detailed branching structure. The present overview of the behavior of branched systems is thus organized according to type of branching structure. Hyperbranched polymers (defined in Chapter 3) are generally unentangled because of the short segments between branch points [56].

Polyethylene, which is the world’s most heavily produced commercial polymer, poses special problems with regard to structure-property studies, because samples with ideal structures cannot be prepared by ionic polymerization. To obtain linear samples with narrow molecular weight distributions, it is necessary to fractionate a polydisperse sample thought to be completely linear. It is also possible to prepare nearly monodisperse polybutadienes having prescribed branching structures, and this polymer can then be hydrogenated to yield a material that is very similar, although not identical, to monodisperse polyethylene. Even before hydrogenation,

Rochefort et al. [57] found that it was not possible to make polybutadiene that had both a polydispersity index less than 1.1 and negligible vinyl content. On the other hand, Raju et al. [58] found that hydrogenation did not disrupt the structure in star polymers.

5.10.2 Ideal Branched Polymers

In Section 3.4 it was explained that polymers having very well defined structures can be prepared by means of anionic polymerization, and this technique has been widely used to prepare samples for rheological study. This has been a particularly fruitful approach to the study of the effects of various types of long-chain branching structure on rheological behavior. Linear viscoelastic properties are very sensitive to branching, and in this section we review what is known about zero-shear viscosity, steady-state compliance, and storage and loss moduli of model branched polymers.

5.10.2.1 Zero-Shear Viscosity of Ideal Stars and Combs

In symmetric stars whose arms are too short to entangle, at constant molecular weight, η_0 decreases further below that of a linear polymer of the same molecular weight. Bueche [59] assumed that in unentangled systems the ratio $[(\eta_0)_B / (\eta_0)_L]_M$ is not affected by the details of the branching structure and proposed that it should be equal to g , the ratio of the mean-square radii of gyration for branched and linear polymers of the same molecular weight. Ham [60] developed a model for stars with unentangled arms that provides a quantitative prediction of this effect. For stars with f arms of equal length, Ham's model gives:

$$g = \frac{3f - 2}{f^2} = \frac{(\eta_0)_B}{(\eta_0)_L} \quad (\text{same } M, \text{ unentangled arms}) \quad (5.39)$$

We see that as f increases, g , and thus η_0 , decrease. (Zimm and Stockmeyer [61] arrived at the same result using a different method; see Eq. 2.17.) This relationship has been found to be reasonably correct as long as the molecular weight of the arm is less than about $M_C/2$. When the arms become long enough to be entangled, we start to see an enhancement of the viscosity, and g is no longer equal to the ratio of the zero shear viscosities. When the arm molecular weight, M_a , reaches two or three times the molecular weight between entanglements, M_e , η_0 increases approximately exponentially with molecular weight. Roovers [62] generalized these observations by use of an *enhancement factor due to entanglements* Γ defined by Eq. 5.40.

$$(\eta_0)_{\text{star}} = (\eta_0)_{\text{lin, same } M} \Gamma g^\alpha \quad (5.40)$$

where:

$$\text{For } 2M < f M_C \quad \alpha = 1 \quad \Gamma = 1$$

$$\text{For } 2M > f M_C \quad \alpha \approx 3.4 \quad \Gamma \propto \exp(2\alpha M/f M_C)$$

Fig. 5.13 shows data of Kraus and Gruver [63] for linear, three-arm and four-arm polybutadiene stars. At moderate molecular weights the data for the stars lie below, but parallel to, the line for linear, entangled polymer with $\alpha = 3.4$, in accord with Eq. 5.4, but when the branch length reaches three ($f = 3$) or four ($f = 4$) times M_e , the data for the stars rise sharply and cross the line for linear polymers described by Eq. 5.4.

In the above expression for the viscosity of entangled stars, we note that M/f is the molecular weight per arm of the star polymer, and this implies that the viscosity of symmetric stars with entangled branches depends only on the length of the branch and not the number of branches. It has been found that this holds for functionalities up to at least 33 [64], except for a modest deviation from the rule for $f = 3$. Thus, data for stars with various numbers of arms can be plotted versus M_a to form a master curve. The dependence of η_0 on M_a is found to be approximately exponential, and theoretical arguments [65, 66] suggest a relationship of the following form:

$$\eta_0 \propto \left(\frac{M_a}{M_e} \right)^\alpha \exp \left(v' \frac{M_a}{M_e} \right) \quad (5.41)$$

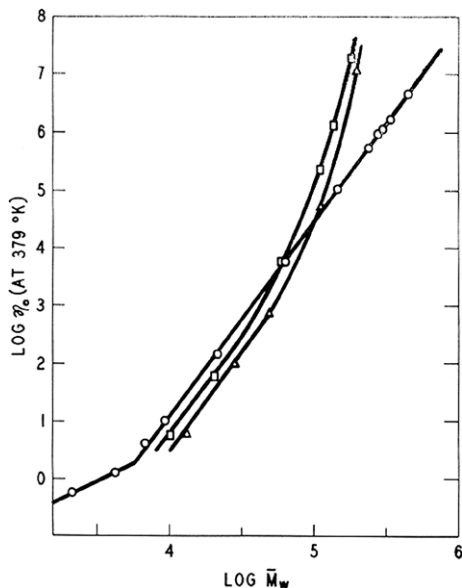


Figure 5.13 Zero-shear viscosity versus molecular weight for polybutadiene linears (circles), three-arm stars (squares), and four-arm stars (triangles). At low M_w , the data for the branched samples fall below the line for linear polymers, while at higher M_w they cross the line and become higher. From Kraus and Gruver [63].

Fetters et al. [67] found that their data for polyisoprene stars followed this relationship with $\alpha = 3/2$ and $v' = 0.47$. Ngai and Roland [68] found that this form also fitted their data for polyisoprene stars but that when M_a/M_e reached 44, the viscosity fell well below that indicated by Eq. 5.41.

The exponential increase of viscosity with M is consistent with the picture in which relaxation occurs primarily by means of primitive path fluctuations (sometimes called arm retraction). In Chapter 9 we will see that this effect can be explained quantitatively by a tube model. The exponential increase of η_0 with M results from the fact that the branch point prevents reptation, so that the principal mechanism of relaxation is primitive path fluctuation, which becomes exponentially slower with increasing arm length. The energy of activation for the zero-shear viscosity is little affected by star branching, except in the case of polyethylene and its close relative, hydrogenated polyisobutylene.

Gell et al. [69] studied a series of asymmetric stars made by adding arms of varying length at the midpoint of a monodisperse backbone for which $M/M_e \approx 40$. They found that even the shortest arm ($M_a/M_e = 0.5$) had the effect of tripling η_0 , and for $M_a/M_e = 2.4$, η_0 was increased by a factor of ten. While there was a modest increase in the backbone length as the arm length increased, this was much too small to account for these large viscosity increases. This finding illustrates the difficulty in relating structural details to viscosity unless the type of structure is known with some precision.

One approach to the analysis of data for a branched polymer is to compare its viscosity with that of a linear polymer having *the same size* (same radius of gyration) rather than the same molecular weight. For unentangled polymers, we expect that the two viscosities will be the same. The factor of g^α in Eq. 5.40, which accounts for the size effect, is thus incorporated into $(\eta_0)_{\text{lin, same size}}$, so that Eq. 5.40 becomes:

$$\Gamma = \frac{(\eta_0)_{\text{br}}}{(\eta_0)_{\text{lin, same size}}} \quad (5.42)$$

The zero-shear viscosity of the same-size of linear polymer can be estimated from the intrinsic viscosity of the branched polymer under theta conditions, which is proportional to hydrodynamic volume; it will be the same as $[\eta]_0$ of a branched polymer having the same size. Using Eqs. 2.86 and 5.42, this leads to:

$$(\eta_0)_{\text{lin, same size}} = k \left([\eta]_0^2 \right)_{\text{br}}^\alpha \quad (5.43)$$

where k is a composite constant. For unentangled, linear molecules, $\alpha = 1$, while for entangled polymers it is about 3.4. If η_0 is plotted as a function of $[\eta]_0^2$, data for the linear and branched polymers should fall on a single line at low molecular weights, where the branches are unentangled, but as its size increases the data

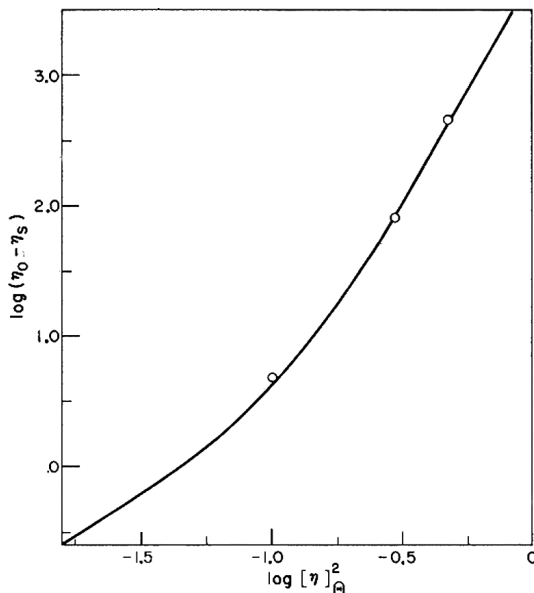


Figure 5.14 Zero-shear viscosity versus the square of the intrinsic viscosity of an H-molecule polystyrene solution (circles) plotted as suggested by Eq. 5.43. The curve is the master curve for star and linear polymers. From Roovers [62].

for the branched molecules will rise above this line. Such a plot for H-shaped polystyrenes [62] is shown in Fig. 5.14. As in the case of stars, the viscosity increases exponentially when the arm molecular weight is sufficiently large. In their study of “pom-pom” polymers (which have two branch points with multiple free arms at each one), Archer and Varshney [70] also found that the zero-shear viscosity increased exponentially with arm length.

Although time-temperature superposition $\eta(\dot{\gamma})$ often fails for branched systems, the variation of η_0 with temperature is generally not sensitive to branching, but an important exception is polyethylene. In hydrogenated polybutadiene stars, for example, the difference between the activation energies for viscosity of star and linear samples is proportional to arm length [63].

5.10.2.2 Steady-State Compliance of Model Star Polymers

For multi-armed stars, where M_a is less than M_e , Ham’s model for unentangled melts [60] indicates that the ratio of J_s^0 values for f -armed stars and linear molecules having the same molecular weight, is given by:

$$\frac{(J_s^0)_B}{(J_s^0)_L} \equiv g_2 = \frac{15f - 14}{(3f - 2)^2} \quad (\text{same } M) \quad (5.44)$$

Combining this with the prediction of the Rouse-Bueche theory for linear, unentangled melts (see Eq. 6.15), we obtain:

$$(J_s^0)_B = \frac{0.4 g_2 M}{\rho R T} \quad (5.45)$$

As the arm length increases above M'_C , we expect the onset of entanglement to cause marked deviations from this relationship. However, for star polymers it is observed that J_s^0 continues to increase linearly with M , in accord with the Rouse-Bueche model for linear, unentangled polymers. This is in contrast to the behavior of entangled, linear, monodisperse melts, for which J_s^0 is independent of M at large M as shown by Eq. 5.8. Figure 5.15 shows data of Graessley and Roovers for four- and six-arm polystyrenes [64]. The horizontal line is based on data for linear polymers, while the dashed lines are the predictions of Eq. 5.44 for f equal to two (linear polymer), four, and six. Ham's theory does a fairly good job, and the surprise is that the data for the stars do not level off at $M_a = M'_C$ but continue, more or less, in accord with Eq. 5.45. Pearson and Helfand [65] proposed the following relationship for stars when the arms are entangled.

$$J_s^0 = \nu' \frac{M_a}{M_e} \frac{1}{G_N^0} \quad (5.46)$$

where the constant factor ν' is the same as in Eq. 5.41.

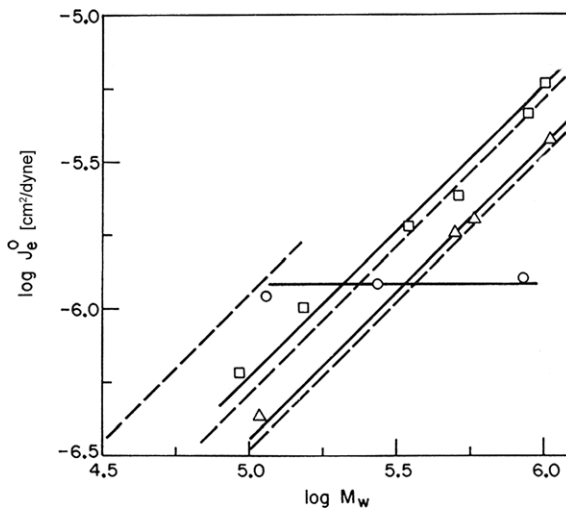


Figure 5.15 Steady-state compliance, determined by measuring the recoverable compliance, versus M_w (log-log plot) for linear polystyrene (circles), four-arm stars (squares), and six-arm stars (triangles). The dashed lines follow Eq. 5.44, while the solid lines are based on data for linear samples. From Graessley and Roovers [64].

Gell et al. [69] found that the steady-state compliance of a symmetric, three-arm star with $M_a/M_e = 18$ was about $18 \cdot 10^{-7} \text{ cm}^2/\text{dyn}$, whereas the value predicted by Eq. 5.44 is about $14 \cdot 10^{-7} \text{ cm}^2/\text{dyn}$ ($g_2 = 0.63$ for $f = 3$). At the same time, the value normally expected for an entangled, monodisperse, linear polymer, as given by Eq. 5.9 (shown again here as Eq. 5.47) is much less than $18 \cdot 10^{-7} \text{ cm}^2/\text{dyn}$.

$$J_s^0 = \frac{0.4 M'_C}{\rho R T} \quad (\text{linear, monodisperse, } M > M'_C) \quad (5.47)$$

We see here once again that the behavior of the branched polymer with entangled arms is much closer to that of an unentangled branched polymer than to an entangled linear polymer.

5.10.3 Storage and Loss Moduli of Model Branched Systems

Figure 5.16 shows the storage and loss moduli of two polyisoprenes, one linear and the other a four-arm star, having similar zero-shear viscosities. These data of Fetter et al. [67] show that for the star polymer, the storage modulus has a greatly extended transition from the “plateau” to the terminal zone and no clearly defined plateau, and a similar stretching out is observed in the loss modulus. As the arms continue to increase in length, the well-defined plateau and the maximum in the storage modulus are not present at all.

Gell et al. [69] looked carefully at the question of when a branch is long enough to have the effects described above. Using a laborious procedure, they prepared samples of poly(ethylene-*alt*-propylene) by hydrogenation of branched polyisoprene, followed by fractionation. The backbone molecular weights were all around 90,000 ($M/M_e \approx 40$), while those of the arms varied from 0 to 42,000. They found that when M_a/M_e was 0.5, the curves of the storage and loss moduli looked much like those for the linear polymer. But for the next longest arm ($M_a/M_e = 2.4$) the effects of the branches were quite obvious. The transition from the plateau to the terminal zone was broadened, and there were two maxima in the loss modulus data. The very small second maximum was associated with branch relaxation. At $M_a/M_e = 7.4$, there was a very broad maximum in G'' , and for $M_a/M_e = 18$, there was no maximum at all. Gell et al. showed master curves of all their data, but for the longer branches, modulus shifts much larger than those prescribed by the Rouse theory (Eq. 4.68) were necessary. And it is likely that a careful analysis of the master curves (e.g., use of linear vertical scale) would reveal that the superposition was not, in fact, very good for the systems with longer branches.

Struglinski et al. [71] and Watanabe et al. [72] studied blends of linear and star polymers and proposed empirical mixing rules for such systems, and Roovers et al. [73, 74] studied the rheology of stars with very large numbers of arms.

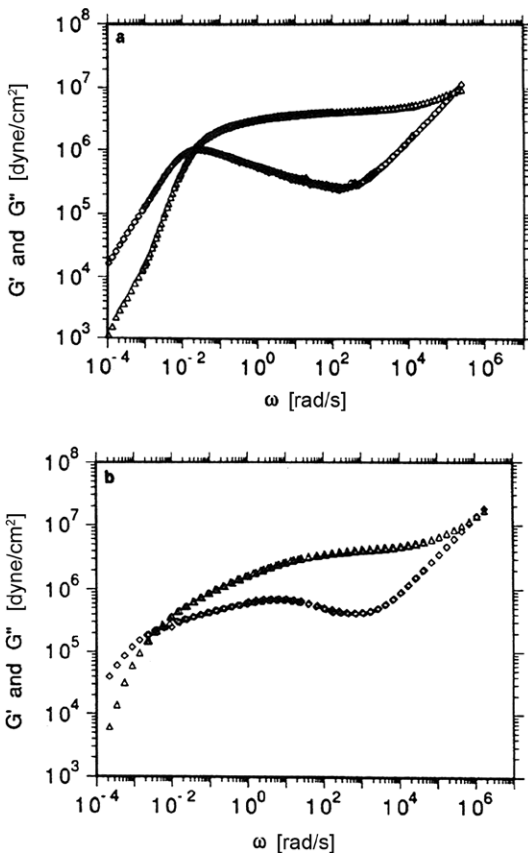


Figure 5.16 Storage and loss moduli for linear (a) and four-arm star (b) polyisoprenes having similar viscosities. There is no clear plateau for the star polymer, and the transition to the terminal zone is greatly lengthened. From Fetters et al. [67].

Comb polymers of several types have been studied, including H-shaped polymers [62], multi-armed combs [75], and “pom-pom” polymers [70] in which there are two branch points connected by a backbone, each having multiple arms. These features are shown in Fig. 5.17, which shows data of Roovers and Graessley [75] for a linear polystyrene with $M_w = 2.75 \cdot 10^5$ and for two 30-armed combs having the same backbone weight as the linear sample. Data for two arm lengths are shown. The storage moduli for all three polymers tend to merge at high frequencies, but the terminal zone is delayed to lower and lower frequencies as the arm length increases. The important feature of these polymers that accounts for the slow-down in terminal relaxation is the presence of at least one backbone segment that is trapped between two branch points. Substantial relaxation of this segment after a deformation cannot take place until sufficient time has passed for the free arms to achieve freedom of motion, and we have seen that this time increases exponentially with arm length.

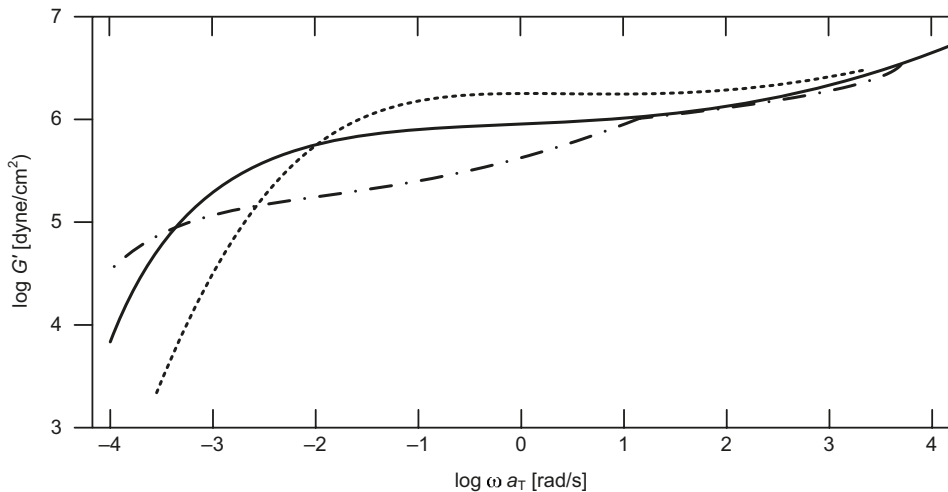


Figure 5.17 Storage moduli versus reduced frequency of a linear polystyrene ($M_w = 8.6 \cdot 10^5$) (dotted curve) and combs having 30 arms with $M_n = 4.7 \cdot 10^4$ (dashed line) and $1.8 \cdot 10^4$ (solid line). The backbone has the same M_w as the linear sample. The terminal zone is delayed to lower frequencies as the arm length increases. Two points of inflection indicate distinct relaxation mechanisms. From Roovers and Graessley [75].

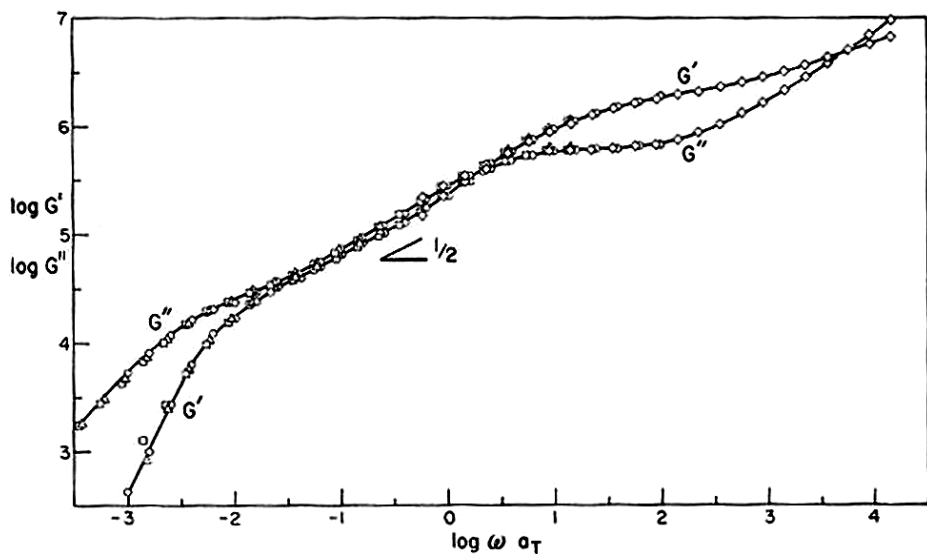


Figure 5.18 Storage and loss moduli versus reduced frequency of a polystyrene comb with a backbone $M_w = 2.75 \cdot 10^5$ and 30 arms with molecular weights of $M_n = 4.7 \cdot 10^4$. Note the substantial portions of both curves that have slopes of one-half on this log-log plot. From Roovers and Graessley [75].

There are two points of inflection in the plateau-terminal region implying that there are two distinct relaxation mechanisms. Figure 5.18 shows master curves for both moduli, and we see that there is a substantial range of reduced frequencies over which both moduli follow a “Rouse-like” relaxation with a one-half power dependency.

By grafting *macromonomers* onto a polymer backbone (see Section 3.4.1) a great variety of comb-like structures have been prepared and studied using rheometry. Bailly et al. [76] made combs (“bottle brushes”) having a 98% grafting density. They found that their plots of storage and loss moduli versus frequency followed power-law dependencies over five decades of frequency with an exponent of 0.6.

$$G' \propto G'' \propto \omega^{0.6} \quad (5.48)$$

The ratio of the two moduli, which is the tangent of the loss angle, was thus constant and equal to 1.43. They proposed two possible models to explain this observation. The first was based on the observation that this behavior is similar to that predicted by the Rouse theory for unentangled polymers, except that the power on the frequency in that theory is 0.5. The second model was inspired by noting that Eq. 5.48 is similar to the criterion proposed by Winter and Chambon [77] to describe a crosslinking system at its gel point. García-Franco et al. [78] reported this gel-like behavior for polyethylene containing low levels of long-chain branching, but over a much narrower range of frequencies.

Namba et al. [79] found that in bottle brushes with high branching levels, intermolecular chain entanglement was suppressed so that there was no plateau. However, Tsukahara et al. [80] reported that if the backbone is long enough, a weak plateau reappears. They found that the entanglement molecular weight, M_e , was very close to that for polystyrene, which was their backbone polymer and concluded that the branches promoted entanglement.

Houli et al. [81] made model “dumbbell” polymers by attaching multi-arm polybutadiene stars onto the ends of a polystyrene connector. If the connector made up less than 10% of the molecule, the behavior was star-like. Finally, we mention that Miros et al. [82] used short polyethylene chains as an “ideal solvent” for multi-arm stars.

5.10.4 Randomly Branched Polymers

Random branching always leads to a broad distribution of structures, making it difficult to distinguish between the effects of branching and polydispersity. In fact, Wood-Adams and Dealy [83] suggested that it should be possible, in principle, to prescribe the molecular weight distribution of a linear polymer that would have a complex viscosity similar to that of any given branched polymer.

Kasehagen and Macosko [84] studied randomly branched polybutadiene. While the precursor PBD was monodisperse, the crosslinker added to produce branching also introduced some polydispersity. Also, it was difficult to establish the precise branching structure on the basis of instrumental analysis. The resulting polymers, with weight percentages of branched material ranging from 5 to 39%, contained chains with one branch point, coupling two precursor chains together, as well as chains with two branch points, coupling three chains together. This was clearly indicated in elution curves for the material with the highest level of branching. The activation energy for viscosity did not depend on branching level, although this is definitely not the case for LDPE. The steady-state compliance, as calculated from the low-frequency value of $[G'/(G'')^2]$, was found to level out at high branching levels. There was a point of inflection in the storage modulus curve between the plateau and the terminal zones, suggesting an intermediate relaxation mechanism. At high frequencies, the $G'(\omega)$ curves for all the polymers merged, showing the expected independence of the branching structure, and the loss modulus had a well-defined maximum for all the samples.

The “constrained geometry catalysts” (CGC) described by Stevens [85] and by Lai et al. [86] constitute a particular class of metallocene, single-site catalysts that can produce polymers having simply described distributions of molecular weight and low levels of long-chain branching (see Section 3.9.2). Wood-Adams et al. [53] reported the rheological properties of a series of polyethylenes made using such a catalyst. The branching levels ranged from 0.01 to 0.08 branches per 1000 carbon atoms. The polydispersities were all very near to 2.0, and the molecular weights were in the neighborhood of 100,000. Wood-Adams and Costeux [54] studied the effect of comonomer on branched polymers of this type. They found that all the long-chain branched polymers were thermorheologically complex and that the activation energy based on the zero-shear viscosity was much higher for branched copolymers than for comparable branched homopolymers.

Torres et al. [87] discussed in detail the structure of a larger group of samples from the same family studied by Wood-Adams et al. [53]. They noted that as the number of branches increases the first branched structures to be formed are stars, followed by combs and then by tree-like molecules with branches on branches. Their plot of zero-shear viscosity versus λ , the number of branches per thousand carbons in the backbone, is shown in Fig. 5.19.

Auhl et al. [88] studied the behavior of a series of polypropylenes that had been subjected to various doses of electron beam radiation to introduce several levels of long-chain branching. The branching factor g of the resulting samples is shown in Fig. 5.20 as a function of radiation dose. Assuming little chain scission occurred, all these samples have about the same molecular weight as the linear precursor material. Thus the point for $d = 0$ corresponds to a branching factor of unity.

These data illustrate nicely the trend of increasing viscosity at low branching levels, reaching a peak and then decreasing and falling to values slightly below unity. Based on all the analytical and rheological data available for these samples, the authors concluded that at low radiation doses, the branched molecules were mainly stars, and the increase in viscosity was thus similar to that shown in Fig. 5.20, whereas the higher doses produced more tree-like structures.

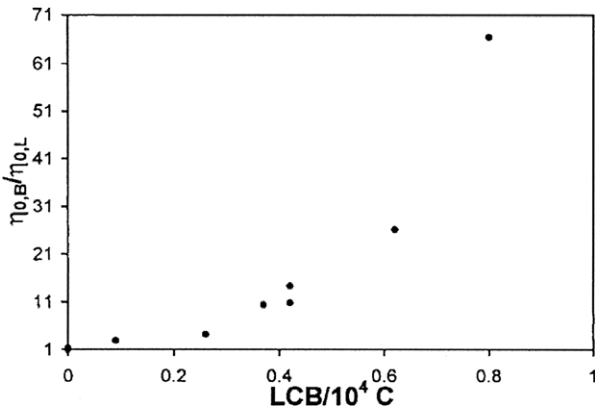


Figure 5.19 Ratio of zero-shear viscosities of branched and linear polyethylenes having the same M_w versus long-chain branching level (linear scales). Even a low level of branching has an important effect on the viscosity. From Torres et al. [87].

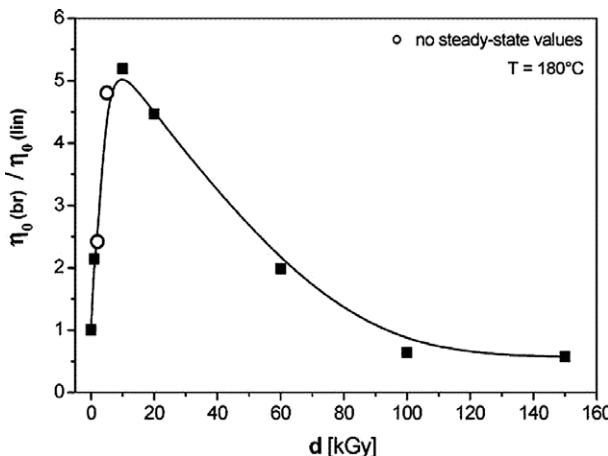


Figure 5.20 The branching factor g (based on η_0 rather than R_g) as a function of radiation dose for a series of polypropylenes subjected to electron beam radiation to introduce various levels of long-chain branching. Assuming little chain scission occurred, all these samples have the same molecular weight as the linear precursor material. Thus the point for $d = 0$ corresponds to a branching factor of unity. These data show the trend of increasing viscosity at low branching levels, reaching a peak and then decreasing and falling to values slightly below unity. From Auhl et al. [88].

5.10.5 Low-Density Polyethylene

The most important commercial branched polymer is LDPE. As was explained in Chapter 3, this polymer is made by high-pressure, free-radical polymerization and has a complex structure that is difficult to reproduce in any detail. The branching is random, and there is a broad range of branching structures, with many short arms as well as complex tree-like molecules. In addition, LDPE made in an autoclave has a distinctly different structure from that made in a tubular reactor. All are strongly shear thinning, and we will see in Chapter 10 that these polymers have a distinctive extensional flow behavior that is associated with long-chain branching rather than polydispersity.

Gabriel and Münstedt [89] compared three types of commercial polyethylene: HDPE, LLDPE, and LDPE. Their η_0 data for the linear materials, i.e., HDPE and LLDPE, fell on the line described by Eq. 5.4, which is repeated below as Eq. 5.49, with the α equal to about 3.4, except when there was a significant amount of unentangled polymer present in the sample.

$$\eta_0 = K M_w^\alpha \quad M_w \leq M_C \quad (5.49)$$

Deviations from this line are often taken to be evidence of long-chain branching, even when these have not been detected by analytical methods. Gabriel et al. [90], and Gabriel and Münstedt [90] found that metallocene polymers with very low levels of branching exhibited a significantly elevated zero-shear viscosity compared with linear polymer having the same molecular weight. Gabriel and Lilge [91] studied several LDPEs produced in the same tubular reactor having similar densities but varying in MFR (melt flow rate). They felt that their results provided evidence of a power-law dependence of viscosity on molecular weight, but these reveal the difficulty in trying to establish such relationships. In general even a modest level of long-chain branching in a well entangled randomly branched polymer causes a viscosity increase in comparison with a linear polymer with the same M_w . However, LDPE should not be looked upon as the result of carrying this trend to very high branching levels.

In fact, the idea of comparing zero-shear viscosities of LDPE with those of linear polyethylenes is questionable. First, the temperature dependence of η_0 is much stronger for LDPE than for HDPE, so changing the temperature will alter η_0 values of the two polymers by different amounts. And differences in temperature dependencies have even been reported for LDPEs made in different types of reactor. But the most serious issue that arises in comparing zero-shear viscosities of the two types of polyethylene is the establishment of a comparable value for molecular weight. The “conventional GPC” value ($\text{gpc-}M_w$) is obtained using an infrared detector and a calibration curve based on linear standards. This value is said to be a “backbone” M_w for any PE sample. On the other hand, the “absolute value” ($\text{abs-}M_w$) is obtained using a light scattering detector and includes the entire molecule: backbone, LCBs

and SCBs. It was noted above that short-chain branches like those in copolymers have a significant effect on η_0 in copolymers when there are no long branches. Furthermore, it is not possible to discern whether a change in viscosity is due simply to the increase in molecular weight or to entangled branches. Wang et al. [92] used both molecular weight values to correlate data for a number of LDPEs made in both types of reactor, and their plots are shown in Fig. 5.21 (top), using abs- M_w , and Fig. 5.21 (bottom), using gpc- M_w . First we note that some points move from one side of the linear PE line to the other when the M_w method is changed. Moreover, using the gpc- M_w results in a clearer trend, especially for the samples from a tubular reactor, for which there is some indication of an exponential dependence.

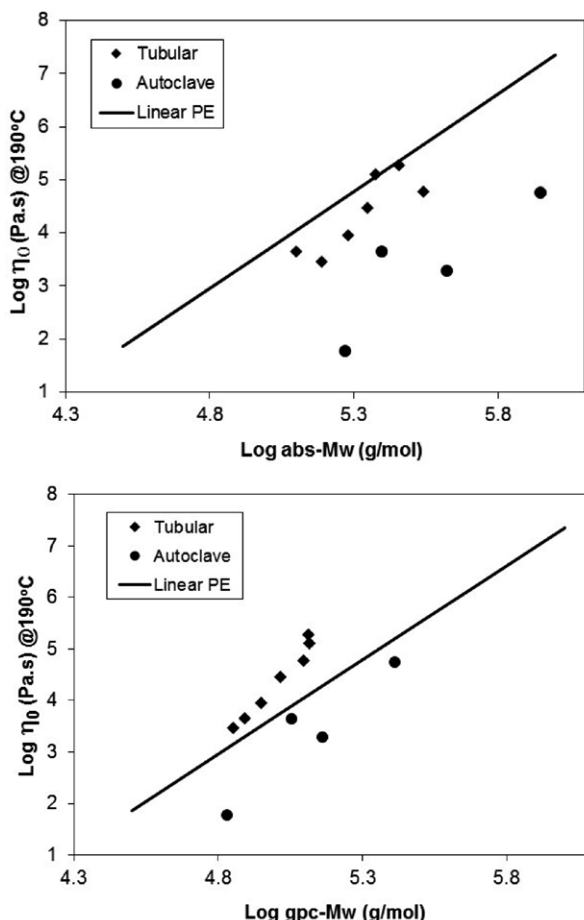


Figure 5.21 Zero -shear viscosity versus Mw of LDPEs made using from both tubular and autoclave reactors. Top: M_w is an “absolute” value determined using a light-scattering detector, which responds to the entire molecule. Bottom: M_w is based on the use of “conventional GPC” using an infrared detector based on linear standards and called a “backbone value.” From Wang et al. [92]

■ 5.11 Use of Linear Viscoelastic Data to Determine Branching Level

5.11.1 Introduction

The difficulty, and often impossibility, of determining the branching structure of a polymer arises from the complexities of possible branching structures that may be present. The quantities that must be determined to obtain a complete characterization of the branching structure of a given sample are as follows [93]:

- Functionality of branch points
- Length of branches
- Separation between branches on the backbone
- Number of branches per backbone
- Presence of branches on branches

Moreover, all of these parameters have distributions that may or not be correlated. As a result, it is not possible to determine the detailed branching structure of a sample of completely unknown structure by any combination of characterization techniques. If information about the structure can be provided *a priori*, for example by detailed modeling of the polymerization reaction, then something might be done. Therefore, a given correlation that relates measurable properties to branching level can only be valid for a specific type of structure. And the more that is known about the structure, the more precise will be the characterization.

For example, if we know that a sample consists entirely of monodisperse, symmetric, three-armed stars, then only the length of the arms is required to fully characterize the structure, and this can be easily accomplished, for example, by measuring the zero-shear viscosity. However, a more challenging objective is the determination of the branching structure of a commercial polymer, and this is currently an issue of intense interest because of the very strong effect of certain branching structures on the processing behavior of polyethylene and its copolymers. In such materials, the branching structure may be almost totally unknown, but rheology can still be used to detect the presence of small levels of branching even if the actual structure cannot be determined [94].

Wood-Adams and Dealy [95] examined the special case of lightly branched metallocene polyethylenes produced using one constrained geometry, single-site catalyst in a single reactor. They used a method for inferring the MWD of linear polymers from complex viscosity data (described in Chapter 8) to obtain a fictitious “viscosity MWD.” The presence of long-chain branches resulted in a shift in the location of the peak molecular weight with respect to its true position, as determined using GPC.

In addition, the viscosity MWD also had a secondary peak. They correlated the shift in the primary peak to the number of branch points per 1000 carbon atoms. He et al. [96] later provided a theoretical basis for this technique by combining a model of the polymerization process with a molecular model of the rheological behavior.

A technique for estimating the degree of branching in monodisperse model long-chain branched polymers inspired by predictions of tube models was described by Daniels et al. [97] and was later used to characterize the structure of commercial polyethylenes [98]. It is based on the observation that the effect of adding a solvent to a polymer on terminal zone behavior is quite sensitive to the presence of branch points. The basic idea is that while linear molecules relax primarily by reptation, branch points prevent reptation, and the limiting relaxation mechanism is the much slower fluctuation of arm length. Dilution reduces the relaxation times of the arms much more than it does those of the linear molecules. The technique is a laborious one requiring terminal zone rheological measurements on a series of samples of varying solvent concentration.

5.11.2 Correlations Based on the Zero-Shear Viscosity

Levels of long-chain branching as low as 0.1 branch per 1,000 carbon atoms can have an important effect on viscosity but are quite difficult to detect using non-rheological techniques. This makes it important to be able to detect such levels, and at the same time it provides a means for doing this. The zero-shear viscosity is particularly sensitive to large molecular structures and has been used along with molecular weight, in a number of empirical correlations [99–104].

It must be kept in mind, however, that it is often impossible to measure the true zero-shear viscosity of polymers with broad molecular weight distributions and/or long chain branching, and if a value is estimated by extrapolation it will seriously compromise the reliability of any correlation. Larson [105] compared several correlations based on η_0 and M_w with model predictions and concluded that "...the zero-shear viscosity of a branched melt is extremely sensitive not only to degree of branching but also to type" and that no single type of correlation could describe all branched systems. Vega et al. [106] evaluated several such correlations and concluded that a correlation for number of branches based on a few rheological and molecular parameters is at best approximately valid for one specific type of branching structure. Using viscosity to characterize branching in LDPE is especially problematic, as is discussed in Section 5.10.5.

■ 5.12 Summary

The linear behavior of well-entangled melts is very sensitive to molecular structure. The threshold for entanglement usually occurs when M_w exceeds the molecular weight between entanglements M_e , which can be estimated from data for a monodisperse polymer whose molecular weight is much larger than M_e . One example of the dramatic effects of entanglement is the change in the dependency of the zero-shear viscosity on molecular weight from a linear proportionality to one involving the molecular weight raised to a power often around 3.5. This occurs at a critical molecular weight M_c . This relationship appears to be valid for polydisperse materials if M_w is used as the independent variable.

For a monodisperse sample, entanglement manifests itself in a prominent plateau in the relaxation and storage moduli and a pronounced minimum in the loss modulus. The plateau is virtually identical to the one observed when a cross-linked elastomer approaches its equilibrium modulus at long times, and this explains why a high molecular weight melt can respond like a rubber to a deformation of short duration. In polydisperse samples, these features are not so clearly exhibited, but the presence of high molecular weight components still results in a delay of the final stage of relaxation to longer times. The accurate determination of the plateau modulus G_N^0 is not straightforward, particularly in case of samples that are not monodisperse, and a number of techniques have been proposed to estimate this important quantity. The molecular weight between entanglements M_e , defined in terms of G_N^0 , plays a key role in molecular models of melt behavior. Techniques for predicting the value of M_e , and thus of G_N^0 , have been proposed, and a parameter of importance in this regard is the packing length p . The creep compliance of monodisperse samples changes from a linear dependence on molecular weight to being constant at a molecular weight M_c' .

Short side branches, such as those introduced by copolymerizing an α -olefin with ethylene, have only a modest effect on rheological behavior, but long chain branches have very profound effects. These include strong influences on the zero-shear viscosity, the steady-state compliance, and the shapes of the curves of storage and loss moduli. However, in order to determine the values of branching parameters, it is necessary to know the type of the branching present, e.g., stars, combs, etc. A fairly good characterization of branching in randomly branched systems is possible when the branching structure has been established by modeling the polymerization or branching reaction. For example, there has been much progress in establishing the detailed branching structure in branched polyethylenes made by use of a constrained geometry catalyst. Low-density polyethylene, however, poses a major challenge because of the complexity of its branching structure. While lightly branched polyolefins such as those made using constrained geometry catalysts have zero-shear

viscosities that are somewhat higher than those of linear material having the same molecular weight, the highly branched LDPEs have zero-shear viscosities that are often well below linear polymer with the same M_w .

Several techniques have been proposed to estimate the level of long-chain branching in randomly branched polymers, but these are only useful within given families of closely related materials.

■ References

- [1] Graessley, W.W. Some phenomenological consequences of the Doi-Edwards theory of viscoelasticity. *J. Polym. Sci., Polym. Phys. Ed.* (1980) 18, pp. 27–34
- [2] Berry, G.C., Fox, T.G. The viscosity of polymers and their concentrated solutions. *Adv. Polym. Sci.* (1968) 5, pp. 261–357
- [3] van Meerveld, J. A method to extract the monomeric friction coefficient from the linear viscoelastic behaviour of linear, entangled polymer melts. *Rheol. Acta* (2004) 43, pp. 615–623
- [4] Kreer, T., Baschnagel, J., Muller, M., Binder, K. Monte Carlo simulation of long chain polymer melts: crossover from Rouse to reptation dynamics. *Macromol.* (2001) 34, pp. 1105–1117
- [5] Harmandaris, V.A., Mavrillas, V.G., Theodorou, D.N., Kröger, M., Ramírez, J., Öttinger, H.C., Vlassopoulos, D. Crossover from the Rouse to the entangled polymer melt regime: Signals from long, detailed atomistic molecular dynamics simulations, supported by rheological experiments. *Macromol.* (2003) 36, pp. 1376–1387
- [6] Colby, R.H., Fetters, L.J., Graessley, W.W. Melt viscosity-molecular weight relationship for linear polymers. *Macromol.* (1987) 20, pp. 2226–2237
- [7] Fetters, L.J., Lohse, D.J., Milner, S.T., Graessley, W.W. Packing length influence in linear polymer melts on the entanglement, critical and reptation molecular weights. *Macromol.* (1999) 32, pp. 6847–6851
- [8] Vega, J.F., Rastogi, S., Peters, G.W.M., Meijer, H.E.H. Rheology and reptation of linear polymers. Ultrahigh molecular weight chain dynamics in the melt. *J. Rheol.* (2004) 48, pp. 663–678
- [9] Sen, S., Kumar, S.K., Kebinski, P. Viscoelastic properties of polymer melts from equilibrium molecular dynamics simulations. *Macromol.* (2005) 38, pp. 650–653
- [10] Zang, Y.H., Muller, R., Froelich, D. Influence of molecular weight distribution on viscoelastic constants of polymer melts in the terminal zone. New blending law and comparison with experimental data. *Polymer* (1987) 28, pp. 1577–1582
- [11] Struglinski, M.J., Graessley, W.W. Effects of polydispersity on the linear viscoelastic properties of entangled polymers, 1. Experimental observations for binary mixtures of linear polybutadiene. *Macromol.* (1985) 18, pp. 2630–2643

- [12] Wood-Adams, P.M., Dealy, J.M., deGroot, A.W., Redwine, O.D. Effect of molecular structure on the linear viscoelastic behavior of polyethylene. *Macromol.* (2000) 33, pp. 7489–7499
- [13] Gabriel, C., Münstedt, H. Influence of long-chain branches in polyethylenes on linear viscoelastic flow properties in shear. *Rheol. Acta* (2002) 41, pp. 232–244
- [14] Wasserman, S.H., Graessley, W.W. Effects of polydispersity on linear viscoelasticity in entangled polymer melts. *J. Rheol.* (1992) 36, pp. 543–572
- [15] Stadler, F.J. et al. Dependence of the zero shear-rate viscosity and the viscosity function of linear high-density polyethylenes on the mass-average molar mass and polydispersity. *Rheol. Acta* (2006) 45, pp. 755–764
- [16] Ansari, M., Hatzikiriakos, S.G., Sukhadia, A.M., Rohlfing, D.C. Rheology of Ziegler-Natta and metallocene high-density polyethylenes: broad molecular weight distribution effects. *Rheol. Acta* (2011) 50, pp. 17–27
- [17] Vega, J.F., Otegui, J., Ramos, J., Martinez-Salazar, J. Effect of molecular weight distribution on Newtonian viscosity of linear polyethylene. *Rheol. Acta* (2012) 51, pp. 81–87
- [18] Plazek, D.J. The temperature dependence of the viscoelastic behavior of poly(vinyl acetate). *Polym. J.* (1980) 12, pp. 43–53
- [19] Wang, S., Wang, S.Q., Halasa, A., Hsu, W.L. Relaxation dynamics in mixtures of long and short chains: Tube dilation and impeded curvilinear diffusion. *Macromol.* (2003) 36, pp. 5355–5371
- [20] Gabriel, C., Münstedt, H. Creep recovery behavior of metallocene linear low-density polyethylenes. *Rheol. Acta* (1999) 38, pp. 393–403
- [21] Gabriel, C., Kaschta, J., Münstedt, H. Influence of molecular structure on rheological properties of polyethylenes. I. Creep recovery measurements in shear. *Rheol. Acta* (1998) 37, pp. 7–20
- [22] Fuchs, K., Friedrich, Chr., Weese, J. Viscoelastic properties of narrow-distribution poly(methyl methacrylates). *Macromol.* (1996) 29, pp. 5893–5901
- [23] Graessley, W.W. Linear viscoelasticity in entangled polymer systems. *J. Chem. Phys.* (1971) 54, pp. 5143–5157
- [24] Montfort, J.P., Marin, G., Arman, J., Monge, Ph. Blending law for binary blends of fractions of linear polystyrene. *Polymer* (1979) 19, pp. 277–284
- [25] Ferry, J.D. *Viscoelastic Properties of Polymers*, 3rd ed. (1980) John Wiley & Sons, New York
- [26] Liu, C., He, J., van Ruymbeke, E., Keunings, R., Bailly, C. Evaluation of different methods for the determination of the plateau modulus and the entanglement molecular weight. *Polymer* (2006) 47 pp. 4461–4479
- [27] Wu, S. Chain structure and entanglement. *J. Polym. Sci., Part B: Polym. Phys.* (1989) 27, pp. 723–741
- [28] Raju, V.R., Smith, G.C., Marin, G., Knox, J.R., Graessley, W.W. Properties of amorphous and crystalline hydrocarbon polymers. I. Melt rheology of fractions of linear polyethylene. *J. Polym. Sci., Polym. Phys. Ed.* (1979) 17, pp. 1183–1195

- [29] Fetters, L.J., Lohse, D.J., Richter, D., Witten, T.A., Zirkel, A. Connection between polymer molecular weight, density, chain dimensions, and melt viscoelastic properties. *Macromol.* (1994) 27, pp. 4639–4647
- [30] Fetters, L.J., Lohse, D.J., Colby, R.H. Chain dimensions and entanglement spacings. In *Physical Properties of Polymers Handbook*, Mark, J.E. (Ed.) (2007) Springer-Verlag, New York, Berlin
- [31] Carella, J.M., Graessley, W.W., Fetters, L.J. Effects of chain microstructure on the viscoelastic properties of linear polymer melts: Polybutadienes and hydrogenated polybutadienes. *Macromol.* (1984) 17, pp. 2775–4647
- [32] Fetters, L.J., Lohse, D.J., García-Franco, C.A., Brant, P., Richter, D. Prediction of melt state poly (α -olefin) rheological properties: The unsuspected role of the average molecular weight per backbone bond. *Macromol.* (2002) 35, pp. 10096–10101
- [33] Liu, C., Yu, J., He, J., Wei, L., Sun, C., Jing, Z. A reexamination of G_N^0 and M_e of syndiotactic polypropylenes with metallocene catalysts. *Macromol.* (2004) 37, pp. 9279–9282
- [34] Huang, C.-L., Chen, Y.-C., Hsiao, T.-L., Tsai, J.-C., Wang, C. Effect of tacticity on viscoelastic properties of polystyrene. *Macromol.* (2011) 44, pp. 6155–6161
- [35] Ahmad, N., Di Grolamo, R., Auriemma, F., De Rosa, C., Grizzuti, N., Relations between stereoregularity and melt viscosity of syndiotactic polypropylene. *Macromol.* (2013) 46, pp. 7940–7946
- [36] Larson, R.G., Sridhar, T., Leal, L.G., McKinley, G.H., Likhtman, A.E., McLeish, T.C.B. Definitions of entanglement spacing and time constants in the tube model. *J. Rheol.* (2003) 47, pp. 809–818
- [37] Brochard, F., deGennes, P.G. Dynamic scaling for polymers in theta solvents. *Macromol.* (1977) 10, pp. 1157–1161
- [38] Colby, R.H., Rubinstein, M. Two-parameter scaling for polymers in θ solvents. *Macromol.* (1990) 23, pp. 2753–2757
- [39] deGennes, P.G. Dynamics of entangled polymer solutions, parts I and II. *Macromol.* (1976) 9, pp. 587–598
- [40] Wolkowicz, R.I., Forsman, W.C. Entanglement in concentrated solutions of polystyrene with narrow distribution of molecular weight. *Macromol.* (1971) 4, pp. 184–192
- [41] Heymans, N. A novel look at models for polymer entanglement. *Macromol.* (2000) 33, pp. 4226–4234
- [42] Edwards, S.F. The statistical mechanics of polymerized material. *Proc. Phys. Sci.* (1967) 92, pp. 9–16
- [43] Colby, R.H., Rubinstein, M., Viovy, J.-L. Chain entanglements in polymer melts. *Macromol.* (1992) 25, pp. 996–998
- [44] Wool, R.P. Polymer entanglements. *Macromol.* (1993) 26, pp. 1564–1569
- [45] Richter, D., Farago, B., Butera, R., Fetters, L.J., Huang, J.S., Ewen, B. On the origins of entanglement constraints. *Macromol.* (1993) 26, pp. 795–804
- [46] Witten, T.A., Milner, S.T., Wang, Z.-G. Theory of stress distribution in block copolymer microdomains. In *Multiphase Macromolecular Systems*, Culbertson, B.M. (Ed.) (1989) Plenum Press

- [47] Fetters, L.J., Lohse, D.J., Graessley, W.W. Chain dimensions and entanglement spacings in dense macromolecular systems. *J. Polym. Sci., Part B: Polym. Phys.* (1999) 37, pp. 1023–1033
- [48] Krishnamoorti, R., Graessley, W.W., Zirkel, A., Richter, D., Hadjichristidis, N., Fetters, L.J., Lohse, D.J. Melt-state polymer chain dimensions as a function of temperature. *J. Polym. Sci., Part B: Polym. Phys.* (2002) 40, pp. 1768–1776
- [49] Graessley, W.W., Edwards, S.F. Entanglement interactions in polymers and the chain contour concentration. *Polymer* (1981) 22, pp. 1329–1334
- [50] Osaki, K., Inoue, T., Uematsu, T., Yamashita, Y. Evaluation methods of the longest Rouse relaxation time of an entangled polymer in dilute solution. *J. Polym. Sci., Part B: Polym. Phys.* (2001) 39, pp. 1704–1712
- [51] Byutner, O., Smith, G.D. Prediction of the linear viscoelastic shear modulus of an entangled polybutadiene melt from simulation and theory. *Macromol.* (2001) 34, pp. 134–139
- [52] Wardhaugh, L.T., Williams, M.C. Blockiness of olefin copolymers and possible microphase separation in the melt. *Polym. Eng. Sci.* (1995) 35, pp. 18–27
- [53] Wood-Adams, P., Dealy, J.M., deGroot, A.W., Redwine, O.D. Rheological properties of metallocene polyethylenes. *Macromol.* (2000) 33, pp. 7489–7499
- [54] Wood-Adams, P., Costeux, S. Thermorheological behavior of polyethylene: Effects of microstructure and long chain branching. *Macromol.* (2001) 34, pp. 6281–6290
- [55] Garcia-Franco, C.A., Harrington, B.A., Lohse, D.J. Effect of short-chain branching on the rheology of polyolefins. *Macromol.* (2006) 39, pp. 2710–2717
- [56] Ye, Z., Zhu, S. Newtonian flow behavior of hyperbranched high-molecular-weight polyethylenes. *Macromol.* (2003) 36, pp. 2194–2197
- [57] Rochefort, W.E., Smith, G.G., Rachapudy, H., Raju, V.R., Graessley, W.W. Properties of amorphous and crystallizable hydrocarbon polymers. II. Rheology of linear and star-branched polybutadiene. *J. Polym. Sci., Polym. Phys. Ed.* (1979) 17, pp. 1179–1210
- [58] Raju, V.R., Rachapudy, H., Graessley, W.W. Properties of amorphous and crystallizable hydrocarbon polymers. IV. Melt rheology of linear and star-branched hydrogenated polybutadiene. *J. Polym. Sci., Polym. Phys. Ed.* (1979) 17, pp. 1223–1235
- [59] Bueche, F. Viscosity of molten branched polymers and their concentrated solutions. *J. Chem. Phys.* (1964) 40, pp. 484–487
- [60] Ham, J.S. Viscosity theory of branched and cross-linked polymers. *J. Chem. Phys.* (1957) 26, pp. 625–637
- [61] Zimm, B.H., Stockmayer, W.H. The dimensions of chain molecules containing branches and rings. *J. Chem. Phys.* (1949) 17, pp. 1301–1314
- [62] Roovers, J. Melt rheology of H-shaped polystyrenes. *Macromol.* (1984) 17, pp. 1196–1200
- [63] Kraus, G., Gruver, J.T. Rheological properties of multichain polybutadienes. *J. Polym. Sci., Part A: Gen. Pap.* (1965) 3, pp. 105–122
- [64] Graessley, W.W., Roovers, J. Melt Rheology of four-arm and six-arm star polystyrenes. *Macromol.* (1979) 12, pp. 959–965

- [65] Pearson, D.S., Helfand, E. Viscoelastic properties of star-shaped polymers. *Macromol.* (1984) 17, pp. 888–895
- [66] Ball, R.C., McLeish, T.C.B. Dynamic dilution and the viscosity of star polymer melts. *Macromol.* (1989) 22, pp. 1911–1913
- [67] Fetters, L.J., Kiss, A.D., Pearson, D.S., Quack, G.F., Vitus, F.J. Rheological behavior of star-shaped polymers. *Macromol.* (1993) 26, pp. 647–654
- [68] Ngai, K.L., Roland, C.M. Terminal relaxation and diffusion of entangled three-arm star polymers: Temperature and molecular weight dependencies. *J. Polym. Sci., Part B: Polym. Phys.* (1997) 35, pp. 2503–2510
- [69] Gell, C.B., Graessley, W.W., Efstratiadis, V., Pitsikalis, M., Kadjichristidis, N. Viscoelasticity and self-diffusion in melts of entangled asymmetric star polymers. *J. Polym. Sci., Part B: Polym. Phys.* (1997) 35, pp. 1943–1954
- [70] Archer, L.A., Varshney, S.K. Synthesis and relaxation dynamics of multiarm polybutadiene melts. *Macromol.* (1998) 31, pp. 6348–6355
- [71] Struglinski, M.J., Graessley, W.W., Fetters, L.J. Effects of polydispersity on the linear viscoelastic properties of entangled polymers. 3. Experimental observations on binary mixtures of linear and star polybutadienes. *Macromol.* (1988) 21, pp. 781–789
- [72] Watanabe, H., Ykoshida, H., Kotaka T. Enganglement in blends of monodisperse star and linear polystyrenes. 1. dilute blends. *Macromol.* (1988) 21, pp. 2175–2184
- [73] Roovers, J. Melt rheology of highly branched polymers. *J. Non-Cryst. Solids* (1991) 131–133, pp. 793–798
- [74] Pakula, T., Vlassopoulos, D., Fytas, G., Roovers, J. Structure and dynamics of melts with multiarm polymer stars. *Macromol.* (1998) 31, pp. 8931–8940
- [75] Roovers, J., Graessley, W.W. Melt rheology of some model comb polystyrenes. *Macromol.* (1981) 14, pp. 766–773
- [76] Bailly, C., Stephaenne, V., Muchtar, Z., Schappacher, M., Deffieux, A. Linear viscoelastic behavior of densely grafted poly(chloroethyl vinyl ether)-g-polystyrene combs in the melt. *J. Rheol.* (2003) 47, pp. 821–827
- [77] Winter, H.H., Chambon, F. Analysis of linear viscoelasticity of a crosslinking polymer at the gel point. *J. Rheol.* (1986) 30, pp. 367–382
- [78] García-Franco, C.A., Srinivas, S., Lohse, D.J., Brant, P. Similarities between gelation on long chain branching viscoelastic behavior. *Macromol.* (2001) 34, pp. 3115–3117
- [79] Namba, S., Tsukahara, Y., Kaeriyama, K., Okamoto, K., Takahashi, M. Bulk properties of multibranched polystyrenes from polystyrene macromomers: rheological behavior I. *Polymer* (2000) 41, pp. 5165–5171
- [80] Tsukahara, Y., Namba, S., Isawa, J., Nakano, Y., Kaerigama, K., Takahashi, M. Bulk properties of polymacromonomers of increased backbone and branch lengths. *Macromol.* (2001) 34, pp. 2624–2629
- [81] Houli, S., Iatrou, H., Hadjichristidis, N., Vlassopoulos, D. Synthesis and viscoelastic properties of model dumbbell copolymers consisting of a polystyrene connector and two 32-arm star butadienes. *Macromol.* (2002) 35, pp. 6592–6597

- [82] Miros, A., Vlassopoulos, D., Likhtman, A.E., Roovers, J. Linear rheology of multiarm star polymers diluted with short linear chains. *J. Rheol.* (2003) 47, pp. 163–176
- [83] Wood-Adams, P., Dealy, J.M. Using rheology to determine the branching level in metallocene polyethylenes. *Macromol.* (2000) 33, pp. 7481–7488
- [84] Kasehagen, L.J., Macosko, C.W. Rheology of long-chain randomly branched polybutadiene. *J. Rheol.* (1996) 40, pp. 680–709
- [85] Stevens, J. *Stud. Surf. Sci. Catal.* (1994) 89, p. 277; (1996) 101, p. 11
- [86] Lai, S.Y., Wilson, J.R., Knight, J.R., Stevens, G.W. Elastic substantially linear olefin polymers. US Patent 5,272,236 (1993)
- [87] Torres, E., Li, S-W., Costeux, S., Dealy, J.M. Branching structure and strain hardening of branched metallocene polyethylenes. *J. Rheol.* (2015) 59, pp. 1151–1172
- [88] Auhl, D., Stange, J., Münstedt, H., Krause, B., Voigt, D., Lederer, A., Lappan, U., Lunkwitz, K. Long-chain branched polypropylenes by electron beam irradiation and their rheological properties. *Macromol.* (2004) 37, pp. 9465–9472
- [89] Gabriel, C., Münstedt, H. Strain hardening of various polyolefins in uniaxial elongational flow. *J. Rheol.* (2003) 47, pp. 619–630
- [90] Gabriel, C., Kokko, E., Löfgren, B., Seppälä, J., Münstedt, H. Analytical and rheological characterization of long-chain branched metallocene-catalyzed ethylene homopolymers. *Polymer* (2003) 43, pp. 6383–6390
- [91] Gabriel, C., Lilge, D. Molecular mass dependence of the zero shear-rate viscosity of LDPE melts: Evidence of an exponential behavior. *Rheol. Acta* (2006) 45, pp. 995–1002
- [92] Wang, J., Mangnus, M., Yau, W., deGroot, W., Karjala, T., Demirors, M. Structure–property relationships of LDPE. Soc. Plast. Engrs., ANTEC (2008), p. 878
- [93] Lohse, D.J., Milner, S.T., Fetter, L.J., Xenidou, M., Hadjichristidis, N., Mendelson, R.A., Garcia-Franco, C.A., Lyon, M.K. Well-defined, model long chain branched polyethylene. 2 Melt rheological behavior. *Macromol.* (2002) 35, pp. 3066–3075
- [94] Vega, J.F., Santamaria, A., Munoz-Escalona, A., Lafuente, P. Small-amplitude oscillatory shear measurements as a tool to detect very low amounts of long chain branching in polyethylenes. *Macromol.* (1998) 31, pp. 3639–3647
- [95] Wood-Adams, P.M., Dealy, J.M. Using rheological data to determine the branching level in metallocene polyethylenes. *Macromol.* (2000) 33, 7481–7488
- [96] He, C., Costeux, S., Wood-Adams, P. A technique to infer structural information for low level long chain branched polyethylenes. *Polymer* (2004) 45, pp. 3747–3754
- [97] Daniels, D.R., McLeish, T.C.B., Kant, R., Crosby, B.J., Young, R.N., Pryke, A., Allgaier, J., Hawkins, R.J., Groves, D.J. Linear rheology of diluted linear, star and model long chain branched polymer melts. *Rheol. Acta* (2001) 40, pp. 403–415
- [98] Crosby, B.J., Mangnus, M., deGroot, W., Daniels, R. McLeish, T.C.B. Characterization of long chain branching: Dilution rheology of industrial polyethylenes. *J. Rheol.* (2003) 46, pp. 401–426
- [99] Lusignan, C.P., Mourey, T.H., Wilson, R.H., Colby, R.H. Viscoelasticity of randomly branched polymers in vulcanization class. *Phys. Rev. E* (1998) 60, pp. 5657–5669

- [100] Janzen, J., Colby, R.H. Diagnosing long-chain branching in polyethylenes. *J. Mol. Struct.* (1999) 485/486, pp. 569–583
- [101] Shroff, R.N., Mavridis, H. Long-chain branching index for essentially linear polyethylenes. *Macromol.* (1999) 32, pp. 8454–8464
- [102] Shroff, R.N., Mavridis, H. Assessment of NMR and rheology for the characterization of LCB in essentially linear polyethylenes. *Macromol.* (2001) 34, pp. 7362–7367
- [103] Robertson, C.G., García-Franco, C.A., Srinivas, S. Extent of branching from linear viscoelasticity of long-chain branched polymers. *J. Polym. Sci., Part B: Polym. Phys.* (2004) 42, pp. 1671–1684
- [104] Tsenoglou, C.J., Gotsis, A.D. Rheological characterization of long chain branching in a melt of evolving molecular architecture. *Macromol.* (2001) 34, pp. 4685–4687
- [105] Larson, L.G. Combinatorial rheology of branched polymer melts. *Macromol.* (2001) 34, pp. 4556–4571
- [106] Vega, J., Aguilar, M., Peon, J., Pastor, D., Martinez-Salazar, J. Effect of long-chain branching on linear viscoelastic melt properties of polyolefins. *E-Polymers* (2002) No. 046

6

Tube Models for Linear Polymers—Fundamentals

■ 6.1 Introduction

The polymer industry has found two practical uses for polymer melt rheology. The first is to characterize molecular structure, e.g., the molecular weight distribution (MWD) and the long-chain branching (LCB) structure. The second is to characterize the processing behavior of the melt. When used to characterize structure, melt rheology can supplement (or even replace) GPC, NMR, light scattering, and other probes of molecular weight distribution and branching structure. When used to characterize processability, rheological measurements can predict how readily a given melt can be shaped into the desired product. These two uses of rheology are synergistic; if rheology can be used both to predict the processability of a melt having a given MWD and branching structure and to determine the MWD and LCB of that polymer, then one can both inform the polymer chemist what polymer structure they should try to make, and determine whether they have succeeded in making that structure, all using rheological methods.

In using rheology as an analytical tool, one wishes to use simple rheological measurements that provide information about molecular structure without the need to invert complicated integral equations. Measurements of linear viscoelastic properties using oscillatory shear (see Section 4.3.1) are usually used for this purpose. To interpret the data, one needs a quantitative molecular theory that can relate the rheological properties of a polymer to its molecular structure. In this chapter, we will describe the basic mechanisms of relaxation that have been found to be most essential in developing models capable of predicting the linear viscoelastic properties of commercial *linear* polymers, i.e., those that lack long-chain branching. The chapter starts with a presentation of a model for unentangled polymers and concludes with a presentation of the *double reptation* scheme for the computation of linear viscoelastic properties of a polymer melt from its molecular weight distribution.

If a rheological theory is truly predictive, then, in principle, the process can be inverted; i.e., given the rheological properties, one can determine the MWD and LCB structure. This use of rheology, called analytical rheology, has already proven useful

for inferring the MWD from the linear viscoelasticity of strictly linear polymers with no LCB. Methods for doing this (some based on the double reptation concept), and a summary of their strengths and weaknesses, are discussed in Chapter 8.

In general, there are multiple relaxation processes in polymers, many of which are much too complex to be described by simple rheological theories (such as the double reptation model presented next), and it is not our objective to describe all such processes in detail. The interested reader can find the details in the book by Doi and Edwards [1], and in the review articles by Watanabe [2] and McLeish [3]. Nevertheless, in Chapter 9 we will present some advanced theories for the linear rheology of polymer melts, developed initially by McLeish, Milner, and coworkers, which include all the known important mechanisms of polymer relaxation. Using such theories, substantial progress has been made for regular branched structures, such as monodisperse stars, H-shaped polymers, more complex combs, and to some extent, mixtures of these with linear polymers. We will proceed to describe how these theories may be combined into computational schemes for monodisperse and polydisperse linear and branched polymers, as well as mixtures of branched and linear polymers. We will demonstrate that (while such studies are in their infancy) these computational schemes are able to make quantitative predictions for more irregularly branched polymers that are typical of some commercial polyolefins. A major current goal is the ability not only to predict the rheology of commercial branched polyolefins, but also to invert rheological data to obtain information on branching structure from viscoelastic data.

When rheology is to be used to predict detailed processing behavior, it is necessary to have a model that can predict the response to complex, multidimensional, time-dependent flows that involve both shear and extension. What is needed for this is a *constitutive equation* capable of predicting nonlinear viscoelastic stresses in arbitrary flows, where the parameters of the constitutive equation can be determined from the molecular structure, i.e., from the MWD and LCB characteristics. The development of a reliable, accurate, nonlinear, viscoelastic constitutive equation that can account for all the effects of both MWD and LCB in complex processing flows is a tall order, to put it mildly. We are not yet at the stage where such molecular constitutive equations can be used routinely in the polymer industry for practical prediction of melt processing. Nevertheless, progress is being made. Detailed molecular models are available to predict nonlinear flow of monodisperse and bidisperse linear polymers (though a full theory for polydisperse linear polymers is still lacking). Also, a good number of simplified, phenomenological models exist, permitting prediction of complex processing flows once model parameters have been fixed by fitting to viscometric data. Finally, encouraged by the success of computational schemes for linear viscoelastic prediction, researchers are beginning to propose similar schemes to predict the nonlinear viscoelastic response of industrial resins based on molecular details such

as MWD and LCB content (though such work is still in its infancy). In Chapter 11, the reader will be apprised of recent progress on these fronts in the development of theories of the nonlinear viscoelastic behavior of polymers. Our principal concern is the relationship between rheological behavior and molecular structure in highly entangled polymers. Thus, the fast, localized molecular motions that dominate the behavior of unentangled systems, such as very dilute solutions and low molecular weight melts, are not of primary interest to us. However, the Brownian motion that every element of a molecule is constantly undergoing is ultimately the cause of all molecular motion in the absence of flow, and some key parameters that arise in the modeling of the dynamics of unentangled polymers will be found to carry through into models of entangled ones. Thus, we begin our treatment of polymer dynamics with a summary of a theory for unentangled polymers.

■ 6.2 The Rouse-Bueche Model for Unentangled Polymers

6.2.1 Introduction

If one attempts to model the dynamics of a single long polymer molecule in a very dilute solution starting from an atomically detailed picture of the molecule, the task rapidly becomes impossibly complicated because of the number of bonds that must be taken into account and the limitations on the motion of the backbone bonds with respect to each other. Fortunately, it is possible to achieve a drastic simplification of the problem if we are not interested in the very short-range motions that are responsible for the initial, very fast stages of relaxation after the imposition of a deformation on the system. In modeling the slower dynamics of a polymer molecule in a dilute solution, many useful results have been derived by use of a model in which the molecule consists of a number of *submolecules*, each containing enough backbone bonds that it behaves like a freely-jointed, Gaussian chain. We saw in Chapter 2 that about ten backbone bonds are required to form a unit that acts like the single link in a freely-jointed chain, so a submolecule must contain many such units.

How many monomer units are required to form a submolecule? It is not necessary to select a specific number of monomer units, but it must be large enough so that there are enough degrees of freedom within the submolecule so that it behaves like a Gaussian chain. It is possible to calculate the minimum length of a submolecule that would allow it to be represented by a freely-jointed chain, and for typical, flexible synthetic polymers this corresponds to about 100 chemical bonds or 100 backbone atoms. On the other hand, a description of the whole molecule sufficiently detailed

for our purposes requires that it contain many submolecules, and hence the size of the submolecule cannot approach that of the entire macromolecule. It follows that this coarse-grained model of a polymer molecule involving submolecules is only appropriate for long molecules containing at least many hundreds of bonds.

The freely-jointed chain picture is used in the next section as the basis for a model for the viscoelastic behavior of a dilute solution. It is important to keep in mind, however, that we cannot expect the model to describe the very short-time behavior involving short-range interactions between segments of the molecule that are within a submolecule, as these are not accounted for in this coarse-grained picture.

6.2.2 The Rouse Model for the Viscoelasticity of a Dilute Polymer Solution

In the Rouse model of the dynamics of a polymer molecule in a dilute solution [4], the mass of a submolecule is assumed to be concentrated in a bead at its center, and the N beads making up the model chain are attached to each other by $N-1$ springs. The elasticity of the submolecule, and thus of the molecule, is an entropic effect that arises from Brownian motion, and thermodynamic arguments show that for small or modest molecular extensions, the spring force should be proportional to kT times the extension, where k is Boltzmann's constant. In the Rouse model, the molecule can be stretched indefinitely, and this reminds us that the Gaussian chain model is only valid when the total extension of the molecule is not too large, i.e., when R (the root-mean-square end-to-end distance) is less than about 0.3 $n l$, where n is the number of backbone bonds, and l is the length of a single backbone bond.

In the Rouse model, the drag force exerted on a bead as it moves through the solvent is assumed to be given by Stokes' equation for the drag on a rigid sphere moving through a Newtonian fluid. This drag force is modeled in terms of a monomeric friction coefficient, ζ_0 , which is the drag force per monomer unit divided by the velocity of the solvent relative to that of the monomer unit and has SI units of kg/s. The subscript zero on the friction coefficient indicates that it applies to a dilute solution in its theta state, i.e., that there are interactions between the polymer and the solvent that cancel out the interactions between the polymer and itself, so that the conformation of the polymer molecule is a random flight, unaffected by these interactions. We note that the definition of ζ_0 used by Berry and Fox in their widely cited article [5] is different from the one used here but is proportional to it.

Relaxation after deformation results from the restoring *entropic-spring* force acting against the viscous resistance of the solvent (indeed, all results in this and subsequent sections assume spring forces are entropic in origin; in practice, there may be enthalpic contributions to spring forces). So, the characteristic time of the relaxation is thus proportional to ζ_0 and inversely proportional to kT .

Because of the many degrees of freedom in the chain, the relaxation process is actually governed by a series of relaxation times. In the Rouse model, there is one relaxation mode, with relaxation time τ_p , for each value of the index p up to N , the number of submolecules in the chain, as shown by Eq. 6.1:

$$G(t) = \frac{\rho R T}{M} \sum_{p=1}^N e^{-2t/\tau_p} = \frac{\rho R T}{M} \sum_{p=1}^N e^{-t/\tilde{\tau}_p} \quad (6.1)$$

The reason for the factor of two appearing in the exponential in Eq. 6.1 is that there is a potentially confusing factor of two difference between two relaxation times that might be defined within the Rouse model. The relaxation time for the *stress* contribution of the p th mode (which we here denote as $\tilde{\tau}_p$) is exactly half the relaxation time of *molecular orientation* from the p th mode (which we here denote as τ_p). That is, $\tau_p = 2\tilde{\tau}_p$. The mathematical reason for this factor of two is that stress depends essentially on the square of the orientation of chain subsegments. In the following, we take care to distinguish these two definitions of relaxation time.

We recall that the number of submolecules N is arbitrary within limits, so if terms for which p approaches N made a significant contribution to the sum, the Rouse model would not be valid, as this would imply that phenomena occurring *within* a submolecule (which are not accounted for in the model) are affecting the stress. It is thus required that the series converge for p somewhat less than N . If the series converges for $p < N/5$, the relaxation times τ_p and $\tilde{\tau}_p$ can be accurately approximated by:

$$\tau_p = \frac{b^2 N^2 \zeta_0}{3 \pi^2 p^2 k T}; \quad \tilde{\tau}_p = \frac{b^2 N^2 \zeta_0}{6 \pi^2 p^2 k T} \quad p = 1, 2, 3, \dots \quad (6.2)$$

where b is the statistical segment length defined in Eq. 2.11 as $(\langle R^2 \rangle_0 / N)^{1/2}$, and N is the degree of polymerization, i.e., the number of monomer units per molecule, M/M_0 . (Ferry [6] uses the symbol a for this length.) These *Rouse relaxation times* play a central role in all the relaxation models discussed in this book, as they govern the time scales for the basic molecular motions that are involved, directly or indirectly, in all relaxation processes.

The Rouse modes of molecular motion are to some degree analogous to the modes of vibration of a string fastened at both ends, as shown in Fig. 6.1. The frequency of vibration is proportional to n/l , where here n is the number of the mode and l is the length of the string. And the wavelength is $2l/n$. Mode one corresponds to a wavelength of $2l$, and this is indicated by the top curve. Mode two corresponds to a wavelength of l , and this is indicated by the second curve. Mode three has a wavelength of $2l/3$, and this is shown by the third curve. Note that as the frequency increases, higher and higher modes are activated, and the corresponding motion of the string involves the coordinated motion of shorter and shorter segments of the string.

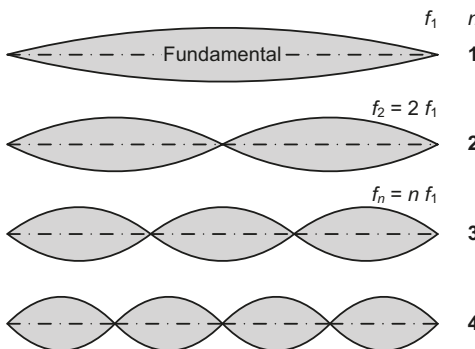


Figure 6.1 Modes of motion in a vibrating string, which are analogous to the modes of motion in a polymer molecule according to the model of Rouse. Modes 1 through 4 are shown. Higher modes involve the coordinated motion of successively shorter segments of the string, as higher Rouse modes represent the coordinated motions of successively smaller groups of submolecules. The analogy is far from perfect, as a molecule is not fixed at its ends

The longest Rouse time, corresponding to $p = 1$, is especially important and is called the *longest Rouse relaxation time*. As with the individual Rouse modes, the longest relaxation time for the stress, and the longest relaxation time for the molecular orientation, are separated by a confusing factor of two (see the previous discussion following Eq. 6.1). Unfortunately, this has led to discrepancies in the literature as to which of the two times should be called “the Rouse time,” with rheologists tending to favor the stress relaxation time, while theoretical physicists often favor the reorientation time. In this book, we shall refer to the two timescales as the *Rouse reorientation time* (giving this the symbol τ_r) and the *Rouse stress relaxation time* (giving this the symbol τ_R). While for dilute polymers and unentangled melts the Rouse stress relaxation time τ_R is the most relevant, when we come to discuss entangled melts we will find the Rouse reorientation time τ_r is the more useful quantity, as it sets the timescale for primitive path fluctuations (Section 6.4.2) and stretch relaxation (Sections 11.2.1 and 11.3.2). The two times are given as:

$$\tau_r = \frac{b^2 N^2 \xi_0}{3 \pi^2 k T}; \quad \tau_R = \frac{b^2 N^2 \xi_0}{6 \pi^2 k T} \quad (6.3)$$

Note that since $N = M/M_0$, both τ_r and τ_R are proportional to M^2 for a given polymer.

Rouse assumed the molecule to be *freely draining*, i.e., that the effect of the flow of solvent past one part of the molecule has no effect on another part. Another way of saying this is that he assumed no *hydrodynamic interaction*. As is noted in Section 2.5.3 on intrinsic viscosity, this led to predictions that were not in accord with observations for dilute polymer solutions. Zimm later developed a model that took into account hydrodynamic interaction, but it is not necessary to consider this here, as it is not relevant to our discussion of melt behavior where there is no solvent.

6.2.3 Bueche's Modification for an Unentangled Melt

While the Rouse model was originally intended to describe dilute polymer solutions, Bueche [7] noted that the freely-jointed chain model should be able to describe the behavior of an unentangled melt. It has been found experimentally that the static interactions between a polymer molecule and its surroundings are normally the same in the melt as in a solution in its theta state, although Krishnamoorti et al. [8] have noted a few cases where chain dimensions are different in the melt and at the theta state. They attribute this to the ability of some theta solvents to "induce a conformer population different from what is favored in the melt state."

In the melt, hydrodynamic interaction is not an issue, as there is no solvent (to be more precise, hydrodynamic interactions are "screened" by interactions with the surrounding polymers, in a similar manner to static interactions). Thus, for a low-molecular-weight melt, it is possible to apply Rouse's results by simply replacing the polymer concentration by the melt density. Since the issue of polymer-solvent interactions does not arise, we will delete the subscript zero from the monomeric friction coefficient ζ in our discussion of melt properties. The monomeric friction coefficient in a melt depends on molecular weight because of the effect of free ends on free volume, but this effect becomes negligible at reasonably high molecular weights (see ref. [6], p. 227). The friction coefficient is also a function of temperature, and this dependency is often described reasonably well by the Volger-Fulcher equation [9]:

$$\ln \zeta = A + B/(T - T_0) \quad (6.4)$$

Majesté et al. [10] fitted their data for high molecular-weight polystyrene to this equation, using the constants shown in Eq. 6.5:

$$\zeta(g/s) = 2.7 \cdot 10^{-11} \exp\left[\frac{1620 \pm 50}{(T - 49.6)}\right] \quad (6.5)$$

where T is expressed in °C. Pattamaprom et al. [11], however, reported that for $T \leq 160$ °C this equation is not accurate.

After replacing ζ_0 by $\zeta(T)$, the relaxation times are still given by Eqs. 6.2 and 6.3, and the viscoelastic moduli are the same as for the Rouse model for a dilute solution under theta conditions. That is,

$$G(t) = \frac{\rho R T}{M} \sum_{p=1}^N e^{-2t/\tau_p} = \frac{\rho R T}{M} \sum_{p=1}^N e^{-t/\tilde{\tau}_p} \quad (6.6)$$

$$G'(\omega) = \frac{\rho R T}{M} \sum_{p=1}^N \frac{\omega^2 \tilde{\tau}_p^2}{1 + \omega^2 \tilde{\tau}_p^2} \quad (6.7a)$$

$$G''(\omega) = \frac{\rho R T}{M} \sum_{p=1}^N \frac{\omega \tilde{\tau}_p}{1 + \omega^2 \tilde{\tau}_p^2} \quad (6.7b)$$

These can also be written in terms of the longest Rouse stress or reorientation relaxation times. For example, Eq. 6.6 becomes:

$$G(t) = \frac{\rho R T}{M} \sum_{p=1}^N e^{-2t p^2 / \tau_r} = \frac{\rho R T}{M} \sum_{p=1}^N e^{-t p^2 / \tau_R} \quad (6.8)$$

The low-frequency, limiting value of the loss modulus must be equal to $\omega \eta_0$, and this fact can be used in combination with Eq. 6.7(b) to show that:

$$\omega \eta_0 = \frac{\rho R T}{M} \omega \sum_{p=1}^N \tilde{\tau}_p = \frac{\rho R T}{M} \omega \tau_R \sum_{p=1}^N \frac{1}{p^2} \quad (6.9)$$

For large values of N , the sum converges as follows:

$$\sum_{p=1}^N \frac{1}{p^2} = \frac{\pi^2}{6} \quad (6.10)$$

Now using Eqs. 6.9 and 6.10, the longest Rouse relaxation times are obtained in terms of other experimentally determined quantities, as (again, taking care to distinguish τ_r for reorientation, and τ_R for stress relaxation):

$$\tau_r = \frac{12 \eta_0 M}{\pi^2 \rho R T}; \quad \tau_R = \frac{6 \eta_0 M}{\pi^2 \rho R T} \quad (6.11)$$

We note that Eq. 6.11 assumes that forces are purely entropic in origin. In a polymer solution the density ρ is replaced by the concentration, expressed in units of mass of polymer per unit volume of solution.

Comparing Eq. 6.11 with 6.3 we see that the viscosity is proportional to the molecular weight, as shown by Eq. 6.12:

$$\eta_0 = \frac{b^2 M \zeta \rho N_A}{36 M_0^2} \quad (6.12)$$

where M_0 is the molecular weight of the monomer (M/N), and N_A is Avogadro's number. Equation 6.12 implies that the monomeric friction coefficient can be determined by measuring the viscosity. However, to do this it is necessary to select the molecular weight of the sample very carefully. One wants a high molecular weight to avoid the effect of M on the friction coefficient due to the effect of free ends. But at the same time, entanglement must be avoided. A value just below M_C , the critical molecular weight for entanglement (see Section 6.3.1), is usually selected, and the

molecular weight distribution must be very narrow. Meerveld [12] proposed two methods for estimating ζ from experimental data, one based on the storage and loss moduli and the other on the zero-shear viscosity.

In the *terminal zone*, when t is a long time after a step strain in a step strain test, or when the frequency ω is very small in oscillatory shear, the viscoelastic moduli take on the limiting forms shown by Eqs. 6.13 and 6.14. These forms are obtained by noting that $\tilde{\tau}_p = \tau_R / p^2$ and letting the frequency approach zero in Eqs. 6.7:

$$G(t) = \frac{\rho R T}{M} e^{-t/\tau_R} \quad (\text{long-time limiting behavior}) \quad (6.13)$$

$$G'(\omega) = \frac{\rho R T}{M} \omega^2 \tau_R^2 \sum_{p=1}^N \frac{1}{p^4} = 1.08 \frac{\rho R T}{M} \omega^2 \tau_R^2 \quad (\text{low } \omega \text{ behavior}) \quad (6.14a)$$

$$G''(\omega) = \frac{\rho R T}{M} \omega \tau_R \sum_{p=1}^N \frac{1}{p^2} = 1.65 \frac{\rho R T}{M} \omega \tau_R \quad (\text{low } \omega \text{ behavior}) \quad (6.14b)$$

The constants, 1.65 ($= \pi^2/6$) and 1.08, are the limiting values of the summations for large N (for example, Eq. 6.10). The steady-state compliance is another property that arises from behavior in the limit of long times and is given by:

$$J_s^0 = 0.40 \frac{M}{\rho R T} \quad (6.15)$$

As in the case of the relaxation modulus, the dependence on temperature is quite weak, because within the experimentally accessible temperature range, the variation of ρT is small.

According to the Bueche-Rouse theory, over some range of times or frequencies away from the terminal zone, where the two or three longest relaxation times can be neglected, the relaxation modulus can be approximated by Eq. 6.16:

$$G(t) = \sqrt{\frac{3 \rho R T \eta_0}{2 \pi M}} t^{-1/2} \quad (6.16)$$

Ferry (see ref. [6], p. 189) reports that the range of validity of this approximation is limited to about three decades of time. Since the viscosity η_0 is proportional to the molecular weight, the modulus in this portion of the transition zone is independent of molecular weight. The reason for this is that, in this time regime, short subsections of chain are relaxing their contribution to the stress, while larger chain sections and whole molecules retain their contribution to the stress. Thus the relaxation depends only on the motion of short subsections, and is independent of the overall size of the chains. We can now write the special form of the relaxation spectrum, $H(\tau)$, that is valid in this region:

$$H(\tau) = \sqrt{\frac{3 \rho R T \eta_0}{2 \pi^2 M}} \tau^{-1/2} \quad (6.17)$$

From this we can show that the storage and loss moduli vary with the square root of the frequency in this region, as shown by Eq. 6.18.

$$G'(\omega) = G''(\omega) = \sqrt{\frac{3 \rho R T \eta_0}{4 M}} \omega^{1/2} \equiv C \omega^{1/2} \quad (6.18)$$

Since Eq. 6.11 gives the longest Rouse time in terms of the zero-shear viscosity, it can be combined with Eq. 6.18 to obtain Eq. 6.19, which shows how the storage or loss modulus data in this region can be used to determine τ_r or τ_R (again, assuming the chain forces are purely entropic in origin).

$$\tau_r = \frac{16}{\pi^2} \left(\frac{C M}{\rho R T} \right)^2; \quad \tau_R = \frac{8}{\pi^2} \left(\frac{C M}{\rho R T} \right)^2 \quad (6.19)$$

Since the size of a submolecule is arbitrary, there is no intrinsic length scale for the Rouse chain. Thus, the relaxation that occurs so quickly that it involves motions within a submolecule cannot be modeled by the Rouse theory, and theories built on it therefore cannot predict behavior at very short times or high frequencies. Moreover, behavior at ever shorter times or ever higher frequencies will reflect more and more the very fast relaxations associated with glassy modes of motion within the molecule. Thus, we cannot use the Rouse model to tell us about viscoelastic responses at very short times after imposition of a strain or at very high frequencies, both of which involve glassy modes of relaxation. These glassy modes involve bond stretching and rotation, which do not depend on large-scale molecular structure and are not of interest to us here.

Figures 6.2 and 6.3 are double-logarithmic plots of the relaxation modulus and the storage and loss moduli predicted by the Rouse model. In the terminal zone, i.e., at long times for $G(t)$ or low frequencies for G' and G'' , the moduli follow Eqs. 6.13 and 6.14. Thus, the limiting slopes for G' and G'' are two and one respectively on these log-log plots, while the limiting, long-time slope on a plot of $(\log G)$ versus t is $-1/\tau_R$ in accordance with Eq. 6.13. At higher frequencies or shorter times, the proportionality of G' and G'' to $\omega^{1/2}$ as indicated by Eq. 6.18 can be seen. The limiting behavior at very high frequency or short time cannot be described by the Bueche-Rouse model, because it does not describe very short-range relative motions within the molecule.

The Bueche-Rouse theory for unentangled melts can be applied to polydisperse systems simply by adding together the concentration-weighted contributions of each molecular weight component, as long as there are no molecules present that are long enough to be entangled (see ref. [6], p. 229).

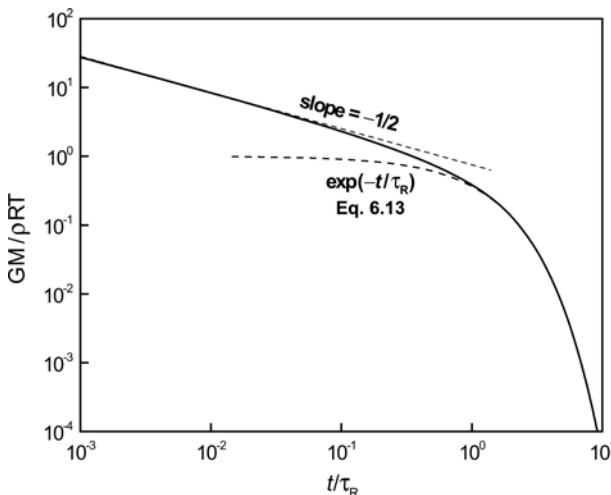


Figure 6.2 Double-logarithmic plot of the dimensionless relaxation modulus as a function of dimensionless time t/τ_R for a melt of linear polymer according to the Rouse model. The molecular weight is less than the entanglement molecular weight, M_e . The slope of $-1/2$ over a range of shorter times is in accord with Eq. 6.16, while the simple exponential corresponds to Eq. 6.13, i.e., to terminal relaxation governed by the longest Rouse stress relaxation time τ_R .

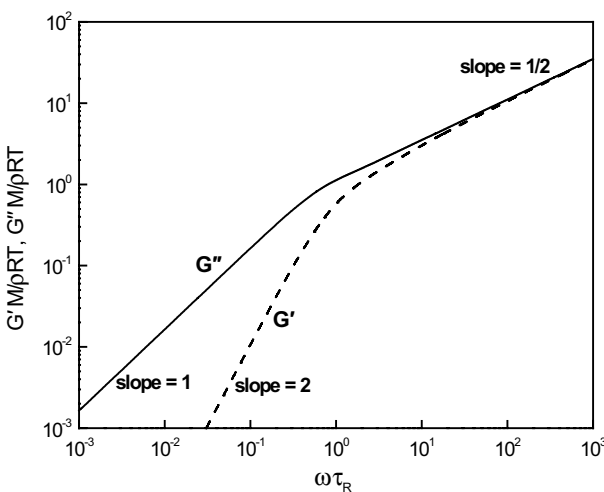


Figure 6.3 Double-logarithmic plot of the dimensionless storage and loss moduli as functions of dimensionless frequency $\omega \tau_R$ for a melt of linear polymer according to the Rouse model. The molecular weight is below the entanglement molecular weight, M_e . The single line with a slope of $1/2$ over a range of higher frequencies is in accord with Eq. 6.18, while the two lines with slopes of 1 and 2 correspond to Eqs. 6.14(b) and 6.14(a) respectively, i.e., to terminal behavior governed by the longest Rouse stress relaxation time τ_R .

Although the Bueche-Rouse theory for undiluted melts is not applicable to systems with entanglements, at sufficiently short times or high frequencies the molecular motions that contribute to relaxation are limited to localized, or uncorrelated, displacements of relatively small portions of the polymer chain. If there is a time span during which these localized displacements are still significantly larger than the size of a submolecule, the Bueche-Rouse theory will describe the resulting relaxation. Thus, the Bueche-Rouse theory is valid for entangled melts at intermediate times, or intermediate frequencies, that are too fast to be in the terminal region, but slow enough that the molecular motion encompasses at least one submolecule, and the linear viscoelastic functions in this region will be given by Eqs. 6.16 to 6.18. In practice, it is found that there is indeed a range of about one decade of time (or frequency) over which the viscoelastic response of an entangled melt is independent of molecular weight (and also independent of long chain branching) and described by Eqs. 6.16 to 6.18. Doi [13] proposed this behavior be called the *Bueche-Ferry law*. Using Eq. 6.20, Osaki et al. [14] used data in this region of frequencies to determine the longest Rouse relaxation time for entangled polymers.

■ 6.3 Entanglements and the Tube Model

Polymers are usually processed as melts or as concentrated solutions, and the molecules are usually of high molecular weight, in the tens of thousands to millions of Daltons. In high-molecular-weight melts or concentrated solutions, flexible polymer molecules are invariably entangled. That is, the motion of a molecule is significantly impeded by topological constraints, i.e., the impediments to motion of a molecule created by its inability to cross through its neighbors (see Fig. 6.4). These constraints are referred to as entanglements. While a precise definition of an entanglement has not been generally agreed upon, we will say that an entanglement is a topological interaction between one polymer molecule and its neighbors that greatly impedes its motion and thus its ability to relax after a deformation is imposed. Like Houdini escaping from a straightjacket, polymer molecules (especially ones with long side branches—see Chapter 9) must undergo rather unusual motions to move or relax in the presence of entanglements with other polymer molecules. These unusual motions are rare and therefore take a long time to occur by random Brownian motion. Therefore, entanglements confer on polymer melts very long relaxation times and high viscosities (often of order a billion or even a trillion times higher than for small molecules of similar chemistry).

A large viscosity is in many cases desirable for the melt to be able to hold its shape long enough after it has been processed for that shape to be *frozen in* by cooling

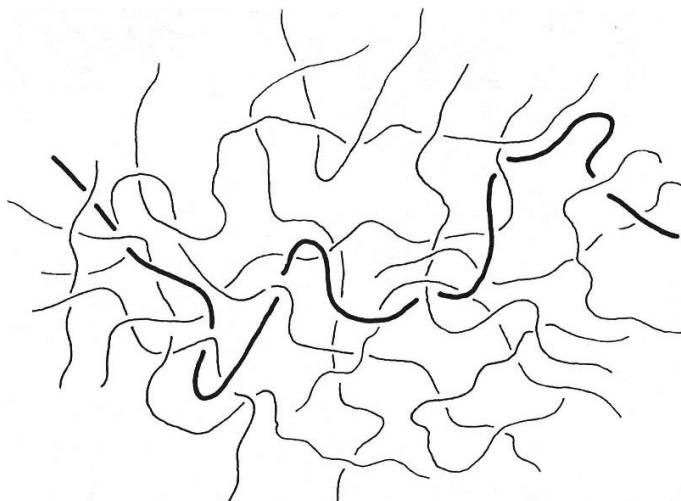


Figure 6.4 A polymer molecule entangled in a mesh of other polymer chains;
adapted from Graessley [15]

into the solid state. In addition, by tinkering with the MWD and LCB characteristics, the relaxation time(s), viscosity, and other rheological properties of the melt can be dramatically altered, and, if done skillfully, this can lead to optimized processing characteristics. Like a skilled glassblower who adjusts the flame conditions to produce exactly the desired viscosity to be able to shape a glass part, the polymer resin manufacturer adjusts polymer molecular characteristics to optimize processing performance. To optimize intelligently, however, it is necessary to predict quantitatively the relationship between molecular structure and rheology. This, in turn, requires a thorough understanding of how entanglements affect rheology.

6.3.1 The Critical Molecular Weight for Entanglement M_C

The most obvious effect of entanglements on polymer rheology involves the dependency of the zero-shear viscosity on molecular weight. As shown by Eq. 6.12, the Rouse theory predicts that the zero-shear viscosity, η_0 , of a melt is proportional to the polymer molecular weight, M . Figure 6.5 shows that this proportionality is, indeed, observed, but only over a limited range of low molecular weights. As discussed in Section 5.2.1, above a critical molecular weight M_C , which varies from one polymer to another, Fig. 6.5 shows that the viscosity has a much steeper, power-law dependence, namely $\eta_0 \propto M^\alpha$. The power α on M is not a universal constant, but for most polymers its value is close to 3.4. This steeper dependence of η_0 on M is due to entanglements. As the molecular weight increases above M_C , the molecule has ever greater difficulty in escaping from its entanglements, and this leads to the increase

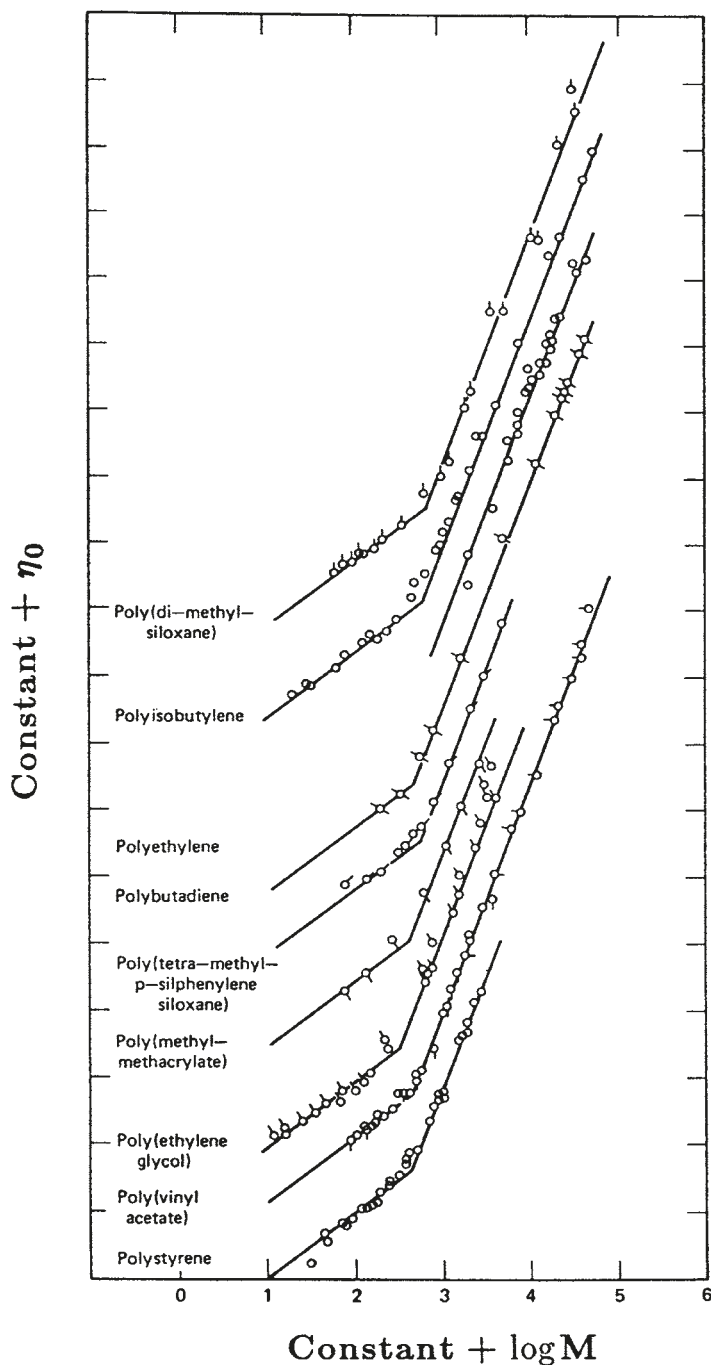


Figure 6.5 Relationship between zero-shear viscosity and molecular weight for several nearly monodisperse melts. For clarity, the curves are shifted relative to each other along both the abscissa and ordinate; adapted from Berry and Fox [5]

in its zero-shear viscosity. The molecular weight M_C is obtained as the intersection of the best-fit lines with power-law slopes of 1 and α on a log-log plot and is called the critical molecular weight for entanglement. Values of M_C are given by Fetters, et al. [16]. Using the relationship $\eta_0 = K M^\alpha$, where K is a constant for a given polymer and temperature, one can infer the molecular weight of a monodisperse polymer from η_0 . The inference of molecular weight and molecular weight distribution from rheology is discussed in much more detail in Chapter 8.

6.3.2 The Plateau Modulus G_N^0

The next most obvious effect of entanglements on polymer rheology is to make a molten polymer act like a rubber when it is deformed more rapidly than the molecules can escape their entanglements. As was pointed out in Sections 5.3 and 5.4, the storage modulus of an entangled, monodisperse, melt shows a plateau over a range of frequencies, which is referred to as the *plateau modulus* G_N^0 , and the relaxation modulus $G(t)$ exhibits this same plateau over a certain range of times. Just as the equilibrium modulus of a rubber is proportional to the density of cross-link points, the plateau modulus of an entangled polymer melt is proportional to the density of entanglements and is a characteristic of the chemical structure of the polymer. It is insensitive to molecular weight and relatively insensitive to temperature, even though the relaxation time and viscosity of the melt are highly sensitive to these variables. This is illustrated in Fig. 6.6, which shows that for the polymer of lowest molecular weight, the curve of $G'(\omega)$ has no plateau and its $G'(\omega)$ curve is similar to that predicted by the Rouse theory, which was presented in Section 6.2. Thus, in this low-molecular-weight sample, the polystyrene molecules are too short to be entangled with each other. However, as the molecular weight increases, Fig. 6.6 shows that a plateau in G' emerges and then grows ever broader, even though the height of the plateau does not change with increasing molecular weight. For polystyrene, the height of the plateau in $G'(\omega)$ is around $2 \cdot 10^5$ Pa, while for polyethylene it is approximately $2.6 \cdot 10^6$ Pa. Values of G_N^0 for several polymers are presented in Appendix A; more complete tabulations have been compiled by Fetters et al. [16].

Comparing Fig. 6.6 with Fig. 6.3, we see that even though the molecular weight is high, the high-frequency portion of the $G'(\omega)$ curve has the shape predicted by the Rouse theory. Thus, even when the molecular weight is much higher than M_C , at high frequencies the polymer relaxes only by Rouse processes. At low frequencies, this Rouse relaxation is interrupted by interference from the entanglements. As the molecular weight increases, the entanglements delay the final relaxation to a greater and greater extent, as is shown by the rapid decrease in the frequency ω_1 at which G' falls off the plateau toward terminal behavior. The reciprocal of the frequency ω_1 is roughly the longest or terminal relaxation time of the polymer τ_1 .

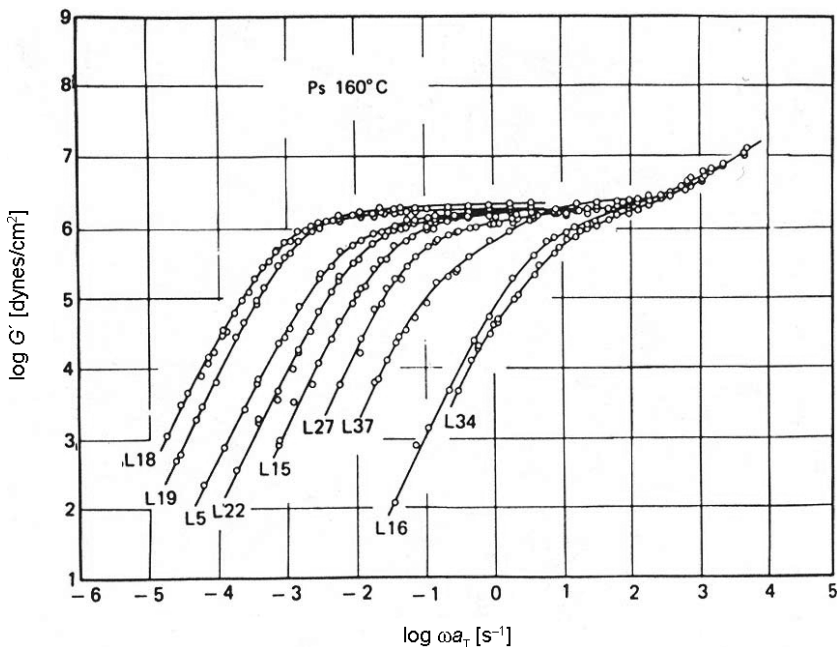


Figure 6.6 Storage modulus, G' , as a function of frequency reduced to 160 °C for nearly monodisperse polystyrenes of molecular weight ranging from 47,000 (L34) to 580,000 (L18), from right to left; adapted from Onogi et al. [17]

And the terminal relaxation time is roughly proportional to the zero-shear viscosity, i.e., $\eta_0 \approx G_N^0 \tau_1$. Thus, a plot of either η_0 or τ_1 against molecular weight shows a steep power-law dependence, namely $\eta_0 \propto \tau_1 \propto M^{3.4}$, as shown in Fig. 6.5. The terminal relaxation time may be very difficult to determine experimentally for melts with a broad molecular weight distribution or a high level of long-chain branching.

Figure 6.6 shows that the flat plateau in $G'(\omega)$, which gives way rather abruptly to terminal relaxation, is characteristic of high-molecular-weight, essentially monodisperse, linear polymers. For polydisperse polymers, the shorter molecules in the melt can escape their entanglements more quickly than the longer molecules. Hence, a component of the melt having a molecular weight M relaxes at its own characteristic frequency, $\omega_1(M)$, and in a polydisperse polymer, such as a commercial polyethylene, the flat plateau in G' is replaced by a region with a gradual slope. The shapes of the $G'(\omega)$ and $G''(\omega)$ curves in this intermediate-frequency region therefore contain information about the molecular weight distribution of the polymer. In principle, the distribution can be extracted from the $G'(\omega)$ and $G''(\omega)$ curves, if we have a theory that quantitatively relates the rate of relaxation of a polymer molecule to its molecular weight, and if an inversion of this theory can be carried out. Methods of carrying out this inversion are described in Chapter 8.

To develop a theory that predicts relaxation from molecular weight and other structural characteristics requires consideration of the ways an entangled polymer can relax. While Brownian motion is the basis for all relaxation processes, the ways in which it operates vary greatly depending on molecular weight, molecular weight distribution and level of long-chain branching. Thus, to some extent, entangled polymers relax in the same way as unentangled polymers, that is, by processes described in the Rouse theory that was presented in Section 6.2. However, entangled polymers cannot relax completely by pure Rouse processes, because these processes are interrupted by entanglements between a chain and its neighbors. Only relatively short-range motions of molecules, which do not encounter much interference from entanglements, continue to be Rouse-like. This is why, as Fig. 6.6 shows, at high frequencies, entangled polymer melts follow the Bueche-Ferry law, which was introduced in Section 6.2.3. However, the low-frequency behavior is dominated by slow, long-range, motions and relaxation is greatly slowed by entanglements, the more so as the molecular weight increases. These slow motions are, nevertheless, the cumulative effect of many short scale motions of the same type as in the Rouse theory. Relaxation at low frequencies is governed by processes in which these local motions add up to allow the escape of a molecule from its entanglements.

6.3.3 The Molecular Weight Between Entanglements M_e

We have seen that the effect of entanglements on the relaxation of a melt is similar in some respects to the effect of cross-links on the relaxation of a rubber. For example, a bouncing ball of silly putty can behave like a cross-linked rubber ball, even though the former has only temporary entanglements and not permanent cross-links. As was explained in Section 5.8, this suggests that the plateau modulus can be related to the entanglement density by analogy with the theory of rubber elasticity. In Section 5.8.1, the entanglement molecular weight M_e was defined by Eq. 5.20 in terms of the plateau modulus. This equation is repeated here as Eq. 6.20, while the alternative definition given there as Eq. 5.21 is reproduced here as Eq. 6.21.

$$M_e \equiv \frac{\rho R T}{G_N^0} \quad (6.20)$$

$$M_e^G \equiv \frac{4}{5} \frac{\rho R T}{G_N^0} \quad (6.21)$$

We recall that the first of the above definitions arose from Ferry's analogy between entangled melts and crosslinked elastomers, while the second definition was based on the fact that fast Rouse modes allow re-equilibration of tension along the chain,

so that one fifth of the initial stress relaxes before the entanglement network interrupts the process.

Both of the above definitions are controversial, and there is even some justification for including another factor of $1/2$ to account for fluctuations of entanglement positions. The relationship between M_e (or M_e^G) and G_N^0 is discussed in detail in Section 5.8.2.

6.3.4 The Tube Diameter a

It has been found that the ways in which entanglements slow down the relaxation of a polymer molecule can be quantitatively predicted by the tube model that was first applied to molten polymers by Doi and Edwards [1]. In this model, the entanglements of a *test chain* with the surrounding *matrix chains* are modeled as a mean-field *tube* to which the test chain is confined, forcing it to move for the most part along the axis of the tube. The axis of the tube is called the *primitive path* of the chain. Figure 6.7(b) shows how the tube is created by entanglements of a test chain with the matrix chains.

If the melt has had plenty of time to relax in the absence of flow, each molecule will have the configuration of a random walk. Thus, the tube is itself also a random walk. Note, however, that the tube in Fig. 6.7(b) is much wider than the diameter of the polymer molecule and that the polymer molecule meanders within the tube, with these meanderings constrained by the diameter of the tube. Thus, the diameter of the tube a is much larger than the statistical segment length b of the molecule itself, which is defined by Eq. 2.11 and just below Eq. 6.2. Consequently, the *primi-*

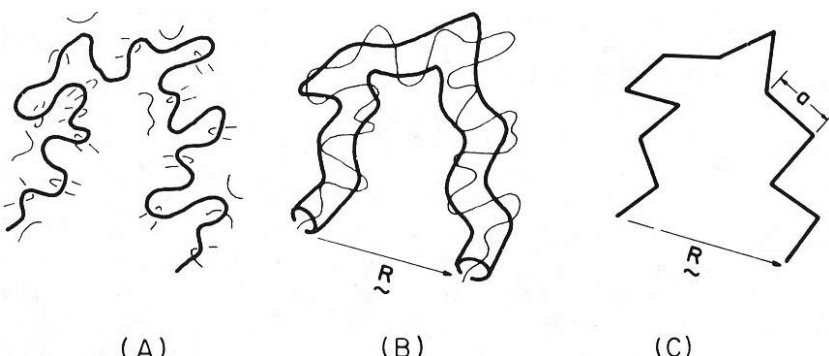


Figure 6.7 (A) Illustration of a polymer molecule entangled with neighboring polymer molecules. (B) The entanglements with surrounding polymers are represented by a tube. (C) The primitive path of the tube, which is a random walk, with step size, a , equal to the diameter of the tube. The contour length of the primitive path is much less than the contour length of the polymer; adapted from Graessley [15]

tive path (or the *contour length*) of the tube is considerably shorter than the contour length of the molecule itself. For a flexible polymer molecule, the diameter of the tube is taken to be equal to the random-walk step length of the tube, and a single random-walk step of the tube is called a *tube segment*. The diameter a (and length) of a tube segment can be shown to be related to the entanglement spacing by [1]:

$$a^2 = \frac{M_e^G}{M_0} b^2 = \frac{4}{5} \frac{\rho R T b^2}{M_0 G_N^0} \quad (6.22)$$

where M_0 is the molecular weight of a monomer. According to Eq. 6.22, the smaller the entanglement spacing M_e , the smaller the tube diameter a . Values for a are 36.8 Å for 1,4-polybutadiene and 76 Å for polystyrene; values for some other polymers are tabulated in Appendix A. These length scales b , a , and the tube length L_t are depicted in Fig. 6.8, illustrating that the tube diameter is typically larger than the segment length, and (correspondingly) the tube path is shorter than the contour length of the molecule.

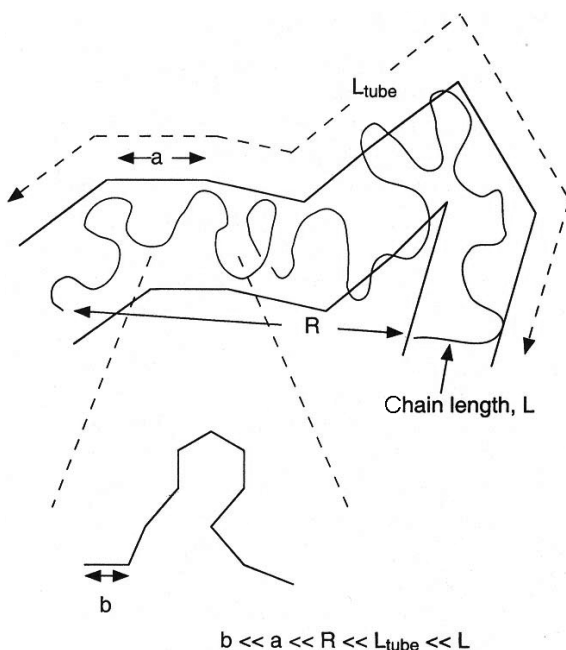


Figure 6.8 Sketch of tube showing definitions of length scales in the tube model, including the random-walk (or freely-jointed chain) step length $b \equiv R/N^{1/2}$, where $R \equiv \sqrt{\langle R^2 \rangle}_0$ is the equilibrium root-mean-square end-to-end length and N the degree of polymerization, a is the tube diameter, or tube segment length, $L_{\text{tube}} = L_t$ is the length of the tube, made up of Z random-walk steps each of length a , and L is the contour length of the polymer molecule itself.

To develop the *tube* theory of polymer motion, we consider the response of the melt, and specifically the dynamics of the entangled molecules, to deformations of the material. A commonly considered deformation is “step” strain. This is an idealized deformation that is so rapid that during the step no polymer relaxation can occur, and the polymer is forced to deform affinely, that is, to the same degree as the macroscopic sample is deformed. The simplest case is when the total deformation, though rapid, is small, so that the chains deform only slightly; this is called a *small amplitude step strain*. Because the deformation is very small, the distribution of chain configurations remains nearly Gaussian, and linear viscoelastic behavior is expected. In Chapter 4, we saw that the assumption of linear behavior makes it possible to use the response to a small step strain experiment to calculate the response to oscillatory shear or any other prescribed deformation.

Given that the *test chain* is trapped in its *tube*, if the polymer is suddenly deformed, we assume that the affine deformation of all the chains causes the tube to be deformed affinely also. As an illustration, consider the extreme case of a tube that has been completely straightened out by the deformation of the melt, as shown in Fig. 6.9(a). While the molecule can meander somewhat within the tube, its coarse-grained path is forced to follow the path of the tube. Since this path has been deformed away from a random walk, the polymer chain is not relaxed, and the melt will therefore be under stress. To relax this stress, each chain must relax its configuration, and to do so it must escape from its tube. Three basic processes have been discovered by which a linear polymer molecule can escape its tube and relax. These processes are: 1) reptation, 2) primitive path fluctuations, and 3) constraint release, which are depicted in Fig. 6.9.

Figure 6.9(a) shows a chain escaping from a straight tube, but the relaxation processes are not changed in the more likely case of a tube that is initially crooked. We also remark that even as a molecule escapes one tube, it re-entangles with other polymers, and so becomes enmeshed in a new tube. If the polymer is not flowing during the escape process, the new tube will be uncorrelated with the old tube, and will have the configuration of a random walk. Thus, if the old tube had been straightened by a flow that has now stopped, when the polymer escapes the old tube, the new polymer configuration will no longer be influenced by the shape of the old tube, and the effect of the flow will have been forgotten. So, in tube theories, polymer configurations and stresses are calculated by assuming that flow straightens out tubes, and thereby straightens out the molecules trapped in the tubes. When the molecules escape their old tubes, the effect of that straightening is lost, and the new tubes in which the polymers become confined have random-walk configurations.

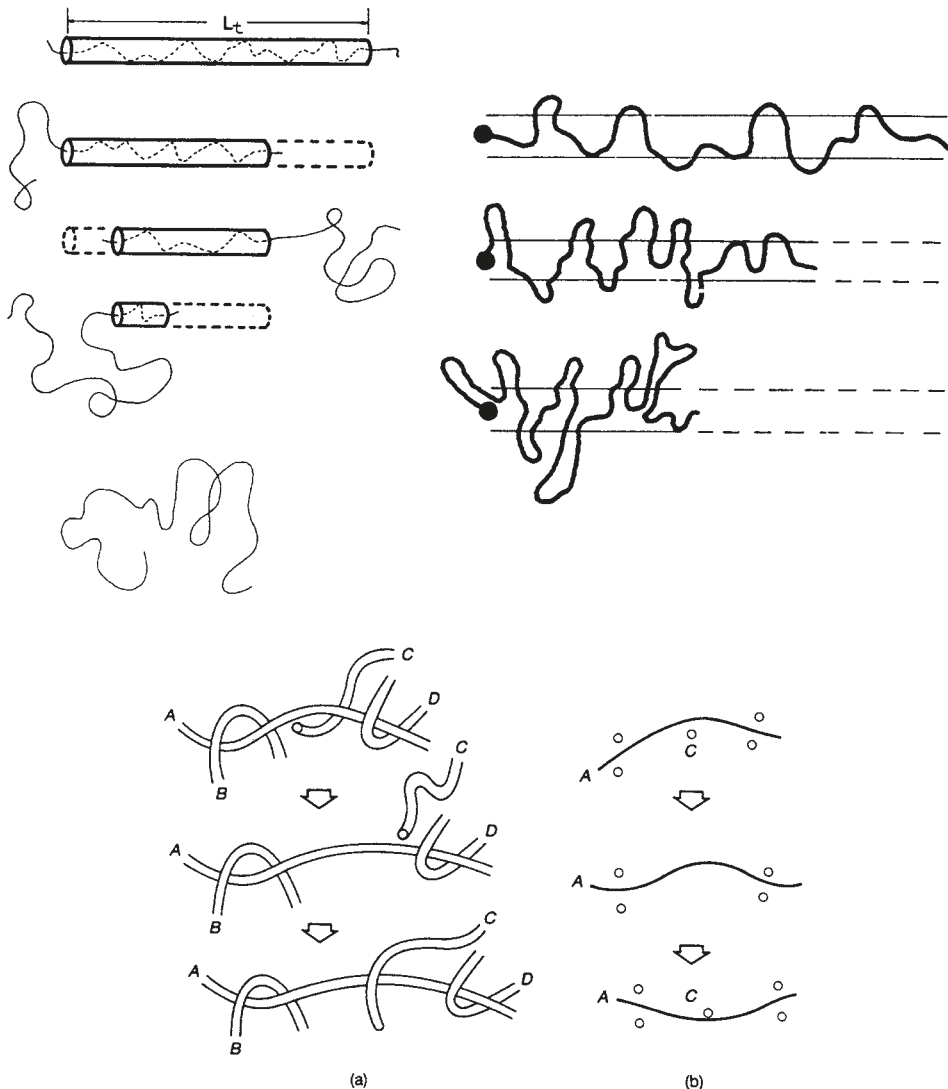


Figure 6.9 Illustration of three relaxation mechanisms in the linear viscoelastic regime.

(a) Upper left: Repetation of a polymer molecule out of its tube. To aid visualization, the tube of Fig. 6.4 has been straightened out; adapted from Graessley [15].

(b) Upper right: Primitive path fluctuations, in which the ends of chains randomly pull away from the ends of the tube, and upon re-expansion the chain ends explore a new regions of space and creates new tube segments; adapted from Doi and Edwards [1].

(c) Lower two pictures: Constraint release, in which chain "C," which presents a topological obstacle to chain A, moves, thus allowing a portion of chain A to relax; adapted from Doi and Edwards [1]

6.3.5 The Equilibration Time τ_e

Tube theories of relaxation share with the Rouse theory the assumption that all relaxation processes are ultimately controlled by the monomeric friction coefficient ζ . The monomeric friction coefficient is essentially independent of molecular weight, and, for a given type of polymer (polystyrene, for instance), depends mainly on temperature and more weakly on pressure. In tube theories, it is convenient to relate this friction coefficient to a fundamental time constant called the *equilibration time* τ_e by

$$\tau_e = \frac{\zeta a^2 M_e^G}{3 \pi^2 k T M_0} \quad (6.23)$$

where k is Boltzmann's constant. The equilibration time τ_e sets the time required to relax the internal configurations for subsections of the chain just large enough to occupy a single tube segment. Hence, on times longer than τ_e the only remaining deformations of the chain are associated with the entanglement restrictions.

More precisely, τ_e is defined as the *Rouse reorientation time* for a short chain with molecular weight equal to the molecular weight between entanglements. We can see this by setting the degree of polymerization N equal to M_e^G/M_0 in τ_r as given in Eq. 6.3. Note that ζ_0 is replaced by ζ , since we are now dealing with melts. Except near the glass transition temperature, τ_e is usually a very short time, and we will find it convenient to relate other, slower, relaxation times to τ_e . Values of τ_e range from around $7 \cdot 10^{-9}$ s for polyethylene at 190 °C, to $5.6 \cdot 10^{-7}$ s for 1,4-polybutadiene at 25 °C, to 0.05 s for polystyrene at 150 °C.

For the purposes of this book, it is not necessary to treat in detail the processes depicted in Fig. 6.9, but we will describe them qualitatively in subsequent sections and present the equations arising from detailed analyses based on the tube model. Before doing this, we discuss further evidence for entanglements in polymers, obtained from recent computer simulations.

6.3.6 Identification of Entanglements and Tubes in Computer Simulation

In the preceding sections, we outlined the basic picture of the tube model and presented some of the experimental evidence for the existence of entanglements in concentrated polymeric liquids (i.e., the behavior of zero shear viscosity with increasing molecular weight, and the emergence of a plateau in the storage modulus). With increases in computational power, it has become possible to simulate the molecular dynamics of polymeric liquids, and it is natural to ask whether such simulations provide further evidence of entanglements, and whether the above tube model parameters might be identified in computer simulations. In fact, since the early

pioneering work of Kremer and Grest [18], substantial evidence for entanglements in computer simulation has emerged, and there is an ongoing effort to quantify the observed chain dynamics. The work of Kremer and Grest is interesting also because they did not attempt to simulate a real chemical polymer chain, but rather a polymer chain comprising beads with relatively simple interaction parameters. So, their model can be thought of as a highly idealized polymer chain. Its relevance lies in the fact that all flexible, entangled polymer chains have similar dynamics (as described in this book). Hence, lessons learned from the Kremer-Grest model are applicable to other real polymers, and their model has become a testing ground for many of the developments described in this section.

A basic question is whether it is possible to directly observe entanglements within simulations of polymeric liquids. Analysis of the trajectories of chains within a molecular dynamics simulation [18, 19] can reveal evidence of the *effect* of entanglements on the chain motion, for example through slowing down of monomer diffusion. So, for example, the entanglement equilibration time τ_e can be inferred from the crossover time between different regimes of diffusion [19] as the point where the monomers feel the effect of entanglements. But this does not allow obvious identification of the entanglements themselves. One solution that has been explored to good effect is via chain-shrinking methods, originally proposed by Everaers et al. [20]. In such methods, chain ends within the simulation are fixed in space, and chain lengths are progressively reduced while preventing chains from crossing. As the chains shrink, apparent entanglement points emerge as points of contact between the chains, so that eventually the chains are reduced to a series of straight lines between these entanglement points (see Figure 6.10). This resulting path of the chain is then considered to be a good approximation to the primitive path of the tube, hence this type of simulation is known as *primitive path analysis*. The ensemble of primitive paths obtained from chain shrinking is visually quite striking, and provides strong qualitative evidence that entanglements are indeed present.

In their original work, Everaers et al. [20] imposed chain shrinking using the molecular dynamics code itself, by switching off repulsive interactions between adjacent monomers on the same chain, causing the chains to shrink under the action of their own spring forces. Since then, several groups have produced alternative algorithms with different shrinking protocols: shrinking under constant tension [21] and more efficient geometric methods to reduce chain length without permitting chain crossing (the Z algorithm of Kröger [22] and the CReTA algorithm of Tzoumanekas and Theodorou [23]). Different protocols do yield different results, but fortunately not too different in terms of the averaged properties (for example differences of order 10% in the average length of the primitive path have been reported [24, 25]).

While these chain-shrinking algorithms do appear to reveal identifiable entanglement points, extraction of parameters suitable for a tube model analysis requires some

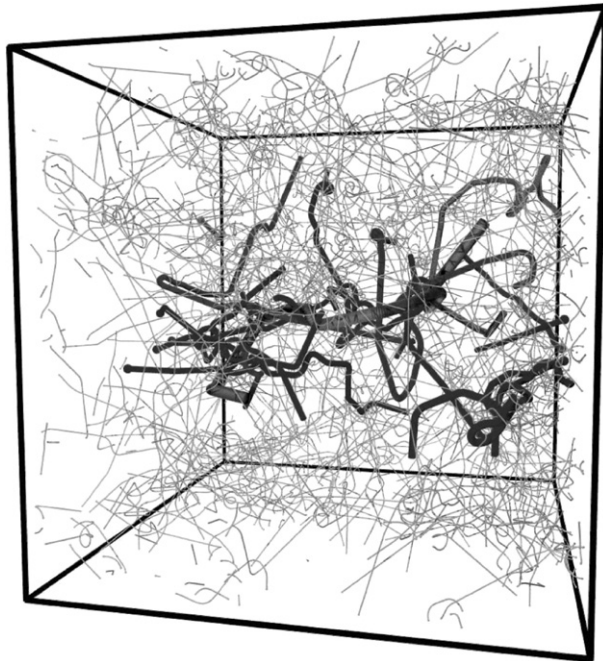


Figure 6.10 Result of a chain-shrinking “primitive-path analysis” for a molecular dynamics simulation for an idealized melt containing 200 chains of 350 beads. In this simulation, beads are not representative of real atoms, but instead the bead-bead interactions are parameterized according to the model of Kremer and Grest [18]. Shown is the primitive path of one chain (thickest gray line) together with all of those it is entangled with (medium thickness lines). The primitive paths of all other chains in the system are shown as thin lines. From Everaers et al. [20]

thought. For example, obtaining the molecular weight between entanglements, as defined in Section 6.3.3, is not so simple as just taking the average weight of chain between the points of contact emerging from the chain-shrinking algorithms. The reason for this is that force balance or similar constraints at the contact points induces correlations in orientation between successive primitive path segments; so, the primitive path emerging from the chain shrinking analysis is not exactly the same as the freely-jointed set of tube segments envisaged as the tube path in Section 6.3.4. Nevertheless, the primitive path must remain a random walk at larger scales, and so it is possible to define a Kuhn length a_{pp} and number of Kuhn segments N_{pp} for primitive paths of average length L_{pp} and mean square end-to-end length $\langle R^2 \rangle$ using equations analogous to Eqs. 2.13 and 2.14:

$$L_{\text{pp}} = a_{\text{pp}} N_{\text{pp}} \quad (6.24)$$

$$\langle R^2 \rangle = a_{\text{pp}}^2 N_{\text{pp}} \quad (6.25)$$

These may be rearranged to obtain:

$$a_{\text{pp}} = \frac{\langle R^2 \rangle}{L_{\text{pp}}} \quad (6.26)$$

$$N_{\text{pp}} = \frac{L_{\text{pp}}^2}{\langle R^2 \rangle} \quad (6.27)$$

For long chains, it is found that N_{pp} provides a good estimate for the total number of entanglements along the chain in the tube model, and hence that a_{pp} is an estimate of the tube diameter [25]. So, the entanglement molecular weight can be estimated as:

$$M_e = \frac{M}{N_{\text{pp}}} = M \frac{\langle R^2 \rangle}{L_{\text{pp}}^2} \quad (6.28)$$

In practice, the number of contact points between chains emerging in chain-shrinking algorithms is roughly twice the number of entanglements calculated on the basis of the above estimates using Kuhn lengths. Everaers [25] offers some rationalization for the above relationships by drawing an analogy with the shear modulus of phantom networks, accounting for fluctuations in junction points.

Although the chain-shrinking algorithms have achieved success both in visualizing topological interactions between chains and in predicting some tube model parameters, they remain open to the criticism that they achieve these results by means of an algorithm which destroys the local melt structure: real polymer chains do not shrink! There is thus a likelihood that the primitive path obtained through chain-shrinking does not exactly correspond to the path along which the chain is constrained to move in the equilibrium melt. It is desirable to have methods that can identify entanglements and tubes “nondestructively,” that is, without strong perturbations to the melt structure.

One such method, which has been used recently, is to consider the tube path as the average position of the monomer in each chain (the “*mean path*”). In their early work, Kremer and Grest [18] obtained a smoothed path by averaging over local monomer positions along the chain, and employed this in order to help visualize the chain motion due to reptation, as shown in Figure 6.11. Recent interest in performing averages over monomer positions to obtain the tube configuration arose following the work of Read et al. [26], who showed that the mean path should be smooth, with an associated bending energy. In practice, this method requires a time average over the position of each monomer during a molecular dynamics trajectory. Better statistics are obtained through the isoconfigurational ensemble (ICE) averaging proposed by Bisbee et al. [27], in which several molecular dynamics trajectories are obtained starting from the same initial configuration, and an average taken over these

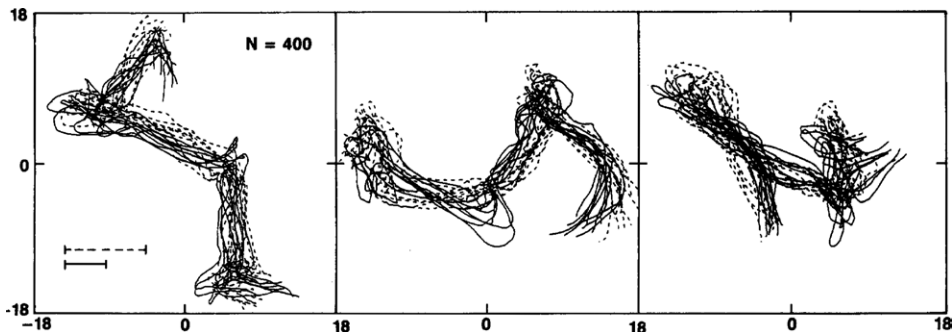


Figure 6.11 Visualization of the motion of a smoothed “primitive chain” obtained by averaging over the positions of neighboring monomers in a simulation of a melt of Kremer-Grest chains with 400 beads. The configurations of this chain are plotted at 20 different times, the first ten plotted as continuous lines, and the second ten as dashed lines. Three projections, along mutually perpendicular directions, are shown. It is clear that the primitive chain remains confined within a tube-like region (from Kremer and Grest [18]).

trajectories (though doing this is obviously more expensive computationally than simply averaging over portions of a single molecular dynamics trajectory). Whether or not the ICE method is used, some decision needs to be made about the interval of time over which to take the average [27, 28]. Evidently averaging times much shorter than the entanglement equilibration time τ_e are unsuitable, since monomers will not have had opportunity to explore the tube locally. Longer averaging times reveal a different problem: as monomers explore back and forth along the tube, they might pass “corners” where the tube is not straight. In three dimensional space, the average position of a monomer passing back and forth across such a corner will “cut the corner.” So, if the averaging time is chosen too long, the mean path ends up too smooth due to this corner-cutting. In practice, an averaging time of order the entanglement equilibration time τ_e seems the best compromise [27, 28]. Likhtman [29] has recently proposed a clever averaging procedure, which finds the center line of the cloud of monomer positions over time, and which allows averaging over much longer times without the corner-cutting problem. So far, this method has been applied only to mutually entangled ring polymers, where the entanglement topology is guaranteed not to change with time.

Finding the tube *mean path* by averaging monomer positions in molecular dynamics is a technique still in its infancy, with only a few publications available. Yet, interesting insights into the dynamics of entangled polymers are already emerging. Inspection of the mean paths of a collection of entangled chains in a simulated melt reveals that these mean paths are often in contact. Some of the contacts seem short-lived and transient (these might, nevertheless, represent interactions between chains which contribute to the overall localization of entangled chains in the melt).

However, some contacts between mean paths seem to be both *tight* (i.e., they are close contacts) and *long-lived* (i.e., they persist for a long time in the simulation of chain dynamics). Some examples of contacts between mean paths are shown in Fig. 6.12. There is an emerging consensus that these long lived contacts between mean paths reveal mutual entanglement between chains, and so might be called *entanglements* [28–30]. The density of close contacts seems commensurate with the expected number of entanglements. Most interactions are binary, though there is some evidence of so-called “triple entanglements.” Likhtman and Ponnurugan [28] have performed a detailed analysis of the dynamics and lifetimes of these entanglements for a simulation of linear polymer chains, revealing that processes of reptation, contour length fluctuation and constraint release indicated in Fig. 6.9 can all be identified. In fact, similar processes can be identified by examining the motion of the mean paths directly [31].

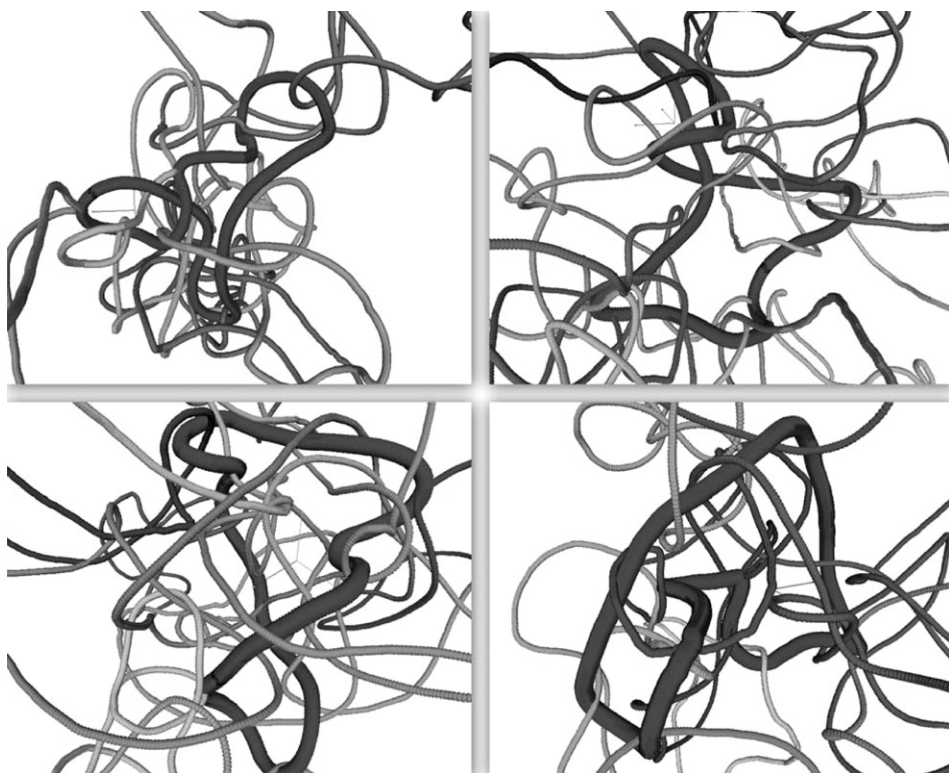


Figure 6.12 Mean paths obtained by the averaging of monomer positions in a simulation of melts of ring polymers comprising 512 Kremer-Grest beads. Four primary mean paths are shown as thick lines, together with the mean paths of other chains which pass within a short distance of the visualized primary paths. It is clear that there are effective interactions between the mean paths, which cause corners to form at positions of close contact. These points of interactions might be considered to be entanglements; from Likhtman [29]

In summary, computer simulations of entangled polymer liquids offer ample evidence for the existence of entanglements. At least two techniques are available for identification of entanglements in such simulations: *primitive path* analysis (i.e., chain shrinking methods) and searching for contacts between *mean paths* of molecular dynamics trajectories. While chain shrinking methods are undoubtedly cheaper computationally, the method strongly changes the local structure of the melt. Mean path methods are more expensive, but allow the study of entanglement dynamics without changing the melt structure. Both methods could, in principle, be used to predict fundamental tube-model parameters, such as entanglement molecular weight, for a new polymer chemistry. It is our estimation that the next decade will see further advances in these methods, and that the insights gained will most likely imply that modifications to the tube model are needed. They might even suggest a better model altogether, though it is likely that it will be some time before the implications are worked out for practical processing of industrial melts. Nevertheless, it is encouraging that molecular dynamics simulations present evidence for the fundamental processes of the tube model—reptation, contour length fluctuation, and constraint release (Fig. 6.9). We now describe these processes in greater detail and present the equations arising from detailed analyses based on the tube model.

■ 6.4 Modes of Relaxation

6.4.1 Reptation

In reptation, a process first described by de Gennes [32], the molecule escapes from its tube by sliding back and forth in it, gradually protruding more and more of its mass outside of the tube. Every time a portion of the tube is vacated by the chain, that portion of the tube is “forgotten,” meaning that the portions of the chain no longer in the tube have freed themselves from their original entanglements. We define the survival fraction $P(t)$ as the fraction of the tube that remains occupied by the molecule at time t , assuming that the whole chain is in the tube at time zero.

An analysis of the reptation process [1] leads to an expression for $P(t)$:

$$P(t) = \frac{8}{\pi^2} \sum_{i \text{ odd}} t^{-2} \exp(-i^2 t/\tau_d) \quad (6.29)$$

The summation is over all odd integers i . If reptation is the only mechanism of relaxation, then the relaxation modulus $G(t)$ is proportional to $P(t)$, i.e., $G(t) = G_N^0 P(t)$, and we have

$$G(t) = \sum_{i \text{ odd}} G_i \exp(-t/\tau_i) \quad (6.30)$$

The distributions of relaxation modes G_i and relaxation times τ_i are given by:

$$G_i = \frac{8}{\pi^2} \frac{G_N^0}{i^2}; \quad \tau_i = \frac{\tau_d}{i^2} \quad i \text{ odd} \quad (6.31)$$

where τ_d is the reptation time or *disengagement time* for the molecule to escape from the tube.

This time constant can be calculated from the monomeric friction coefficient ζ , the statistical segment length, b , the degree of polymerization N , and the tube diameter, a , by noting that it is the time taken to diffuse over a distance L (the length of the tube) by a process with diffusion constant D where:

$$L = \frac{N b^2}{a}; \quad D = \frac{k T}{N \zeta} \quad (6.32)$$

These may be rewritten in terms of “entanglement variables,” that is, the tube diameter, a , and entanglement time τ_e , as:

$$L = Z a; \quad D = \frac{a^2}{3 \pi^2 Z \tau_e} \quad (6.33)$$

Here, and throughout this book, $Z = M/M_e^G$ is the number of entanglements per molecule. The reptation time, or disengagement time, τ_d , is then given by Eq. 6.34 [1].

$$\tau_d = \frac{L^2}{\pi^2 D} = \frac{\zeta N^3 b^4}{\pi^2 k T a^2} = 3 Z^3 \tau_e \quad (6.34)$$

The zero-shear viscosity, η_0 , can be obtained from the discrete spectrum of relaxation times given by Eq. 6.30 by using Eq. 4.16:

$$\eta_0 = \sum_{i \text{ odd}} G_i \tau_i \quad (6.35)$$

Using the expressions for G_i and τ_i given in Eq. 6.31, and noting that the sum converges very rapidly, we find that the zero shear viscosity is given by Eq. 6.36.

$$\eta_0 = \frac{\pi^2}{12} G_N^0 \tau_d \approx 0.822 G_N^0 \tau_d \quad (6.36)$$

The original tube model predicts that the spectrum of relaxation times, defined by Eq. 6.31, is quite narrow, i.e., it is dominated by the largest relaxation time τ_d . In fact, 98% of the zero-shear viscosity can be attributed to the slowest relaxation mode, which is controlled by the longest relaxation time τ_d , that is, to the first term in Eq. 6.35. Note that the reptation time, τ_d , is very sensitive to the number of entanglements per molecule Z , or, equivalently, to the molecular weight $M = Z M_e^G$, since τ_d scales with the third power of Z , and therefore with the third power of M .

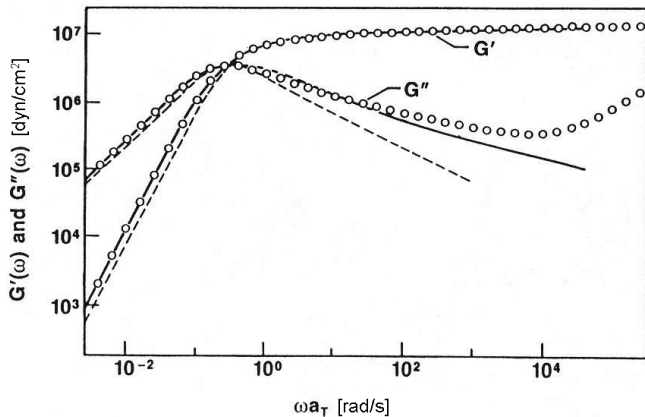


Figure 6.13 Linear moduli G' and G'' versus reduced frequency for a nearly monodisperse polybutadiene melt of molecular weight 360,000. The dashed lines are the predictions of the reptation theory. The solid lines include the effects of primitive path fluctuations; adapted from Pearson [33]

However, the relaxation of real polymers is not well described by reptation alone. Figure 6.13 compares the predictions of $G'(\omega)$ and $G''(\omega)$ for pure reptation with data for a nearly monodisperse polymer. As is explained in Section 4.3, the predictions of $G'(\omega)$ and $G''(\omega)$ can be obtained from the discrete spectrum parameters $\{G_i, \tau_i\}$ by use of Eqs. 4.40.

For relaxation by reptation only, the values of G_i are zero for even values of i . Note in Fig. 6.13 that the $G''(\omega)$ predicted by pure reptation decreases too rapidly with increasing frequency compared to the experimental response. This implies that real polymers have additional relaxation mechanisms besides reptation.

6.4.2 Primitive Path Fluctuations

One such additional relaxation mechanism is primitive path fluctuation. Since the tube diameter is much wider than the diameter of the chain, and the chain meanders within the tube, the chain is “wrinkled up” within its tube as shown in Fig. 6.9(b). The degree of wrinkling changes constantly, due to Brownian motion. Hence, by wrinkling more than usual (see Fig. 6.9(b)), the chain can pull its ends inside, thus vacating the ends of the tube. When the chain then “unwrinkles” a little, it pushes its ends out again, but these ends emerge into new, randomly created tube segments, and the stress associated with the now-vacated end tube segments is lost. Thus, the occupied tube (primitive path or contour length) fluctuates in length due to the Brownian motion of the polymer molecule, and stress is thereby relaxed. As one can readily imagine, primitive path fluctuations (PPF), otherwise known as contour

length fluctuations (CLF), relax the ends of the chain very rapidly, but relaxation of the center of the molecule by this mechanism is slow, because the chain must take on a highly wrinkled, and hence unlikely, conformation to vacate the center of the tube. For this reason, primitive path fluctuations are described by a very broad spectrum of relaxation times, much broader than for reptation. For primitive path fluctuations, each small portion of the tube is characterized by its own fluctuation relaxation time, the time required for that portion of the tube to be vacated by fluctuations. We therefore define a *tube coordinate* z that counts the length of chain, in units of the number of entanglements, from the chain ends towards the center of the chain. So, as shown in Fig. 6.14, z increases from 0 to $Z/2$ from the end of the tube to its center, where $Z = M/M_e^G$ is the number of entanglements per molecule. The typical time at which the portion of tube having coordinate value z is vacated by primitive path fluctuations is denoted by $\tau_{\text{fluc}}(z)$.

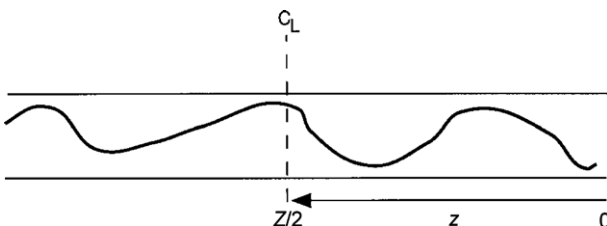


Figure 6.14 Definition of the tube coordinate z first used in Eq. 6.37.

For linear chains, only the portions near the chain ends relax by primitive path fluctuations, and we will use the symbol $\tau_{\text{early}}(z)$ in our development of a model for this fast relaxation. The interior parts of the chain, however, require quite deep fluctuations to reach them, and the time required to do this is slower than the time at which these portions of the chain will have already relaxed by reptation. We will later use the symbol $\tau_{\text{late}}(z)$ in our discussion of this process. For the parts of the chain near the ends, i.e., for z near zero, τ_{fluc} is equal to τ_{early} and is controlled by fast Rouse processes involving motion of the little bit of polymer near the end of the tube. This relaxation time was first estimated by Doi [34], and a more precise model was later proposed by Milner and McLeish, who called the motions involved “early-time chain end fluctuations” [35]:

$$\tau_{\text{early}}(z) = \frac{9}{16} \pi^3 \tau_e z^4 \quad (6.37)$$

Notice in Eq. 6.37 that the relaxation time of the tip of the chain (which is at $z = 0$) is very fast; i.e., it approaches zero in proportion to z^4 . Equation 6.37 applies for times less than the Rouse reorientation time, τ_r , which sets the longest time for “early” primitive path fluctuations.

While Eq. 6.37 gives the impression that there is a single effective relaxation time for the chain at tube coordinate z , with a relaxation profile that is single exponential, the reality is more complicated. Likhtman and McLeish [36] report that for early times the relaxation process is “strongly nonexponential.” Hence, Eq. 6.37 can be considered (at best) to be an estimate of the typical relaxation time for early fluctuations. It has, nevertheless, been widely applied in the literature for linear polymers [35] and (as will be seen in Chapter 9) branched polymers.

6.4.3 Reptation Combined with Primitive Path Fluctuations

For linear polymers, primitive path fluctuations (PPF or CLF) occur simultaneously with reptation. At short times (or high frequencies) the ends of the chain relax rapidly by primitive path fluctuation. But primitive path fluctuations are too slow to relax portions of the chain near the center, and these portions therefore relax only by reptation. However, the relaxation of the center by reptation is speeded up by primitive path fluctuations, because the tube remaining to be vacated by reptation is shortened, since its ends have already been vacated by primitive path fluctuations. Thus, the distance needed to reptate is less. The distance by which the tube is shortened can be estimated by noting that the typical time for primitive path fluctuations for tube coordinate z is given by Eq. 6.37. The typical time for moving a distance za along the tube by reptation (with diffusion constant given by Eq. 6.33) is estimated in Eq. 6.38 (ignoring numerical prefactors):

$$\tau_{\text{rep}}(z) \approx \frac{(za)^2}{D} \approx z^2 Z \tau_e \quad (6.38)$$

Equating Eq. 6.37 with Eq. 6.38 shows that primitive path fluctuations and reptation are competitive processes when $z \approx Z^{1/2}$; for smaller z PPF is the dominant process, while for larger z reptation is faster. The time at which this crossover occurs is, roughly, the Rouse reorientation time, τ_r . Thus we estimate that primitive path fluctuations relax the outer $Z^{1/2}$ entanglements, or a fraction $Z^{-1/2}$ of the length of the chain. So, the fraction of chain remaining to be relaxed by reptation is $(1 - X Z^{-1/2})$ where X is a constant that is somewhat greater than 1.47 [1, 34].

As a result, the longest reptation time τ_1 (i.e., the terminal relaxation time) and zero-shear viscosity are lower than in the absence of the fluctuations and can be approximated by the following equations [1]:

$$\tau_1 = \tau_d (1 - X Z^{-1/2})^2 \quad (6.39)$$

where τ_d is the reptation time in the absence of fluctuations, and the factor $(1 - X Z^{-1/2})$ is squared because the relaxation time, due to diffusion, depends on

the square of the distance travelled (as in Eq. 6.34). The zero-shear viscosity can then be calculated as follows:

$$\eta_0 = \eta_{0,\text{NF}} \left(1 - X Z^{-1/2}\right)^3 \quad (6.40)$$

where $\eta_{0,\text{NF}}$ is the zero-shear viscosity in the absence of fluctuation effects. Equation 6.40 contains a further factor of $(1 - X Z^{-1/2})$ beyond Eq. 6.39 because, in addition to the reduction in terminal time, the terminal modulus is also reduced because of the shortened tube. A slightly more accurate formula for the corrections to the longest relaxation time was given by Likhtman and McLeish [36], namely:

$$\frac{\tau_1}{\tau_d} = 1 - \frac{3.38}{\sqrt{Z}} + \frac{4.17}{Z} - \frac{1.55}{Z^{1.5}} \quad (6.41)$$

Figure 6.15 compares the prediction of Eq. 6.40 (thick line) with that for pure reptation, which is given by Eqs. 6.34 and 6.36 (thin line). Note that the two predictions merge at high molecular weight, where the influence of primitive path fluctuations becomes small. Over the range $5 \ll M/M_e \ll 200$, the prediction of Eq. 6.40 can be approximated by a power law, $\tau_1 \propto M^\alpha$ where α is roughly 3.4, which is shown by the dashed line in Fig. 6.15. The particular exponent that fits best will depend on

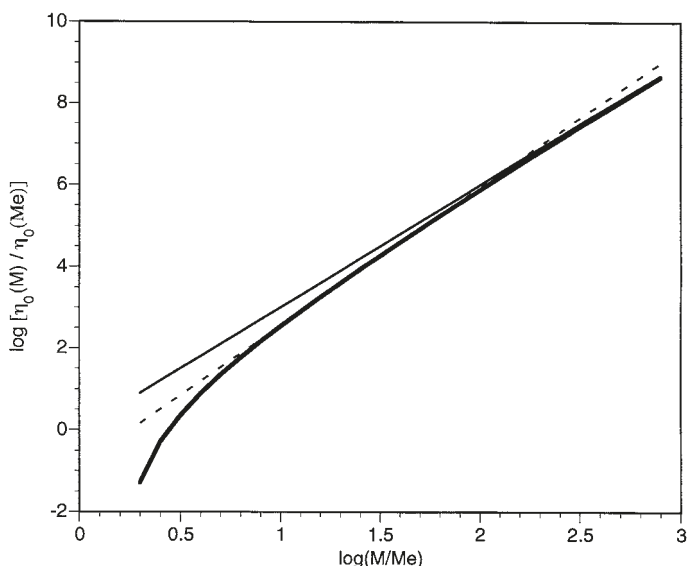


Figure 6.15 Prediction of the zero-shear viscosity η_0 , normalized by the zero-shear viscosity of a polymer with molecular weight corresponding to one entanglement, as a function of normalized molecular weight $Z = M/M_e$ for pure reptation (solid thin line), reptation with fluctuations, given by Eq. 6.40 with $X = 1.3$ (solid thick line) and the empirical formula $\eta_0 \propto M^{3.4}$ (dashed line).

the range of molecular weights over which the fit is made, and so there is nothing sacred about the precise value 3.4. Indeed, while the “3.4 power law” has achieved a certain iconic status in the field of polymer rheology, experimental values for the exponent range from 3.3 to 3.6. Thus, the combination of reptation and primitive path fluctuations explains the molecular weight dependence of the longest relaxation time τ_1 and thus of the zero-shear viscosity of linear polymers [34]. This explanation of the long-mysterious “3.4 power law” for the viscosity of highly entangled melts is one of the major achievements of the tube model, and of polymer physics in general.

Primitive path fluctuations (PPF or CLF) also broaden the spectrum of relaxation times. Note that in Fig. 6.13, the inclusion of PPF results in a less steep decrease in G'' with frequency (at frequencies just above the one where G'' has a local maximum) than is predicted by reptation alone. This is a manifestation of the broader distribution of relaxation times.

The combination of reptation and primitive path fluctuations (PPF) with fast Rouse relaxation also explains almost quantitatively the linear viscoelasticity of monodisperse melts of linear chains. Figure 6.16 shows $G''(\omega)$ data for three nearly monodisperse polystyrene melts along with the predictions of Milner and McLeish [35], which account for reptation, primitive path fluctuations, and high frequency Rouse modes. With only the equilibration time τ_e and the plateau modulus G_N^0 as adjustable parameters, the agreement between predictions and experiments shown in Fig. 6.16 was obtained. This excellent agreement shows that quantitative molecular theories of linear viscoelasticity are possible. Other quantitative theories for linear polymers have been developed using similar ideas to those contained in the Milner-McLeish theory. These related theories include the *dual constraint model*, described in Pattamaprom et al. [11, 37], as well as a detailed and comprehensive model by Likhtman and McLeish [36]. More recent works suggest that Likhtman and McLeish marginally overestimated the effects of primitive path fluctuations [38, 39]. Similar ideas have been incorporated into the theories of Marin and coworkers [40, 41], Carrot et al. [42], and others, as will be discussed in Chapter 8. These have all been generally successful in predicting the linear rheology of nearly monodisperse melts, including melts of polystyrene, 1,4-polybutadiene, 1,4-polyisoprene, and hydrogenated 1,4-polybutadiene. The latter melt is very similar to high density polyethylene. These theories could, in principle, be used in an inverse fashion to infer molecular weights and molecular weight distributions from rheological data. Methods for doing this are described in Chapter 8.

Although reptation and primitive path fluctuations together provide a nearly quantitative prediction of the linear viscoelasticity of monodisperse melts of linear chains, for polydisperse melts it is clear that these are not the only important relaxation mechanisms. To develop quantitative, or even qualitative, theories for polydisperse melts, *constraint release* must be taken into account.

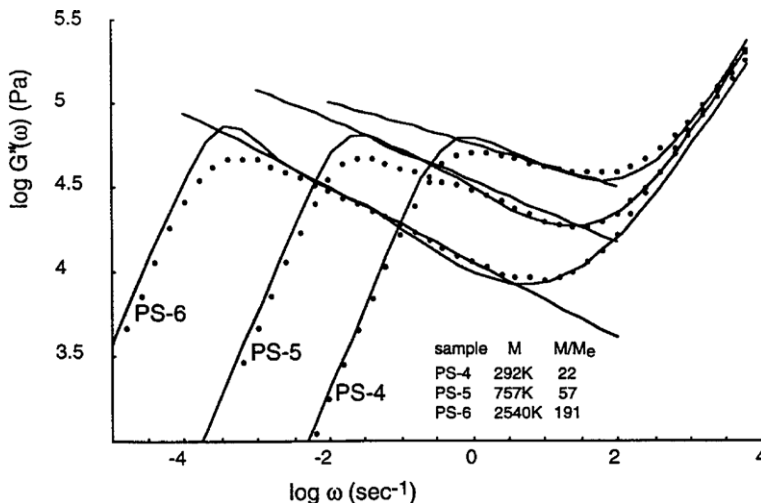


Figure 6.16 Storage modulus data (symbols) of Schausberger et al. [43] for three nearly monodisperse polystyrene samples having the molecular weights shown. The curves through the data are the predictions of the theory of Milner and McLeish [35], which includes both reptation and primitive path fluctuations. The straight lines, drawn to aid the eye, have slopes of $-1/8$, $-1/5.5$, and $-1/4.5$. The slope in this frequency region deviates from the Doi-Edwards [1] prediction of $-1/2$, because of the increasing importance of primitive path fluctuations, as the molecular weight decreases. The plateau modulus G_N^0 and the equilibration time τ_0 were adjusted to obtain the best fit. The upturn in the moduli at high frequency are produced by high frequency Rouse modes within the tube, discussed in Section 6.4.5; from Milner and McLeish [35]

6.4.4 Constraint Release—Double Reptation

So far we have taken the tube to be fixed and have assumed that the relaxation of a polymer chain requires that it escape from its tube. However, the tube is defined by the matrix chains surrounding the test chain in the tube, and these matrix chains are all also moving. So, while the test chain is undergoing reptation and primitive path fluctuation, the matrix chains are undergoing similar motions. To view it another way, at the same time that the test chain is constrained by entanglements with surrounding matrix chains, it is also imposing topological constraints on those chains. When the test chain reptates, it therefore releases constraints on the matrix chains, and when the matrix chains reptate, they release their constraints on the test chain. The process of constraint release therefore accelerates the relaxation of the melt. It turns out that the effect of this constraint release on monodisperse, linear, polymers is rather minor. But for polydisperse linear polymers (or branched polymers), its effects cannot be ignored.

The process of constraint release is in general very complex, and a completely general, rigorous, theory has not yet been developed. Nevertheless, there is a simple description of constraint release called *double reptation* that is reasonably accurate for many cases of practical importance. More rigorous, general theories of constraint release are presented in Chapter 7.

The theory of double reptation was derived in somewhat different ways by Tuminello [44], Tsenoglou [45], and des Cloizeaux [46]. In each version, an entanglement is viewed as an interaction of two chains, both of which must continue to participate in the interaction for it to remain intact. If reptation causes a chain end on either chain to pass through the entanglement point, then that entanglement is lost to both chains. If the unrelaxed stress at time t is assumed to be proportional to the fraction of surviving entanglement points at that time, and if the two chains participating in the entanglement reptate independently, then it follows that the relaxation modulus should be simply proportional to the square of the tube survival probability $P(t)$ for a single chain. This idea is expressed by Eq. 6.42.

$$G(t) = G_N^0 P^2(t) \quad (6.42)$$

6.4.4.1 Monodisperse Melts

The simple replacement of $P(t)$ by P^2 as shown in Eq. 6.42 (which does not account for primitive path fluctuations) does not have much effect on the relaxation modulus of monodisperse linear chains, as mentioned previously. This is because the relaxation spectrum for reptation is dominated by a single, longest relaxation time. If all relaxation times except the longest are neglected, we find from Eqs. 6.29 and 6.42 that

$$G(t) = G_N^0 \exp(-2t/\tau_d) \quad (6.43)$$

where the factor of two in the exponential comes from the squaring of the survival probability $P(t)$. From the definition of the relaxation time, we see from Eq. 6.43 that the longest relaxation time in double reptation is $\tau_1 = \tau_d/2$, which is half the reptation time of a chain in the absence of constraint release. The predicted reduction of the relaxation time as a result of constraint release agrees to some extent with observations, which indicate that the relaxation time of a polymer chain in a monodisperse melt is about one third that in a matrix of very long chains that reptate too slowly to release constraints [2]. Although the factor of one third is different from the predicted factor of one half, the double reptation prediction is qualitatively correct. Apart from changing the longest relaxation time by this modest factor, constraint release, as described by double reptation, has little effect on the shape of the relaxation spectrum of a monodisperse linear polymer.

6.4.4.2 Bidisperse Melts

For polydisperse polymers, double reptation, as modeled by Eq. 6.42, has a much stronger effect. To illustrate this, consider the case of a mixture of two monodisperse polymers, a long chain and a short chain, with volume fractions ϕ_L of the long chain and $\phi_S = 1 - \phi_L$ of the short one. Although this example of a “binary” mixture of two monodisperse polymers is rather academic and of little commercial interest, it is useful for illustrating how double reptation works. Let us again neglect all relaxation modes except the slowest for each chain. If we imagine that all chains are in fixed tubes, i.e., that there is no constraint release, then the tube survival probability $P(t)$ for the whole melt is just the weighted average over the two types of chain, as shown by Eq. 6.44.

$$P(t) = \phi_L \exp(-t/\tau_{d,L}) + \phi_S \exp(-t/\tau_{d,S}) \quad (6.44)$$

Here $\tau_{d,L}$ and $\tau_{d,S}$ are the reptation times of the long and short chains, respectively. If we neglect constraint release, the relaxation modulus $G(t)$ is just $P(t)$ times the plateau modulus G_N^0 . To calculate the stress relaxation modulus, including the effects of constraint release using the double reptation theory, we merely square $P(t)$ as follows:

$$\begin{aligned} G(t)/G_N^0 &= P^2(t) = [\phi_L \exp(-t/\tau_{d,L}) + \phi_S \exp(-t/\tau_{d,S})]^2 \\ &= \phi_L^2 \exp(-2t/\tau_{d,L}) + \phi_S^2 \exp(-2t/\tau_{d,S}) + 2\phi_L\phi_S \exp\left[-t\left(\frac{1}{\tau_{d,L}} + \frac{1}{\tau_{d,S}}\right)\right] \end{aligned} \quad (6.45)$$

This relaxation modulus is different from the one obtained without constraint release, Eq. 6.44, in three ways. First, the factor of two appears in the exponents of the first and second terms of Eq. 6.45, just as it did for monodisperse polymers in Eq. 6.43. Second, the weighting of the contributions to the modulus from the long and short chains is proportional to the concentration of those chains squared in Eq. 6.45, rather than as the first power in Eq. 6.44. And third, with double reptation there is a cross-term that depends on the relaxation times of both components. If, however, the short chain is considerably shorter than the long chain, then because of the steep power-law dependence of the reptation time on chain length, the contribution of $1/\tau_{d,L}$ in the third term will be negligible compared to that of $1/\tau_{d,S}$. Thus, the time constant governing the third term will be approximately $\tau_{d,S}$, the relaxation time of the short chain. The contribution from this cross-term thus occurs on a time scale that is not too far separated from that of the second term. Crudely, then, double reptation predicts that a binary blend of two monodisperse polymers with widely separated molecular weights will show two prominent relaxations. One of these is due to entanglements of the long chain with other long chains and is of relative magnitude ϕ_L^2 .

The other is due to relaxation of entanglements between two short chains, or entanglements of short chains with long chains. This second relaxation has a relative magnitude of $(1 - \phi_L^2)$.

This prediction of double reptation theory has been verified. The most useful data for this purpose are those for the loss modulus, which shows a peak at any frequency where there is a prominent relaxation process. Figure 6.17 shows the loss modulus as a function of frequency, with G'' plotted on a linear scale, for binary blends of a long- and a short-chain polybutadiene [47] where the fractions ϕ_L of long chains are equal to 1.0, 0.882, 0.768, and 0.638. The squares of these values are: 1.0, 0.777, 0.589, and 0.407. Figure 6.14 reveals two peaks in the loss modulus. The height of the low-frequency one is indeed proportional to ϕ_L^2 . Thus, the simple double reptation formula captures some important aspects of constraint release in polymer melts.

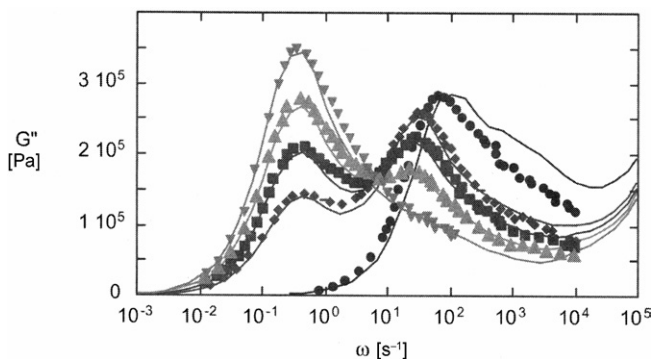


Figure 6.17 Loss modulus data for bidisperse polybutadienes ($MW = 70,900$ and $335,000$) at 30°C on a log-linear scale (from Rubinstein and Colby [47]). The volume fractions of the high molecular weight component (x_L) from right to left are 0.0, 0.638, 0.768, 0.882, and 1.0, respectively. The lines are predictions of the “dual constraint model”; adapted from Pattamaprom et al. [11].

The simple double reptation theory presented above, while qualitatively predicting the existence of two peaks in the $G''(\omega)$ curve, does a poor job of describing the precise shapes of these curves for bidisperse polymers. A number of more sophisticated models, founded on the double reptation concept, are available (e.g., [11, 37, 41, 48, and 49]). The curves in Fig. 6.17 are the predictions of one such model, the *dual constraint model* [11, 37], which is similar to the Milner-McLeish theory but extended to allow bidisperse or polydisperse molecular weight distributions. The double reptation prediction for a binary blend of polystyrenes is plotted in Fig. 6.18, which shows that the predicted peaks in $G''(\omega)$ are too sharp, and the high-frequency upturn in the data is missing from the predictions. The high-frequency upturn is missing because of the omission of the high-frequency Rouse modes (see Section 6.4.5 below).

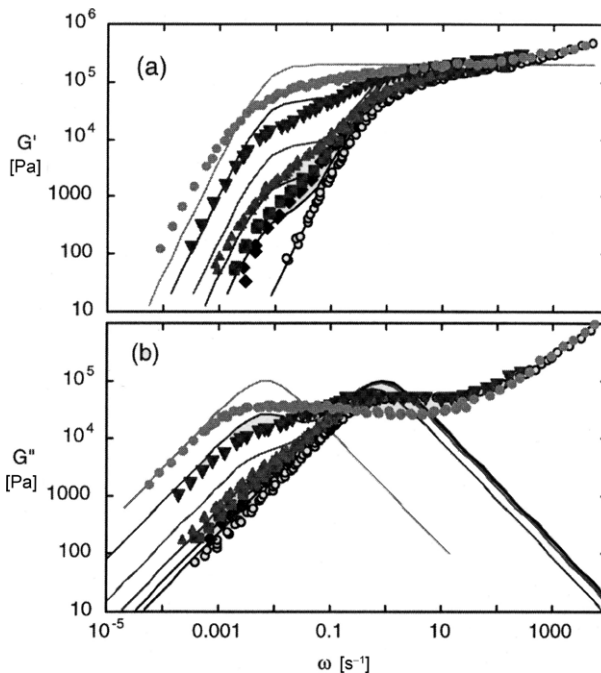


Figure 6.18 Comparison of the predictions of the double reptation model (lines) to experimental data (symbols) for (a) the storage modulus G' , and (b) the loss modulus G'' , for bidisperse polystyrenes ($\text{MW} = 160,000$ and $670,000$) at $160\text{ }^{\circ}\text{C}$ [50]. The volume fractions of the high molecular weight component (ϕ_L) from right to left are $0.0, 0.05, 0.1, 0.2, 0.5$, and 1.0 , respectively. The parameter values are $G_N^0 = 2 \cdot 10^5 \text{ Pa}$ and $K = 4.6 \cdot 10^{-18} \text{ s}/(\text{mol})^{3.4}$. The latter value, obtained by a best fit to the data for monodisperse samples, is almost identical to the value ($K = 4.55 \cdot 10^{-18} \text{ s}/(\text{mol})^{3.4}$) obtained using Eq. 7.13 with $\tau_e = 0.00375$; adapted from Pattamaprom and Larson [37]

The sharpness of the predicted peaks is partly due to the use of a single relaxation time for each component of the bidisperse melt. This deficiency can easily be fixed by including the full reptation relaxation spectrum for each component. That is, for $P(t)$ we can generalize Eq. 6.29 for the double reptation model to include two components:

$$P(t) = \phi_L \frac{8}{\pi^2} \sum_{i_{\text{odd}}} i^{-2} \exp(-t^2 t/\tau_{d,L}) + \phi_S \frac{8}{\pi^2} \sum_{i_{\text{odd}}} i^{-2} \exp(-t^2 t/\tau_{d,S}) \quad (6.46)$$

This will broaden the spectrum of relaxation times compared to the single-relaxation-time approximation. Nevertheless, because the Doi-Edwards relaxation spectrum is so narrow (i.e., the modes higher than the first mode have very little weight), inclusion of these extra modes does not improve the predictions of the double reptation theory very much. More significant improvements in describing the

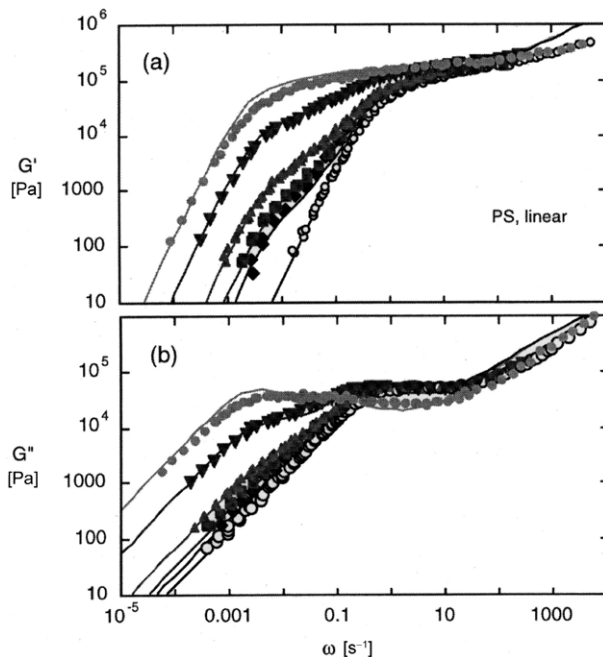


Figure 6.19 Comparison of the predictions of the dual constraint model (lines) to experimental data (symbols) in Fig. 6.18. The parameter values are $G_N^0 = 2 \cdot 10^5$ Pa and $\tau_e = 0.01$ s. The latter value gave the best fit to the data for the monodisperse samples; adapted from Pattamaprom and Larson [37]

shape of the peaks in $G''(\omega)$ can be made by including the fast modes of primitive path fluctuation. These were required to obtain a good prediction of the $G'(\omega)$ and $G''(\omega)$ curves for monodisperse polymers, as shown by Fig. 6.16, and they are also required for good predictions of the behavior of bidisperse polymers. In Fig. 6.19, the dual constraint model predictions of G' and G'' are compared to data for the same binary blend of polystyrenes, displaying improved predictions in the moderate frequency region, due to inclusion of primitive path fluctuations. The upturn in G' and G'' in the high-frequency region is correctly predicted by the dual constraint model, because it also includes high frequency Rouse relaxation modes (see section 6.4.5). Despite what we said previously, in one sense fluctuations have been included in the double reptation predictions of Fig. 6.18. As was explained in connection with Fig. 6.15, primitive path fluctuations affect even the longest relaxation time of a polymer, changing the 3.0 power-law exponent for the dependence of viscosity on molecular weight predicted by pure reptation to a somewhat higher exponent of around 3.4 power or so. Thus, if we neglect fluctuations entirely, we cannot hope to predict the correct peak positions in $G''(\omega)$. So in the predictions shown in Fig. 6.18, the longest relaxation times used for the short and long chains in Eq. 6.45 were not

those for pure reptation, Eq. 6.34, but were calculated using the following empirical formula proposed by Mead [51]:

$$\tau_{d,i}^{\text{eff}} = K Z_i^{3.4} \quad (6.47)$$

where K is an empirical constant typically obtained by fitting experimental data for monodisperse samples. This expression implicitly accounts for the effect of fluctuations on the longest relaxation time, since it is primitive path fluctuations that change the exponent 3.0 for pure reptation to around 3.4 for reptation combined with PPF. The predictions of the basic double reptation theory shown in Fig. 6.18 were obtained by using Eq. 6.47 for the relaxation times of the two components of the melt. Of course, this correction only fixes the predictions of the peak locations in $G''(\omega)$ and cannot correct the shapes of those peaks for bidisperse polymers, because the additional relaxation modes produced by primitive path fluctuations are still neglected by the basic double reptation theory.

While the basic double reptation theory, with a single-exponential relaxation *kernel* function for each molecular weight component, does not predict very accurately the shapes of linear viscoelastic moduli, des Cloizeaux [48] has suggested a more sophisticated kernel function that provides much more accurate predictions for nearly monodisperse or bidisperse polymers. Still other kernel functions have also been suggested, which, when combined with the double reptation ansatz, have been shown to be quite successful in matching linear viscoelastic data, especially when the double reptation exponent is made slightly higher (around 2.25) than its canonical value of two [49]. In addition to the canonical value of two, a theoretical value for this exponent of around 7/3 could also be rationalized; see Section 9.3.2.

However, a more fundamental problem of the double reptation concept is the assumption, implicit in Eqs 6.44 and 6.46, that the relaxation times and relaxation kernel functions for the long and short chains are unaffected by the presence of the other chain lengths. This assumption implies that the relaxation functions, determined by measurements on pure melts of the long or short chains, can then be used to predict the relaxation of all blends of the two components. For the particular blends of Fig 6.17, this assumption turns out to be reasonable, especially for the longer chains (for example, the peak in the loss modulus corresponding to relaxation of the long chains remains at approximately the same frequency for all the blends). However, this observation does not apply to all bidisperse melts, and it is frequently observed that the relaxation of the long chains is significantly accelerated by dilution in short chains (even when those short chains are still long enough to be entangled) [52–54]. As an illustration of this, Fig. 6.20 shows the storage and loss moduli for two series of polyisoprene bidisperse melts (a blend of MW = 483 kg/mol and 33.6 kg/mol, and a blend of MW = 226 kg/mol and 23.4 kg/mol). In each case, the terminal relaxation of the long chains is observed to move to higher frequencies with increasing dilu-

tion, indicating that the relaxation function of the long chains is indeed affected by the short chains. Similarly, there are indications that the presence of long chains marginally slows down the relaxation of the short chains. This serves to illustrate that the relaxation of bidisperse entangled melts is subtler than implied by double reptation theory, and requires careful consideration. We will discuss constraint release effects in bidisperse melts in more detail in Chapter 7.

Fortunately, many of the subtleties exposed through a detailed consideration of bidisperse systems are hidden in the broader relaxation spectra associated with fully polydisperse melts, where double reptation theory is more practically applied.

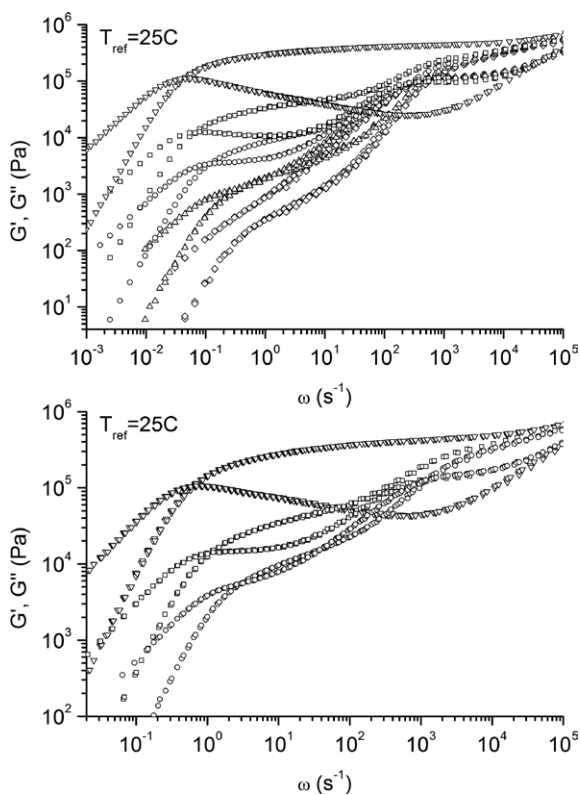


Figure 6.20 The upper graph shows the storage and loss modulus as a function of frequency for polyisoprene melts which are mixtures of 483 kg/mol and 33.6 kg/mol linear chains, at concentrations of (from top to bottom) 100%, 40%, 20%, 10%, and 4% of the long chains by weight. The lower graph shows similar data for polyisoprene melts, which are mixtures of 226 kg/mol and 23.4 kg/mol chains, at concentrations of 100%, 40% and 20% long chains by weight. For reference, the entanglement molecular weight of polyisoprene is considered to be in the range of 4–5 kg/mol. In both cases, dilution of the long chains with shorter (but still entangled) chains results in a decrease in the terminal relaxation time of the longer chains, in contradiction to double reptation predictions.

6.4.4.3 Polydisperse Melts

Commercial melts are neither monodisperse nor bidisperse, but usually have a broad, continuous, distribution of relaxation times with polydispersity ratios, M_w/M_n , greater than or equal to 2.0. We will start our discussion of the effect of polydispersity by replacing the exponential in Eq. 6.43 with a dimensionless relaxation function $F(t, M)$ to obtain a general expression for the relaxation modulus (reptation only) of a monodisperse polymer:

$$G(t) = G_N^0 F(t, M) \quad (6.48)$$

If we were to naïvely apply this theory to a polydisperse polymer, we would simply sum the weighted relaxation functions for the various molecular weights present and write:

$$G(t) = G_N^0 \sum_i w_i F(t, M_i) \quad (6.49)$$

In Eq. 6.49, $F(t, M_i)$ is the normalized relaxation modulus for a monodisperse melt composed of molecules of molecular weight M_i , and w_i is the weight fraction (or equivalently, the volume fraction) of component i in the mixture. However, Eq. 6.49 fails to account for the fact that the shorter molecules reptate faster than the longer ones, so the tube cannot be assumed to be fixed during the entire period of relaxation of a long molecule. This is where the double reptation theory can be employed to great advantage.

Actually, it is the performance of the double reptation theory for broad molecular weight distributions that is of the greatest practical importance. The double reptation model predicts the shapes of the $G'(\omega)$ and $G''(\omega)$ curves rather well for such melts, better than it does for monodisperse or bidisperse melts. The reason for this is that when the molecular weight distribution is broad, the peak in $G''(\omega)$ is smeared out, or entirely eliminated, and the omission of the fast fluctuation modes for a given molecular weight is masked by the longest-relaxation-time contributions of the other molecular weights. For polydisperse polymers, the double reptation formula for the relaxation modulus is written as:

$$G(t) = G_N^0 \left[\sum_i w_i F(t, M_i)^{1/2} \right]^2 \quad (6.50)$$

Thus, according to Eq. 6.50, if one knows the normalized relaxation modulus $F(t, M_i)$ of a monodisperse polymer as a function of molecular weight within the appropriate range, one can compute the relaxation modulus for any polydisperse polymer containing molecules with molecular weights within that range. Equation 6.50 can therefore be thought of as a simple mixing formula analogous to mixing formulas for viscosities.

From the tube model with simple reptation, the function $F(t, M_i)$ is given by

$$F(t, M_i)^{1/2} = P_i(t, M_i) = \frac{8}{\pi^2} \sum_{j \text{ odd}} j^2 \exp(-j^2 t/\tau_{d,i}) \quad (6.51)$$

The subscript i on P designates this function is for component i in a fixed tube, and the time constant $\tau_{d,i}$ depends on the molecular weight M_i of component i .

As was noted earlier, the summation in Eq. 6.51 is dominated by the term with the longest relaxation time, $\tau_{d,i}$, and a reasonable approximation is to retain just the first term of the series (with the prefactor $8/\pi^2$ changed to unity):

$$P_i(t, M_i) \approx \exp(-t/\tau_{d,i}) \quad (6.52)$$

Hence, the function $F(t, M_i)$ used in the double reptation expression, Eq. 6.50, is just the square of this:

$$F(t, M_i) = \exp(-2t/\tau_{d,i}) = \exp(-t/\tau'_{d,i}) \quad (6.53)$$

where $\tau'_{d,i} = \tau_{d,i}/2$ is the longest relaxation time of chain i in a monodisperse melt, with constraint release effects included via double reptation.

As mentioned in Section 6.4.4.1, the double reptation theory contains no explicit treatment of primitive path fluctuations, and if the theoretical expression Eq. 6.34 is used for the reptation time, it will predict that a monodisperse melt will have a longest relaxation time proportional to the third power of molecular weight, in disagreement with the observed 3.4 power-law dependence. A simple way of dealing with this is to use the empirical formula, Eq. 6.47, for the longest relaxation time. More sophisticated ways are available for dealing with this limitation [49], but here we confine ourselves to this simple fix, which is adequate for many commercial polymers with broad (but not too broad) molecular weight distributions.

With this correction, double reptation theory automatically gives the correct terminal relaxation behavior of monodisperse melts. We shall see shortly that when K is fitted using data for monodisperse melts, double reptation theory fits data for polydisperse polymer melts quite well at low and modest frequencies, if the molecular weight distribution is moderately broad, (M_w/M_n between 2 and 3), and has no more than a few percent by weight of chains that are too short to be well entangled. As is explained in Chapter 8, empirical “mixing rules” other than Eq. 6.50 for the linear relaxation modulus have sometimes been used to give better agreement with experimental data.

To illustrate this, in Figs. 6.21(a) and (b) we compare the predictions of the double reptation model against data for both a monodisperse and a polydisperse polystyrene of nearly the same molecular weight at 150 °C [37]. The sample of Fig. 6.21(a) is a nearly monodisperse polystyrene, with $M_w = 363,000$, and $M_w/M_n = 1.03$.

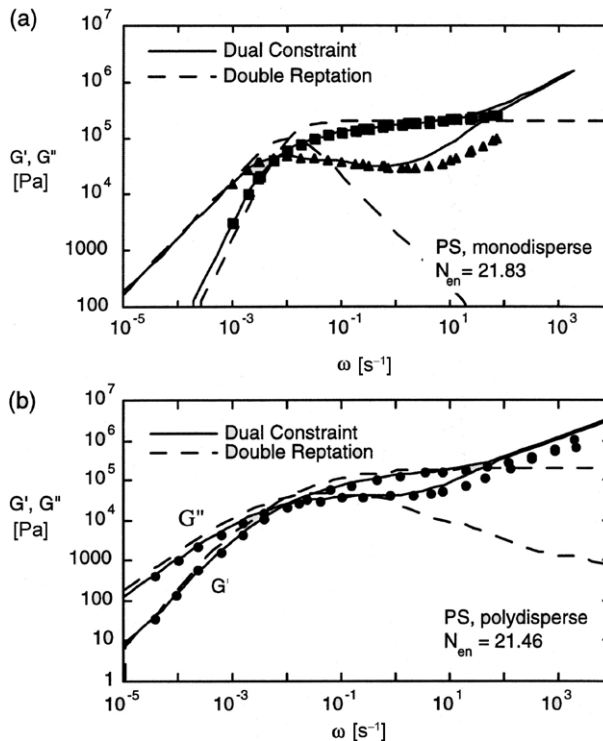


Figure 6.21 (a) Comparison of the predictions of the dual constraint model (solid lines) and the double reptation model (broken lines) to experimental data (symbols) for the storage modulus, G' , and the loss modulus, G'' , for monodisperse linear polystyrene ($M_w = 363,000$) at 150 °C. The parameter values are: $G_N^0 = 2 \times 105 \text{ Pa}$ and $\tau_e = 0.05 \text{ s}$, the latter value being obtained as a best fit. From this value of τ_e , after multiplying it by the correction factor of 0.375 in footnote (g) of Table 7.1, the value $K = 2.275 \times 10^{-17} \text{ s}/(\text{mol})^{3.4}$ for the double reptation model is obtained from Eq. 7.13 (from Pattamaprom and Larson [37]). (b) The same as (a), except the sample is a polydisperse polystyrene ($M_w = 357,000$; $M_w/M_n = 2.3$) constructed from 11 monodisperse components, again at 150 °C. The parameter values are the same as in (a). (In the predictions of the dual constraint model, a factor of 1/3 replaced the factor of 1/5 in Eq. 6.54 for the Rouse modes); adapted from Pattamaprom and Larson [37]

The linear rheology for this sample has been fitted by the double reptation theory in the terminal region, yielding a value of $K = 2.275 \times 10^{-17}$ at 150 °C for the double reptation constant. Using this value of K , we make the *a priori* predictions shown in Fig. 6.21(b) (at 150 °C) of the linear moduli of the polydisperse sample ($M_w/M_n = 2.3$) with $M_w = 357,000$, which is very close to the molecular weight of the monodisperse sample. This polydisperse sample is a special “cocktail” prepared by Wasserman and Graessley [55] that contains 11 nearly monodisperse polystyrenes mixed together to produce a polydisperse sample with $M_w/M_n = 2.3$.

Since the latter sample was made from known monodisperse fractions, its polydispersity is accurately known *a priori*, without recourse to a GPC determination. Note that the *a priori* prediction of the linear behavior of the polydisperse sample is remarkably good in the vicinity of the terminal zone.

Note also in Figs. 6.21(a) and (b), while the double reptation model (dashed lines) predicts the terminal region well, the prediction for $G''(\omega)$ plunges to very low values at high frequency because of the neglect of high-frequency primitive path fluctuations and Rouse motion within the tube. Hence, for monodisperse polymers, the double reptation model provides a good prediction only over a rather limited range of frequencies. The predictions of the *dual constraint* model [11, 37], introduced in Section 6.4.4.2, are also shown in Figs. 6.21(a) and (b). Predictions in the intermediate and high frequency regions are improved through inclusion of primitive path fluctuations (Section 6.4.2) and Rouse relaxation modes (Section 6.4.5) respectively. These are similar to the improvements in the bidisperse melt predictions of Fig. 6.19. We note that the high-frequency Rouse relaxation terms could be added to the double reptation theory simply by adding the appropriate terms (Section 6.4.5) to the double reptation expressions.

While the double reptation model does give reasonable predictions of the terminal relaxation of mildly polydisperse melts, it does predict a weak increase in zero shear viscosity η_0 with increasing polydispersity [37]. This prediction of the double reptation model is in slight disagreement with experiments, which show essentially no effect of molecular weight distribution for small polydispersities $M_w/M_n < 4$. More sophisticated treatments, such as the dual constraint model [37], correct this slight discrepancy, which seems (once again) to be due to incorrect treatment of primitive path fluctuations in the double reptation model. The effect of polydispersity on the relationship between zero-shear viscosity and M_w is discussed in detail in Section 5.2.2.

We also note that similar predictions can be obtained for other polydisperse linear melts, including polyethylene; see, for example, Figs. 7.13 and 9.5(a). And other, related models appear to give predictions roughly equivalent to those of the dual constraint model. Of particular note is the work of Marin and coworkers [40, 41], whose model is described in more detail in Chapter 8, and the double reptation model with a more complex kernel relaxation function $F(t)$ [49].

6.4.5 Rouse Relaxation within the Tube

The final relaxation mechanism to be considered is Rouse relaxation within the tube. The Rouse model was described in Section 6.2 for unentangled polymers. For entangled polymers, Rouse relaxation is hindered by the presence of the entangle-

ment tube, which blocks long-range Rouse motions that would cause the chain to escape through the walls of the tube. However, Rouse motions are not completely quenched by entanglements and can still contribute to relaxation. One way in which this can occur has already been discussed; Rouse motions that occur at a chain end lead to evacuation of tube segments near the end of the tube and are responsible for relaxation by *primitive path fluctuations*, discussed in Section 6.4.2. In addition, however, Rouse motions can also occur in the interior of the tube, away from the ends, where they relax stress either within a single tube segment, or they shuttle monomers longitudinally from one tube segment to another. Rouse motions within a single tube segment, because of their short range, involve only the higher frequency components of the Rouse spectrum and have relaxation times shorter than τ_e , the time at which the chain segments first feel the constraints imposed by the tube. The slower *longitudinal* Rouse motions that shuttle monomers along the axis of the tube have longer relaxation times. The slowest of these longitudinal Rouse motions is governed by the longest Rouse reorientation time, $\tau_{r,i}$ for a molecule with $M = M_i$, which can be obtained from Eq. 6.3. As discussed in Section 6.3.5, the equilibration time τ_e is the Rouse reorientation relaxation time for an entanglement segment of a chain and is independent of chain length, i.e., of the molecular weight of the polymer. τ_e is related to $\tau_{r,i}$ by $\tau_e = \tau_{r,i} / Z_i^2$ (see ref. [1], p. 214).

The division of spatial scales separating the very high-frequency, local Rouse processes (with time scales less than τ_e) from the longitudinal Rouse modes (with time scales greater than τ_e) has been represented by Likhtman and McLeish [36] using an approximate *fragmented* Rouse spectrum to calculate the Rouse relaxation modulus $G_{R,i}$ of chain i :

$$G_{R,i}(t) = w_i \frac{5 G_N^0}{4 Z_i} \left[\frac{1}{5} \sum_{p=1}^{Z_i-1} \exp\left(-\frac{p^2 t}{\tau_{r,i}}\right) + \sum_{p=Z_i}^{N_i} \exp\left(-\frac{2 p^2 t}{\tau_{r,i}}\right) \right] \quad (6.54)$$

The first term accounts for the slow longitudinal modes that re-equilibrate chain density along the one-dimensional tube coordinate, rather than in three-dimensional space, as in the ordinary Rouse theory. Their magnitude is therefore reduced by a factor of five relative to ordinary Rouse relaxation. Likhtman and McLeish [36] showed that this factor of 1/5 included in Eq. 6.54 is more accurate than the value of 1/3 suggested earlier by Milner and McLeish, and is related to the factor of 4/5 in Eq. 6.21 for the relation between entanglement molecular weight and plateau modulus. (That is, the longitudinal Rouse relaxation relaxes 1/5 of the stress that would otherwise contribute to the plateau modulus G_N^0 .) The second term in Eq. 6.54 accounts for fast Rouse relaxation of portions of the chain that are small enough to reside within a single tube segment and hence experience full three-dimensional motion; therefore, there is no fractional numerical pre-factor in front of this term. The factor of two in the exponential has the same origin as the factor of two in Eq. 6.1:

this second term is dealing with stress relaxation within the Rouse model, and $\tau_{r,i}$ is the Rouse reorientation time (see also Eq 6.3). The relaxations comprising the second term have time constants of $\tau_e/2$ or less. The inclusion of Rouse relaxation within the tube adds an upturn to G' and G'' at high frequency, as can be seen in the data and predictions in Figs. 6.16 through 6.21.

■ 6.5 An Alternative Picture for Entangled Polymers: Slip-Links

The above description of relaxation processes was framed wholly by using the language of the “tube model,” which has been the dominant paradigm for discussion and modeling of entangled polymer dynamics since the pioneering work of Doi and Edwards [1]. The tube model provides a useful picture for imagining the dynamics of entangled polymers, and for developing a mathematical description of those dynamics. However, it is not a “model” in the very strictest sense, in that it does not provide a precisely defined and agreed-upon set of dynamical rules that could (for example) be implemented within a computer simulation. Hence, different groups sometimes produce different mathematical results which seem consistent with the tube picture, but giving different predictions. For example, there remains debate as to the correct mathematical description of constraint release, discussed in more detail in Chapters 7 and 9.

In one of their celebrated papers, Doi and Edwards [56] discussed a second model that they claimed could be used interchangeably with the tube picture: the slip-link model (see Fig. 6.22). In this model, entanglements are represented as small “rings” (the slip-links) through which a polymer chain can pass freely. The vector from one ring to the next then becomes equivalent to the “*tube segment*” in the tube theory, so that adjacent rings are typically a distance a apart (the tube diameter), and the chain between two rings contains typically M_e^G monomers (the entanglement molecular weight). Thus, there seems at least a strong equivalence between the slip-link model and the tube model: free motion of the chain through slip-links permits the exact equivalent of reptation and contour-length fluctuations. However, an advantage of the slip-link model (over the tube model) is that it is easier to write down a clear set of dynamical variables to represent a chain constrained by slip-links, and so it is correspondingly easier to define computational algorithms to simulate the chain dynamics within a slip-link model. With recent increases in computational power, slip-links have become a useful tool for investigation of entangled polymer dynamics and prediction of viscoelasticity.

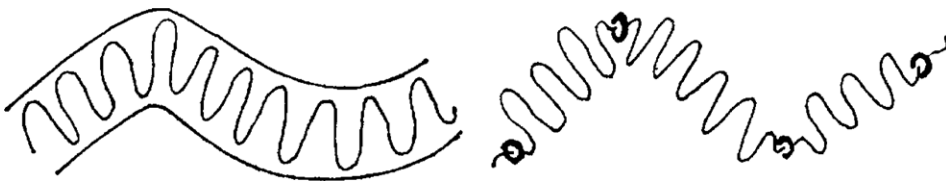


Figure 6.22 Two model pictures considered to be equivalent and used interchangeably in the work of Doi and Edwards; left: the tube model; right: the slip-link model; from Doi and Edwards [56]

There is not, however, a universally agreed set of rules for slip-link models either! Different authors have chosen alternative sets of dynamical variables to describe the chain dynamics. Here is a brief summary of several of the main models described in the literature:

- Early work by Hua and Schieber [57] implemented Brownian dynamics of bead-spring chains along a primitive path (though this is often referred to as a “slip-link” model, it is actually closer to the tube model in origin). Later models by Schieber and coworkers [e.g., 58–60] retain only the slip-link positions and the number of monomers between slip-links as dynamical variables, and so do not resolve chain motion on scales smaller than the tube segment. Reptation and contour length fluctuation are implemented by allowing a stochastic exchange of the number of monomers between adjacent slip-links. In their latest implementation [60], constraint release is included via a stochastic and self-consistent creation and destruction of slip-links (e.g., if a slip-link is lost at a chain end, then a corresponding slip-link is deleted from another chain). All these dynamics are built on a model with an explicit underlying free energy, and are designed to satisfy detailed balance so as to produce the correct equilibrium distribution of chain and slip-link configurations.
- Doi and Takimoto presented a similar, but simpler model [61] in which only slip-link positions and the total primitive path length of the chain were treated as dynamical variables. A related model was created by Shanbhag and Larson [62, 63] for star and branched polymers.
- The “slip-spring” model of Likhtman [64, 65] treats slip-links as rings tethered to a fixed background by short springs, so that they can fluctuate in position by a short distance. The chain is treated as Brownian beads connected by springs, which can pass through the slip-springs creating reptation and contour length fluctuation. Constraint release is again modeled through creation and destruction of slip-springs. An advantage of this approach is that the model predicts dynamics on a range of length-scales, including motion below the tube diameter, which can be compared with multiple experimental observations such as viscoelastic measurements, neutron spin-echo, and dielectric spectroscopy [64], as well as with molecular dynamics simulations [65].

The above models are all “single chain” models, in that they simulate dynamics of isolated chains that communicate with one-another only through the self-consistent creation and destruction of slip-links used to model constraint release. A second family of “multichain” slip-link models aims to capture the three-dimensional arrangement of chains with respect to one another, so that chains are entangled only with their direct neighbors within the simulation:

- The so-called “NAPLES” code of Masubuchi and coworkers [66, 67] can be considered a direct analogue of the single-chain models by Schieber and coworkers [e.g., 58–60], in that their dynamical variables are the slip-link positions and number of monomers between slip-links. The substantive difference is that in the NAPLES code the chains are linked in an explicit three-dimensional arrangement, with slip-links connecting neighboring chains. One result of this is that the relationship between plateau modulus and average number of monomers between slip-links is changed. Typically, a multichain slip-link model requires roughly a factor of two more slip-links per chain to achieve the same plateau modulus, when compared to the equivalent “single chain” model [67]. In common with a similar issue in chain-shrinking algorithms for entanglement detection (see above, Section 6.3.6), this is most likely due to force balance and fluctuations of the linking points [25].
- Other multichain approaches are analogues of Likhtman’s slip-spring model [64, 65]. Several authors have proposed models in which neighboring chains in a three-dimensional simulation are linked together with slip-springs: these include Brownian bead-spring chains [68, 69], chains modeled using dissipative particle dynamics [70, 71], and Brownian chains in a self-consistent field [72, 73]. In most cases, these models can be viewed as methods to introduce entangled chain dynamics into coarse-grained simulation techniques where chains would otherwise pass through one another. To preserve the statistics of chain configurations from the original coarse-grained technique, some authors have noted that bead-bead repulsion should be added so as to compensate for the effective attraction due to slip-springs [68, 70].

While there are evidently close relationships between many of these slip-link models, no two are exactly identical in terms of the precise microscopic rules used to determine the chain dynamics. One distinct advantage of these models, however, is that once the microscopic rules are fixed, then the rich array of chain dynamics described earlier in this chapter (reptation, contour length fluctuations, constraint release, and the interactions between these different mechanisms) emerge naturally from the simulation. Hence, a prediction of linear viscoelasticity is obtained without any need for further mathematical developments to describe each of these processes. In this sense, slip-link simulations are very different from the tube model: the tube model is always used as a convenient picture allowing such mathematical descriptions to be developed; slip-links provide a means to avoid these mathematical descriptions altogether!

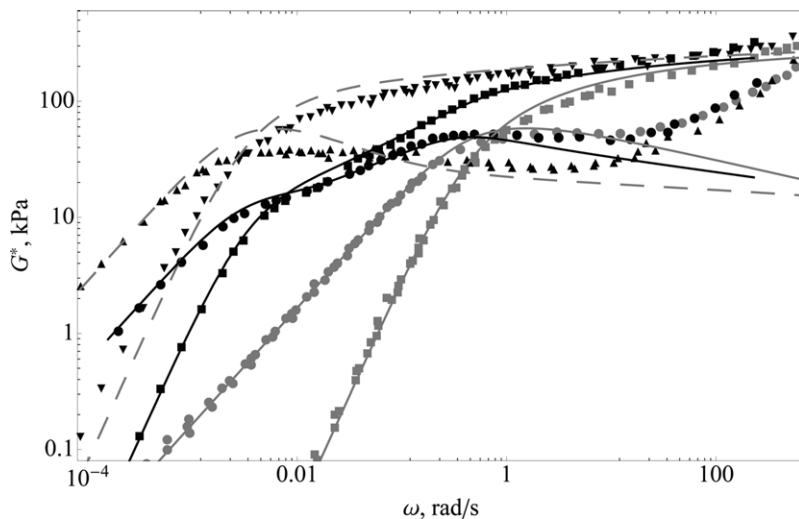


Figure 6.23 Linear viscoelasticity of two monodisperse polystyrenes with molecular weights 670 kg/mol (black triangles) and 160 kg/mol (gray squares and circles), and a 50% mixture by weight of the two (black squares and circles) together with predictions of the discrete slip-link model of Schieber and coworkers for the pure melts and the blend; from Khaliullin and Schieber [60]

This distinction becomes quite obvious when considering polydisperse systems, in particular binary blends of long and short polymers. Slip-link simulations can be parameterized so that they are able to predict the linear viscoelasticity for monodisperse linear polymers of a given chemistry, across a broad range of molecular weights. Then, once these parameters are fixed, the linear viscoelasticity for blends of different molecular weights is predicted without any further need for parameterization. As an example of this, Fig. 6.23 shows predictions using the model of Khaliullin and Schieber [60] for the linear viscoelasticity of two monodisperse polystyrenes with molecular weights 670 kg/mol and 160 kg/mol and a 50% mixture by weight of the two. Similarly, Fig. 6.24 shows linear viscoelasticity for monodisperse polyisoprenes with molecular weights 308 kg/mol and 21 kg/mol, together with a series of blends of the two at different weight fractions. The predictions, using a variant of Likhtman's slip-spring model [64, 74], capture the data for both the monodisperse melts and for all blend compositions. Both sets of predictions are very good.

As we will see below in Chapter 7, the corresponding tube-model description for rheology of binary blends requires much more thought about the subtle interplay between constraint release at different rates and the motion of the chain along the confining tube. While these interactions are undoubtedly taking place within the slip-link simulations, their algorithmic implementation removes the need to think about exactly what dynamics are occurring. So, provided enough computing power to obtain results in reasonable time, slip-link models are rapidly becoming a fast and

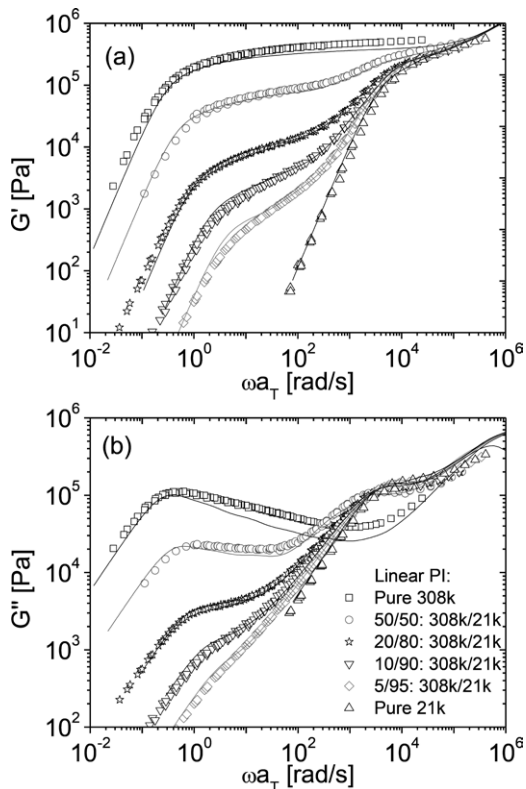


Figure 6.24 (a) Storage modulus and (b) loss modulus for monodisperse polyisoprenes with molecular weights 308 kg/mol and 21 kg/mol, together with a series of blends of the two at different weight fractions as indicated in the legend; lines are predictions from the slip-spring model of Likhdtman with parameters matched to fit the data from monodisperse polyisoprenes; from Shivokin et al. [74]

reliable method for linear rheology prediction. They are readily applicable to linear polymers of moderate degree of entanglement. Additionally, slip-spring models, which resolve chain motion below the entanglement scale, are perhaps the only available method for addressing the motion of short chains near the entanglement threshold.

In Chapter 9 we will discuss the application of slip-link simulations to branched polymers. We will see that to proceed beyond the simplest case of symmetric star polymers requires the introduction of further dynamical rules governing branch-point motion through slip-links. Presently, predictions for highly branched polymers are beyond the most advanced slip-link models. So, tube models, and the thought that goes with them, still seem to be necessary. It is likely that future developments may fruitfully explore the relationship between tube and slip-link models, in particular using insights from slip-link simulations to guide mathematical description of the tube model [74].

■ 6.6 Summary

In this chapter, we started by summarizing the predictions of the Bueche-Rouse model for unentangled polymers. The Rouse model represents the polymer molecule as a bead-spring chain moving in a viscous solvent, whereas in the Bueche-Rouse model, the “viscous solvent” is a melt of similar chains. The Rouse-Bueche model is also valid for entangled chains, but only within a window of frequencies that is high enough that the chain does not “feel” its entanglements, but not so high as to enter the glassy frequency regime, where the assumption that the polymer can be thought of as a bead-spring chain breaks down.

At low frequencies, the polymer molecule does feel its entanglements with other chains, and these entanglements act to confine the molecule to a tube-like region, from which it can only very gradually escape. We then presented tube-based models for the linear viscoelasticity of entangled melts and solutions of linear polymers, i.e., polymers without long side branches. In the linear viscoelastic regime, the important relaxation mechanisms that can be included in the tube model include reptation, primitive path fluctuations, and constraint release. As mentioned in the last paragraph, there are also Rouse motions within the tube that can occur even for entangled polymers. Reptation is a sliding motion of the chain along the tube that eventually allows it to completely escape the tube, and primitive path fluctuations are wrinkling movements of the chain that allow it to vacate the ends of the tube very rapidly. Constraint release is the loss of entanglements on a given chain due to motion of the surrounding chains. It is essential to take this into account in dealing with polydisperse polymers. Constraint release can be described simply in certain cases by assuming that an entanglement is produced by a topological interaction between a pair of chains, a test chain and a matrix chain; when either chain escapes this entanglement, by reptation for example, the entanglement is lost. This simple picture, known as double reptation, is inadequate for monodisperse and bidisperse polymers, but provides reasonably accurate predictions for some polymers with polydispersities typical of commercial melts.

Finally, we discussed an alternative picture for describing the motion of entangled polymer chains, the slip-link model. This picture enables the definition of computational algorithms to simulate the random chain dynamics, allowing accurate predictions to be made for linear viscoelasticity of monodisperse, bidisperse and polydisperse linear polymers. Dynamics such as reptation, contour length fluctuations and constraint release emerge naturally from these simulations, meaning that predictions can be made without detailed mathematical description, but perhaps reducing the impetus to understand these processes.

■ References

- [1] Doi, M., Edwards, S.F. *The Theory of Polymer Dynamics* (1986) Clarendon Press, Oxford
- [2] Watanabe, H. Viscoelasticity and Dynamics of Entangled Polymers. *Prog. Polym. Sci.* (1999) 24, pp. 1253–1403
- [3] McLeish, T.C.B. Tube theory of entangled polymer dynamics. *Adv. Phys.* (2002) 51, pp. 1379–1527
- [4] Rouse, P. A theory of the linear viscoelastic properties of dilute solutions of coiling polymers. *J. Chem. Phys.* (1953) 21, pp. 1272–1280
- [5] Berry, G.C., Fox, T.G. The viscosity of polymers and their concentrated solutions. *Adv. Polym. Sci.* (1967) 5, pp. 261–357
- [6] Ferry, J.D. *Viscoelastic Properties of Polymers* (1980) Wiley, New York
- [7] Bueche, F. Viscosity self-diffusion and allied effects in solid polymers. *J. Chem. Phys.* (1952) 20, pp. 1959–1964
- [8] Krishnamoorti, R., Graessley, W.W., Zirkel, A., Richter, D., Hadjichristidis, N., Fetters, L.J., Lohse, D.J. Melt-state polymer chain dimensions as a function of temperature. *J. Polym. Sci., Part B: Polym. Phys.* (2002) 40, pp. 1768–1776
- [9] Strobl, G.R. *The Physics of Polymers* (1997) Springer-Verlag, Berlin
- [10] Majesté, J.-C., Montfort, J.-P., Allal, A., Marin, G. Viscoelasticity of low-molecular weight polymers and the transition to the entangled state. *Rheol. Acta* (1998) 37, pp. 486–499
- [11] Pattamaprom, C., Larson, R.G., Van Dyke, T.J. Quantitative predictions of linear viscoelastic properties of entangled polymers. *Rheol. Acta* (2000) 39, pp. 517–531
- [12] Meerveld, J.A. Method to extract the monomer friction coefficient from the linear viscoelastic behavior of linear, entangled polymer melts. *Rheol. Acta* (2004) 43, pp. 615–623
- [13] Doi, M. Basic principle in the viscoelasticity of polymeric liquids. *J. Non-Newtonian Fl. Mech.* (1987) 23, pp. 151–162
- [14] Osaki, K., Inoue, T., Uematsu, T., Yamashita, Y. Evaluation methods of the longest Rouse relaxation time of an entangled polymer in dilute solution. *J. Polym. Sci., Part B: Polym. Phys.* (2001) 39, pp. 1704–1712
- [15] Graessley, W.W. Entangled linear, branched and network polymer systems—molecular theories. *Adv. Polym. Sci.* (1982) 47, pp. 67–117
- [16] Fetters, L.J., Lohse, D.J., Colby, R.H. Chain dimensions and entanglement spacings. *Physical Properties of Polymers Handbook*. Mark, J.E. (Ed.) (2005) Springer-Verlag, New York, Berlin
- [17] Onogi, S., Masuda, T., Kitagawa, K. Rheological properties of anionic polystyrenes. I. Dynamic viscoelasticity of narrow-distribution polystyrenes. *Macromol.* (1970) 3, pp. 109–116
- [18] Kremer, K., Grest, G.S. Dynamics of entangled polymer melts: a molecular-dynamics simulation. *J. Chem. Phys.* (1990) 92, pp. 5057–5086

- [19] Sukumaran, S.K., Likhtman, A.E. Modeling entangled dynamics: comparison between stochastic single-chain and multichain models. *Macromol.* (2009) 42 pp. 4300–4309
- [20] Everaers, R., Sukumaran, S.K., Grest, G.S., Svaneborg, C., Sivasubramanian, A., Kremer, K. Rheology and microscopic topology of entangled polymeric liquids. *Science* (2004) 303, pp. 823–226
- [21] Zhou, Q., Larson, R.G. Primitive path identification and statistics in molecular dynamics simulations of entangled polymer melts. *Macromol.* (2005) 38, pp. 5761–5765
- [22] Kröger, M. Shortest multiple disconnected path for the analysis of entanglements in two- and three-dimensional polymeric systems. *Comput. Phys. Commun.* (2005) 168, pp. 209–232
- [23] Tzoumanekas C., Theodorou, D.N. Topological analysis of linear polymer melts: a statistical approach. *Macromol.* (2006) 39, pp. 4592–4604
- [24] Hoy, R.S., Foteinopoulou, K., Kröger, M. Topological analysis of polymeric melts: Chain-length effects and fast-converging estimators for entanglement length. *Phys. Rev. E* (2009) 80, article no. 031803
- [25] Everaers, R. Topological versus rheological entanglement length in primitive-path analysis protocols, tube models, and slip-link models. *Phys. Rev. E* (2012) 86, article no. 022801
- [26] Read, D.J., Jagannathan, K., Likhtman, A.E. Entangled polymers: Constraint release, mean paths, and tube bending energy. *Macromol.* (2008) 41, pp. 6843–6853
- [27] Bisbee, W. Qin, J., Milner, S.T. Finding the tube with isoconfigurational averaging. *Macromol.* (2011) 44, pp. 8972–8980
- [28] Likhtman, A.E., Ponnurugan, M. Microscopic definition of polymer entanglements. *Macromol.* (2014) 47, pp. 1470–1481
- [29] Likhtman, A.E. The tube axis and entanglements in polymer melts. *Soft Matter* (2014) 10, pp. 1895–1904
- [30] Cao, J., Qin, J., Milner, S.T. Finding entanglement points in simulated polymer melts. *Macromol.* (2015) 48, pp. 99–110
- [31] Qin, J., Milner, S.T., Stephanou, P.S., Mavrntzas, V.G. Effects of tube persistence length on dynamics of mildly entangled polymers. *J. Rheol.* (2012) 56, pp. 707–723
- [32] de Gennes, P.G. Reptation of a polymer chain in the presence of fixed obstacles. *J. Chem. Phys.* (1971) 55, pp. 572–579
- [33] Pearson, D.S. Recent advances in the molecular aspects of polymer viscoelasticity. *Rubber Chem. Technol.* (1987) 60, pp. 439–496
- [34] Doi, M. Explanation for the 3.4 Power law of viscosity of polymeric liquids on the basis of the tube model. *J. Polym. Sci., Polym. Phys. Ed.* (1983) 21, pp. 667–684
- [35] Milner, S.T., McLeish, T.C.B. Reptation and contour-length fluctuations in melts of linear polymers. *Phys. Rev. Lett.* (1998) 81, pp. 725–728
- [36] Likhtman, A.E., McLeish, T.C.B. Quantitative theory for linear dynamics of linear entangled polymers. *Macromol.* (2002) 35, pp. 6332–6343

- [37] Pattamaprom, C., Larson, R.G. Predicting the linear viscoelastic properties of monodisperse and polydisperse polystyrenes and polyethylenes. *Rheol. Acta* (2001) 40, pp. 516–532
- [38] Hou, J.X., Svaneborg, C., Everaers, R., Grest, G.S. Stress relaxation in entangled polymer melts. *Phys. Rev. Lett.* (2010) 105, article no. 068301
- [39] Liu, C.Y., He, J.S., Keunings, R., Bailly, C. Do tube models yield consistent predictions for the relaxation time and apparent plateau modulus of entangled linear polymers? *Macromol.* (2006) 39, pp. 3093–3097
- [40] Benallal, A., Marin, G., Montfort, J.P., Derail, C. Linear viscoelasticity revisited: The relaxation function of monodisperse polymer melts. *Macromol.* (1993) 26, pp. 7229–7235
- [41] Léonardi, F., Majesté, J.-C., Allal, A., Marin, G. A rheological model based on the double reptation concept: the effects of a polydisperse environment. *J. Rheol.* (2000) 44, pp. 675–692
- [42] Carrot, C., Guillet, J. From dynamic moduli to molecular weight distribution: a study of various polydisperse linear polymers. *J. Rheol.* (1997) 41, pp. 1203–1220
- [43] Schausberger, A., Schindlauer, G., Janeschitz-Kriegl, H. Linear elastico-viscous properties of molten standard polystyrenes. I. Presentation of complex moduli; Role of short range structural parameters. *Rheol. Acta* (1985) 24, pp. 220–227
- [44] Tuminello, W.H. Molecular-weight polydispersity effects on the viscoelasticity of entangled linear-polymers. *Polym. Eng. Sci.* (1986) 26, pp. 1339–1347
- [45] Tsengoglou, C. Viscoelasticity of binary homopolymer blends. *ACS Polym. Prepr.* (1987) 8, pp. 185–186
- [46] des Cloizeaux, J. Double reptation vs. simple reptation in polymer melts. *Europhys. Lett.* (1988) 5, pp. 437–442
- [47] Rubinstein, M., Colby, R.H. Self-consistent theory of polydisperse entangled polymers: Linear viscoelasticity of binary blends. *J. Chem. Phys.* (1988) 89, pp. 5291–5306
- [48] des Cloizeaux, J. Relaxation and viscosity anomaly of melts made of long entangled polymers: time-dependent reptation. *Macromol.* (1990) 23, pp. 4678–4687
- [49] van Ruymbeke, E., Keunings, R., Stéphenne, V., Hagenaars, A., Bailly, C. Evaluation of reptation models for predicting the linear viscoelastic properties of entangled linear polymers. *Macromol.* (2002) 35, pp. 2689–2699
- [50] Montfort J.P., Marin G., Arman J., Monge Ph. Viscoelastic properties of high molecular weight polymers in the molten state II. Influence of the molecular weight distribution on linear viscoelastic properties. *Rheol. Acta* (1979) 18, pp. 623–628
- [51] Mead, D.W. Determination of molecular weight distributions of linear flexible polymers from linear viscoelastic material functions. *J. Rheol.* (1994) 38, pp. 1797–1827
- [52] Park, S.J., Larson, R.G. Long-chain dynamics in binary blends of monodisperse linear polymers. *J. Rheol.* (2006) 50, pp. 21–39
- [53] Read, D.J., Jagannathan, K., Sukumaran, S.K., Auhl, D. A full-chain constitutive model for bidisperse blends of linear polymers. *J. Rheol.* (2012) 56, pp. 823–873

- [54] van Ruymbeke, E., Shchetnikava, V., Matsumiya, Y., Watanabe H. Dynamic dilution effect in binary blends of linear polymers with well-separated molecular weights. *Macromol.* (2014) 47, pp. 7653–7665
- [55] Wasserman, S., Graessley, W.W. Effects of polydispersity on linear viscoelasticity in entangled polymer melts. *J. Rheol.* (1992) 36, pp. 543–572
- [56] Doi, M., Edwards S.F. Dynamics of concentrated polymer systems: Part 2—molecular motion under flow. *J. Chem. Soc., Faraday Trans. 2* (1978) 74, pp. 1802–1817
- [57] Hua, C.C., Schieber, J.D. Segment connectivity, chain-length breathing, segmental stretch, and constraint release in reptation models. I. Theory and single-step strain predictions. *J. Chem. Phys.* (1998) 109, pp. 10018
- [58] Schieber, J.D., Neergaard, J., Gupta, S. A full-chain, temporary network model with sliplinks, chain-length fluctuations, chain connectivity and chain stretching. *J. Rheol.* (2003) 47, pp. 213–233
- [59] Nair, D.M., Schieber, J.D. Linear Viscoelastic predictions of a consistently unconstrained brownian slip-link model. *Macromol.* (2006), 39, pp. 3386–3397
- [60] Khalilullin, R.N., Schieber J.D. Application of the slip-link model to bidisperse systems. *Macromol.* (2010) 43, pp. 6202–6212
- [61] Doi, M., Takimoto, J.-I. Molecular modelling of entanglement. *Philos. Trans. R. Soc., A* (2003) 361, pp. 641–652
- [62] Shanbhag, S., Larson, R.G., Takimoto, J.-I., Doi, M. Deviations from dynamic dilution in the terminal relaxation of star polymers. *Phys. Rev. Lett.* (2001) 87, article no. 195502
- [63] Shanbhag, S., Larson, R.G. A slip link model of branch-point motion in entangled polymers. *Macromol.* (2004) 37, pp. 8160–8166
- [64] Likhtman, A.E. Single-chain slip-link model of entangled polymers: simultaneous description of neutron spin-echo, rheology, and diffusion. *Macromol.* (2005) 38, pp. 6128–6139
- [65] Sukumaran, S.K., Likhtman A.E. Modeling entangled dynamics: comparison between stochastic single-chain and multichain models, *Macromol.* (2009) 42, pp. 4300–4309
- [66] Masubuchi, Y., Takimoto, J.-I., Koyama, K., Ianniruberto, G., Marrucci, G., Greco, F. Brownian simulations of a network of reptating primitive chains. *J. Chem. Phys.* (2001) 115, pp. 4387–4394
- [67] Masubuchi, Y., Ianniruberto, G., Greco, F., Marrucci, G. Entanglement molecular weight and frequency response of sliplink networks. *J. Chem. Phys.* (2003) 119, pp. 6925–6930
- [68] Uneyama, T. and Masubuchi, Y. Multi-chain slip-spring model for entangled polymer dynamics. *J. Chem. Phys.* (2012) 137, article no. 154902
- [69] Masubuchi, Y., Effects of degree of freedom below entanglement segment on relaxation of polymer configuration under fast shear in multi-chain slip-spring simulations. *J. Chem. Phys.* (2015) 143, article no. 224905
- [70] Chappa, V., Morse, D.C., Zippelius, A., Müller, M. Translationally invariant slip-spring model for entangled polymer dynamics, *Phys. Rev. Lett.* (2012) 109, article no. 148302

- [71] Langeloth, M., Masubuchi, Y., Böhm, M.C., Müller-Plathe, F. Recovering the reptation dynamics of polymer melts in dissipative particle dynamics simulations via slip-springs. *J. Chem. Phys.* (2013) 138, article no. 104907
- [72] Ramírez-Hernández, A., Müller, M., de Pablo, J.J. Theoretically informed entangled polymer simulations: linear and non-linear rheology of melts. *Soft Matter* (2013) 9, pp. 2030–2036
- [73] Ramírez-Hernández, A., Peters, B.L., Andreev, M., Schieber, J.D., de Pablo, J.J. A multichain polymer slip-spring model with fluctuating number of entanglements for linear and nonlinear rheology. *J. Chem. Phys.* (2015) 143, article no. 243147
- [74] Shivokhin, M.E., Read, D.J., Kocen, R., Bailly, C., Kouloumasis D., Hadjichristidis, N., Likhtman, A.E. Understanding effect of constraint release environment on end-to-end vector relaxation of linear polymer chains *Macromol.* (2017) 50, pp. 4501–4523

7

Tube Models for Linear Polymers—Advanced Topics

■ 7.1 Introduction

In Chapter 6, polymer deformation and relaxation in entangled melts were discussed using the “tube” model. Chapter 6 culminated with a discussion of the “double reptation” model, which can predict reasonably well the orientation and stress in the linear viscoelastic regime for some polydisperse linear polymers; i.e., polymers without long side branches. The double reptation model deals with the difficult problem of constraint release using a very simple-minded idea that if a constraint on a “test” chain is released by movement of a surrounding “constraint” chain, then the test chain can relax the stress associated with that constraint immediately. However, at the end of Chapter 6 we noted that there are flaws in the predictions of at least some versions of the double reptation theory. In particular, the theory predicts that at fixed weight average molecular weight, the zero shear viscosity should increase with increasing polydispersity, a prediction not supported by experimental data, at least for modest levels of polydispersity ($M_w/M_n < 4$ or so). In addition, as discussed in Chapter 6, the simplest version of the double reptation model (with a single exponential kernel) works poorly for monodisperse and bidisperse polymer melts. Finally, double reptation assumes that the relaxation function of polymers of a given molecular weight is unaffected by the presence of polymers with different molecular weights; this turns out to be not true, though it may hold approximately in many circumstances.

In this chapter and in Chapter 9, we wish to introduce more advanced constraint-release concepts, which can be applied to cases for which the double reptation model works poorly, including monodisperse and bidisperse linear polymers. We will show that when the advanced concepts of “constraint-release Rouse” relaxation and “dynamic dilution” are introduced into the tube model, then successful predictions of the linear rheology of bidisperse melts can be achieved. While bidisperse melts are not of great commercial interest, the concepts we will introduce in this chapter are also important for polymers with long side branches, which are of great commercial interest, and are discussed in Chapter 9.

■ 7.2 Limitations of Double Reptation Theory

Let us start by illustrating the conceptual limitations of the double reptation idea. Consider the case of a polymer of high molecular weight at a volume concentration ϕ_L in a matrix of a polymer of much lower molecular weight. This case was considered in Section 6.4.4.2, and we found that the double reptation model predicts two relaxation peaks in G'' , a peak at a high frequency roughly equal to the inverse of the reptation time, $\tau_{d,S}$, of the short chains, and a low-frequency peak, whose frequency is the inverse of half the reptation time, $\tau_{d,L}/2$, of the long chains. The height of the low-frequency peak is predicted by double reptation to be proportional to the square of the volume fraction of long chains ϕ_L^2 . These predictions were found to be in good agreement with data for some binary blends of polybutadiene. For those data, the concentration of long chains was high enough that each long chain was entangled with other long chains.

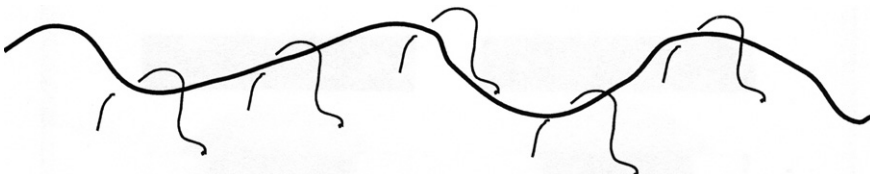


Figure 7.1 Illustration of a long polymer (artificially straightened for illustrative purposes) entangled with much shorter chains, where the long-chain concentration is too low to permit entanglements between long chains

Let us now consider a more severe test of double reptation in which the long chains are dilute, meaning that entanglements of the long chains with other long chains are negligible; see Fig. 7.1. This is the case if the product of the concentration ϕ_L of the long chains and their molecular weight M_L is less than the entanglement threshold for the melt; i.e., $\phi_L M_L < M_C$. Figure 7.2 shows experimental $G'(\omega)$ data for this case. The volume fraction of long chain in this binary blend of monodisperse polystyrenes is only $\phi_L = 0.015$, and its molecular weight is held fixed at $M_L = M_2 = 1,810,000$, while the molecular weight of the short matrix chains is varied from $M_S = M_1 = 71,400$ to $775,000$ [1]. Notice from Fig. 7.2 that, as expected, there is a fast relaxation mode at high frequency with a high plateau modulus. The frequency at which $G'(\omega)$ begins to decrease from this plateau decreases with increasing molecular weight of the short chain. Thus, the relaxation time associated with the “fast” relaxation mode clearly increases with increasing molecular weight of the short chain. This much is expected from double reptation theory.

There is also a second relaxation mode that is revealed by the “shoulder” in the data at low frequency. This second mode, which is generated by the relaxation of the

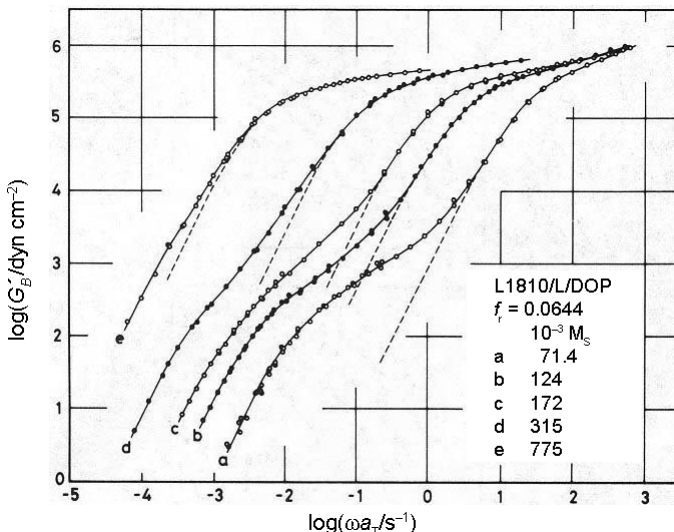


Figure 7.2 Storage modulus of 60 vol% solutions of bidisperse polystyrene in diethylphthalate. The molecular weight M_L is 1,810,000 and M_S values are shown. The volume fraction ϕ_L of long chain is 0.015, which is low enough to be unentangled with itself. The dashed lines are G' of monodisperse, low molecular weight polystyrenes at 60% concentration; adapted from Watanabe [1]

long chains, is expected to be present, according to double reptation theory, but in double reptation theory it would appear as a relatively flat plateau, rather than as a more gradual “shoulder”. In addition, the relaxation time associated with this mode would in double reptation theory be independent of the molecular weight of the short chains, since it is caused by reptation of the long chains. However, in Fig. 7.2, the long chain molecular weight is held fixed, yet the “shoulder” clearly shifts its location with the molecular weight of the short chains. Thus the relaxation time of the slow mode depends on the molecular weight of the short chain, in contradiction to double reptation theory. Clearly, double reptation theory cannot apply to this case. Double reptation also predicts that the magnitude of the slow relaxation mode should be proportional to ϕ_L^2 , while these experiments instead show proportionality to ϕ_L [2]. The dashed lines in Fig. 7.2 are the $G'(\omega)$ curves for the pure short chains. If these dashed curves are subtracted from the data for the binary blends in Fig. 7.2, the contribution from the long chains is obtained, and this is plotted in normalized form in Fig. 7.3 for several different dilute blends of long chains in short chains [3]. These long-chain contributions to $G'(\omega)$ are proportional to ϕ_L , not ϕ_L^2 , and the relaxation of the long chain clearly is described by multiple relaxation modes, not a single mode, which would produce a flat plateau. Both of these findings disagree with predictions of double reptation theory. Notice, however, that the shapes of the curves for the long-chain contribution to $G'(\omega)$ in Fig. 7.3 are similar to those of

the curves predicted by the Rouse theory in Fig. 6.3. Thus, when the long chains are dilute, the long-chain contribution to the linear viscoelasticity is similar to that predicted by the Rouse theory, which was obtained by neglecting entanglements (see Section 6.2). While the solution considered in Figs. 7.2 and 7.3 has entanglements of long chains with short chains, it lacks significant entanglements of long chains with other long chains, and it is the lack of such long-chain/long-chain entanglements that produces the Rouse-like response observed in Fig. 7.3. Thus, when the long chains are dilute, double reptation theory fails, but a version of the Rouse theory, describing “constraint-release Rouse” relaxation, becomes applicable.

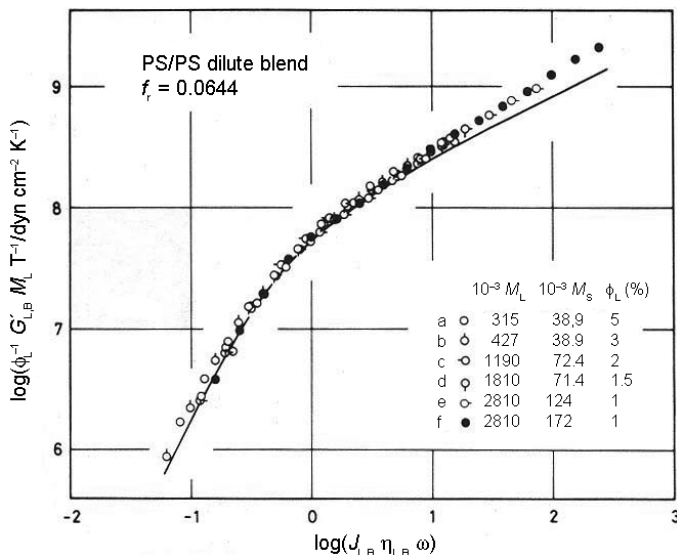


Figure 7.3 Dependence of the normalized storage modulus $M_L G'_{L,B} / c_L RT$ on reduced frequency $\langle \tau_{L,G} \rangle = \omega J_{L,B} \eta_{L,B}$ for dilute blends of high-molecular weight polystyrene at volume fraction ϕ_L in a matrix of much shorter polystyrene chains, or of dilute polyisoprene in polybutadiene. Here, G'_B is the contribution of the long chain to the storage modulus, i.e., the storage modulus of the dilute blend with the matrix contribution subtracted off, and ϕ_L is the concentration of the long chain in units of mass/volume. R is the gas constant. $\langle \tau_{L,G} \rangle$ is an average relaxation time defined in Watanabe [2]. The molecular weights M_L and M_S of the long and short chains are given in the figure. The dashed line is the prediction of Rouse theory. Adapted from Watanabe et al. [1].

■ 7.3 Constraint-Release Rouse Relaxation in Bidisperse Melts

7.3.1 Non-Self-Entangled Long Chains in a Short-Chain Matrix

The key problem with the double reptation theory in the above example is that it assumes that a long chain can relax as fast as the entanglement constraints on it are removed. This assumption may be acceptable if there are only a limited number of entanglements between the short and long chains, so that when the entanglements between short and long chains are removed, the long chains need only relax *locally*, see Fig. 7.4. This local relaxation is rapid, and leads to partial stress relaxation, which is accounted for by double reptation. But when all the chains that entangle with the long chain are short chains, double reptation predicts that the long chain will relax completely, *as soon as the short chains have relaxed*, since all entanglements restraining the long chain will have disappeared. However, in reality, as illustrated in Fig. 7.5, the removal of all constraints imposed by these short-chain neighbors still produces only modest relaxation of the *overall* chain conformation. It cannot lead to *complete global* reconfiguration of the entire long chain on the short time scale of the reptation of the short chains. Instead, before the long chain has moved very far, it will become re-entangled with short-chain neighbors again; again see Fig. 7.5. To relax further, the long chain will have to wait for its short chain neighbors to reptate out of the way again. Complete global relaxation of the long chain will require many cycles of relaxation of short chains and local movement of the long chain. In effect, the long chain remains trapped in a tube, *but this tube containing the long chain is itself relaxing at a rate controlled by the reptation of the short chains*. Once the tube containing the long chain has relaxed its conformation, the long chain within the tube will also be relaxed.

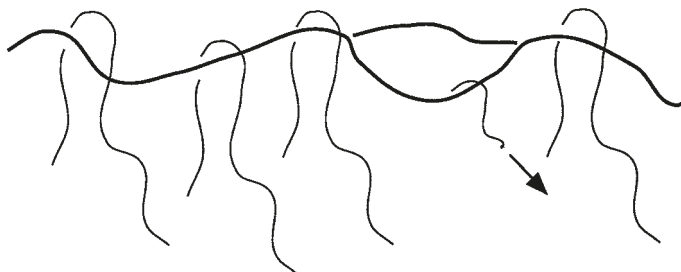


Figure 7.4 A long polymer chain entangled with both long and short chains. At times greater than the reptation time of the short chain, i.e., $t > \tau_{d,S} \propto Z_S^3 \tau_e$, the short polymer releases a constraint by reptation, and the long chain can then relax its configuration *locally*. Global relaxation can only occur at $t > \tau_{d,L} \propto Z_L^3 \tau_e$, when the entangling long chains have also relaxed

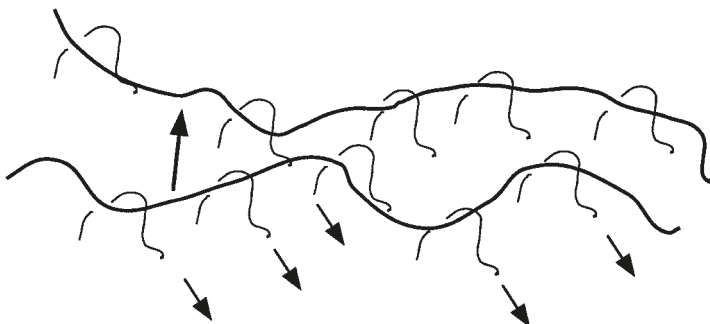


Figure 7.5 A long molecule entangled only with short polymers can relax locally at each point along its entire contour at times $t \approx \tau_{d,S} \propto Z_S^3 \tau_e$, when all surrounding short chains have reptated away, but globally relaxation is only partial in that the global conformation of the chain changes only modestly. This is illustrated by the modest change in conformation of the long chain that occurs even though all short chains have released their entanglements. Complete global relaxation of the long chain requires many cycles of relaxation (reptation) of the short chains and local motion of the long chain; therefore complete global relaxation occurs over a Rouse constraint-release time $\tau_{CR,L} \propto Z_S^3 Z_L^2 \tau_e$

Thus, the tube containing the long chain can be thought of as a “polymer” that moves through a “solvent” consisting of the entanglements with short chains, and this motion is described by the Rouse theory for unentangled polymers, described in Section 6.2. However, the relaxation of the tube containing the long chain differs from ordinary Rouse relaxation in that the rate at which the tube can execute local motion is not set simply by a monomeric friction coefficient (as in ordinary Rouse relaxation), but by the rate at which short chains release constraints on the tube by short-chain reptation. For this reason, the process of relaxation of the tube containing the long chain due to repeated short-chain constraint release is nowadays usually called *constraint-release Rouse*, or CR-Rouse, relaxation; it is really a higher-order Rouse process. This mechanism was earlier called “tube reorganization” by Viovy et al. [4], and the basic idea goes back to Klein [5] and Daoud and de Gennes [6]. The following discussion is similar to the work presented by Viovy et al. [4]. The Rouse-like character of constraint release for the case of dilute long chains in a matrix of short chains is confirmed in Fig. 7.3, which shows that the long-chain contribution to $G'(\omega)$ is well described by the Rouse relaxation spectrum, which is given by the solid line. Since the time scale for a single cycle of this higher-order Rouse process is roughly the reptation time of the short chains, a single constraint-release Rouse cycle will require a time proportional to $\tau_{d,S} \propto Z_S^3 \tau_e$, i.e., proportional to the cube of the number of entanglements Z_S of a short chain. (Here for simplicity we ignore the fluctuation correction, which produces a higher power law, with exponent around 3.4.) However, this single cycle must be repeated over and over again before complete relaxation of the tube containing the long chain can occur. From the Rouse theory described in

Section 6.2.2, we infer that the number of cycles required for complete relaxation of the tube containing the long chain must be proportional to the square of the molecular weight of the long chain (see Eq. 6.3). Combining this with the time for a single cycle gives the following scaling law for the *constraint-release Rouse time* for complete relaxation of the tube containing the long chain [4]:

$$\tau_{\text{CR,L}} \propto Z_s^3 Z_L^2 \tau_e \quad (7.1)$$

where Z_L is the number of entanglements in the long chain. (One can obtain this proportionality from Eq. 6.3 for ordinary Rouse relaxation by noting the friction coefficient ζ_0 in Eq. 6.3 is proportional to $Z_s^3 \tau_e$ and the effective number of monomers N is the number of tube segments Z_L .) Obviously, if the long chain is long enough, $\tau_{\text{CR,L}}$ can be much longer than the reptation time of the short chain, which is proportional only to $Z_s^3 \tau_e$. As reviewed by Watanabe [2], detailed theories to predict $\tau_{\text{CR,L}}$ more precisely have been proposed by Graessley [7], Klein [5], and Daoud and de Gennes [6]. For our purposes, it is sufficient to note that constraint-release Rouse relaxation is an important process that is ignored by double reptation.

Constraint-release Rouse motion (abbreviated here as CR-Rouse) is a possible mechanism for complete relaxation of the stress carried by the long chains. Of course, it is not the only mechanism available, and reptation of the long chains along their tube is perfectly possible. Neglecting the fluctuation correction, the reptation time is $\tau_{d,L} \propto Z_L^3 \tau_e$. In order to decide whether CR-Rouse relaxation or reptation governs the final relaxation of the long chains, we consider the ratio of $\tau_{d,L}$ to $\tau_{\text{CR,L}}$:

$$\frac{\tau_{d,L}}{\tau_{\text{CR,L}}} \propto \frac{Z_L^3 \tau_e}{Z_s^3 Z_L^2 \tau_e} = \frac{Z_L}{Z_s^3} = Gr \quad (7.2)$$

The ratio, $Gr = Z_L / Z_s^3 = M_L (M_e^G)^2 / M_s^3$ (sometimes called the “Graessley parameter” or “Struglinski-Graessley parameter”), is an important quantity in the physics of entangled bidisperse polymer melts. If Gr is small, then reptation of the long chains is faster than the longest constraint-release Rouse time; so reptation governs the final relaxation. Conversely, if Gr is large, then constraint-release Rouse motion is the faster mechanism for relaxing the long chain stress. The critical value Gr_c has been estimated to be around 0.06–0.5 [8–10].

Figure 7.6(a) is an illustration adapted from Viovy et al. [4] showing how CR-Rouse relaxation affects the stress relaxation modulus $G(t)$ in the case of large $Gr > Gr_c$. The predicted relaxation modulus according to the double reptation theory is shown by the bold dashed line; it has two steep drops in $G(t)$, one at time $\tau_{d,S}/2$, and the other at time $\tau_{d,L}/2$. The steep drops are really exponential decays, but are represented as step functions in Fig. 7.6 to distinguish them from the more gradual power-law Rouse-type relaxation, represented by a “Rouse ramp”, that is, a downward-sloping line with a slope of $-1/2$ on a log-log scale, describing a $t^{-1/2}$ time dependence.

(This power law is an approximation to Rouse relaxation; more accurate formulas for CR-Rouse relaxation can be found in Watanabe [10, 11].) When CR-Rouse relaxation is considered (bold solid lines), the first step is no longer a drop from $G(t)/G_N^0 = 1$ to ϕ_L^2 , but a drop only to ϕ_L due to relaxation of the short chains. Thereafter, the long chains start relaxing by the CR-Rouse process. This follows a power law in time, $G(t)/G_N^0 \propto \phi_L (t/\tau_{d,S})^{-1/2}$, which continues until the longest CR-Rouse relaxation time is reached, occurring roughly at the time $\tau_{CR,L} \propto \tau_{d,S} Z_L^2 = Z_S^3 Z_L^2 \tau_e$. At this point, exponential terminal relaxation occurs, which is again represented by a step in Fig. 7.6(a). Notice the differences in the relaxation characteristics of CR-Rouse relaxation relative to that of double reptation. First, in CR-Rouse, relaxation of the

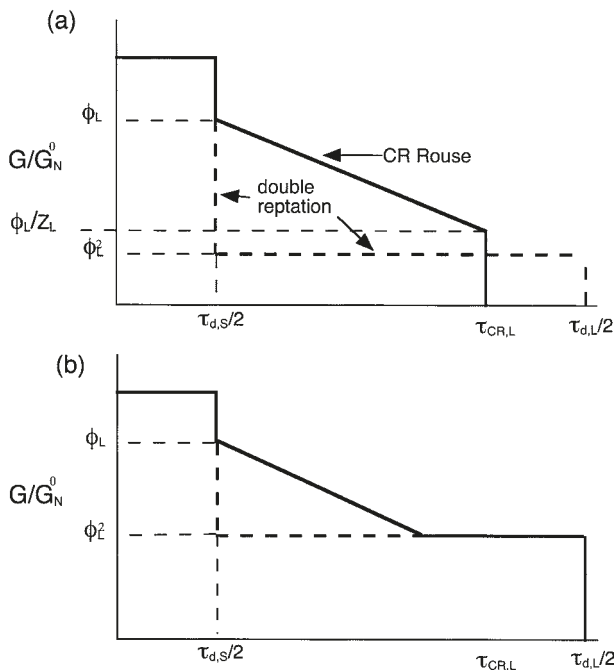


Figure 7.6 Relaxation moduli of entangled binary blends of long and short chains according to the double reptation theory (bold dashed line) and the constraint-release Rouse picture (bold solid line) when the reptation time of the long chain exceeds its constraint-release Rouse time; i.e., $\tau_{d,L} > \tau_{CR,L} \propto Z_S^3 Z_L^2$. In both (a) and (b), double reptation predicts two “step” decreases in the relaxation modulus, at times $\tau_{d,S}/2$ and $\tau_{d,L}/2$. In (a), which is the situation sketched in Fig. 7.5, the concentration of the long chain is too dilute for it to entangle with itself; i.e., $\phi_L < 1/Z_L = M_C/M_L$. In this case, the constraint-release Rouse relaxation, represented by the sloping solid line, comes to completion at the terminal Rouse time $\tau_{CR,L} \propto Z_S^3 Z_L^3$. In (b), the situation shown in Fig. 7.7, ϕ_L is large enough that the entanglements of long chains with themselves bring constraint-release Rouse relaxation to a halt before relaxation is complete. Final relaxation occurs by reptation of the long chains. Both abscissa and ordinate should be considered logarithmic scales

long chains is a smoother, more continuous, process than is predicted by double reptation. Second, for $Gr > Gr_c$, the terminal time for final relaxation of the long chains will be $\tau_{CR,L}$, which is shorter than the relaxation time $\tau_{d,L}/2$ predicted by double reptation. Finally, the modulus of the melt just prior to terminal relaxation is higher (ϕ_L/Z_L compared to ϕ_L^2) in CR-Rouse than in double reptation. The illustration in Fig. 7.6(a) thus applies to the example where the long chains are dilute and $Gr > Gr_c$, as is the case for the smallest three short chain molecular weights in Fig. 7.2 and for all blends in Fig. 7.3. The data presented in Fig. 7.2 can be interpreted using Fig. 7.6(a) if one remembers that frequency corresponds to inverse time, so that, qualitatively, if one inverts the log time axis in Fig. 7.6(a) one obtains a qualitative depiction of the shape of the curve of G' versus frequency ω . The $t^{-1/2}$ time dependence in Fig. 7.6(a) then becomes a Rouse-like $\omega^{1/2}$ frequency-dependence, as observed in Figs. 7.2 and 7.3.

If $Gr < Gr_c$, then reptation of the long chains precedes the terminal time for CR-Rouse relaxation. In this case, the expectation is that CR-Rouse relaxation will begin in exactly the same manner as in Fig. 7.6(a), that is, a drop in $G(t)/G_N^0$ to ϕ_L upon relaxation of the short chains, after which the long chains start relaxing by the CR-Rouse process with $G(t)/G_N^0 \propto \phi_L (t/\tau_{d,S})^{-1/2}$. However, before the CR-Rouse time $\tau_{CR,L}$ can be reached, the long chains reptate in their tubes and all remaining stress is relaxed at time $\tau_{d,L}$ (which is now less than $\tau_{CR,L}$). In Fig. 7.6(a), this would be represented by a vertical line ending the CR-Rouse region at time $\tau_{d,L}$, as discussed by Viovy et al. [4]. For the data in Fig. 7.2, this is likely to be the process governing the terminal relaxation for the two blends with short chain lengths $M_S = 315,000$ and $775,000$.

7.3.2 Self-Entangled Long Chains in a Short-Chain Matrix

Now suppose that the concentration of long chains is low, but not so low as to be dilute in the matrix of short chains, i.e., $\phi_L M_L > M_C$. Defining the number of long-chain entanglements along a long chain as $\tilde{Z}_L = \phi_L Z_L$, we are now considering the case where $\tilde{Z}_L > 1$, that is, there are now a significant number of long-chain/long-chain entanglements. This situation is depicted in Fig. 7.7(a). In this case, repeated reptation of the short chains will again lead to CR-Rouse motion of the long chain (and the tube containing it). However, this CR-Rouse motion can no longer relax the whole long-chain configuration, because entanglements with other long-chains will get in the way, arresting the CR-Rouse motion. There are then numerous possible relaxation pathways for the long chains, and this leads to a rich physics of binary blend rheology, the details of which are still not completely settled in the literature. Here we shall continue to follow the work of Viovy et al. [4, 12, 13], initially ignoring fluctuation corrections to reptation.

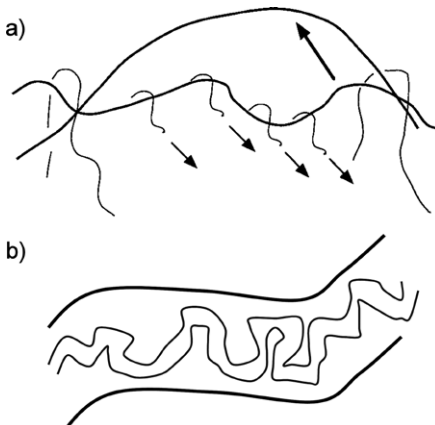


Figure 7.7 (a) A long molecule entangled mostly with short chains, but also with some other long chains, can relax locally by constraint-release Rouse motion on short timescales, with local constraint-release events dictated by short chain reptation. On longer time scales, the long molecule is constrained by entanglements with other long chains, which restrict its motion. (b) The equivalent picture in terms of fat and thin tubes. The thin tube represents entanglements with all other chains, and undergoes constraint-release Rouse motion, until it locally explores the fat tube, which represents entanglements with long chains only

A relevant question to ask is how long can CR-Rouse motion of the long chains proceed before being arrested by entanglements with other long chains? This is the time at which the effects of long chain entanglements will become apparent. Returning again to Fig. 7.7(a), for every long-chain entanglement there are a certain number, n , of short-chain entanglements (and double reptation theory suggests $n = \phi_L^{-1}$). The subsection of chain between two long chain entanglements can still undergo local CR-Rouse motion as the short chains repeatedly entangle and disentangle with the long chain. This motion relaxes the internal configurations of the chain subsection and occurs over a time $\tau_{\text{CR,loc}} \propto \tau_{d,S} n^2 = Z_S^3 \phi_L^{-2} \tau_e$, because the time for Rouse motion depends on the square of the number of chain segments. At times that are shorter than this, local CR-Rouse relaxation can proceed. At times that are longer than this, the CR-Rouse relaxation is arrested by the presence of long-chain entanglements.

While CR-Rouse motion alone cannot relax the long chains, reptation of long chains along their tube (on timescale $\tau_{d,L}$) can still fully relax the long chains. It is possible that $\tau_{d,L} < \tau_{\text{CR,loc}}$, in which case the terminal relaxation due to reptation of the long chains occurs before the local CR-Rouse motion has completed. This happens if the constraint release from short chains is slow. If this is the case, long chain entanglements will never impact on the relaxation pathway at all, and the situation is analogous to the relaxation of dilute long chains, terminated by chain reptation, as described at the end of Section 7.3.1. In order to decide whether this occurs, we consider the ratio of $\tau_{d,L}$ to $\tau_{\text{CR,loc}}$:

$$\frac{\tau_{d,L}}{\tau_{CR,loc}} \propto \frac{Z_L^3 \tau_e}{Z_S^3 \phi_L^{-2} \tau_e} = \frac{Z_L}{Z_S^3} Z_L^2 \phi_L^2 = Gr \tilde{Z}_L^2 \quad (7.3)$$

The ratio depends only on the Graessley parameter Gr and the entanglement number $\tilde{Z}_L = \phi_L Z_L$. If $Gr \tilde{Z}_L^2 < 1$, then we expect reptation to occur before local equilibration due to CR-Rouse motion. If $Gr \tilde{Z}_L^2 > 1$, then we expect local equilibration due to CR-Rouse motion to be completed before terminal relaxation; so, we also expect the effects of entanglements between long chains to be visible.

If we assume the more typical situation that $\tau_{d,L} > \tau_{CR,loc}$, that is, $Gr \tilde{Z}_L^2 > 1$, then the expected time-dependent modulus is illustrated in Fig. 7.6(b), which again schematically compares the double reptation prediction to the predictions of CR-Rouse relaxation. In both cases, the terminal relaxation of the long chain occurs at the time $\tau_{d,L}$. The CR-Rouse process simply adds an intermediate gradual relaxation process, indicated by the “Rouse ramp” with a power-law slope of $-1/2$, which produces a gradual relaxation of $G(t)/G_N^0$ from ϕ_L to ϕ_L^2 between times $\tau_{d,S}$ and $\tau_{CR,loc}$. If the relaxation is as depicted in Fig. 7.6(b), then neglect of this additional “Rouse ramp” by the double reptation theory is not too serious an omission, and double reptation theory may be expected to make reasonable predictions for the linear viscoelastic response.

7.3.3 Thin Tubes, Fat Tubes, and the Viovy Diagram

Up to now, in our discussion of constraint release, we have assumed that for nondilute concentrations of long chains, the reptation time of the long-chain component of a bidisperse melt is unaffected by relaxation of the other components (except for the factor of two correction predicted by double reptation). This is not always true. To take an extreme example, if a monodisperse polymer melt is diluted with a small-molecule solvent, entanglements will become less dense, and the plateau modulus G_N^0 will drop, thus increasing the tube diameter a as indicated by Eq. 6.22, reproduced here:

$$a^2 = \frac{M_e^G}{M_0} b^2 = \frac{4}{5} \frac{\rho N_A k T b^2}{M_0 G_N^0} \quad (7.4)$$

Then the reptation time of the polymer will be reduced, as can be seen in the expression for the reptation time, Eq. 6.34, reproduced here:

$$\tau_d = \frac{\xi N^3 b^4}{\pi^2 k T a^2} \quad (7.5)$$

Equation 7.5 shows that the reptation time τ_d is affected by the entanglement tube diameter a . In general, if ϕ_p is the concentration of polymer in a polymer solution containing solvent, the plateau modulus decreases with decreasing ϕ_p roughly as $G_N^0 \propto \phi_p^2$. More generally, it has been suggested that $G_N^0 \propto \phi_p^{1+\alpha}$, where the exponent α

might be slightly greater than unity, in particular, $\alpha = 4/3$ [2, 10, 14, and 15]. For purposes of this discussion, we will take $\alpha = 1$, which is a value consistent with the double reptation theory. From Eq. 7.4, noting that the polymer density ρ is proportional to ϕ_p , Eq. 7.4 then implies that the tube diameter a scales as $a \propto \phi_p^{-1/2}$, that is, the tube diameter is proportional to the inverse square root of the polymer concentration. From Eq. 7.5, the reptation time therefore decreases as the polymer concentration decreases, if the monomeric friction coefficient is constant.

Now, let us suppose that the “solvent” is really polymer, chemically identical to the “solute” polymer, but of much smaller molecular weight. Therefore, this is just an extreme case of a bidisperse melt of two polymer lengths, one of them having a very low molecular weight. If the low-molecular-weight component in a binary blend is of low enough molecular weight to be effectively a “solvent” (i.e., if it is unentangled) then the reptation time of the high-molecular-weight component will certainly be reduced by the presence of the low molecular-weight component.

On the other hand, if the low molecular weight component is itself entangled, then this is exactly the situation we have been considering so far in Section 7.3.2. The question is, to what extent can the short chains be considered as solvent, and do they speed up the terminal relaxation of the long chains? The preceding discussion suggests that we need to define two tubes for the long chains, both a “thin” tube, which is defined by all entanglements—entanglements with both short and long chains—and a “fat” tube, which is defined by the entanglements with the long chains only (the fat tube would be the only tube present if the short chains were truly unentangled solvent). This picture of thin and fat tubes, illustrated in Fig. 7.7(b), is equivalent to the description in terms of entanglements with long and short chains (Fig. 7.7(a)).

In the case of unentangled short chains, the motion of the long chain along the fat tube is unhindered by entanglements, i.e., it proceeds at a rate determined by monomeric friction only, with terminal time as given by Eq. 7.5. But, if the short chains are entangled, then motion along the fat tube must proceed at a rate determined by constraint release from the short chains. The situation is equivalent to the case of dilute long chains: in an unentangled solvent the long chains relax via Rouse motion (Section 6.2.2, ignoring hydrodynamic effects). However, if the “solvent” consists of short, entangled chains, then dilute long chains relax by CR-Rouse motion (Section 7.3.1). When long chains are more concentrated and entangled with each other, then this CR-Rouse motion is further restricted by the presence of long chain entanglements. Nevertheless, the CR-Rouse motion can still carry the long chains along the contour of fat tube, because such motion is not prevented by long-chain entanglements. Viovy et al. [4] called this process “tube reptation” since it is, in a sense, reptation of the thin tube along the fat tube. They determined the time for reptation along the fat tube to be:

$$\tau_{\text{dfat,L}} \propto \tau_{\text{d,S}} Z_L^3 \phi_L \propto \tau_e Z_S^3 Z_L^3 \phi_L \propto \tau_{\text{CR,L}} \tilde{Z}_L \quad (7.6)$$

The factor $\tau_{d,S} \propto \tau_e Z_S^3$ enters this expression because short chain reptation sets the timescale for the constraint release “hops” of the thin tube, which carry the chain along the fat tube. Reptation along the fat tube (with timescale set by CR-Rouse motion of the chain in the thin tube) competes with the unhindered reptation of the chain along the thin tube, at time $\tau_{d,L}$. We can compare the two processes by taking the ratio of their terminal times:

$$\frac{\tau_{d,L}}{\tau_{dfat,L}} \propto \frac{Z_L^3 \tau_e}{Z_S^3 Z_L^3 \phi_L \tau_e} = \frac{Z_L}{Z_S^3 \tilde{Z}_L} = Gr \tilde{Z}_L^{-1} \quad (7.7)$$

Once again, the ratio depends only on the Graessley parameter Gr and on the entanglement number $\tilde{Z}_L = \phi_L Z_L$. If $Gr \tilde{Z}_L^{-1} > 1$ then tube reptation along the fat tube is the faster process, and is expected to speed up the terminal relaxation of the long chains. Conversely, if $Gr \tilde{Z}_L^{-1} < 1$ then reptation along the thin tube remains the faster process, and this suggests the short chains cannot significantly accelerate the terminal relaxation of the longer chains, which is consistent with the double reptation assumption. The relaxation would then proceed in the manner illustrated in Fig. 7.6(b).

So far in Section 7.3 we have considered numerous possible effects of CR-Rouse motion, both for dilute and more concentrated long chains in a bidisperse melt. In doing this, we have compared the reptation time of the long chain along the thin tube with the timescales of various possible relaxation processes driven by CR-Rouse motion: (i) CR-Rouse relaxation of the whole chain, (ii) local CR-Rouse motion of a chain subsection between long-chain/long-chain entanglements, and (iii) tube reptation. The results of these comparisons are found, respectively, in Eqs. 7.2, 7.3, and 7.7, and these depend only on two significant parameters: the Graessley parameter Gr and the diluted entanglement number $\tilde{Z}_L = \phi_L Z_L$. It is therefore possible to produce a “map” of the two dimensional space spanned by the parameters Gr and \tilde{Z}_L . Such a map was first suggested by Viovy et al. [4], hence, we refer to it as a “Viovy diagram.” This diagram provides a very useful summary of all our preceding discussion of CR-Rouse motion.

We reproduce the Viovy diagram schematically in Fig. 7.8. Different regions of the diagram are separated by lines obtained by setting each of the Eqs. 7.2, 7.3, and 7.7 equal to unity. Along each of these lines, two different relaxation pathways have similar relaxation times and are therefore competing with one another. Within each region of the map, a single relaxation pathway is expected to be dominant. The left hand side of the map (low values of \tilde{Z}_L) concerns dilute long chains, as discussed in Section 7.3.1. In region 1 (at high values of Gr), CR-Rouse motion dominates the whole of the relaxation of the long chains, and we expect stress relaxation as depicted in Fig. 7.6(a). Increasing the molecular weight of the short chains (for example, as shown in the data of Fig. 7.2) results in a reduction in the value of Gr and slows

down the CR-Rouse motion. Eventually, a transition into region 2 of the diagram occurs, where the terminal relaxation of the long chains occurs via reptation along the thin tube.

The right hand side of the Viovy diagram in Fig. 7.8 concerns bidisperse melts with more concentrated long chains, where the effects of entanglements between the long chains become apparent. In both regions 3 and 4, the stress relaxation is expected to be qualitatively as depicted in Fig. 7.6(b). The initial CR-Rouse ramp is halted when $G(t)/G_N^0$ equals ϕ_L^2 , because the long chain entanglements prevent further relaxation by CR-Rouse motion. $G(t)/G_N^0$ then remains at this plateau value until terminal relaxation of the chains by reptation. In region 3, the presence of the short chains is not expected to affect the terminal relaxation, which occurs by reptation of the long chains along the thin tube at time $\tau_{d,L}$. This gives exactly the relaxation profile depicted in Fig. 7.6(b), and is very close to the prediction of double reptation theory (save for the initial CR-Rouse “ramp”). In region 4, however, “tube reptation” along the fat tube, occurring at time $\tau_{dfat,L}$, is expected to accelerate the terminal relaxation.

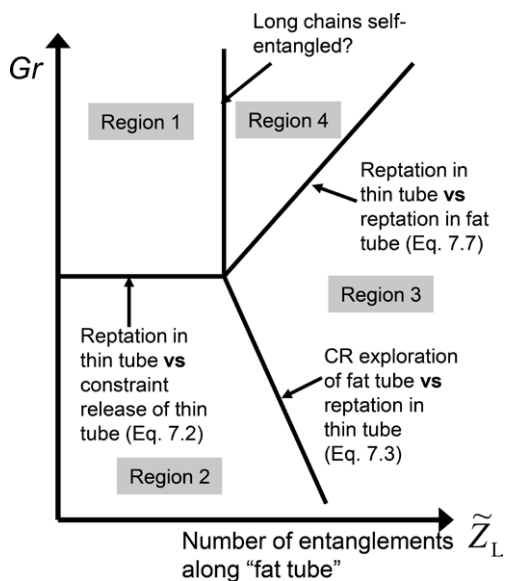


Figure 7.8 Schematic representation of a Viovy diagram, which delineates different regions of parameter space for binary blends of entangled polymers. The vertical axis is the Graessley parameter, Gr , while the horizontal axis is the number of entanglements along the fat tube of the longer chains, \tilde{Z}_L . Both axes are logarithmic in this schematic diagram. In region 1, CR-Rouse motion dominates the whole of the relaxation of the long chains, as in Fig. 7.6(a). In region 2, CR-Rouse motion of the long chains is terminated by reptation. In region 3, the terminal modulus is set by entanglements between long chains, but the terminal time is set by reptation along the thin tube as in Fig. 7.6(b). In region 4, the terminal time is set by “tube reptation” along the fat tube

Here, the presence of the short chains does affect the final relaxation of the long chains, in contradiction to double reptation theory. However, going deep into region 4 of the diagram is (in practice) very difficult to realize experimentally, requiring long chains of extremely high molecular weight. There is, therefore, a sizeable region of the Viovy diagram (region 3) in which double reptation theory might be expected to be successful.

Ignoring the CR-Rouse ramp, there are two features depicted schematically in Fig. 7.6(b), consistent with double reptation, that have been found valid for at least some of the available experimental data, such as the data shown in Fig. 6.17:

1. The time (or frequency) at which the long chain relaxes in Fig. 7.6(b) is set by the reptation time of the long chain $\tau_{d,L}$ and is unaffected by the concentration or molecular weight of the short chain.
2. The magnitude of the plateau in $G(t)$ in Fig. 7.6(b) at times near $\tau_{d,L}$ scales roughly as ϕ_L^2 .

While these features characterize the experimental data shown in Fig. 6.17, neither of them hold when the long chain is dilute in the short-chain matrix (i.e., the left hand side of the Viovy diagram) as illustrated in Figs. 7.2 and 7.6(a).

More seriously, these features do not even hold for all data where the long chains are more concentrated and self-entangled. For example, the data shown in Fig. 6.20 illustrate a case in which the long chain relaxation is accelerated by the presence of short chains, i.e., the terminal time decreases, contrary to the prediction of double reptation theory and of Fig. 7.6(b). Unfortunately, if one attempts to locate the melts from Fig. 6.20 on the Viovy diagram, they appear to be within region 3 where no significant change to the terminal time is expected. For example, the polyisoprene blends of MW = 483,000 and 33,600 have a Graessley number $Gr = Z_L/Z_S^3 \approx 0.3$ and diluted entanglement numbers ranging from $\tilde{Z}_L \approx 1$ at 1% dilution (i.e., barely entangled) to $\tilde{Z}_L \approx 40$ at 40% dilution. The ratio $Gr\tilde{Z}_L^{-1}$ (from Eq. 7.7) is thus significantly less than 1 for all the blends. One may allow for the fact that the critical value Gr_c for dilute chains has been estimated to be in the range 0.06–0.5 [8–10], and this may place the most dilute blends in Fig. 6.20 on the boundary of region 4 of the Viovy diagram. However, the more concentrated blends are firmly in region 3. Yet, the experimental data show evidence of a change in the terminal time with dilution of the long chains even when they are at their most concentrated. Similar behavior is found for other data in the literature [9]. It seems, then, that one of the predictions of the Viovy diagram is wrong: double reptation theory is expected to hold well in region 3, where it is predicted that the terminal time of the long chains is unaffected by the presence of short chains, but experimental data indicate more frequent deviation from double reptation predictions.

One suggestion found in the literature, going back to early work of Doi et al. [16], is that above a critical Graessley number long chains always reptate in the diluted fat tube, completely unhindered by the presence of short chains (i.e., the short chains are considered to be equivalent to unentangled solvent). This gives, simply, $\tau_{\text{dfat,L}} \propto \tau_e Z_L^3 \phi_L$, i.e., a reptation time in the fat tube independent of the short chain length, because CR-Rouse motion is ignored. This suggestion has the strong merit that it has been used successfully to predict experimental data for the stress relaxation for a wide range of bidisperse blends (as was demonstrated by Park and Larson [9, 17]). However, the suggestion must be rejected on conceptual grounds. Suggesting that the long chain can reptate along the fat tube, unhindered by the entanglement constraints of the short chains, is conceptually equivalent to suggesting that a dilute long chain, in a matrix of entangled short chains, is able to relax via free, unhindered Rouse motion. But, this is not the case: we know that such dilute long chains relax via CR-Rouse motion, at a timescale set by the release of short chain constraints (see Fig. 7.2 and Section 7.3.1). In the same way, motion of the long chain along the fat tube must proceed at a rate determined by constraint release from the short chains, giving Eq. 7.6.

A more recent suggestion [13, 18, 19] notes the fact that the Viovy diagram [4] was constructed by considering pure reptation and ignoring the corrections due to primitive path fluctuations. As discussed in Section 6.4.3, primitive path fluctuations (PPF) produce a significant correction to the simple reptation theory for monodisperse entangled polymers, relaxing a fraction of order $Z^{-1/2}$ of the length of the chain and so speeding up the terminal reptation so that it can be approximated as $\tau_1 = \tau_d (1 - X Z^{-1/2})^2$ where X is a constant (see Eq. 6.39). For bidisperse melts, there is potential for the PPF mechanism to produce yet more significant corrections. As the long chains explore the fat tube via CR-Rouse motion, this provides greater freedom for primitive path fluctuations. PPF can now, potentially, relax a fraction of order $\tilde{Z}_L^{-1/2}$ of the length of the chain, and since the number of entanglements between long chains \tilde{Z}_L is significantly smaller than the total number of entanglements Z_L then the fraction of chain relaxed by PPF becomes larger with increasing dilution. Because the distance to reptate is consequently smaller, the terminal reptation time is potentially accelerated, so that it might now be approximated as:

$$\tau_1 = \tau_d (1 - X \tilde{Z}_L^{-1/2})^2 \quad (7.8)$$

This terminal time is predicted to decrease as the long chains are further diluted with short chains, in qualitative agreement with the data in Figure 6.20, but in disagreement with double reptation predictions.

All of this assumes that there is sufficient time available for the deeper primitive path fluctuations in the fat tube. Read et al. [13] predicted that, in many circumstances, the timescale for fat tube PPF is simply obtained as the chain Rouse reorientation

time divided by the volume concentration of long chains, $\tau_{r,L}/\phi_L$ (the same timescale was obtained by Auhl et al. [20] for the stretch relaxation time relevant in nonlinear rheology). Provided this PPF timescale is longer than the time $\tau_{CR,loc}$ obtained above for local exploration of the fat tube by CR-Rouse motion, then the increased freedom for PPF in the fat tube is available to the long chains, and Eq. 7.8 should apply for their terminal relaxation. Expressing this condition in terms of the parameters of the Viovy diagram, we find that fat tube PPF should occur under the condition $Gr > \tilde{Z}_L^{-1}$, which represents a sizeable portion of region 3 in the diagram (Figure 7.8) and all of region 4. This explains why data for bidisperse melts at higher values of the Graessley parameter Gr often exhibit an accelerated terminal relaxation with increasing dilution, as noted by Park and Larson [9, 17]. In order to illustrate the significant effect of fat tube PPF, we show in Figure 7.9 predictions of the linear rheology for one of the blend series in Fig. 6.20, using theory developed in Read et al. [13].

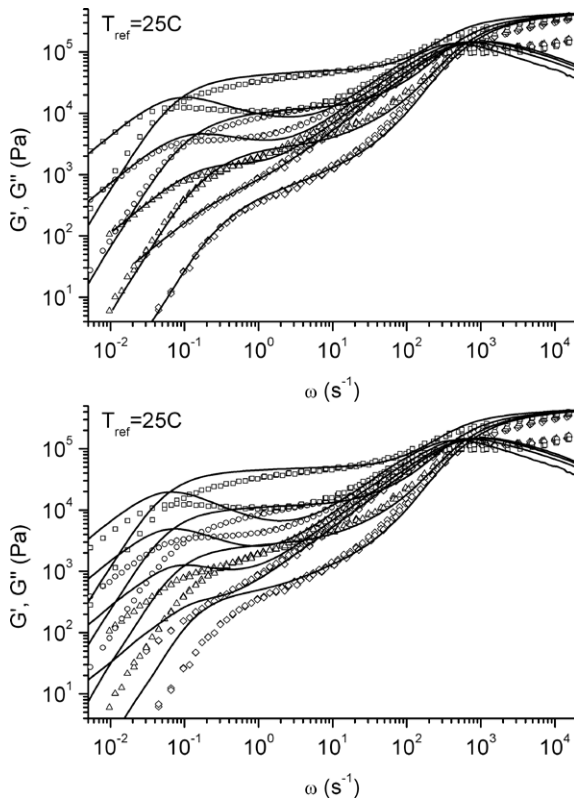


Figure 7.9 Storage and loss modulus for blends of 483 kg/mol with 33.6 kg/mol polyisoprene at concentrations of 40%, 20%, 10%, and 4% long chains. Also shown are predictions using the model of Read et al. [13] both (top) including primitive path fluctuations along the fat tube, and (bottom) including only primitive path fluctuations along the thin tube. From Read et al. [13].

The upper graph shows predictions taking account of the enhanced PPF in the fat tube, whilst the lower graph shows predictions when the fat tube PPF is not accounted for (whilst PPF for the thin tube is included). It is clear that correct prediction of the terminal time of the long chains requires the fat tube PPF mechanism. Similar conclusions, and predictions for other datasets, were obtained by van Ruymbeke et al. [18].

■ 7.4 Polydisperse Melts and “Dynamic Dilution”

7.4.1 Polydisperse Chains

It is clear from Section 7.3 that bidisperse polymer melts produce a rich and interesting behavior in their linear viscoelastic response, with many subtleties. We might summarize the discussion in that section as follows: CR-Rouse relaxation differs from double reptation in that for the latter, the relaxation modulus at any time t is taken to be proportional to the fraction of tube segments occupied, i.e., $G(t) \propto P^2(t)$, while when CR-Rouse relaxation is accounted for, $G(t) \propto P(t) P_{\text{CR}}(t)$, where the constraint-release function $P_{\text{CR}}(t)$ is proportional to $t^{-1/2}$, producing the “Rouse ramp” of Fig. 7.6.

Thus, for both double reptation and CR-Rouse relaxation, the modulus is the product of two functions: one describing relaxation due to motion of the “test” chain, and the other, due to movement of the matrix chains. In double reptation, the two functions are identical and both are taken to be the relaxation function $P(t)$ for a chain in a fixed tube. When CR-Rouse relaxation is occurring, the function describing relaxation due to the matrix takes the form $P_{\text{CR}}(t) \propto t^{-1/2}$.

The CR-Rouse behavior in Fig. 7.6(b) can then be captured heuristically as follows: (i) whenever CR-Rouse motion is not occurring, for example in Fig. 7.6(b) at early times $t < \tau_S$ before the short chains reptate, we can set the function $P_{\text{CR}}(t) = P(t)$; (ii) whenever CR-Rouse motion is occurring, for example shortly after the short chains reptate, we can set $P_{\text{CR}}(t) = P(\tau_S)(t/\tau_S)^{-1/2}$. We note that, at still later times when $P_{\text{CR}}(t)$ drops down to $P(t)$ again, CR-Rouse relaxation comes to a halt as the long chain has now explored the entire tube defined by entanglements with other long chains, and we set $P_{\text{CR}}(t) = P(t)$ again; see Fig. 7.6(b). Thus, the matrix function $P_{\text{CR}}(t)$ can never be smaller than $P(t)$, but it can exceed $P(t)$ whenever $P(t)$ decreases rapidly due to sudden relaxation of matrix chains. In no case can $P_{\text{CR}}(t)$ relax faster than $P_{\text{CR}}(t) \propto t^{-1/2}$.

Depending on the molecular weights of the long and short chains and their concentrations, it may also be the case that the relaxation function $P(t)$ for the long

chains is accelerated by the presence of the short chains, for example by allowing “tube reptation” or primitive path fluctuations along the fat tube (Section 7.3.3).

Now, consider a polydisperse polymer with a continuous distribution of molecular weights. Given the subtleties for the bidisperse melts just discussed, why might the double reptation concept work at all? If we represent the distribution of reptation times for the different components by a set of discrete, but closely spaced relaxation times, we obtain the relaxation modulus shown schematically in Fig. 7.10. Here, in the double reptation theory (bold dashed lines) we have a series of steps, each representing the exponential relaxation of a component of a given molecular weight. When CR-Rouse relaxation is considered, a portion of each step is replaced by a “Rouse ramp.” We can again represent this behavior by setting $G(t) \propto P(t) P_{\text{CR}}(t)$, with $P_{\text{CR}}(t) = P(t)$ along the plateaus in $P(t)$ where relaxation is slow, and with $P_{\text{CR}}(t) = P(\tau_i)(t/\tau_i)^{-1/2}$ whenever a time τ_i is reached at which $P(t)$ begins to decrease rapidly, i.e., more rapidly than as $t^{-1/2}$. It is clear from Fig. 7.10 that if the number of discrete molecular weights is large enough and the size of each step is small enough, then the difference between the double reptation description and the CR-Rouse description will become small and can then be neglected. That is, if the intervals of time during which $P_{\text{CR}}(t) = P(t)$ are brief, we can ignore CR-Rouse motion and simply set $P_{\text{CR}}(t) = P(t)$ for all t and recover the double reptation theory. This argument helps explain why the double reptation theory can work well in predicting the shape of the linear viscoelastic modulus of linear polymers with a *continuous* distribution of molecular weights, even though its predictions for monodisperse and bidisperse melts are rather poor.

Milner [21] has given a more complete argument that defines the requirements that the molecular weight distribution must meet for double reptation to be a reasonable approximation. There remains the consideration of the conditions under which the contribution to $P(t)$ from long chains is significantly accelerated by the presence of shorter chains. To our knowledge, this has not yet been addressed in the literature,

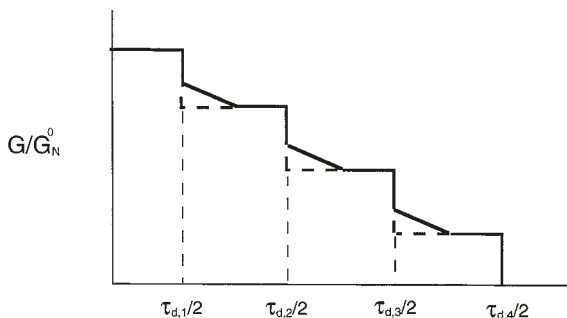


Figure 7.10 Relaxation modulus of entangled polydisperse melts according to the double reptation theory (bold dashed line) and the constraint-release Rouse theory (bold solid line)

though it is likely that (as with bidisperse melts) an enhancement of primitive path fluctuations will play a role.

7.4.2 Tube Dilation or “Dynamic Dilution”

So far, in Chapter 6 and in Section 7.3, we have discussed several effects of constraint release, illustrating these for the case of a bidisperse melt. These effects can be classed into two categories:

1. Relaxation of stress due to constraint release.
2. Speeding up of relaxation by constraint release.

The first effect occurs because the long chains can partially relax their configurations, and so relax their contribution to the stress, when the surrounding shorter chains reptate and release their constraints on the long chains. This relaxation is only partial because some of the constraints on long chains are produced by entanglements with other long chains, and these constraints do not relax on the short timescale of reptation of the short chains. This effect of stress relaxation is accounted for by double reptation, which, however, assumes that this partial relaxation of the long chain occurs as fast as a single reptation time of the short chains. CR-Rouse relaxation corrects this picture, incorporating the fact that, after reptation of the short chains, the long chain can only move a short distance before re-entangling with the other short chains. The gradual relaxation produced by successive constraint-release and re-entanglement processes is accounted for by the inverse square root scaling law discussed in Section 7.3. CR-Rouse relaxation comes to an end when the stress has relaxed to a residual level set by the density of entanglements of long chains with other long chains. In the case of polydisperse melts, just discussed in Section 7.4.1, the CR-Rouse relaxation may be “hidden” due to the gradual release of constraints at the different reptation times of the different molecular weight components, so recovering the double reptation picture. In all these cases, the relaxation modulus can be written as $G(t) \propto P(t) P_{\text{CR}}(t)$, where the factor $P(t)$ represents the fraction of material constrained by the initial set of entanglements, and $P_{\text{CR}}(t)$ represents the release of those constraints through reptation of the shorter chains.

The stress relaxation as just described can be represented through a very appealing conceptual picture, in which the effective tube diameter is envisaged to increase gradually during the relaxation (this is somewhat similar to the picture of thin tubes and fat tubes introduced in Section 7.3.3). Within this picture, the fraction of remaining stress-carrying polymer strands is given by the function $P(t)$, and these are constrained by an effective tube represented by entanglement molecular weight $M_e^G(t)$, or equivalently, the tube diameter $a(t)$, both of which increase with time such that:

$$M_e^G(t) = \frac{M_e^G(0)}{P_{CR}(t)}, \quad a^2(t) = \frac{a^2(0)}{P_{CR}(t)} \quad (7.9)$$

The relaxation modulus is then given by:

$$G(t) = \frac{4}{5} \frac{\rho R T}{M_e^G(t)} P(t) = G_N^0 P(t) P_{CR}(t) \quad (7.10)$$

which is exactly consistent with the arguments given in Section 7.4.1. Within the constraint-release Rouse regions of stress relaxation, the effective tube diameter for stress relaxation increases with a quarter power of time. At other times, the tube diameter is obtained from the remaining fraction of stress carrying polymer strands, since $P_{CR}(t) = P(t)$.

So, a picture of a gradually widening tube seems to be a helpful, and quite accurate, way of envisaging the effect of constraint release, discussed above, i.e., stress relaxation due to local rearrangement of chains from constraint release events.

A second effect of constraint release, which is linked to the first one, is that it provides a mechanism to accelerate the relaxation of the constrained chains, because motion of the chain along the path of the wider tube becomes a possibility. For example, in discussing bidisperse melts in Section 7.3.3, we introduced the concept of a thin tube and a fat tube, and showed that under some circumstances, it can be accurate to consider the motion of the chain as taking place along the fatter tube. In region 4 of the Viovy diagram (Fig. 7.8), the fastest terminal relaxation mechanism is “tube reptation,” i.e., the motion of the thin tube along the fat tube by constraint release hops. Similarly, the deeper primitive path fluctuations permitted along the fat tube contour can accelerate the terminal relaxation. So, the concept of a widening tube can also provide a helpful picture to envisage this second effect of constraint release: accelerated relaxation.

The set of tube model theories that make use of this picture of an increasing tube diameter are collectively known as “tube dilation,” “dynamic dilution” [22], or sometimes “tube enlargement” [23] theories, since the relaxation of the short chains essentially enlarges or dilates the diameter of the tube surrounding the long chains. This dilution is “dynamic,” since it occurs only at times much longer than the reptation time of the short chains, i.e., times long enough that the entanglement constraints imposed by the short chains are released so frequently relative to the motion of the long chains that the short chains might be regarded as “diluent” for the long chains. At times comparable to, or shorter than, the reptation time of the short matrix chains, the entanglements imposed by the short matrix chains are still intact, and the tube that the long chain “feels” is the original nondiluted tube.

However, some care is necessary when constructing arguments using the dynamic dilution picture. Even if the stress is well represented by a diluted tube using Eq. 7.10,

it does not necessarily follow that motion along that tube gives the fastest relaxation mechanism. For example, in region 3 of the Viovy diagram (Fig. 7.8), during the terminal relaxation of the long chains the stress level is given by the “diluted” (fat) tube, yet the fastest reptation relaxation is given by motion along the thin tube (and not via “tube reptation” of the thin tube along the fat tube). At the same time, primitive path fluctuations within the fat tube are possible, and may speed up reptation by shortening the distance required to diffuse in order to relax the stress [13]. Consequently, the picture of “dynamic dilution” is helpful in describing some, *but not all*, aspects of the relaxation pathway.

In particular, we draw attention to a common error in dynamic dilution theories. It is sometimes argued that motion of a chain along the “dynamically diluted” tube proceeds as though the shorter chains act purely as solvent, so that the effective friction associated with chain motion along the diluted tube is obtained by including only the monomer friction. Unfortunately, this cannot be the case, unless the short chains are actually so short as to be unentangled (and truly acting as solvent chains). In all other cases, entanglements with the shorter chains slow down the motion of the longer chains along the diluted tube path. Constraint release permits motion along the diluted tube, but this is subject to an increased effective friction associated with the constraint release events, i.e., the repeated disentanglement and re-entanglement with shorter chains (e.g., as considered in deriving Eq. 7.6). Nevertheless, it may yet be the case that motion along the diluted tube is faster than motion along the thin tube, despite the increased friction, since the diluted tube path is shorter and less tortuous than the thin tube path (and this is the case in region 4 of the Viovy diagram of Figure 7.8).

To summarize, dynamic dilution, or tube dilation, is the name given to a set of theories based on the tube model in which a picture of a gradually increasing tube diameter is used. This picture can be used to signify two distinct concepts: (1) the stress relaxation associated with local chain rearrangements from constraint release events, and (2) the opportunity for chain motion along tube paths with increased diameter and shorter path length, providing the possibility of faster relaxation. It is important *not* to assume that, just because the first of these applies, then the second must necessarily follow.

Dynamic dilution or tube dilation is an especially important concept in describing the relaxation of branched polymer chains, where there is typically a broad distribution of constraint release timescales. We shall discuss these theories for branched polymer chains in Chapter 9, but we note here that the assumption of “short chains acting as solvent” (criticized above) has been frequently made in the literature of branched polymer rheology, even by the authors of this book. Despite the many successes of the current theoretical framework for branched polymers, it may be that aspects of these theories need to be revised in the coming years.

While the simple theories of CR-Rouse motion and dynamic dilution discussed above greatly improve the predictions of the tube model, especially when the distribution of molecular weights is bimodal, these theories are not always quantitatively accurate (see, for example, Lee et al. [24]). More advanced, but also more complex theories of constraint release are available; see, for example, Rubinstein and Colby [25], Likhtman and McLeish [26], and Watanabe et al. [10]. For a thorough discussion of the successes and failures of the available theories, see Watanabe et al. [1, 10, 11].

■ 7.5 Input Parameters for Tube Models

The constraint-release models just discussed have been tested by comparing their predictions to experimental data, for example, as shown in Fig. 7.9. For linear polymers where the molecular weight distribution is unimodal and not too broad, dynamic dilution is not very important, and theories that account for some stress relaxation from constraint release without assuming any acceleration of relaxation from “tube dilation” are adequate. Such is the case with the version of the Milner-McLeish theory [27] for linear polymers used to make the predictions shown in Fig. 6.16. Similarly, the double reptation theory also neglects acceleration of relaxation from tube dilation. The “dual constraint” theory mentioned in Chapter 6 does include dynamic dilution effects, although they are not very important for narrowly dispersed linear polymers. As just described, the different aspects of dynamic dilution become important for some bimodal blends, for example leading to enhanced primitive path fluctuations as included by Read et al. [13] and van Ruymbeke et al. [18]. Dynamic dilution is certainly extremely important for branched polymers, as discussed in Chapter 9.

In general, within the tube model, there should be only two parameters that need to be specified prior to such predictions. These are the *plateau modulus* G_N^0 (or equivalently, the *entanglement spacing* M_e) and the *monomeric friction coefficient* ζ . The value of G_N^0 should be independent of polymer molecular weight and branching structure, and only slightly dependent on temperature; values of G_N^0 for many polymer melts have been tabulated by Fetters et al. [28] and Ferry [14], and a few of the values from Fetters et al. [28] are reproduced in Table 7.1. It should be noted that there are differences between the values of M_e as tabulated by Ferry and by Fetters et al., due mainly to the differing conventions used in the definition relating M_e to the plateau modulus G_N^0 ; see Section 6.3.3. This accounts for a factor of 4/5 smaller value of M_e in Fetters et al. [28] relative to Ferry. The Fetters definition is given in Eq. 6.21 of Chapter 6, namely $M_e^G = (4/5) \rho R T / G_N^0$, where ρ is the polymer mass density and $R = k N_A$ is the gas constant (N_A is Avogadro’s number).

Table 7.1 Tube Model Parameters for Various Polymer Melts

Polymer	^a G_N^0 (Pa)	^b M_e^G (g/mol)	^c a (cm)	ξ (g/s)	^d τ_e (s)
1,4PBD (25 °C) (28 °C) (30 °C)	$1.15 \cdot 10^6$	1543	$36.8 \cdot 10^{-8}$	$10^{-6.75} =$	
				^e $1.78 \cdot 10^{-7}$	$5.6 \cdot 10^{-7}$
					^f $4.9 \cdot 10^{-7}$
PS (140 °C) (150 °C) (160 °C) (170 °C) (180 °C)	$2 \cdot 10^5$	13,309	$76.0 \cdot 10^{-8}$		
					^g $5 \cdot 10^{-2}$ (fit)
					^h $1 \cdot 10^{-2}$ (fit)
				ⁱ $2.66 \cdot 10^{-5}$	$1.61 \cdot 10^{-3}$
				ⁱ $8.99 \cdot 10^{-6}$	$5.45 \cdot 10^{-4}$
1,4PI (25 °C)	$3.5 \cdot 10^5$	5097	$55.1 \cdot 10^{-8}$	$10^{-6.41} =$	
				^j $3.89 \cdot 10^{-7}$	$7.3 \cdot 10^{-6}$
^k H-1,4PB (190 °C)	^l $2.31 \cdot 10^6$	^m 932			ⁿ $7 \cdot 10^{-9}$ (fit)
					^p $7 \cdot 10^{-9}$ (fit)

^a data taken from Fettters et al. [28]^b using values and the G definition from Fettters et al. [28], i.e., $M_e^G = (4/5) \rho R T / G_N^0$, except where noted otherwise^c from $a^2 = M_e \langle R^2 \rangle_0 / M$ using experimental M_e , $\langle R^2 \rangle_0 / M$ and Eq. 17 from Fettters et al. [28]^d from $\tau_e = (M_e^G / M_0) \xi a^2 / (3 \pi^2 k_B T)$, unless noted otherwise^e from Ferry et al. [14] for poly-1,4-butadiene^f data obtained from WLF shifting, Eq. 4.58, with $c_1^0 = 3.64$; $c_2^0 = 186.5$ K; $T_0 = 25$ °C, from Ferry [14, p. 277], polybutadiene, “cis-trans”^g from fit to dual constraint model [33] in Fig. 6.21 (see correction of τ_e by factor of 0.375 discussed in [34])^h from fit to dual constraint model [33] in Fig. 6.18 (see correction of τ_e by factor of 0.375 discussed in [34])ⁱ from formula of Majesté [35] given by Eq. 7.12^j from Ferry et al. [14, p. 330] for Hevea rubber^k hydrogenated 1,4-polybutadiene; typically contains around 2% ethyl side branches resulting from the 7% vinyl content in most nominally 1,4-polybutadienes^l given by Raju et al. [36]^m taken from the value for HDPE times inverse ratio of values of G_N^0 for hydrogenated 1,4-polybutadiene relative to HDPEⁿ from fit to dual constraint model [33] in Fig. 7.12 (see correction of τ_e by factor of 0.375 discussed in [34])^p from fits of dual constraint model [33] to zero-shear viscosity correlation of Arnett and Thomas [37], Eq. 7.14 at 190 °C (see correction of τ_e by factor of 0.375 discussed in [34])

We should also note that the relationship between M_e^G and G_N^0 is dependent on assumptions in the tube model, including neglect of fluctuations in the positions of entanglement points. Although the molecular dynamics simulations of Everaers et al. [29] (as also discussed in Section 6.3.6) support the validity of the formula $M_e^G = (4/5) \rho R T / G_N^0$, in some “slip link” models (see Chapter 6, Section 6.5) fluctuations in entanglement positions appear to lead to a reduction in M_e by a factor of 2, for a given value of G_N^0 [30, 31]. Some of these differences can be resolved using the arguments of Everaers [32]. Nevertheless, because of such issues (and further, because there may be nonentropic contributions to the stress) the value of M_e used

in theoretical predictions is sometimes taken as an independent third adjustable parameter, besides the standard parameters of G_N^0 and ζ . Here, we will ignore the relatively weak temperature dependences of M_e and G_N^0 .

If ζ is given, the *equilibration time* τ_e can be obtained from Chapter 6, Eq. 6.23, reproduced here:

$$\tau_e = \frac{\zeta a^2 M_e^G}{3 \pi^2 k T M_0} \quad (7.11)$$

where a is the tube diameter (given in terms of M_e^G by Eq. 6.22), and M_0 is the molecular weight of a monomer. Given literature values for G_N^0 (or M_e) and ζ specified in Table 7.1, the predictions of the tube models can in principle, be made *a priori*, i.e., without any adjustable parameters, beyond the fits used in the literature to obtain G_N^0 and ζ .

In Section 6.2.3, we briefly alluded to methods of obtaining ζ *a priori*, i.e., independently of fits to rheological data for entangled melts, and additional discussion of this issue can be found in Ferry [14]. Typically, ζ is obtained through measurements of viscosity or diffusivity for unentangled melts. However, for unentangled melts the chains are often so short that corrections to the glass transition temperature due to chain ends are important, and these affect ζ . The unreliability of methods for obtaining ζ has been asserted, or at any rate used as a rationale, to justify adjusting the value τ_e (and implicitly of ζ through the dependence of τ_e on ζ in Eq. 7.11). Thus, many of the tube model predictions presented in Chapters 6 through 11 use τ_e as a fitting parameter to help match the model to experimental data.

Normally, however, τ_e must be kept fixed if molecular weight or branching structure is changed, and τ_e should change with temperature in the same way as does ζ and the *shift factor* $a_T(T)$, discussed in Section 4.5. In addition, if the value of τ_e required to fit rheological data differs greatly (more than a factor of two or so) from the value inferred from a measured value of ζ this casts some doubt on the validity of the tube model used to obtain the fit.

As discussed in Section 4.5, there are two functional forms commonly used to express the temperature dependence of $a_T(T)$ and these should be used to shift τ_e to account for changes in temperature. These are the *Arrhenius* and the *WLF* dependences given, respectively, by Eqs. 4.57 and 4.58. The Arrhenius form is appropriate when the polymer is far above its glass transition temperature T_g . It is often used for polymers, such as polyethylene or polypropylene, that crystallize at temperatures far above their glass transition, and so exist in the melt state only at temperatures well above T_g . The WLF form is used when the polymer is closer to its glass transition temperature. Consider, for example, 1,4-polybutadiene, whose glass transition temperature is around 205 K, or -68°C [14]. At 25°C , the monomeric friction coefficient is reported to be $\zeta = 10^{-6.75} = 1.78 \cdot 10^{-7}$ (see ref. [14], p. 330).

Since 25 °C is close enough to the glass transition temperature for the WLF form to be most appropriate, for temperatures other than 298 K (25 °C), this value of ζ and the value of τ_e tabulated in Table 7.1 can be time-temperature shifted using Eqs. 4.54 and 4.58. For 1,4-polybutadiene, the fitted values of the WLF parameters are $c_1^0 = 3.64$; $c_2^0 = 186.5$ K; $T_0 = 25$ °C (see ref. [14], p. 277).

For polystyrene, Majesté et al. [35] have extracted from rheological data the following temperature dependence of the monomeric friction coefficient:

$$\zeta = \zeta_\infty \exp \left[\frac{B}{\alpha(T - 322.6)} \right] \quad (7.12)$$

where $\zeta_\infty = 2.7 \cdot 10^{-11}$ g/s, $B/\alpha = 1620 \pm 50$, and T is again the absolute temperature in Kelvin. These values of $\zeta = \zeta_0$ can be converted to τ_e using Eq. 7.11; see Table 7.1. For lower temperatures, $T \leq 160$ °C, the correlation of Majesté et al. seems to be inaccurate [33], but the values of τ_e can be obtained by fitting to the rheological data.

For linear polymers, fits of rheological data to the tube model are often used to obtain τ_e , with literature values (for example from Fetters et al. [28]) used to assign values of G_N^0 and M_e . As discussed in Larson et al. [38], inconsistent definitions, errors in assignment or calculation of the values of G_N^0 , M_e and τ_e have been common in the literature. For reference, a table giving three sets of self-consistent definitions of the parameter values M_e and τ_e , taken from Larson et al. [38], is reproduced as Table 7.2. In this book, we adhere to the G definitions. However, if one consistently uses the definitions from only one column of this table, and is careful to be sure that any literature values used were defined using the same definitions, or are corrected to be consistent with them, one can avoid these errors. For linear polymers, even when errors have been made in the literature, they can usually be absorbed, more or less, into the fitted value of τ_e . Hence, even with erroneous or inconsistent definitions or parameters, the resulting predictions are similar to those obtainable from the correct parameter assignments, only with a different value of τ_e . For branched polymers, however, correct assignment of parameter values is much more crucial, especially if one insists (as one should) that the same parameter values used to predict the rheology of linear polymers of a given chemical type be applied to the predictions for stars and other branched polymers as well. Obtaining fits, simultaneously, of the tube model to data for melts of linear polymers, star polymers, and binary blends of linear/linear, star/star, or linear/star with the same set of parameter values (G_N^0 , M_e^G , τ_e) has frequently required treating not only τ_e , but also M_e^G as a fitting parameter, even though this requires abandoning the theoretical relationship between G_N^0 and M_e^G , given by Eq. 6.21. It is fair to note, however, that some adjustment of the value of M_e^G (maybe by 10–20%) can be justified by the fact that predictions of the rheology of branched polymers are very sensitive to the value of M_e^G , well beyond the accuracy of measurements of G_N^0 .

Table 7.2 Summary of Alternative Definitions of Tube Parameters

	G Definitions (Fetters <i>et al.</i>) Based on Eq. 6.21 for M_e^G and Eq. 6.23 for τ_e	F Definitions (Ferry) Based on Eq. 6.20 for M_e and Eq. 6.23 for τ_e	MM Definitions (Milner-McLeish) Based on Eq. 6.20 for M_e and Eq. 6.20 for M_e
M_e Entanglement molecular weight	$M_e^G \equiv \frac{4}{5} \frac{\rho R T}{G_N^0}$	$M_e \equiv \frac{\rho R T}{G_N^0}$	$M_e \equiv \frac{\rho R T}{G_N^0}$
Z Number of tube segments	$Z = \frac{M}{M_e^G}$	$Z = \frac{5}{4} \frac{M}{M_e}$	$Z = \frac{5}{4} \frac{M}{M_e}$
τ_e Equilibration time	$\tau_e = \left(\frac{M_e^G}{M_0} \right) \frac{\xi b^2}{3 \pi^2 k T}$	$\tau_e = \left(\frac{4}{5} \right)^2 \left(\frac{M_e}{M_0} \right)^2 \frac{\xi b^2}{3 \pi^2 k T}$	$\tau_e^{MM} = \left(\frac{M_e}{M_0} \right)^2 \frac{\xi b^2}{3 \pi^2 k T}$
τ_r ($= 2 \tau_R$) Rouse reorientation time	$\tau_r = Z^2 \tau_e$	$\tau_r = \left(\frac{4}{5} \right)^2 Z^2 \tau_e^{MM}$	$\tau_r = \left(\frac{4}{5} \right)^2 Z^2 \tau_e^{MM}$
τ_d Reptation time	$\tau_d = 3 Z^3 \tau_e$	$\tau_d = 3 Z^3 \tau_e$	$\tau_d = 3 \left(\frac{4}{5} \right)^2 Z^3 \tau_e^{MM}$

Finally, we remark that there are other parameters in tube models whose values are believed to be universal but that are uncertain or controversial. One of these, the “dilution exponent” α introduced in Section 9.3.2, and above in Section 7.3.3, has been assigned values of either $\alpha = 1$ or $\alpha = 4/3$ [2, 10, 14, 15]. This difference, while not large, turns out to have big effects on the predicted rheological properties of branched polymers, as will be shown in Chapter 9. A second parameter whose value has been disputed is an exponent ν that appears in the theory for branched polymer relaxation, namely in Eq. 9.2. This parameter is assigned the value $3/2$ in most theories, but might arguably have a different value [12] (see, however, [39] and [40]). There is, additionally, a parameter p^2 , associated with the hop length for branch points upon relaxation of a polymer side-arm (see Chapter 9 and [41]).

The other constants of the tube models, including the reptation time $\tau_{d,i} = 3 \tau_e Z_i^3$ and the Rouse reorientation time $\tau_{r,i} = \tau_e Z_i^2$, are typically given in terms of τ_e and the number of entanglements per molecule $Z_i = M_i / M_e^G$, as discussed in Chapter 6. For the double reptation model, on the other hand, the “reptation time” is usually not given by a physically-based equation, but at least in some treatments is given by the empirical formula $\tau_{d,i}^{\text{eff}} = K Z_i^{3.4}$ that includes implicitly effects of primitive path fluctuations [42]. To use this formula, the constant K must be specified. The principle of time-temperature superposition implies that K must have the same temperature dependence as does τ_e , i.e., an Arrhenius or WLF form. Therefore, the value of K can be found at any temperature as soon as it is specified for a single temperature. One might obtain K at a single temperature for a given type of polymer by fitting the double reptation model to a single sample of that polymer, for example of monodisperse sample of a particular molecular weight. If the theory is accurate, it then ought to predict the behavior of any other well-entangled sample of that polymer, regardless of its molecular weight or molecular weight distribution, and the effect of temperature can be accounted for using the tabulated time-temperature shift formula. Thus, for each type of polymer, one should only need to perform data fitting once, to a single polymer sample at a single temperature.

Since the constant K must be related somehow to the monomeric friction coefficient, one should, in principle, be able to do even better than this. In fact, one can obtain the parameter K *a priori* by relating it to the more fundamental parameters G_N^0 and τ_e of the tube model. For example, for the dual constraint model or Milner-McLeish model, one can produce a *universal plot* of the dimensionless quantity $\eta_0 / (G_N^0 \tau_e)$ versus M/M_e for an arbitrary monodisperse polymer, and match this prediction to that of the double reptation model by adjusting the value of K . Tube models, such as the Milner-McLeish or dual constraint models, that explicitly include the effects of primitive path fluctuations, give roughly a 3.4 power-law dependence of zero-shear viscosity on molecular weight over the range of typical molecular weights for melts, which is the same power law that is assumed by fiat in the double reptation model.

One can therefore fit the predictions of the double reptation model to the Milner-McLeish or dual constraint model with fluctuations, and thereby extract the value of K in terms of τ_e . For the dual constraint model, Pattamaprom et al. [33, 34] performed this exercise and obtained the formula:

$$K = 0.127 \tau_e / (M_e^G)^{3.4} \quad (7.13)$$

(the formula given by Pattamaprom et al. used the Ferry definition of M_e). To the extent that the dual constraint model accurately predicts real data, Eq. 7.13 can be regarded as a microscopic formula for the parameter K . Thus, by using Eq. 7.13, the one “adjustable” parameter of the double reptation theory is fixed without any prior data fitting. A similar equation could be extracted by matching double reptation to the Milner-McLeish theory.

So far, in Chapter 6, and in this chapter, we have compared predictions of various versions of the tube model to data for monodisperse, bidisperse, and polydisperse samples of polystyrene and polyisoprene. While polystyrene, and, to a lesser extent, polyisoprene, have significant commercial value, the most important commercial polymer in the world, measured by either volume of product or total revenue, is polyethylene. Polyethylene constitutes some 40% of the total volume of commercial polymers, amounting to around 10^{11} pounds sold annually worldwide [43]. Hence the need for methods of rheological characterization of polyethylenes is especially high. The need is made all the more acute by the relative difficulty in applying non-rheological methods of characterization to polyethylene. Characterization of molecular weight distributions by GPC or light scattering, for example, requires dissolution of the polymer in a solvent. While polystyrene, polyisoprene, polybutadiene, and many other polymers are readily soluble in many solvents at room temperature, polyethylene is especially intractable, dissolving only under rather extreme solvent conditions, such as in xylene at near-boiling conditions. To make matters worse, polyethylene cannot be synthesized directly by anionic polymerization, and hence ordinary polyethylene samples are invariably of high polydispersity, often with M_w/M_n well above 2. A further complication is that one cannot always be sure that such polyethylenes are completely free of long-chain branching. Thus, molecular interpretation of rheological data for polyethylenes is still controversial, despite the fact that polyethylene has been the single most important commercial polymer worldwide for more than half a century!

Fortunately, there is an indirect method of producing an ideal, monodisperse, close approximation to polyethylene that is free of long-chain branching, namely, via hydrogenation of 1,4-polybutadiene [36]. When anionically synthesized monodisperse 1,4-polybutadiene is hydrogenated, the product is chemically equivalent to simple polyethylene (except for the presence of an occasional ethyl branch in hydrogenated

1,4-polybutadiene; see below). Thus, hydrogenated 1,4-polybutadiene is a good model material for developing an understanding of commercial polyethylenes.

Figure 7.11 shows predictions of G' and G'' from the dual constraint model compared with experimental data for nearly monodisperse hydrogenated polybutadiene [33, 36] of molecular weights 4.39, 6.02, 7.15, 11.9, 17.4, 20.2, and $35.9 \cdot 10^4$. In this case, the value of the parameter $\tau_e = 7 \cdot 10^{-9}$ s was obtained by fitting the model to the data. For hydrogenated 1,4-polybutadiene, the value of the plateau modulus, $G_N^0 = 2.31 \cdot 10^6$ Pa [36], is a little lower than that for ordinary polyethylene ($G_N^0 = 2.60 \cdot 10^6$ Pa; see Table 7.1), apparently because of the presence of a few ethyl branches in the former; see below. The agreement of the dual constraint model with the data is good except at very low frequencies, where deviations from terminal relaxation behavior in G' are observed in some of the samples. Such deviations are probably caused by non-idealities in the samples, such as a high-molecular-weight tail in the molecular weight distribution or a low level of long-chain branching.

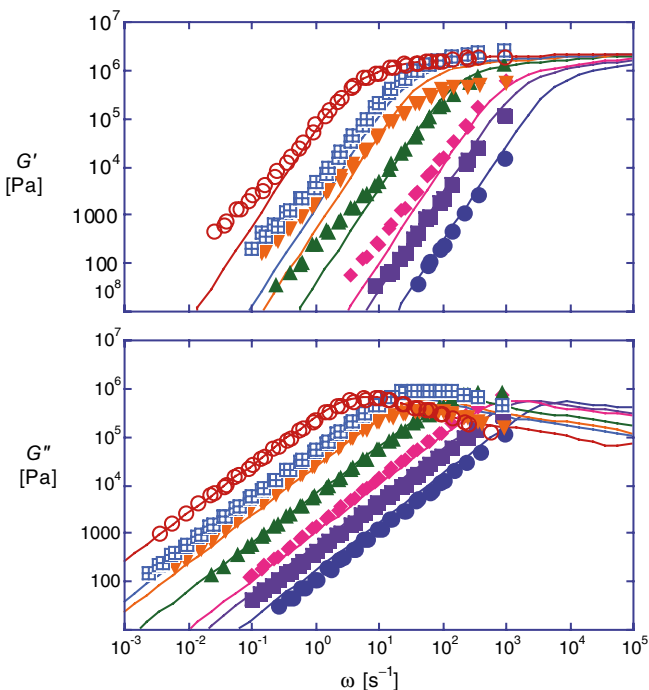


Figure 7.11 Comparison of the predictions of the dual constraint model (lines) to experimental data (symbols) for the loss modulus of monodisperse, linear, hydrogenated polybutadienes of molecular weights 4.39, 6.02, 7.15, 11.9, 17.4, 20.2, and $35.9 \cdot 10^4$, from right to left, at 190 °C. The parameter values are: $G_N^0 = 2.31 \cdot 10^6$ Pa and $\tau_e = 7 \cdot 10^{-9}$ s, the latter value being obtained as a best fit. From Pattamaprom and Larson [33]; see correction to τ_e by factor of 3/8 in [34].

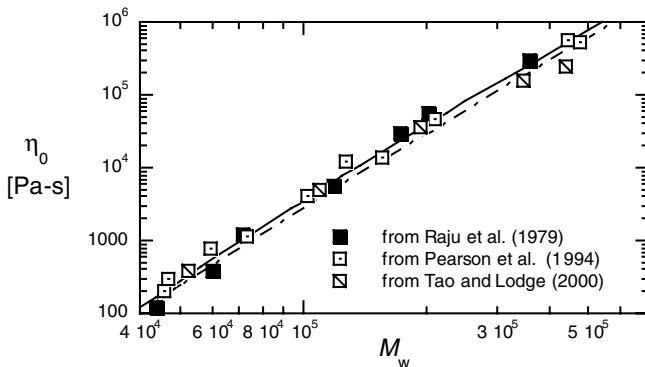


Figure 7.12 Predictions of $\eta_0(M_w)$ by the dual constraint model (solid lines) compared with experimental data (symbols) from the sources listed for monodisperse, linear, hydrogenated polybutadienes at 190 °C. The parameter values are: $G_N^0 = 2.31 \cdot 10^6$ Pa and $\tau_e = 7 \cdot 10^{-9}$ s. The dashed line is the correlation of Arnett and Thomas [37]. From Pattamaprom and Larson [33]; see correction to τ_e by factor of 3/8 in [34]

Figure 7.12 shows zero-shear viscosities measured for three series of monodisperse hydrogenated polybutadienes [36, 44, 45] at 190 °C. The data of Tao and Lodge [45] were shifted from 140 °C to 190 °C and those of Pearson et al. [44] were shifted from 175 °C to 190 °C using the following Arrhenius correlation [37]:

$$\ln(\eta_0) = \ln(M^{3.41}) + \frac{3523 \pm b}{T} \exp[(2.36 \pm 0.08) \cdot b] - 37.04 \quad (7.14)$$

where M is the molecular weight, T is absolute temperature (in Kelvin), and b is the fraction of ethyl branches in the sample. Ethyl branches are present because polybutadiene is almost never purely 1,4 addition, but typically contains around 7% vinyl addition (see ref. [14], p. 279). When hydrogenated, these become ethyl side-branches, because each monomer of butadiene contains four carbons, 7% vinyl addition, when hydrogenated, will yield a little less than 2% ethyl side branches per backbone carbon. Thus, for the samples considered in Fig. 7.12, b in Eq. 7.14 is estimated to be 0.02. The solid line in Fig. 7.12 is the prediction of the dual constraint model using the same values of $G_N^0 = 2.31 \cdot 10^6$ Pa and $\tau_e = 7 \cdot 10^{-9}$ s used in Fig. 7.11. The dot-dashed line is the correlation of Arnett and Thomas [37] for monodisperse hydrogenated 1,4-polybutadiene.

The agreement of the dual constraint model with the experimental data and with the correlation of Arnett and Thomas is excellent.

As shown in Fig. 7.13(a), the tube model (in this case the dual constraint model) is also reasonably successful in predicting the linear viscoelastic response of *Polydisperse* polyethylene melts, as long as they do not contain long side branches.

The rheological properties are extremely sensitive to long-chain branching; Fig. 7.13(b) shows the linear viscoelastic response of an LLDPE melt with almost the same molecular weight distribution as in Fig. 7.13(a), but with long-chain branching. The theory, which assumes no long-chain branching, obviously grossly underestimates the magnitude of the elastic modulus in the terminal regime when long-chain branching is present. In Chapter 9, another example of this is given (Fig. 9.5), and methods are presented for including the effect of long-chain branching on the linear rheology of polymer melts.

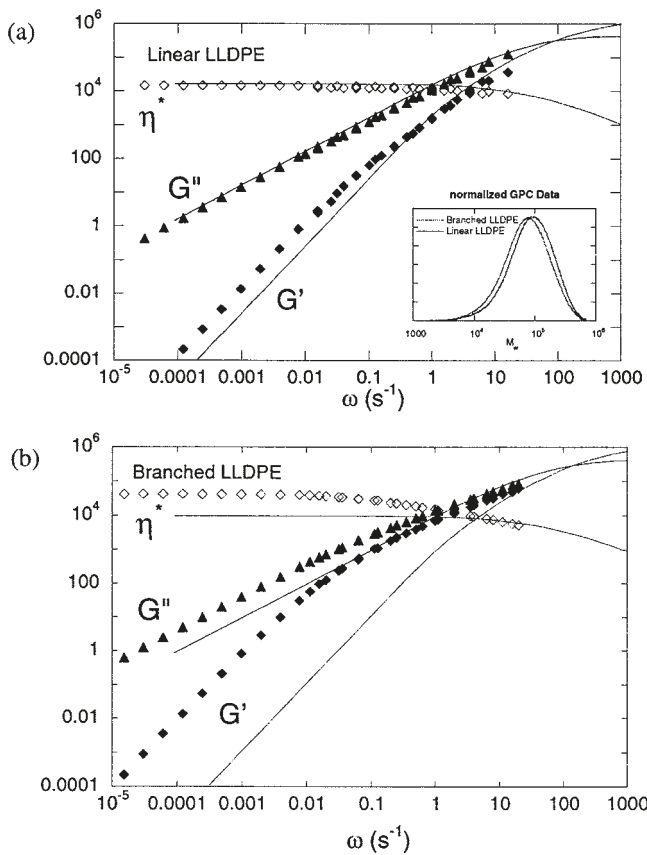


Figure 7.13 Predictions of G' , G'' , and $\eta \equiv \left[(G')^2 + (G'')^2 \right]^{1/2} / \omega$ by the dual constraint model compared with data of Gabriel and Münstedt [46] for two LLDPE melts. In (a), the melt ($M_w = 1.14 \cdot 10^5$; $M_w/M_n = 2.07$) has no long side branches, while in (b) the melt ($M_w = 9.86 \cdot 10^4$; $M_w/M_n = 2.05$) has long side branches. Both melts have nearly the same MWD, as shown by the insert in (a). For both melts, dual constraint predictions were carried out using the experimental molecular weight distribution, with parameter values of $G_N^0 = 2.6 \cdot 10^6$ Pa, $M_e = 1035$, and $\tau_e = 11 \cdot 10^{-9}$ s. From Pattamaprom and Larson [33]; see correction to τ_e by factor of 3/8 in [34].

■ 7.6 Summary

The linear viscoelastic behavior of melts of linear polymers can be predicted accurately using “tube” theories that account for reptation, primitive path fluctuations, and constraint release. The physics of constraint release is complex; however, semi-empirical methods that account for it are available. The crudest method, “double reptation,” assumes instantaneous loss of stress whenever a “matrix” chain releases a constraint on a “test” chain. This method gives fairly accurate predictions of storage and loss moduli $G'(\omega)$ and $G''(\omega)$ at low and moderate frequencies, as discussed in Chapter 6. However, we saw in Chapter 6 that the simplest version of double reptation predicts that increasing polydispersity at fixed weight average molecular weight M_w should increase the zero-shear viscosity η_0 , a prediction not supported by the data. This failure may arise from conceptual flaws in the double reptation concept that are exposed when one considers in detail the relaxation of bidisperse entangled melts. More sophisticated treatments of constraint release include “constraint-release Rouse” relaxation and “dynamic dilution.” Constraint-release Rouse relaxation is a time-delayed relaxation by which the test chain gradually explores a wider tube once constraints have been released. Dynamic dilution is the name given to a set of theories which make use of this picture of a widening tube, both as a description of stress relaxation and of acceleration of relaxation timescales due to constraint release. Dynamic dilution theories are perhaps most appropriate when some constraints are relaxed very much more rapidly than the time scale for motion of the test chain, or portions of the test chain. In such a case, the density of matrix constraints at long times may be considered to be “diluted” relative to the density of constraints at short times. When these processes are included, accurate predictions are obtained of the linear viscoelasticity of bidisperse blends, even when the high molecular weight component of the blend is either very dilute or very much higher in molecular weight than the low-molecular-weight component. As we will see in Chapter 9, dynamic dilution is especially important for star polymers, even monodisperse stars, because of their very wide distribution of relaxation times.

■ References

- [1] Watanabe, H., Yamazaki, M., Yoshida, H., Kotaka, T. Viscoelastic properties of binary blends of linear polystyrenes: Further examination of constraint release models. *Macromol.* (1991) 24, pp. 5573–5581
- [2] Watanabe, H. Viscoelasticity and dynamics of entangled polymers. *Prog. Polym. Sci.* (1999) 24, pp. 1253–1403
- [3] Watanabe H., Urakawa, O., Kotaka, T. Slow dielectric-relaxation of entangled linear cis-polyisoprenes with asymmetrically inverted dipoles. 2. Behavior in a short matrix. *Macromol.* (1994) 27, pp. 3525–3536
- [4] Viovy, J.L., Rubinstein, M., Colby, R.H. Constraint release in polymer melts: Tube reorganization versus tube dilution. *Macromol.* (1991) 24, pp. 3587–3596
- [5] Klein, J. Onset of entangled behavior in semidilute and concentrated polymer solutions. *Macromol.* (1978) 11, pp. 852–858
- [6] Daoud, M., de Gennes, P.G. Some remarks on the dynamics of polymer melts. *J. Polym. Sci., Polym. Phys. Ed.* (1979) 17, pp. 1971–1981
- [7] Graessley, W.W. Entangled linear, branched and network polymer systems—molecular theories. *Adv. Polym. Sci.* (1982) 47, pp. 67–117
- [8] Green, P.F., Mills, P.J., Palmstrom, C.J., Mayer, J.W., Kramer, E.J. Limits of reptation in polymer melts. *Phys. Rev. Lett.* (1984) 53, pp. 2145–2148
- [9] Park, S.J., Larson, R.G. Tube dilation and reptation in binary blends of monodisperse linear polymers. *Macromol.* (2004) 37, pp. 597–604
- [10] Watanabe, H., Ishida, S., Matsumiya, Y., Inoue, T. Test of full and partial tube dilation pictures in entangled blends of linear polyisoprenes. *Macromol.* (2004) 37, pp. 6619–6631
- [11] Watanabe, H., Ishida, S., Matsumiya, Y., Inoue, T. Viscoelastic and dielectric behavior of entangled blends of linear polyisoprenes having widely separated molecular weights: Test of tube dilution picture. *Macromol.* (2004) 37, pp. 1937–1951
- [12] McLeish, T.C.B. Tube theory of entangled polymer dynamics. *Adv. Phys.* (2002) 51, pp. 1379–1527
- [13] Read, D.J., Jagannathan, K., Sukumaran S.K., Auhl, D. A full-chain constitutive model for bidisperse blends of linear polymers. *J. Rheol.* (2012) 56 pp. 823–873
- [14] Ferry, J.D. *Viscoelastic Properties of Polymers* (1980) Wiley, New York
- [15] Colby, R.H., Rubinstein, M. 2-Parameter scaling for polymers in theta-solvents. *Macromol.* (1990) 23, pp. 2753–2757
- [16] Doi, M., Graessley, W., Helfand, E., Pearson, D.S. Dynamics of polymers in polydisperse melts. *Macromol.* (1987) 20, pp. 1900–1906
- [17] Park, S.J., Larson, R.G. Long-chain dynamics in binary blends of monodisperse linear polymers. *J. Rheol.* (2006) 50, pp. 21–39
- [18] van Ruymbeke, E., Shchetnikova, V., Matsumiya, Y., Watanabe, H. Dynamic Dilution Effect in Binary Blends of Linear Polymers with Well-Separated Molecular Weights. *Macromol.* (2014) 47, pp. 7653–7665

- [19] Wang, S., Wang, S.Q., Halasa, A., Hsu, W.-L., Relaxation Dynamics in Mixtures of Long and Short Chains: Tube Dilation and Impeded Curvilinear Diffusion. *Macromol.* (2003) 36, pp. 5355–5371
- [20] Auhl, D., Chambon, P., McLeish, T.C.B., Read, D.J. Elongational flow of blends of long and short polymers: Effective stretch relaxation time. *Phys. Rev. Lett.* (2009) 103, article no. 136001
- [21] Milner, S.T. Relating the shear-thinning curve to the molecular weight distribution in linear polymer melts. *J. Rheol.* (1996) 40, pp. 303–315
- [22] Ball, R.C., McLeish T.C.B. Dynamic dilution and the viscosity of star polymer melts. *Macromol.* (1989) 22, pp. 1911–1913
- [23] Marrucci, G. Relaxation by reptation and tube enlargement: A model for polydisperse polymers. *J. Polym. Sci., Polym. Phys. Ed.* (1985) 23, pp. 159–177
- [24] Lee, J.H., Fetters, L.J., Archer, L.A., Halasa, A.F. Tube dynamics in binary polymer blends. *Macromol.* (2005) 38, pp. 3917–3932
- [25] Rubinstein, M., Colby, R.H. Self-consistent theory of polydisperse entangled polymers—linear viscoelasticity of binary blends. *J. Chem. Phys.* (1988) 89, pp. 5291–5306
- [26] Likhtman, A.E., McLeish, T.C.B. Quantitative theory for linear dynamics of linear entangled polymers. *Macromol.* (2002) 35, pp. 6332–6343
- [27] Milner, S.T., McLeish, T.C.B. Reptation and contour-length fluctuations in melts of linear polymers. *Phys. Rev. Lett.* (1998) 81, pp. 725–728
- [28] Fetters, L.J., Lohse, D.J., Richter, D., Witten, T.A., Zirkel, A. Connection between polymer molecular weight, density, chain dimensions, and melt viscoelastic properties. *Macromol.* (1994) 27, pp. 4639–4647
- [29] Everaers, R., Sukumaran, S.K., Grest, G.S., Svaneborg, C., Sivasubramanian, A., Kremer, K. Rheology and microscopic topology of entangled polymeric liquids. *Science* (2004) 303, pp. 823–826
- [30] Masubuchi, Y., Ianniruberto, G., Greco, F., Marrucci, G. Entanglement molecular weight and frequency response of sliplink networks. *J. Chem. Phys.*, (2003) 119, pp. 6925–6930
- [31] Pütz, M., Kremer, K., Grest, G.S. What is the entanglement length in a polymer melt? *Europhys. Letts.* (2000) 49, pp. 735–741
- [32] Everaers, R. Topological versus rheological entanglement length in primitive-path analysis protocols, tube models, and slip-link models. *Phys. Rev. E* (2012) 86, article no. 022801
- [33] Pattamaprom, C., Larson, R.G. Predicting the linear viscoelastic properties of monodisperse and polydisperse polystyrenes and polyethylenes. *Rheol. Acta* (2001) 40, pp. 516–532
- [34] Pattamaprom, C., Larson, R.G., Siriwat, A. Determining polymer molecular weight distributions from their rheological properties using the dual constraint model. *Rheol. Acta* (2008) 47, pp. 689–700
- [35] Majesté, J.C., Montfort, J. P., Allal, A., Marin, G. Viscoelasticity of low molecular weight polymers and the transition to the entangled regime. *Rheol. Acta* (1998) 37, pp. 486–499

- [36] Raju, V.R., Rachapudy, H., Graessley, W.W. Properties of amorphous and crystallizable hydrocarbon polymers. IV. Melt rheology of linear and star-branched hydrogenated polybutadiene. *J. Polym. Sci., Polym. Phys. Ed.* (1979) 17, pp. 1223–1235
- [37] Arnett, R.L., Thomas, C.P. Zero-shear viscosity of some ethyl branched paraffinic model polymers. *J. Phys. Chem.* (1980) 84, pp. 649–652
- [38] Larson, R.G., Sridhar, T., Leal, L.G., McKinley, G.H., Likhtman, A.E., McLeish, T.C.B. Definitions of entanglement spacing and time Constants in the tube model. *J. Rheol.* (2003) 47, pp. 809–818
- [39] Shanbhag, S., Larson, R.G. The chain retraction potential in a fixed entanglement network. *Phys. Rev. Lett.* (2005) Art. No. 076001
- [40] Zhou, Q., Larson, R.G. Primitive path identification in molecular dynamics simulations of entangled polymer melts. *Macromol.* (2005) 38, pp. 5761–5765
- [41] Read, D.J., From reactor to rheology in industrial polymers. *J. Polym. Sci., Part B: Polym. Phys.* (2015) 53, pp. 123–141
- [42] Mead, D.W. Determination of molecular weight distributions of linear flexible polymers from linear viscoelastic material functions. *J. Rheol.* (1994) 38, pp. 1797–1827
- [43] Reisch, M.S. Plastics makers remold industry. *Chem. Eng. News*, May 26 (1997) pp. 14–16
- [44] Pearson, D.S., Fetter, L.J., Graessley, W.W., Ver Strate, G., von Meerwall, E. Viscosity and self-diffusion coefficient of hydrogenated polybutadiene. *Macromol.* (1994) 27, pp. 711–771
- [45] Tao, H., Lodge, T.P., von Meerwall, E.D. Diffusivity and viscosity of concentrated hydrogenated polybutadiene solutions. *Macromol.* (2000) 33, pp. 1747–1758
- [46] Gabriel, C., Münstedt, H. Influence of long-chain branches on shear creep and recovery behaviour of polyethylene melts. *XIIith Intern. Congr. Rheol.* (2000), pp. 1–231

8

Determination of Molecular Weight Distribution Using Rheology

■ 8.1 Introduction

In Chapter 2 it was pointed out that the primary tool for determination of molecular weight distribution (MWD) is gel permeation chromatography (GPC), also called size exclusion chromatography (SEC). But sometimes GPC is not an option, as some polymers of commercial importance dissolve either with difficulty or not at all in a solvent so that the chromatography column must be operated at high temperature or is not an option at all. In addition rheological properties are much more sensitive to high molecular weight fractions than GPC elution curves, and these fractions have an important effect on the melt processing behavior. Finally, the viscosity and storage and loss moduli are easier to measure than GPC elution curves. For these reasons it is sometimes useful to consider rheological information as source of molecular weight information.

■ 8.2 Viscosity Methods

Bersted and Slee [1] based their method on the idea that each molecule makes a contribution to the bulk viscosity equal to its zero-shear viscosity but that as the shear rate increases from zero, the maximum length of molecule that makes such a contribution decreases [2, 3]. A similar approach was that of Malkin and Teishev [4, 5] who made use of Eq. 5.6. The final result of their derivation is a relationship that involves the first and second derivatives of viscosity with respect to shear rate. To make use of it, it is necessary to know α , η_0 , and the high-shear-rate power law slope, i.e., to have viscosity data over a wide range of shear rates. And the data must have a high precision, since they are differentiated twice to determine the MWD. Most often complex viscosity $|\eta^*|$ versus frequency data are used in place of viscosity versus shear rate, since precision, accuracy, and range are all enhanced in this way. One can look at this as an application of the Cox-Merz rule or as an alternative

empirical procedure based on a different measurable property. This method was used by Shaw and Tuminello [6] and by Wood-Adams and Dealy [7]. Tuminello and Cudré-Mauroux [11] found it useful in the solution of industrial problems but noted that it is essential to use a sufficient number of data points. Shaw and Tuminello [6] found that 50 points are usually adequate, but increasing this number improves the precision of the resulting MWD. Wood-Adams and Dealy [7] proposed seven points per decade as a minimum. Liu et al. [12] made a study of the effect of point density and noise level on the ability of the technique to resolve a bimodal distribution. Both they and Wood-Adams and Dealy [7] point out that the most important portions of the viscosity curve are those where changes in shape occur, as reflected by the second derivative of viscosity. They recommend the use of a plot of the second derivative versus reduced frequency to evaluate the reliability of the MWD calculation and found that the region around the minimum is most important. If the measured points, as opposed to extrapolated points, include this minimum, then the peak in the MWD is well within the experimental window. Multiple peaks in the MWD should show up in the data as multiple minima in the second derivative of the viscosity. Figure 8.1 is an example of such a curve for a polyethylene studied by Wood-Adams and Dealy [7]. Noise levels up to 2% do not appear to cause serious degradation of the effectiveness of the method, but exceptional care and skill are required to obtain data of this quality. In response to problems arising in the differentiation of data, Liu et al. [13] proposed a variation of this method.

In comparison with the other methods discussed below, we note that viscosity methods require neither a value for the plateau modulus nor an assumption regarding a mathematical form for the molecular weight distribution. Another advantage is

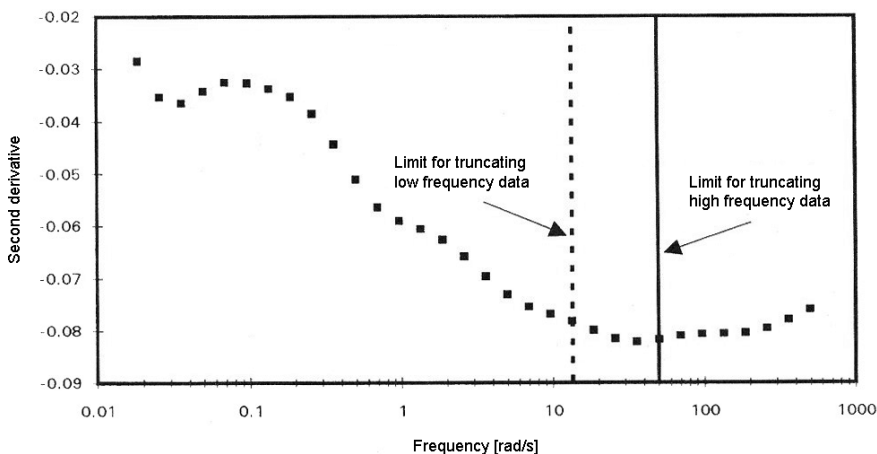


Figure 8.1 Second derivative of complex viscosity versus frequency for a commercial polyethylene. The region around the minimum corresponds to the peak in the MWD, and it is essential that experimental data cover this region.
From Wood-Adams and Dealy [7].

that by forcing the viscosity to approach a power law at high shear rate, the effects of high-frequency relaxation mechanisms that are not related to molecular weight are automatically suppressed.

■ 8.3 Empirical Correlations Based on the Elastic Modulus

Wu [15] noted the similarity of a plot of $[G'(\omega)/G_N^0]$ versus ω to that of the cumulative molecular weight distribution for the same polymer and developed a method for estimating the MWD. Tuminello [16] improved the accuracy of this method by using $[G'(\omega)/G_N^0]^{0.5}$ in place of the simple ratio of the moduli, and he assumed that a plot of $[1 - (G'/G_N^0)^{0.5}]$ versus $(1/\omega)^{1/3.4}$ is closely related to the cumulative molecular weight distribution. Tuminello et al. [20, 21] used this technique to determine the MWD of several fluoropolymers that could not be analyzed using GPC due to their insolubility. McGrory and Tuminello [22] tried using the relaxation modulus in place of the storage modulus to determine MWD and found that this worked well except in the case of materials with narrow molecular weight distributions.

Figure 8.2 compares molecular weight distributions calculated by the viscosity method and the modulus method with experimental data for a blend of LLDPE and HDPE. The viscosity method provides a better result in this case [7].

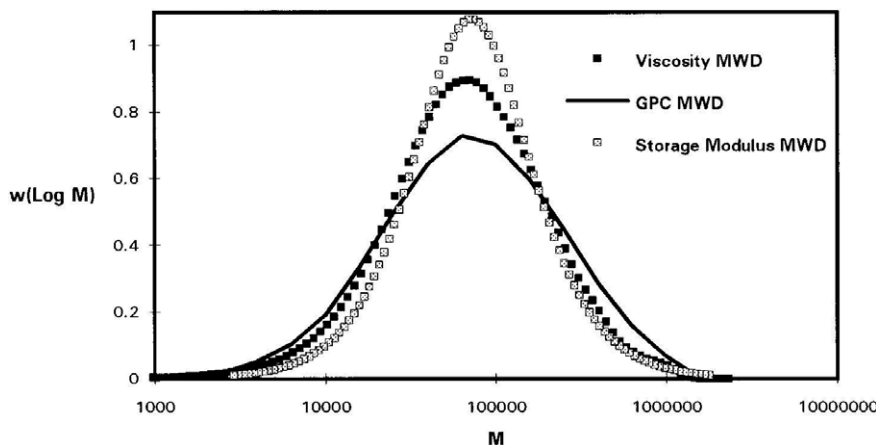


Figure 8.2 Comparison of molecular weight distributions calculated using the viscosity method and the modulus method for a blend of HDPE and LLDPE.
From Wood-Adams and Dealy [7].

■ 8.4 Methods Based on Double Reptation

In Chapter 6, the *double reptation* modification of the Doi-Edwards model for polydisperse systems was introduced in Chapter 6, and we repeat the basic idea here as Eq. 8.1.

$$\frac{G(t)}{G_N^0} = \left\{ \int_{M_e}^{\infty} w(M) [F(t, M)]^{1/2} dM \right\}^2 \quad (8.1)$$

This was introduced as a simple method to account for constraint release, and in its original form it does not account for contour length relaxation, so that it predicts that the zero-shear viscosity is proportional to M^3 rather than to $M^{3.4}$. As an empirical correction to the model, Mead [23] suggested simply making the relaxation time in the relaxation function proportional to $M^{3.4}$ instead of M^3 . Of course this does not constitute a full modeling of contour length fluctuations, but it does guarantee the correct dependence of η_0 on M as calculated from $F(t, M)$. For a single exponential relaxation function with the relaxation time equal to $K M^{3.4}$:

$$F(t, M) = \exp\left(\frac{-t}{K M^{3.4}}\right) \quad (8.2)$$

If Eq. 8.1 were a good model for polydisperse systems, and if the integral could be inverted, the molecular weight could be determined once $G(t)$ had been measured. But to accomplish this, several issues must be addressed.

1. The relaxation modulus must be fitted by an equation.
2. The relaxation function for monodisperse polymer $F(M, t)$ must be specified.
3. Since the model only applies to the plateau and the terminal relaxations, other mechanisms, particularly the high frequency (short-time) Rouse modes, will pollute the curve of $G(t)$ and interfere with the MWD determination, as these do not depend on the molecular weight.

However, the properties most often used to characterize linear viscoelastic behavior are the storage and loss moduli rather than the relaxation modulus. In Section 4.4 we described several techniques for inferring continuous or discrete relaxation spectra from such data. However it is important to note that in the transformation to a discrete spectrum, some information is always lost, and this can affect the reliability of subsequent calculations.

As for the form of the monodisperse relaxation function, several models have been proposed. First, since double reptation is a direct descendent of the Doi-Edwards reptation model, it seems appropriate to use the original D-E modulus, which is given by Eq. 8.3.

$$F(t, M) = \frac{8}{\pi^2} \sum_{n=1(\text{odd})}^{\infty} \frac{e^{-t n^2 / \tau_0(M)}}{n^2} \quad (8.3)$$

Noting that this series is dominated by the first term and that in a polydisperse system, the details of the spectrum will be smeared out to some degree, Tsenoglu [24] suggested the use of a single exponential (Eq. 8.4).

$$F(t, M) = e^{-t/\tau_0(M)} \quad (8.4)$$

And there is an even simpler possibility. Mead (see ref. [23], App. A) points out that Tuminello's method, which is based on the curve of $[G'(\omega)/G_N^0]^{0.5}$ versus frequency, can be considered to be a special case of double reptation in which the relaxation function is a step function (Eq. 8.5).

$$\begin{aligned} F(t, M) &= 1 & t < \tau_0 \\ F(t, M) &= 0 & t > \tau_0 \end{aligned} \quad (8.5)$$

A two-parameter empirical equation (the BSW function) was proposed by Baumgaertel et al. [25], and des Cloizeaux [26] developed a more complex form from a theory. The most popular choice, however, has turned out to be the single exponential, as it is simple but often adequate. Wasserman and Graessley [27] made a critical comparison of the four forms of $F(t, M)$ mentioned above.

The problem remains of inverting the integral, and it is the most difficult one. Equation 8.1 is of a form that arises often in applied physics and is called a Fredholm integral equation of the first kind. It is an example of an "ill-posed" problem, which means, in this case, that noise or incompleteness in data generally result in a system that has no unique solution for $w(M)$. The same type of problem arises in the inference of a relaxation spectrum from data for the storage and loss moduli as was explained in Section 4.4.

Mead [23] noted that to overcome the ill-posedness it is necessary to provide additional information and to use specialized numerical methods. In the case of the step function choice for $F(t, M)$ he was able to find an analytical solution to the inversion problem, while for other choices, he recommended the use of the CONTIN software, originally designed for use in treating light scattering data [28]. This makes use of a non-linear regularization parameter that is adjusted in accord with the noise level in the data.

In order to guide the problem to the correct solution, several normalization conditions are imposed, for example that the weight fractions sum to one.

$$\int_0^{\infty} w(M) dM = 1 \quad (8.6)$$

Comparing the MWD determined using this technique to GPC results for several systems, the agreement was quite good for higher molecular weight species, but the amount of low molecular weight material present was overestimated. In general, Mead found that the broader the MWD, the harder it is to resolve low molecular weight material using rheology. In general, a broad MWD will cause his method to indicate too low a value of M_w , because the low molecular weight species “dilute” the larger molecules, an effect that is not accounted for in the model. Also the model predicts that the MWD has a significant effect on η_0 , but as noted in Section 5.2.2 this is counter to most observations.

Wasserman [29] also developed a method for calculating MWD that is based on the double reptation model. However, whereas Mead [23] chose to use the integral form of the equation and employed various mathematical transforms to manipulate it, Wasserman used discrete variables and numerical techniques. Thus, he writes the double reptation relationship as:

$$G(t) = G_N^0 \left[\sum_{i=1}^c w_i \sqrt{F(t, M_i)} \right]^2 \quad (8.7)$$

He chose to use the BSW empirical relaxation function [25], which was implemented in the manner described by Wasserman and Graessley [27]. Each datum (G_k, t_k) thus yields an algebraic equation in which all the $F(M_i, t_k)$ coefficients are known, and the system of such equations can, in principle, be solved by linear regression for the variables (w_i). Wasserman [29] discusses the problems that arise in this procedure. He notes that since experimental data are available only over a limited range of frequencies, MWD can only be determined within certain limits, and he provides equations for estimating the molecular weight limits.

But the problem is still ill-posed, and Wasserman [29] used Tikhonov-Mallows regularization to obtain a solution. He used the same technique to infer a discrete spectrum $\{G_k, t_k\}$ from experimental data in the form of $\{G_k^*, \omega_k\}$. Wasserman [31] points out that the selection of the regularization parameter, λ_R , is subjective and depends on whether one wants a smooth solution, with a high degree of certainty in the calculated weight functions (large λ_R), or less certainty and a theoretically more accurate distribution (small λ_R). If λ_R is too high, the solution indicates too much high MW material, but if it is too small, artificial maxima and minima appear in the MWD. The problem of selecting the best value for λ_R was addressed by Honerkamp and Weese [30], who compared several methods and concluded by recommending the “self-consistent” method, in which the value is set in accord with the noise level in the data. Weese [31] developed a “Fast Tikhonov Regularization (FTIKREG)” algorithm based on this method. This tool has been used to determine MWD, for example by Léonardi et al. [32], who discuss the method in more detail.

Nobile and Cocchini [33] used the double reptation model to calculate the relaxation modulus, the zero-shear viscosity and the steady-state compliance for a given MWD. They compared three forms of the relaxation function for monodisperse systems: the step function, the single integral, and the BSW. In the BSW model, they set the parameter β equal to 0.5, which gives $J_s^0 G_N^0$ equal to 1.8. The molecular weight data were fitted to a Gex function to facilitate the calculations (see Section 2.2.4 for a description of distribution functions). For the step function form of $F(M, t)$, the relaxation function is given by Eq. 8.8.

$$G(t) = G_N^0 \Gamma^2 \left[\left(\frac{a+1}{b} \right), \left(\frac{t}{\tau} \right)^{b/\alpha} \right] / \Gamma^2 \left(\frac{a+1}{b} \right) \quad (8.8)$$

where: $\tau = K M_0^\alpha$, $K = \eta_0 / M^\alpha$, a , b , and c are parameters of the Gex distribution, and $\Gamma(x)$ is the gamma function.

Using the analytical result (Eq. 8.8), they found that for mildly polydisperse systems, the zero-shear viscosity depended only on the weight average molecular weight as has often been reported, but that for broader distributions, the zero-shear viscosity varied with the polydispersity. They reported an approximate form of this dependency, valid when $M_w/M_n > 1.5$, which is shown here as Eq. 8.9.

$$\eta_0 = k \left(\frac{M_z}{M_w} \right)^{0.8} M_w^{3.4} \quad (8.9)$$

Nobile and Cocchini [34] then used the step relaxation function in the double reptation integral, together with the Gex molecular weight distribution, to calculate the parameters of the latter for several polymers. In order to obtain $G(t)$ from dynamic data, they approximated the former by a series of linear segments. Comparing their results with GPC distributions they found that their predicted values of M_z/M_w were fairly accurate but that the values of M_w/M_n were not. It must be recalled here that in order to arrive at an analytical form for the relationship between $G(t)$ and MWD, a number of simplifying assumptions must be made. These include neglecting Rouse modes, tube length fluctuations, and “dynamic dilution.” In addition, the step relaxation function and the Gex molecular weight distribution were assumed. Cocchini and Nobile [35] later improved their method by using the relaxation function proposed by Thimm et al. [36] and accounting for the contribution of Rouse modes. Another method that makes use of the double reptation model and the assumption of a Gex MWD is that of Guzmán et al. [37]. They also account for the effect of unentangled chains. Their method avoids the use of a regularization technique to infer $G(t)$ from dynamic data, and their analysis provides an estimate of the reliability of the results.

■ 8.5 Generalization of Double Reptation

Anderssen and Mead [38] considered a generalized mixing rule that includes both the Doi-Edwards relaxation modulus and that of double reptation as special cases. The dual-constraint assumption was described in Section 6.4.3, and the basic concept is shown by Eq. 8.10.

$$G(t) = G_N^0 \left[\int_{\ln M_e}^{\infty} F^{1/\beta}(t, M) w(M) d(\ln M) \right]^{\beta} \quad (8.10)$$

Obviously $\beta = 1$ gives the Doi-Edwards function, and $\beta = 2$ gives double reptation. Anderssen and Mead reported that the scaling of rheological properties with respect to molecular weight averages, e.g., $\eta_0 \propto M_w^\alpha$, is not sensitive to the value of β .

Maier et al. [39] took β to be a material-dependent parameter and determined its value for several polymers by fitting data for binary blends of samples having different molecular weight distributions. They assumed a single-exponential form for $F(t, M)$ and found $\beta = 3.3$ for PMMA and $\beta = 3.8$ for polystyrene. The terminal relaxation time was assumed to be proportional to M_w^α , where $\alpha > 3$. As we have seen, this can be interpreted as a very crude way of accounting for tube length fluctuations.

Two procedures based on Eq. 8.10 have been proposed to infer the molecular weight distribution from the relaxation modulus. Maier et al. [39] used Tikhonov regularization to invert the integral, whereas Thimm et al. [36] used an analytical relation between the relaxation function, $H(t)$ and the molecular weight distribution.

Thimm et al. [40] later reported that their conclusion that the best value for β in Eq. 8.10 was in the range of 3 to 4 for the polymers studied was incorrect, because the rheological data analyzed to obtain these values included Rouse contributions. After they “corrected” the data to delete the portion of the spectrum function $h(\tau)$ due to Rouse modes, the optimal value for β was found to be close to two, the value for double reptation [41].

■ 8.6 Dealing with the Rouse Modes

A problem that arises with all methods for inferring the molecular weight distribution from rheological data is avoiding the contamination of information about the plateau and terminal relaxation by the effects of faster relaxation mechanisms. We recall that these faster relaxations due to Rouse modes reflect short-range motions that are not related to the size of the molecule.

There is no precise way to distinguish between the contributions of various relaxation mechanisms to the complex modulus, but various more or less empirical procedures have been used. Tuminello [42] simply omitted data for which $G' > 0.8 G_N^0$ before using Mead's [23] method. In his earlier modulus method [16], Tuminello fitted his data to an arbitrary function whose shape did not accommodate the type of behavior observed in the transition zone. Another empirical procedure for eliminating the effect of Rouse modes on the relaxation spectrum was that of Thimm et al. [40, 43].

■ 8.7 Models that Account for Additional Relaxation Processes

A more sophisticated way of dealing with relaxation mechanisms not related to MWD is to use a model that includes these. The first methods based on molecular mechanisms focused attention on reptation, as this is the one most affected by the length of the molecule. But except in the case of monodisperse polymers, there is no reliable way to separate the relaxation modes related to motions of the whole molecule from those related to motions of segments between entanglements in a precise way. Furthermore, there are other important aspects of the relaxation that were neglected in the early applications of the double reptation concept. In particular, longitudinal Rouse relaxation, which involves the entire chain, and tube length ("primitive path") fluctuations were omitted.

A rational approach to this problem is to model all aspects of the relaxation process, including the high-frequency (short-time) processes. This was the approach taken by Benallal et al. [44] in their model for a monodisperse polymer. They considered the relaxation modulus to be the sum of four contributions as follows:

$$G(t) = G_{\text{HF}}(t) + G_A(t) + G_B(t) + G_C(t) \quad (8.11)$$

where:

HF: High-frequency glassy (alpha) relaxation process

A: Fast Rouse modes involving only chain segments between entanglements

B: Longitudinal Rouse modes

C: Reptation with constraint release and tube length fluctuations

The HF relaxation is normally not a factor in the rheology of melts and solutions, but for completeness, the simple empirical relaxation function proposed by Davidson and Cole [45] was used.

$$G_{\text{HF}}(t) = G_\infty \left[1 - \text{erf} \left(\sqrt{t/\tau_{\text{HF}}} \right) \right] \quad (8.12)$$

The relaxation time, τ_{HF} , depends only on very localized features of the chain.

The A mode relaxation used by Benallal et al. is shown as Eq. 8.13.

$$G_A(t) = \frac{4}{5} G_N^0 \sum_{p=1}^{p=N_e} \exp\left(-\frac{t p^2}{\tau_A}\right) \quad (8.13)$$

In the above, τ_A is one-half the *equilibration time* defined in Chapter 5.

The B process is represented by the Viovy model [46], although the more recent model of Likhtman and McLeish [47] could also be used. The Viovy model is:

$$G_B(t) = \frac{4}{5} G_N^0 \sum_{p=1}^{\infty} \frac{1}{N} \exp\left(-\frac{t p^2}{\tau_B}\right) \quad (8.14)$$

where τ_B is the longest Rouse relaxation time, given by Eq. 6.3 in Chapter 6, except that Benallal, et al. incorrectly used the *Rouse reorientation time*, which is twice the *Rouse stress relaxation time*. The relaxations arising from the “A” and “B” processes are given, respectively, by the second and first terms within the brackets on the right side of Eq. 6.54, except that in Eq. 6.54, there is a pre-factor of unity for the term corresponding to the A process and a pre-factor of 1/5 for that corresponding to the B process, while the above expressions (incorrectly, we believe) have factors of 4/5 for both terms. A discussion of these terms, and their pre-factors can be found in Section 6.4.5

For the monodisperse system, the Doi-Edwards relaxation function, including contour length fluctuations, is used for $G_C(t)$. Benallal et al. add a final term $G_{\text{Rouse}}(t)$ to account for the presence of molecules that are too short to be entangled ($M < M_c = 2 M_e$)

$$G_{\text{Rouse}}(t) = G_N^0 M_e \int_{-\infty}^{\ln M_c} \left[\sum_{p=1}^{p=r} \exp\left(-\frac{t p^2}{\tau_{\text{Rouse}}(M)}\right) \right] \frac{P(\ln M)}{M} d \ln M \quad (8.15)$$

The upper limit on the summation is r , the degree of polymerization, which is M/M_0 . In a polydisperse system, this approach must be modified. Montfort et al. [48] account for the effects of polydispersity in two ways. First, they use the double reptation concept with the Doi-Edwards kernel function to account for constraint release, but they also let the relaxation times depend on the molecular weight distribution, a concept originally proposed by Graessley [49]. Specifically, they represent the terminal relaxation time in a polydisperse system as the harmonic average of the reptation time and a tube renewal time, τ_t , which depends on the molecular weight distribution.

$$\frac{1}{\tau[M, P(\ln M)]} = \frac{1}{\tau_C(M)} + \frac{1}{\tau_t[M, P(\ln M)]} \quad (8.16)$$

Where $\tau_c(M)$ is the reptation time of a linear, monodisperse polymer having a molecular weight M . Léonardi et al. [50] assembled a complete model of $G(t)$ for polydisperse systems by combining the ideas of Benallal et al. [44] and Montfort et al. [48]. The final model for $G(t)$ is similar to one published by Carrot and Guillet [51], except that the latter do not account for tube length fluctuations and use a different modeling of the Rouse processes.

Léonardi et al. [52] then inverted their $G(t)$ model to obtain the molecular weight distribution by assuming that the distribution is either bi-Gaussian for binary blends or Gex for commercial polymers. (These distributions are described in Chapter 2.) A numerical procedure was used to determine the best values for the parameters of the model selected. They concluded that the inclusion of tube length fluctuations and the effect described by Eq. 8.16 are essential for accurate determinations when there are significant amounts of low molecular weight material present.

The model of Mead [23] includes only the terminal zone, and here the key difference from the models of Carrot and Guillet [51] and Léonardi et al. [52] is that the latter authors include the dependence of the terminal relaxation time on the molecular weight distribution. Léonardi et al. [52] compare the predictions of their comprehensive model with those of Mead's model [23] and with experimental data. They conclude that Mead's approach is useful when the average molecular weight is high, i.e., when the $M_w \gg M_e$ and when the polydispersity index is small ($M_w/M_n < 4$). In other cases, they say that *tube renewal* (Eq. 8.16) must be included for accurate predictions.

Like Léonardi et al. [52] van Ruymbeke et al. [53] accounted for non-reptational mechanisms in their method, but they used different models for the relaxation processes. They inverted a model that they had previously proposed [54] for the calculation of rheological behavior from the molecular weight distribution. For the Rouse modes they used a modified version of an expression proposed by Pattamaprom et al. [55]. Their modified equation is shown below.

$$F_{\text{Rouse}}(t, M) = \frac{1}{N} \left\{ \sum_{i=N}^{\infty} \exp \left[\frac{-i^2 t}{\tau_R(M)} \right] + \frac{1}{3} \sum_{i=1}^N \exp \left[\frac{-i^2 t}{\tau_R(M)} \right] \right\} \quad (8.17)$$

where $N \equiv M/M_e$, and τ_R is inversely proportional to M . The first term is the basic Rouse term, while the second describes longitudinal motion in the tube.

For $F(t, M)$ they used the des Cloizeau form [26] but modified it to give better agreement with data for samples containing significant fractions of material with $M < 4 M_e$. They used the generalized form of double reptation (Eq. 8.10) with $\beta = 2.25$. The Gex molecular weight distribution was assumed for unimodal distributions and a “double Gex” distribution for bimodal samples. The latter is defined as follows:

$$w_{\text{DGex}}(M) \equiv p w_{\text{Gex}}^{(1)}(M) + (1-p) w_{\text{Gex}}^{(2)}(M) \quad (8.18)$$

where $0 \leq p \leq 1$. Since each of the Gex functions has three parameters, there are all together seven parameters that must be determined by fitting the model to experimental data. The authors tested their method using data for polystyrene, polycarbonate and HDPE. The comparisons were good except for HDPE, for which it was necessary to use the double Gex distribution, and the agreement was only fair. Pattamaprom and Larson [56] used the dual-constraint model described in Chapter 6, which includes additional relaxation processes, to arrive at a better prediction of molecular weight distribution than double reptation. Figure 8.3 compares the two results for a blend of two polystyrenes. The distribution was assumed to be bi-log-Gaussian.

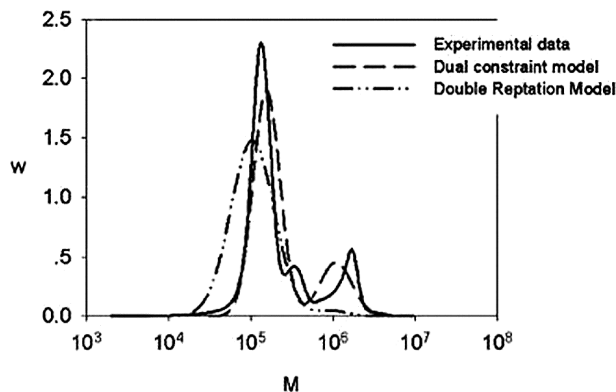


Figure 8.3 Comparison of molecular distribution calculations for a blend of two polystyrenes using dual-constraint and a double reptation models. From Pattamaprom and Larson [56].

■ 8.8 Determination of Polydispersity Indexes

Shroff and Mavridis [57] examined the simpler problem of inferring a single polydispersity parameter from various types of rheological data. They considered several parameters in addition to the polydispersity index (M_w/M_n), including the “polydispersity index of relaxation times” originally defined by Graessley [58].

■ 8.9 Summary

It is useful to group the various methods into three categories.

1. Models based on an empirical transformation from rheological material function to molecular weight distribution (viscosity models and modulus models)
2. Models based on double reptation that do not take into account other relaxation mechanisms. (Mead, Wasserman)
3. Models including additional relaxation mechanisms. (Rouse relaxation)

Each of these has its advantages and disadvantages, which are summarized below.

The models based on empirical transformations lead directly to a molecular weight distribution without the need to assume a form for it or to use a regularization technique. In addition, the viscosity technique does not require a value for the plateau modulus. On the other hand, such models do not give reliable results for systems containing significant amounts of low molecular weight material.

The models based on double reptation that do not take other relaxation mechanisms into account have the decided advantage of being readily subject to mathematical manipulation. For example, a powerful regularization technique can be used to invert the single integral of the model. Or a form for the molecular weight distribution can be assumed. Such models work well when the polydispersity is modest ($PI < 4$) and when there is very little material present for which M is near or below M_e .

The models that take into account all the relaxation processes are the most versatile in terms of the types of system that they can describe, but they are complex mathematically. Because direct inversion to obtain the MWD is not possible, it is necessary to assume a form for the molecular weight distribution due to the nonlinearity of the model with regard to MWD.

■ References

- [1] Bersted, B.H., Slee, J.D. A relationship between steady-state shear melt viscosity and molecular weight distribution in polystyrene. *J. Appl. Polym. Sci.* (1977) 21, pp. 2631–2644
- [2] Bersted, B.H. An empirical model relating the molecular weight distribution of high-density to the shear dependence of the steady shear viscosity. *J. Appl. Polym. Sci.* (1975) 19, pp. 2167–2177
- [3] Bersted, B.H. A model relating the elastic properties of high-density polyethylene melts to the molecular weight distribution. *J. Appl. Polym. Sci.* (1976) 20, pp. 2705–2714
- [4] Malkin, A.Ya., Teishev, A.Ye. Can the MWD of polymers be determined uniquely from the flow curve of its melt? *Polym. Sci. USSR* (1988) 29, pp. 2449–2455

- [5] Malkin, A.Ya., Teishev, A.Ye. Flow curve-molecular weight distribution: Is the solution of the inverse problem possible? *Polym. Eng. Sci.* (1991) 31, pp. 1590–1596
- [6] Shaw, M.T., Tuminello, W.H. A closer look at the MWD-viscosity transform. *Polym. Eng. Sci.* (1994) 34, pp. 159–165
- [7] Wood-Adams, P.M., Dealy, J.M. Use of rheological measurements to estimate molecular weight distribution of linear polyethylene. *J. Rheol.* (1996) 40, pp. 761–778
- [8] Berker, A., Driscoll, J.J. Comment on “Obtaining molecular-weight distribution from the viscosity data of linear polymer melts” *J. Rheol.* (1998) 42, pp. 1555–1562
- [9] Liu, Y., Shaw, M.T., Tuminello, W.H. Response to “Comment on ‘Obtaining molecular-weight distribution ...’ ” *J. Rheol.* (1998) 42, pp. 1563–1564
- [10] Malkin, A.Ya. Some inverse problems in rheology leading to integral equations. *Rheol. Acta* (1990) 29, pp. 512–518
- [11] Tuminello, W.H., Cudré-Mauroux, N. Determining molecular weight distributions from viscosity versus shear rate curves. *Polym. Eng. Sci.* (1991) 31, pp. 1496–1507
- [12] Liu, Y., Shaw, M.T., Tuminello, W.H. Optimized data collection for determination of the MWD from the viscosity data of polymer melts. *Polym. Eng. Sci.* (1996) 38, pp. 169–176
- [13] Liu, Y., Shaw, M.T., Tuminello W.H. Obtaining molecular-weight distribution information from the viscosity data of linear polymer melts. *J. Rheol.* (1998) 42, pp. 453–476
- [14] Nobile, M.R., Cocchini, F., Lawler, J.V. On the stability of molecular weight distributions as computed from the flow curves of polymer melts. *J. Rheol.* (1996) 40, pp. 363–382
- [15] Wu, S. Polymer molecular-weight distribution from dynamic melt viscoelasticity. *Polym. Eng. Sci.* (1985) 25, pp. 122–128
- [16] Tuminello, W.H. Molecular weight and molecular weight distribution from dynamic measurements of polymer melts. *Polym. Eng. Sci.* (1986) 26, pp. 1339–1347
- [17] Ferry, J.D. *Viscoelastic properties of polymers*. 3rd ed. (1980) John Wiley & Sons, New York, p. 503
- [18] de Gennes, P.G. Dynamics of entangled polymer solutions *Macromol.* (1976) 9, pp. 587–598
- [19] Colby, R.H., Rubinstein, M. 2-Parameter Scaling for Polymers in Theta-Solvents. *Macromol.* (1990) 23, pp. 2753–2757
- [20] Tuminello, W.H., Treat, T.A., English, A.D. Poly(tetrafluoroethylene): Molecular weight distributions and chain stiffness. *Macromol.* (1988) 21, p. 2606
- [21] Tuminello, W.H. Molecular weight distributions of tetrafluoroethylene-hexafluoropropylene copolymers. *Polym. Eng. Sci.* (1989) 29, pp. 645–653
- [22] McGrory W.J., Tuminello, W.H. Determining the molecular weight distribution from stress relaxation properties of a melt. *J. Rheol.* (1990) 34, pp. 867–890
- [23] Mead, D.W. Determination of the molecular weight distributions of linear flexible polymers from linear viscoelastic material functions. *J. Rheol.* (1994) 38, pp. 1797–1827

- [24] Tsenoglu, C. Molecular weight polydispersity effects on the viscoelasticity of entangled linear flexible polymers. *Macromol.* (1991) 24, pp. 1762–1767
- [25] Baumgaertel, M.A. Schausberger, A., Winter, H.H. Relaxation of polymers with linear flexible chains of uniform length. *Rheol. Acta* (1990) 28, pp. 400–408
- [26] des Cloizeaux, J. Relaxation and viscosity anomaly of melts made of entangled polymers: time dependent reptation. *Macromol.* (1990) 23, pp. 4678–4687
- [27] Wasserman, S.H., Graessley, W.W. Effects of polydispersity on linear viscoelasticity in entangled polymer melts. *J. Rheol.* (1992) 36, pp. 543–572
- [28] Provencher, S.W. CONTIN: A general purpose constrained regularization program for inverting noisy linear algebraic and integral equations. *Comput. Phys. Commun.* (1982) 27, pp. 229–242
- [29] Wasserman, S.H. Calculating the molecular weight distribution from linear viscoelastic response of polymer melts. *J. Rheol.* (1995) 39, pp. 601–625
- [30] Honerkamp, J., Weese, J. Tikhonov's regularization method for ill-posed problems. *Continuum Mech. Thermodyn.* (1990) 2, pp. 17–30
- [31] Weese, J. A reliable and fast method for the solution of Fredholm integral equations of the first kind based on Tikhonov regularization. *Comput. Phys. Commun.* (1992) 69, pp. 99–111
- [32] Léonardi, F., Allal, A., Marin, G. Determination of the molecular weight distribution of linear polymers by inversion of a blending law on complex viscosities. *Rheol. Acta* (1998) 37, pp. 199–213
- [33] Nobile, M.R., Cocchini, F. Predictions of linear viscoelastic properties for polydisperse entangled polymers. *Rheol. Acta* (2000) 39, pp. 152–162
- [34] Nobile, M.R., Cocchini, F. Evaluation of molecular weight distribution from dynamic moduli. *Rheol. Acta* (2001) 40, pp. 111–119
- [35] Cocchini, F., Nobile, M.R. Constrained inversion of rheological data to molecular weight distribution for polymer melts. *Rheol. Acta* (2003) 42, pp. 232–242
- [36] Thimm, W., Friedrich, Ch., Marth, M., Honerkamp, J. An analytical relation between relaxation time spectrum and molecular weight distribution. *J. Rheol.* (1999) 43, pp. 1663–1672
- [37] Guzmán, J.D., Schieber, J.D., Pollard, R. A regularization-free method for the calculation of molecular weight distributions from dynamic moduli data. *Rheol. Acta* (2005) 44, pp. 342–351
- [38] Anderssen, R.S., Mead, D.W. Theoretical derivation of molecular weight scaling for rheological parameters. *J. Non-Newtonian Fluid Mech.* (1998) 76, pp. 299–306
- [39] Maier, D., Eckstein, A. Friedrich, Ch., Honerkamp, J. Evaluation of models combining rheological data with the molecular weight distribution. *J. Rheol.* (1998) 42, pp. 1153–1173
- [40] Thimm, W., Friedrich, Ch., Marth, M. On the Rouse spectrum and the determination of the molecular weight distribution from rheological data. *J. Rheol.* (2000) 44, pp. 429–438
- [41] Thimm, W., Friedrich, Ch., Roths, T. Molecular weight distribution dependent kernels in generalized mixing rules. *J. Rheol.* (2000) 44, pp. 1353–1361

- [42] Tuminello, W.H. Determining molecular weight distribution from the rheological properties of polymer melt. *Rheol. Bull.* (Soc. of Rheology) (2000) 69 (2), pp. 8–15
- [43] Dealy, J.M. Comment on ‘The Rouse spectrum and the determination of the molecular weight distribution’ and Author’s response *J. Rheol.* (2001) 45, pp. 603–604
- [44] Benallal, A., Marin, G., Montfort, J.-P., Derail, C. Linear viscoelasticity revisited: the relaxation function of monodisperse polymer melts. *Macromol.* (1993) 26, pp. 7229–7236
- [45] Davidson, D.W., Cole, R.H. Dielectric relationship in glycerol, propylene glycol, and n-propanol. *J. Chem. Phys.* (1951) 19, pp. 1484–1951
- [46] Viovy, J.L. Tube relaxation: a quantitative molecular model for the viscoelastic plateau of entangled polymer media. *J. Polym. Sci., Polym. Phys. Ed.* (1985) 23, pp. 2423–2442
- [47] Likhtman, A.E., McLeish, T.C.B. Quantitative theory for linear dynamics of linear entangled polymers. *Macromol.* (2002) 35, pp. 6332–6343
- [48] Montfort, J.-P., Marin, G., Monge, Ph. Molecular weight distribution dependence of the viscoelastic properties of linear polymers: the coupling of reptation and tube-renewal effects. *Macromol.* (1986) 19, pp. 1979–1988
- [49] Graessley, W.W. Entangled linear, branched and network polymer systems—molecular theories. *Adv. Polym. Sci.* (1982) 47, pp. 67–117
- [50] Léonardi, F., Majesté, J.-C., Allal, A., Marin, G. Rheological models based on the double reptation mixing rule: the effects of a polydisperse environment. *J. Rheol.*, (2000) 44, pp. 675–692
- [51] Carrot, C., Guillet, J. From dynamic moduli to molecular weight distribution: a study of various polydisperse linear polymers. *J. Rheol.* (1997) 41, pp. 1203–1220
- [52] Léonardi, F., Allal, A., Marin, G. Molecular weight distribution from viscoelastic data: The importance of tube renewal and Rouse modes *J. Rheol.* (2001) 46, pp. 209–224
- [53] van Ruymbeke, E., Keunings, R., Bailly, C. Determination of the molecular weight distribution of entangled linear polymers from linear viscoelasticity data. *J. Non-Newtonian Fluid Mech.* (2002) 105, pp. 153–175
- [54] van Ruymbeke, E., Keunings, R., Stéphenne, V., Hagenaars A., Bailly, C. Evaluation of reptation models for predicting the linear viscoelastic properties of entangled polymers. *Macromol.* (2002) 35, pp. 2689–2699
- [55] Pattamaprom, C., Larson, R.G., van Dyke, T.J. Quantitative predictions of linear viscoelastic rheological properties of entangled polymers. *Rheol. Acta* (2000) 39, pp. 517–531
- [56] Pattamaprom, C., Larson, R.G., Sirivat, A. Determining polymer molecular weight distributions from rheological properties using the dual-constraint model. *Rheol. Acta* (2008) 47, pp. 689–700
- [57] Shroff, R., Mavridis, H. New measures of polydispersity from rheological data on polymer melts. *J. Appl. Polym. Sci.* (1995) 57, pp. 1605–1626
- [58] Graessley, W.W. The entanglement concept in polymer rheology. *Adv. Polym. Sci.* (1974) 16, p. 25

9

Tube Models for Branched Polymers

■ 9.1 Introduction

In Chapter 6, various versions of the “tube” model were presented, which can predict the linear viscoelasticity of monodisperse and polydisperse *linear* polymers, i.e., polymers without long-chain branching (LCB). To be quantitatively accurate, these models need to include several mechanisms of polymer motion, namely:

- Reptation
- Primitive path fluctuations
- Constraint release
- Rouse relaxation within the tube

As shown in Chapter 6, theories containing appropriate forms for all these mechanisms have often proved to be accurate in predicting the linear viscoelastic properties of *linear* polymers. (In Chapter 11 we will show that even the nonlinear properties of linear polymers can be predicted accurately in some cases.) In fact, theories for the linear viscoelasticity of polydisperse linear polymers are now well-enough developed that one can (at least in principle) invert them to infer the molecular weight distribution from linear viscoelastic data; see Chapter 8.

However, many of most useful commercial polymers contain long side branches. This is especially true of polyethylenes. Low-density polyethylenes (LDPEs) made by old-style high-pressure gas-phase methods have been known for decades to contain significant numbers of irregularly spaced long-chain branches. High-density polyethylenes (HDPEs) made using conventional Ziegler-Natta catalysts contain short-chain branches, and are frequently assumed to have no long-chain branches, that is, no branches that are long enough to become entangled with other polymers. However, even HDPEs sometimes have long-chain branches, especially if they are made by the chromium-catalyst method pioneered by Phillips Petroleum Company. “Linear” low-density polyethylenes (LLDPEs) are, as their name implies, low in density, yet supposedly nearly free of long-chain branches. The low density of these polymers is produced by the short branches present, which interfere with crystallization

and hence lower the solid density. More recently, commercial synthesis of polyethylenes and other polymers has been carried out by a new class of catalysts, namely the *metallocene* or *single-site* catalysts; see Section 3.9. These catalysts give better control not only of molecular weight distributions, but also of branching density and branch length. Since, as we will see, linear and nonlinear rheological properties can be strongly affected by LCB, rheological measurements are powerful both because they can tell us about how branching affects processing behavior and because they are an indicator of the presence and degree of LCB in a polymer. Janzen and Colby summarized the experience of many when they wrote the following [1]:

"The flow behavior ('rheology') of [polyethylenes] is enormously sensitive to LCB [long-chain branching] concentrations far too low to be detectable by spectroscopic (NMR, IR) or chromatographic techniques. Thus polyethylene manufacturers are often faced with 'processability' issues that depend directly upon polymer properties that are not explainable with spectroscopic or chromatographic characterization data. Rheological characterization becomes the method of last resort, but when the rheological data are in hand, we often still wonder what molecular structures gave rise to those results."

Thus, perhaps one of the most important potential practical uses of rheology in the entire field of polymer science is as a method to detect and quantify the presence of long-chain branching. This potential use of rheology is more important than its use in measuring molecular weight distributions, because there are analytical methods for the latter, but for the measurement of LCB there is simply no alternative method that can detect minute levels of LCB (i.e., less than about 0.1 branch per 1,000 carbons); see Section 5.11.2.

While rheology is exquisitely sensitive to LCB, the inverse process of inferring the degree and type of LCB from rheology is far from a solved problem. Nevertheless, rapid progress is being made, now that the problem of inferring MWD from rheology for linear polymers has been largely solved. Additional impetus to determine quantitatively the link between rheology and LCB comes from the rapid commercialization of metallocene polymers. The ability to exploit the versatility of metallocene catalysts to control the level and type of LCB will only be consummated when a quantitative understanding is achieved of the relationship between LCB and rheology.

In this chapter, we will explore the relationship between LCB and rheology in the linear viscoelastic regime. In Section 9.2, we will describe the general effect of long-chain branching on rheology. In Section 9.3, we will present molecular theories based on the four relaxation mechanisms listed above that can quantitatively predict the influence of branching on rheology for a simple, ideal, branching architecture, namely that of a star polymer. In Section 9.4, we will discuss recent progress that has enabled quantitative, or at least semi-quantitative, predictions to be made for more complex, but still ideal, branched polymer structures. Then, in Section 9.5, we

will discuss ideas and theories that enable predictions to be made for very general classes of branched polymers, containing broad distributions of molecular weights and molecular branching structures. Finally, in Section 9.6 we discuss recent insights into branched polymer rheology from slip-link models. Theories for the nonlinear viscoelastic properties of branched polymers will be presented in Chapter 11.

■ 9.2 General Effect of LCB on Rheology

The presence of long-chain branching makes it hard for a polymer molecule to move or relax its conformations. This is already true even for polymers with the simplest long-chain branched architecture, that of a star polymer, depicted in Fig. 9.1 (top). It is intuitively obvious that a star molecule will have difficulty moving by reptation. To reptate, it would have to drag one of the arms into the tube formed by the other two arms, as illustrated in Fig. 9.1 (bottom). Thus, long-chain branching might be expected to greatly slow the relaxation of an entangled molecule. This has proved to be true in many circumstances. However, there are cases in which the presence of long-chain branching can speed up relaxation, even if the branched and unbranched polymers are of the same chemical character and the same molecular weight.

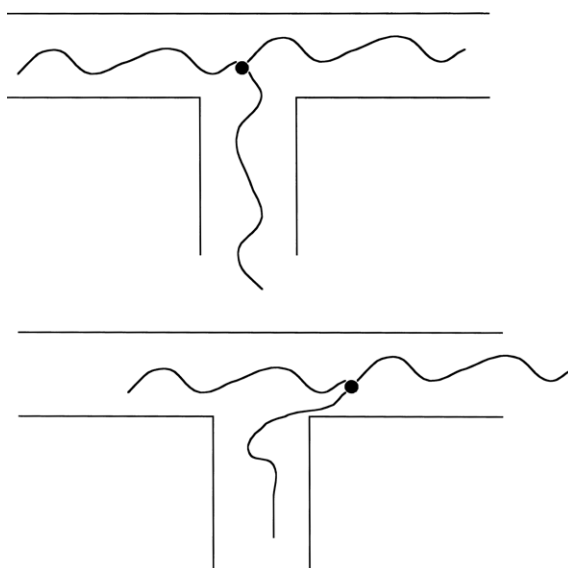


Figure 9.1 Sketch of a three-arm star polymer trying to reptate out of its three-armed tube. To escape by reptation, two arms will have to be dragged into the same arm of the tube, which is entropically disfavored.

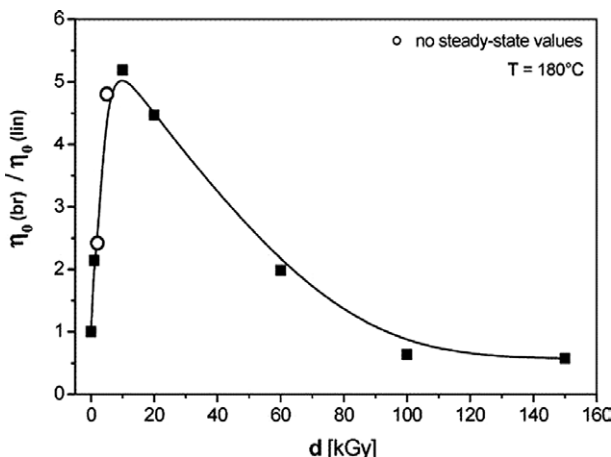


Figure 9.2 Ratio of zero-shear viscosity to the value for the precursor linear material for a series of polypropylenes subjected to electron beam radiation to introduce various levels of long-chain branching. Assuming little chain scission occurred, all these samples have the same or similar molecular weight as the linear precursor material. These data show the trend of increasing viscosity at low branching levels, reaching a peak and then decreasing and falling to values slightly below the viscosity of the initial linear material. From Auhl et al. [2].

An example is shown in the data of Auhl et al. [2], using an initially linear polypropylene that was irradiated by an electron beam to introduce long-chain branching (see Fig. 9.2). The radiation did not greatly change the average molecular weight of the samples, but increased radiation dose increased the degree of long-chain branching. As seen in Fig. 9.2, a small increase in branching resulted in a substantial increase of viscosity. However, at increased levels of branching the viscosity falls again, signifying a speeding up of the relaxation processes. Similar results were obtained previously by Mendelson et al. [3]. Any description of the rheology of long-chain-branched polymers must be able to explain this non-monotonic behavior of relaxation time and viscosity with increased branching. A simple, and rather superficial, reason that a branched polymer might relax faster than a linear molecule of the same molecular weight is that the linear molecule has a longer *span* than does the branched molecule. The span is the distance from the tip of one end of the molecule to the most distant other tip, where distance is measured along the molecular contour; see Fig. 9.3. Since complete relaxation of the linear molecule requires that its tube be completely vacated, the distance along its contour that the center of the molecule must move to escape the tube is greater in the case of the linear molecule than for the star. This shorter distance of motion required of the star is offset by the slower rate of motion of the star's branch point, so that, depending on the molecular details, complete relaxation of a star can be either faster, or slower, than that of an equal-mass linear.

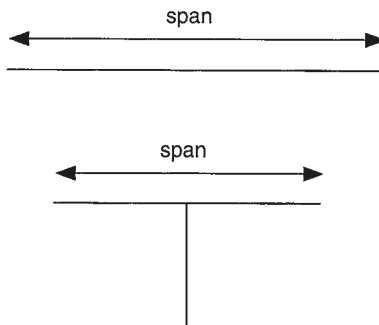


Figure 9.3 Definition of the molecular span, which is the maximum distance from one end of the molecule to the most distant other end, when the molecule is fully extended. For the same total molecular mass, a linear molecule has a longer span than a star.

Another way of looking at this is that molecular ends are highly mobile and accelerate relaxation of the polymer molecule, while branch points are sluggish and hence retard relaxation. Thus, depending on the balance of these effects, for the same total molecular weight, either a star—with three or more molecular ends and one branch point—or a linear molecule—with two molecular ends and no branch point—might have the longer relaxation time. It has been found that small star molecules, which are not well entangled, have shorter terminal relaxation times than linear polymers of the same weight-averaged molecular weight, while large, well-entangled stars have larger terminal times than their linear counterparts. Even if the star molecule has the longer terminal relaxation time, the early stages of relaxation of the star are likely to be faster than the early stages of relaxation of the linear polymer, since at early times the presence of the additional fast moving branch tip(s) is more important than is the presence of the sluggish branch point. Thus, the effect of LCB on relaxation rates is non-monotonic.

These complications exist already for the star, which is the simplest branched architecture. For more complicated structures, such as an H molecule, a pom-pom, or a comb (see Fig. 9.4) the relaxation behavior is even more complex. This is because a molecule with more than one branch point contains a “backbone” segment that lies between the branch points on either end of the molecule. This backbone segment has great difficulty relaxing, since it is “pinned down” on both ends by branch points. Hence, the backbone is expected to be especially slow to relax. In addition, backbone segments readily produce pronounced nonlinear effects in extensional flow, especially *strain hardening*, as will be discussed in Chapters 10 and 11. Finally, there are tree-like branched polymers, with branches on branches. Unlike stars, high-molecular-weight polymers with tree-like architecture generally have a reduced zero-shear viscosity relative to linear polymers of the same molecular weight [2, 4]. Generally, for high-molecular-weight polymers, light branching,

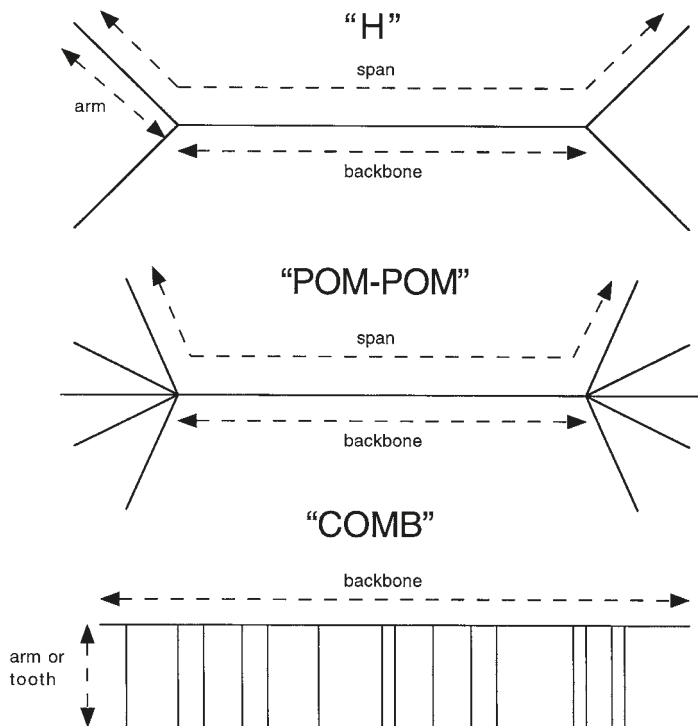


Figure 9.4 Illustration of branched polymers: H, pom-pom, and comb molecular architectures.

which produces star-like architectures, increases the molecule's longest relaxation time, while heavy branching, which produces tree-like architectures, decreases it [4]. Thus, for high-molecular-weight polymers, the zero-shear viscosity initially increases as long branches are added, but eventually decreases when branching density gets high enough [2, 4]. Rheological modeling indicates that the maximum zero-shear viscosity at a fixed overall molecular weight is achieved at roughly one long branch per molecule [5, 6].

Despite their complexity, enough progress has been made in describing and predicting the rheology of model branched polymers that it is now possible to predict the linear, or even nonlinear, viscoelasticity of some commercial branched polymers with reasonable success [5–10]. If such predictions are accurate enough, one might be able to use rheology, combined with other analytic methods, to infer important branching characteristics. Still, it remains highly unlikely that the exact branching structure of any resin could be inferred in this manner, in the absence of further information. However, if something extra is known about the type of branching present, then rheology may be able to provide a measure of the level of such branching. So, for example, if the type of reactions involved in the production of long-chain branches are known, then this gives clues as to the types of branching structures present,

information which can then be used in conjunction with rheology to determine the branching level. The success in predicting the linear viscoelastic properties of polydisperse linear polymers, documented in Chapters 6 and 7, encourages us to pursue similar predictions for polymers with long-chain branching.

It is certainly possible to use existing tube theories for linear polymers to infer at least the existence of long-chain branches in polymers. This can be done simply by comparing the measured linear viscoelastic response with that predicted under the assumption of no LCB. Given the broad reliability of the theories such as the double reptation or “dual constraint” model for polymers with no long-chain branching, a significant deviation between the predicted and measured linear viscoelasticity can then be attributed to LCB. This is illustrated in Fig. 9.5 (top), which shows a curve of the complex viscosity $\eta^*(\omega)$ (defined in Eq. 4.37) for a metallocene high-density polyethylene that is expected to be free of long-chain branching. Using the molecular weight distribution determined by gel permeation chromatography (or GPC—see Section 2.6.3), the prediction of one particular linear viscoelastic model, the “dual constraint” model mentioned in Section 6.4 for linear polymers, is shown to be in excellent agreement with the measured $\eta^*(\omega)$ curve. Reasonable agreement would also likely be achieved using the double reptation model. When long-chain branching is introduced by treatment of this melt with peroxide, the $\eta^*(\omega)$ curve is increased at low frequencies, and no longer follows the model. (Although the theoretical prediction in Fig. 9.5 (top) does not correct for the change in molecular weight distribution produced by the peroxide treatment, this change is believed to be too small, by itself, to account for the large change in low-frequency rheological properties.) Another example is given in Fig. 9.5 (bottom), which shows two $\eta^*(\omega)$ curves for polyethylenes with different, but relatively small, long-chain branching levels. Again, using measured polydispersity, the $\eta^*(\omega)$ curves predicted by the “dual constraint” theory for linear polyethylenes with these molecular weight distributions are shown in Fig. 9.5 (bottom). Yet another example of the profound effect of long-chain branching on the linear viscoelastic properties of polymer melts was given in Chapter 7 (Fig. 7.13(b)). These predictions, which take the molecules to be linear, disagree with the experimental data at low and moderate frequencies, again showing that the rheological data can be used to infer the presence of long-chain branching. However, without theories that explicitly consider the effect of long-chain branching on rheology, we can say nothing beyond affirming that the samples contain LCB. In what follows, we will describe some recently developed theories for predicting the linear viscoelasticity of long-chain-branched polymer melts. Theories for the non-linear viscoelasticity of branched polymers are covered in Sections 11.5 and 11.6.

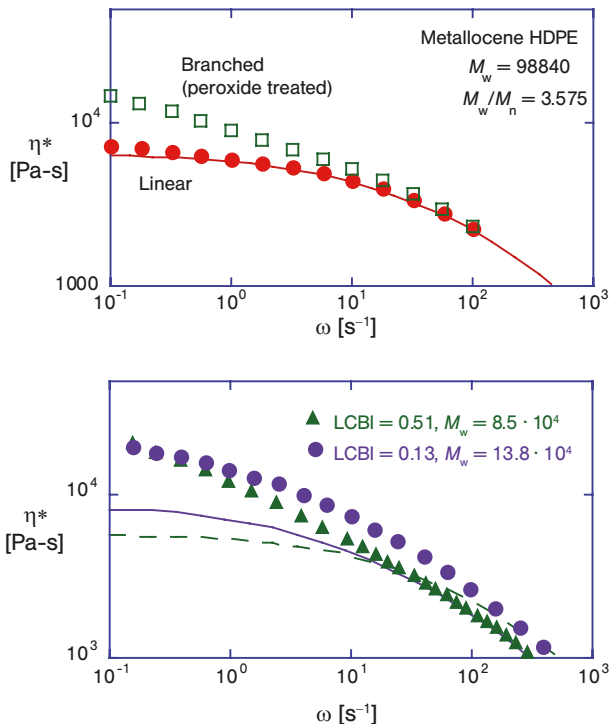


Figure 9.5 Dynamic viscosity $\eta^*(\omega)$ of polyethylenes at 190 °C (symbols) compared to predictions of the dual constraint model, with $G_N^0 = 2.6 \cdot 10^6$ Pa and $\tau_e = 7 \cdot 10^{-9}$ s. In (a), the circles are for metallocene-synthesized HDPE ($M_w = 9.88 \cdot 10^4$, $M_w/M_n = 3.6$), and the squares are for the same sample treated with peroxide to induce long-chain branching (data of Rohlfing and Janzen [11]). The effect of the peroxide on the molecular weight distribution was ignored in these calculations. In (b), the polymers are an LLDPE (data: circles, theory: solid line; $M_w = 13.8 \cdot 10^4$, $M_w/M_n = 4.2$, with LCBI = 0.13), and a metallocene-catalyzed polyethylene (data: triangles, theory: dashed line; $M_w = 8.5 \cdot 10^4$, $M_w/M_n = 2.4$, with LCBI = 0.51). Data of Shroff and Mavridis [12]; figure from Pattamaprom and Larson [13].

9.2.1 Qualitative Description of Relaxation Mechanisms in Long-Chain-Branched Polymers

Before embarking on a mathematical description of relaxation mechanisms in long-chain-branched polymers, we consider qualitatively the types of behavior that might be expected. The simplest possible type of branched polymer is a monodisperse star. In some respects, monodisperse stars are actually easier to consider than linears, because for stars one can neglect reptation. This leaves only the relaxation mechanisms of primitive path fluctuations, constraint release, and high-frequency Rouse modes.

At the shortest relaxation timescales, or equivalently the highest frequencies, Rouse relaxation within a tube (as discussed in Section 6.4.5 for linear polymers) provides the dominant relaxation mechanism. Since this relaxation mechanism is essentially *local*, relaxing short subsections of the chain, it is insensitive to the long-chain-branched structure or molecular weight of the chains. So, to good approximation, all entangled polymer melts of the same local chemistry and composition relax in an identical manner at short timescales, resulting in largely identical viscoelastic response at high frequencies. Differences between different LCB structures emerge in the response at longer timescales or lower frequencies.

We already discussed primitive path fluctuations in Section 6.4.2, as a mechanism for the fast relaxation of the tips of a linear polymer. For a linear polymer, primitive path fluctuations are cut off once reptation sets in. For a star polymer, however, reptation is quenched, and so primitive path fluctuations must be relied upon to relax the entire star arm, all the way to the branch point. At early times, we anticipate that these primitive path fluctuations proceed in a manner similar to linear polymers, as described in Section 6.4.2 and by Eq. 6.37. However, this equation is appropriate only for shallow fluctuations, relaxing a fraction of order $Z_a^{-1/2}$ of the star arm (where Z_a is the number of entanglements along the arm). Deeper fluctuations require substantial, and unlikely, rearrangements of the chain configuration so as to allow the chain end to travel a longer distance up the tube contour. So, deep fluctuations incur a substantial entropy (or free energy) penalty and must be described as an activated process, using mathematics as described below in Section 9.3.1. Relaxation of monodisperse star polymers thus occurs over a wide distribution of timescales, from fast relaxations of the arm tips to much slower relaxations for chain sections near the branch point, giving a broad “shoulder” in the loss modulus as a function of frequency (see below, Fig. 9.8). This contrasts with the nearly single-timescale relaxation associated with monodisperse linear polymer reptation.

Since relaxation of star polymers occurs over such a broad range of timescales, it is possible, and helpful, to invoke the concept of *dynamic dilution* discussed earlier in Section 7.4.2. The arm tips relax very much more quickly than the chain near the branch point. As a result, the entanglement constraints imposed by the arm tips appear and disappear very rapidly, compared to the timescale on which the arm centers relax. The resulting constraint release motion allows the chain near the arm centers to explore a gradually widening tube as relaxation proceeds. This is exactly the picture of dynamic dilution outlined in Section 7.4.2, and it affects the relaxation of stress in star polymers in both the ways described there:

- It provides a means of describing the stress relaxation associated with local chain rearrangements from constraint release events. As the tube “widens,” the entanglement constraints on the trapped chain are diluted and so the stress they carry is reduced.

- It provides a mechanism to accelerate the rate of stress relaxation due to chain motion along the tube. This effect is much stronger for branched polymers, such as stars, than it is for linear polymers. As described above, primitive path fluctuations are the only available relaxation mechanism for star polymers, and deep fluctuations are an activated process, incurring a substantial entropy penalty. However, fluctuations in a *wider* tube do not require such substantial or unusual chain rearrangements, and therefore incur a lower entropy penalty. So, deep fluctuations in a wider tube are more likely and can occur more often, and they provide a faster relaxation mechanism. For this reason, dynamic dilution in branched polymers gives rise to an *enormous* acceleration of stress relaxation, often by several orders of magnitude in relaxation time.

These principles of dynamic dilution were first applied to star polymers by Ball and McLeish [14], and we shall describe their results in Section 9.3.

More complicated branched polymers may be expected to relax via similar mechanisms, initially via primitive path fluctuations starting at the tips of arms and working their way in towards the center of the molecule as the fluctuations become deeper. At the same time, constraint release from entanglements with arm tips can be described using the picture of “dynamic dilution.” However, consideration of other branched structures reveals that further relaxation mechanisms must be active. As a particular example, consider the “comb” molecule shown in Fig. 9.4. The initial relaxation of these proceed as just described: the arms of the comb, and the tips of the backbone, can relax via primitive path fluctuations. However, most of the backbone consists of chain that is trapped *between* multiple branch points, and so cannot immediately relax via fluctuation modes. Relaxation of the backbone requires motion of the branch points, and for this the backbone must wait until the arms are relaxed. The complete relaxation of an arm permits it to explore a new path through the entanglement mesh, which then allows the branch point freedom to take a hop forward or backward along the path of the backbone. Over a longer timescale, many such hops of the branch points permit the backbone, eventually, to escape its tube in a process analogous to reptation, but with friction effectively concentrated at the branch points. Hence, the viscoelastic spectrum of comb polymers contains two major relaxation processes, corresponding to fluctuation of the arms at higher frequencies and reptation of the backbone at lower frequencies. For some well-defined comb molecules it is possible to observe these as two separate peaks in the loss modulus, as illustrated in Fig. 9.16.

So, relaxation of more complicated branched polymers can still be thought of as occurring *from the outside inwards* (this “hierarchical” picture of polymer relaxation was described by McLeish [15]). Relaxation begins at the arm tips and proceeds inwards, through a combination of primitive paths fluctuations, branch point hopping and, often, a terminal relaxation via a motion akin to reptation. At the same time, the wide

distribution of relaxations give rise to constraint release motion, which can usefully be described using the picture of dynamic dilution. This set of relaxation pathways can be easily visualized, and so it is often straightforward to predict, qualitatively, how the relaxation of a particular branched structure might be expected to proceed. To make predictions more quantitative, we will examine dynamic dilution, branch point hopping and reptation in idealized branched polymers in Sections 9.3 and 9.4. In Section 9.5 we discuss the generalization of these ideas towards computer algorithms, designed to predict the linear viscoelastic spectrum of general mixtures of branched polymers, which open up the possibility of quantitative prediction for industrial resins.

■ 9.3 Star Polymers

9.3.1 Deep Primitive Path Fluctuations

We now aim to furnish the qualitative description of branched polymer relaxation, just given in the preceding section, with a more detailed mathematical treatment. We return to the simplest branched polymer, a monodisperse star, for which we noted that relaxation occurs via primitive path fluctuations, described for linear polymers in Section 6.4.2. We will need to extend this treatment to include the deeper primitive path fluctuations required to relax a whole star arm. We first consider the relaxation of a star in a fixed entanglement network, i.e., ignoring the effects of constraint release, before discussing dynamic dilution in Section 9.3.2.

We noted in Eq. 6.37 that the relaxation time for a piece of chain a distance z (measured as number of entanglements) from the tip of the arm scales as the fourth power of z if the fluctuation is shallow enough that the fluctuating piece of chain not big enough to appreciably “feel” its connection to the molecule as a whole beyond the branch point. However, if the fluctuation is deeper than an entanglement spacing or so, the chain must maneuver around the entanglements in order to fluctuate, and this begins to incur an entropic penalty, as noted Doi and Kuzuu [16]. Thus Eq. 6.37 only accounts for the drag required to move portions of the chain near the tips. It does not account for the highly improbable configurations that are required if the chain is to wrinkle up enough to contract its tip all the way to the center of the tube. These deep fluctuations are much slower than can be accounted for by Eq. 6.37. The relaxation time of a deep fluctuation is given instead by Eq. 9.1 [14, 16, 17].

$$\tau_{\text{late}}(z) = \tau_{\text{pre}} \exp(U(z)) \quad (9.1)$$

where the prefactor τ_{pre} is a time constant that is roughly of order the Rouse reorientation time τ_r , the function $U(z)$ describes the free energy, in units of the thermal entropic barrier to deep fluctuations that predominate at late times, and z runs from zero at the tip of the arm to Z_a at the branch point, where $Z_a = M_a / M_e^G$ is the number of entanglements per star arm. This barrier is given approximately by [17, 18]

$$U(z) = \nu \frac{z^2}{Z_a} \quad (9.2)$$

where ν is a numerical constant found to be equal to $3/2$ for a straight, impenetrable tube [18]. Thus, deep fluctuations, where z approaches Z_a , become exponentially slower as the arm molecular weight and number of arm entanglements increases. At early times, the fluctuations continue to be described by $\tau_{\text{early}}(z)$, given by Eq. 6.37. Milner and McLeish [19] presented a *cross-over function*, which reduces to $\tau_{\text{early}}(z)$ at small z , near zero, and to $\tau_{\text{late}}(z)$ at z near Z_a , namely:

$$\tau_z(z) = \frac{\tau_{\text{early}}(z)}{\exp(-U(z)) + \frac{\tau_{\text{early}}(z)}{\tau_{\text{late}}(z)}} \quad (9.3)$$

Because of the exponential dependence of relaxation time on the potential, the relaxation of star polymers is extremely sensitive to the strength of the potential and therefore to the value of ν and of M_e^G , which sets the value of Z_a . The correct value of ν has been controversial; a discussion of this and of non-quadratic corrections to Eq. 9.2 can be found in McLeish [20]. Fine-scale simulations using lattice models and real-space pearl necklace models of entangled polymers provide some justification for the quadratic potential and for the value $\nu = 3/2$ [21, 22]. As mentioned in Sections 6.3 and 7.5, the relationship between M_e^G and G_N^0 is also open to revision [23]. One may add to these complications the observation that relaxation at a given value of z from early time fluctuations are not single exponential (but cover a range of timescales) [24]. Additionally, recent work [25] has noted that the prefactor τ_{pre} calculated by Milner and McLeish using a single-bead approximation [19] is not exact when compared to full simulations of a Rouse chain. So, whilst prediction of relaxation of branched polymers is a relatively mature field, with many successful theories, there remains scope for improvement in even the simplest case of star polymers. It is likely that adjustments of either M_e^G or ν have been used to obtain quantitative predictions of the rheology of star polymers, compensating for some of the above inaccuracies in the theory.

9.3.2 Dynamic Dilution

Once the “early time” relaxation governed by $\tau_{\text{early}}(z)$ is complete, further relaxation is governed entirely by $\tau_{\text{late}}(z)$, given by Eq. 9.1. Ball and McLeish [14] noted that Eq. 9.1 implies that the outer portions of the star arms relax much faster than the inner parts that are closest to the branch point. Thus, at a given time t after a small step strain, the arm contains an inner core that is completely unrelaxed, and an outer tip that is completely relaxed. The value of $z(t)$ separating this inner core from the outer tip is obtained from Eq. 9.1 by equating the relaxation time $\tau_{\text{late}}(z)$ with the time t . Thus, as t increases, the position z along the tube that separates the relaxed from the unrelaxed part of the arm moves in towards the branch point. The rate at which this position z moves inward can be obtained from Eq. 9.1 by replacing $\tau_{\text{late}}(z)$ with t , taking a logarithm, and differentiating, to obtain:

$$d(\ln t) = \frac{2\nu z}{Z_a} dz \quad (9.4)$$

The very much faster relaxation of the branch tips compared to the branch “cores” means that constraints imposed by the branch tips disappear and reappear very quickly compared to the longer times at which the inner parts of the arms relax. This means that the number of entanglement constraints effective in restricting the chain motion during relaxation of star arms diminishes with time. As noted above in Section 9.2, this corresponds exactly to the set of assumptions in *dynamic dilution* or *tube dilation* theories, which were discussed in connection with polydisperse linear polymers in Section 7.4.2.

Ball and McLeish [14] accounted for dynamic dilution using a clever argument. They noted that, at a given time t , the density of entanglements that are actually effective is reduced below the initial entanglement density Z_a by dynamic dilution. In fact, at time t , the density of remaining entanglements per chain is just $Z_a \phi_{p,\text{eff}}(t)$, where $\phi_{p,\text{eff}}(t)$ is the “effective” volume fraction of polymer that still contributes to the entanglement mesh at time t .

More generally, it has been suggested that the density of entanglements per chain should be given by $Z_a \phi_{p,\text{eff}}^\alpha(t)$ where the *dilution exponent* α can be slightly greater than unity, in particular, $\alpha = 4/3$ [26, 27]. This means that the entanglement molecular weight M_e^G is then proportional to $\phi_{p,\text{eff}}^{-\alpha}$, and so Eq. 6.22 then implies that the tube diameter a scales as $a \propto \phi_p^{-\alpha/2}$, that is, for $\alpha = 1$, the tube diameter is proportional to the inverse square root of the polymer concentration (see Eq. 7.9). For simplicity, we shall continue our argument here with the dilution exponent α taken to be unity. The final results are easily generalized to arbitrary α .

Since, as noted above, each arm consists of two parts, a completely relaxed outer part at tube-coordinate values less than $z(t)$, and an unrelaxed inner part at tube

coordinate values greater than $z(t)$, and all the arms are identical in length for a monodisperse star, Ball and McLeish made the approximation $\phi_{p,\text{eff}}(t) \approx 1 - z/Z_a$. This approximation is based on the observation that for long arms, the relaxation time of the part of the arm at coordinate z is so much longer than the relaxation time at coordinate values smaller than z that the latter parts of the chains act as mere solvent for the former. With Z_a replaced by $Z_a \phi_{p,\text{eff}}(t)$ (and, correspondingly, z replaced by $z \phi_{p,\text{eff}}(t)$ since this also counts the number of entanglements), Eq. 9.4 becomes

$$d(\ln t) = \frac{2\nu z \phi_{p,\text{eff}}}{Z_a} dz = \frac{2\nu z}{Z_a} \left(1 - \frac{z}{Z_a}\right) dz \quad (9.5)$$

Now, integrating this expression, and equating t with $\tau_{\text{late}}(z)$ using the prefactor τ_{pre} from Eq. 9.1 as the initial condition for the integration, we obtain

$$\tau_{\text{late}}(z) = \tau_{\text{pre}} \exp \left[\nu Z_a \left(\frac{z^2}{Z_a^2} - \frac{2z^3}{3Z_a^3} \right) \right] \quad (9.6)$$

The longest relaxation time for the star polymer is therefore

$$\tau_{\text{late}}(z = Z_a) = \tau_{\text{pre}} \exp \left[\frac{1}{3} \nu Z_a \right] \quad (9.7)$$

Comparing this result with Eq. 9.2, we find that dynamic dilution speeds up relaxation of a star arm by the exponential of an order unity prefactor times a large number Z_a . Thus, the degree of acceleration of the relaxation can be truly enormous, i.e., factors of millions or billions. Ball and McLeish point out that inclusion of the dynamic-dilution effect is essential if truly quantitative, or even qualitative, predictions of the relaxation of star polymers are to be obtained.

Equation 9.5 captures the “dynamic dilution hypothesis” as it is presently applied in the context of branched polymers, and it includes two separate ideas: (i) the effective decrease in entanglement with relaxation of the surrounding chains, and (ii) the ingenious *ansatz* of Ball and McLeish, of incrementing the relaxation time in a differential manner. This second idea corresponds to updating the free energy for retraction $U(z)$ in a differential form:

$$\frac{dU}{dz} = \frac{2\nu z \phi_{p,\text{eff}}}{Z_a} \quad (9.8)$$

The modification of the relaxation potential via Eq. 9.8 is not so obvious, and remains open to question. We note, for example, that any effects of constraint release on the prefactor τ_{pre} have been wholly ignored in the above derivation; this contrasts strongly with the more nuanced discussion of chain motion in bidisperse blends

of linear polymers in Sections 7.3 and 7.4 (see, also, McLeish [28]). Nevertheless, it is by no means an understatement to say that virtually all modeling of branched polymer relaxation and rheology since the work of Ball and McLeish [14] is based upon the dynamic dilution hypothesis as expressed in Eqs. 9.5 and 9.8, giving rise to a family of immensely successful theories. So, in what follows for the remainder of the chapter we shall follow this prevailing (but likely imperfect) wisdom, and assume that these equations correctly capture the effects of constraint release and dynamic dilution in branched polymer relaxation.

We noted in Section 7.4 that, in dynamic dilution theories, the loss of effective entanglements and corresponding tube dilution gives rise to a relaxation of stress from the remaining entangled chains, so that the relaxation modulus takes the form $G(t) = G_N^0 P(t) P_{CR}(t)$ (Eq. 7.10). The factor $P(t)$ represents the fraction of material constrained by the initial set of entanglements, and $P_{CR}(t)$ represents the release of those constraints through relaxation. Within the above star theory, it is thus appropriate to set $P(t) = P_{CR}(t) = \phi_{p,eff}(t)$ so that the change in modulus associated with relaxation of a small increment dz of the star arm can be written as

$$dG = G_N^0 d\phi_{p,eff}^2 = 2 G_N^0 \phi_{p,eff} d\phi_{p,eff} = -2 G_N^0 \left(1 - \frac{z}{Z_a}\right) \frac{dz}{Z_a}. \quad (9.9)$$

Ball and McLeish assumed this increment in modulus relaxes at timescale given by Eq. 9.6 (the relaxation time for each portion of the star arm), and so obtained an expression for the relaxation modulus $G(t)$ for stars:

$$G(t) = 2 G_N^0 \int_0^{Z_a} \exp\left[-\frac{t}{\tau_z(z)}\right] \left(1 - \frac{z}{Z_a}\right) \frac{dz}{Z_a}. \quad (9.10)$$

Further refinements of this basic theory for star polymers were made by Milner and McLeish [19], who took the dilution exponent to be $\alpha = 4/3$, rather than $\alpha = 1$. Following this, theories combining reptation, primitive path fluctuations, and constraint release by dynamic dilution were derived and applied successfully by Milner, McLeish, and coworkers to monodisperse linear polymers [29], monodisperse stars [19], bimodal star/star blends [30], and star/linear blends [31], as well as H-branched polymers [32], and combs [33]. The approach taken for all these cases is similar and follows the qualitative description given in Section 9.2.1. We shall describe some of the additional considerations required for relaxation of H-polymers, combs, and other structures with multiple branch points in Section 9.4. We refer to this collective set of theories for stars, linears, and mixtures thereof as the “Milner-McLeish theory.” The details of the Milner-McLeish theory are beyond the scope of this work, but the interested reader can learn more from the original articles as well as from McLeish and Milner [34], McLeish [20], Park and Larson [35], and Watanabe [27].

While the Milner-McLeish theory is successful for the cases described above, in comparisons with data, the adjustable constants of the model were often changed from one case to the next, the polymer studied was not always chemically the same for all cases considered, and there were inconsistencies in the choice of the entanglement molecular weight. (An explanation of the alternative definitions used in the literature for the entanglement spacing can be found in Larson et al. [36].) In what follows, we detail a study comparing the predictions of the Milner-McLeish theory to data for 1,4-polybutadiene linear, star, star/star, and star/linear blends, using in all comparisons the same values of the parameters: plateau modulus G_N^0 , entanglement spacing M_e , and equilibration time τ_e , except where τ_e was shifted to account for the slightly different temperatures used in some of the experiments (e.g., 29 °C vs. 25 °C). The details of these calculations can be found in Park and Larson [35].

9.3.3 Comparison of Milner-McLeish Theory to Linear Viscoelastic Data

9.3.3.1 Monodisperse Stars

Figure 9.6 compares the predictions of the Milner-McLeish theory with $\alpha = 1$ and $\alpha = 4/3$ compared to the zero-shear viscosities for linear and star 1,4-polybutadienes from several different sources. Figures 9.7 and 9.8 show similar comparisons to G' and G'' data for nearly monodisperse linear and star 1,4-polybutadienes.

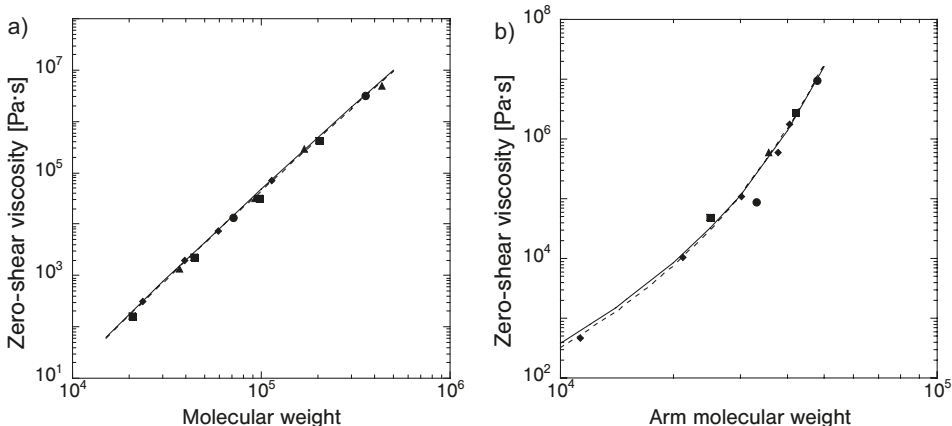


Figure 9.6 Zero-shear viscosity vs. molecular weight of nearly monodisperse 1,4-polybutadienes at $T = 25$ °C for (a) linear molecules: ▲: Struglinski and Graessley [39]; ◆: Roovers [40, 41]; ●: Rubinstein and Colby [42]; ■: Baumgaertel et al. [43]; and for (b) stars: ●: Raju et al. [44]; ◆: Roovers [40]; ▲: Roovers [41]; ■: Struglinski, et al. [45]. The solid line is the prediction of the Milner-McLeish theory using $\alpha = 1$ with $\tau_e = 9.5 \cdot 10^{-7}$ s, $M_e^G = 2200$ and the dashed line using $\alpha = 4/3$, $\tau_e = 3.7 \cdot 10^{-7}$, $M_e^G = 1650$. The value of $G_N^0 = 1.15 \cdot 10^6$ Pa is obtained from Fetters et al. [37]; see Table 7.1. From Park and Larson [35].

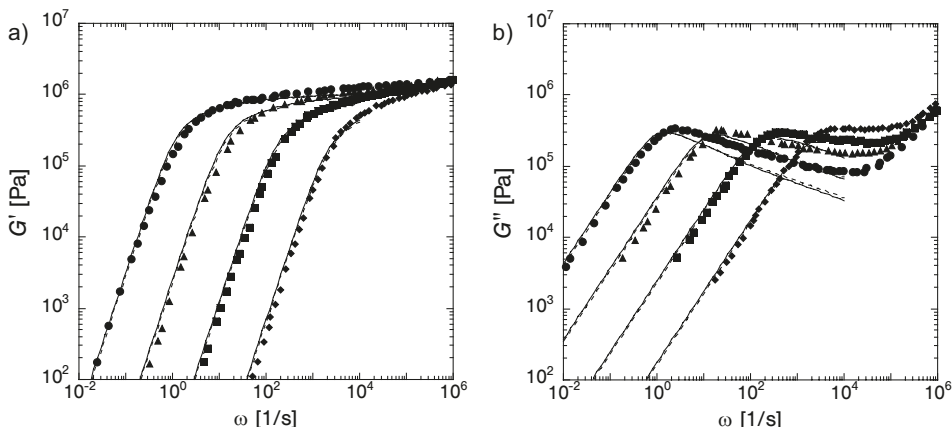


Figure 9.7 Comparison of predictions of theory of Milner and McLeish [21] with measurements of (a) G' and (b) G'' for nearly monodisperse linear 1,4-polybutadienes with molecular weights, from right to left, of 20,700, 44,100, 97,000, and 201,000 at $T = 28$ °C. The symbols are experimental data from Baumgaertel et al. [43]; the solid lines are the predictions using $\alpha = 1$ and the dashed lines using $\alpha = 4/3$. The parameter values are the same as in Fig. 9.6 for these respective values of α , except that τ_e has been time-temperature shifted from $T = 25$ °C to $T = 28$ °C (Table 7.1). From Park and Larson [35].

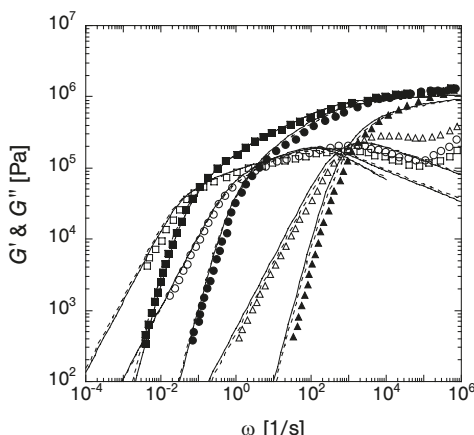


Figure 9.8 Comparison of predictions of theory of Milner and McLeish [19] with measurements of G' (filled symbols) and G'' (unfilled symbols) for nearly monodisperse 1,4-polybutadiene four-arm stars with total molecular weights, from right to left, of 45,200, 121,000, and 162,000 at $T = 27$ °C. (The arm molecular weight are one-quarter of the total molecular weight.) The symbols are experimental data for samples F, D, and B of Roovers [40]. The solid lines are model predictions using $\alpha = 1$, the dashed lines using $\alpha = 4/3$. The parameter values are the same as in Fig. 9.6, with a small shift in τ_e to account for the change in temperature (Table 7.1). From Park and Larson [35].

These very accurate predictions were made using the *same algorithm for both star and linear polymers*. Also, the same parameter values (G_N^0 and τ_e) were used in Figs. 9.6 through 9.8, except for a small shift in τ_e (see Table 7.1) to account for small differences in temperatures for the star polymers (28 °C) and linear ones (27 °C). Furthermore the value for the parameter M_e for $\alpha = 4/3$ was set to 1650, which is rather close to the value, 1543, given in Fetters et al. [37], and calculated from the plateau modulus using the formula $M_e^G = \frac{4}{5} \frac{\rho R T}{G_N^0}$. For $\alpha = 1$, a significantly higher value, $M_e^G = 2200$, is required to give the good fits to data shown in Figs. 9.6 through 9.8; this value disagrees with that inferred from the experimental plateau modulus, suggesting that $\alpha = 1$ might be a less appropriate value for the dilution exponent. However, we noted above that aspects of the theory of star polymer relaxation remain open to criticism and revision (see, e.g., refs. [25, 28]) and it might yet be that future corrections to the theory lead to reconsideration of the “best” value for the dilution exponent.

With M_e determined, only τ_e is left as an adjustable parameter. A best-fit value in the case $\alpha = 4/3$ leads to $\tau_e = 2.8 \cdot 10^{-7}$ s, while $\alpha = 1$ leads to $\tau_e = 5.5 \cdot 10^{-7}$ s, compared to the value $\tau_e = 5.6 \cdot 10^{-7}$ s inferred from Eq. 6.23, using the value of ζ given by Ferry et al. [38] and tabulated in Table 7.1. (The calculation yielding a predicted value of $\tau_e = 8.3 \cdot 10^{-7}$ s, given in Park and Larson [35], is in error.) The very encouraging agreement of the theory with linear viscoelastic data for both star and linear polymers using a unified set of parameter values that are physically reasonable suggests that the basic molecular physics of the tube model accurately describes molecular motion in both branched and unbranched polymers. Thus, we have reason to hope that the relaxation mechanisms we have already described in Chapter 6, might, with appropriate adaptation, allow quantitative prediction of rheological properties of even complex, commercial, branched polymers.

Comparing the data in Figs. 9.7 and 9.8, we note the *qualitative* difference between relaxation of linear and star polymers. This is readily apparent in the shape of the loss modulus as a function of frequency. For linear polymers, a clearly defined peak in the loss modulus corresponds to the reptation of the chains, a relaxation process dominated by a single relaxation time. In contrast, the star polymer melts do not exhibit such a peak; rather, a broad “shoulder” signifies a broad spectrum of relaxation times, from very fast relaxation of the arm tips, to much slower relaxation of chain sections near the branch point. The terminal relaxation time of the star polymer with molecular weight 162,000 (Fig. 9.8) is two orders of magnitude slower than the linear polymer with a higher molecular weight 201,000 (Fig. 9.7). This illustrates the exponentially slow relaxation associated with star polymer relaxation.

In the theory for star polymers, the linear viscoelasticity is independent of the number of arms, because the branch point is assumed to be motionless so that

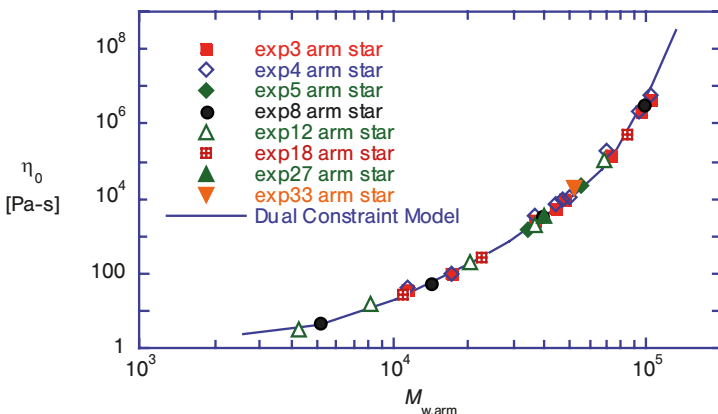


Figure 9.9 Zero-shear viscosity versus arm M_w of star polyisoprenes. Symbols are data of Fetters et al. [46] at a reference temperature of 60 °C. The line is the prediction of the dual constraint model with parameters $G_N^0 = 4.34 \cdot 10^6$ Pa from Pearson et al. [47], and $\tau_e = 1.2 \cdot 10^{-5}$ s gives the best fit to the data. From Pattamaprom and Larson [13].

each arm relaxes independently of the others. Figure 9.9 confirms this prediction, showing that the zero-shear viscosity versus arm molecular weight for a series of polyisoprene stars, containing from 3 to 33 arms per molecule, depends exponentially on the length of the arm, but is nearly independent of the number of arms per molecule. This remarkable finding shows that if the molecular weight of a star is raised 10-fold by increasing the length of each branch, the viscosity can rise by six orders of magnitude, while if it is increased to the same extent by increasing the number of arms, the viscosity rises hardly at all! *Thus, for branched polymers, the rheology is extremely sensitive to the arrangement and length of the branches, and not just to the overall molecular weight of the molecule.* The independence of viscoelasticity on the number of branches is consistent with the assumption that the branch point is immobile; an assumption made by the Milner-McLeish and other theories (such as the “dual constraint” theory). This assumption seems to be accurate when the number of arms equals four or more, but a modest (20%) decrease in the zero-shear viscosity has been observed when the number of arms is decreased from four to three [46, 48]; this indicates that for three arms, the branch point is slightly mobile. Models such as the Milner-McLeish or dual constraint model appear to give good agreement with experimental star data for 1,4-polybutadiene, 1,4-polyisoprene, and polystyrene [13]. However, the most common commercial polymer for which long-chain branching is found is polyethylene, and it is therefore of great interest to see if similarly good agreement is obtained for star polyethylenes as well. Direct synthesis of polyethylenes cannot be carried out anionically, however, so ideal, model branched (or for that matter linear) polyethylenes cannot be made directly.

Fortunately, as mentioned in Section 7.5, there is an indirect method of producing a nearly ideal, monodisperse, polyethylene via hydrogenation of 1,4-polybutadiene [49–51]. Plots of zero-shear viscosities for monodisperse linear and two- and three-arm star hydrogenated 1,4-polybutadiene are shown in Figs. 9.10 and 9.11. The lines are the predictions of the Milner-McLeish theory with the same set of parameters for both linear and star molecules. The agreement of the theory with the measurements is reasonably good; however, there is considerable scatter in the star data, especially when one considers the very large range of viscosities covered. Furthermore, Pattamaprom et al. [13] found that large adjustments of the parameter values were required to obtain good fits to some of the G' and G'' star data.

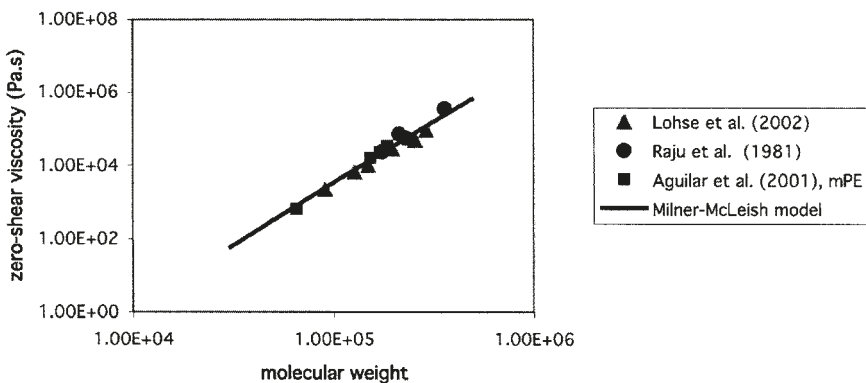


Figure 9.10 Zero-shear viscosity versus molecular weight for nearly monodisperse linear hydrogenated 1,4-polybutadienes at 190 °C. The lines show the fits of the data to the Milner-McLeish model with $M_e^G = 1167$, $G_N^0 = 2.0 \cdot 10^6$ Pa, $\tau_e = 6 \cdot 10^{-6}$ s. From Park [52].

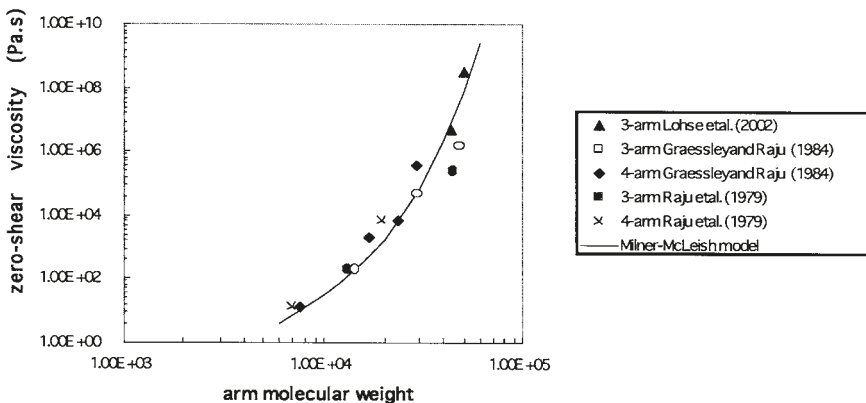


Figure 9.11 Zero-shear viscosities of 3-arm and 4-arm hydrogenated polybutadiene stars at 190 °C as functions of arm molecular weight. The line is the prediction of the Milner-McLeish theory with the same parameter values as in Fig. 9.10. From Park [52].

It has been observed that star hPBs have unusual thermorheological behavior. As discussed in Section 4.5, when attempting to superpose linear viscoelastic data for star hPBs by time-temperature shifting, one finds that the terminal region can be superposed, but that the shift factor is described by an Arrhenius form, $\tau_e = \tau_{e,0} \exp(E_a/R T)$, with an activation energy E_a that is *higher* than for linear hPB [49–51]. The failure of time-temperature superposition observed in star hPBs has also been observed in commercial long-chain-branched polyethylenes, such as LDPE [3, 53]. Thus, predicting the effect of LCB on the rheology of polyethylenes will require not only the development of general theories of relaxation in branched polymers, but also an accounting of the peculiar features of branched polyethylenes. Some progress on this latter problem has been made by considering the changes in relative proportions of trans and gauche bonds that occur during “deep” primitive path fluctuations [54, 55], but much more work is required.

9.3.3.2 Bidisperse Stars

In Chapter 6, good agreement was obtained between tube theories and experiments for linear polymers, not only monodisperse ones, but also for polydisperse polymers as well; see for example Fig. 6.21(b). Since, as we have just seen, tube theories can predict linear viscoelastic data for monodisperse *star* polymers, logically the next step is to compare the theory to data for bidisperse and polydisperse stars. Figure 9.12 shows the results of such a comparison of the dual constraint theory [56] to data for binary blends of polyisoprene stars of two different arm molecular weights, where, as usual, the parameter values were obtained from other data sets, in this case a set of monodisperse stars at the same temperature, 25 °C. The agreement between theory and experiment is excellent at low and moderate frequencies, except for the pure star of low arm molecular weight. This low-molecular-weight star has only around 5.4 entanglements per arm, which is probably too low for a tube model to be quantitatively accurate.

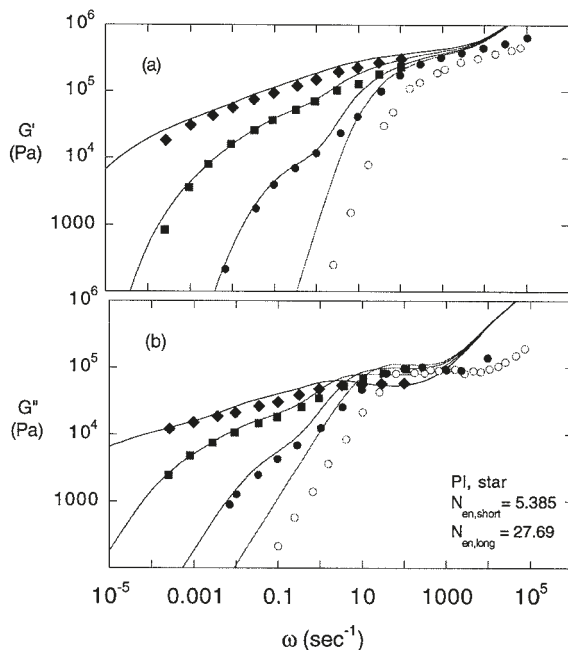


Figure 9.12 Predictions of the dual constraint model (lines) compared to experimental data (symbols) for (a) the storage modulus, and (b) the loss modulus, for bimodal star polyisoprenes ($M=2.8 \cdot 10^4/1.44 \cdot 10^5$) at the reference temperature 25 °C (from Blottière et al., [30]). The volume fraction of the high-molecular-weight component (χ_i) from right to left are 0.0, 0.2, 0.5, and 0.8, respectively. The model parameters were obtained from fits to data for linear polyisoprenes at the same temperature: $G_N^0 = 1.25 \cdot 10^6$ Pa and $\tau_e = 2 \cdot 10^{-4}$ s. From Pattamaprom et al. [56].

9.3.3.3 Star/Linear Blends

The case of star/linear blends is a challenging one. The description of constraint release used for pure star polymers is the very simple version of dynamic dilution outlined in Section 9.3.2. In contrast, for pure linear polymers, “double reptation,” supplemented by the more detailed descriptions of constraint release Rouse motion detailed in Section 7.3, seems to be the better description. However, Milner, McLeish, and coworkers [31] have developed a seemingly successful theory for the case of star/linear blends, which combines at least some of these concepts. In the Milner-McLeish theory, at early times after a step strain both the star branches and the ends of the linear chains relax by primitive path fluctuations combined with dynamic dilution, the latter causing the effective tube diameter to slowly increase with time. Then, at a time corresponding to the reptation time of the linear chains, a large number of the constraints on the unrelaxed star arms are suddenly released, because of the sudden reptation of the linear chains. The increase in the tube diameter would be very abrupt,

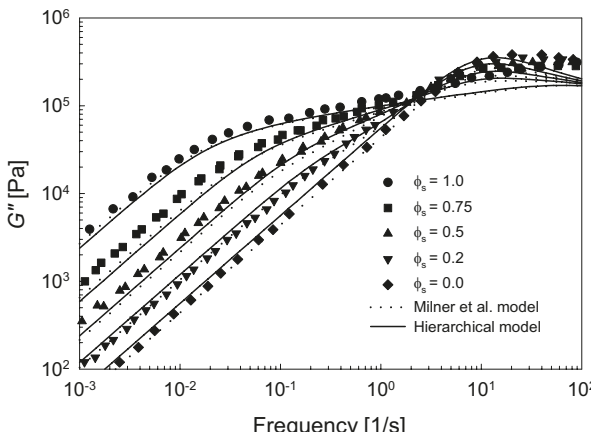


Figure 9.13 Comparison of theory with data for the loss moduli of binary blends of nearly monodisperse, linear 1,4-polybutadiene ($MW = 105,000$) and three-arm star 1,4-polybutadiene ($MW = 127,000$) at $T = 25^\circ\text{C}$. The star volume fractions, from right to left, are: 0, 0.2, 0.5, 0.75, and 1. The data are from Struglinski et al. [45]. The dashed lines are the Milner-McLeish model predictions, while the solid lines were obtained from the hierarchical model (see Section 9.5.1) both using $\alpha = 4/3$. The parameter values are the same as in Fig. 9.6. From Park and Larson [57].

if it were not slowed by inclusion of the constraint release-Rouse processes, which leads to a square-root-in-time decay in the relaxation modulus (in a manner exactly equivalent to the discussion in Sections 7.3 and 7.4, with $G(t) \propto P(t) P_{\text{CR}}(t)$ and $P_{\text{CR}}(t) \propto t^{-1/2}$). A more subtle consideration is the functional form of $\phi_{p,\text{eff}}(t)$ which should be applied in Eqs. 9.5 and 9.8 during the constraint release-Rouse processes. Milner, McLeish, and coworkers [31] argued that, whilst constraint release-Rouse motion is active, $\phi_{p,\text{eff}}(t)$ should be held *constant* at a value equal to the fraction of unrelaxed material just prior to the reptation of the linear chains. With this formulation, the Milner-McLeish theory yields very favorable predictions of polybutadiene data for star/linear blends; see Fig. 9.13, where the parameters have the same values as were used for pure linears and pure stars.

There is, however, a problem with the Milner-McLeish theory which becomes apparent at low volume fractions of stars. In this case, the window in time over which constraint release Rouse motion is active becomes very long, and the suggestion [31] that $\phi_{p,\text{eff}}(t)$ should be held constant during the entirety of this time window means that dynamic dilution is barely permitted to accelerate the relaxation of the stars at all. Then, the predicted terminal relaxation time of the stars becomes very long indeed, and the predictions are both unphysical and in contradiction to experiments. Similar problems are evident in predictions of mixtures of linear polymers with other branched species. There are several possible ways to fix this issue, at least qualitatively. Park and Larson [35] introduced a “disentanglement relaxation”

process for the star polymers, which enforced terminal relaxation of the star arms when constraint release Rouse motion relaxes sections of chain corresponding to a significant fraction of the arm molecular weight. An alternative is to relax the insistence that that $\phi_{p,\text{eff}}(t)$ should be held fixed during constraint release Rouse motion; one possibility which may be considered is to allow $\phi_{p,\text{eff}}(t) \approx P_{\text{CR}}(t) \propto t^{-1/2}$. This is another area where further work, both theoretical and experimental, is required. It is likely that insights from slip-link simulations, which we discuss below in Section 9.6, will be a key component of further theoretical development in this area.

The theories considered thus far have been limited to linear and star polymers, which have no more than a single branch point. Theories for polymers with more than one branch point require consideration of branch point motion, and of how this is coupled to the effects of constraint release and dynamic dilution.

■ 9.4 Multiply Branched Polymers

9.4.1 Dynamic Dilution for Polymers with Backbones

In this section, we will consider an idealized branched polymer which consists of a “backbone” with a number of side arms. Examples of such polymers are the “comb,” “H-polymer,” or “pom-pom” depicted in Fig. 9.4. As described qualitatively in Section 9.2.1, such polymers are expected to relax first via primitive path fluctuations of the arms, followed by a reptation-like process of the backbone mediated by hopping of the branch points.

We focus first on the relaxation of the arms, noting that we have to reconsider the role of “dynamic dilution” when both arms and backbones are present. For a melt of pure monodisperse stars, the Ball-McLeish theory for dynamic dilution predicts that the effective volume fraction of entangling chains $\phi_{p,\text{eff}}(t)$ decreases towards zero as the arms relax; see Section 9.3.2. However we now consider the case of arms attached to backbones, where the backbones remain unrelaxed at timescales shorter than or equal to the arm relaxation time. These unrelaxed backbones, then, do *not* become equivalent to solvent during the arm relaxation, but continue to serve as constraints on the arms until the arms have fully relaxed. Let us suppose that the volume fraction of melt contained in the arms is ϕ_a , while the volume fraction in the backbone is ϕ_b where $\phi_a + \phi_b = 1$. Now, we recall that in the absence of dynamic dilution, the “late-time” relaxation time for a star arm is given by Eqs. 9.1 and 9.2:

$$\tau_{\text{late}}(z) = \tau_{\text{pre}} \exp\left(\nu \frac{z^2}{Z_a}\right) \quad (9.11)$$

where z is the distance (counted as number of entanglements) along the star arm from the free end to the branch point. Since the relaxation time $\tau_{\text{late}}(z)$ is a very strong function of z , at any time t , the outer portion of the arm, which has relaxation time less than t , is almost entirely relaxed, while the inner portion with relaxation time greater than t is almost entirely unrelaxed. Thus, at any time t , there is a position z_c that separates the relaxed outer portion from the unrelaxed inner portion, where z_c is defined by the relationship

$$t = \tau_{\text{late}}(z_c) = \tau_{\text{pre}} \exp\left(\nu \frac{z_c^2}{Z_a}\right) \quad (9.12)$$

We now take the logarithm of Eq. 9.12, and differentiate, giving

$$d(\ln t) = \frac{2\nu z_c}{Z_a} dz_c \quad (9.13)$$

Eq. 9.12 can be recovered by integrating Eq. 9.13 with the initial condition $z = 0$ at $t = \tau_{\text{pre}}$.

To account for “dynamic dilution” in the case of pure monodisperse stars, Ball and McLeish [14] noted that the fraction of entanglements still unrelaxed at time t is given by $1 - z_c/Z_a$ (where we are here taking $\alpha = 1$). Multiplying the right side of Eq. 9.13 by this factor, and integrating, yields the formula for the longest arm relaxation time, $\tau_a = \tau_{\text{pre}} \exp(\nu Z_a/3)$, wherein a factor of one-third enters the exponential, due to dynamic dilution. However, when the backbones are present, these do not participate in dynamic dilution. Hence the fraction of unrelaxed melt at time t during arm relaxation for a comb molecule will be given by $1 - \phi_a z_c/Z_a$. Multiplying this factor on the right side of Eq. 9.13, and integrating, gives

$$\tau_{\text{late}}(z) = \tau_{\text{pre}} \exp\left[\nu Z_a \left(\frac{z^2}{Z_a^2} - \phi_a \frac{2z^3}{3Z_a^3}\right)\right] \quad (9.14)$$

where, for convenience, we have dropped the subscript c from z . The longest arm relaxation time, obtained at $z = Z_a$, is then

$$\tau_a = \tau_{\text{pre}} \exp\left[\nu Z_a (1 - 2\phi_a/3)\right] \quad (9.15)$$

The corresponding formula for $\alpha \neq 1$ is easily derived. Notice that when the volume fraction of arms ϕ_a approaches unity, Eq. 9.15 yields the expression for dynamically diluted star arms, while when ϕ_a approaches zero, Eq. 9.15 reverts to the arm relaxation time in the absence of dynamic dilution.

As discussed in Section 9.2.1, complete relaxation of the side arms opens up the possibility that the branch points can move, ultimately resulting in the relaxation of the main backbone of the branched chain.

9.4.2 Branch Point Motion

How can a branch point move? The repertoire of polymer movements that we have so far considered in detail: reptation, primitive path fluctuations, and Rouse motion within the tube; do not allow for branch point motion, at least not directly. Yet, clearly, the branch points do move, for if they did not, branched polymers, including stars, would have zero center-of-mass diffusivity. As noted qualitatively in Section 9.2.1, branch point motion is also critical to the relaxation of polymer backbones trapped between branch points.

For a three-arm star, one can imagine that the branch point might move whenever one of the three arms is in a state of complete retraction, so that the remaining two arms are free to slide, or reptate, carrying the now unentangled branch with them, at least a short distance before the arm becomes re-entangled again. If the star is trapped in a fixed matrix of entanglements (i.e., neglecting the effects of constraint release), the arm must become completely disentangled, at least briefly, and this requires that the tip of the arm retract by primitive path fluctuations all the way to the branch point. The time required for this is the longest relaxation time of the arm, as given (for example) in Eq. 9.15. However, after disentangling itself from the matrix, the arm will quickly become re-entangled again, and will have to wait to disentangle again before it will have another chance to migrate. Thus, in an entangled polymer, the diffusivity of a branch point is related to the relaxation time of the arms that are attached to it. In fact, one can view the diffusion of a branch point as a slow “hopping” process: the arm disentangles from the matrix by primitive path fluctuations in a time τ_a , the branch point then hops a short distance before the arm re-entangles, and the process repeats itself.

With this picture, the diffusion coefficient of the branch point is approximately $D_a = x^2/(2 \tau_a)$, where x is the “hopping distance” that the branch point moves every time the arm disentangles itself [58, 59]. An estimate of the “hopping distance” is the tube diameter a , since the tube diameter is the distance over which the branch point is localized by the entanglements with its neighbors. Hence, we can estimate that

$$D_a = (p a)^2 / (2 \tau_a) \quad (9.16)$$

where p is a prefactor expected to be of order unity or so. However, values for p used in the literature range by a surprisingly large amount, from $p^2 = 1$ [60] to $p^2 = 1/60$ [59]. Most likely, the reason for this wide range of values has to do with different assumptions which are made in the models used, both in their description of branch point motion and in other competing relaxation pathways. Two particular issues which have been contentious are the effects of varying number of arms at a branch point (the functionality), and the effects of constraint release or “dynamic dilution.”

Let us briefly consider the effect of functionality. What if the star has more than three arms? In a star with q arms, a naïve extension of the above picture would suggest that $q - 2$ of the arms must retract simultaneously to allow the chain to reptate along the path defined by the remaining two unretracted arms. This would imply that the time between hops would be of the order $\tau_h = \tau_{\text{pre}} [\exp(\nu Z_a)]^{q-2} = \tau_{\text{pre}} \exp[(q-2)\nu Z_a]$, which, for large q and large Z_a , would be an enormously long time. However, the center of mass diffusivity of a star polymer, measured by Shull et al. [61], is only modestly dependent on the number of arms in the star, decreasing by a factor of around 40 as the number of arms (q) in a polystyrene star increases from 3 to 12. This modest dependence of star diffusivity on the number of branches shows that the above naïve picture of branch point motion must be wrong.

An alternative view is that entanglements with the surrounding arms hold the branch point in a “trap” of size a , the entanglement spacing. The center of the trap is the centroid of the positions of the innermost entanglements of each of the arms; see Fig. 9.14. When a single arm retracts completely, and then re-entangles, the location of the innermost entanglement of that arm will shift to a new position, typically separated from its old position by a distance of order the tube diameter a . Since this is only one of the q arms attached to the branch point, the centroid will only shift a distance a/q , since the new location of the innermost entanglement of the one relaxed arm must be averaged in with the locations of the other $q - 1$ arms which have not moved their innermost entanglements. When another arm retracts completely, its innermost entanglement will also shift, and so forth for all the arms.

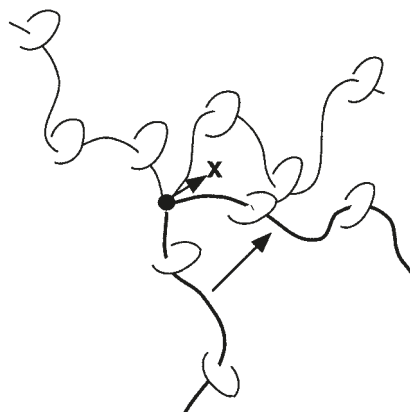


Figure 9.14 Sketch showing branch point motion. The entanglements of the arms with neighboring invisible chains are shown as loops that represent “slip-links” that confine each arm. The location of the branch point, on average, is taken to be the centroid of the three locations of the innermost entanglements of each of the three arms. When the arm shown as a bold line relaxes and re-entangles, the slip-links, including the innermost slip-link on this arm, move to a new position. Hence the centroid of the three innermost slip-links, and therefore the average location of the branch point, shifts to the position marked with an “X”, as shown.

Thus, after all the arms have retracted once, the branch point will have shifted q times, each time by a distance a/q in a random direction. In an arm relaxation time τ_a each of the q arms will have moved its innermost entanglement once, each time producing a random movement of the centroid by a distance a/q . Since the motion is diffusive, the net effect is that the centroid will move a distance $\sqrt{q(a/q)^2} = a/\sqrt{q}$ in the time τ_a . This implies that for a q -arm star, the “hopping distance” in Eq. 9.1 should be a/\sqrt{q} rather than a . In other words, the prefactor p^2 in Eq. 9.16 should be inversely proportional to the number of arms q per star. Since the measured diffusivity actually decreases with q somewhat more rapidly than as $1/q$, this argument is evidently still not quite right.

Whilst the effect of branch point functionality is interesting, and important for testing our understanding of branch point motion, it is of marginal importance in most commercial branched polymers where the functionality is usually low (typically either three or four polymer chains meet at a branch point). Of more critical importance is the effect of constraint release on branch point motion. For branched polymers, the effects of constraint release are usually pictured using the concept of dynamic dilution, introduced in Sections 7.4.2 and 9.3.2. Within this framework, the tube is envisaged to increase gradually in diameter as relaxation progresses. This begs the question: when an arm relaxes, and a branch point takes a hop, which tube diameter should be used in Eq. 9.16? Should we use the original tube diameter, or the dynamically diluted tube diameter, or something else? The answer to this question remains controversial, but an answer is required because the differences in tube diameter can easily give rise to factors of 10 or more difference in the predictions of branch point diffusivity.

In order to illustrate the conceptual difficulties involved, we consider the simple case of a three-functional branch point, attaching a short side arm to a much longer backbone. In this case, we wish to assess the diffusivity of the branch point along the one-dimensional path of the tube containing the backbone. We imagine that, each time the side arm relaxes, the branch point takes a “hop” along a tube of diameter a_{hop} along the backbone. In this case, the diffusivity along this tube (with diameter a_{hop}) should be given by Eq. 9.16, with the tube diameter set to $a = a_{\text{hop}}$. Different assumptions are made in the literature as to the size of a_{hop} . It is sometimes assumed that hopping takes place in the undiluted tube diameter (see e.g. [5]), or in the dynamically diluted tube diameter at the time of arm relaxation (see, e.g., refs. [6, 32]). Sometimes the assumption made at this point is not very explicit. To clarify the situation, in a recent work Bacova et al. [62] examined branch point motion in several molecular dynamics simulations of asymmetric stars, in some cases mixed with shorter entangled linear polymers. They concluded that the most consistent description of their data corresponds to the assumption that the branch point “hops” in the diluted tube diameter. This conclusion makes conceptual sense if it is imagined

that the branch point is able to change position through constraint release motion, in the same way that a linear chain section explores space through constraint release as described in Section 7.3. Then, even when the side arm is not in a retracted configuration, the branch point explores the dynamically dilating tube. At the point of arm retraction, the displacement obtained by the branch point, from prior constraint release motion, becomes permanently fixed when the arm pushes back out into the surrounding matrix of entanglements. So, whilst the arm might only be able to move a small distance during the short instant when the arm is actually in a retracted configuration, the net effect of the constraint release motion occurring in the time *between* two successive retracted configurations of the arm means the effective hop size per arm retraction event is given by the diluted tube. Nevertheless, this question of which tube diameter fixes the hop size remains contested in the literature.

Now, suppose there are multiple side arms on a backbone, which are of different lengths and so relax on different timescales. We assume the hopping occurs on a lengthscale set by the dynamically dilated tube at the timescale of the side arm relaxation: then, the lengthscale for hopping is potentially different for each arm. In order to be able to calculate the total effect of these side arms on the motion of the backbone, we need to consider the *effective* diffusion constant of all branch points along the *same* tube path, defined by some chosen diameter a . The situation is as depicted in Fig. 9.15 for the case where $a > a_{\text{hop}}$. Although the branch point “hops” along the tube with diameter a_{hop} , this motion corresponds to a different distance along the smoother path of the tube with diameter a . Hence, the effective diffusion constant along this tube is rescaled, and is found to be:

$$D_{\text{eff},a} = \frac{(p a_{\text{hop}})^2}{2 \tau_a} \left(\frac{a_{\text{hop}}}{a} \right)^2 = \frac{p^2 a_{\text{hop}}^4}{2 \tau_a a^2} \quad (9.17)$$

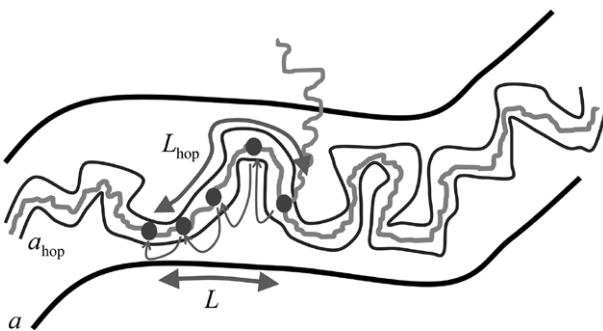


Figure 9.15 A branch point diffuses by taking a series of hops along a tube of diameter a_{hop} , so that the total distance traveled along that tube is L_{hop} . This diffusive motion can be projected onto an effective motion along a tube with larger diameter a . Since the projected distance traveled along that tube, L , is smaller than L_{hop} , the effective diffusion constant for projected motion along the larger tube is also smaller, and is as given by Eq. 9.17.

The extra factor of a_{hop}^2/a^2 comes from the fact that motion a long distance along a thin tube path is equivalent to motion a shorter distance along a fatter tube path, because the thin tube is more tortuous than the fatter tube.

9.4.3 Backbone Relaxation

Branch point diffusivity is relevant to viscoelastic relaxation because branch point motion is required to allow the backbone of an H, pom-pom, or comb molecule to relax. For a comb polymer, all branches are of low functionality, but there are many branch points. In this case, the polymer will not relax completely until the backbone has relaxed, and this requires all the branch points to hop many times over. Since all branch points hop randomly, if there are many branch points on the chain, and the backbone is entangled with other backbones, then on timescales long compared to the hopping time of the branch points the motion of the backbone will be like that of a linear polymer, except much slower. Since the backbone is confined to a tube created by entanglements with other backbones, the motion of the backbone must be by reptation. But the rate of reptative motion is greatly slowed by the need for each branch to relax before the piece of the backbone containing that branch can move. We would like, then, to compute the reptation time of the backbone τ_b from the diffusion coefficient $D_{\text{eff},a}$ of the branch points. We can do this by first rewriting Eq. 6.34 for the reptation time of a linear polymer as

$$\tau_d = \frac{\zeta N^3 b^4}{\pi^2 k T a^2} = \frac{\zeta N Z^2 a^4}{\pi^2 k T a^2} = \frac{\zeta_{\text{tot}} Z^2 a^2}{\pi^2 k T} \quad (9.18)$$

where we have used the fact that the end-to-end vector $\langle R^2 \rangle$ of the chain can be written as either $N b^2$ or $Z a^2$, and we have defined $\zeta_{\text{tot}} = N\zeta$ to be the total frictional drag on the linear polymer. In Eq. 9.18, ζ is the monomeric friction coefficient and N is the number of monomers in the chain, while Z is the number of entanglements. The final expression in Eq. 9.18 makes clear the role of frictional drag in determining the reptation time.

The final expression in Eq. 9.18 can also be used in dynamic dilution theories *provided all quantities are calculated self-consistently*. For example, reptation may be calculated in terms of an effective motion along a diluted tube, or along the undiluted tube. If a is taken to be the tube diameter of the diluted tube, then Z must be the effective number of entanglements along that tube, and (crucially) ζ_{tot} is the *effective* friction constant for motion along that tube (including appropriate rescaling of friction as given in Eq. 9.17). We illustrate this now for the case of comb polymers.

For a comb polymer with many arms, most of the drag comes not from the backbone itself, but from the entangled arms that slow the motion of the backbone, the

branch point for each arm having a diffusion coefficient $D_{\text{eff,a}}$. According to the Stokes-Einstein law, an object with a diffusion coefficient $D_{\text{eff,a}}$ has a drag coefficient $\zeta_{\text{eff,a}}$, given by

$$\zeta_{\text{eff,a}} = \frac{k T}{D_{\text{eff,a}}} \quad (9.19)$$

Thus, if there are q_{tot} identical arms attached to the backbone, each of which takes “hops” along a tube of diameter a_{hop} each time the side arm relaxes, then the drag that these arms add to that of the backbone for effective motion along tube of diameter a is

$$\zeta_{\text{tot}} = q_{\text{tot}} \zeta_{\text{eff,a}} = \frac{q_{\text{tot}} k T}{D_{\text{eff,a}}} = \frac{2 q_{\text{tot}} k T a^2 \tau_a}{\pi^2 p^2 a_{\text{hop}}^4} \quad (9.20)$$

where we have used Eq. 9.17 for $D_{\text{eff,a}}$. If the arms are the main source of drag slowing down the motion of the backbone, then Eq. 9.20 can be substituted into Eq. 9.18 to give the backbone relaxation time τ_b :

$$\tau_b = \frac{2 q_{\text{tot}} Z_b^2 a^4 \tau_a}{\pi^2 p^2 a_{\text{hop}}^4} = \frac{2 q_{\text{tot}} N_b^2 b^4 \tau_a}{\pi^2 p^2 a_{\text{hop}}^4} \quad (9.21)$$

In the above expression, a is the tube diameter along which we are considering the diffusion to take place, and Z_b is the effective number of entanglements in the backbone, self-consistently calculated for that tube diameter. But, since the end-to-end vector $\langle R^2 \rangle$ of the backbone can be written as either $N_b b^2$ or $Z_b a^2$ irrespective of which tube diameter a is chosen, the result Eq. 9.21 does not depend on this (actually arbitrary) choice of tube diameter, a , but only on the tube diameter along which branch point hops occur, a_{hop} . We can, for simplicity, use the undiluted values for tube diameter a and number of entanglements Z_b in Eq. 9.21. Then, if we assume that hopping occurs in the diluted tube at the timescale of arm relaxation, then $a_{\text{hop}} = a/\phi_b^{1/2}$ and so (making use of Eq. 9.15):

$$\tau_b = \frac{2 q_{\text{tot}} Z_b^2 \phi_b^2 \tau_a}{\pi^2 p^2} = \frac{2 q_{\text{tot}} Z_b^2 \phi_b^2}{\pi^2 p^2} \tau_{\text{pre}} \exp\left[\nu Z_a (1 - 2 \phi_a / 3)\right] \quad (9.22)$$

If, on the other hand, hopping is assumed to occur along the undiluted tube, i.e., $a_{\text{hop}} = a$, then the factor of ϕ_b^2 is absent from Eq. 9.22. There are several instances in the literature in which the size of hops is considered to be given by the undiluted tube diameter, whilst the *path* along which hops occur is given by the diluted tube: this perhaps inconsistent approach results in a single factor of ϕ_b , instead of ϕ_b^2 , in the numerator of Eq. 9.22.

Equation 9.22 could be used to estimate the longest relaxation time of a comb molecule with q_{tot} arms, each arm having a relaxation time τ_a . In practice, one should also consider a fluctuation correction which can be incorporated into the above,

since the ends of the backbone can relax partially by primitive path fluctuations in a manner equivalent to linear polymers; see Section 6.4.3. If the relaxation time of the comb backbone is significantly longer than the arm relaxation time, then the backbone relaxation can be observed as a low-frequency peak in the loss modulus, separate from the higher frequency shoulder from arm relaxation, as shown (for example) in Fig. 9.16.

The above calculation assumes all arms of the comb are identical and relax at the same time. In polydisperse polymers, different side arms relax at different times, and (depending on what assumptions are made) take hops in tubes of different diameter. In such cases, we must sum the friction from all arms in a self-consistent manner. It then becomes crucial to rescale the motion of all branch points onto an effective motion along the same tube diameter, in the manner of Eq. 9.17.

For especially short side arms, it may also be the case that the friction from branch point hopping is comparable to the monomeric friction of the backbone itself, in which case the monomer friction must also be self-consistently added to ζ_{tot} in Eq. 9.18. Again, in such cases it is important to consider the optimal path for motion of the backbone chain. As noted in Section 7.3, motion of the chain along the diluted tube requires multiple constraint release events of the thin tube, which is usually a slow process. It is most likely that the fastest path for chain motion is by chain sliding along the thin tube. So, even in cases where the branch points “hop” along the diluted tube, it may be that the chain between branch points moves most efficiently via motion along the thin tube.

These considerations serve to reiterate the words of caution given in Section 7.4 for dynamic dilution theories. In the branched polymer literature, it is often asserted that the “comb backbone relaxes by reptation along the diluted tube.” This is usually written to mean that (i) the diluted tube gives the effective relaxation modulus at the timescale of backbone relaxation, and (ii) we should picture the chain as diffusing along the diluted tube. The first of these is almost certainly true, but the second requires more care. A more common situation is that different length side arms relax at different times, taking hops along different diameter tube paths. The easiest path for motion of the chain sections between branch points is usually along the thin tube. So, motion actually takes place along a multiplicity of different tube diameters. Despite this complexity, in the situation where all side arms relax at the same time, and where branch points dominate the friction, then the simple dynamic dilution “cartoon” of motion along the diluted tube is applicable.

More generally, for polydisperse polymers, and certainly for industrial polymers, it would be impossible to perform the necessary calculations for chain relaxation analytically. Fortunately, the last decade has seen the development and improvement of algorithms which can perform these calculations numerically and automatically. We now describe several of these algorithms.

■ 9.5 Tube Model Algorithms for Polydisperse Branched Polymers

We would like to have a general theory for the linear viscoelasticity of *commercial* long-chain-branched polymers. Such polymers are irregularly branched, and polydisperse in overall molecular weight distribution as well as in their molecular weight and location of the branches. Equally, we have begun to appreciate that even “model” branched polymers are less regular than we would like. Always the reactions used to make H-shaped polymers, combs, and Cayley trees are imperfect, resulting in unwanted byproducts with different structures. The arms and backbones of these polymers are not fully monodisperse. Placement of side arms in a comb polymer is usually a random process, resulting in distributions of arm number and placement. In the context of the extreme irregularity of industrial polymers or the more moderate irregularity of “model” polymers, quantitative application of the principles of branched polymer relaxation, outlined above in Sections 9.2 to 9.4, is difficult to achieve using simple pen-and-paper calculations. Fortunately, the last decade and a half has seen the development of several promising attempts to codify the above relaxation mechanisms into computational algorithms which, in principle, promise to predict the linear viscoelasticity of arbitrary mixtures of polydisperse branched and linear polymers. These models hold the possibility of designing polymer branching structures to produce the desired linear viscoelastic response. They could also potentially be used to infer, from linear viscoelastic data, information about the type of branching present in the melt [5, 63, 64]. This latter use of linear viscoelastic data is referred to as *analytical rheology*. We shall review the available models in this section.

Nevertheless, we note from the outset that all of these models are based, in essence, on the dynamic dilution hypothesis as expressed mathematically by Ball, McLeish, and Milner [14, 19], shown in its fundamental form in Eq. 9.5; hence they are subject to the same criticisms as may be leveled at the Ball-McLeish theory discussed above. Likewise, whilst each model seeks to codify all of the above relaxation mechanisms for branched polymers, each makes different (but self-consistent) assumptions about these physical processes and how they might be expressed mathematically. As a result, whilst all of them can be successfully used to describe experimental data, they usually do so using different parameters. It is to be hoped that this, somewhat unsatisfactory, situation may be resolved as our understanding of branched polymer relaxation continues to improve.

9.5.1 “Hierarchical” and “BoB” Dynamic Dilution Models

The first attempt to specify a computational algorithm for relaxation of arbitrary branched polymers was made by Larson [5]. Subsequent developments made by the same group [7, 8, 57, 65] produced a series of algorithms collectively known as the “Hierarchical” model. In a parallel development, Das et al. [6] also modified the Larson algorithm, producing the so-called “BoB” (Branch-on-Branch) algorithm. Whilst there are differences between the specific implementations by Larson et al. and by Das et al., they are founded on the same principles, and may be considered together. Both algorithms are also freely available to download [66, 67].

The basis of Larson’s algorithm is the recognition that the “dynamic dilution” equations such as Eq. 9.5 and Eq. 9.13, for branched polymer arm relaxation, are cast in a differential form. From Eq. 9.5, the increment in logarithmic time for relaxation of an increment dz of a branched polymer arm (measured in units of number of initial entanglements) is given as:

$$d(\ln t) = \frac{2\nu z \phi_{p,\text{eff}}}{Z_a} dz \quad (9.23)$$

where Z_a is the number of entanglements along the relaxing arm, and $\phi_{p,\text{eff}}$ is the “effective” volume fraction of polymer that still contributes to the entanglement mesh at the current time t , which must be self-consistently calculated from the polymer chains which are relaxing. This formula can straightforwardly be rearranged to obtain the amount dz of arm relaxation in an increment of logarithmic time:

$$dz = \frac{Z_a}{2\nu z \phi_{p,\text{eff}}} d(\ln t) \quad (9.24)$$

This is the basis of the iterative scheme proposed by Larson [5]. The scheme operates by storing a representative set of polymer architectures in computer memory. It takes increments in logarithmic time, and keeps track of which portions of the polymers are relaxed after each timestep. As described qualitatively in Section 9.2.1, the branched polymers relax from the outside segments first. For each time increment, the relaxed portion of every free polymer arm is updated according to Eq. 9.24. The volume fraction $\phi_{p,\text{eff}}$ is calculated self-consistently from the relaxing polymers, and is usually set to be equal to the total unrelaxed fraction $P(t)$ (other than in the constraint release Rouse regime, which we mention below). Hence, $\phi_{p,\text{eff}}$ is updated before taking the next step in logarithmic time. In this way, the relaxation time of all outer sections of the polymer chains can, in principle, be obtained. With the inclusion of branch point hopping, inner sections can be allowed to relax also. Thus the linear relaxation modulus as a function of time can in principle be predicted.

In order to implement such a scheme for complex polymer architectures, and to produce quantitative predictions, a number of additional physical processes, as outlined above for model polymers, need to be included:

- (i) Early time relaxation due to sub-tube diameter motion of the chains, and local Rouse motion of chains along tube contour, can be included in the same manner as implemented by Likhtman and McLeish [24] for linear polymers, using a formula equivalent to Eq. 6.54.
- (ii) Equations such as Eq. 9.6 or Eq. 9.14 for arm relaxation have a prefactor τ_{pre} which should be adjusted according to the arm length, and which effectively gives an initial condition for the numerical iteration [5]. Similarly, the early time fluctuations of the arms (Eq. 6.37) should be included via a cross-over formula, in line with the theory of star polymers of Milner and McLeish [19] as indicated in Eq. 9.3. Fortunately, it is possible to adjust the iterative numerical scheme to accomplish this, as detailed by Park et al. [57] and Das et al. [6].
- (iii) During the relaxation of most branched polymer architectures, “compound arms” are formed: side arms fully relax, so that their branch points are now able to move, and this in turn affects the relaxation of the main polymer arm. In the original algorithm, Larson [5] introduced the concept of a “waiting time” to handle this situation. Later developments gave alternative proposals. Subsequent versions of the hierarchical model modified the effective prefactor τ_{pre} to account for extra friction of the side arms [57, 65]. The “BoB” model of Das et al. modified the iterative scheme to update the effective retraction potential [6]. These contrasting approaches each have a physical basis, and most likely a combination of the two approaches would be more appropriate.
- (iv) As discussed in Section 9.3.2, when matrix chains relax, they cease to act as constraints on test chains. However, if a large number of chains relax suddenly (e.g., the linear chains in a blend of linear and branched polymers—see Section 9.3.3), then the wider tube that is created can only gradually be explored via the “constraint release Rouse” process discussed in Section 7.3. Thus, the contribution of constraint release to stress relaxation is controlled not by $P(t)$ directly, but through a “constraint release volume fraction” $P_{\text{CR}}(t)$. This is equal to $P(t)$ whenever $P(t)$ is relaxing no faster than as $t^{-1/2}$, but if $P(t)$ relaxes faster than $t^{-1/2}$ (for example, if it relaxes exponentially fast), then $P_{\text{CR}}(t)$ is given by (see Section 7.4.1):

$$P_{\text{CR}}(t) = P(t_0) \left(\frac{t}{t_0} \right)^{-1/2} \quad (9.25)$$

Here, t_0 is the time at which $P(t)$ first begins to relax faster than $t^{-1/2}$. If the relaxation of $P(t)$ later slows down, so that $P_{\text{CR}}(t)$ drops down to equal $P(t)$, then we set $P_{\text{CR}}(t)$ again equal to $P(t)$, until such time as $P(t)$ again relaxes faster than $t^{-1/2}$.

We note that in case α is not unity, the above arguments all apply with the exponent $-1/2$ replaced by $-1/(2\alpha)$.

As discussed above in Section 9.3.3.3, a further consideration to be made is the functional form of $\phi_{p,\text{eff}}(t)$ which should be applied in Eq. 9.24 during the constraint release-Rouse processes. Milner, McLeish, and coworkers [31] argued that, whilst constraint release-Rouse motion is active, $\phi_{p,\text{eff}}(t)$ should be held *constant* at a value equal to the fraction of unrelaxed material just prior to the reptation of the linear chains, $P(t_0)$. However, this formulation is known to cause problems (i.e., prediction of unphysically long relaxation times) when the volume fraction of branched species is low. So, alternative prescriptions may be sought. One possibility is to allow $\phi_{p,\text{eff}}(t) \approx P_{\text{CR}}(t) \propto t^{-1/2}$, which removes the problem, but may not always give quantitatively correct predictions: further work, both theoretical and experimental, is required.

(v) The terminal relaxation of most branched polymers is via a reptation-like process of an effectively linear segment, but subject to extra friction arising from relaxed side arms, as detailed above for the case of combs in Section 9.4.3. In both Hierarchical models [5, 7, 8, 57, 65] and the BoB model [6], polymer chains relax by fluctuation until the time when reptation is possible (and the distance required to reptate is adjusted to account for relaxation of the chain ends by the fluctuation modes). At the reptation time, any remaining unrelaxed portions of the chain are assumed to relax with that timescale.

With respect to calculating the friction for reptation, different assumptions are made by the different groups. The BoB model of Das et al. [6] assumes that branch point hopping occurs in a tube with dilution commensurate with side arm relaxation, using Eq. 9.17 to rescale the friction constant so as to project the motion along tubes with different diameters. Additionally, they assume that the (usually minor) contribution from chain friction should be calculated for motion along the thin tube, since this usually gives lower friction than tube reptation (as discussed in Sections 7.3.3 and 7.4.2). In contrast, the Hierarchical models of Larson et al. [5, 7, 8, 57, 65] calculate friction for branch point hopping, assuming the hop size is the *undiluted* tube diameter, and add this to the monomeric friction from the backbone. They then use this summed friction constant, but calculate the distance required for reptation using a partially diluted tube. These differing prescriptions are one reason why the Hierarchical and BoB models recommend different values of the hopping parameter p , introduced in Section 9.4.2.

Having considered all the above relaxation mechanisms, the computational implementation of both the Hierarchical and BoB models is quite similar. First, a data structure must be implemented which allows the sizes and branched connectivity of a set of “representative” molecules to be stored in computer memory. Here, the Branch-on-Branch (“BoB”) model has a flexible data structure which permits any

branched structure—with the exclusion of structures containing loops—to be represented (i.e., including “Branch-on-Branch” structures). In contrast, the Hierarchical models are coded so as to allow only comb-like architectures (though there is no reason why they could not be suitably generalized). Since many industrial polymers, especially highly branched resins such as LDPE, are thought to contain structures with multiple levels of branching, this confers a practical advantage to the BoB model in industrial application.

Having stored a representative set of molecules in memory, the next task is to integrate numerically equations of form Eq. 9.24, starting at the outermost branches and working inwards. At each time increment, the fraction of unrelaxed polymer $P(t)$ may be calculated from the stored polymers, and from this the “constraint release volume fraction” $P_{\text{CR}}(t)$ and the function $\phi_{p,\text{eff}}(t)$ in Eq. 9.24 can be self-consistently calculated (see (iv) above), permitting further iterations of Eq. 9.24.

At various increments in time, complete relaxation of side arms occurs, giving rise to “compound arms” (see (iii) above) and ultimately resulting in unrelaxed linear sections of chain which can relax via reptation (see (v) above). Thus, the complete relaxation pathway of the representative set of polymers can be numerically predicted and stored. In this sense, the set of algorithms based on Larson’s original work [5] give quantitative predictions corresponding to the qualitative description of branched polymer relaxation discussed in Section 9.2.1.

From the functions, $P(t)$ and $P_{\text{CR}}(t)$ the linear viscoelastic properties of the melt can be computed. The entanglement contribution to the storage and loss moduli G' and G'' are approximated by

$$G'(\omega)/G_{\text{N}}^0 = \int_0^1 \frac{\omega^2 t'^2}{1 + \omega^2 t'^2} P_{\text{CR}}(t') dP(t') + \int_0^1 \frac{\omega^2 t'^2}{1 + \omega^2 t'^2} P(t') dP_{\text{CR}}(t') \quad (9.26)$$

and

$$G''(\omega)/G_{\text{N}}^0 = \int_0^1 \frac{\omega t'}{1 + \omega^2 t'^2} P_{\text{CR}}(t') dP(t') + \int_0^1 \frac{\omega t'}{1 + \omega^2 t'^2} P(t') dP_{\text{CR}}(t') \quad (9.27)$$

When the dilution exponent α is not unity, these formulas become [57]:

$$G'(\omega)/G_{\text{N}}^0 = \left[\int_0^1 \frac{\omega^2 t'^2}{1 + \omega^2 t'^2} P_{\text{CR}}^\alpha(t') dP(t') + \alpha \int_0^1 \frac{\omega^2 t'^2}{1 + \omega^2 t'^2} P(t') P_{\text{CR}}^{\alpha-1}(t') dP_{\text{CR}}(t') \right] \quad (9.28)$$

$$G''(\omega)/G_{\text{N}}^0 = \left[\int_0^1 \frac{\omega t'}{1 + \omega^2 t'^2} P_{\text{CR}}^\alpha(t') dP(t') + \alpha \int_0^1 \frac{\omega t'}{1 + \omega^2 t'^2} P(t') P_{\text{CR}}^{\alpha-1}(t') dP_{\text{CR}}(t') \right] \quad (9.29)$$

To these is added a contribution from sub-tube diameter Rouse motion, and tension equilibration along the tube, using a formula equivalent to Eq. 6.54.

In Section 9.5.3 we present some applications of the Hierarchical and BoB models to polymer melts. Before that, we briefly discuss a third tube-based algorithm for prediction of linear viscoelasticity.

9.5.2 The “Time-Marching” Algorithm

Whilst the Hierarchical and BoB algorithms very much belong to the same immediate family (descended directly from Larson’s work [5]), the time-marching algorithm of van Ruymbeke [60, 68] is more distantly related. Within this model, the relaxation function $P(t)$ is written as:

$$P(t) = \int p_{\text{rept}}(x, t) p_{\text{fluc}}(x, t) dx \quad (9.30)$$

where $p_{\text{rept}}(x, t)$ is the probability that a given segment (labeled with x) has not relaxed by reptation, and $p_{\text{fluc}}(x, t)$ is the probability that it has not relaxed by arm fluctuations. These two probabilities are updated as a function of time by a set of iterative steps over time, accounting for the current value of $P(t)$ at each iterative step (hence the term “time-marching”). The integral represents a sum over all chain sections. A significant difference compared to the algorithms based on the work of Larson [5] is that within the time-marching algorithm the reptation and fluctuation processes are considered independent processes (though they can indirectly affect one another through $P(t)$). In contrast, within the Hierarchical and BoB models, reptation is considered to be the terminal process of relaxation for a molecule, occurring sequentially after arm fluctuation. As a result, arm fluctuation speeds up the terminal reptation relaxation by shortening the distance required to reptate (this is in qualitative agreement with the Likhtman-McLeish [24] and similar models for linear rheology of linear chains). Within the time-marching algorithm, no such shortening of the distance required to reptate is included. Thus, reptation is often a slower process within the time-marching algorithm, and this may be one reason why it is possible to use $p^2 = 1$ to describe branch point hopping within the algorithm [60].

A second feature of the time-marching algorithm is that it enforces continuity of the fluctuation relaxation time for segments on either side of a branch point, by introducing an effective chain length for fluctuations of inner segments [60]. This chain length is adjusted at each branch point so as to enforce continuity of relaxation times, a process which becomes complicated for combs [69]. For multiply branched molecules, the algorithm also considers multiple retraction pathways. These may be the reasons why the algorithm has not yet been applied to arbitrarily branched polymers of commercial origin; the automation of such detailed considerations

within a computer algorithm is likely to be difficult. Nevertheless, the time-marching algorithm has been applied to a number of different model architectures such as stars [68], pom-poms [60], Cayley trees [70], and combs [69], and also to mixtures of these inspired by Temperature Gradient Interaction Chromatography (TGIC) results on a “model” polymer melt [71].

In summary, there are some clear differences between the time-marching algorithm and the hierarchical algorithms based on the work of Larson, and there remains scope for discussion about which (if either) is the better approximation to the underlying physics. At present, the time-marching algorithm does not appear to have the flexibility to deal with the huge complexity and polydispersity of industrial polymer resins.

9.5.3 Data and Predictions for Model Polymers and Randomly Branched Polymers

Each of the above models (Hierarchical, BoB and Time-Marching) has enjoyed success in matching experimental data from branched polymer resins. At a qualitative level, for a given molecular architecture all three algorithms typically make similar predictions for the overall shape of the viscoelastic spectrum. For an individual resin their parameters may be adjusted to obtain a quantitative match to data.

For example, Fig. 9.16 shows the linear viscoelastic spectrum of a polyisoprene comb polymer (backbone molecular weight $M_b = 121 \text{ kg/mol}$, arm molecular weight $M_a = 18.8 \text{ kg/mol}$ with an average of 7.1 arms per polymer—randomly grafted to the backbone) [62]. These data exhibit the expected series of relaxations for a comb-like polymer as detailed qualitatively in Section 9.2.1. At high frequencies, the storage and loss modulus follow the power-law relaxation expected from Rouse modes on scales smaller than the tube diameter. At intermediate frequencies, between 10^0 rad/s and 10^2 rad/s , a broad shoulder in the loss modulus is observed, corresponding to the relaxation of the arms of the comb. The terminal relaxation, between 10^{-3} rad/s and 10^{-2} rad/s , is due to reptation of the backbone. In some comb polymers, a distinct peak in the loss modulus is observed in the terminal relaxation, a characteristic signature of reptation. More commonly, the peak is less distinct, or absent, due to a combination of polydispersity and a relatively low terminal modulus associated with the comb backbones after dilution from the relaxed comb arms.

We may briefly consider the approximate application of Eq. 9.22 to these data. Given the backbone and arm molecular weights, and number of arms per polymer, we might estimate $\phi_b \approx 0.5$. Literature values for entanglement molecular weight of polyisoprene are of order $M_e^G = 4\text{--}5 \text{ kg/mol}$, indicating the number of backbone entanglements may be around $Z_b \approx 25$. Based on the lowest frequency for the “shoulder” in the loss modulus for arm relaxation, the arm relaxation time is roughly $\tau_a \approx 1 \text{ s}$.

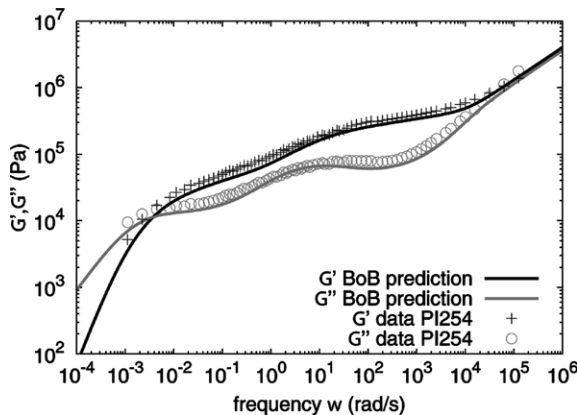


Figure 9.16 Predictions of the BoB model (lines) compared to experimental data (symbols) for the linear viscoelastic spectrum of a polyisoprene comb polymer (backbone molecular weight $M_b = 121$ kg/mol, arm molecular weight $M_a = 18.8$ kg/mol with an average of 7.1 arms per polymer) at reference temperature 0 °C. BoB model parameters are $M_e^G = 4.1$ kg/mol, $G_N^0 = 0.4$ MPa, $\tau_e = 10^{-4}$ s, $\alpha = 1$, and $p^2 = 1/40$. From Bacova et al. [62].

Taking, for example, $p^2 = 1/20$ gives, from Eq. 9.22, $\tau_b \approx 4000$ s, a value which is certainly larger than the terminal time suggested by the data (a little less than 1000 s based on the frequency of terminal relaxation). The main correction to our estimate from Eq. 9.22 is due to primitive path fluctuations (Section 6.4.3). For linear polymers at this degree of entanglement (taking into account the dilution $\phi_b \approx 0.5$) the fluctuation correction, according to Eq. 6.41, speeds up reptation by a factor of roughly 3. For sparsely branched combs, the fluctuation correction is typically yet more significant, due to relatively rapid fluctuation of the unbranched sections of backbone beyond the outer branch points. Whilst it is possible to estimate these fluctuation corrections, it is now perhaps easier to rely on the predictions of automatic computational algorithms.

Also shown in Fig. 9.16 is a prediction of these data using the BoB model [6, 62] using a numerical ensemble of molecules generated with the assumption of random addition of side arms to the polymer backbone, and reasonable estimates of arm and backbone polydispersities. The rheological parameters for this prediction were $M_e^G = 4.1$ kg/mol, $G_N^0 = 0.4$ MPa, and $\tau_e = 10^{-4}$ s at the reference temperature of 0 °C, which are in reasonable agreement with literature values. The prediction also uses the “recommended” BoB parameters of $\alpha = 1$ for the dilution exponent, and $p^2 = 1/40$ for the branch point hopping parameter (see Section 9.4.2). These latter parameters were “fixed” in the original work of Das et al. [6] through comparison to literature data available at the time from a wide range of polymer architectures.

Any such exercise in establishing universal parameters is limited by the quality of polymer samples and data available. It is also influenced strongly by the physical assumptions made in the algorithm. For example, the Hierarchical models [5, 7, 8, 57, 65] recommend $p^2 = 1/12$ for the hopping parameter (the Hierarchical and BoB models make different assumptions for branch point hopping and reptation, as detailed in Section 9.5.1). Conversely, the Time-Marching algorithm uses $p^2 = 1$ [60] (most likely because contour length fluctuations do not reduce the distance required to reptate in that model). It is to be expected that the recommended parameters will evolve with further advances in our understanding of branched polymer relaxation (e.g., through computer simulation [62]), with improved algorithms, and with the availability of more accurate experimental data.

The hierarchical nature of branched polymer relaxation is also illustrated in Fig. 9.17, which shows data for a two generation “Cayley tree” polybutadiene sample, in which the outer arms have molecular weight 7.25 kg/mol, and the inner arms have molecular weight 15.2 kg/mol [72]. These molecules were designed using the BoB algorithm before their synthesis using anionic polymerization (Section 3.4.1). The design criterion used was that the linear rheology should exhibit clearly separated relaxations of the outer arms, and inner arms, visible as well-separated “broad peaks” in the loss modulus as a function of frequency. Figure 9.17 confirms the success of this design, with the broad peaks appearing at frequencies of roughly 10^0 s^{-1} (inner arm relaxation) and $10^3\text{--}10^4 \text{ s}^{-1}$ (outer arm relaxation). This corresponds well to the qualitative description of hierarchical relaxation of branched polymers outlined in Section 9.2.1.

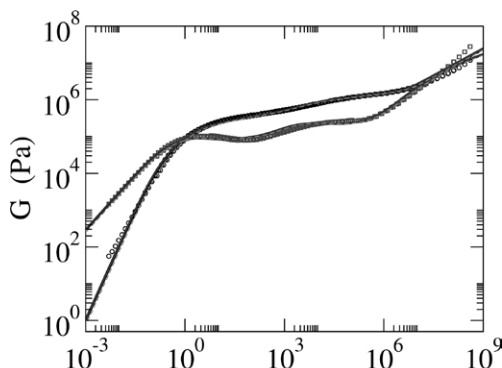


Figure 9.17 Predictions of the BoB model (lines) compared to experimental data (symbols) for the linear viscoelastic spectrum of a polybutadiene Cayley tree polymer (outer arms molecular weight 7.25 kg/mol, inner arms molecular weight 15.2 kg/mol) at reference temperature 25 °C. BoB model parameters are $M_e^G = 1.84 \text{ kg/mol}$, $G_N^0 = 1.2 \text{ MPa}$, $\alpha = 1$, and $p^2 = 1/40$. Solid lines are predictions with impurities from TGIC analysis, the dashed line is the prediction for the pure Cayley tree. From Hutchings et al. [72].

Analysis of the synthesized Cayley tree polymers, using temperature gradient interaction chromatography (TGIC—see Section 2.6.3.4) revealed some impurities were present. Roughly 14% by weight of the molecules had a lower molecular mass, most likely corresponding to one of the outer arms missing. There were hints also of a higher mass impurity, at a level of perhaps 4% by weight, which might correspond to molecules in which one of the outer arms had the length of an inner arm. In fact, for a molecule of this complexity, this represents a triumph of painstaking synthesis. Such low levels of impurity are rare: normally one would expect a wider range of defects, and a lower fraction of the target architecture to be present. An advantage of the hierarchical algorithms is that such defects can be accounted for in the numerical ensemble of molecules used as input. The predictions using the BoB algorithm in Fig. 9.17 (using rheology parameters $M_e^G = 1.84 \text{ kg/mol}$, $G_N^0 = 1.2 \text{ MPa}$, $\tau_e = 2.75 \times 10^{-7} \text{ s}$) agree well with the data. Additionally, the BoB algorithm was used to show that these levels of impurity have a negligible effect on the predicted linear viscoelasticity.

More commonly, impurity levels from anionic synthesis are higher. As noted in Section 3.4.1, TGIC reveals the presence of molecules with a substantial range of defects, which do sometimes influence their linear rheology, as revealed by a series of studies on “model” H-shaped polymers [71, 73–76]. In such cases, educated guess-work is needed in order to decide what structures correspond to the peaks in the TGIC separation. Usually this exercise can be informed by the likely side reactions anticipated by chemists for the chosen synthetic route. As an example of such work, Li and Dealy [76] studied a series of polybutadienes with H-shaped target structure with TGIC characterization used to determine the actual mixture of structures in the melts. They constrained their predictions using $G_N^0 = 1.15 \text{ MPa}$ and by insisting that Eq. 6.21 hold exactly (a requirement that is sometimes relaxed in fitting rheology data), giving $M_e^G = 1.54 \text{ kg/mol}$. They compared their data with predictions from both the Hierarchical and BoB model. Within each model they explored recommended parameters for polybutadiene from both the BoB model ($\alpha = 1$, $p^2 = 1/40$, and $\tau_e = 2.75 \times 10^{-7} \text{ s}$) and Hierarchical model ($\alpha = 4/3$, $p^2 = 1/12$, and $\tau_e = 3.7 \times 10^{-7} \text{ s}$). As can be seen from the results in Figs. 9.18 and 9.19, quantitative prediction was possible in some cases, and qualitatively the predictions follow the measured trends from one resin to the next. However, none of the tested combinations of model and recommended parameters gave accurate predictions for all four measured melts. It may be that, through further adjusting the parameterization of either of the two models, a better fit might be obtained. There is also the possibility that some of the educated guesses of structures from TGIC were incorrect.

In all of the above examples, the target molecular architectures dominate the rheology, so reasonable progress in predicting the rheology could be made using pen-and-paper calculations, whilst computational algorithms allow consideration of polydispersity

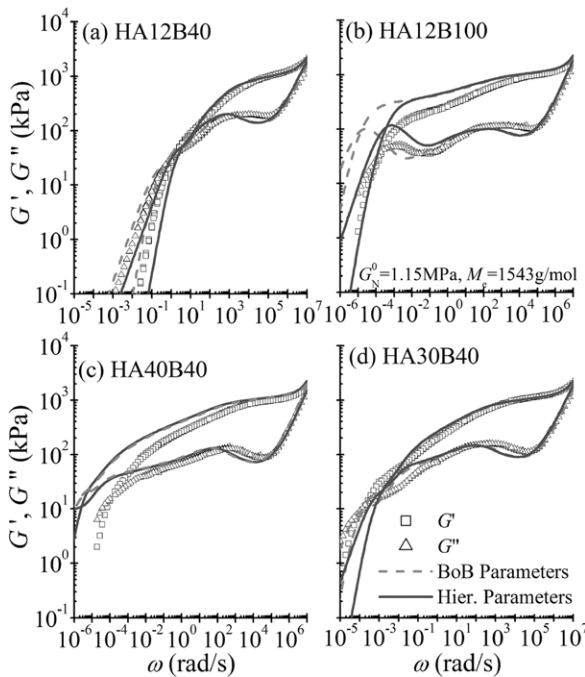


Figure 9.18 Predictions of the BoB model (lines) compared to experimental data (symbols) for the linear viscoelastic spectrum of four polybutadiene H-polymer melts, with impurities characterized by TGIC. The sample codes designate approximate arm (A) and backbone (B) molecular weights, in kg/mol. Theory parameters were $G_N^0 = 1.15 \text{ MPa}$, and recommended parameters from both the BoB model ($\alpha = 1$, $p^2 = 1/40$, and $\tau_e = 2.75 \times 10^{-7} \text{ s}$ —dashed lines) and Hierarchical model ($\alpha = 4/3$, $p^2 = 1/12$, and $\tau_e = 3.7 \times 10^{-7} \text{ s}$ —solid lines). From Li and Dealy [76].

and variations in branched shape. However, the real power in computational models for linear rheology is in their ability to make predictions in cases where pen-and-paper theory would be impossible, where random reactions produce a huge variety of different structures in the resin. An intermediate example, halfway between the “model” polymers considered above and randomly structured industrial resins, is the data obtained by Nicol et al. [77] for linear rheology of end-linked polypropylene sulfide (PPS) stars, shown in Fig. 9.20. Three-arm stars, with arm molecular weight 23 kg/mol, were randomly end-linked, producing four different resins with different extent of reaction. In modeling these data, den Doelder et al. [78] created a numerical ensemble of polymers by simulating the random reaction process, with each star arm being end-linked with probability p . The reaction probability was found to be strongly constrained by the available GPC data. Nevertheless, the rheology data could be predicted by the BoB model, with reasonable accuracy, using a consistent set of parameters for all four resins, as shown in Fig. 9.20. Both data and predictions exhibit a high-frequency “shoulder” in the loss modulus, corresponding to the relaxation of

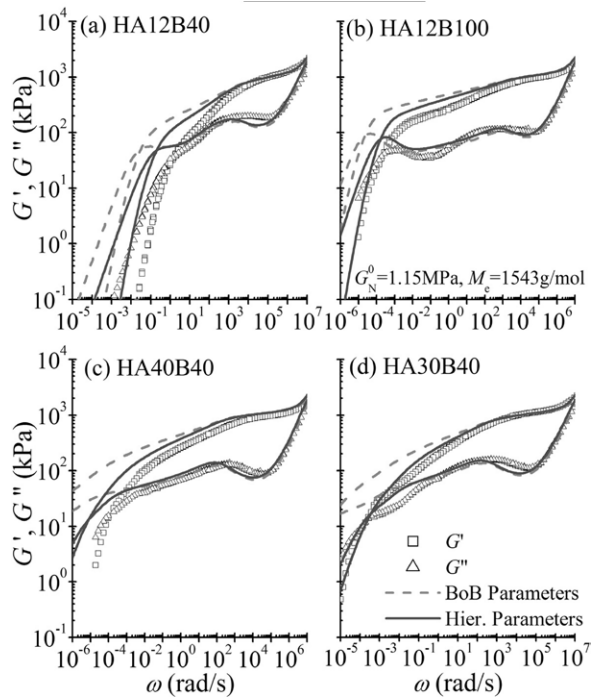


Figure 9.19 Predictions of the Hierarchical model (lines) compared to experimental data (symbols) for the linear viscoelastic spectrum of four polybutadiene H-polymer melts, with impurities characterized by TGIC. The sample codes designate approximate arm (A) and backbone (B) molecular weights, in kg/mol. Theory parameters were $G_N^0 = 1.15$ MPa, and recommended parameters from both the BoB model ($\alpha = 1$, $p^2 = 1/40$, and $\tau_e = 2.75 \times 10^{-7}$ s—dashed lines) and Hierarchical model ($\alpha = 4/3$, $p^2 = 1/12$, and $\tau_e = 3.7 \times 10^{-7}$ s—solid lines).

From Li and Dealy [76].

the monodisperse star arms, together with a longer tail at lower frequencies, corresponding to hierarchical relaxation of the large end-linked structures; in this sense these data combine features of both model and structurally polydisperse polymers.

Finally, we examine predictions for an extremely well-characterized set of “industrial” resins: the HDB 1-7 series of high-density polyethylene resins synthesized using a constrained geometry catalyst (CGC) by Dow Chemicals for research purposes. As discussed in Section 3.9.2, just two parameters are thought to be required to specify the statistical distribution of molecular architectures in solution-synthesized CGC resins: (1) a measure of molecular weight, and (2) a measure of the level of long-chain branching. An advantage of the HDB series of resins is that they were synthesized without comonomer, so that an accurate determination of long-chain branching level could be made using NMR analysis. This, together with a determination of molecular weight using GPC, is sufficient to specify the two required parameters,

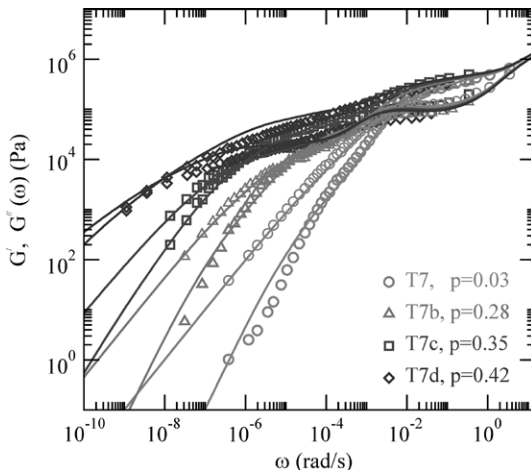


Figure 9.20 Comparison of BoB model (lines) and experimental data (symbols) at 363 K for end-linked PPS three-arm star polymers of Nicol et al. [77]. The probability (ρ) used for end-linking in the modeling is given in the legend. Star arms were generated with molecular weight 23 kg/mol and dispersity 1.12. Other parameters used in the calculations are $M_e^0 = 5.18$ kg/mol, $\tau_e = 3 \times 10^{-3}$ s, and $\rho = 0.9 \text{ g} \cdot \text{cm}^{-3}$. From den Doeler et al. [78].

and the measured set of parameters for the HDB series are listed in Table 3.1. This, then, allowed Das et al. [6] to construct a recursive statistical algorithm to generate a representative set of polymers for each resin—this algorithm is included as part of the released BoB code [67]. Figure 9.21 shows comparisons between the measured linear rheology data and predictions of the BoB model, using a consistent set of rheology parameters resins ($M_e^G = 1.12$ kg/mol, $G_N^0 = 1.97$ MPa, $\tau_e = 1.05 \times 10^{-8}$ s) for all the HDB resins and for a melt of linear polymers (HDL) with molecular weight of 93 kg/mol and dispersity of approximately 2. As can be seen, compared to the data of model polymers discussed earlier in the chapter, the linear rheology of each of these randomly branched polymers, taken on their own, is quite featureless (there are not, for example, peaks or shoulders in the loss modulus). However, the constraints imposed by using the same tube model parameters, together with the independent determination of molecular structure through NMR and GPC, mean that the data taken as a whole can be viewed as a good test of theoretical modeling. In this context, the description of the data can be considered as good. As Das et al. [6] point out, the small discrepancy between model and data for HDB4 may be explained by noting that this resin lies in a region of parameter space where the terminal viscosity is very sensitive to branching level. A small error in determination of degree of branching then produces a large change in predicted rheology. The Hierarchical model was also used to model the rheology of a subset of the resins (HDB1-3 and HDL) [7]. For the more branched resins, the constraint that the Hierarchical model is coded only

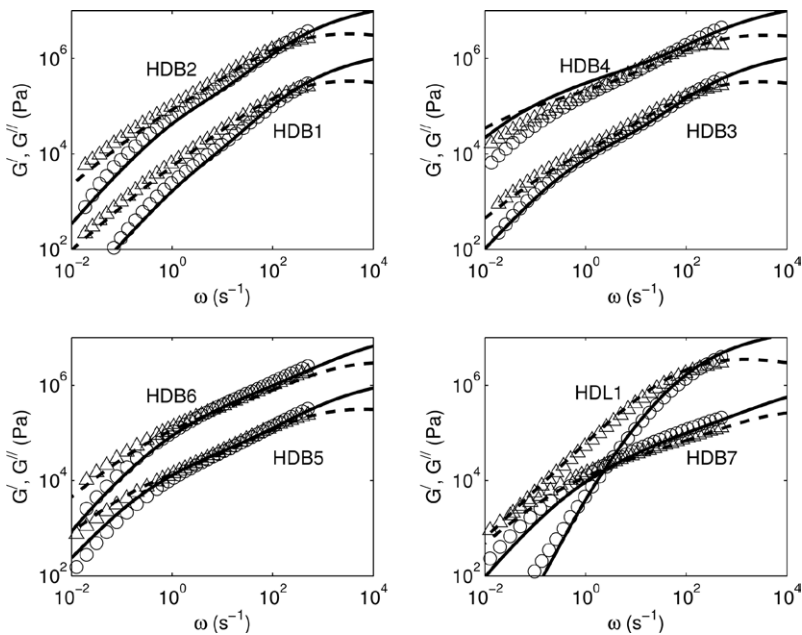


Figure 9.21 Linear rheology data together with BoB model predictions for the HDB series of metallocene catalyzed polyethylene resins (Table 3.1) and a linear resin (HDL) with molecular weight of 93 kg/mol and dispersity of approximately 2. Circles/solid lines and triangles/dashed lines, respectively, are the experimental/predicted values for storage and loss modulus. For clarity, the data on HDB2, HDB4, HDB6, and HDL1 have been shifted by a factor of 10 vertically. Parameters for BoB predictions are $M_e^G = 1.12 \text{ kg/mol}$, $G_N^0 = 1.97 \text{ MPa}$, and $\tau_e = 1.05 \times 10^{-8} \text{ s}$. From Das et al. [6].

for comb-like molecules becomes more serious, as the number of molecules with a branch-on-branch structure becomes significant (e.g., for HDB7, 10% by mass of the molecules have a branch-on-branch structure which is not comb-like [6]).

More recently, Chen et al. [8] successfully used the Hierarchical model to explore the rheology of a series of blends between branched and unbranched metallocene resins. Since the resins were only lightly branched, they were able to show that the effect of branch-on-branch molecules on the resin were negligible.

Similar approaches have been used to predict the linear rheology of melts made from polycondensation reactions [79, 80] and for LDPE [9, 10, 81]. As noted in a recent review [82], successful modeling in the arena of such randomly branched, polydisperse melts requires, at the very least:

- A statistical model for the polymerization reaction, including branch formation.
- As much structural information as can be gained on (i) the molecular weight distribution and (ii) degree of branching.

Ideally, both should be available prior to use of computational algorithms for rheology prediction. A polymerization reaction model is necessary in order to constrain the type of distribution of branching and molecular weight, since typically many possible distributions will be consistent with the experimental characterization data, taken on their own. Structural information can help to parameterize and further constrain the reaction model. As previously noted, both of these elements were in place for the HDB metallocene resins discussed above, and we may have some confidence in the distribution of molecular shapes and sizes used in rheology prediction. In other cases, the available data and reaction modeling is less perfect. For example, in their studies of a series of LDPE resins manufactured in tubular reactors, Read et al. [9, 10] did not have access to detailed reactor parameters for the resins. Instead, they made use of a generic and simplified Monte Carlo scheme for LDPE synthesis [83], which might be expected to predict the typical shapes of LDPE molecules. They constrained the Monte Carlo scheme by fitting to GPC-MALLS data, giving information on molecular weight distribution, and indirect information on degree of branching via measurement of molecular radius through light scattering. This combination of imperfect reaction modeling and imperfect structural data indicates that the distribution of LDPE molecular shapes and sizes could not be exactly known. Nevertheless, Read et al. [9, 10] were able (i) to rank successfully their six LDPE resins in order of viscosity, and (ii) through small adjustments in reactor parameters, to match simultaneously the linear rheology and GPC-MALLS data with a consistent set of tube model parameters, allowing them to proceed towards prediction of nonlinear rheology (see Section 11.6.2). Therefore, in the absence of exact characterization of the molecular distribution, it appears to be possible, still, to make some progress on the basis of incomplete and approximate information.

■ 9.6 Slip-Link Models for Branched Polymers

In Section 6.5, we discussed slip-link models as an alternative picture to the tube model for calculations of entangled polymer dynamics and rheology. We noted that an advantage of slip-link models is that, once the microscopic rules for chain dynamics within the slip-link model are decided, simulation of the model provides rheological predictions without need for further mathematical development. Relaxation mechanisms such as reptation, primitive path fluctuations, and constraint release (described by both constraint release Rouse motion and dynamic dilution) are all captured as a direct consequence of repeated application of the microscopic dynamical rules for chain motion through slip-links.

Slip-link models can also be applied to branched polymers, though a disadvantage in this context is that the extremely long relaxation times typical of branched polymers can lead to large computational time and expense. Nevertheless, slip-link models are both a predictive tool in their own right for branched polymer rheology, and a potential testing-ground for tube model developments. In particular, the “dynamic dilution” theory (detailed above in Section 9.3 for symmetric stars and their blends with linear polymers) can be checked using slip-link models without introducing any extra assumptions beyond those already used for linear polymers. However, in parallel with the tube model development for multiply branched polymers and asymmetric stars (detailed above in Section 9.4), simulation of branch point motion within slip-link models requires extra rules to be introduced. We shall first discuss application of slip-link models to symmetric stars, before considering the additional rules that might be introduced for multiply branched polymers.

9.6.1 Symmetric Star Polymers and Blends with Linear Polymers

An early application of a slip-link model to star polymers was presented by Shanbhag et al. [84]. Their slip-link model was somewhat simplified (as compared to more recent slip-link implementations) in that it did not store positions of slip-links in three-dimensional space. Rather, it maintained a list of the ordering of slip-links along each star polymer arm, allowing the number of slip-links to fluctuate through a quadratic potential (mimicking the deep fluctuations of tube path length discussed in Section 9.3.1). Instead of handling constraint release through the dynamic dilution *ansatz* (Section 9.3.2), they implemented constraint release directly by pairing together slip-links on different chains, i.e., the destruction of a slip-link through length fluctuation of one chain results in the deletion of a paired slip-spring in the middle of another chain. Correspondingly, the creation of a slip-link at the end of one chain results also in the creation of a paired slip-link on another chain. It is important in such an algorithm to maintain a record of pairs of slip-links so that this constraint release algorithm can be applied consistently.

Once these microscopic dynamical rules are specified, stochastic simulation of the individual dynamics of an ensemble of chains (typically several hundred or more) is performed, and predictions of linear viscoelasticity and other measures of chain relaxation (such as dielectric spectroscopy) can be made based on the simulated dynamics, in particular from the distribution of slip-link creation and destruction rates.

While the slip-link model includes, by construction, a constraint release process, it is not immediately apparent that the constraint release included in the slip-link model is in any sense “equivalent” to dynamic dilution, which has been so successfully used to describe the relaxation of star polymers. However, simulations with

the slip-link model of Shanbhag et al. [84] show that the longest relaxation time predicted by the model is proportional to $\exp(\beta \nu N_0)$, with $\beta \approx 0.25$. That is, the constraint release effect included in the slip-link model acts to create an effective softening of the fluctuation potential, much as does dynamic dilution. In the classical Ball-McLeish form of dynamic dilution, in which $\alpha = 1$, the equivalent factor β is just $1/3$; see Eq. 9.7, while in the Milner-McLeish form, for which $\alpha = 4/3$, the factor β is $2/(1+\alpha)(2+\alpha) = 0.257$, almost the same “softening” factor as is inferred from the slip-link model (despite the fact that the slip-spring model, by construction, uses pairwise constraint release events which implies $\alpha = 1$). Since the Milner-McLeish model with this softened potential is quite successful in predicting the linear viscoelasticity of star polymers, one might expect similar success with the slip-link model, and such is indeed the case. Figure 9.22 shows predictions of the slip-link model for the dynamic dielectric moduli as functions of frequency, compared to data from Watanabe and coworkers [85]. Agreement between simulations and experimental data is good, except at high frequency, which is dominated by Rouse motions within the tube, and which are not included in the slip-link model. Agreement similar to that shown in Fig. 9.22 is obtained for the mechanical moduli G' and G'' , for this sample and polyisoprene star polymers with other molecular weights [86].

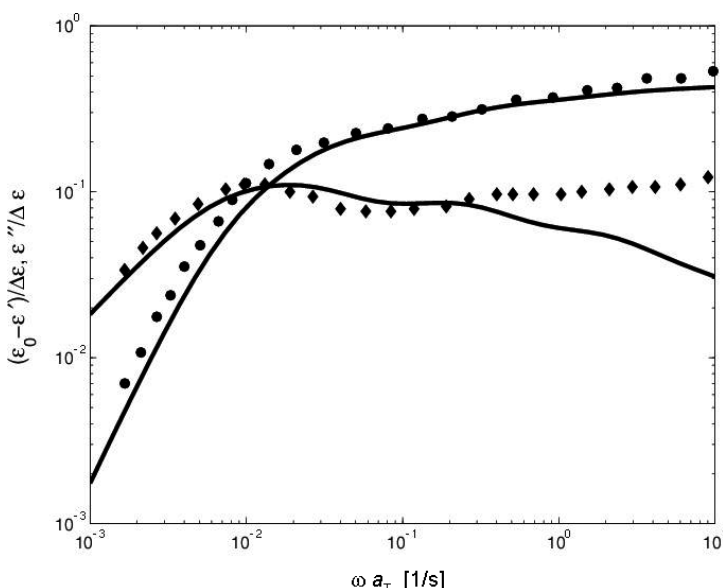


Figure 9.22 Normalized dielectric constant $\epsilon_0 - \epsilon'$ (●), where ϵ_0 is the zero-frequency dielectric constant, and dielectric loss constant (◆) at 40 °C for a 6-arm polyisoprene star with $M_w = 459,000$. Symbols are data of Watanabe et al. [85], and the lines are predictions of the slip-link model. The parameters of the model $M_e^G = 4650$ and $\tau_0 = 42$ s, are used for all calculations with the slip-link model for 1,4-polyisoprene. From Shanbhag and Larson [86].

This agreement of the slip-link model with dielectric relaxation data is particularly significant, because the dynamic dilution concept, included in the Milner-McLeish theory, breaks down for star polymers in the terminal region [28, 84, 87], and is not able to predict correctly the dielectric relaxation, although it is successful for the mechanical relaxation data (because they are much less sensitive to the failure of dynamic dilution in the terminal regime). The terminal relaxation behavior of a star polymer, according to the slip-link model, is dominated by rare events, in which *new entanglements* are created between the branch point and the slip-link originally closest to the branch point, thereby allowing a relatively shallow fluctuation of the chain end to release this slip-link. Since slip-links originally nearest the branch point represent the “deepest,” most slowly relaxing, entanglements in a star polymer, this relaxation mechanism dominates the terminal regime [84], and while qualitatively similar to the tube widening process envisioned in dynamic dilution, may not be identical to it. McLeish [28] has discussed some reasons why the original tube dilution picture successfully predicts linear rheology but not dielectric relaxation for stars. The Ball-McLeish [14, 19] implementation of dynamic dilution has been immensely successful in terms of quantitative predictions for branched polymer rheology. However, there appears to be a need to reformulate and rethink their mathematical implementation of dynamic dilution for branched polymers, perhaps including more detailed descriptions of constraint release as discussed in Chapter 7. It is likely that analysis of chain dynamics in slip-link simulations will help to inspire such developments in the future.

More recent, and sophisticated, slip-link simulations of star polymers retain the pairing of slip-links used to simulate constraint release used by Shanbhag et al. [84], but implement more detailed descriptions of chain dynamics, and specify the position of slip-links in three-dimensional space. They retain the ability to predict, simultaneously, both linear viscoelasticity and dielectric relaxation, as was demonstrated recently by Pilyugina et al. [88], using Schieber’s implementation of the slip-link model (Section 6.5). They also hold the ability to predict, without any additional parameters or further mathematical development, the linear rheology of linear polymers, star polymers and their blends. As an example of this, Fig. 9.23 shows predictions by Shivokhin et al. [89], using Likhtman’s slip-spring model (Section 6.5), for the linear viscoelasticity of polybutadiene 3-arm star polymers with arm molecular weight 24.5 kg/mol, for linear polybutadiene chains with molecular weight 7.5 kg/mol, and for blends of these two polymers. It can be seen that the rheology of both the pure components and their blends are predicted with a high degree of accuracy, suggesting that the complex constraint release dynamics from fast moving linear chains and slow star polymers is well handled by this slip-link implementation. In the same paper, Shivokhin et al. [89] also show successful predictions for star polymers of a range of arm molecular weights.

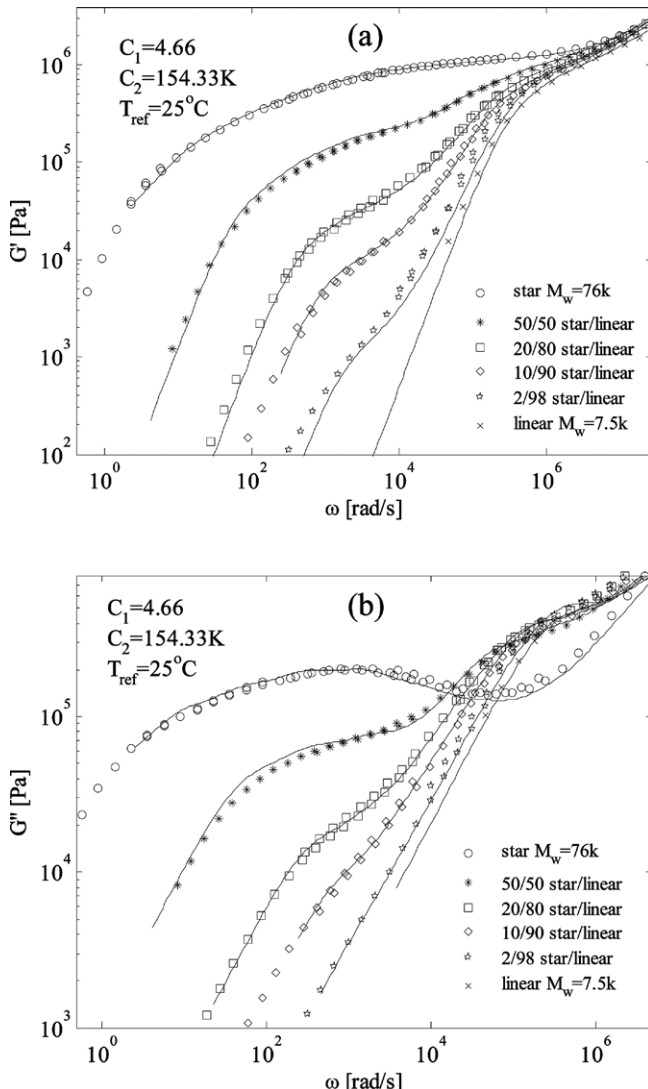


Figure 9.23 Linear rheology data for (a) storage modulus and (b) loss modulus of polybutadiene 3-arm star polymers with arm molecular weight 24.5 kg/mol, linear polybutadiene chains with molecular weight 7.5 kg/mol, and of blends of these two polymers. From Shivokhin et al. [89].

More recent work by Desai et al. [90] has studied a broader range of star-linear blends. Their work emphasizes the success of both the Schieber and Likhtman slip-link implementations in describing the linear viscoelastic data, and the corresponding difficulties in describing those same data using existing tube theories, as encoded in the Hierarchical and BoB models discussed in Section 9.5. It is clear that work is required, still, to improve the tube theory and especially the dynamic dilution approximation.

Interestingly, Shivokhin et al. [89] also use their slip-spring model to compare the terminal relaxation of stars in their blend with entangled linear chains with stars in an unentangled solvent at the same concentration. They find that the form of the terminal relaxation is identical, but shifted in time by a factor that can be predicted using models [91] based the constraint release Rouse picture of binary blends, discussed earlier in Chapter 7. Such a finding indicates some consistency between slip-link models and more detailed treatments of constraint release. This may provide clues to help improve our mathematical description of constraint release in branched polymers beyond the dynamic dilution approximation.

9.6.2 Branch Point Hopping in Slip-Link Simulations

In Section 9.4 we considered the application of tube models to multiply branched polymers, noting that a critical issue is the physics of branch point motion. As discussed in Sections 9.4.2 and 9.4.3, the assumption employed in tube models is that complete relaxation of a side arm allows branch points to take a “hop” through the entanglement network, and that enough such hops can lead to relaxation of whole chains.

Slip-link models also face the issue of branch point motion, and specifically the problem of defining dynamical rules to govern this. It presently seems difficult to define multiple options for hopping rules in slip-link algorithms, corresponding to the various options available within tube models (such as hopping in a diluted or undiluted tube). In fact, only one hopping rule has been proposed in the literature, perhaps because it is the easiest option to define and implement within a slip-link framework. For three-functional branch points, this rule is to wait until all slip-links from a side arm have been *completely* removed by arm fluctuation, and then to allow the branch point to hop, one way or the other, past the adjacent slip-links on the two unrelaxed arms. This rule was first implemented for asymmetric stars and H-shaped polymers by Shanbhag and Larson [86] and later generalized to branch points of higher functionality by Masubuchi et al. [92] within their NAPLES code (Section 6.5), applying it to asymmetric stars [93], pom-pom polymers [94], and combs [95].

Figure 9.24 shows the storage modulus versus frequency for a series of asymmetric star polymers with short-arm lengths ranging from around 2 up to around 20 entanglements, the latter corresponding to the length of the two long arms, together with predictions made using the slip-link algorithm of Shanbhag and Larson [86]. Note that the experimental results show a very dramatic retardation of relaxation induced by attachment of even the shortest arm, and the relaxation becomes nearly as slow as a symmetric star already when the short arm molecular weight is 17,000, only 3.5 entanglements. This feature, whereby short side arms dramatically retard the relaxation of asymmetric stars, has been found to cause problems for tube

models, as demonstrated by Frischknecht et al. [59]—though a reasonable prediction of these data was made by Das et al. [6]. However, it is interesting to note that the slip-link algorithm yields the results shown in Fig. 9.24, which are in remarkably good agreement with the experimental data, especially considering the lack of any adjustable parameters (since all parameters were determined in simulations with symmetric stars). The success of the slip-link model in predicting these data where tube models face greater difficulty has been traced in part to a distinction between the longest relaxation time of the short arm, which is the time it takes to free itself of all *original* entanglements (or slip-links), and the longer time it takes to free itself of *all* entanglements, both original and those created during the relaxation process. The latter, longer, time controls branch point motion in the slip-link model, and in particular leads to slower-than-expected branch point motion for the asymmetric stars with short side arms. For longer side arms, the branch point is practically immobile with respect to branch point hopping, and so the entire relaxation comes from deep fluctuation of the long arms. This point has been discussed in detail by Masubuchi et al. [93] in application of their model to asymmetric stars. The conclusion that the timescale for branch point motion is substantially slower than the longest relaxation time of the attached arms is also supported by experiments of Juliani and Archer [96].

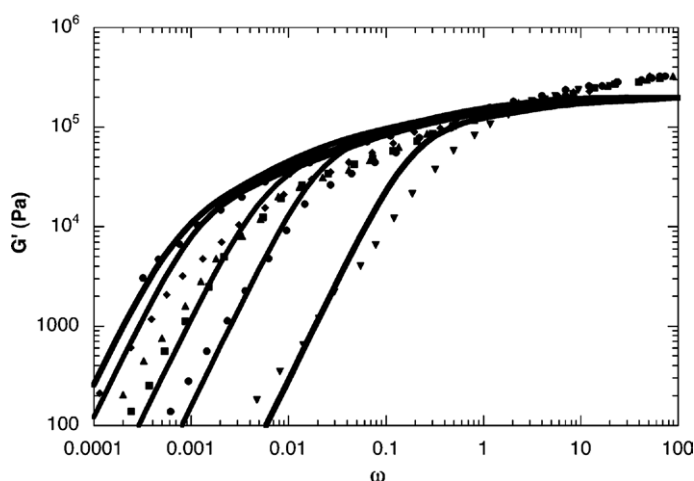


Figure 9.24 Comparison of predictions of slip-link simulations with data for asymmetric stars having two long arms of molecular weight $1.05 \cdot 10^5$, and a short arm. The data, from right to left are for: a linear chain of molecular weight $2 \cdot (1.05 \cdot 10^5)$ with no arm (∇), and for arm molecular weights of 11,000 (\bullet), 17,000 (\blacktriangle), 37,000 (ρ), 47,000 (\blacklozenge). The final data set on the left is for a symmetric three-arm star with arm molecular weight $1.05 \cdot 10^5$ (\bullet). The simulation curves for short-arm molecular weights of 37,000 and 47,000 are almost coincident. In the simulations, $G_N^0 = 0.25$ MPa, $M_e^G = 4650$ (Frischknecht et al. [59]), and $\tau_0 = 42$ s. From Shanbhag and Larson [86]

For branched polymers with more than one branch point, such as combs [95] and H-shaped polymers [86], relaxation of the polymer backbone is impossible without branch point motion taking place, so these polymers are perhaps a stronger test slip-link implementation of this algorithm. For the most part, algorithms have been tested in situations where side arms are relatively short, and where there are only a few slip-links per arm. In such cases it is not so unlikely to find side arms in which all slip-links have been removed, and so branch point hopping occurs with reasonable regularity within the algorithm. In these cases, it seems to be that slip-link algorithms can predict the linear rheology of multiply branched polymers with good accuracy [86, 94, 95].

However, there is evidence that the slip-link model fails for H polymers with longer arms [86]. The reason for this is again because of the distinction between the longest relaxation time of the short arm, the longer time it takes to free itself of *all* entanglements. The first of these is accelerated by the dynamic dilution process, but the latter is not accelerated, and becomes exponentially more unlikely as the number of entanglements on the side arm is increased. It is likely that branch points with a substantial number of such entanglements will be practically immobile in any slip-link algorithm using the above model for branch point motion. Shanbhag and Larson [86] found this to become a significant effect in modeling H-polymers with around 11 entanglements per arm. If slip-link models are to be applied to industrial polymers, which often contain many more entanglements in the largest molecules, then more accurate models of branch point motion will need to be developed.

■ 9.7 Summary

The rheology of polymers with long-chain branching (LCB) is a very complex, yet vital, field of study. Because each branch emanating from a branch point can entangle with other molecules, the motions of branch points are slow, and polymers with long-chain branches can have very slow relaxation. Hence, measurement of rheology is perhaps the most precise means of detecting the presence of small levels of long-chain branching. Quantifying the level and type of LCB with the assistance of rheology requires the development of quantitative theories that can be used to interpret the rheological data. Most of the basic concepts required to develop such theories now seem to be in place. In the linear viscoelastic regime, branched polymers relax by a combination of primitive path fluctuations, constraint release, and, in multiply branched polymers, a high-order reptation process, in which each step of the reptation requires hopping of the branch point. Theories for the linear viscoelasticity of branched polymers are well developed for singly branched polymers, such as monodisperse and bidisperse stars, and even mixtures of star and linear polymers.

Theories have been developed for the linear viscoelasticity of the simplest polymers with more than one branch point, including H, pom-pom, and comb polymers.

More recently, computational algorithms have been developed that can predict the linear viscoelasticity of arbitrary mixtures of long-chain-branched polymers of various architectures—these include the Hierarchical model of Larson and co-workers [5, 7, 8, 57, 65, 66], the “BoB” model of Das and co-workers [6, 67], and the “Time-marching algorithm” of van Ruymbeke [60, 68]. These use a hierarchical approach, suggested by McLeish, in which the relaxation is envisioned as starting from the tips of the branches, which relax by primitive path fluctuations, working inwards towards the backbone, which finally relaxes by reptation. Constraint release can be accounted for during these processes by a combination of dynamic dilution and constraint-release Rouse motion. The most important unknown aspect of hierarchical theories is the rate at which branch points diffuse for arbitrary branched architectures. Even with theoretical knowledge still incomplete, these algorithms have been able to make successful quantitative predictions for the linear rheology of polydisperse mixtures of branched polymers from both academic and industrial origin. They require, as input, information about the distribution of molecular size and branching architecture, which can to sometimes be obtained from knowledge of the synthesis procedure and from characterization methods such as TGIC and GPS with light scattering or viscometry. More often, knowledge of the molecular shapes is incomplete. In such cases the synthesis and characterization information provides *constraints* on the range of viable molecular shapes; then, these algorithms (in conjunction with rheology measurements) can help to infer the molecular architectures. For example, it is now possible to use the zero-shear viscosity of a polymer, combined with a measured molecular weight distribution, to infer the level of branching present, at least for some cases, such as when branches are introduced by peroxide, or are introduced randomly by a single-site metallocene catalyst.

An alternative simulation strategy is to make use of slip-link models. These have been successful in making quantitative predictions for star polymers, blends of stars with linear polymers, asymmetric stars, H-polymers, and combs. In the case of stars and their blends with linear polymers, slip-link models provide a test for theories describing the interaction between constraint release and primitive path fluctuations. These suggest that our present mathematical description of “dynamic dilution” may not be wholly accurate, and that more work is needed (this has strong implications for the previously discussed computational algorithms). For asymmetric stars, H-polymers, and combs, sliplink simulations require additional assumptions about motion of branch points. The current strategy in slip-link models, to allow a “hop” only when the side arm is completely free of slip-links, appears effective for short side arms. It is likely to prove incorrect for well-entangled or hierarchically branched side arms, predicting much too long relaxation times. Slip-link models

are not yet sufficiently fast to deal with the large, multiply branched, and highly polydisperse molecules found in many industrial resins.

■ References

- [1] Janzen, J., Colby, R.H. Diagnosing long-chain branching in polyethylenes. *J. Mol. Struct.* (1999) 485–486, pp. 569–583
- [2] Auhl, D., Stange, J., Münstedt, H., Krause, B., Voigt, D., Lederer, A., Lappan, U., Lunkwitz, K. Long-chain branched polypropylenes by electron beam irradiation and their rheological properties. *Macromol.* (2004) 37, pp. 9465–9472
- [3] Mendelson, R.A., Bowles, W.A., Finger, F.L. Effect of molecular structure on polyethylene melt rheology, I. Low-shear behavior. *J. Polym. Sci., Part A-2* (1970) 8, pp. 105–126
- [4] Gabriel, C., Münstedt, H. Strain hardening of various polyolefins in uniaxial elongational flow. *J. Rheol.* (2003) 47, pp. 619–630
- [5] Larson, R.G. Combinatorial rheology of branched polymer melts, *Macromol.* (2001) 34, pp. 5229–5237
- [6] Das, C., Inkson, N.J., Read, D.J., Kelmanson, M.A., McLeish, T.C.B. Computational linear rheology of general branch-on-branch polymers. *J. Rheol.* (2006) 50, pp. 207–234
- [7] Park, S.J., Larson, R.G. Modeling the linear viscoelastic properties of metallocene-catalyzed high density polyethylenes with long-chain branching. *J. Rheol.* (2005) 49, pp. 523–536
- [8] Chen, X., Costeux, C., Larson, R.G. Characterization and prediction of long-chain branching in commercial polyethylenes by a combination of rheology and modeling methods. *J. Rheol.* (2010) 54, pp. 1185–1205
- [9] Read, D.J., Auhl, D., Das, C., den Doelder, J., Kapnistos, M., Vittorias, I., McLeish, T.C.B. Linking models of polymerization and dynamics to predict branched polymer structure and flow. *Science* (2011) 333, pp. 1871–1874
- [10] Das, C., Read, D.J., Auhl, D., Kapnistos, M., den Doelder, J., Vittorias, I., McLeish, T.C.B. Numerical prediction of nonlinear rheology of branched polymer melts. *J. Rheol.* (2014) 58, pp. 737–757
- [11] Rohlfing, D.C., Janzen, J. Melt-rheological characteristics of metallocene-catalyzed polyethylenes. in *Metallocene-Based Polyolefins-Preparation, Properties and Technology*, Vol. 2 (1999) John Wiley & Sons, Ltd., Chichester, pp. 419–434
- [12] Shroff, R.N., Mavridis, H. Long-chain-branched index for essentially linear polyethylenes. *Macromol.* (1999) 32, pp. 8454–8464
- [13] Pattamaprom, C., Larson, R.G. Predicting the linear viscoelastic properties of monodisperse and polydisperse polystyrenes and polyethylenes. *Rheol. Acta* (2001) 40, pp. 516–532
- [14] Ball, R.C., McLeish, T.C.B. Dynamic dilution and the viscosity of star polymer melts. *Macromol.* (1989) 22, pp. 1911–1913

- [15] McLeish, T.C.B. Hierarchical relaxation in tube models of branched polymers. *Europhys. Lett.* (1988) B6, pp. 511–516
- [16] Doi, M., Kuzuu, N.Y. Rheology of star polymers in concentrated-solutions and melts. *J. Polym. Sci., Polym. Lett. Ed.* (1980) 18, p. 775
- [17] Pearson, D.S., Helfand, E. Viscoelastic properties of star-shaped polymers. *Macromol.* (1984) 17, pp. 888–895
- [18] Doi, M., Edwards, S.F. *The Theory of Polymer Dynamics* (1986) Clarendon Press, Oxford
- [19] Milner, S.T., McLeish, T.C.B. Parameter-free theory for stress relaxation in star polymer melts. *Macromol.* (1997) 30, pp. 2157–2166
- [20] McLeish, T.C.B. Tube theory of entangled polymer dynamics. *Adv. Phys.* (2002) 51, pp. 1379–1527
- [21] Shanbhag, S., Larson, R.G. The chain retraction potential in a fixed entanglement network. *Phys. Rev. Lett.* (2005) 94, article no. 076001
- [22] Zhou, Q., Larson, R.G. Primitive path identification and statistics in molecular dynamics simulations of entangled polymer melts. *Macromol.* (2005) 38, pp. 5761–5765.
- [23] Masubuchi, Y., Ianniruberto, G., Greco, F., Marrucci, G. Entanglement molecular weight and frequency response of sliplink networks. *J. Chem. Phys.*, (2003) 119, pp. 6925–6930
- [24] Likhtman, A.E., McLeish, T.C.B. Quantitative theory for linear dynamics of linear entangled polymers. *Macromol.* (2002) 35, pp. 6332–6343
- [25] Cao, J., Zhu, J., Wang, Z., Likhtman, A.E. Large deviations of Rouse polymer chain: First passage problem. *J. Chem. Phys.*, (2015) 143, p. 204105
- [26] Colby, R.H., Rubinstein, M. 2-Parameter scaling for polymers in theta-solvents. *Macromol.* (1990) 23, pp. 2753–2757
- [27] Watanabe, H. Viscoelasticity and dynamics of entangled polymers. *Prog. Polym. Sci.* (1999) 24, pp. 1253–1403
- [28] McLeish, T.C.B. Why, and when, does dynamic tube dilation work for stars? *J. Rheol.* (2003) 47, pp. 177–198
- [29] Milner, S.T., McLeish, T.C.B. Reptation and contour-length fluctuations in melts of linear polymers, *Phys. Rev. Lett.* (1998) 81, pp. 725–728
- [30] Blottière, B., McLeish, T.C.P., Hakiki, A., Young, R.N., Milner, S.T. The rheology of bimodal blends of star polymer melts. *Macromol.* (1998) 31, pp. 9295–9304
- [31] Milner, S.T., McLeish, T.C.B., Young, R.N., Hakiki, A., Johnson, J.M. Dynamic dilution, constraint-release, and star-linear blends. *Macromol.* (1998) 31, pp. 9345–9353
- [32] McLeish, T.C.B., Allgaier, J., Bick, D.K., Bishko, G., Biswas, P., Blackwell, R., Blottière, B., Clarke, N., Gibbs, B., Groves, D.J., Hakiki, A., Heenan, R.K., Johnson, J.M., Kant, R., Read, D.J., Young, R.N. Dynamics of entangled H-polymers: Theory, rheology, and neutron-scattering. *Macromol.* (1999) 32, pp. 6734–6758
- [33] Daniels, D.R., McLeish, T.C.B., Crosby, B.J., Young, R.N., Fernyhough, C.M. Molecular rheology of comb polymer melts. Linear viscoelastic response. *Macromol.* (2001) 34, pp. 7025–7033

- [34] McLeish, T.C.B., Milner, S.T. Entangled dynamics and melt flow of branched polymers. *Adv. Polym. Sci.* (1999) 143, pp. 195–256
- [35] Park, S.-J., Larson, R.G. Dilution exponent in the dynamic dilution theory for polymer melts. *J. Rheol.* (2003) 47, pp. 199–211. (This paper contains a typographical error in Section II-C, where it reports that the disentanglement transition occurs at a value of $S_a \Phi = 3$; the correct statement is that this transition occurs at $S_a \Phi^\alpha = 3$.)
- [36] Larson, R.G., Sridhar, T., Leal, L.G., McKinley, G.H., Likhtman, A.E., McLeish, T.C.B. Definitions of entanglement spacing and time constants in the tube model. *J. Rheol.* (2003) 47, pp. 809–818
- [37] Fetters, L.J., Lohse, D.J., Richter, D., Witten, T.A., Zirkel, A. Connection between polymer molecular weight, density, chain dimensions, and melt viscoelastic properties. *Macromol.* (1994) 27, pp. 4639–4647
- [38] Ferry, J.D. *Viscoelastic Properties of Polymers* (1980) Wiley, New York
- [39] Struglinski, M.J., Graessley, W.W. Effects of polydispersity on the linear viscoelastic Properties of entangled polymers. 1. Experimental observations for binary mixtures of linear polybutadiene. *Macromol.* (1985) 18, pp. 2630–2643
- [40] Roovers, J. Properties of the plateau zone of star-branched polybutadienes and polystyrenes. *Polymer* (1985) 26, pp. 1091–1095
- [41] Roovers, J. Tube renewal in the relaxation of 4-arm star polybutadienes in linear polybutadienes, *Macromol.* (1987) 20, pp. 148–152
- [42] Rubinstein, M., Colby, R.H. Self-consistent theory of polydisperse entangled polymers: Linear viscoelasticity of binary blends. *J. Chem. Phys.* (1988) 89, pp. 5291–5306
- [43] Baumgaertel, M., De Rosa, M.E., Machado, J., Masse, M., Winter, H.H. The relaxation time spectrum of nearly monodisperse polybutadiene melts. *Rheol. Acta* (1992) 31, pp. 75–82
- [44] Raju, V.R., Menezes, E.V., Marin, G., Graessley, W.W. Concentration and molecular weight dependence of viscoelastic properties in linear and star polymers. *Macromol.* (1981) 14, pp. 1668–1676
- [45] Struglinski, M.J., Graessley, W.W., Fetters, L.J. Effects of polydispersity on the linear viscoelastic properties of entangled polymers. 3. Experimental observations on binary mixtures of linear and star polybutadienes. *Macromol.* (1988) 21, pp. 783–789
- [46] Fetters, L.J., Kiss, A.D., Pearson, D.S., Quack, G.F., Vitus, F.J. Rheological behavior of star-shaped polymers. *Macromol.* (1993) 26, pp. 647–654
- [47] Pearson, D.S., Mueller, S.J., Fetters, L.J., Hadjichristidis, N. Comparison of the rheological properties of linear and star-branched polyisoprenes in shear and elongational flows. *J. Polym. Sci., Polym. Phys. Ed.* (1983) 21, pp. 2287–2298
- [48] Hadjichristidis, N., Roovers, J. Linear viscoelastic properties of mixtures of 3- and 4-arm polybutadiene stars. *Polymer* (1985) 26, pp. 1087–1090
- [49] Raju, V.R., Rachapudy, H., Graessley, W.W. Properties of amorphous and crystallizable hydrocarbon polymers. IV. Melt rheology of linear and star-branched hydrogenated polybutadiene. *J. Poly. Sci., Polym. Phys. Ed.* (1979) 17, pp. 1223–1235

- [50] Graessley, W.W., Raju, V.R. Some rheological properties of solutions and blends of hydrogenated polybutadiene. *J. Polym. Sci., Polym. Symp.* (1984) 71, pp. 77–93
- [51] Lohse, D.J., Milner, S.T., Fetter, L.J., Xenidou, M., Hadjichristidis, N., Mendelson, R.A., Garcia-Franco, C.A., Lyon, M.K. Well-defined, model long chain branched polyethylene. 2. Melt rheological behavior. *Macromol.* (2002) 35, pp. 3066–3075
- [52] Park, S.-J. private communication (2005)
- [53] Laun, H.M., Schuch, H. Transient elongational viscosities and drawability of polymer melts. *J. Rheol.* (1989) 33, pp. 119–175
- [54] Graessley, W.W. Effect of long branches on the temperature-dependence of viscoelastic properties in polymer melts. *Macromol.* (1982) 15, pp. 1164–1167
- [55] Levine, A.J., Milner, S.T. Star polymers and the failure of time-temperature superposition. *Macromol.* (1998) 31, pp. 8623–8637
- [56] Pattamaprom, C., Larson, R.G., Van Dyke, T.J. Quantitative predictions of linear viscoelastic rheological properties of entangled polymers. *Rheol. Acta* (2000) 39, pp. 517–531
- [57] Park, S.-J., Larson, R.G. A hierarchical algorithm for predicting the linear viscoelastic properties of polymer melts with long-chain branching. *Rheol. Acta* (2005) 44, pp. 319–330
- [58] McLeish, T.C.B., Larson, R.G. Molecular constitutive equations for a class of branched polymers: The pom-pom polymer. *J. Rheol.* (1998) 42, pp. 81–110
- [59] Frischknecht, A.L., Milner, S.T., Pryke, A., Young, R.N., Hawkins, R., McLeish, T.C.B. Rheology of three-arm asymmetric star polymer melts. *Macromol.* (2002) 35, pp. 4801–4819
- [60] van Ruymbeke, E., Bailly, C., Keunings, R., Vlassopoulos, D. A general methodology to predict the linear rheology of branched polymers. *Macromol.* (2006) 39, pp. 6248–6259
- [61] Shull, K.R., Kramer, E.J., Fetter, L.J. Effect of number of arms on diffusion of star polymers. *Nature* (1990) 345, pp. 790–791
- [62] Bacova, P., Lentzakis, H., Read, D.J., Moreno, A.J., Vlassopoulos, D., Das, C. Branch-point motion in architecturally complex polymers: estimation of hopping parameters from computer simulations and experiments. *Macromol.* (2014) 47, pp. 3362–3377
- [63] Wood-Adams, P.M., Dealy, J.M. Using rheological data to determine the branching level in metallocene polyethylenes. *Macromol.* (2000) 33, pp. 7481–7488
- [64] Wood-Adams, P.M., Dealy, J.M. Effect of molecular structure on the linear viscoelastic behavior of polyethylene. *Macromol.* (2000) 33, pp. 7489–7499
- [65] Wang, Z., Chen, X., Larson, R.G. Comparing tube models for predicting the linear rheology of branched polymer melts. *J. Rheol.* (2010) 54, pp. 223–260
- [66] <http://chereresearch.engin.umich.edu/larson/software.html>
- [67] <http://sourceforge.net/projects/bob-rheology>
- [68] van Ruymbeke, E., Keunings, R., Bailly, C. Prediction of linear viscoelastic properties for polydisperse mixtures of entangled star and linear polymers: Modified tube-based model and comparison with experimental results. *J. Non-Newtonian Fluid Mech.* (2005) 1, pp. 7–22

- [69] Ahmadi, M., Bailly, C., Keunings, R., Nekoomanesh, M., Arabi, H., van Ruymbeke, E. Time marching algorithm for predicting the linear rheology of monodisperse comb polymer melts. *Macromol.* (2011) 44, pp. 647–659
- [70] van Ruymbeke, E., Orfanou, K., Kapnistos, M., Iatrou, H., Pitsikalis, M., Hadjichristidis, N., Lohse, D.J., Vlassopoulos, D. Entangled dendritic polymers and beyond: Rheology of symmetric cayley-tree polymers and macromolecular self-assemblies. *Macromol.* (2007) 40, pp. 5941–5952
- [71] Snijkers, F., van Ruymbeke, E., Kim, P., Lee, H., Nikopoulou, A., Chang, T., Hadjichristidis, N., Pathak, J., Vlassopoulos, D. Architectural dispersity in model branched polymers: analysis and rheological consequences. *Macromol.* (2011) 44, pp. 8631–8643
- [72] Hutchings, L.R., Kimani, S.M., Hoyle, D.M., Read, D.J., Das, C., McLeish, T.C.B., Chang, T., Lee, H., Auhl, D. In silico molecular design, synthesis, characterization, and rheology of dendritically branched polymers: Closing the design loop. *ACS Macro Lett.* (2012) 1, pp. 404–408
- [73] Li, S.W., Park, H.E., Dealy, J.M., Maric, M., Lee, M.H., Im, K., Chopi, H., Chang, T., Rahman, M.S., Mays, J. Detecting structural polydispersity in branched polybutadienes. *Macromol.* (2011) 44, pp. 208–214
- [74] Van Ruymbeke, E., Chang, H.K., Nikopoulou, A., Hadjichristidis, N., Snijkers, F., Vlassopoulos, D. Molecular rheology of branched polymers: Decoding and exploring the role of architectural dispersity through a synergy of anionic synthesis, interaction chromatography, rheometry and modeling. *Soft Matter* (2014) 10, pp. 4762–4777
- [75] Chen, X., Shahinur Rahman, M., Lee, H., Mays, J., Chang, T., Larson, R. Combined synthesis, TGIC characterization, and rheological measurement and prediction of symmetric H polybutadienes and their blends with linear and star-shaped polybutadienes. *Macromol.* (2011) 44, pp. 7799–7809
- [76] Li, S.W., Dealy, J.M. Evaluation of molecular linear viscoelastic models for polydisperse H-polybutadienes. *J. Rheol.* (2011) 55, pp. 1341–1373
- [77] Nicol, E., Nicolai T., Durand, D. Effect of random endlinking on the viscoelastic relaxation of entangled star polymers. *Macromol.* (2001) 34, pp. 5205–5215
- [78] den Doelder, J., Das, C., Read, D.J. Exploration of branching topology effects on polymer melt rheology using hierarchical calculation schemes. *Rheol. Acta* (2011) 50, pp. 469–484
- [79] Das, C., Read, D.J., Kelmanson, M.A., McLeish, T.C.B. Dynamic scaling in entangled mean-field gelation polymers. *Phys. Rev. E* (2006) 74, p. 011404
- [80] van Ruymbeke, E., Slot, J.J.M., Kapnistos, M., Steeman P.A.M. Structure and rheology of branched polyamide 6 polymers from their reaction recipe. *Soft Matter* (2013) 9, pp. 6921–6935
- [81] Pladis, P., Meimarooglou, D., Kiparissides, C. Prediction of the viscoelastic behavior of low-density polyethylene produced in high-pressure tubular reactors. *Macromol. React. Eng.* (2015) 9, pp. 271–284
- [82] Read D.J. From reactor to rheology in industrial polymers. *J. Polym. Sci., Part B* (2015) 53, pp. 123–141

- [83] Tobita, H. Simultaneous long-chain branching and random scission: I. Monte Carlo simulation. *J. Polym. Sci., Part B* (2001) 39, pp. 391–403
- [84] Shanbhag, S., Larson, R.G., Takimoto, J., Doi, M. Deviations from dynamic dilution in the terminal relaxation of star polymers. *Phys. Rev. Lett.* (2001) 87, article no. 195502
- [85] Watanabe, H., Matsumiya, Y., Inoue, T. Dielectric and viscoelastic relaxation of highly entangled star polyisoprene: Quantitative test of tube dilation model. *Macromol.* (2002) 35, pp. 2339–2357
- [86] Shanbhag, S., Larson, R.G. A slip link model of branch-point motion in entangled polymers. *Macromol.* (2004) 37, pp. 8160–8166
- [87] Watanabe, H., Matsumiya, Y., Osaki, K. Tube dilation process in star-branched cis-polyisoprenes. *J. Polym. Sci.* (2000) 38, pp. 1024–1036
- [88] Pilyugina, E., Andreev, M., Schieber, J.D. Dielectric relaxation as an independent examination of relaxation mechanisms in entangled polymers using the discrete slip-link model. *Macromol.* (2012) 45, pp. 5728–5743
- [89] Shivokhin, M.E., van Ruymbeke, E., Bailly, C., Kouloumasis, D., Hadjichristidis, N., Liktman, A.E. Understanding constraint release in star/linear polymer blends. *Macromol.* (2014) 47, pp. 2451–2463
- [90] Desai, P.S., Kang, B.-G., Katzarova, M., Hall, R., Huang, Q., Lee, S., Shivokhin, M., Chang, T., Venerus, D.C., Mays, J., Schieber, J.D., Larson, R.G. Challenging tube and slip-link models: Predicting the linear rheology of blends of well-characterized star and linear 1,4-polybutadienes. *Macromol.* (2016) 49, pp. 4964–4977
- [91] Read, D.J., Jagannathan, K., Sukumaran, S.K., Auhl, D. A full-chain constitutive model for bidisperse blends of linear polymers. *J. Rheol.*, (2012) 56, pp. 823–873
- [92] Masubuchi, Y., Ianniruberto, G., Greco, F., Marrucci, G. Primitive chain network simulations for branched polymers. *Rheol. Acta* (2006) 46, pp. 297–303
- [93] Masubuchi, Y., Yaoita, T., Matsumiya, Y., Watanabe, H. Primitive chain network simulations for asymmetric star polymers. *J. Chem. Phys.* (2011) 134, p. 194905
- [94] Masubuchi, Y., Yaoita, T., Matsumiya, Y., Watanabe, H., Marrucci, G., Ianniruberto, G. Primitive Chain Network Simulations for Pom-Pom Polymers in Uniaxial Elongational Flows. *Macromol.* (2014) 47, pp. 3511–3519
- [95] Masubuchi, Y., Matsumiya, Y., Watanabe, H., Shiromoto, S., Tsutsubuchi, M., Togawa, Y. Primitive chain network simulations for comb-branched polymer under step shear deformations *Rheol. Acta* (2012) 51, pp. 193–200
- [96] Juliani, Archer, L.A. Relaxation dynamics of entangled and unentangled multiarm polymer solutions: Comparisons with theory. *Macromol.* (2002) 35, pp. 10048–10053

10

Nonlinear Viscoelasticity

■ 10.1 Introduction

In Chapter 4, it was noted that linear viscoelastic behavior is observed only in deformations that are very small or very slow. The response of a polymer to large, rapid deformations is nonlinear, which means that the stress depends on the magnitude, rate and kinematics of the deformation. The Boltzmann superposition principle is no longer valid, and nonlinear viscoelastic behavior cannot be predicted from linear properties. There exists no general model, i.e., no universal *constitutive equation* or *rheological equation of state* that describes all nonlinear behavior. The constitutive equations that have been developed are of two basic types; empirical continuum models, and those based on a molecular theory. We will briefly describe several examples of each type in this chapter, but since our primary objective is to relate rheological behavior to molecular structure, we will be most interested in models based on molecular phenomena. The most successful molecular models to date are those based on the concept of a molecule in a tube or of slip links, which were introduced in Chapter 6. We therefore begin this chapter with a brief exposition of how nonlinear phenomena are represented in tube models. A much more complete discussion of these models is provided in Chapter 11.

■ 10.2 Nonlinear Phenomena—A Tube Model Interpretation

As was explained in Chapter 6, tube models are based on a picture in which the constraints imposed on a highly entangled polymer molecule (*test chain*) by the surrounding ones are modeled as a *tube* having a characteristic length and diameter [1]. This is an example of a mean-field theory, in which the effects of surrounding molecules on the test chain are averaged together, drastically reducing the computational effort that is required to make rheological predictions compared to that required

for a detailed molecular dynamics model. Tube models have shown promise in the prediction of linear viscoelastic behavior and some types of nonlinear behavior for certain types of molecular structure.

In response to a sudden deformation, the tube is deformed, i.e., the distribution of orientations of the chain segments is shifted from its equilibrium distribution, and the relaxation of a molecule back to its undeformed configuration is constrained by its confinement in the tube. When the imposed deformation is very small, the first relaxation process that occurs is equilibration within the tube, as mentioned briefly in Section 6.3.5. Equilibration involves the redistribution of stress along the chain within the tube. Further relaxation can only occur as a result of the molecule escaping the constraints of the tube, and this requires it to slither along or *reptate* out of its tube. This is a much slower process and is the reason that there is a plateau in the relaxation modulus for entangled polymers with a very narrow molecular weight distribution. This shows up in the linear relaxation spectrum $H(\tau)$ in the form of two peaks, one for each relaxation mechanism. If the molecular weight is not narrow, the shorter molecules making up the tube will relax fast enough to cause a blurring of the tube. In Chapter 6 we called this *constraint release* and noted that it speeds up the relaxation of a longer molecule in its tube. This results in significant relaxation in what would be the plateau zone for a monodisperse sample of the same polymer.

10.2.1 Large Scale Orientation—The Need for a Finite Strain Tensor

The relaxation processes described above apply to linear viscoelastic behavior. If the deformation is not small or slow, the *orientation* of the chain segments may be sufficiently large to cause a nonlinear response. We will see that this effect *alone* can be accounted for in rheological models by simply replacing the infinitesimal strain tensor by one able to describe large deformations; no new relaxation mechanism needs to be invoked. Nonlinear effects related to orientation, such as normal stress differences, can be described qualitatively in this manner.

10.2.2 Chain Retraction and the Damping Function

In a perfect “step” strain, the deformation is so rapid that no polymer relaxation can occur, and the chain is forced to deform affinely. Unless the strain is very small, this requires the chain to stretch beyond its equilibrium tube contour length, and this gives rise to a new relaxation mechanism, *retraction of the chain within its tube*. (Doi and Edwards [1] call this *contour length relaxation*.) Figure 10.1 illustrates this phenomenon schematically. The chain segment on the left having an initial length of R_1 is stretched affinely by a large strain but then retracts to its original length.

This is a fast relaxation process, and once it is completed, the remainder of the relaxation process occurs as in the case of a linear response, i.e., via reptation. The result is a relaxation modulus curve that has an early, rapid decrease, due to retraction, followed by a curve that has the same shape as that for linear behavior. These features can be seen in Fig. 10.2, which shows relaxation modulus data obtained using several strains for a solution of monodisperse polystyrene with $cM = 5 \cdot 10^5$ [2]. Except at the shortest times and the smallest strains, the modulus curves drop to successively lower levels as the strain is increased. Furthermore, the shear stress versus time curves appear to be superposable by a vertical shift on this log-log plot, again except at quite short times.

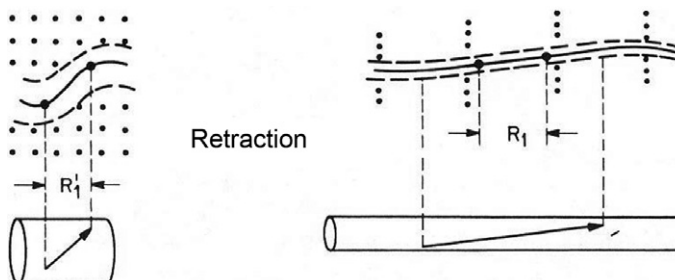


Figure 10.1 Sketch illustrating chain retraction. We see affine deformation of the matrix of constraints (represented by dots) as well as the tube, followed by retraction of the chain within the tube. Affine deformation implies that the microscopic deformation equals the macroscopic strain. After retraction, the chain deformation is non-affine, and the primitive path equals that at equilibrium (drawing from [5]).

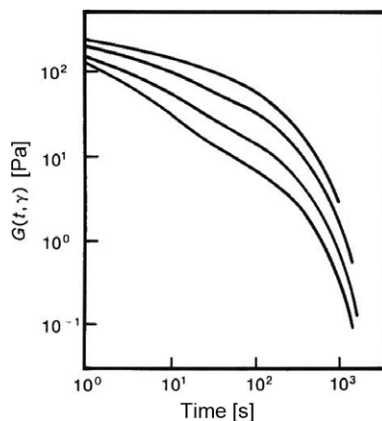


Figure 10.2 Relaxation moduli at several step-strain amplitudes for a polystyrene solution with $cM = 5 \cdot 10^5 \text{ g cm}^{-3}$. At the smallest strain (top curve), the behavior is linear, but as the strain increases, the modulus is reduced except at very short times (off scale). From Osaki et al. [2].

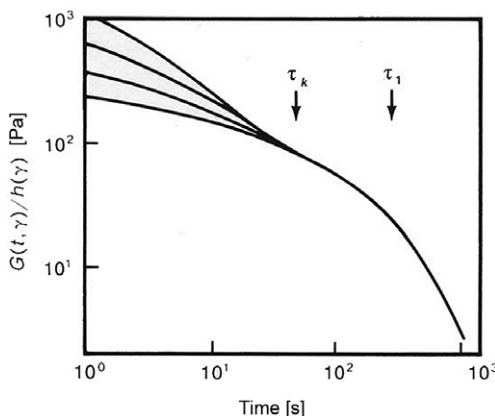


Figure 10.3 Data of Fig. 10.2 replotted as $G(t)/h(\gamma)$. Superposition is achieved by vertical shifting except at times less than τ_k . The longest relaxation time τ_1 is also shown. From Osaki et al. [2].

This implies that the nonlinear relaxation modulus can be separated into time-dependent and strain-dependent factors, as shown by Eq. 10.1.

$$G(t, \gamma) = G(t) h(\gamma) \quad (10.1)$$

The data of Fig. 10.2 are replotted in Fig. 10.3 as the ratio $G(t, \gamma)/h(\gamma)$ versus time. At times greater than τ_k the data superpose demonstrating time-strain separability. The value of τ_k was about 30 s in this case, so the duration of the initial ramp was not a problem in the experiments. Also indicated by an arrow is the longest relaxation time. The superposability implies that the nonlinear relaxation modulus can be separated into time-dependent and strain-dependent factors as shown by Eq. 10.1. This type of stress relaxation is said to exhibit *time-strain separability*, and the factor $h(\gamma)$ is called the *damping function*, which can be thought of as the fraction of the initial stress that is not relaxed by retraction. The behavior of this function for typical melts is discussed in Section 10.4.3, and a quantitative model of the retraction process is described in Chapter 11.

The interpretation of nonlinear stress relaxation using a tube model can be summarized as follows. The small step strain that generates a linear response orients but does not stretch chains. Relaxation then occurs at short times due to equilibration between entanglements within the tube, and at longer times by reptation of the chain out of its tube, with some acceleration of this process due to primitive path fluctuations (contour length fluctuations) (see ref. [1], p. 238). In response to large deformations that cause chain stretch, retraction (contour length relaxation) relaxes the stretch simultaneously with equilibration. Well after the completion of these processes, reptation relaxes the stress arising from the orientation of chain segments in the same way as for small deformations, and the time-dependency of

this final relaxation is therefore the same as in linear viscoelasticity. In this way, the tube-model explains time-strain separability.

10.2.3 Convective Constraint Release and Shear Thinning

We have seen that nonlinear viscoelastic behavior can arise from the orientation of chain segments and from the retraction of the entire chain in its tube. There is one more important new process that can occur, particularly in fast shearing deformations. A serious failure of the original Doi-Edwards theory of nonlinear viscoelasticity (presented in Chapter 11) was its prediction that the shear stress in steady simple shear has a maximum as a function of shear rate. A modification of the model that eliminates this defect was proposed by Marrucci [3] many years later. He proposed a new relaxation mechanism called *convective constraint release* (CCR). (An early version of this idea was proposed in 1965 by Graessley [4].) In steady shear flow, molecules on neighboring streamlines are moving at different speeds, and this carries away entanglements at a rate comparable to the reciprocal of the shear rate. Figure 10.4 illustrates this process schematically. This concept will be used in the interpretation of viscosity data presented later in this chapter. In addition, in steady shear flow this powerful new relaxation mechanism becomes dominant, delaying the onset of chain stretch to shear rates that are generally beyond the limits imposed by flow instabilities and viscous heating in the rheometer.

Convective constraint release strongly suppresses chain stretch in simple shear except at very high strain rates. The degree of stretch depends on the product of the shear rate and a characteristic time governing chain stretch, and this time is expected to be close to the longest Rouse stress relaxation time, τ_R . Since this is often a very small number, and $\dot{\gamma}\tau_R$ must be greater than unity to generate stretch, for many polymers, e.g., linear polyethylene, the shear rate required to generate stretch is not experimentally accessible unless the molecular weight is exceptionally large [4].

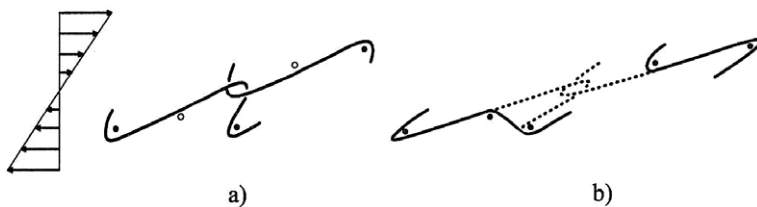


Figure 10.4 Convective constraint release mechanism as envisioned by Ianniruberto and Marrucci. A simple shear field is shown at left and has the effect of sweeping away entanglements originally present in a) allowing the molecules of interest to relax to a new, less constraining entanglement. Filled dots are molecules providing active entanglements; unfilled dots become entanglements after the constraint release.

■ 10.3 Constitutive Equations

The most fundamental approach to calculating the stresses arising in a given deformation is to use a molecular dynamics model based on the principles governing the behavior of individual polymer molecules. Such a model generally consists of the following components:

1. A description of the deformation of chain segments,
2. Calculation of the subsequent relaxation via Brownian motion, and
3. A rule for computing the stresses from the segmental orientation distribution function.

The computational requirements of a molecular dynamics model can be greatly reduced if we make use of averaging to produce a *mean-field model* such as those based on the concept of a molecule in a tube. Here, instead of starting from a detailed picture of the interactions between individual molecules, we focus attention on a single molecule, a *test chain*, and represent the effect of all the surrounding molecules by an average field of constraints. Such models can be used to calculate the response to homogeneous deformations such as step shear and steady-simple shear.

For the simulation of more complex flows, one needs a *constitutive equation (rheological equation of state)*. Most of the many equations that have been proposed over the past 60 years are basically empirical in nature, and only in the last 30 years have such equations been developed on the basis of mean-field molecular theories, *e.g.*, tube and slip-link models. The earlier empirical equations are referred to as continuum models, as they start from fundamental principles of continuum mechanics. The relaxation mechanisms invoked build on concepts such as “network rupture” or “anisotropic friction,” without the molecular detail required to predict *a priori* the dependence of viscoelastic behavior on molecular structure. While these lack a firm molecular basis and thus do not have universal validity or predictive capability, they have been useful in the interpretation of experimental data. In more recent times, constitutive equations have been derived from mean-field models of molecular behavior, and these are described in Chapter 11. We describe in this section a few constitutive equations that have proven useful in one or another way. More complete treatments of this subject are given by Larson [5] and by Bird et al. [6].

Equation 4.4, repeated here as 10.2, can be looked upon as a constitutive equation that describes linear viscoelastic behavior, although it is not a predictive model unless $G(t)$ is specified.

$$\sigma_{ij}(t) = \int_{-\infty}^t G(t-t') \dot{\gamma}_{ij}(t') dt' \quad (10.2)$$

where $\sigma_{ij}(t)$ is the extra stress tensor of a fluid element at time t , and $G(t - t')$ is the relaxation modulus evaluated at a time equal to that which elapsed from previous times t' up to t . As is explained in Section 4.1.1, the extra stress is that part of the stress that is related to deformation and does not include an isotropic contribution to the stress that is not related to deformation in an incompressible material. In a fluid at rest, we call this contribution the pressure, although it is actually the negative of the pressure, since according to the standard sign convention, a compressive stress is a negative quantity. Both the stress and the strain rate tensors have nine components that are functions of time and position in space, but they are symmetrical tensors, so only six components are independent. We recall that the second index on the stress indicates the direction of the force, while the first index indicates the face of a fluid element on which it acts. In this book, we adopt the sign convention that a tensile stress has a positive value. Shear stresses ($i \neq j$) always generate deformation in liquids, but an isotropic normal stress ($i = j$) generates no deformation in an incompressible material, and. Constitutive equations for incompressible materials involve only the extra stress.

Continuum models are usually written as closed-form integral or differential equations. These are empirical equations whose tensorial forms are inspired by the general principles of continuum mechanics [5]. Like all empirical equations, their validity can only be established by the comparison of predictions with experimental data. However, experimental techniques only allow us to study the response of melts to a few simple, homogeneous deformations, *e.g.*, simple shear and uniaxial extension at low deformation rates. Thus, such a model can only be evaluated under these conditions at modest rates of deformation, and there is no certainty that it will be able to describe more complex flows.

10.3.1 Boltzmann Revisited

Before we see how we might modify the Boltzmann superposition principle to deal with large or fast deformations, it will be useful to review the basic elements of this model. This principle was given in the form of Eq. 10.2. It is implicit in this model that the total deformation be sufficiently small that it does not alter the conformation of the molecules to a significant degree. In other words, the response of the material to any new deformation is unaffected by previous deformations. However, molten polymers have a “fading memory,” which means that deformations that occurred sufficiently long ago no longer affect the present state of the melt. This implies that for melts $G(\infty) = 0$. Thus, it is not actually the total strain over all time that is important for linearity but only that which has occurred sufficiently recently that it has not been “forgotten.” This means that a linear response can also be expected if the deformation is sufficiently slow. One way of looking at this is to note that Brownian

motion is always tending to return the molecule to its equilibrium configuration after a deformation, and if the deformation occurs sufficiently slowly, this process is able to “keep up” with the deformation so that the molecule is never significantly removed from its equilibrium or “rest” state.

The most fundamental deficiency of Eq. 10.2 that prevents it from describing nonlinear behavior is that the product of the strain rate tensor and the time interval dt' is not able to describe large strains. In preparation for the introduction of a strain tensor describing finite strain into Eq. 10.2 to correct this deficiency, in an *ad hoc* manner, we rewrite Eq. 10.2 in terms of the infinitesimal strain **tensor**, whose components are γ_{ij} . This tensor is derived in Ref. [7] (see p. 121 therein), and it is totally adequate to describe any type of very small or very slow deformation.

It is important here to recall that a strain tensor is a *relative tensor* that describes the configuration (shape and, for a compressible fluid, volume) of a material element at a given time t_1 relative to its configuration at some reference time t_0 . Thus, the strain is a measure of the amount of deformation that has occurred in a material element between times t_0 and t_1 . A typical component of the infinitesimal strain tensor is $\gamma_{ij}(t_0, t_1)$. If the components of the strain rate tensor at intermediate times are $\dot{\gamma}_{ij}(t'')$, the components of the strain tensor at time t_1 are given by Eq. 10.3.

$$\gamma_{ij}(t_0, t_1) = \int_{t_0}^{t_1} \dot{\gamma}_{ij}(t'') dt'' \quad (10.3)$$

For a cured rubber, there is a unique configuration of a material element that it will always return to when the extra stress is zero, and a time when the element was in this configuration is an obvious choice for the reference time. For a melt, there is no such unique, unstrained state, so some other reference time must be selected. In a laboratory experiment in which the sample is initially in a stress-free configuration, the time at which the deformation begins is an obvious reference time. For example, for a step strain experiment, the relaxation modulus $G(t)$ is measured as a function of the time from the instant of the initial strain ($t = 0$). Thus it is convenient to let the reference time be $t_0 = 0$.

However, in general, as time passes, the configuration at any given time in the past will have less and less relevance to the present state of stress in the sample, which is reflected in the fact that $G(t - t_0 \rightarrow \infty) = 0$. This is because, unlike purely elastic rubbers, a melts have a *fading* memory. Thus, for purposes of writing a general description of linear viscoelastic behavior, i.e., a constitutive equation, the only time during the strain history that is unique and continues to be relevant as time passes is the current time t , i.e., the time at which the stress is being evaluated. Thus, we adopt this as the reference time for use in describing large strains so that the independent strain variable is that occurring at previous times, t' , relative to the

configuration of a fluid element at the present time t . We note that from Eq. 10.1 if the strain rate is always positive:

$$\gamma_{ij}(t,t') = 0 \quad \text{when } t' = t$$

$$\gamma_{ij}(t,t') < 0 \quad \text{when } t' < t$$

We can now write the basic principle of linear viscoelasticity in tensorial form, which gives any component of the stress tensor at time t resulting from strains occurring at past times t' , by integrating Eq. 10.2 by parts and recalling that $G(\infty) = 0$:

$$\sigma_{ij}(t) = \int_{-\infty}^t m(t-t') \gamma_{ij}(t,t') dt' \quad (10.4)$$

where $m(t-t')$ is the linear memory function that is related to $G(t-t')$ as follows:

$$m(t-t') = \frac{dG(t-t')}{dt'} = -\frac{dG(s)}{ds} \quad (10.5)$$

with $s \equiv t - t'$.

10.3.2 Integral Constitutive Equations

Starting from Eq. 10.4, we will see how it might be modified to deal with nonlinear phenomena. The first step is to replace the infinitesimal strain tensor with one able to describe finite strains. But there is no unique way to do this, as there are a number of tensors that can describe the configuration of a material element at one time relative to that at another time. In this book we will make use of the Finger and Cauchy tensors, \mathbf{B} and \mathbf{C} , respectively, which have been found to be most useful in describing nonlinear viscoelasticity. We note that the Finger tensor is the inverse of the Cauchy tensor, i.e., $\mathbf{B} = \mathbf{C}^{-1}$. A strain tensor that appears in constitutive equations derived from tube models is the Doi-Edwards tensor \mathbf{Q} , which is defined below and used in Chapter 9. The definitions of these tensors and their components for shear and uniaxial extension are given in Appendix B.

Lodge [8] started from rubber elasticity models by replacing permanent elastic network strands by temporary strands. He replaced the infinitesimal strain tensor by the Finger tensor to arrive at what he called the *rubberlike liquid model*, which is shown below.

$$\sigma_{ij}(t) = \int_{-\infty}^t m(t-t') B_{ij}(t,t') dt' \quad (10.6)$$

This behavior is sometimes called *finite linear viscoelasticity*. If the memory function in the rubberlike liquid is taken to be the relaxation modulus of a single Maxwell element [$G(t) = G_0 \exp(t/\tau)$], we obtain the special case of the rubberlike liquid that we will call Lodge's equation; this is shown as Eq. 10.7.

$$\sigma_{ij}(t) = G_0 \int_{t'=-\infty}^t \frac{1}{\tau} \exp[-(t-t')/\tau] B_{ij}(t,t') dt' \quad (10.7)$$

This is also the integral form of the differential constitutive equation called the “upper convected Maxwell model,” which is given in the next section. Eq. 10.7 can be generalized to accommodate a spectrum of relaxation times as follows:

$$\sigma_{ij}(t) = \int_{t'=-\infty}^t \sum_{p=1}^N \frac{G_p}{\tau_p} \exp[-(t-t')/\tau_p] B_{ij}(t,t') dt' \quad (10.8)$$

The use of the Finger tensor to build a model for the response of a material to large deformations implies that the deformation is *affine*. This means that the strain at the microscopic level, i.e., of the molecules, is the same as that imposed on the sample. This will require the segments of the chain to orient accordingly and to be stretched or compressed beyond its equilibrium contour length.

The rubberlike liquid model provides qualitative predictions of a few nonlinear phenomena, including a non-zero (but constant) first normal stress difference and strain hardening in all extensional flows. All shear stress responses to simple shear deformations, regardless of time dependency, are the same as in linear viscoelasticity. The use of the Cauchy strain in place of the infinitesimal strain tensor is also unable to describe nonlinearities in a useful way.

An important feature of the rubberlike liquid is that it assumes time-strain separability, meaning that the functions describing the time and strain dependencies are independent of each other. We saw this type of behavior in the response to step shear strain where time dependency is described by the linear relaxation spectrum, and strain dependency is described by a damping function that depends only on strain. All the integral equations introduced in this section have this feature.

The damping function used so far is based on step-shear strain. To generalize this concept to deal with any type of deformation Wagner [9] defined a generalized damping function to deal with any type of deformation. The independent variable needs to involve all the components of the strain tensor, and to accomplish this Wagner let the damping function depend of the first and second *scalar invariants* of the Finger strain tensor. Whereas a vector has one scalar invariant, its magnitude, a tensor has three, one of which is zero for incompressible fluids. The other two are shown below.

$$I_1(\mathbf{B}) = \text{tr } \mathbf{B} = B_{11} + B_{22} + B_{33} \quad (10.9)$$

$$I_2(\mathbf{B}) = \text{tr } \mathbf{C} = C_{11} + C_{22} + C_{33} \quad (10.10)$$

The result, which we call Wagner's equation, is then:

$$\sigma_{ij}(t) = \int_{-\infty}^t m(t-t') h(I_1, I_2) B_{ij}(t, t') dt' \quad (10.11)$$

The damping function $h(I_1, I_2)$ is determined by fitting it to experimental data. The difficulty with this is that data are available only for uniform flows that can be readily generated in the laboratory. Thus, Eq. 10.11 does not have broad predictive capabilities but can be used to reduce a multitude of experimental data to only two material functions, a time-dependent function, e.g. the memory function $m(t) = -dG(t)/dt$, and the strain-dependent function $h(I_1, I_2)$. As a result it has been found useful in the interpretation of experimental data.

Unlike Lodge's rubberlike liquid, Wagner's model predicts shear thinning. We will see later in this chapter that any form of the damping function $h(\gamma)$ that decreases monotonically to a small value at a modest value of strain can provide a rough estimate of the viscosity function. Thus, the form of the damping function has a very weak effect on shear thinning, and this is consistent with predictions of tube models that incorporate convective constraint release.

Eq. 10.11 predicts that the second normal stress difference is zero, and to correct this, it is necessary to introduce the Cauchy stress tensor, and this was the approach of Wagner and Demarmels [10] which is shown below.

$$\sigma_{ij}(t) = \int_{-\infty}^t m(t-t') h(I_1, I_2) [(1+\beta) B_{ij}(t, t') + \beta C_{ij}(t, t')] dt' \quad (10.12)$$

They assumed that the parameter β is constant and found that a value of -0.27 fitted their planar extension data. While it is now understood that the normal stress ratio is a function of strain, it is noted in Section 10.4.5 that it does approach a specific limiting value as $\gamma \rightarrow 0$.

The K-BKZ model [5] also involves both the Finger and Cauchy tensors, but the coefficients of these tensors are derivatives of a strain energy function like the one that describes the free energy of a deformed rubber. A number of variations on the K-BKZ model have been proposed [5].

A constitutive equation developed from a molecular model is that of Doi and Edwards, which was based on the molecule in a tube concept introduced by deGennes. Assuming a system of well-entangled monodisperse linear chains, the predicted memory function is shown by Eq. 10.13.

$$m(t-t') = \frac{8G}{5\tau_d \pi^2} \sum_{p \text{ odd}} \exp\left[-(t-t') p^2 / \tau_d\right] \quad (10.13)$$

The strain dependency is given by the Doi-Edwards strain tensor, $\mathbf{Q}(t', t)$, whose components can be represented in terms of the components of the Finger and Cauchy tensors as follows:

$$Q_{ij}(t) = \varphi_1(I_1, I_2) B_{ij}(t, t') + \varphi_2(I_1, I_2) C_{ij}(t, t') \quad (10.14)$$

The two scalar functions of the invariants of the Finger tensor are described in Section 11.3.1, where the Doi-Edwards equation is discussed in more detail.

The Doi-Edwards equation is able to predict in a semi-quantitative way several nonlinear phenomena, but does not take into account chain stretch. Therefore the tube model on which it is based has been amended in several ways over the past 30 years in order to bring its predictions closer to observations. However, the results are molecular models too complex to be reduced to a single-integral constitutive equation.

To deal with the issue of chain stretch and also take into account polydispersity and branching, Wagner proposed a generalized tube model with strain-dependent tube diameter [11–13]. In his *Molecular Stress Function* (MSF) model, the tube segment stretch f is directly related to the tube diameter a , which decreases from its equilibrium value a_0 with increasing stretch. Thus, the scalar molecular stress function $f(t, t')$ is the inverse of the relative tube diameter, $a_0/a(t, t')$, and depends on the deformation history between the time t' of the creation of a tube segment and the time t of the stress determination. This results in the modification of the Doi-Edwards equation shown below.

$$\sigma_{ij}(t) = \int_{-\infty}^t m(t-t') f^2(t, t') Q_{ij}(t, t') dt' \quad (10.15)$$

The evolution equation for $f(t, t')$ depends on the type of system (solution, melt, linear, branched, monodisperse, polydisperse, etc.), and in the polydisperse case requires two (extensional flows) or three (flows with shear contributions) fitting parameters that are determined from experimental data. A useful review of work using the MSF model is that of Rolón-Garrido [14].

A recent development is the Hierarchical Multi-mode MSF model (HMMSF), which in the polydisperse case allows reduction of the number of parameters to one in extensional flows and two in shear flows. It is based on hierarchical dilution of tube segments with long relaxation times by those with shorter relaxation times, and on interchain tube pressure increasing with decreasing tube diameter. Many examples of its application have been published [15–18].

10.3.3 Differential Constitutive Equations

Equation 10.4, for shear flow with $G(t)$ described by a single Maxwell element (Eq. 4.1), can be written in the form of the differential equation shown below.

$$\tau \frac{d\sigma}{dt} + \sigma = G_0 \tau_0 \dot{\gamma} \quad (10.16)$$

Note that for a step shear strain of γ_0 at $t = 0$, the resulting shear stress is:

$$\sigma(t) = G_0 \gamma_0 e^{-t/\tau_0} \quad (10.17)$$

And for steady simple shear the long-time steady-state stress is:

$$\sigma = G_0 \tau_0 \dot{\gamma} \quad (10.18)$$

The viscosity η_0 is thus $G_0 \tau_0$.

To generalize Eq. 10.16 to describe slow or small deformations having any kinematics, we replace the shear stress and shear rate by the corresponding tensorial quantities to obtain the generalized *Maxwell model*:

$$\tau_0 \frac{d\sigma_{ij}}{dt} + \sigma_{ij} = G_0 \tau_0 \dot{\gamma}_{ij} \quad (10.19)$$

And this simple, two-constant model can be further generalized to accommodate a discrete spectrum of relaxation times by writing Eq. 10.19 for each relaxation mode and summing the stresses resulting from solving each equation.

Just as there are various possible finite strain tensors, there are various time derivatives that can be used in place of the ordinary derivative of stress in Eq. 10.19 to satisfy the continuum mechanics requirements for a model to be able to describe large, rapid deformations in arbitrary coordinate systems. The derivative that yields a differential model equivalent to Lodge's Eq. 10.6 is the *upper convected time derivative* (defined by Eq. 11.19), and the resulting model is called the *upper-convected Maxwell model*. Other possibilities include the *lower-convected derivative* and the *corotational derivative*. Furthermore, a weighted sum of two of these derivatives can be used to formulate a differential constitutive equation for polymeric liquids. In particular, the Gordon-Schowalter convected derivative [5] is defined in this manner.

Differential models obtained by replacing the ordinary time derivative in Eq. 10.19 by one that can describe large, rapid deformations are able to describe some nonlinear viscoelastic phenomena, but only qualitatively. To improve on such models, it is necessary to introduce additional nonlinearity into the equation. In the popular Phan-Thien/Tanner model, the Gordon-Schowalter convected derivative is used, and nonlinearity is introduced by multiplying the stress term by a function of the trace of the stress tensor. The Giesekus and Leonov models are other examples of

nonlinear differential models. All of these models are described in the monograph by Larson [5], and differential equation models based on tube models are presented in Section 11.3.4. Because they are much easier to use to calculate responses to various flows, differential constitutive equations are much preferred and are the principal focus in Chapter 11.

■ 10.4 Nonlinear Stress Relaxation

In the remainder of this chapter we define the principal material functions used to describe nonlinear behavior and describe methods for measuring them. The data presented are interpreted qualitatively in terms of tube model concepts that are developed in detail in Chapter 11. Of particular interest is how nonlinear behavior is influenced by molecular structure. It is demonstrated in Chapter 8 that there is a close relationship between the molecular weight distribution of a linear polymer and its linear viscoelastic behavior. The nonlinear behavior of linear polymers is, in general, not as closely related to MWD as linear behavior, but both the linear and nonlinear properties are strongly affected by long-chain branching structure. Using only data from steady-shear shear experiments, it is difficult to distinguish between the effects of molecular weight distribution and long-chain branching, but extensional flow behavior is quite sensitive to branching, especially when tree-like structures are present.

In defining the material functions that describe responses to simple-shear deformations, a standard frame of reference has been adopted. This is shown in Fig. 10.5. The shear stress σ is the component σ_{21} (equal to σ_{12} because of the symmetry of the stress tensor), and the three normal stresses are: σ_{11} , in the direction of flow (x_1), σ_{22} in the direction of the gradient (x_2), and σ_{33} , in the *neutral* (x_3) direction.

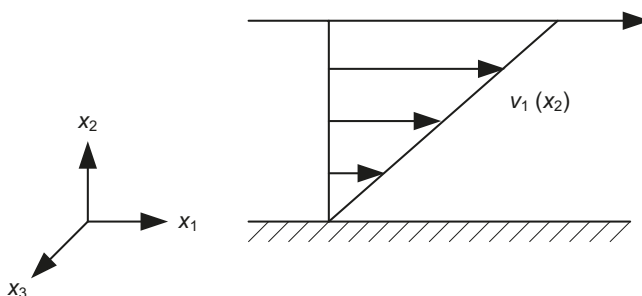


Figure 10.5 Standard coordinate frame for describing simple shear flow. The x_1 coordinate is in the flow direction, x_2 is in the direction of the velocity gradient, and x_3 is in the neutral direction in this two-dimensional flow.

As this is by definition a two-dimensional flow, there is no velocity and no velocity gradient in the x_3 direction. However, in describing shear flow behavior, we will follow the conventional practice of referring to the shear stress as σ , and the shear strain as γ , without subscripts.

10.4.1 Doi and Edwards Predictions of the Damping Function

In order to derive their original constitutive equation, Doi and Edwards assumed that chain stretch is instantly relieved by retraction, so that in effect the chain is never stretched at all and thus does not undergo affine deformation. This model gives a quantitative prediction of the shear damping function for a linear, entangled, mono-disperse polymer that is independent of molecular weight. In fact, there are two DE predictions, one with and one without the “independent alignment” (IA) simplifying assumption, although these damping functions are similar to each other. While avoiding the use of the IA assumption gives a better mathematical representation of the original DE theory, predictions made using DE (with IA) continue to be most commonly compared with observations, perhaps because these were the first to be published and have become, in a sense, the canonical DE predictions. Furthermore, DE (with IA) is also used because it leads to a K-BKZ equation, and without IA, the constitutive equation is much more complicated. In the following, the term DE will be used to refer to predictions with IA. In any event, a number of refinements have been made over the years since the original theory was presented, so neither DE nor DE without IA are the latest word in tube models.

Shown in Fig. 10.6 are the predictions of the DE model, with and without the IA assumption [19]. The experimentally determined values of the damping function were found to lie a bit above the curve of the DE prediction and to be independent of molecular weight when M was greater than about $40 M_e$. The data for the narrow MWD polymer fall very close to the DE prediction, although great importance should not be attached to this quantitative agreement in the light of the discussion above about tube models. Nonetheless, the original theory does a good job of describing the essential features of nonlinear stress relaxation except at short times.

Later developments of the Doi-Edwards theory include relaxation during retraction, and we are interested in how the time scale of this process is related to molecular structure. We also want to compare this time scale with those of the other relaxation processes that follow step strain. A fast process that was first described in Chapter 6 in connection with linear relaxation is equilibration within the tube, which involves only the motion of chain portions between entanglements, i.e., within a single tube segment. This occurs on a time scale of τ_e , which was given by Eq. 6.23. When the strain is large and rapid, the sudden deformation stretches the chain beyond

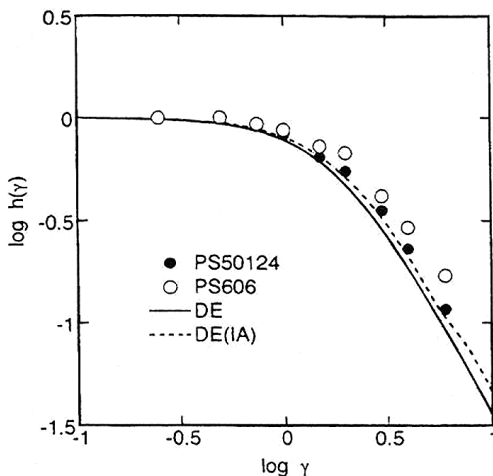


Figure 10.6 Damping functions for polystyrene melts with polydispersity indexes of 1.1 (PS50124) and 2.5 (PS606). Also shown are the DE model predictions with and without the IA assumption which are quite similar to each other. The data for the broad MWD sample are higher, and those for the narrow distribution sample conform more closely to the predicted curves. From Urakawa et al. [19].

its equilibrium contour length. The chain responds to this by retracting back to its equilibrium length, thus relaxing the stress associated with chain stretch. For high-molecular-weight chains, retraction is much faster than reptation, although it is slower than equilibration within the tube, so the chain is still constrained in its tube at the end of the process. The final, much slower relaxation process is reptation, which occurs on a time scale τ_d .

The time after which time-strain superposability is observed is τ_k , and it is of interest to relate this empirically determined quantity to molecular parameters. We noted above that according to the tube model, time-strain separability occurs after the retraction process is completed. The retraction process involves the entire molecule while it is still constrained inside its tube. Thus, since retraction does not require that the chain escape from any entanglements, we expect τ_k to be approximated by the longest Rouse time τ_R of a hypothetical unentangled chain having the molecular weight of the entangled chain of interest. We would also expect that in steady flows, chain stretch will occur when the rate of deformation is greater than $1/\tau_R$.

The damping function is expected to be independent of molecular weight. But since τ_R increases with M , for a sufficiently broad molecular weight distribution, the retraction time of long molecules eventually overlap with the reptation times of the short chains leading to the failure of time-strain separability.

10.4.2 Estimating the Rouse Time of an Entangled Chain

Since the longest Rouse reorientation time τ_r of a hypothetical unentangled molecule with $M \gg M_e$ is not related to the longest relaxation time of an entangled molecule with the same M because of entanglement coupling, it is necessary to estimate its value. Inoue et al. [20] and Roland et al. [21] compared several methods for doing this. These methods are based on various ways of extrapolating the behavior of unentangled polymers to molecular weights well above M_e . One method is based on the viscosity [22, App.]. The Rouse reorientation time of an unentangled polymer was given by Eq. 6.11, which is repeated here as Eq. 10.20. Note that Rouse reorientation time τ_r is equal to the stretch relaxation time, for which we will use the symbol τ_s (see Sections 11.2.1 and 11.3.2). The Rouse reorientation time is two times the Rouse stress relaxation time, τ_R (See Eq. 6.11).

$$\tau_r(M) = \frac{12 \eta_0 M}{\pi^2 \rho R T} \quad (M < M_e) \quad (10.20)$$

where η_0 is the zero-shear viscosity of an unentangled polymer. Thus, if we could estimate the viscosity of a hypothetical unentangled molecule with $M > M_C$, we could use Eq. 10.20 to determine $\tau_r(M)$.

According to the Rouse model the viscosity is proportional to the molecular weight for an unentangled molecule, as was indicated by Eq. 6.12 which is repeated here as Eq. 10.21.

$$\eta_0 = \frac{b^2 M \zeta \rho N_A}{36 M_0^2} \quad (10.21)$$

Now we assume that this linear relationship is valid up to $M = M_C$, where M_C is the critical molecular weight for entanglement introduced in Section 5.2.1. This implies that:

$$\eta_0(M) = \eta_0(M_C) \left(\frac{M}{M_C} \right) \quad (M \leq M_C) \quad (10.22)$$

Then we further assume that this equation describes the hypothetical, unentangled melt with $M > M_C$, and we call the zero-shear viscosity of this hypothetical material η_R .

$$\eta_R = \eta_0(M_C) \left(\frac{M}{M_C} \right) \quad (M \geq M_C) \quad (10.23)$$

For an entangled polymer, we know that the zero-shear viscosity is proportional to M^a , where $a \approx 3.4$, and if this relationship holds at $M = M_C$, then:

$$\eta_0(M) = \eta_0(M_C) \left(\frac{M}{M_C} \right)^a \quad (M \geq M_C) \quad (10.24)$$

We now eliminate $\eta_0(M_C)$ from the above two equations to give:

$$\eta_R(M) = \eta_0(M) \left(\frac{M_C}{M} \right)^{a-1} \quad (M > M_C) \quad (10.25)$$

Inserting this expression for $\eta_R(M)$ into Eq. 6.11 in place of the η_0 of the unentangled melt, we obtain:

$$\tau_r(M) = \frac{12 M \eta_0(M)}{\pi^2 \rho R T} \left(\frac{M_C}{M} \right)^{a-1} \quad (M > M_C) \quad (10.26)$$

Thus, by measuring the zero-shear viscosity of the entangled polymer, we can estimate its longest Rouse reorientation time. A similar method was proposed by Pattamaprom and Larson [23].

10.4.3 Damping Functions of Typical Polymers

The damping function is expected to be independent of molecular weight. But since τ_R increases with M , for a sufficiently broad molecular weight distribution the retraction time of long molecules eventually overlaps with the reptation times of the short chains leading to the failure of time-strain separability.

The study that produced the data shown in Fig. 10.2 [2] included several other solutions, and it was found that molecular weight and concentration had little effect on the damping function for cM around $5 \cdot 10^5$.

Various empirical functions have been used to describe the damping function. Two popular types are shown by Eqs. 10.27 and 10.28.

$$h(\gamma) = e^{-n\gamma} \quad (10.27)$$

$$h(\gamma) = \frac{1}{1 + a\gamma^2} \quad (10.28)$$

Because it leads to expressions that can be evaluated analytically, the power law function given by Eq. 10.27 has been used with integral constitutive equations to predict responses to various shear histories. We note, however, that it approaches its limiting value of one with a non-zero slope as the strain approaches zero.¹ Equation 10.28 does have the correct limiting slope and is often used to describe experimental data for purposes of material characterization. The DE prediction of

¹ The slope should be one according to the general theory of weak viscoelasticity, which is derived by assuming smooth rheological functions. This “simple fluid” theory requires that the first deviation of $h(\gamma)$ from unity should be quadratic in the strain.

$h(\gamma)$ cannot be expressed in a simple explicit form, but Larson (see ref. [5], p. 143) has shown that the DE shear damping function is closely approximated by Eq. 10.28 with $a = 0.2$.

The damping functions of linear, entangled, monodisperse polymers have been found to be in good agreement with the DE prediction for solutions with cM in the range of 40 to 50 M_e , but polydispersity complicates the picture. Venerus et al. [24] found that $h(\gamma)$ for an entangled polystyrene solution with $M_w/M_n = 1.26$ fell slightly above the DE(IA) prediction, while that for a sample with $M_w/M_n = 2.9$ was significantly further from the prediction. And Wagner et al. [25] observed that a commercial HDPE had a damping function that lay significantly above the DE curve. Figure 10.6 shows damping functions of two polystyrene melts one with a narrow MWD and one with a broad one [19]. We note that broadening the molecular weight distribution decreases the damping, i.e., the damping function is higher for the broad-distribution polymer.

There have been some reports of damping much stronger than the DE prediction in melts with $M/M_e > 50$. Figure 10.7 shows this type of behavior as reported by Morrison and Larson [26]. There is apparently a very sharp decrease in the modulus followed by a sudden reversion to separable behavior, sometimes described as a “kink”. This behavior is now known to result from interfacial slip that takes place between bulk polymer and molecules that are strongly adsorbed at the wall [27]. This phenomenon will be mentioned again in Sections 10.9.1.1 and 10.9.4.

In Chapter 5, it was pointed out that the relaxation modulus of linear viscoelasticity is strongly affected by molecular weight, by MWD and by the presence of branches.

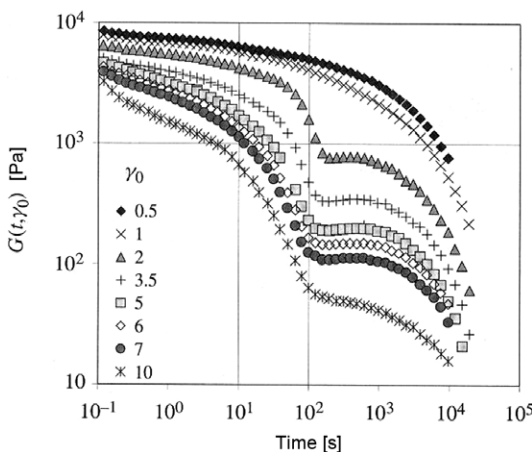


Figure 10.7 Stress relaxation data showing “kinks” when the step strain becomes sufficiently large. It is now believed that this effect results from slip of the sample at the wall of the rheometer. After slip, relaxation proceeds in response to the reduced strain. From Morrison and Larson [26].

However, for linear, entangled polymers, we saw that the damping function is independent of molecular weight over some range of molecular weights, and while it does depend on MWD and branching structure, the dependence is not strong, i.e., the damping function is not very sensitive to molecular structure. Yamaguchi and Takahashi [28] compared low-density polyethylenes produced by autoclave and tubular reactors. These two polymers were known to have markedly different molecular structures, although this did not have a strong effect on the shear damping function. The tubular product has a simpler branching structure, and its damping function did not differ notably from that predicted by the DE prediction. The more complex autoclave product exhibited significantly less damping, i.e., $h(\gamma)$ closer to unity. This was also the observation of Wagner et al. [24] for an autoclave LDPE. Turning to the effect of long-chain branching in model polymers, the damping function for regular star molecules is expected to be the same as that for linear molecules (see ref. [29], p. 1291). This is because the arm of a star recovers its equilibrium length by the same process as a linear chain. Osaki et al. [30], however, observed a modest difference between the damping functions of four-armed stars and linear polystyrene. For more complex branching structures, particularly when there are chain segments with branch points at both ends, there is a definite effect on the damping function, as has been demonstrated by Islam et al. [31], who found that pom-pom molecules and combs exhibit less damping, i.e., h is somewhat closer to unity than it is in linear molecules. McLeish et al. [32] compared experimental data with tube model predictions for H-polymers, which have two arms at each end of a cross-bar segment (see Fig. 2.4). The initial retraction relaxation mechanism for H-molecules involves only the arms, but there is now a new nonlinear relaxation time τ_s that governs the stretch of the cross-bar or backbone of the H. At times greater than τ_s , i.e., in the terminal zone, the behavior is close to the DE prediction, as reptation of the cross-bar is the only remaining relaxation mechanism.

Kasehagen and Macosko [33] used Eq. 10.28 to fit their data for a linear polybutadiene and for several randomly branched samples derived from it. For the linear sample they reported that a value of $a = 0.26$ fitted their data, while for the branched samples, the value of a decreased, reaching $a = 0.07$ for a sample with 39 wt.% branched molecules.

10.4.4 Normal Stress Relaxation

In an incompressible material, normal stresses are themselves of no rheological significance, because if they are equal in all directions they cause no deformation. However, differences between normal stress components are significant, because they cause deformation. For simple shear, the two rheologically significant differ-

ences are the *first and second normal stress differences* N_1 and N_2 , which are defined by Eqs. 10.29 and 10.30.

$$N_1 \equiv \sigma_{11} - \sigma_{22} \quad (10.29)$$

$$N_2 \equiv \sigma_{22} - \sigma_{33} \quad (10.30)$$

For the relaxation of the first normal stress difference following a step strain, the rubberlike liquid model (Eq. 10.6) predicts that:

$$N_1(t) = \gamma^2 G(t) = \gamma \sigma(t) \quad (10.31)$$

This suggests that at sufficiently small strains, the stress ratio (N_1/σ) should become equal to the strain. This relationship is known as the Lodge-Meissner rule [34].

This is similar to the result for an isotropic, perfectly elastic solid (see ref. [8], p. 78), which has a constant modulus of elasticity. This behavior is called neoHookeian.

$$\sigma = G \gamma \quad (10.32)$$

$$N_1 = G \gamma^2 \quad (10.33)$$

Thus, the stress ratio (N_1/σ) is equal to the strain for the perfectly elastic solid.

The Doi-Edwards theory (see ref. [1], p. 253) predicts that the stress ratio is equal to the strain for *all* strains.

$$\frac{N_1(t, \gamma)}{\sigma(t, \gamma)} = \gamma \quad (10.34)$$

This implies that the Lodge-Meissner rule (Eq. 10.31) continues to be valid at large strains. We note that if time-strain superposability is valid, this implies that the transient first normal stress difference is given by Eq. 10.35.

$$N_1(t, \gamma) = \gamma^2 h(\gamma) G(t) \quad (10.35)$$

Or, in terms of the first normal stress relaxation coefficient:

$$\Psi_1(t, \gamma) \equiv \frac{N_1(t, \gamma)}{\gamma^2} = h(\gamma) G(t) \quad (10.36)$$

In fact, this relationship had been previously found to describe experimental data for LDPE for γ up to 30 [35], a polystyrene solution for γ up to at least 8 [36] and polybutadiene solution for γ up to at least 3.3 [37]. It should be noted that the precise measurement of transient normal stress differences requires great care, as it is very difficult to avoid errors due to instrument compliance and temperature variations associated with the operation of the heating/cooling system [33].

It was pointed out in Section 10.4.3 that wall slip can cause a large error in the determination of the strain in step-strain experiments, and the true strain may be much less than the nominal strain inferred from the displacement of a rheometer surface. The observation that N_1/σ is independent of time does not, by itself, imply that there is no slip unless this ratio is also equal to the nominal strain applied. And when the Lodge-Meissner rule is not obeyed, it is often taken as evidence that slip is occurring, and the stress ratio N_1/σ is used in place of the nominal strain as the independent variable in reporting shear stress and normal stress difference data [38].

The second normal stress difference has been found to be negative with a magnitude less than that of N_1 . It is quite sensitive to the assumptions used in deriving a tube model of rheological behavior. A useful material function is the *normal stress relaxation ratio* $\Psi(t, \gamma)$ defined as follows:

$$\Psi(t, \gamma) \equiv \frac{-N_2(t, \gamma)}{N_1(t, \gamma)} = \frac{-\Psi_2(t, \gamma)}{\Psi_1(t, \gamma)} \quad (10.37)$$

The normal stress ratio is predicted by the DE model to be independent of time during a relaxation experiment. In fact, any separable constitutive equation of the BKZ type predicts this result, which implies that:

$$\Psi_2(t, \gamma) = -\Psi(\gamma) \Psi_1(t, \gamma) \quad (10.38)$$

For strains less than one, $\Psi(\gamma)$ approaches a limiting, zero-strain value $\Psi(0)$, often around 0.25. At larger strains it decreases with strain. These trends are revealed in Fig. 10.8, which shows the DE and DE (without IA) predictions together with data for a polystyrene solution and a polyisoprene melt [41]. The predictions of

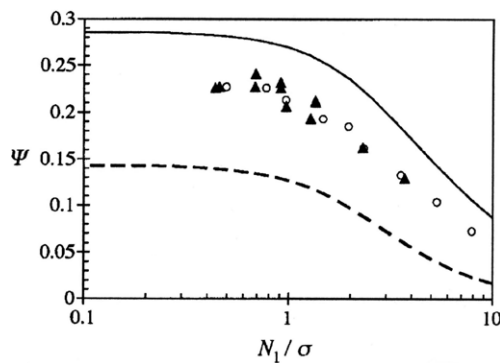


Figure 10.8 Average values of the normal stress ratio over times from 0.1 to 2 s during stress relaxation as a function of the stress ratio, which is assumed to be equal to the strain (Eq. 10.34). Data for a polystyrene solution (circles) and for a polyisoprene melt (triangles) are shown. Also shown are the DE predictions with (dashed) and without (solid) the IA assumption, which show that N_2 is the property most affected by the IA simplification. From Olson et al. [39].

the zero-strain value are 2/7 (DE without IA) and 1/7 (DE). This reflects the fact that among the viscometric functions, the IA approximation affects primarily the second normal stress difference. Because slip is always a potential hazard in step strain experiments with entangled polymeric liquids, the abscissa in Fig. 10.8 is not the imposed strain but that calculated using the Lodge-Meissner relation, i.e., $\gamma = N_1/\sigma$. The experimental data fall between the two predictions but follow their trend very closely. Also, this function appears to be universal for well-entangled systems. Venerus et al. [24] reported values for $\Psi(\gamma)$ for solutions of monodisperse and polydisperse polystyrenes. The data for the monodisperse solution are similar to those of Olson et al. [39], while values for the sample with a broad MWD sample are somewhat higher and closer to the DE prediction.

10.4.5 Double-Step Strain

A deformation history that provides a critical test of constitutive equations is stress relaxation following double-step strain. In this experiment, a strain of γ_1 is introduced at $t = 0$, and a second strain is introduced at $t = t_1$ such that the final total strain is γ_2 . The resulting stress is a function of four parameters, i.e., $\sigma = \sigma(\gamma_1, \gamma_2, t, t_1)$ and is reported only for $t > t_1$. If $\gamma_2 < \gamma_1$, it is a reversing double-step, and if $\gamma_2 = 0$, the second step is equal and opposite to the first one. For the latter test, it has been shown that many constitutive equations, including the DE equation, predict that the shear stress and first normal stress difference obey a relationship that is very similar to the Lodge-Meissner relationship, *viz*,

$$\frac{N_1(\gamma_1, 0, t, t_1)}{\sigma(\gamma_1, 0, t, t_1)} = -\gamma_1 \quad (10.39)$$

This relation, which Venerus et al. [24] call the Osaki-Lodge equation, has been found to be valid for entangled polystyrene solutions [24, 40, 41]. Another quantity of interest is the normal stress ratio defined as:

$$\Psi = -\frac{N_2(\gamma_1, \gamma_2, t, t_1)}{N_1(\gamma_1, \gamma_2, t, t_1)} \quad (10.40)$$

Tube models predict that this ratio is independent of both t and t_1 , and Venerus et al. [24] found it to be valid with $\gamma_1 = 2\gamma_2 = 4$ for a polystyrene solution.

■ 10.5 Dimensionless Groups Used to Plot Rheological Data

10.5.1 The Deborah Number

In plotting the nonlinear response to a transient strain other than step strain, and for comparing data with theoretical predictions, it is sometimes useful to show results in terms of a ratio of times called the *Deborah number* (De). This is a measure of the degree to which elastic behavior is expected in a flow that is unsteady from the point of view of a material element. In other words, it reflects the rate at which elastic energy is either stored or released during an experiment. This dimensionless group is the ratio of a time arising from the fluid's viscoelasticity, i.e., a relaxation time, to a time that is a measure of the duration of the deformation. In simple shear, at steady state when all stresses (and the stored elastic energy) are constant with time, the duration of the flow is unlimited, and De is zero. More generally, De is zero in deformations with constant stretch history (steady from the point of view of a material element) when the stresses are steady. Thus, it is only in transient flows, i.e., when the deformation is unsteady from the point of view of a fluid element, that the Deborah number has a non-zero value. The characteristic time of the deformation depends on the kinematics of the flow. For example, in oscillatory flow it is the reciprocal of the frequency, and in a start-up flow, it is the time t , since at long times no further energy storage occurs. In the case of "silly putty" when we form it into a ball and drop it on a hard surface, the time the ball is in contact with the surface is a small fraction of a second, and this results in a high value of De and purely elastic behavior. But when we squeeze it in our hand, the deformation time is much longer, and the low value of De results in purely viscous behavior. We therefore define De in general terms as follows:

$$\text{De} \equiv \frac{\tau_r}{\text{char. time of transient deformation}} \quad (10.41)$$

The *Weissenberg number* is introduced in the following section to describe the extent of nonlinearity in connection with flows with constant stretch history, i.e., flows in which the deformation rate and all the stresses are constant with time. These are flows in which De is zero. And for deformations in which linear viscoelastic behavior is exhibited, Wi is zero. However, there are also flows of practical importance in which both Wi and De are non-zero, as in LAOS, and are sometimes even directly related to each other. This causes confusion, as authors often use the two groups interchangeably. This situation arises, for example, in the flow from a reservoir into a much smaller channel, either a slit or capillary. A Weissenberg number can readily be defined for this flow as the product of the characteristic time of the fluid and

the shear rate at the wall of the flow channel. However, entrance flow is clearly not a flow with constant stretch history, and the Deborah number is thus non-zero as well and depends on the rate of convergence and length of the channel. The choice of the time constant varies with the phenomenon of interest; for example, it might be τ_R or τ_e . The one used is indicated by a subscript on De.

10.5.2 The Weissenberg Number

The Weissenberg number Wi is the product of a time scale governing the onset of nonlinearity, let's call it λ , and a characteristic rate of strain. We will see in the next section that a fluid that has a shear-rate dependent viscosity must have at least one material constant with units of time. This time then characterizes the nonlinearity of the response. The degree to which a melt deviates from Newtonian behavior depends on how this time constant compares with the rate of the deformation. Thus, the Weissenberg number in steady simple shear is defined as follows:

$$Wi \equiv \dot{\gamma} \lambda \quad (10.42)$$

For steady uniaxial extension with Hencky strain rate $\dot{\varepsilon}$, $Wi = \dot{\varepsilon} \lambda$.

For oscillatory shear the characteristic rate is the shear rate amplitude $\omega\gamma_0$. For single-phase, low-molecular-weight fluids, the time constant of the material is extremely short, so that the Weissenberg number is essentially zero. But for molten, high-molecular-weight polymers, λ can be quite large.

The Weissenberg number also indicates the degree of anisotropy generated by the deformation, i.e., the normal stress differences, which are manifestations of nonlinear viscoelasticity.

■ 10.6 Transient Shear Tests at Finite Rates

10.6.1 Stress Growth and Relaxation in Steady Shear

In *start-up of steady simple shear* under conditions where linear viscoelastic behavior is observed, the shear stress growth function is given by Eq. 4.8, repeated here as Eq. 10.43, and the first and second normal stress differences are zero.

$$\eta^+(t) \equiv \frac{\sigma}{\dot{\gamma}} = \int_0^t G(s) ds \quad (10.43)$$

According to the rubberlike liquid model, the first normal stress difference is given by Eq. 10.44.

$$N_1^+(t) = 2 \dot{\gamma}^2 \int_0^t G(s) s \, ds \quad (10.44)$$

It has, in fact, been observed that both the first and second normal stress differences become quadratic in shear rate in the limit of vanishing shear rate, so that the ratios of normal stress differences to the square of the shear rate have limiting non-zero values as the shear rate approaches zero. This behavior inspired the definitions of the first and second normal stress growth coefficients shown below.

$$\Psi_1^+(t, \dot{\gamma}) \equiv N_1(t, \dot{\gamma}) / \dot{\gamma}^2 \quad (10.45)$$

$$\Psi_2^+(t, \dot{\gamma}) \equiv N_2(t, \dot{\gamma}) / \dot{\gamma}^2 \quad (10.46)$$

And the *shear stress growth coefficient* also becomes a function of shear rate.

$$\eta^+(t, \dot{\gamma}) \equiv \sigma(t, \dot{\gamma}) / \dot{\gamma} \quad (10.47)$$

Linear, low-shear-rate behavior is usually plotted along with the nonlinear data, and the data should approach this at low shear rates. As the shear rate increases, the nonlinear data fall below the linear envelope at shorter and shorter times resulting in a maximum, i.e., an overshoot in the stress [42, 43]. These features can be seen in Fig. 10.9, which shows the data of Menezes and Graessley [44] for shear and first normal stress difference in start-up of simple shear for a solution. The dashed lines are calculated from the linear spectrum using Eqs. 10.43 and 10.44. Start-up shear and normal stress data have been reported for monodisperse polystyrene melts [45]. It is important to note that start-up data are particularly sensitive to edge distortions, often called edge fracture, and this issue is addressed in detail in a later section of this chapter.

The strains γ_S and γ_N at which the maxima occur in the shear stress and first normal stress difference are sometimes used as empirical measures of nonlinearity. Using the exponential damping function (Eq. 10.31) in Wagner's equation (Eq. 10.10) Osaki et al. [40] derived the following relationships:

$$\gamma_S = 1/n$$

$$\gamma_N = 2/n$$

Osaki et al. [42] reported that their data for an entangled polystyrene solution followed closely the prediction that $\gamma_N/\gamma_S = 2$. Schweizer et al. [45] reviewed the results of several studies involving both mono- and polydisperse, entangled solutions and melts. The results of their own and other studies can be summarized as follows. The peak strains for the shear stress, as well as the two normal stress differences level off to constant values below $\dot{\gamma}\tau_d = 10$. For shear stress the peak strain value is between

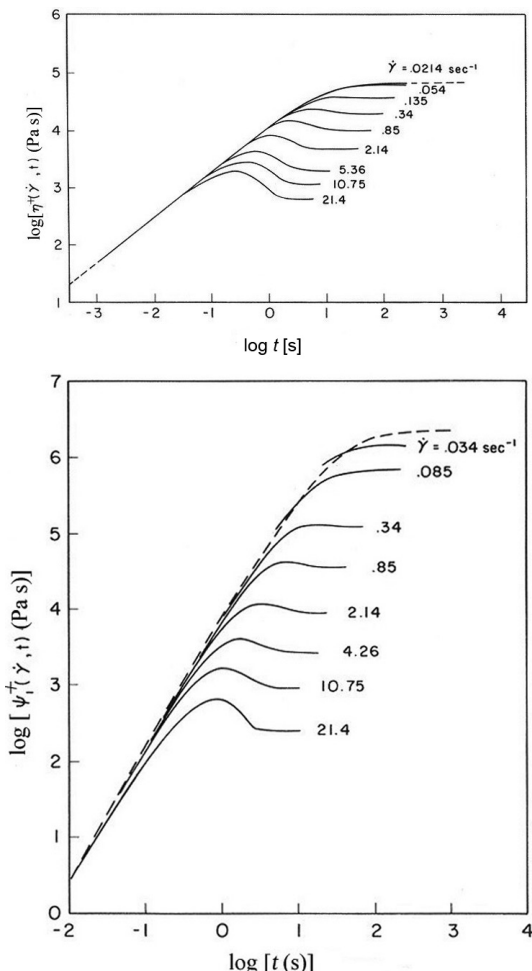


Figure 10.9 Shear (a) and normal stress (b) start-up functions for an entangled polystyrene solution at the shear rates shown (log-log plot). As the shear rate is increased, departures from linear viscoelasticity occur at shorter times, and the overshoot becomes more pronounced. From Menezes and Graessley [44].

2 and 2.3, for N_1 it is between four and five, and for N_2 it is about three. The last value noted is based on data for a monodisperse polystyrene melt. The review [45] also used the ratios of the peak shear stress and normal stress differences to their steady-state values to characterize the nonlinear response and make comparisons with model predictions. There has been some debate as to whether the overshoot arises solely from chain orientation or from chain stretch. Pearson [46] carried out simultaneous shear stress and birefringence measurements on a concentrated polystyrene solution and found that the stress-optical rule held even when $\dot{\gamma} > 1/\tau_R$ and that there is a direct correlation between segment orientation and stress overshoot.

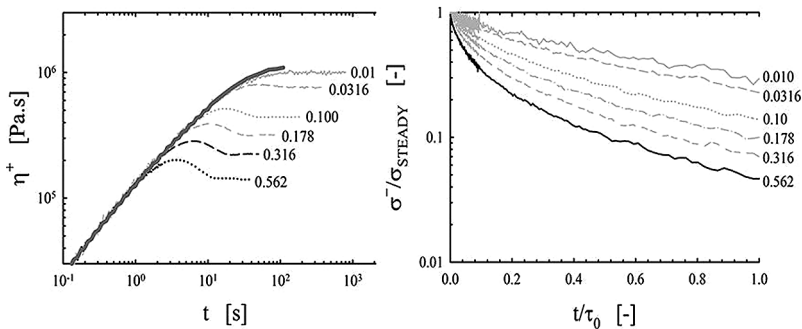


Figure 10.10 Shear stress growth coefficient and shear stress decay stress divided by steady-state stress for a four-armed polystyrene star. From Snijkers et al. [48]

Masubuchi and Watanabe [47] later used a primitive chain network model (PCN) to simulate shear stress start-up flow, and their results verified that the overshoot arises from orientation and not from stretch.

At long times, the stress growth coefficients approach constant values equal to the corresponding viscometric functions of shear rate. These *viscometric functions* are the viscosity and the first and second normal stress differences, which are described in Section 10.7.

There is also a *shear stress decay coefficient* $\eta^- (t, \dot{\gamma})$ that tracks the relaxation of stress after cessation of steady simple shear at a new start time $t = 0$. Figure 10.10 shows the shear stress growth and decay coefficients of a four-armed polyisoprene star [48] with an arm molecular weight of 56 kg/mol at 20 °C for several shear rates. The thick gray line shows the linear viscoelastic behavior. Similar data have been reported for comb polyisoprenes [49]. Stress decay after steady-state shear has been little used as it has turned out to be a sensitive probe of nonlinear behavior.

An interesting variant on start-up and cessation of steady shear is *interrupted shear*, which is used to monitor relaxation processes that occur at very long times. The time at which data can no longer be obtained in a relaxation experiment is governed by the sensitivity of the stress or strain transducer used to monitor the process. In order to obtain information about relaxation that occurs after the stress signal has fallen into the noise level, a series of start-up and cessation tests are performed with increasing *rest time*, i.e., the time between one cessation and the next start-up of flow, t_r . The start-up flow is allowed to continue until the steady-state stress σ_{ss} is reached. In the nonlinear regime, there will be a peak stress $\sigma_m(t_r)$ that is a function of the rest time t_r . This stress will have its maximum in the first test, which takes place when the sample has not been previously sheared, $\sigma_m(\infty)$, and if the rest time is fairly short, the maximum stress in the second test, started at a time t_r after the first ended, will be smaller. In the limit of zero rest time, there is no overshoot, and the stress returns immediately to its steady-state value, i.e., $\sigma_{ss} = \sigma_m(0)$.

Only after a long rest time is the initial maximum stress recovered. Stratton and Butcher [50] first proposed this experiment to characterize entangled polymers and fitted their data to Eq. 10.48.

$$\frac{\sigma_m(t_r) - \sigma_{ss}}{\sigma_m(\infty) - \sigma_{ss}} = \left(1 - e^{-t_r/t_e}\right) \quad (10.48)$$

The fitting parameter, t_e , was found to be much larger than the time required for relaxation after cessation of steady shear. Interrupted shear data have also been reported by Tsang and Dealy [51] for an HDPE.

Robertson et al. [52] reported that for entangled polybutadiene solutions t_e is more than 10 times the disengagement time of the DE theory and that it increases with molecular weight in about the same way as the viscosity. It should be noted, however, that these two characteristic times, τ_d and t_e , are defined in quite different ways and represent different weightings of the fluid's relaxation time spectrum. The fact that they are substantially different, therefore, does not necessarily imply that a new relaxation mechanism is involved.

Roy and Roland [53] studied the interrupted shear behavior of concentrated polyisobutylene and also reported that the characteristic time of the reentanglement process was much longer than that associated with stress relaxation, i.e. that zero-stress does not imply a return to the equilibrium state. They also reported the curious observation that the recovery time did not seem to be related to the shear rate used during the stress growth stages, which is not what molecular theories predict. Furthermore, the time dependencies of the stress growth and recovery processes were the same. Figure 10.11 shows the stress growth coefficient, $\eta + (t, t_r)$ versus time for several values of the rest time, t_r . After a rest time of 240 s, the stress growth behavior has nearly recovered to that starting from a true rest state.

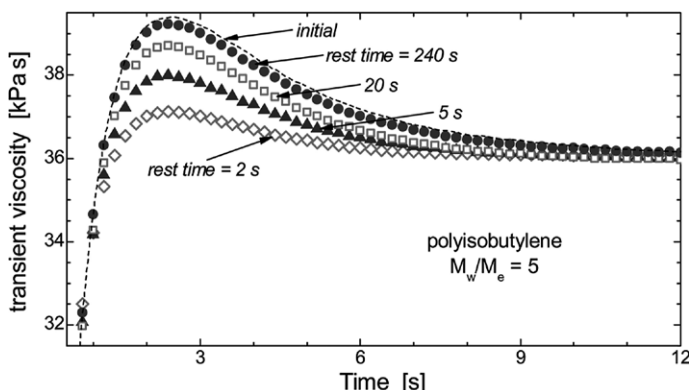


Figure 10.11 Shear stress start-up coefficient after various rest times. The dashed line shows the initial start-up, which is approached after long rest times. From Roy and Roland [53]

10.6.2 Large- and Medium-Amplitude Oscillatory Shear

Over the last decade, many articles have been published on the use of large-amplitude oscillatory shear (LAOS) to study nonlinear viscoelastic behavior. The data are thought to provide information not obtainable from other transient tests such as stress relaxation, start-up of steady shear or creep. In addition, tests can be easily carried out using a standard, rotational, strain-controlled rheometer. The shear strain is sinusoidal, resulting in a Delta peak in frequency space for the displacement. If the strain amplitude is sufficiently large the response is not governed by the Boltzmann superposition principle. Thus the torque is not sinusoidal and cannot be interpreted in terms of the storage and loss moduli. For many years LAOS data were interpreted using a sum of principal and higher harmonics in the torque signal.

It is the view of the authors that only deformations resulting in significant chain stretch provide useful information about molecular structure beyond what can be learned from data in linear regime. Furthermore, shear flow does not generate significant stretch. However, because so much attention has been focused on LAOS and MAOS, a full treatment of this technique and its use is provided here.

Wilhelm et al. [54, 55] proposed a quick and convenient method for determining the higher harmonics using high-sensitivity Fourier transform, a technique that he called “FT-Rheology.” And this provided a convenient method for the interpretation of LAOS data in terms of ratios of higher harmonics to the first harmonic in a spectrum. Figure 10.12 is a sketch showing the appearance of a typical Fourier analysis. During the last decade, there has been an explosion of publications dealing with LAOS, and Hyun et al. [56] published a review of the subject as of 2011.

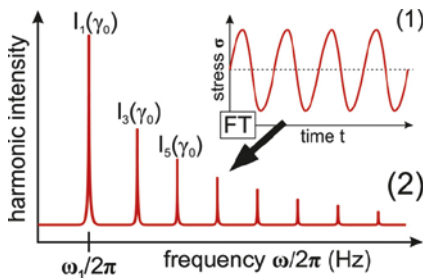


Figure 10.12 Sketch showing appearance of FFT harmonics. From Cziep et al. [63]

LAOS has the interesting feature that the Weissenberg and Deborah numbers can be varied independently. The Weissenberg number, which indicates the degree of nonlinearity expected, is $\tau \dot{\gamma}_0$, where τ is a relaxation time, one choice for which is τ_d in the tube model. The Deborah number, which indicates the degree to which elastic behavior is exhibited, is $\omega \tau$, where τ is the relevant relaxation time, which might be τ_d . A convenient way of representing the parameter space of large-ampli-

tude oscillatory shear is a Pipkin diagram, which is a graph of shear rate amplitude or Weissenberg number ($\dot{\gamma}_0 \tau$) versus frequency or Deborah number ($\omega \tau$) [57]. At very low De we expect behavior consistent with viscometric flow, while at very low Wi linear behavior is expected. Where these two regions overlap, in the lower, left-hand corner we expect to see Newtonian behavior.

The technique usually employed in the past for nonlinear shear studies makes use of cone-plate fixtures in a standard rotational rheometer, since the strain and strain rate, and thus shear stress, are practically uniform throughout the field of flow. But because sample loading is much simpler in parallel disk flow, these have been used in nearly all LAOS tests. However, the use of parallel disks significantly attenuates higher harmonics, since the strain amplitude decreases linearly with r to zero at the center. Data are reported in terms of ratios of higher harmonics to the first, principal, harmonic. It is often assumed that ratios of harmonics in the torque signal using parallel disks are the same as those that would be observed in uniform, cone-plate, shearing, but this is not correct, since the shear stress is not proportional to radius. The general relationship for the torque is given by Eq. 10.49 [58].

$$T = \frac{2\pi R^3}{\gamma_R^3} \int_0^{\gamma_R} \sigma(\gamma) \gamma^2 d\gamma \quad (10.49)$$

When the stress is not linear with radius, its value at $r = R$ can be inferred from the variation of torque with strain at the rim as shown by Eq. 10.50 [59].

$$\sigma(t) = \frac{1}{2\pi R^3} \left[\gamma_R \frac{\partial T(\gamma_R)}{\partial \gamma_R} + 3T(\gamma_R) \right] \quad (10.50)$$

The validity of this relationship to infer shear stress from torque in LAOS tests was verified by Ng et al. [60].

However, numerical differentiation of data amplifies random experimental error (noise). Famini et al. [61] avoid this problem by carrying out a Fourier transform of the torque data, reconstructing the data, and then applying Eq. 10.50 to the in-phase and out-of-phase components of each harmonic.

For a material that is isotropic in structure in its rest state, reversing the direction of shear will change the sign of the shear stress, which means that a Fourier decomposition of the shear stress in oscillatory shear contains only odd harmonics. On the other hand, the sign of the normal stresses and normal stress differences do not change with a reversal of the flow, so that the Fourier decompositions of these quantities have only even harmonics. But even harmonics in the shear stress Fourier spectrum can also result from fixture misalignment, random noise in the data, crosstalk between the torque and normal force sensors or flow instabilities such as slip and edge effects.

The shear stress in LAOS can be expressed as expansions of odd powers of the strain amplitude. One example is as shown below [54].

$$\sigma(t) = \sum_{m=1}^{\infty} \sum_{n=1}^m \gamma_0^n \left[G'_{mn}(\omega) \sin(n\omega) + G''_{mn}(\omega) \cos(n\omega) \right] \quad (10.51)$$

odd odd

The component that has attracted the most attention is the third harmonic of the shear stress series, which can be observed at strain amplitudes in a region just above that for linear behavior, generally between 0.1 and 1.0, although this depends on the polymer, MW and temperature. This region has come to be called *medium amplitude oscillatory shear* (MAOS) [62]. Results are most often reported in terms of the ratio of the third to principal harmonics, $I_{3/1} \equiv I_3/I_1$. Because the Nth Fourier harmonic of the stress increases with the Nth power of γ_0 the ratio of the third to the first harmonics should scale with γ_0^2 at low strain amplitudes, and the *intrinsic nonlinearity* $Q_0(\omega)$ (also called the *zero-strain nonlinearity*) is thus defined as follows:

$$Q_0(\omega) \equiv \lim_{\gamma_0 \rightarrow 0} \frac{I_3/I_1}{\gamma_0^2} \quad (10.52)$$

The symbol ${}^{3/1}Q_0(\omega)$ is also used for the intrinsic nonlinearity of the third harmonic. At sufficiently low frequencies, i.e., in the terminal zone, which is not always experimentally accessible, the intrinsic nonlinearity depends on the frequency and the zero-shear viscosity as shown below [63].

$$Q_0 \propto \frac{\omega^2}{\eta_0}$$

Returning to the problem of inferring stress ratios from those of torque measured using parallel disks, Wagner et al. [64] and Giacomin et al. [65] considered the low Wi regime where the third and fifth harmonics are dominant and assumed that the harmonic amplitudes and their ratios can be described by power laws. This approach resulted in simple “correction factors” for the conversion of torque (T) harmonic ratios to shear stress (σ) harmonic ratios, which Giacomin et al. [65] verified by comparison with experimental data and results for a simple constitutive equation.

$$\frac{\sigma_3}{\sigma_1} = \frac{3}{2} \frac{T_3}{T_1} \quad (10.53)$$

$$\frac{\sigma_5}{\sigma_1} = 2 \frac{T_5}{T_1} \quad (10.54)$$

Thus, in the MAOS regime,

$$Q_0 = \frac{3}{2} \frac{T_3}{T_1} \quad (10.55)$$

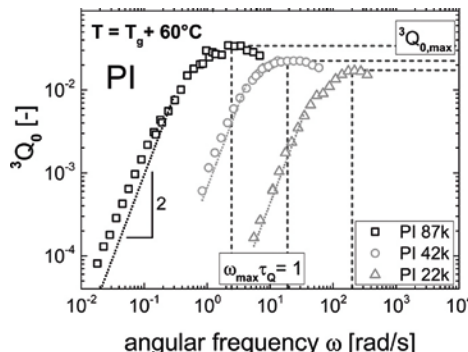


Figure 10.13 Intrinsic nonlinearity of three polyisoprenes having different molecular weights. The maximum values are noted, and the slopes approach two at low frequencies. From Czep et al. [63].

Czep et al. [63] demonstrated the use of this material function to study the behavior of several polymers and compared their results with the predictions of two constitutive equations, the molecular stress function (MSF) model of Wagner and one derived from the “pom-pom” tube model. Figure 10.13 shows their data for three polyisoprenes, where the low frequency data fall close to lines with slopes of two. They also discuss in detail the difficulties involved in making this type of measurement and describe ways of dealing with these. Hoyle et al. [66] reviewed work on the use of MAOS to characterize model branched polymers.

Some reports of LAOS and MAOS work take the view that these shear flows can generate chain stretch, for example [64, 66], but it seems unlikely that significant stretch would occur. As explained in detail in Section 10.4.1 this would require a shear rate greater than the reciprocal of the Rouse stretch time τ_s , i.e., a Weissenberg number ($\omega \tau_s$) greater than unity. Except for samples of very high molecular weight, such a shear rate cannot be achieved due to the occurrence of edge flow instabilities. And such instabilities have been observed in melts during MAOS [67].

An interesting way to visualize LAOS data is to plot the stress versus strain or stress versus strain rate. Such plots are called Lissajous or Lissajous-Bowditch curves. For a Newtonian fluid, stress versus shear rate is a diagonal line in the first and third quadrants. For a shear thinning inelastic fluid, the curve is S-shaped with skew symmetry in the same two quadrants. For a Newtonian fluid a stress versus strain curve would be an ellipse with its major and minor axes vertical and horizontal. For a simple purely elastic material, stress versus strain is a diagonal line, and stress versus rate of strain is an ellipse with its major and minor axes vertical and horizontal. Figure 10.14 shows a group of such plots used by Ewoldt and McKinley [68] to illustrate model predictions. In particular they addressed the origins of secondary loops that sometimes appear. However, the Fourier harmonics provide a much more precise and quantitative picture of the nonlinearity.

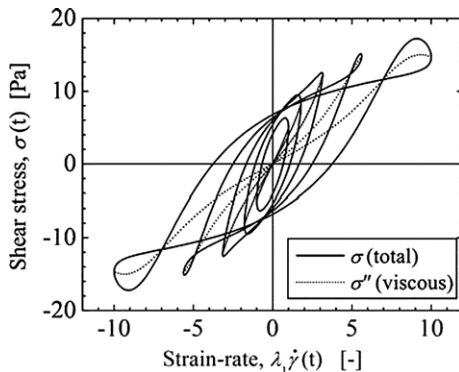


Figure 10.14 Lissajou figures created by plotting shear stress versus Weissenberg number for several levels of nonlinearity. From Ewoldt and McKinley [68].

Ewoldt et al. [69] believe that using Fourier components to characterize nonlinearity fails to reveal important features of the data and propose in its place the use of Chebyshev polynomials, the coefficients of which they use to quantify nonlinear behavior via Lissajous–Bowditch plots. To filter noise, a Fourier transform is first applied to the data, and the data are then reconstructed.

■ 10.7 The Viscometric Functions

If a creep or start-up shearing test is continued until the stresses reach their steady-state values, the rheological response of the material is described completely by three functions of the shear rate. These are the viscosity and the first and second normal stress differences, which were defined by Eqs. 10.29 and 10.30. The three material functions of steady simple shear $\eta(\dot{\gamma})$, $N_1(\dot{\gamma})$, and $N_2(\dot{\gamma})$ are called the *viscometric functions*, and they provide a complete description of the behavior in steady simple shear of an *isotropic* polymer, i.e., one that does not form a liquid crystal or another ordered phase at rest.

10.7.1 Dependence of Viscosity on Shear Rate

Of the viscometric functions, the viscosity is the easiest to measure and the one most often reported. As in the case of Newtonian fluids, the viscosity of a polymer depends on temperature and pressure, but for polymeric fluids it also depends on shear rate, and this dependency is quite sensitive to molecular structure. In particular, the curve of viscosity versus shear rate can be used to infer the molecular weight

distribution of a linear polymer, as is explained in Chapter 8. And in certain cases it can also tell us something about the level of long-chain branching. This curve is also of central importance in plastics processing, where it is directly related to the energy required to extrude a melt.

At sufficiently high shear rates, the viscosity often approaches a power-law relationship with the shear rate. Figure 10.15 is a plot of viscosity versus shear rate for a molten LDPE, and it shows both a low-shear-rate Newtonian region and a high-shear-rate power-law region. This highly branched polymer is valued for the ease with which it can be extruded. This is because the decrease in its viscosity begins at a very low shear rate. This makes the zero-shear viscosity of LDPE very difficult, or impossible, to measure. These data were reported by J. Meissner [70] many years ago but still represent the ultimate in rheometrical technique. He developed a special rheometer to obtain these data.

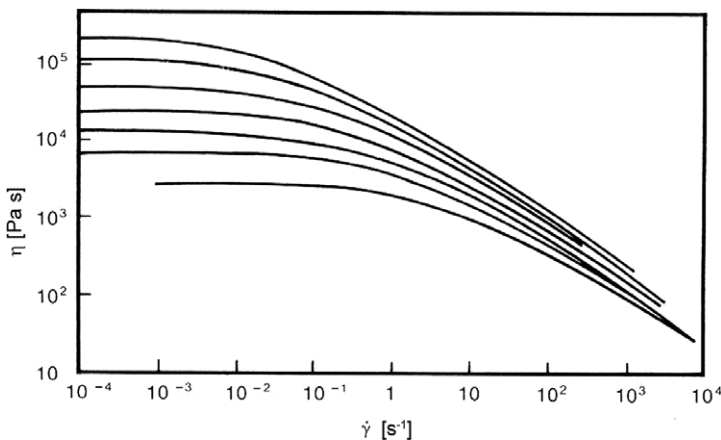


Figure 10.15 Double logarithmic plot of viscosity as a function of shear rate for an LDPE. From top to bottom, the temperatures are: 115, 130, 150, 170, 190, 210 and 240 °C. These data were obtained using a specially modified rotational rheometer that made it possible to reach exceptionally low shear rates.
From Meissner [70].

10.7.1.1 Empirical Viscosity Models

At the highest shear rates shown in Fig. 10.15, the curves tend toward a linear relationship on the log-log plot, implying that a “power law” can be used to represent the variation of viscosity with shear rate at sufficiently high shear rates, as shown by Eq. 10.56.

$$\eta = k(\dot{\gamma})^{n-1} \quad (10.56)$$

It is important to note that this model contains no characteristic time. It thus implies that the power-law parameters are independent of shear rate. Of course such a model cannot describe the low-shear-rate portion of the curve, where the viscosity approaches a constant value. Several empirical equations have been proposed to allow for a transition to Newtonian behavior over a range of shear rates. It was noted in the discussion of the Weissenberg number earlier in this chapter that the variation of η with $\dot{\gamma}$ implies the existence of at least one material property with units of time. The reciprocal of the shear rate at which the extrapolation of the power-law line reaches the value of η_0 is one such characteristic time. Models that can describe the approach to η_0 thus must involve a characteristic time. Examples include the Cross equation [71] and the Carreau equation [72], shown below as Eqs. 10.57 and 10.58 respectively.

$$\eta(\dot{\gamma}) = \eta_0 \left[1 + (\lambda |\dot{\gamma}|)^m \right]^{-1} \quad (\text{Cross equation}) \quad (10.57)$$

$$\eta(\dot{\gamma}) = \eta_0 \left[1 + (\lambda \dot{\gamma})^2 \right]^{-p} \quad (\text{Carreau equation}) \quad (10.58)$$

These models approach power-law behavior at high shear rates, and the dimensionless material constants m and p are simply related to the power law exponent. Hieber and Chiang [73] compared the ability of these two models to fit data for a variety of commercial polymers for purposes of flow simulation. They reported that the Cross equation provided a better fit for the polymers they considered. For more flexibility in fitting data, Yasuda et al. [74] generalized Eq. 10.58 by adding an additional parameter as shown in Eq. 10.59 in order to adjust the curvature in the transition region.

$$\eta(\dot{\gamma}) = \eta_0 \left[1 + (\lambda \dot{\gamma})^a \right]^{(n-1)/a} \quad (10.59)$$

This is often called the Carreau-Yasuda equation.

We note the appearance in these models of a material constant λ with units of time. As mentioned above, such a constant is an essential feature of a rational model for the shear rate dependency of viscosity. Elberli and Shaw [75] compared a number of empirical viscosity equations and found that time constant values obtained by fitting data to two-parameter viscosity models were less sensitive to experimental error than those based on more complex models. The data at low shear rates and in the neighborhood of the reciprocal of the time constant are most critical in obtaining meaningful values of the parameters, while the high shear rate data are important only in regard to the power-law exponent.

Plumley-Karjala et al. [76] evaluated the ability of the models presented above to describe data for a large number of linear and branched metallocene polyethylenes.

They found that the Cross equation gave a good fit to the data and that adding parameters did not lead to a significant improvement. There is no unique procedure for inferring parameter values from data, and different procedures lead to different parameter values. When such equations are fitted to experimental data, information is lost. For example, it is not possible to use such an equation to infer the molecular weight distribution using the methods described in Chapter 8.

Viscosity models are sometimes used to estimate the zero-shear viscosity when no experimental data are available at shear rates sufficiently low that the viscosity is constant. However, this is an unreliable procedure, as there is no fundamental basis for any of these equations, and the resulting value of η_0 should be deemed at best a rough estimate. For example, Kataoka and Ueda [77] found that the Cross equation yielded extrapolated values of η_0 that were about 50% less than measured values.

Graessley [78] suggested that it should be possible to describe the viscosity of all monodisperse, linear, entangled polymers by a single universal curve, if data are plotted as:

$$\frac{\eta}{\eta_0} \text{ versus } \eta_0 J_s^0 \dot{\gamma} \quad (10.60)$$

Berry et al. [79] and Attané et al. [80] published generalized plots based on Eq. 10.60.

10.7.1.2 Viscosity Function in Terms of Tube Models

The original Doi-Edwards model predicted that the shear stress in steady shear increases with shear rate from zero and goes through a maximum. This type of behavior has never been observed, and this remained a basic deficiency of tube models until Ianniruberto and Marrucci [81] introduced the concept of *convective constraint release* (CCR). In steady shear flow, molecules on neighboring streamlines are moving at different speeds, and this carries away entanglements at a rate comparable to the reciprocal of the shear rate. An early version of this idea that predates the tube model was presented in 1965 by Graessley [4].

Ianniruberto and Marrucci [81] interpret the variation of viscosity with shear rate for an entangled, linear, monodisperse polymer as follows. At sufficiently slow shear rates, Brownian motion has plenty of time to keep the molecule in its unstressed configuration, so there is no significant orientation and certainly no chain stretch. This is the limiting, slow-flow, linear viscoelastic behavior in which the shear stress is equal to the zero-shear viscosity times the shear rate. As the shear rate increases and approaches the reciprocal of the reptation time, there is a substantial departure from the zero-shear behavior, with the shear stress becoming nearly independent of the shear rate. In this portion of the stress curve, convective constraint release (CCR) is dominant, and as the flow rate is increased, CCR also increases in pro-

portion to the shear rate, relaxing orientation as fast as it is produced, leading to a saturation of orientation. The shear stress increases slowly with shear rate in this region, with a pseudo-plateau at about $0.6 G_N^0$. This portion of the stress curve is often described by a power law with a small exponent, although this is only an approximation, and the power-law exponent varies from one polymer to another. If the shear rate could be increased to a level near the reciprocal of the Rouse time of the chain, chain stretch would become active, as the rate would be too fast for CCR to keep the chains from stretching. Eventually, chain stretch would also saturate, leading to an upper plateau in the shear stress. Such a stress increase due to chain stretch has rarely been observed, because of the very large value of M/M_e required for $1/\tau_R$ to be within the range of shear rates that are experimentally accessible. However, Bercea et al. [82] were able to reach the chain stretch region by studying a solution of poly(methyl methacrylate) having a molecular weight of about $2.4 \cdot 10^7$.

10.7.1.3 Effect of Molecular Weight Distribution on Viscosity

The effect of molecular weight distribution, MWD, is somewhat more subtle but still very important. In general, commercial polymers have broad molecular weight distributions, although materials produced using metallocene catalysts can have polydispersities (M_w/M_n) as low as two. Figure 10.16 is a sketch of typical viscosity curves for two polymers having the same weight average molecular weight but different molecular weight distributions. The upper curve is for a nearly monodisperse sample, while the lower one is for a sample with a moderately broad MWD. The broadening of the distribution stretches out the range of shear rates over which the transition from the zero-shear viscosity to the power law region occurs. Chapter 8 describes methods for using rheological data to infer the MWD of a linear polymer,

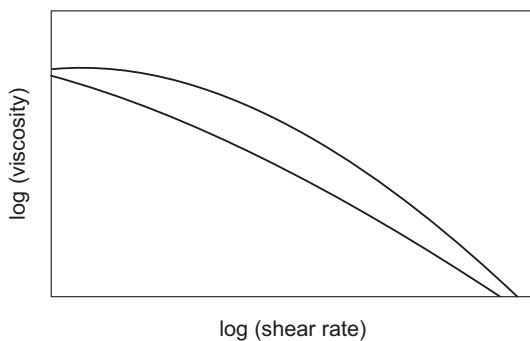


Figure 10.16 Sketch of viscosity versus shear rate curves for samples with narrow (upper curve) and broad (lower curve) molecular weight distributions; both have the same M_w . The narrow MWD sample undergoes the transition from Newtonian to power-law behavior over a narrow range of shear rates, while this range is much broader for the highly polydisperse sample.

but it is to be noted that this requires data of very high accuracy. In the plastics industry it is often desired to estimate polydispersity from easily measured quantities. Shroff and Mavridis [83] compared several empirical correlations that had been proposed to do this.

10.7.1.4 Effect of Long-Chain Branching on Viscosity

In Section 5.10 the effect of branching on the zero-shear viscosity was discussed, and it was pointed out that when the length of the branches of a star are more than about $3 M_e$, η_0 increases approximately exponentially with weight-average molecular weight. The presence of long-chain branching, even at quite low levels, also has a very important effect on the shape of the viscosity curve. This effect is similar to that of broadening the molecular weight distribution, and for this reason, it is not possible, using viscosity data alone, to distinguish between the effect of MWD and that of long-chain branching (LCB), if no other information about molecular structure is available.

Figure 10.17 shows the complex viscosity data of Robertson et al. [84] as a function of frequency for one linear and four branched ethylene/1-butene copolymers. All five samples have nearly the same absolute molecular weight ($M_w \approx 155$ kg/mol), MWD ($M_w/M_n \approx 2$), and comonomer content. Sample A is linear, and the level of long-chain branching increases in the order B-C-D-E. Based on the Cox-Merz

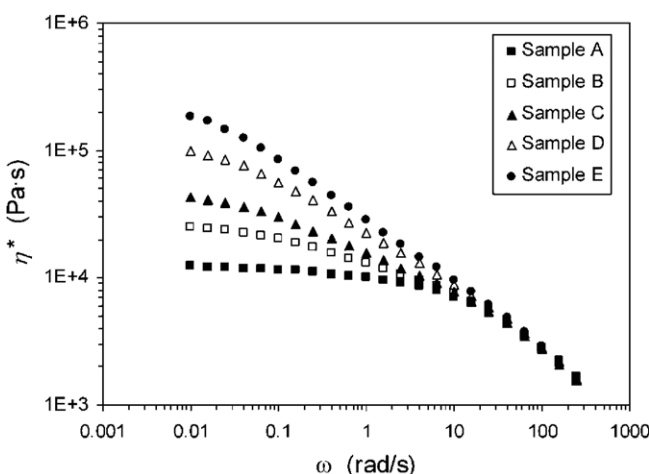


Figure 10.17 Complex viscosity as function of frequency for one linear and four branched ethylene/1-butene copolymers at 190 °C. For all samples $M_w \approx 155$ kg/mol and $M_w/M_n \approx 2$. Sample A is linear, and the level of LCB increases in the order B-C-D-E. As branching increases, the onset of shear thinning shifts to lower frequencies, and the low-shear-rate viscosity increases. At high frequencies, the data for all the samples come together. From Robertson et al. [84].

relationship (Section 10.9.5) it is reasonable to assume that these curves are very similar to those of viscosity versus shear rate. We see that the zero-shear viscosity increases sharply with the level of branching but that all the data converge onto one curve at high shear rates.

Several methods of estimating LCB levels using linear viscoelastic data are described in Section 5.11. A technique based on the shape of the viscosity curve has been proposed for single-site polyethylenes with low levels of LCB. Lai et al. [85] found that for strictly linear polyethylenes prepared using a single-site catalyst, the Cross equation (Eq. 10.57) gives a reasonably good fit to viscosity data. They further showed that the characteristic time λ of the cross equation is proportional to the zero shear viscosity for these materials:

$$\eta_0 = 3.65 \cdot 10^6 \lambda \quad (10.61)$$

They noted that the Cross model (Eq. 10.57) could also be fitted to viscosity data for similar polymers into which a small level of long-chain branching has been introduced but that the presence of the branches caused a departure from the Cross model. They proposed the use of this departure as an indicator of the level of long-chain branching in such materials. To this end, they defined the *Dow Rheology Index*, DRI, as follows:

$$\text{DRI} \equiv \frac{\left(\frac{3.65 \cdot 10^6 \lambda}{\eta_0} - 1 \right)}{10} \quad (10.62)$$

We note that for any material obeying Eq. 10.61, the value of the DRI would be zero, and Lai et al. [85] found that the introduction of long-chain branching resulted in positive values of the DRI and that the value increased with the level of LCB.

Highly branched, heterogeneous polymers such as LDPE have very broad relaxation time spectra, and this results in a very broad range of shear rates over which viscosity data make the transition from the Newtonian limiting value to a power-law region. In fact, it is often impossible to reach the Newtonian value using commercial rheometers, because the shear rate required is extremely low.

It was observed many years ago that when LDPE is sheared, the effect on its rheological behavior is very long-lasting [94]. This phenomenon is called *shear modification*. For example, if this polymer is extruded and immediately converted to pellets, when these pellets are re-melted the properties of the melt are different from those of the polymer originally fed to the extruder. However, if the extruded polymer is allowed to stand in the molten state for a sufficiently long time, it regains its original properties. Shearing in a mixer for a period of one hour was observed to reduce the viscosity, first normal stress difference, and extrudate swell by about 30% [95]. The effect of shearing on extensional flow behavior is particularly strong.

Leblans and Bastiaansen [96] found that five passes through a twin-screw extruder substantially decreased the tendency for strain hardening and reduced the steady-state extensional viscosity by a factor of three.

It has been hypothesized that this phenomenon results from the alignment of the long branches along the backbone. In terms of the tube picture, the branches are drawn into the tube of the backbone during deformation, and a long time is required for the complex molecule to recover its equilibrium configuration. Leblans and Bastiaansen [96] found that the Doi-Edwards strain measure provided a good description of the extensional behavior of sheared LDPE, making its response very similar to that of linear HDPE. This supports the idea that the long branches are drawn into the tube with the backbone by pre-shearing. Bourrigaud et al. [97] modified the tube model for a pom-pom polymer to simulate this phenomenon. Their results indicated that strain hardening can be eliminated by sufficient shear modification and that extensional flow itself should have a much stronger modifying effect than shear.

Yamaguchi and Gogos [98] observed a strong effect of pre-shearing on melt strength. Yamaguchi et al. [99] compared several shearing devices and reported that the continuous shearing that occurs in a twin-screw extruder with conveying screws or in an internal batch mixer much more effective for shear modification than that in a two-roll mill or an extruder equipped with kneading blocks. Yamaguchi and Takahashi [28] found that the melt strength of autoclave LDPE is significantly more sensitive to shear history than that produced in a tubular reactor.

10.7.2 Normal Stress Differences in Steady Simple Shear

From the basic axioms of continuum mechanics, it is possible to show that for a *simple fluid* subjected to a perfectly smooth (infinitely differentiable) strain history the stress tensor is given by an infinite series in terms of Rivlin-Ericksen strain tensors. The first three terms of this series show the earliest departures from Newtonian behavior as the strain rate increases from zero. This truncated series is said to model the behavior of a *second-order fluid*, although this is a misnomer, as it does not describe the behavior of any actual fluid but is rather an approximation of the behavior of a simple fluid in a flow that differs only infinitesimally from the rest state. According to the second-order truncation, in simple shear flow the shear stress is proportional to the shear rate, while the first and second normal stress differences are quadratic in the shear rate. This inspired the definitions of the *first* and *second normal stress coefficients* as follows.

$$\Psi_1(\dot{\gamma}) \equiv N_1(\dot{\gamma})/\dot{\gamma}^2 \quad (10.63)$$

$$\Psi_2(\dot{\gamma}) \equiv N_2(\dot{\gamma})/\dot{\gamma}^2 \quad (10.64)$$

The rubberlike liquid model (Eq. 10.6), predicts that Ψ_1 is independent of shear rate and related to the linear relaxation modulus:

$$\Psi_1 = 2 \int_0^\infty G(s) s \, ds \quad (\text{rubberlike liquid}) \quad (10.65)$$

Experimental observations indicate that at very low shear rates Ψ_1 does, indeed, become independent of shear rate and that its value is given by Eq. 10.65. Its limiting, low-shear-rate value is assigned the symbol $\Psi_{1,0}$. Thus, although the Boltzmann superposition principle indicates that N_1 is zero, $\Psi_{1,0}$ appears as a material constant of linear viscoelasticity. By use of Eqs. 4.30 and 10.63 it can be related to other material constants of linear viscoelasticity:

$$\Psi_{1,0} \equiv \lim_{\dot{\gamma} \rightarrow 0} [\Psi_1(\dot{\gamma})] = 2 \int_0^\infty G(s) s \, ds = 2 \eta_0^2 J_s^0 \quad (10.66)$$

We recall from Chapter 5 that for an entangled, monodisperse polymer J_s^0 is independent of molecular weight. Thus, since viscosity is proportional to M^a , Eq. 10.66 implies that:

$$\Psi_{1,0} \propto M^{2a} \quad (\text{monodisperse}) \quad (10.67)$$

For example, if $a = 3.4$, then $\Psi_{1,0}$ should be proportional to $M^{6.8}$. Wood-Adams [86] reported that even low levels of long branching enhance Ψ_1 much more than the viscosity, especially at low shear rates.

At shear rates beyond those where N_1 is second order in $\dot{\gamma}$ it increases less rapidly with shear rate. Laun [87] found that the empirical relationship given below as Eq. 10.68 was valid for several commercial polymers, and it has also been found to describe data for a narrow-distribution polybutadiene [88].

$$\Psi_1(\dot{\gamma}) = 2 \frac{G'}{\omega^2} \left[1 + \left(\frac{G'}{G''} \right)^2 \right]^{0.7} \quad \text{for } \omega = \dot{\gamma} \quad (10.68)$$

We note that this is like the Cox-Merz relationship presented in Section 10.9.5 in that it relates a nonlinear viscometric function to linear behavior.

At very high shear rates that are generally beyond the range of rotational rheometers, Bercea et al. [82] reported that there is a region of further rapid increase in N_1 . This is in general agreement with the tube model of Ianniruberto and Marrucci [81], which predicts that the first normal stress difference increases little in the region of shear rates where convective constraint release is dominant, and then enters a high-shear-rate region where it becomes proportional to $\dot{\gamma}^{1/2}$.

The dimensionless quantity $N_1(\dot{\gamma})/\sigma(\dot{\gamma})$ is called the *stress ratio*, SR, and indicates the relative importance of orientation or stored elastic energy at a given shear rate. The orientation angle χ , which describes the average orientation of chain segments with respect to the x_1 axis (direction of flow), is related to σ and N_1 as shown below:

$$\tan(2\chi) = \frac{2\sigma}{N_1} = \frac{2}{SR} \quad (10.69)$$

Note that for a Newtonian fluid, in which $N_1 = 0$, the orientation angle is 45 degrees, while for an elastic fluid, beyond the low-shear-rate Newtonian regime, it is less than 45 degrees. Islam et al. [89] reported that the orientation angle for a polybutadiene was constant over an intermediate range of shear rates and equal to about 18 degrees.

A shear-rate dependent relaxation time $\tau(\dot{\gamma})$ is sometimes used to describe the state of a polymer in steady-simple shear. This function is defined as follows:

$$\tau(\dot{\gamma}) = \frac{\Psi_1(\dot{\gamma})}{2\eta(\dot{\gamma})} = \frac{SR}{2\dot{\gamma}} = \frac{N_1(\dot{\gamma})}{2\dot{\gamma}\sigma(\dot{\gamma})} \quad (10.70)$$

In the limit as the shear rate approaches zero, the equations of Chapter 4 can be used to show that the relaxation time $\tau(\dot{\gamma})$ defined by Eq. 10.70 is given by Eq. 10.71.

$$\lim_{\dot{\gamma} \rightarrow 0} \tau(\dot{\gamma}) \equiv \frac{\Psi_{1,0}}{2\eta_0} = J_s^0 \eta_0 = \frac{1}{\eta_0} \sum G_i \tau_i^2 \quad (10.71)$$

The ratio $N_1(\dot{\gamma})/2\sigma(\dot{\gamma})$, i.e., SR/2, is often called the *recoverable shear*. However, it is only equal to the actual ultimate recoil γ_∞ , i.e., the strain recovered after sudden release of the shear stress during steady shear, in the low shear rate limit, as indicated by Eq. 10.72, which is the behavior predicted by the rubberlike liquid model.

$$\lim_{\dot{\gamma} \rightarrow 0} \gamma_\infty(\dot{\gamma}) = \frac{N_1}{2\sigma} = \frac{\Psi_{1,0}}{2\eta_0} \dot{\gamma} \quad (10.72)$$

Laun [87] measured the ultimate recoil (recoverable strain) of an autoclave LDPE, and his data are shown in Fig. 10.18 along with the “recoverable shear,” defined above as $N_1(\dot{\gamma})/2\sigma(\dot{\gamma})$, and the predictions of Wagner’s equation, Eq. 10.11, with an exponential damping function [90]. While there is good agreement with Wagner’s equation, the recoverable strain data fall well above the “recoverable shear.” He also found that there was good agreement with the following empirical equation, which has some similarity to Eq. 10.68:

$$\gamma_\infty(\dot{\gamma}) = \frac{G'}{G''} \left[1 + \left(\frac{G'}{G''} \right)^2 \right]^{1.5} \quad \text{for } \omega = \dot{\gamma} \quad (10.73)$$

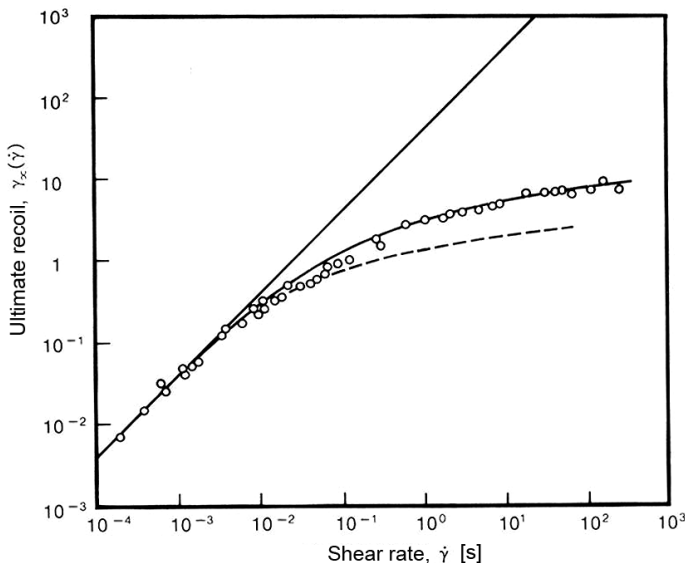


Figure 10.18 Recoverable shear for steady simple shear for an LDPE. Also shown is the shear-rate dependent recoverable shear $N_2(\dot{\gamma})/2\sigma(\dot{\gamma})$ (dashed line), the predictions of the rubberlike liquid model (straight line, from Eq. 10.6) and Wagner's equation (solid curve, from Eq. 10.11). From Laun [87].

The second normal stress difference is usually reported in relation to the first normal stress difference using the shear-rate dependent normal stress ratio:

$$\Psi(\dot{\gamma}) \equiv \frac{-\Psi_2(\dot{\gamma})}{\Psi_1(\dot{\gamma})} = \frac{-N_2(\dot{\gamma})}{N_1(\dot{\gamma})} \quad (10.74)$$

We indicate the dependence on shear rate to avoid confusion with the functions used to describe stress relaxation functions, which are functions of time and *strain*. The DE model predicts that $\Psi(\dot{\gamma})$ is a universal function of $(\dot{\gamma}\tau_d)$ for all entangled polymers (see ref. [91], p. 44). The predicted limiting zero-shear rate values are 2/7 or 0.29 (DE-IA) and 1/7 or 0.14 (DE). Based on their low-shear rate data Magda et al. [92] reported that this limiting value was about 0.2 for linear polymer solutions, and Schweizer et al. [45] found it to be 0.24 in linear melts, while Lee et al. [93] reported that it was about 0.3 for stars. Given the uncertainties in the data and the weak dependencies on the molecular weight and its distribution, a safe conclusion is that for entangled polymers, the limiting, low-shear-rate value of the normal stress ratio is in the range of 0.2 to 0.3. As in the case of stress relaxation, the IA approximation affects the second normal stress much more than it does the first normal stress difference or the shear stress.

■ 10.8 Experimental Methods for Shear Measurements

It is important to understand the capabilities of various melt rheometers, as these limit our ability to explore structure-property relationships, and in particular to evaluate molecular models for rheological behavior. A rotational rheometer with cone-plate fixtures is the instrument universally used for the study of nonlinear shear behavior, since the strain and shear rate are, in principle, uniform throughout the field of flow. But deviations from this ideal flow limit precision and shear rate range, as is discussed in detail below.

10.8.1 Rotational Rheometers

Shear stress is inferred from the torque M , and the first normal stress difference is inferred from the normal force F , as shown by Eqs. 10.75 and 10.76. Measurement of the second normal stress difference is discussed in Section 10.8.1.3.

$$\sigma = 3 M / 2 \pi R^3 \quad (10.75)$$

$$N_1 = 2 F / \pi R^2 \quad (10.76)$$

$$\dot{\gamma} = \Omega / \Theta_0 \quad (10.77)$$

where Ω is the rotational speed (rad/s) and Θ_0 is the cone angle in radians.

Controlled strain is the preferred mode of operation for nonlinear studies. A fundamental uncertainty in cone-plate data arises from the precision with which the cone can be fabricated and its final geometry established. In order to avoid problems arising from a sharp apex, the cones are always truncated, and in setting the gap, the virtual height of the missing cone must be calculated. This requires the precise measurement of the cone angle and the diameter of the circular area exposed by the truncation. Mackay and Dick sent a cone to several laboratories for measurement and reported the results [100]. Their conclusion was that the absolute minimum error in the measured shear stress due to uncertainties in the cone angle and truncation height is $\pm 2.5\%$. For a given cone, this represents a constant bias, or error in accuracy, and random errors would be superposed on this. Inserting a sample and setting the gap are sources of random error. Minimizing random errors requires many repeat measurements so that the statistical significance of each point can be evaluated.

Instrument compliance is another cause of concern in making mechanical measurements, since the forces generated by the fluid in response to a deformation will tend to twist, bend, or compress the rheometer components that also experience these forces.

These include shear and normal force transducers as well as the frame of the instrument. Instrument manufacturers compensate for this using one of several techniques, one of which was described by Vermant et al. [101]. In the case of torsional motion, there remains some compliance due to the twisting of the shafts supporting the fixtures. And thermal expansion resulting from the power consumed by the transducer can affect the gap spacing.

The measurement of normal stress differences in transient deformations is extremely sensitive to small variations in gap spacing, which can arise from instrument compliance or small temperature variations. Venerus and Kahvand [41] showed how to evaluate the effect of instrument compliance by measuring the response using several sets of cone-plate fixtures. If a Force Rebalance Transducer is used for a transient normal stress measurement to compensate continuously for compliance in order to keep the gap constant, the response time of the transducer may affect the data. Also, the thermal expansion that results from the power dissipated in the transducer is of particular concern when normal stresses are being measured.

For the shearing to be homogeneous the edge surface should be a segment of a sphere centered at the tip of the cone, but it is impossible to achieve this condition precisely. A common practice is to use a sample large enough to fill the rheometer with its gap set a bit larger than the one to be used. The sample is then trimmed even with the edges of the fixtures and the gap set to its final value. (This requires the cone and plate to have the same diameters.) The second normal stress difference is especially sensitive to the edge condition. There are also uncertainties associated with trimming the edges of the sample and controlling the temperature of the sample. Overall, even with the best possible practice, using commercial rheometers, the best accuracy that can be achieved is about $\pm 3\%$.

10.8.1.1 Generating Step Strain

While step strain is the deformation used to determine the relaxation modulus it is not possible, in practice, to impose a truly instantaneous strain. The moving rheometer components and the fluid have mass and cannot be instantaneously accelerated. Even if a powerful motor is used to generate the deformation, there remains the problem of controlling its motion. If the motor controller is tuned to give a very fast response, there will be an overshoot and ringing, and if it is tuned to avoid this entirely, the result will be a rounded ramp instead of a step. Laun [102] and Venerus and Kahvand [41] discussed this problem and how it might be addressed. To analyze the effect of the initial transient, one approach is to model the “step” as a ramp with a duration of δ , so that the actual shear rate is taken to be γ/δ rather than infinity. The law of the mean tells us that the stress response $\sigma(t)$ is related to that for an ideal step strain $\gamma G(t)$ as follows:

$$\sigma(t) = \gamma G(t + \epsilon \delta) \quad (10.78)$$

where ε is a number between zero and one. Thus, for $t \gg \delta$, the measured response becomes indistinguishable from the ideal response. From a practical point of view this means that as long as the first data point used in the viscoelastic characterization of the material corresponds to a time much greater than δ , the non-zero duration of the step will have no significant effect on the result. A useful rule of thumb is that data should not be deemed to represent the true behavior of the melt until $t > 10 \delta$. For high-molecular-weight melts, this is generally not a problem, because these materials have relatively slow relaxation mechanisms. Laun [102] proposed a procedure to correct data at shorter times ($t < 10 \delta$) to approximate the initial portion of relaxation modulus curve. Venerus and Kahvand [41] also discussed this problem, as did Flory and McKenna [103], who compared two methods for estimating the true relaxation modulus from experimental data.

Wall slip occurs in all shear flows of entangled polymers when the shear stress is sufficiently large for a sufficient length of time, and this phenomenon limits the strains that can be used in stress relaxation experiments. Figure 10.7 showed anomalous behavior in step shear that has been shown to result from wall slip [27]. Archer et al. [104, 105] used tracer particles to examine the detailed velocity distribution in a cone-plate rheometer and demonstrated that at large strains, much of the strain imposed by the rotating member is “lost due to slip or, more-likely, stress-induced disentanglement within a micron-thick layer of each wall.”

10.8.1.2 Flow Irregularities in Cone-Plate Rheometers

Several flow irregularities occur in the cone-plate flow of molten polymers, and these limit the use of these fixtures to use at low shear rates [106]. The circular streamlines assumed for cone-plate flow can become unstable when N_2 is large. This instability leads to a secondary flow that increases in strength as the cone angle is increased [106]. Other flow irregularities manifest themselves as visible distortions at the edge of the sample. Edge fracture starts as an axisymmetric indentation in the meniscus [107], and as the shear rate increases the indentation develops into a crack that penetrates into the sample, leading eventually to severe breakup and debonding [108]. Chen et al. [109] observed “fractures” in oscillatory shear using cone-plate fixtures at both large and small strain amplitudes, even in unentangled melts, leading to a decrease in the stress amplitude and the appearance of higher harmonics in the stress waveform. The onset of this instability has been associated with the second normal stress difference, occurring when $(-N_2)$ exceeds a critical value [110]. A second irregularity whose effects can be observed at the edge of the sample involves *edge vortices*, which are the ends of cone-shaped eddies that extend to the flow axis [111, 112]. This instability appears to be associated with the first normal stress difference [106]. This type of irregularity has also been observed in large-amplitude oscillatory shear.

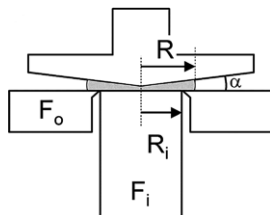


Figure 10.19 Cone partitioned plate fixture designed to eliminate edge effects. Torque is measured only on the inner surface with radius R_i . From Schweizer [114].

Another observation that may be related to this was made by Larson [113] while studying the response of a LDPE to step strain in a cone-plate rheometer. He found that for strains larger than two the edge took on a “braided” appearance and that it was necessary to wait several hours after this had happened to again obtain reproducible results with the same sample.

Schweizer [114] showed that it is possible to avoid the effect of edge fracture by use of a cone-partitioned plate (CPP) fixtures to determine the viscosity at shear rates up to 100 s^{-1} for a commercial polystyrene. This device is sketched in Fig. 10.19. Only the torque on the inner plate is measured. The use of the CPP fixture requires an SMT (separate motor, transducer) rheometer and is not yet in wide use.

The selection of a cone angle requires a compromise between a small angle, to prevent edge fracture and minimize viscous heating, and a large angle to minimize gap variation due to instrument compliance. An angle above six degrees is usually selected, although this accelerates edge fracture.

Schweizer and Stöckli [115] measured the velocity profile near the edge of polystyrene melts and found that the velocity profile is nonlinear immediately and that the nonlinearity increases with time; it also depends on the cone angle and relaxation time of the polymer. They provide advice on shaping the rim.

The first normal stress difference is usually determined by measuring the normal thrust F exerted on the plate using Eq. 10.76. The normal thrust is strongly affected by changes in the gap and by axial instrument compliance, as these can cause squeezing or stretching of the sample. It also varies with temperature much more than the shear stress, so temperature control and measurement are critical.

10.8.1.3 Measurement of the Second Normal Stress Difference

The second normal stress difference is the most difficult to measure of the three viscometric functions. One technique that has been used is based on the following relationship.

$$\frac{\partial \sigma_{\theta\theta}}{\partial \ln r} = N_1 + 2 N_2 \quad (10.79)$$

The stress component shown is the normal stress acting on the plate, and this method requires the measurement of the radial distribution of this stress. Miller and Christiansen [116] mounted very small pressure transducers in the plate to determine this distribution, but the development of a plate incorporating micro miniature sensors makes this measurement much easier and more reliable [117]. Alcoutlabi et al. [118] compared results for a polyisobutylene using two pressure-distribution methods, one using cone-plate geometry and the other using plate-plate geometry. They also evaluated a method involving total force measurements made using both cone-plate and plate-plate fixtures.

Another method makes use of the CPP (cone partitioned plate) fixture mentioned above, which is based on Eq. 10.79. But instead of making a direct measurement of the radial normal stress gradient, the usual monolithic plate is replaced by one partitioned into two concentric parts, an inner disk with a radius R_i , and an outer ring whose radius R_0 the same as that of the cone [119]. The normal force transducer responds only to the thrust F_i on the inner disk. Data are collected for several samples having radii R between R_i and R_0 and the measured thrust F_i is related to N_1 and N_2 as shown by Eq. 10.80:

$$\frac{2 F_i}{\pi R_i^2} = N_1 + 2(N_1 + 2 N_2) \ln\left(\frac{R}{R_i}\right) \quad (10.80)$$

When $R_i = R$, N_1 can be calculated from F_i using Eq. 10.80, which reduces to Eq. 10.76. Schweizer [114] reported that a cone angle of 0.148 rad minimized instrument compliance while generating a nearly homogeneous strain. He noted that this technique requires great skill, as the fixtures are delicate and the experiments are time consuming. Also a number of samples are required. Schweizer [114] used this technique to study a polystyrene melt and found that the normal stress ratio Ψ was 0.24 at a shear rate of 0.1 s^{-1} and decreased to 0.05 at 30 s^{-1} . Schweizer et al. [45] used the cone/partitioned plate method to obtain transient normal stress data for a polystyrene melt and reported that axial compliance and the normal force range caused problems. Schweizer and Schmidheiny [120] added a third plate partition (CPP3) to suppress edge effects, and this improved the accuracy of the steady state value of N_2 , but it was not suitable for use with melts because of rheometer frame compliance.

10.8.2 Sliding Plate Rheometers

The sliding plate melt rheometer was developed to make measurements of nonlinear viscoelastic behavior under conditions where cone-plate flow is unstable, i.e., in large, rapid deformations [121]. The sample is placed between two rectangular

plates, one of which translates relative to the other, generating, in principle, an ideal rectilinear simple shear deformation. In order to avoid edge and end effects associated with total force measurements, a shear stress transducer was introduced to detect the shear stress directly in the center of the sample rather than inferring it from the x-direction force on a plate. Such instruments have been used to determine the shear stress response to large, transient deformations [122, 123] as well as the first normal stress difference at high shear rates [90]. In addition they have been used to determine the effect of pressure on the viscosity and nonlinear behavior of melts [124, 125]. Their advantage over capillary instruments for high-pressure measurements is that the pressure and shear rate in the sample are uniform [126]. Many years of experience with sliding plate rheometers have revealed several phenomena that limit their utility under certain conditions. First, normal stress differences create a pressure gradient in the sample that tends to pump melt in from the ends of the sample and out toward the edges [122, 123]. This flow can be eliminated by the use of fluorocarbon side-rails. More serious limitations are imposed by slip and rupture, which interrupt experiments at sufficiently high strains and strain rates. High-molecular-weight elastomers are particularly resistant to shearing deformations and even the use of deep grooves in the plates does not ensure their adherence [124].

At the same time, sliding plate rheometers have been found to be useful tools for the study of melt slip [127–130]. Wall slip is known to be time-dependent, and sliding plate rheometers are the ideal tools to explore this phenomenon and provide data to formulate models of time-dependent slip [131]. Because the plate velocity, which is the sum of the wall velocity and the slip velocity, can be varied continuously, it is possible to produce a continuous curve of shear stress versus slip velocity showing clearly that there is a maximum followed by minimum [132]. This explains the origin of the “spurt flow” and oscillatory flow phenomena that occur in capillary flow.

10.8.3 Optical Methods—Flow Birefringence

Techniques used for shear flow experiments and for extensional flow measurements are quite different. However, one technique that is applicable to both types of flow is polarimetry. This is a nonmechanical method for measuring stresses when the sample is transparent and polarizable and its molecules become oriented under stress. Such a material is said to be birefringent under deformation. The components of the birefringence tensor are often proportional to the components of the stress tensor, and this relationship is called the *stress-optic law*. The orientation angle in Eq. 10.69 can be measured using this technique. Fuller's monograph [133] is a valuable source on this subject, and a useful introduction is that of T.P. Lodge [134].

This technique is useful with transparent materials that have reasonably large values of the stress-optic coefficient. It has been used successfully to study both shear and extensional flows [135], but if the deformation generates significant chain stretch, the stress-optic rule is no longer valid [135]. Olson et al. [136] measured the second normal stress difference using beams inclined at several angles to find the components of the refractive index tensor.

To determine transient normal stress difference, the phase-modulated polarization technique was developed by Frattini and Fuller [137]. Kalogrianitis and van Egmond [138] used this technique to determine the shear stress and both normal stress differences as functions of time in start-up of steady simple shear. Optical techniques are particularly attractive for measurements of normal stress differences, since such methods do not require the use of a mechanical transducer that is subject to compliance error.

10.8.4 Capillary and Slit Rheometers

Pressure-driven rheometers, particularly capillary instruments, are the rheological workhorses of the plastics industry, as they are relatively simple and easy to use, even for melts at high temperatures. In most capillary rheometers, the flow is generated by a piston moving in a cylindrical reservoir to drive the melt through a small capillary, which often has a diameter of about one millimeter. Also used are instruments in which the driving pressure is the controlled variable, and the flow rate is measured. The latter are often referred to as constant-stress rheometers, but this is not an accurate description, because, as explained below, the driving pressure is not proportional to the true wall shear stress in the capillary. After a short entrance length, the flow becomes fully developed, i.e., the velocity profile and shear stress become independent of the distance from the entrance, if the flow is assumed isothermal and we neglect the effect of pressure on viscosity. Raw data consist of the reservoir driving pressures P_d corresponding to various volumetric flow rates Q , and these are often reported in terms of plots of apparent wall shear stress σ_A versus apparent wall shear rate $\dot{\gamma}_A$, which are defined as follows:

$$\sigma_A \equiv \frac{P_d R}{2 L} \quad (10.81)$$

$$\dot{\gamma}_A \equiv \frac{4 Q}{\pi R^3} \quad (10.82)$$

The equation for the shear stress ignores the entrance and barrel pressure drops, and the equation for the shear rate is only correct for a Newtonian fluid in the absence

of wall slip. There are well-established methods for using these data to calculate the true shear stress and true shear rate at the wall of a capillary [7, 58]. The true shear rate at the wall is generally determined using the Rabinowich correction for shear thinning, which requires the differentiation of data obtained using several radii. A much simpler procedure that yields good results is the Schümmmer shifting procedure [139], which is based on the power-law viscosity model. Determination of the true wall shear stress requires a correction for the entrance pressure drop. Making use of these techniques, capillary rheometers can be used to measure melt viscosity at moderate to high shear rates.

Slit rheometers are more difficult to build and use but are preferred for research, because the flat flow channel makes it possible to mount pressure sensors and to make optical measurements. As in the case of capillary rheometers, there are established methods for calculating the true wall shear stress and shear rate from experimental slit data [7, 58, 140].

The standard methods for interpreting capillary and slit rheometer data to determine the viscosity are based on the assumptions that the temperature and density are uniform and that the axial variation in pressure has no effect on the viscosity. However, at sufficiently high shear rates, variations in these parameters have significant effects on the calculated viscosity. Laun [141] studied capillary flow thoroughly and showed that the effects of pressure-dependent viscosity and dissipative heating are important and can be taken into account in analyzing data. Hay et al. [142] analyzed slit flow and came to a similar conclusion. The variation in melt density arising from the pressure drop is also a source of error, but Laun [141] estimated that the effect of this variation on the calculated pressure and temperature coefficients is less than 5%, even at high driving pressures. Dees et al. [143] studied the capillary flow of a very pressure-sensitive linear polycarbonate and proposed a method for analyzing the data to obtain the pressure coefficient of viscosity and correct values of viscosity.

A final source of uncertainty in the analysis of data from pressure-driven rheometers is the possibility of wall slip [144]. In fact, well-entangled, linear polymers nearly always slip at a sufficiently high wall shear stress. A large slip velocity often announces itself by the occurrence of an oscillatory shear regime in constant-piston-speed rheometers, or a sudden large jump in flow rate (“spurt”) in pressure-controlled instruments. However, the presence of slip velocities at pressures below those at which these phenomena occur may not be apparent from an inspection of data. This issue was discussed in Section 10.8.2, where we saw that sliding plate rheometer data have revealed the origin of the spurt and oscillatory flow phenomena that occur in capillaries.

We note in conclusion that capillary and slit rheometers are useful for the determination of melt viscosity at shear rates well above those accessible in rotational

rheometer. However, at some shear rate, pressure and temperature variations become important and must be taken into account in the analysis of data. Also, the occurrence of slip may limit the shear rate at which data can be obtained.

The time required to reach steady melt flow in a capillary can be quite long [145]. It is sometimes claimed that the start-up pressure transient in capillary flow can provide information on viscoelastic behavior, but it can be easily demonstrated that this transient arises mainly from melt compressibility [146].

10.8.5 The Cox-Merz Rule

Oscillatory shear measurements provide more precise data than capillary rheometry and require smaller samples. In addition, capillary viscometers are limited to use at moderate to high shear rates and do not provide accurate results at shear rates below 10 s^{-1} for most materials. It would thus be useful to be able to estimate the viscosity curve using data from oscillatory shear measurements. Based on their data for two polystyrenes, Cox and Merz [147] reported that the curve of *apparent viscosity* versus shear rate, as determined using a capillary viscometer, lay very close to the curve of complex viscosity versus frequency. While the apparent viscosity measured in a capillary viscometer is usually defined as the apparent wall shear stress divided by the apparent wall shear rate, it is likely that the entrance pressure drop was nearly negligible for the polystyrenes studied by Cox and Merz. This led to the custom of taking the viscosity as a function of shear rate to be the same as $|\eta^*(\omega)|$, and this relationship is called the “Cox-Merz rule.”

$$\eta(\dot{\gamma}) = |\eta^*(\omega)| \quad \text{when } \dot{\gamma} = \omega \quad (10.83)$$

This relationship is often said to be obeyed by experimental data, but this conclusion is usually based on data plotted on a small log-log graph, where significant deviations can easily hide. An example can be found in the report by Ferri and Lomellini [148] of their study of linear and branched polystyrenes. In their plots for linear polystyrenes, the data seem to follow Eq. 10.83 fairly well, but they note that the viscosity was always less than $|\eta^*(\omega)|$ with the discrepancy reaching 25% at high shear rates for the sample with the highest molecular weight. For their branched samples, the viscosity was greater than the complex viscosity by about 15%.

The Cox-Merz “rule” has been examined critically by Utracki and Gendron [149] and by Venkatraman et al. [150]. The latter authors reported that Eq. 10.83 worked fairly well for LDPE, but not for HDPE, and they pointed out the pressure dependence of viscosity can affect capillary results when the viscosity is high or the capillary is long. Finally, we recall that Cox and Merz based their report on observations of only two polystyrenes in which the entrance pressure drop was probably quite small.

There have been several attempts to provide a theoretical basis for the Cox-Merz rule. Early approaches were based on the relationship between the damping function and the viscosity function. Booij et al. [151] started with a relationship equivalent to Wagner's equation (Eq. 10.11) and showed that the viscosity function is rather insensitive to the detailed form of the damping function. In addition, the damping function does not vary greatly from one polymer to another, and they found that any function that is even roughly similar to the ones reported for entangled polymers leads to a result that is essentially the Cox-Merz rule. Milner took a similar approach to this question [152].

Marrucci [3] proposed convective constraint release (CCR) as an addition to the Doi-Edwards model to provide a theoretical basis for the Cox-Merz rule.

■ 10.9 Extensional Flow Behavior of Melts and Concentrated Solutions

10.9.1 Introduction

Most experimental studies of melt behavior involve shearing flows, and we saw in Chapter 5 that linear viscoelastic behavior is a rich source of information about molecular structure. However, no matter how many material functions we determine in shear, outside the regime of linear viscoelasticity such information cannot be used to predict behavior in other types of deformation, i.e., for any other flow kinematics. A class of flows that is of particular importance in commercial processing is extensional flow. In this type of flow, material elements are stretched very rapidly along streamlines. Nonlinear behavior in extensional deformations provides information about structural features of molecules that are not revealed by shear data. In particular, long-chain branching is known to have an important effect on the response of a melt to a stretching flow that is not revealed in shear flows.

From the point of view of tube models, the two key elements of nonlinear behavior are molecular orientation and chain stretch. Orientation can be probed using shear flow, but shear flows are not effective in generating significant chain stretch. As we have seen, chain stretch in shear is strongly suppressed by the mechanism of convective constraint release (CCR) up to extremely high shear rates. The CCR mechanism of relaxation is qualitatively much less important in extensional flows than in shear flows, because in the former molecules on neighboring streamlines move at the same velocity. Thus, extensional flows are of particular importance in the study of nonlinear viscoelasticity.

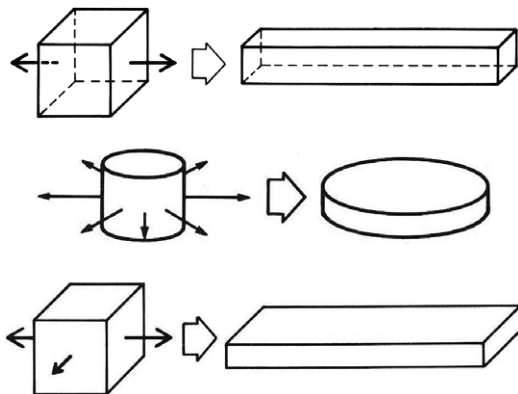


Figure 10.20 Sketch showing the three simplest types of extensional deformation: uniaxial, equibiaxial, and planar.

As in the case of shear, when using large, rapid stretching deformations for polymer characterization, the preferred test modes are those that generate a homogeneous strain. Uniaxial (tensile), equibiaxial (usually called simply biaxial), and planar extension have all been used. These are illustrated in Fig. 10.20. There have been only two or three reports of devices that generate asymmetric biaxial stretching, which is intermediate between tensile and (axisymmetric) biaxial extension. All of these are of potential interest in the simulation of plastics forming operations, but uniaxial extension is the easiest to generate, and the response to this deformation has been found to be quite sensitive to certain aspects of the molecular structure. Because homogeneous extensional flows are more difficult to generate than shear flows, one would not use an extensional flow to measure linear properties. However, it is useful to compare extensional flow data to the behavior predicted by the theory of linear viscoelasticity. This provides a criterion for evaluating the reliability of the data and also serves as a basis for describing the type of nonlinearity exhibited by a particular polymer.

Because step extensional strain is not practical for melts, the experiment usually carried out to study uniaxial extension is start-up of steady simple extension at a constant *Hencky strain rate* $\dot{\epsilon}$. The Hencky strain rate can be defined in terms of the length L of a sample as shown by Eq. 10.84.

$$\dot{\epsilon} = d \ln L / dt \quad (10.84)$$

This strain rate is a measure of the speed with which material elements on a streamline are separated from each other. Note that both the velocity of the end of a sample and the sample length increase exponentially with time when the sample is subjected to a constant Hencky strain rate.

$$L(t) = L(0) \exp(\dot{\epsilon} t) \quad (10.85)$$

But at a fixed distance z from a $z = 0$ plane where $v_z = 0$, the velocity is constant and proportional to the Hencky strain rate:

$$v_z = \dot{\epsilon} z \quad (10.86)$$

We will see in Section 10.11, which describes experimental techniques, that this relationship provides the basis for an experimental technique that does not require the exponential increase of the effective length of the sample.

The material function usually reported in extensional flow rheometry is the *tensile stress growth coefficient* defined by Eq. 10.87.

$$\eta_E^+ (t, \dot{\epsilon}) \equiv \sigma_E (t, \dot{\epsilon}) / \dot{\epsilon} \quad (10.87)$$

The Boltzmann superposition principle can be used to derive the linear response, which should be exhibited at sufficiently small strain rates:

$$\lim_{\dot{\epsilon} \rightarrow 0} \eta_E^+ (t, \dot{\epsilon}) = \eta_E^+ (t) = 3 \int_0^t G(s) ds = 3 \eta^+ (t) \quad (10.88)$$

If steady extensional flow is achieved, the *extensional viscosity* can be determined:

$$\lim_{t \rightarrow \infty} \eta_E^+ (t, \dot{\epsilon}) \equiv \eta_E (\dot{\epsilon}) \quad (10.89)$$

and in the limit of vanishing strain rate, the extensional viscosity becomes simply three times the zero-shear viscosity:

$$\lim_{\dot{\epsilon} \rightarrow 0} \eta_E (\dot{\epsilon}) = 3 \int_0^\infty G(s) ds = 3 \eta_0 \quad (10.90)$$

This Newtonian fluid behavior was first noted by Trouton, and the quantity $\eta_E (\dot{\epsilon}) / 3 \eta_0$ is sometimes referred to as the Trouton ratio and used to normalize extensional viscosity data. The reader should be aware, however, that this name is also used for several other ratios, including $\eta(\dot{\epsilon})/\eta_0$; $\eta(\dot{\epsilon})/\eta(\dot{\gamma} = \dot{\epsilon})$ and $\eta(\dot{\epsilon})/\eta(\dot{\gamma} = \sqrt{3} \dot{\epsilon})$, the last of which compares the extensional and shear viscosities at equal values of the second invariant of the rate of strain tensor.

We noted in Section 10.7.2 that the second-order fluid approximation for flows only marginally removed from the rest state indicates that the first and second normal stress differences are second order in the shear rate, so that the first and second normal stress coefficients $\Psi_{1,0}$ and $\Psi_{2,0}$ approach non-zero limiting values at vanishing shear rate. The second-order approximation also predicts that the net stretching stress in uniaxial extension is second order in the Hencky strain rate, and this implies that the extensional viscosity approaches its limiting zero-strain-rate value $3 \eta_0$ with a non-zero slope:

$$\lim_{\dot{\varepsilon} \rightarrow 0} \frac{\eta_E(\dot{\varepsilon})}{\dot{\varepsilon}} = \frac{3}{2} (\Psi_{1,0} + 2 \Psi_{2,0}) \quad (10.91)$$

And since $\Psi_{2,0}$ is negative, with a magnitude less than half that of $\Psi_{1,0}$, this slope is positive. However, its effect on a logarithmic plot of $\eta_E(\dot{\varepsilon})$ is quite small.

It is almost universal practice when reporting the results of an extensional flow experiment to compare the nonlinear material function $\eta_E^+(t, \dot{\varepsilon})$ with the linear response given by Eq. 10.88. If both data sets are accurate, the nonlinear response should agree with the linear one at short times and low strain rates. Furthermore, the way in which the nonlinear response departs from the linear one is used to classify the extensional flow behavior. If the nonlinear data rise above the linear curve at some point, the melt is said to be *strain hardening*, and if they fall below, it is said to be *strain softening*. Figure 10.21 shows the data of Münstedt and Laun [153] for a low-density polyethylene made in a tubular reactor, and we see that this material is strain hardening. Linear polymers containing no very high-molecular-weight components usually exhibit strain softening. This classification system has inspired the use of a “reduced” stress growth coefficient [154] $\eta_{ER}^+(t, \dot{\varepsilon})$, or “degree of strain hardening” χ [155], defined as follows:

$$\eta_{ER}^+(t, \dot{\varepsilon}) \equiv \frac{\eta_E^+(t, \dot{\varepsilon})}{3 \eta^+(t)} \quad (10.92)$$

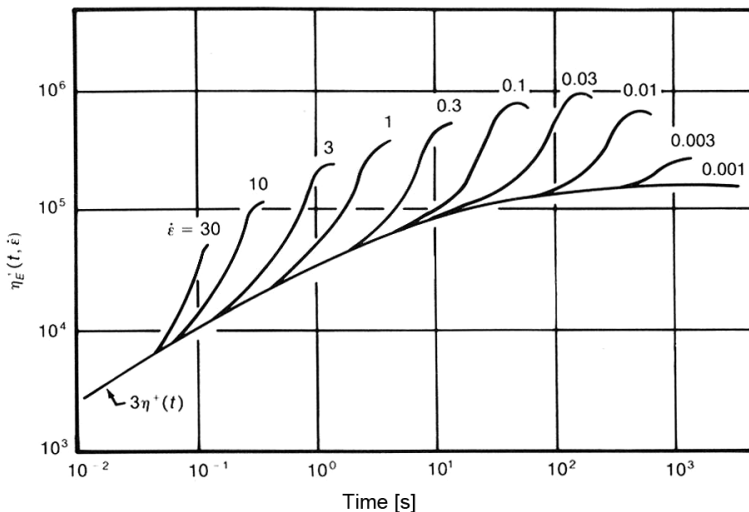


Figure 10.21 Stress growth coefficient in uniaxial extension at strain rates from 0.001 to 30 s^{-1} for an LDPE (IUPAC A) at 150°C . As the strain rate increases, the data rise above the linear envelope curve at progressively shorter times. The steady-state value (extensional viscosity) first increases with strain rate and then decreases. From Münstedt and Laun [153].

When there is strain hardening, the value of this function is greater than one and *vice versa*. The use of this function to compare data for several polymers shows the comparative strain hardening but normalized with respect to the effect of differences in the linear relaxation spectra. Wood-Adams et al. [154] used this function to compare data for a series of metallocene polyethylene homopolymers having various, low levels of long-chain branching and found that once the effect of the linear spectrum was eliminated in this way, the differences between the samples became insignificant except at the longest times.

When comparing extensional flow data with the LVE prediction, care must be taken in the calculation of the linear prediction. If the data used to establish the relaxation spectrum do not include very short-time (high-frequency) data, the initial portion of the curve will not be correct. It may thus be better to use data from start-up of steady simple shear to measure $\eta^+(t)$ directly rather than inferring it from complex modulus data.

While the term “strain hardening” is widely used to describe the extensional flow behavior of some polymeric liquids, it lacks any basis in polymer physics. It was introduced by G.I. Taylor in 1934 [156] to describe the plastic flow of crystalline metals. It has also been used to describe the behavior of glassy and semicrystalline polymers, where it is said to arise from the effect of strain on solid-state structural features. Its use for melts is based solely on the shape of the curve of $\eta_E^+(t, \dot{\epsilon})$ versus time with strain rate as a parameter.

Strain-softening polymers are very prone to a necking instability in extension leading to ductile failure, and this poses a major challenge for the experimentalist. If there is a small variation in diameter along the sample, the resistance to further deformation will be reduced at that point, leading to instability and failure. This makes it difficult to continue an experiment to steady-state for determination of a value of the extensional viscosity. A theoretical treatment of this instability making use of the Considère criterion [157] indicates that if the stress passes through a smooth maximum before undergoing ductile failure, this maximum is the steady-state stress, and the extensional viscosity $\eta_E(\dot{\epsilon})$ can be calculated from it. However, a more recent analysis by Fielding [158] concludes that the Considère criterion is not applicable to this problem and that the downward curvature of the stress is related to necking.

If the tensile stress, rather than the Hencky strain rate, is held constant, the extensional creep compliance $D(t, \sigma_E)$ can be determined, and if steady state is achieved, the compliance becomes linear with time, and the intercept of this line with the vertical axis is the steady-state extensional creep compliance $D_s(\sigma_E)$.

$$D(t, \sigma_E) \equiv \frac{\epsilon(t)}{\sigma_E} = D_s(\sigma_E) + \frac{t}{\eta_E(\sigma_E)} \quad (10.93)$$

where η_E is the extensional viscosity corresponding to the steady stress, σ_E . At sufficiently low stresses, the response is linear, and the extensional compliance is just one-third of the shear compliance as shown by Eq. 10.94.

$$D(t) = D_s^0 + \frac{t}{3\eta_0} = \frac{1}{3} J(t) \quad (10.94)$$

It has been observed that steady state is achieved substantially faster in a constant stress experiment than in a constant strain rate experiment, and this is advantageous because of the very large sample length and very small diameter that are involved in continuing a constant rate experiment to steady state. If the extensional viscosity is the property of interest, the use of tensile creep is therefore advantageous. However, most of the data that have been reported were measured at constant strain rate.

If the sample is cut into segments of known length during stretching, and the equilibrium lengths of the segments are measured after they have recoiled to their equilibrium lengths, the recoverable strain ε_r can be calculated. If the segments are cut at a time t after start-up of steady extension, the recoverable strain is a function of strain rate and time or strain. If the cutting and measuring occur during a creep experiment, the recoverable strain is a function of time and extensional stress. At sufficiently long times, the recoverable strain approaches a steady-state value.

Because of the difficulties involved in continuing extensional flow start-up experiments to steady state, few reliable extensional viscosity data have been published. While plastics processing operations never involve steady-state extensional flow, the behavior of $\eta_E(\dot{\epsilon})$ is of considerable importance with regard to the relationship between molecular structure and rheological behavior.

There are three possible types of behavior of the extensional viscosity function. It can exhibit the Newtonian/second order behavior shown by Eqs. 10.90 and 10.91; it can exhibit *extension thickening* (η_E increasing strongly with $\dot{\epsilon}$); or it can exhibit *extension thinning* (η_E decreasing with $\dot{\epsilon}$). It is important not to confuse this classification scheme with that used to describe the transient response to the start-up of steady simple extension. For example, a material can be strain hardening in its start-up behavior but extension thinning in its steady-state behavior over the same range of strain rates.

Tube models have been used to predict this material function for linear, monodisperse polymers, and a so-called “standard molecular theory” [159] gives the prediction shown in Fig. 10.22. This theory takes into account reptation, chain-end fluctuations, and thermal constraint release, which contribute to linear viscoelasticity, as well as the three sources of nonlinearity, namely: orientation, retraction after chain stretch and convective constraint release, which is not very important in extensional flows.

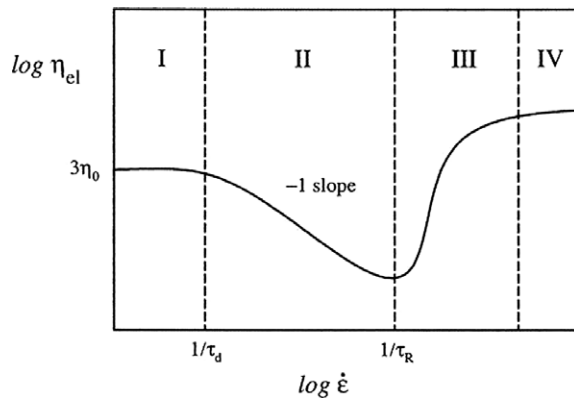


Figure 10.22 Standard tube-model prediction of the extensional viscosity function. In zone I the Trouton ratio is three ($\eta_E = 3 \eta_0$), while in zone II there is orientation but no stretch, and CCR has little effect, so the stress is constant. When the strain rate reaches $1/\tau_R$, chain stretch occurs and the extensional viscosity rises until maximum stretch is achieved, and the stress becomes proportional to the strain rate. From Marrucci and Ianniruberto [159].

At strain rates less than the reciprocal τ_d^{-1} of the disengagement (reptation) time, molecules have time to maintain their equilibrium state, and the Trouton ratio is one, i.e., $\eta_E = 3 \eta_0$ (zone I in Fig. 10.22). For rates larger than this, but smaller than the reciprocal of the Rouse time, the tubes reach their maximum orientation, but there is no stretch, and CCR has little effect, with the result that the stress is predicted to be constant so that the viscosity decreases with the inverse of the strain rate, as shown in zone II of Fig. 10.22. When the strain rate becomes comparable to the inverse of the Rouse time, chain stretch occurs, leading to an increase in the viscosity, until maximum stretch is obtained, and the viscosity becomes constant again. Deviations from this prediction are described above, and possible reasons for them are discussed in Chapter 11.

Another stretching flow that has been used to characterize the nonlinear behavior of melts is equibiaxial extension, usually called simply biaxial extension. This flow can be generated by clamping a circular sample around its rim and stretching it radially, as demonstrated by Hachmann and Meissner [160]. The biaxial strain ε_B is given by:

$$\varepsilon_B(t) \equiv \ln \left[R(t)/R(0) \right] = \ln(\lambda_B) \quad (10.95)$$

If the radius increases exponentially with time, the experiment is start-up of biaxial extension. However, a simpler technique is lubricated squeeze flow in which the thickness of a sample d decreases with time, and the biaxial strain is given by:

$$\varepsilon_B = -\frac{1}{2} \ln \left(\frac{d}{d_0} \right) \quad (10.96)$$

For small or slow equibiaxial extension, the biaxial start-up function can be found using the Boltzmann superposition principle:

$$\eta_B^+(t) = 6 \int_0^t G(s) ds \quad (10.97)$$

10.9.2 Solutions versus Melts

It was once thought that polymer solutions and melts having the same degree of entanglement should have the same rheological behavior in extension and in shear, and this was found to be true for linear properties. But it was later suggested that this universality principle was not valid for strongly nonlinear behavior [161, 162]. Wingstrand et al. [163] pointed out that based on our current understanding of polymer physics, solutions and melts should exhibit the same behavior if they have: (i) the same number of entanglements, (ii) the same flexibility based on the number of Kuhn segments per entanglement, and (iii) the same potential for monomeric friction reduction. They observed that the failure to observe universality resulted from the difficulty of satisfying conditions (ii) and (iii) using the same system. Wingstrand et al. demonstrated using PMMA that when all three are fulfilled, universality is, indeed, observed for both linear viscoelastic and extensional flow behavior.

10.9.3 Linear, Monodisperse Polymers

For well-entangled, linear, monodisperse melts, tube models predict that chain stretch and thus strain hardening will occur when the rate of deformation exceeds the reciprocal of the stretch relaxation time, which is equal to τ_r and to $2\tau_R$ where τ_R is the longest Rouse stress relaxation time. Eq. 10.26 provides a rough estimate of τ_r for an entangled polymer showing it is proportional to $(M_c/M)^{a-1}$ where a is approximately 3.4. For a polyethylene with a molar mass of M of 100 kg/mol, $\tau_R \approx 5 \times 10^{-5}$ s at 190 °C, the strain rate needed to achieve significant strain hardening at this temperature would have to be greater than 10,000 s⁻¹, which is far beyond rates achievable in practice. But for polystyrene, $\tau_R \approx 3$ s, and one can achieve chain stretch and thus strain hardening in practical experiments. Studies of highly entangled, monodisperse, linear polystyrene melts by Bach et al. [164] revealed a modest degree of strain hardening starting when the strain rate was somewhat above $1/\tau_R$, especially for a sample with high molar mass at strain rates above 0.01 s⁻¹. Hassager et al. [165] used stress and neutron scattering measurements to study PS chain stretch in uniaxial extension and reported that finite chain extensibility seemed to play no role in strain hardening.

Bhattacharjee et al. [166, 167] studied entangled solutions of linear, high-molecular-weight polystyrene. Like Bach et al. they used a filament-stretching rheometer, but their solutions had $c M/M_e$ values up to about 20, and they were able to reach Hencky strains of about five. Their data show the initial extension thinning followed by strong extension thickening that is predicted by older tube models and shown in Fig. 10.22. However, the slope of the data in the extension thinning zone seems to be weaker than the -1.0 predicted by that model. A more detailed discussion of this behavior in terms of tube models is presented in Chapter 11.

10.9.4 Effect of Polydispersity

It has been observed that a sample with a modest peak in the MWD well above that of the bulk of the sample can exhibit strong strain hardening. Münstedt [168] compared the behavior of four linear polystyrenes, one of which exhibited strong strain hardening. This sample had an M_w of 39 kg/mol but also a much smaller MWD peak at about 70 kg/mol. However, neither a PS with $M_w = 74$ kg/mol and a small high-molecular-weight tail nor a commercial polymer with $M_w = 219$ kg/mol and $M_w/M_n = 2.3$ exhibited significant strain hardening. Nielsen et al.[169] studied binary blends of monodisperse, linear polystyrenes. Both the monodisperse samples exhibited strain hardening and strain-rate thickening at low strain rates, but became strain-rate thinning at higher strain rates. The maximum extensional viscosity $\eta_E(\dot{\epsilon})$ of the monodisperse samples divided by $3 \eta_0$ were about two, while for the blends this ratio was as much as seven. A blend containing 86 wt% ($M = 50$ kg/mol) and 14% ($M = 390$ kg/mol) exhibited very strong strain hardening, much more so than a sample with 96% (50 kg/mol) and 4% (390 kg/mol). These have been compared with predictions of a tube model by van Ruymbeke et al. [170]. Auhl et al. [171] studied strain hardening in binary blends of long and short chains. Their model predicted that dilution by short chains increases the effective stretch relaxation time of the long chains, and this was confirmed experimentally. A general conclusion regarding binary blends of linear polymers is that strain hardening is governed by the high-molecular-weight component, and to maximize hardening while keeping the MW of the blend constant, one needs to add a relatively small amount of very high-molecular-weight polymer.

10.9.5 Linear Low-Density Polyethylene

The behavior of ethylene/ α -olefin copolymers depends markedly on the catalyst used. As was explained in Section 3.8, in copolymers made using Ziegler-type catalysts the comonomer tends to end up primarily in the shorter chains. Münstedt et al. [172] and

Gabriel and Kaschta [171] observed unusual behavior in such a copolymer. First, it was found that the LLDPE they studied was thermorheologically complex. In addition, it was markedly strain hardening in extension at the lowest strain rates and long times but less so at higher rates. Creep experiments permitted the determination of the extensional viscosity, and this was found to be about seven times the expected zero shear rate value of $3 \eta_0$ at the lowest stress accessible, decreasing with stress to become equal to $3 \eta_0$ at the highest stresses used. Since the extensional viscosity at very low, but often inaccessible, extension rates must approach $3 \eta_0$, this implies that this sample is strongly extension thickening at very low shear rates, with the extensional viscosity rising from $3 \eta_0$, going through a maximum, and then decreasing back to its Newtonian value $3 \eta_0$ at high strain rates.

However, this is not the end of this strange story. When the Hencky strain rate during a creep test was plotted versus time, in addition to the long-time plateau from which the extensional viscosity was determined, another well-defined plateau appeared at a much earlier time. When this strain rate was used to calculate an extensional viscosity, the resulting values were very close to $3 \eta_0$! The authors felt that this unusual behavior was related to the fact that the comonomer was located almost exclusively in the shorter molecules, leaving a distinct high-molecular-weight, linear fraction. This fraction did not show up in the MWD inferred from GPC data, but it did show up in data from DSC and TREF measurements, which revealed the presence of two components that melted at significantly different temperatures [173]. Based on these observations, Münstedt et al. [172] hypothesized that the two components were immiscible, with the linear component forming the dispersed phase and the comonomer the matrix. Evidence of phase separation in a very-low-density copolymer made using a Ziegler catalyst was reported by van Ruiten and Boode [174].

By contrast, LLDPE polymers made using metallocene catalysts do not exhibit this unexpected behavior, acting essentially like HDPE but having a narrower MWD than commercial HDPE. This is presumably a result of the fact that in these polymers the comonomer is much more uniformly distributed among the molecules.

10.9.6 Model Branched Systems

For a star we expect the uniaxial extensional flow behavior to be qualitatively similar to that of linear polymers, but with a stretch relation time dependent on the number of entanglements per arm. This difference between linear and star molecules is due to the fact that a linear chain can retract from two ends, while star arms can retract from only one. Data on asymmetric, polystyrene star melts obtained using a filament stretching rheometer [175] revealed strong strain hardening in asymmetric polystyrene stars.

For a molecule with more than one branch point, there are internal segments without free ends, whose retraction is impeded so that strain hardening is much more likely to be exhibited. The simplest structure is an H molecule, which has two branch points connected by a backbone or tie-bar. An H is the simplest example of a comb, which has two or more branch points on a single backbone. Hepperle and Münstedt [176] studied polystyrene combs with various numbers and lengths of grafted side chains. They found that strain hardening became more prominent as the average number of side chains increased as long as the branches had lengths greater than M_e .

Lentzakis et al. [177] studied carefully synthesized comb polymers and determined the effects of the length and number of branches and the length of segments between branches on rheological properties. At very high $\dot{\epsilon}$ all the samples exhibited strain hardening, regardless of these molecular parameters. This occurs when the rate of deformation is faster than either the Rouse time or the effective backbone stretch time of the combs. By contrast, at lower strain rates, increasing M/M_e of the backbone segments and/or the branches enhanced strain hardening, but M/M_e of the branches was found to be the key parameter for strain hardening.

Van Ruymbeke et al. [178] studied a series of trees starting with generation 1 (G1), a four-armed star, moving to G2 by adding a branch point at the end of each star arm to yield a tree with 8 arms, and so on for higher generations. They found that at large Hencky strain rates the inner and middle generations of segments are stretched, while at low $\dot{\epsilon}$ only the inner generation is stretched. But because the inner segments have long stretch relaxation times, strain hardening can occur when $\dot{\epsilon}$ is less than $1/\tau_R$. Recognition of the essential role of deep inner backbones in strain hardening was the inspiration for the modelling of LDPE by simulating it as a pom-pom polymer, which has two branch points but multiple arms at each one. (The added arms increase the stretch time of the backbone by making it more difficult for the branch points to be drawn into its tube.) This impedes the relaxation of the backbone much more than in an H polymer, thus enhancing strain hardening [179].

Thus, pure combs of sufficient molar mass entangled with each other should exhibit strain-hardening. But in polydisperse systems containing both linear and branched molecules, the situation is much more complex, since the occurrence of strain hardening depends on the mutual influence of all species in the polymer, which affects their relaxation, and on the rate of deformation. Combs in metallocene polyethylenes are diluted by short linear chains and stars, which limit their degree of entanglement with other combs. There is little reported evidence of strain hardening in diluted combs. Lohse et al. [180] observed strain hardening for a linear metallocene polyethylene to which 3 wt% combs were added. However, these combs had 26 arms and an M_w of 730 kg/mol and were thus much larger than the typical combs, and Lohse et al. were not able to measure properties of the pure combs because they were “too elastic.”

The next step in complexity is a branch-on-branch or tree-like structure. Large molecules containing many tree-like molecules are well-known to exhibit pronounced strain hardening. This behavior often persists after dilution with linear chains; for example, the presence of LDPE in a blend with linear PE can generate strain hardening at concentrations below 10% [181]. And Stange et al. [182] found that as little as 3% of a highly branched polypropylene in a linear matrix was sufficient to generate strain hardening.

10.9.7 Long-Chain Branched Metallocene Polyethylenes

Long-chain branched copolymers are *architecturally polydisperse* systems containing molecules of various sizes and molecular structures, and the situation is much more complex than in the simpler model polymers, since strain hardening depends on the mutual influence of all species in the polymer. In Section 3.9.2 the synthesis of a group of polyethylenes (the HDB samples) made with one single-site catalyst and having varying levels of long-chain branching was described. We recall that these materials consist of linear chains, stars, H polymers, and molecules with inner backbones. Figure 5.19 was a plot of the zero-shear viscosity of these materials.

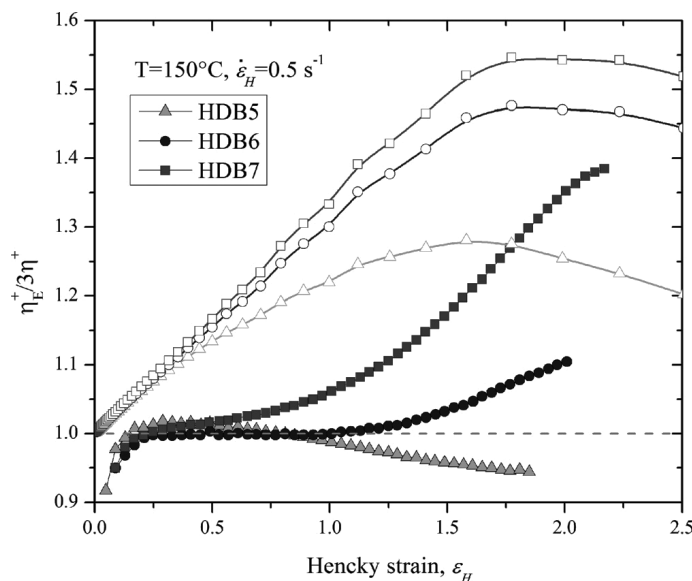


Figure 10.23 Extensional stress growth coefficients of samples HDB 5–7 divided by $3 \eta^+ (t = \varepsilon_- / \dot{\varepsilon})$ to show the degree of strain hardening. Use of linear scales reveals weak strain hardening. Solid symbols are data, and open symbols are predictions of branch-on-branch (BoB) model, version 2.5. From Torres et al. [183].

Wood-Adams et al. [154] carried out a thorough structural and rheological analysis of four of these polymers, and Torres et al. [183] examined the behavior of a larger group of seven samples, including three that had more long-chain branches than those studied earlier. The first four samples with the lowest level of long-chain branching exhibited no significant strain hardening but Torres et al. [183] found that samples HDB6 and 7 exhibited strain hardening. This is shown in Fig. 10.23. Note that since the hardening is weak, linear scales were used to reveal it.

As was explained in section 3.9.2, molecules with branches on branches, i.e., trees, only appear in significant quantities in samples 6 and 7. The strain hardening of samples 6 and 7 was thus attributed to the presence of tree-like molecules with inner backbones, whose extremely slow relaxations allow strain hardening to persist even after dilution by linear chains. A mass fraction of trees exceeding about 3 wt% was deemed sufficient to produce the required deep inner backbones (high seniority segments) similar to the higher generation segments of Van Ruymbeke et al. [178], which have long stretch relaxation times. The number of inner backbones appeared to be much more important than their lengths in enhancing strain hardening.

Malmberg et al. [184] studied branched copolymers made using several catalysts and found marked differences between the samples. Moreover, some samples exhibited very large values of $[\eta_E(\dot{\varepsilon})/3\eta_0]$ at the lowest strain rates followed by strong extension thinning, bringing this ratio close to unity at the highest strain rate used. This behavior is very similar to that observed by Münstedt et al. [172] for an LLDPE made using a Ziegler type catalyst. Malmberg et al. concluded from their study that extensional flow behavior depends primarily on the distribution of long-chain branches rather than the number of branches. In particular, the presence of multiple branch points on a few molecules is much more effective for strain hardening than many branches evenly distributed among many molecules. On the other hand, evenly distributed branches have a larger effect on the zero-shear viscosity. This is consistent with observations of the difference between the behaviors of star and comb polymers.

10.9.8 Randomly Branched Polymers and LDPE

A basic problem in dealing quantitatively with randomly branched polymers is the competing effects of branching and polydispersity, the latter of which is always present in commercial polymers and increases when monodisperse linear polymers are treated with cross-linking agents. Linear polymers that are known to be strain-softening can be made strongly strain-hardening by the introduction of long-chain branches. Kurzbeck et al. [185] used electron-beam radiation to introduce branching into a linear polypropylene and obtained a polymer that was strongly

strain-hardening and extension thickening. The thickening was already present at the lowest stress used, and there was a maximum in the curve of $\eta_E(\dot{\epsilon})$. The same behavior was observed by Hingmann and Marcinke [186] in polypropylenes treated with a chemical crosslinking agent. The degree of hardening was even greater than that predicted by the Lodge rubberlike liquid model. They estimated that fewer than three branches per molecule were required to produce this pronounced strain hardening. Kasehagen and Macosko [187] used a chemical crosslinking agent to add branches to polybutadiene and obtained similar results. The extreme strain hardening observed in these partially cross-linked samples has never been produced by polydispersity alone, without any long-chain branching, even if there is a high-molecular-weight “tail”, and must therefore be attributed to the presence of the long branches.

The structure and rheology of low-density polyethylene (LDPE) is of practical interest because of its importance as a commercial polymer, especially in film-blown and extrusion-coating. It has been known for many years that the extensional behavior of LDPE is quite different from that of linear HDPE, and this suggests the possibility of a correlation between the level of long-chain branching and the extensional flow properties. However, while a general trend of increased strain hardening with the introduction of long-chain branching has been observed, it has not been possible to develop a quantitative correlation between the level of branching and degree of strain hardening, in part because of the substantial difficulties involved in obtaining extensional flow data of sufficient accuracy. But a greater difficulty is the potential complexity of branched systems, particularly LDPE. Moreover, as explained in Chapter 3, LDPE can have a variety of structures depending on how it was manufactured. In particular, autoclave LDPE has a much more complex branching structure than that produced in a tubular reactor.

Yamaguchi and Takahashi [28] compared two LDPE samples that had similar values of M_n ; one was a tubular reactor product, and the other was made in an autoclave and had a broader MWD. The branching factors g' of both polymers were much less than one, but that of the tubular reactor material was larger than that of the autoclave product, especially in low-molecular-weight fractions, implying less branching in the tubular product. The linear viscoelastic properties and viscosities of the two samples were not markedly different, but the autoclave polymer exhibited substantially greater strain-hardening in uniaxial extension. This result was attributed to the strong stretching action of the flow field together with the suppression of chain contraction by the many branch points. Differences between the two samples were not as marked in start-up of biaxial extension, and the authors concluded that biaxial stress-growth data are not as sensitive to molecular structure as uniaxial data.

Figure 10.24 shows the extensional viscosity data of Laun and Münstedt [188] for several low-density polyethylenes made in a tubular reactor. We note that these

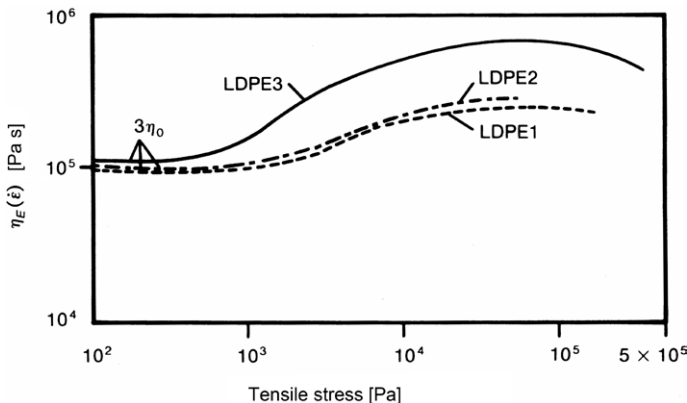


Figure 10.24 Extensional viscosity versus tensile stress (log-log plot) for three LDPEs made in a tubular reactor. The viscosity rises above $3\eta_0$ at low stresses then decreases at higher stresses. The zero-shear viscosities of the three polymers are very similar, but LDPE 3 has a much broader MWD (24 compared to 7 and 8) than the other materials. From Laun and Münstedt [188].

branched polymers are Newtonian at low strain rates, become extension thickening at higher strain rates, and finally exhibit extension thinning. This is similar to the behavior observed by Kurzbeck et al. [185] for a crosslinked polypropylene. In Chapter 11, it will be shown that the pom-pom model predicts this type of extensional viscosity curve. We will see in the following section that there has been some controversy about the interpretation of maxima in the extensional stress growth curves as steady states, and there is now evidence that these maxima actually lead on to lower steady-state extensional viscosities.

Gabriel and Münstedt [189] carried out a thorough comparative study of polyolefins having various branching structures. They concluded that both the number of branches per molecule and the number of entanglements per branch play crucial roles in strain hardening. They also concluded that if a polyethylene exhibits strain hardening but has the zero-shear viscosity dependence on M_w that is typical of linear polymers (Eq. 5.4), it is very likely a linear polymer containing some very high-molecular-weight material.

10.9.9 Stress Overshoot in Extensional Flow

In Section 10.10.1 it was explained that the necking instability that is likely to occur when the extensional stress decreases makes it difficult to identify a steady state value for calculating an extensional viscosity. Uncertainty arises regarding whether a maximum in $\eta_E^+(t, \dot{\epsilon})$ is the result of necking or is an overshoot leading to a lower steady-state value. We take up this issue again here, because most studies of this

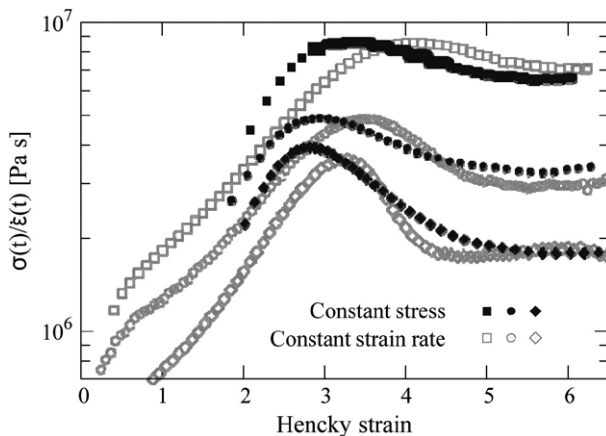


Figure 10.25 Extensional stress growth coefficient of a LDPE at three strain rates. Controlled stress and controlled rate tests yield similar extensional viscosities after going through maxima and reaching steady states. From Alvarez et al. [192].

issue have involved LDPE. Rasmussen et al. [190] and Burgelea et al. [191] carried out a detailed experimental study of the occurrence in LDPE of sample diameter non-uniformity using the Münstedt tensile rheometer (MTR) described in Section 10.11 below. Using a filament stretching rheometer (also described in Section 10.11) Alvarez et al. [192] were able to avoid necking to move beyond the stress maximum, and their data indicate a true plateau at a lower stress, which they used to determine the extensional viscosity as a function of strain rate. They performed both constant strain rate and constant stress experiments, and both yielded similar values of $\eta_E(\dot{\gamma})$. Their extensional viscosity plot is shown in Fig. 10.25.

■ 10.10 Experimental Methods for Extensional Flows

10.10.1 Introduction

It is much more difficult to measure the response of a melt to a stretching deformation than to a shearing deformation. However, without a reliable constitutive equation based on a molecular model, there is no way to predict how a melt will behave in a large, rapid extensional flow, based only on knowledge of its response to shearing deformations. Therefore, the essential criterion for the success of an extensional flow technique is the degree of departure from linear viscoelastic behavior that can be generated.

In order to evaluate the significance of published data, we need to know something about the capabilities and limitations of the experimental technique used. We present here a brief review of experimental methods. As in the case of shear, a sample does not always undergo the desired deformation in response to the tractions applied to its exposed surfaces, but the challenge is all the greater when tensile forces must be applied to stretch a molten sample. Also, the sample thickness decreases rapidly at a constant strain rate. Melt behavior has been studied using uniaxial (also called simple or tensile), biaxial, and planar extensional flows. However, only the first two of these have been used to a significant extent. A uniaxial extensional rheometer is designed to generate a deformation in which either the net tensile stress σ_E or the Hencky strain rate is maintained constant. The material functions that can, in principle, be determined are the tensile stress growth coefficient $\eta_E^+(t, \dot{\epsilon})$, the tensile creep compliance, $D(t, \sigma_E)$ and the tensile (uniaxial) extensional viscosity $\eta_E(\dot{\epsilon})$, which is the long-time, steady-state value of $\eta_E^+(t, \dot{\epsilon})$ as well as the reciprocal of the slope of the steady-state portion of the creep compliance curve.

In the early stages of a start-up of steady simple extension when the deformation is still very small, or when the strain rate is very small, the behavior should follow the prediction of the Boltzmann superposition principle. This can be calculated using the linear relaxation modulus, as shown by Eq. 10.88, thus providing a valuable criterion for the accuracy of data, at least at short times or low rates.

10.10.2 Rheometers for Uniaxial Extension

Over a period of more than 50 years there have been many attempts to build devices able to generate extensional flow, and nearly all of this effort involved uniaxial extension. Such measurements pose major problems not encountered in studying shear deformations. In particular, a molten sample has somehow to be clamped at its ends to facilitate stretching and cannot be supported by a solid surface and is thus subject to sag due to gravity. Joachim Meissner devoted much of his career to the development of extensional rheometers. In his first device [193], the stretching stress was applied by “rotary clamps,” and sample sag was avoided by floating the sample on a hot oil bath. Later improvements were made by Laun and Münstedt [194]. In a later design, which was commercialized as the RME, the sample was a strip and was supported on a bed of air flowing from a porous surface [195]. The capabilities of these instruments and their limitations were the subject of several studies [196–198].

Münstedt [199] later developed a more compact instrument, the MTR, in which the sample is gripped at its ends by adhering it to small metal end plates and is mounted vertically in an oil bath. It is shown in Fig. 10.26. One of the end metal plates is

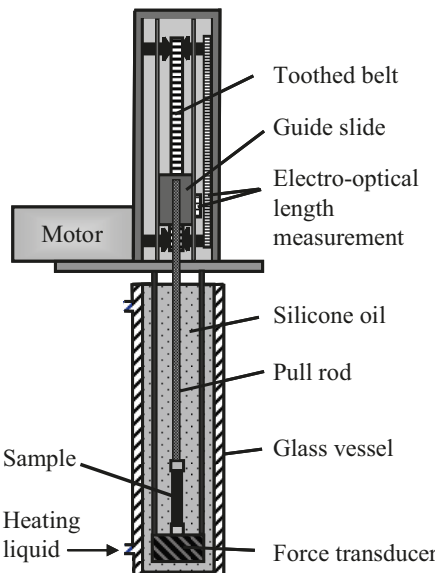


Figure 10.26 Sketch showing the principle of operation of the Münstedt tensile rheometer (MTR). The cylindrical sample is glued to metal plates, one of which is mounted on a force transducer while the other is coupled to a linear actuator system. The sample and transducer are immersed in a vertical oil bath. Sketch courtesy of Jen Shueng Tiang.

attached to a force transducer at the bottom of the bath, and the other is coupled to a pull rod that is vertically displaced by a toothed belt driven by a motor. The MTR can reach strain rates of 5 s^{-1} and can be used for creep measurements.

A much simpler device for measuring the response of melts and elastomers to uniaxial extension is the Sentmanat Extensional Rheometer (SER) [200]. A sketch is shown in Fig. 10.27. The sample is a small rectangular plaque that is clamped at each end to a rotating drum. Both drums are rotated by the motor of a rotational rheometer, and the force in the sample is calculated from the torque. In addition to start-up of steady, simple extension, creep and stress relaxation experiments can be carried out. The entire device is designed to fit within the thermostatted chamber of a standard rotational rheometer, and the sample can be viewed through a window in the chamber. This instrument has been found to yield data that are in good agreement with those from other types of instrument [201]. Sentmanat et al. [202] evaluated the capabilities of the SER for the study of a linear low density polyethylene, a low density polyethylene, and an ultra-high molecular weight polyethylene. Strain rates ranged from 0.3 to 30 s^{-1} . They also carried out stress relaxation tests to explore necking instabilities. The total strain is limited to about 4, but this can be increased by avoiding the use of the sample clamps and simply pressing the ends of a sample onto the hot cylinders.

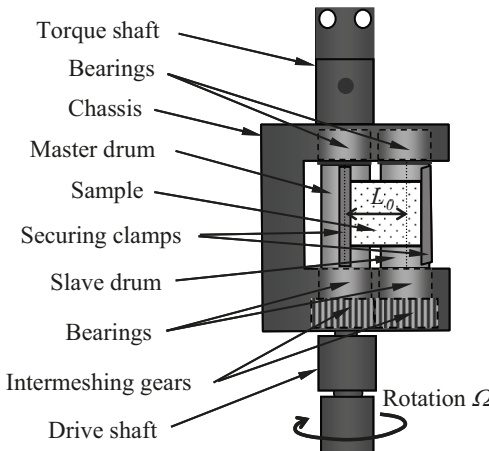


Figure 10.27 Sketch showing the principle of operation of the Sentmanat extensional rheometer (SER), which is designed to be used as a fixture in a standard rotational melt rheometer. One of two cylinders is driven directly by the rheometer motor, while a gear train drives the slave drum. The thin, rectangular sample is clamped at its ends to the cylinders. The torque on the drive shaft is proportional to the tensile stress in the sample. (Sketch courtesy of Jen Shueng Tiang.)

To remove a sample, load a new one, heat the sample, and carry out a test requires only a few minutes. Because of its low cost and ease of use, the SER is the most widely used extensional rheometer for molten polymers, as versions are available for use in many commercial rotational rheometers. Aho et al. [203] evaluated the SER for the study of a low-density polyethylene. They found it necessary to make corrections to determine the true sample dimensions. The resulting data agreed with those using other test methods if measurements were made without using the sample clamps. Lin and Wang [204] estimated the temperature rise due to viscous heating in the SER and found that for high-viscosity melts at high strain rates, the temperature rise can be significant.

A device somewhat similar to the SER is the EVF, a fixture designed for use in a TA Instruments rheometer. The mechanism is simpler than that of the SER, but the sample rotates and cannot be viewed through the window of the heating chamber. The SER has been used in several studies of commercial polyethylenes [205, 206].

The filament stretching rheometer (FSR) is an elaborate and elegant instrument designed to improve precision and reach higher strains. Used initially for the study of polymer solutions [207–209], a somewhat modified version was later used to study melts [218–221]. Its use to determine the long-time final plateau in the stress growth behavior of LDPE was discussed above [190, 192]. As shown in Fig. 10.28 the filament is formed from a small sample by stretching it between two cylindrical, steel fixtures to which it is attached by the direct adhesion of the sample to the metal.

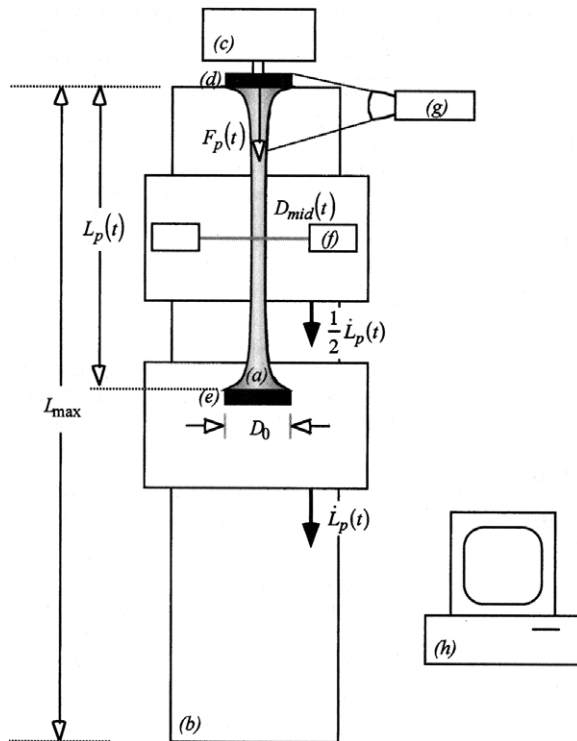


Figure 10.28 Sketch showing the principle of operation of the filament stretching rheometer described by McKinley and Sridhar [209]. (a) filament, (b) linear motor, (c) force transducer, (d) top endplate, (e) bottom endplate, (f) diameter sensor, (g) camera. Drawing from Anna et al. [208].

The strain in this device is not uniform, and the measurement is based on the portion of the filament midway between the end fixtures, where its diameter is a minimum. As a result, several preliminary experiments are required to establish an empirical relationship between the radius at this point, where the Hencky strain is $-2[\ln(R/R_0)]$, and the distance between the fixtures, $L(t)$. The data for $\epsilon < 1.0$ are not reliable, but steady state was reached in experiments by Bach et al. for an LDPE and an LLDPE, making it possible to determine the extensional viscosity [210]. The results agreed with data from an RME. This technique has also been used to demonstrate extension thickening in linear polystyrene [211]. It is necessary to correct data for the effect of gravity on the lower half of the sample and the shear stress resulting from the adhesion of the sample to the end-plates.

Because of its ability to reach the largest strains and lowest strain rates of any extensional rheometer, the FSR has been used in many fundamental studies, as mentioned in Section 10.9. A commercial version, the VADR1000, is now available (www.rheofilament.com).

Nielsen et al. [212] carried out a thorough comparison of the FSR, EVF, and SER based on the study of a highly entangled polyisoprene. The data from all three were within 15% of each other. For the units that are fixtures for rotational rheometers, it is advantageous to use samples with the smallest possible aspect ratio, but they have the advantage of being able to reach strain rates up to 5 s^{-1} , require a small sample and are easy and fast to use. The FSR, on the other hand can reach significantly higher strains, has better control of test variables, and can operate at very low strain rates. Nielsen et al. [213] used the FSR to study chain stretch in polyisoprene melts.

10.10.3 Uniaxial Extension—Approximate Methods

The extensional rheometers described above are limited to use at Hencky strain rates well below 10 s^{-1} . In order to reach higher strain rates, the drawdown of an extruded filament (melt spinning) and converging flow into an orifice die or capillary have been used to determine an apparent extensional viscosity. Such tests are often used in industry since commercial melt processing involves high stretching rates. Since the stress and strain are not uniform in these flows, it is necessary to model the flow in order to interpret data in terms of material functions. And such a simulation must incorporate a rheological model for the melt under study. This is the basic problem with techniques in which the kinematics is neither controlled nor known with precision. It is necessary to make a greatly simplified flow analysis to interpret the data in terms of an approximate material function.

In converging flow, one knows only the overall pressure drop and the flow rate, and results are very sensitive to die exit shape [214, 215]. Models used to interpret these data range from the simple, but still popular, approach of Cogswell [216] based on power laws. Simulations incorporating viscoelastic constitutive equations have also been attempted [217, 218]. Genieser et al. [219] carried out a detailed simulation of entrance flow and concluded that it is not possible to generate a significant degree of chain stretch using this technique. On the other hand, Laun and Schuch [220] compared average extensional viscosities calculated using Cogswell's equations with values determined using a reliable extensional rheometer. They found that there was some agreement for certain samples over narrow ranges of strain rate but that for other materials there was no correlation between the data from the two devices. And Hingmann and Marcinke [186] concluded from their study that converging flow is of very limited value for distinguishing between degrees of long-chain branching in commercial polymers.

In the “melt strength” test, usually carried out using the Göttfert Rheotens, a commercial version of an instrument developed by Meissner [221], a filament extruded from a capillary is drawn down by a rotary gear clamp. The melt is exposed to the

surroundings, so stretching is not isothermal. In this test, only the flow rate and tensile force are known, and several factors affect the behavior of the filament [222]. However, because the melt strength test is widely used in industry, considerable attention has been given to methods of interpreting test results [223, 224]. Laun and Schuch [220] concluded from their study that for film resins the tensile stress at break is a meaningful tool for characterizing such materials.

10.10.4 Rheometers for Biaxial and Planar Extension

To generate equibiaxial extension sheet inflation, lubricated squeeze flow, and rotary clamps have all been used. The most reliable of these is the one based on the rotary clamp technique, the latest version of which was described by Hachmann and Meissner [160]. But it was a very complex and difficult to use device, requiring very large samples and having no heating system. Lubricated squeezing flow is much simpler, although there are limitations on its capabilities due the difficulty of maintaining uniform lubrication [225–228]. Planar extension is the most difficult to generate, although one technique for doing so has been described [160]. In summary, biaxial or planar extensional rheometers are not suitable for routine use.

■ 10.11 Summary

When a deformation is neither very slow nor very small, the mechanical behavior of a polymer moves into the realm of nonlinear viscoelasticity. While the Boltzmann superposition principle provides a unifying principle for all linear viscoelastic behavior, there is no such unifying principle for nonlinear behavior. Before the advent of molecular theories, data were interpreted using empirical, continuum mechanics constitutive models, but the fitting of parameters to data is required so that these models are not predictive. In recent years, the advent of mean-field theories, particularly those based on the concept of a molecule in a tube or slip links, have provided a framework for understanding nonlinear behavior, and we have made reference to these in discussing nonlinear behavior in this chapter. Models based on this concept were introduced in Chapters 6 and 9, and their application to nonlinear behavior is described in detail in Chapter 11. One new element that is introduced into the models for large, rapid deformations is chain stretch followed by retraction, a very fast relaxation mechanism that does not occur in small or slow deformations. This mechanism is most apparent in stress relaxation following step strain. The remainder of the relaxation is found to progress as in the case of a small strain.

This phenomenon is described as time-strain superposability. Another relaxation mechanism that contributes to nonlinearity is convective constraint release, which is most prominent in steady simple shear at significant shear rates.

Constitutive equations describe quantitatively the response of a continuum to any type of deformation. There exists no universally applicable equation, but various models have been widely used to interpret experimental data and to predict behavior in complex flows based on data obtained using laboratory rheometers. A simple nonlinear model can be obtained by replacing the infinitesimal strain tensor in the Boltzmann principle by a finite measure of strain. If the Finger tensor is used, we obtain Lodge's rubberlike liquid model. This model predicts a non-zero first normal stress difference and strain hardening in extension, but it fails to predict any other nonlinear phenomena. The rubberlike liquid model can be modified by adding empirical constants or functions to describe more types of nonlinear behavior. In the tube model, the response to a large strain is understood to arise from retraction following the chain stretch caused by the large and very fast deformation.

Constitutive equations are now based on molecular models, and since the parameters in these models are related to basic molecular parameters, these models should be truly predictive, but their ability to make quantitative predictions is limited because of the simplifying assumptions necessary to derive them. These equations and their strengths and weaknesses are presented in detail in Chapter 11.

Turning to the behavior of typical melts, it is found that the damping function is not nearly as sensitive to molecular structure as linear viscoelastic properties, e.g. the storage and loss moduli. The rubberlike liquid, as well as the tube model, predict that the ratio of the first normal stress difference to the shear stress in step shear should be equal to the strain at all strains, and this is in fact observed. The other quantity measured in simple shear experiments is the second normal stress difference, but this is very difficult to measure and few data are available. Of the shear histories other than step strain than have been used to study nonlinear viscoelasticity, start-up of steady simple shear has been the most used.

The viscosity as a function of shear rate is the material function most often measured for melts; it is very similar to the complex viscosity as a function of the frequency, and both functions are quite sensitive to the molecular weight distribution in linear polymers as shown in Chapter 8. The shear thinning that is observed is not as strong as was predicted by the original tube model, and this is now explained as the result of convective constraint release. Long-chain branching results in greatly enhanced shear thinning, although this can also arise from a sufficiently broad molecular weight distribution, so in the absence of knowledge about the type of branching present, it is not possible to infer the level of branching from viscosity data.

While capillary rheometers are widely used to determine the viscosity at moderate to high shear rates, other nonlinear material functions require the use of an exper-

iment in which the strain and stress are uniform throughout the sample and can be varied with time in a well-controlled manner. Cone-plate rheometers are the most-used choice, but flow instabilities limit their use with melts to relatively low shear rates. Experiments can be carried to higher shear rates if the modulus is reduced by the addition of a large volume fraction of solvent. Sliding-plate instruments are useful at higher shear rates and when all three of the meaningful rheological stress quantities can be determined using birefringence, but wall slip occurs at sufficiently large strains and shear rates. Normal stress differences are more difficult to measure than the shear stress, particularly when these are varying with time.

Extensional flows yield information about rheological behavior that cannot be inferred from shear flow data. The test most widely used is start-up of steady, uniaxial extension. It is common practice to compare the transient tensile stress with the response predicted by the Boltzmann superposition principle using the linear relaxation spectrum; a nonlinear response should approach this curve at short times and low strain rates. A transient response that rises significantly above this curve is said to reflect strain-hardening behavior, while a material whose stress falls below the linear response is said to be strain softening. At a sufficiently long time, the stress becomes constant, and its steady-state value allows the calculation of the extensional viscosity as a function of strain rate. If the extensional viscosity increases with strain rate, the material is said to be extension thickening, while if it decreases, it is extension thinning.

Tube models predict that in a linear, monodisperse polymer, the extensional viscosity should decrease with strain rate at moderate rates, pass through a minimum, and then rise as chain stretch begins to occur. At a sufficiently high rate, the chain reaches its maximum stretch, and the extensional viscosity should approach a final plateau. However, strain rates capable of generating chain stretch in linear molecules are out of the range of most experimental methods. Some aspects of this behavior, however, have been observed in experimental data.

The extensional flow behavior of polydisperse, linear polymers is more complex. The presence of some higher molecular-weight material in a system consisting primarily of polymer having a moderate molecular weight can give rise to strain hardening. Tube models are so far unable to explain this behavior, a matter that is discussed in detail in Chapter 11.

While reliable data for a wide variety of branched systems is not yet available, it is known that extensional flow behavior is sensitive to branching structure. Stars behave like linear polymers, but when there is more than one branch point on at least some of the chains present, strain hardening is always observed. This observation has given rise to the expectation that extensional flow data would provide quantitative information about branching structure. However, the difficulties of obtaining reliable, precise data on a routine basis have so far limited the use of such tests for this purpose.

The most commonly used experiment is start-up of steady simple extension, and the main problems that arise are the support of the sample and the marked decrease in sample cross section at Hencky strains sufficient to generate nonlinear information. The small cross-section gives rise to necking and rupture that prematurely terminate experiments. Two commercial extensional rheometers are designed for use as fixtures in standard rotational rheometers. These are easy to use and inexpensive, but the stability of the flow at large strains remains a limitation. A relatively new device is the filament stretching rheometer, which is more complex but yields more precise data up to higher strains.

Since chain stretch is known to play a central role in nonlinear viscoelasticity, it is of interest to know the degree to which various experiments can generate stretch. It is clear that large-strain step shear generates stretch, the rapid relaxation of which, by retraction, precedes the time at which relaxation modulus data start to superpose and the damping function can be used to describe the data. In steady shear flow, convective constraint release is the dominant relaxation mechanism in the modestly nonlinear region; chain stretch can in theory be accessed at very high shear rates that are generally beyond the limits imposed by flow instabilities and viscous heating, unless the molecular weight is very high. Extensional flows at rates that can be reached using available instruments can generate significant chain stretch in many polymers.

■ References

- [1] Doi, M., Edwards, S.F. *The Theory of Polymer Dynamics*. Oxford Univ. Press, Oxford, 1986
- [2] Osaki, K., Nishizawa, K., Kurata, N. Material time constant characterization of nonlinear viscoelasticity of entangled polymeric solutions. *Macromol.* (1982) 15, pp. 1068–1071
- [3] Marrucci, G. Dynamics of entanglements: A nonlinear model consistent with the Cox-Merz rule. *J. Non-Newtonian Fluid Mech.* (1996) 62, pp. 279–289
- [4] Graessley, W.W. Molecular entanglement theory of flow behavior in amorphous polymers. *J. Chem. Phys.* (1965) 43, pp. 2696–2703
- [5] Larson, R.G. *Constitutive Equations for Polymer Melts and Solutions*. (1988) Butterworths, Boston
- [6] Bird, R.B., Armstrong, R.C., Hassager, O. *Dynamics of Polymeric Liquids, Vol. 1., Fluid Mechanics*, 2nd ed. (1986), John Wiley & Sons, New York
- [7] Dealy, J.M., Wang, J. *Melt Rheology and its Applications in the Plastics Industry*. Springer, New York, 2013
- [8] Lodge, A.S. *Elastic Liquids*. (1964) Academic Press, New York, Chapter 6

- [9] Wagner, M.H. Zur Netzwerktheorie von Polymer-Schmelzen. *Rheol. Acta* (1979) 18, pp. 33–50
- [10] Wagner, M.H., Demarmels, A.A. Constitutive analysis of extensional flows of polyisobutylene. *J. Rheol.* (1990) 36, pp. 943–958
- [11] Wagner, M.H., Schaeffer, J. Nonlinear strain measures for general biaxial extension of polymer melts, *J. Rheol.* (1992) 36, pp. 1–26
- [12] Wagner, M.H., Schaeffer, J. Rubbers and Polymer melts: universal aspects of non-linear stress-strain relations. *J. Rheol.* (1993) 37, pp. 643–661
- [13] Wagner, M.H., Schaeffer, J. Assessment of non-linear strain measures for extensional and shearing flows of polymer melts. *Rheol. Acta* (1994) 33, pp. 506–516
- [14] Rolón-Garrido, V.H. The molecular stress function (MSF) model in rheology. *Rheol. Acta* (2014) 53, pp. 663–700
- [15] Narimissa, E., Rolón-Garrido, V.H., Wagner, M.H. A Hierarchical Multi-Mode MSF Model for Long-Chain Branched Polymer Melts Part I: Elongational Flow. *Rheol. Acta* (2015) 54, pp. 779–791
- [16] Narimissa, E., Wagner, M.H. A Hierarchical Multi-Mode MSF Model for Long-Chain Branched Polymer Melts Part III: Shear Flows. *Rheol. Acta* (2016) 55, pp. 633–639
- [17] Narimissa, E., Wagner, M.H. A hierarchical multimode molecular stress function model for linear polymer melts in extensional flows. *J. Rheol.* (2016) 60, pp. 625–636
- [18] Narimissa, E., Wagner, M.H. From linear viscoelasticity to elongational flow of polydisperse linear and branched polymer melts: The hierarchical multi-mode molecular stress function model. *Polymer* (2016) 104, pp. 204–214
- [19] Urakawa, O., Takahashi, M., Masuda, T., Ebrahimi, N.G. Damping functions and chain relaxation in uniaxial and biaxial extensions: Comparison with the Doi-Edwards Theory. *Macromol.* (1995) 28, pp. 7196–7201
- [20] Inoue, T., Uematsu, T., Yamashita, Y., Osaki, K. Significance of the longest Rouse relaxation time in the stress relaxation process at large deformation of entangled polymer solutions. *Macromol.* (2002) 35, pp. 4718–4724
- [21] Roland, C.M., Archer, L.A., Mott, P.H., Sanchez-Reyes, J. Determining Rouse relaxation times from the dynamic modulus of entangled polymers. *J. Rheol.* (2004) 48, pp. 395–403
- [22] Menezes, E.V., Graessley, W.W. Nonlinear rheological behavior of polymer systems for several shear-flow histories. *J. Polym. Sci., Part B: Polym. Phys.* (1992) 20, pp. 1817–1833
- [23] Pattamaprom, C., Larson, R.G., Constraint Release Effects in Monodisperse and Bidisperse Polystyrenes in Fast Transient Shear Flows. *Macromol.* (2001) 34, pp. 5229–5237
- [24] Venerus, D.C., Brown, E.F., Burghardt, W.R. The nonlinear response of a polydisperse polymer solution to step strain deformations. *Macromol.* (1998) 31, pp. 9206–9212
- [25] Wagner, M.H., Rubio, P., Bastian, H. The molecular stress function model for polydisperse polymers melts with dissipative convective constraint release. *J. Rheol.* (2001) 45, pp. 1387–1412

- [26] Morrison, F.A., Larson, R.G. A study of shear-stress relaxation anomalies in binary mixtures of monodisperse polystyrenes. *J. Polym. Sci., Part B: Polym. Phys.*, (1992) 30, pp. 943–950
- [27] Sanchez-Reyes, J., Archer, L.A. Step shear dynamics of entangled polymer liquids. *Macromol.* (2002) 35, pp. 5194–5202
- [28] Yamaguchi, M., Takahashi, M. Rheological properties of low-density polyethylenes produced by tubular and vessel processes. *Polymer* (2001) 42, pp. 8663–8670
- [29] Watanabe, H. Viscoelasticity and dynamics of entangled polymers. *Prog. Polym. Sci.* (1999) 24, pp. 1253–1403
- [30] Osaki, K., Takatori, E., Kurata, M., Watanabe, H., Yoshida, H., Kotaka T. viscoelastic properties of solutions of star-branched polystyrene. *Macromol.* (1990) 23, pp. 4392–4396
- [31] Islam, M.T., Archer, L.A., Varshney, S.K. Linear rheology of entangled six-arm and eight-arm polybutadienes. *Macromol.* (2001) 34, pp. 6438–6449
- [32] McLeish, T.C.B. et al. Dynamics of entangled H-polymers: Theory, Rheology, and Neutron Scattering. *Macromol.* (1999) 32, pp. 6734–6758
- [33] Kasehagen, L.J., Macosko, C.W. Nonlinear shear and extensional rheology of long-chain randomly branched polybutadiene. *J. Rheol.* (1998) 42, pp. 1303–1327
- [34] Lodge, A.S., Meissner, J. On the use of instantaneous strains to test the Gaussian network hypothesis. *Rheol. Acta* (1972) 11, pp. 351–352
- [35] Laun, H.M. Description of the non-linear shear behavior of a low-density polyethylene melt. *Rheol. Acta* (1978) 17, pp. 1–15
- [36] Osaki, K., Bessho, N., Kojimoto, T., Kurata, M. Flow birefringence of polymer solutions in time-dependent field. *J. Rheol.* (1979) 23, pp. 617–624
- [37] Vrentas, C.M., Graessley, W.W. Relaxation of shear stress and normal stress components in step-strain experiments. *J. Non-Newtonian Fluid Mech.* (1981) 9, pp. 339–355
- [38] Brown, E.F., Burghardt, W.R., Kahvand, H., Venerus, D.C. Comparison of optical and mechanical measurements of second normal stress difference relaxation following step strain. *Rheol. Acta* (1995) 34, pp. 221–234
- [39] Olson, D.J., Brown, E.F., Burghardt, W.R. Second normal stress difference relaxation in a linear polymer melt following step-strain. *J. Polym. Sci., Part B: Polym. Phys.* (1998) 36, pp. 2671–2675
- [40] Osaki, K., Ohta, S., Fukada, M., Kurata, M. Nonlinear viscoelasticity of polystyrene solutions. III. Start of steady shear flow. *J. Polym. Sci., Polym. Phys. Ed.* (1976) 14, pp. 1701–1715
- [41] Venerus, D.C., Kahvand, H. Normal stress relaxation in reversing double-step flows. *J. Rheol.* (1994) 38, pp. 1297–1315
- [42] Osaki, K., Inoue, T., Isomura, T. Stress overshoot of polymer solutions at high rates of shear. *J. Polym. Sci., Part B: Polym. Phys.* (2000) 38, pp. 1917–1925
- [43] Graessley, W.W., Park, W.S., Crawley, R.L. Experimental tests of constitutive relations for polymers undergoing uniaxial shear flows. *Rheol. Acta* (1977) 16, pp. 291–301

- [44] Menezes, E.V., Graessley, W.W. Study of the nonlinear response of a polymer solution to various uniaxial shear flow histories. *Rheol. Acta* (1980) 19, pp. 38–50
- [45] Schweizer, T., van Meerveld, J., Öttinger, H.C. Nonlinear shear rheology of polystyrene melt with narrow molecular weight distribution—Experiment and theory. *J. Rheol.* (2004) 48, pp. 1345–1363
- [46] Pearson, D.S. Flow-birefringence of concentrated polystyrene solutions. *J. Rheol.* (1989) 33, pp. 517–535
- [47] Masubuchi, Y., Watanabe, H. Origin of Stress Overshoot under Start-up Shear in Primitive Chain Network Simulation. *ACS Macro Lett.* (2014) 3, pp. 1183–1186
- [48] Snijkers, F., Ratkanthwar, K., Vlassopoulos, D., Hadjichristidis, N. Viscoelasticity, nonlinear shear start-up, and relaxation of entangled star polymers. *Macromol.* (2013) 46, pp. 5702–5713
- [49] Snijkers, F., Kirkwood, K.M., Vlassopoulos, D., Leal, L.G., Nikopoulou, A., Hadjichristidis, N., Coppola, S. Viscoelasticity and nonlinear simple shear flow behavior of an entangled asymmetric exact comb polymer solution. *J. Rheol.* (2016) 60, pp. 451–463
- [50] Stratton, R.A., Butcher, A.F. Stress relaxation upon cessation of steady flow and the overshoot effect of polymer solutions. *J. Polym. Sci., Polym. Phys. Ed.* (1973) 11, pp. 1747–1758
- [51] Tsang, W.K.W., Dealy, J.M. The use of large transient deformations to evaluate rheological models for molten polymers. *J. Non-Newtonian Fluid Mech.* (1981) 9, pp. 203–222
- [52] Robertson, C.G., Warren, S., Plazek, D.J., Roland, C.M. Re-entanglement kinetics in sheared polybutadiene solutions. *Macromol.* (2004) 37, pp. 10018–10022
- [53] Roy, D., Roland, C.M. Reentanglement kinetics in polyisobutylene. *Macromol.* (2013) 46, pp. 9403–9408
- [54] Wilhelm, M., Maring, D., Spiess, H.W. Fourier-Transform Rheology. *Rheol. Acta* (1998) 37, pp. 399–405
- [55] Wilhelm, M., Reinheimer, P., Ortseifer, M. High sensitivity Fourier-transform rheology, *Rheol. Acta* (1999) 38, pp. 349–356
- [56] Hyun, K., Wilhelm, M., Klein, C.O., Kwang, S.C., Nam, J.G., Ahn, K.H., Leed, S.J., Ewoldt, R.H., McKinley, G.H. A review of nonlinear oscillatory shear tests: Analysis and application of large amplitude oscillatory shear (LAOS). *Prog. Polym. Sci.* (2011) 36, pp. 1697–1753
- [57] Pipkin, A.C. *Lectures in Viscoelastic Theory*. (1972) Springer-Verlag, New York
- [58] Macosko, C.W. *Rheology: Principles, Measurements, and Applications*. (1994) VCH, New York
- [59] Phan-Thien, N., Newberrys, M., Tanner, R.I. Nonlinear oscillatory flow of a soft solid-like viscoelastic material. *J. Non-Newtonian Fluid Mech.* (2000) 92, pp. 67–80
- [60] Ng, T.S.K., McKinley, G.H., Ewoldt, R.H. Large amplitude oscillatory shear flow of gluten dough: a model power-law gel. *J. Rheol.* (2011) 55, pp. 627–654

- [61] Famini, Z., Broedersz, C.P., van Kempen, T.H.S., Florea, D., Peters, G.W.M., Wyss, H.M. A new approach for calculating the true stress response from large amplitude oscillatory shear (LAOS) measurements using parallel plates. *Rheol. Acta* (2014) 53, p. 75–83
- [62] Hyun, K., Wilhelm, M. Establishing a new mechanical nonlinear coefficient Q from FT-rheology: First investigation of entangled linear and comb polymer systems. *Macromol.* (2009) 42, pp. 411–422
- [63] Cziep, M.A., Abbasi, M., Heck, M., Arens, L., Wilhelm, M. Effect of molecular weight, polydispersity, and monomer of linear homopolymer melts on the intrinsic mechanical nonlinearity if MAOS. *Macromol.* (2016) 49, pp. 3566–3579
- [64] Wagner, M.H., Rolón-Garrido, V.H., Hyun, K., Wilhelm, M. Analysis of medium amplitude oscillatory shear data of entangled linear and model comb polymers. *J. Rheol.* (2011) 55, pp. 495–516
- [65] Giacomin, A.J., Gilbert, P.H., Merger, D., Wilhelm, M. Large-amplitude oscillatory shear: Comparing parallel-disk with cone-plate flow. *Rheol. Acta* (2015) 54, pp. 263–285
- [66] Hoyle, D.M., Auhl, D., Harlen, O.G., Barroso, V.C., Wilhelm, M., McLeish, T.C.B. Large amplitude oscillatory shear and Fourier transform rheology analysis of branched polymer melts. *J. Rheol.* (2014) 58, pp. 969–997
- [67] Pearson, D.S., Rochefort, W.E. Behavior of concentrated polystyrene solutions in large-amplitude oscillating shear fields. *J. Polym. Sci.* (1982) 20, pp. 83–98
- [68] Ewoldt, R.H., McKinley, G.H. On secondary loops in LAOS via self-intersection of Lissajous–Bowditch curves. *Rheol. Acta* (2010) 49, pp. 213–219
- [69] Ewoldt, R.H., Hosoi, A.E., McKinley, G.H. New measures for characterizing nonlinear viscoelasticity in large amplitude oscillatory shear. *J. Rheol.* (2008) 52, pp. 1427–1458
- [70] Meissner, J. Deformationsverhalten der Kunststoffe im flüssigen und im festen Zustand. *Kunststoffe* (1971) 61, pp. 576–582
- [71] Cross, M.M. in *Polymer Systems: Deformation and Flow* Wetton and Whorlow, Eds. (1968) Macmillan, London
- [72] Carreau, P.J. Rheological equations from molecular network theories. *Trans. Soc. Rheol.* (1972) 16, pp. 99–127
- [73] Hieber, C.A., Chiang, H.H. Shear-rate-dependence modeling of polymer melt viscosity. *Polym. Eng. Sci.* (1992) 14, pp. 931–938
- [74] Yasuda, K.Y., Armstrong, R.C., Cohen, R.E. Shear flow properties of concentrated solutions of linear and star-branched polystyrenes. *Rheol. Acta* (1981) 20, pp. 163–178
- [75] Elberli, B., Shaw, M.T. Time constants from shear viscosity data. *J. Rheol.* (1978) 22, pp. 561–570
- [76] Plumley, T.A., Lai, S., Betso S.R., Knight, G.W. Rheological modeling of Insite technology polymers. *SPE ANTEC Tech. Papers* (1994) 40, pp. 1221–1224
- [77] Kataoka, T., Ueda, S.J. Flow properties of polyethylene melt. *J. Appl. Polym. Sci.* (1968) 12, pp. 939–953

- [78] Graessley, W.W. The entanglement concept in polymer rheology. *Adv. Polym. Sci.* (1974) 16, pp. 1–179
- [79] Berry, G.C., Hager, B.L., Wong, C.-P. *Macromol.* (1977) 10, pp. 361–365
- [80] Attané, P., Pierrard, J.M., Turrell, G. Steady and transient shear flows of polystyrene solutions. *J. Non-Newtonian Fluid Mech.* (1985) 18, pp. 295–317
- [81] Ianniruberto, G., Marrucci, G. A multi-mode CCR model for entangled polymers with chain stretch. *J. Non-Newtonian Fluid Mech.* (2002) 102, pp. 383–395
- [82] Bercea, M., Peiti, C., Simionescu, B., Navard, P. Shear rheology of semidilute poly(methyl methacrylate) solutions. *Macromol.* (1993) 26, pp. 7095–7096
- [83] Shroff, A.R., Mavridis, H. New measures of polydispersity from rheological data on polymer melts. *J. Appl. Polym. Sci.* (1995) 57, pp. 1605–1626
- [84] Robertson, C.G., García-Franco, C.A., Srinivas, S. Extent of branching from linear viscoelasticity of long-chain branched polymers. *J. Polym. Sci., Part B: Polym. Phys.* (2005) 42, pp. 1671–1684
- [85] Lai, S., Plumley, T.A., Butler, T.I., Knight, G.W., Kao, C.I. Dow rheology index (DRI) for Insite technology polyolefins. *SPE ANTEC Tech. Papers* (1994) 40, pp. 1814–1815
- [86] Wood-Adams, P.M. The effect of long chain branches on the shear flow behavior of polyethylene. *J. Rheol.* (2001) 45, pp. 203–210
- [87] Laun, H.M. Prediction of elastic strains of polymers melts in shear and elongation. *J. Rheol.* (1986) 30, pp. 459–501
- [88] Xu, J., Costeux, S., Dealy, J.M., De Decker, M.N. Use of a sliding plate rheometer to measure the first normal stress difference at high shear rates. *Rheol. Acta* (2007) 46, pp. 815–824
- [89] Islam, M.T., Sanchez-Reyes, J., Archer, L.A. Step and steady shear responses of nearly monodisperse highly entangled 1,4-polybutadiene solutions. *Rheol. Acta* (2003) 42, pp. 191–198
- [90] Laun, H.M. Elastic properties of polymer melts at high shear rates with respect to extrusion. *Rheol. Acta* (1982) 21, pp. 464–469
- [91] Doi, M., Edwards, S.F. Dynamics of concentrated polymer systems. *J. Chem. Soc., Faraday Trans. II* (1979) 75, pp. 38–54
- [92] Magda, J.J., Lee, C.-S., Muller, S.J., Larson, R.G. Rheology, flow instabilities and shear-induced diffusion in polystyrene solutions. *Macromol.* (1993) 26, pp. 1696–1706
- [93] Lee, C.-S., Magda, J.J., DeVries, K.L., Mays, J.W. Measurements of the second normal stress difference for star polymers with highly entangled branches. *Macromol.* (1992) 25, pp. 4744–4750
- [94] Hanson, D.E. Shear modification of polyethylene. *Polym. Eng. Sci.* (1969) 9, pp. 405–414
- [95] Rodudai, M., Mihara, S., Fujiki, T.J. Influence of shearing history on the rheological properties and processability of branched polymers. *J. Appl. Polym. Sci.* (1979) 32, pp. 463–471
- [96] Leblans, P.J.R., Bastiaansen, C. Shear modification of low-density polyethylene: its origin and its effect on the basic rheological functions of the melt. *Macromol.* (1989) 22, pp. 3312–3317

- [97] Bourrigaud, S., Marin, G., Poitou, A. Shear modification of long-chain branched polymers: A theoretical approach using the pom-pom model. *Macromol.* (2003) 36, pp. 1388–1394
- [98] Yamaguchi, M., Gogos, C.G. Quantitative relation between shear history and rheological properties of LDPE, *Adv. Polym. Technol.* (2001) 20 (4), pp. 261–269
- [99] Yamaguchi, M., Todd, D., Gogos, C.G. Rheological properties of LDPE processed by conventional processing machines. *Adv. Polym. Technol.* (2003) 22 (3), pp. 179–187
- [100] Mackay, M.E., Dick, G.K. A comparison of the dimensions of a truncated cone measured with various techniques: The cone measurement project. *J. Rheol.* (1995) 39, pp. 673–677
- [101] Vermant, J., Moldenaers, P., Mewis, J., Ellis, M., Garritano, R. Orthogonal superposition measurements using a rheometer equipped with a force rebalance transducer. *Rev. Sci. Instrum.* (1987) 68, pp. 4090–4096
- [102] Laun, H.M. Description of the non-linear shear behavior of a low density polyethylene melt by means of an experimentally determined strain dependent memory function. *Rheol. Acta* (1978) 17, pp. 1–15
- [103] Flory, A., McKenna, G.B. Finite step rate corrections in stress relaxation experiments: A comparison of two methods. *Mech. Time-Depend. Mater.* (2004) 8, pp. 17–37
- [104] Archer, L.A., Chen, Y.-L., Larson, R.G. Delayed slip after step strains in highly entangled polystyrene solutions. *J. Rheol.* (1995) 39, pp. 519–525
- [105] Archer, L.A. Comments on “A critical evaluation of step strain flows of entangled polymer melts”. *J. Rheol.* 49, pp. 277–295
- [106] Larson, R.G. Instabilities in viscoelastic flows. *Rheol. Acta* (1992) 31, pp. 213–263
- [107] Hutton, J.F. Fracture and secondary flow of elastic liquids. *Rheol. Acta* (1969) 8, pp. 54–59
- [108] Gleissle, W. Schub-und Normalspannungsmessungen an Silikonölen bei hohen Scherfällen mit einem neuen Kegel-Platte-Rheometer. *Colloid Polym. Sci.* (1974) 252, pp. 848–853
- [109] Chen, Y.L., Larson, R.G., Patel, S.S. Shear fracture of polystyrene melts and solutions. *Rheol. Acta* (1994) 33, pp. 243–256
- [110] Lee, C.S., Tripp, B.C., Magda, J.J. Does N1 or N2 control the onset of edge fracture? *Rheol. Acta* (1992) 31, pp. 306–308
- [111] Kulicke, W.M., Porter, R.S. Irregularities in steady flow of non-Newtonian fluids between cone and plate. *J. Appl. Polym. Sci.* (1979) 23, pp. 953–965
- [112] Kulicke, W.M., Jeberien, H.E., Kiss, H., Porter, R.S. Visual observation of flow irregularities in polymer solutions. *Rheol. Acta* (1979) 18, pp. 711–716
- [113] Larson, R.G. Nonlinear shear relaxation modulus for a linear low-density polyethylene. *J. Rheol.* (1985) 29, pp. 823–831
- [114] Schweizer, T. Comparing cone-partitioned plate and cone-standard plate shear rheometry of a polystyrene melt. *J. Rheol.* (2003) 47, pp. 1071–1085
- [115] Schweizer, T., Stöckli, M. Departure from linear velocity profile at the surface of polystyrene melts during shear in cone-plate geometry. *J. Rheol.* (2008) 523, pp. 713–727

- [116] Miller, M.J., Christiansen, E.B. The stress state of elastic fluids in viscometric flow. *AICHE J.* (1972) 18, pp. 600–608
- [117] Baek, S.-G., Magda, J.J. Monolithic rheometer plate fabricated using silicon micro-machining technology and containing miniature pressure sensors for N_1 and N_2 measurements. *J. Rheol.* (2003) 47, pp. 1249–1260
- [118] Alcoutlabi, M., Baek, S.G., Magda, J.J., Shi, X., Hutcheson, S.A., McKenna, G.B. A comparison of three different methods for measuring both normal stress differences of viscoelastic liquids in torsional rheometers. *Rheol. Acta* (2009) 48, pp. 191–200
- [119] Meissner, J., Garbella, R.W., Hostettler, J. Measuring normal stress differences in polymer melt shear flow. *J. Rheol.* (1989) 33, pp. 843–864
- [120] Schwiezer, T., Schmidheiny, W. A cone-partitioned plate rheometer cell with three partitions (CPP3) to determine shear stress and both normal stress differences for small quantities of polymeric fluids. *J. Rheol.* (2013) 57, pp. 841–856
- [121] Giacomin, A.J., Samurkas, T., Dealy, J.M. A novel sliding plate rheometer for molten polymers, *Polym. Eng. Sci.* (1989) 29, pp. 499–504
- [122] Reimers, M., Dealy, J.M. Sliding plate rheometer studies of concentrated polystyrene solutions; Large amplitude oscillatory shear of a very high molecular weight polymer in diethyl phthalate. *J. Rheol.* (1996) 40, pp. 167–186
- [123] Reimers, M., Dealy, J.M. Sliding plate rheometer studies of concentrated polystyrene solutions: Nonlinear viscoelasticity and wall slip of two high molecular weight polymers in tricresyl phosphate. *J. Rheol.* (1998) 42, pp. 527–548
- [124] Koran, F., Dealy, J.M. A high-pressure sliding plate rheometer for polymer melts. *J. Rheol.* (1999) 43, pp. 1279–1290
- [125] Park, H.E., Dealy, J.M. Effect of pressure and supercritical CO₂ on the viscosity of polyethylene. *Macromol.* (2006) 39, pp. 5438–5452
- [126] Park, H.E., Lim, S.T., Laun, M.H., Dealy, J.M. Measurement of pressure coefficient of polymer viscosity: Drag flow versus capillary flow. *Rheol. Acta* (2008) 47, pp. 1023–1038
- [127] Koran, F., Dealy, J.M. Wall slip of polyisobutylene: interfacial and pressure effects. *J. Rheol.* (1999) 43, pp. 1291–1306
- [128] Mhetar, V.R., Archer, L.A. Secondary flow of entangled polymer fluids in plane couette shear. *J. Rheol.* (1996) 40, pp. 549–571
- [129] Hatzikiriakos, S.G., Dealy, J.M. Wall slip of molten high density polyethylene. I. Sliding plate rheometer studies. *J. Rheol.* (1991) 35, pp. 497–523
- [130] Hatzikiriakos, S.G., Stewart, C.W., Dealy, J.M. Effect of surface coatings on the wall slip Of LLDPE, *Int. Polym. Process.* (1993) 8, pp. 30–35
- [131] Hatzikiriakos, S.G., Kalogerakis, N. A dynamic slip velocity model for molten polymers based on a network kinetic theory. *Rheol. Acta* (1994) 33, pp. 38–47
- [132] Park, H.E., Lim, S.T., Smillo, F., Dealy, J.M., Robertson, C.G. Wall slip and spurt of polybutadiene. *J. Rheol.* (2008) 52, pp. 1201–1239
- [133] Fuller, G.G. *Optical rheometry of complex fluids*. (2005) Oxford Univ. Press, NY

- [134] Lodge, T.P. Rheo-Optics: Flow Birefringence, Chap. 9 of: Macosko, C.W. *Rheology Principles, Measurements and Applications*. (1994) VCH Publishers, NY, Weinheim.
- [135] Venerus, D.C., Zhu, S.H., Öttinger, H.C. Stress and birefringence measurements during the uniaxial elongation of polystyrene melts *J. Rheol.* (1999) 43, pp. 795–813
- [136] Olson, D.F., Brown, E.F., Burghardt, W.R. Second normal stress difference relaxation in a linear polymer melt following step-strain. *J. Polym. Sci., Part B: Polym. Phys.* (1998) 36, pp. 2671–2675
- [137] Frattini, P.L., Fuller, G.G. A note on phase-modulated flow birefringence: A promising rheo-optical method. *J. Rheol.* (1984) 28, pp. 61–70
- [138] Kalogrianitis, S.G., van Egmond, J.W. Full tensor optical rheometry of polymer fluids. *J. Rheol.* (1997) 41, pp. 343–364
- [139] Schümmel, P., Worthoff, R.H. An elementary method for the evaluation of a flow curve. *Chem. Eng. Sci.* (1978) 33, pp. 759–763
- [140] Laun, H.M., Polymer melt rheology with a slit die. *Rheol. Acta* (1983) 22, pp. 171–185
- [141] Laun, H.M. Pressure dependent viscosity and dissipative heating in capillary rheometry of polymer melts. *Rheol. Acta* (2003) 42, pp. 295–308
- [142] Hay, G., Mackay, M.E., Awati, K.M., Park, Y. Pressure and temperature effects in slit rheometry. *J. Rheol.* (1999) 43, pp. 1099–1116
- [143] Dees, M., Mangnus, M., Hermans, N., Thaens, W., Hanot, A.-S., Van Puyvelde, P. On the pressure correction of capillary melt rheology data. *Rheol. Acta* (2011) 50, pp. 117–124
- [144] Hatzikiriakos, S.G., Dealy, J.M. Wall slip of molten high density polyethylene. II. Capillary rheometer studies. *J. Rheol.* (1992) 36, pp. 703–741
- [145] Hatzikiriakos, S.G., Dealy, J.M. Start-up pressure transients in a capillary rheometer. *Polym. Eng. Sci.* (1994) 34, pp. 493–499
- [146] Dealy, J.M. On the Significance of Pressure Relaxations in Capillary and Slit Flow. *Rheol. Acta* (1995) 34, pp. 115–116
- [147] Cox, W.P., Merz, E.H. Correlation of dynamic and steady flow viscosities. *J. Polym. Sci.* (1958) 28, pp. 619–621
- [148] Ferri, D., Lomellini, P. Melt rheology of randomly branched polystyrenes. *J. Rheol.* (1999) 43, pp. 1355–1372
- [149] Utracki, L.A., Gendron, R. Pressure oscillation during extrusion of polyethylenes. *J. Rheol.* (1984) 28, pp. 601–623
- [150] Venkatraman, S., Okano, M., Nixon, A. A comparison of torsional and capillary rheometry for polymer melts: The Cox-Merz rule revisited. *Polym. Eng. Sci.* (1990) 30, pp. 308–313
- [151] Booij, H.C., Leblans, P., Palmen, J., Tiemersma-Thoone, G. Nonlinear viscoelasticity and the Cox-Merz relations for polymeric fluids. *J. Polym. Sci., Polym. Phys. Ed.* (1983) 21, pp. 1703–1711
- [152] Milner, S.T. Relating the shear-thinning curve to the molecular weight distribution in linear polymer melts. *J. Rheol.* (1996) 40, pp. 303–315

- [153] Münstedt, H., Laun, H.M. Elongational behavior of a low density polyethylene melt II. Transient behavior in constant stretching rate and tensile creep experiments. *Rheol. Acta* (1979) 18, pp. 492–504
- [154] Wood-Adams, P.M., Dealy, J.M., deGroot, A.W., Redwine, O.D. Effect of molecular structure on the linear viscoelastic behavior of polyethylene. *Macromol.* (2000) 33, pp. 7489–7499
- [155] Vega, J.F., Fernández, M., Santamaráa, A., Muñoz-Escalona, Lafuente, P. Rheological criteria to characterize metallocene catalyzed polyethylenes. *Macromol. Chem. Phys.* (1999) 200, pp. 2257–2268
- [156] Taylor, G.I. The mechanism of plastic deformation in crystals. Part I. Theoretical. *Proc. R. Soc. London, Ser. A* (1934) 145, pp. 362–404
- [157] McKinley, G.H., Hassager, O. The Considère condition and rapid stretching of linear and branched polymer melts. *J. Rheol.* (1999) 43, pp. 1195–1212
- [158] Fielding, S.M. Criterion for Extensional Necking Instability in Polymeric Fluids. *Phys. Rev. Lett.* (2011) 107, 258301, pp. 1–5
- [159] Marrucci, G., Ianniruberto, G. Interchain pressure effect in extensional flows of entangled polymer. *Macromol.* (2004) 37, pp. 3934–3942
- [160] Hachmann, P., Meissner, J. Rheometer for equibiaxial and planar elongations of polymer melts. *J. Rheol.* (2003) 47, pp. 989–1010
- [161] Rasmussen, H.K., Huang, Q. The missing link between the extensional dynamics of polymer melts and solutions. *J. Non-Newtonian Fluid Mech.* (2014) 204, pp. 1–6
- [162] Sridhar, T., Acharya, M., Nguyen, D.A., Bhattacharjee, P.K. On the extensional rheology of polymer melts and concentrated solutions. *Macromol.* (2014) 47, pp. 379–386
- [163] Wingstrand, S.L., Alvarez, N.J., Huang, Q., Hassager, O. Linear and nonlinear universality in the rheology of polymer melts and solutions. *Phys. Rev. Lett.* (2015) 115, 78302, pp. 1–5
- [164] Bach, A., Almdal, K., Rasmussen, H.K., Hassager, O. Elongational viscosity of narrow molar mass distribution polystyrene. *Macromol.* (2003) 36, pp. 5174–5179
- [165] Hassager, O., Mortensen, K., Bach, A., Almdal, K., Rasmussen, H.K., Pyckhout-Hintzen, W. Stress and neutron scattering measurements on linear polymer melts undergoing steady elongational flow. *Rheol. Acta* (2012) 51, pp. 385–394
- [166] Bhattacharjee, P.K., Nguyen, D.A., McKinley, G.H., Sridhar, T. Extensional stress growth and stress relaxation in entangled polymer solutions. *J. Rheol.* (2003) 47, pp. 269–290
- [167] Bhattacharjee, P.K., Oberhauser, J.P., McKinley, G.H., Leal, L.G., Sridhar, T. Extensional rheometry of entangled solutions. *Macromol.* (2002) 35, pp. 10131–10148
- [168] Münstedt, H. Dependence of the elongational behavior of polystyrene melts on molecular weight and molecular weight distribution. *J. Rheol.* (1980) 24, pp. 847–867
- [169] Nielsen, J.K., Rasmussen, H.K., Hassager, O., McKinley, G.H. Elongational viscosity of monodisperse and bidisperse polystyrene melts. *J. Rheol.* (2006) 50, pp. 453–476

- [170] van Ruymbeke, E., Nielsen, J., Hassager, O. Linear and nonlinear viscoelastic properties of bidisperse linear polymers: Mixing law and tube pressure effect. *J. Rheol.* (2010) 54, pp. 1155–1172
- [171] Auhl, D., Chambon, P., McLeish, T.J.B., Read, D.J. Elongational Flow of Blends of Long and Short Polymers: Effective Stretch Relaxation Time. *Phys. Rev. Lett.* (2009) 103, 136001, pp. 1–4
- [172] Münstedt, H., Kurzbeck, S., Egersdörfer, L. Influence of molecular structure on rheological properties of polyethylenes. Part II. Elongational behavior. *Rheol. Acta* (1998) 37, pp. 21–29
- [173] Gabriel, C., Kaschta, J., Münstedt, H. Influence of molecular structure on rheological properties of polyethylenes. I. Creep recovery measurements in shear. *Rheol. Acta* (1998) 37, pp. 7–20
- [174] van Ruiten, J., Boode, J.W. Mixing and demixing of heterogeneous ethylene-octene copolymers. *Polymer* (1992) 33, pp. 2548–2552
- [175] Nielsen, J.K., Rasmussen, H.K., Denberg, M., Almdal, K., Hassager, O. Nonlinear branch-point dynamics of multiarm polystyrene. *Macromol.* (2006) 39, pp. 8844–8853
- [176] Hepperle, J., Münstedt, H. Rheological properties of branched polystyrenes: nonlinear shear and extensional behavior. *Rheol. Acta* (2006) 45, pp. 717–727
- [177] Lentzakis, H., Vlassopoulos, D., Read, D.J., Lee, H., Chang, T., Driva, P., Hadjichristidis, H. Uniaxial extensional rheology of well-characterized comb polymers. *J. Rheol.* (2013) 57, pp. 605–625
- [178] van Ruymbeke, E., Muliawan, E.B., Hatzikiriakos, S.G., Watanabe, T., Hirao, A., Vlassopoulos, D. Viscoelastic and extensional rheology of model Cayley-tree polymers of different generations. *J. Rheol.* (2010) 54, pp. 643–662
- [179] Das, C., Read, D.J., Auhl, D., Kapnistos, M., den Doelder, J., Vittorias, I., McLeish, T.C.B. Numerical prediction of nonlinear rheology of branched polymer melts. *J. Rheol.* (2014) 58, pp. 737–757
- [180] Lohse, D.J., Milner, S.T., Fetter, L.J., Xenidou, M., Hadjichristidis, N., Mendelson, R.A., Garcia-Franco, C.A., Lyon, M.K. Well-defined model long chain branched polyethylene. 2. Melt Rheological Behavior. *Macromol.* (2002) 35, pp. 3066–3075
- [181] Münstedt, H., Steffl, T., Malmberg, A. Correlation between rheological behavior in uniaxial elongation and film blowing properties of various polyethylenes. *Rheol. Acta* (2005) 45, pp. 14–22
- [182] Stange, J., Uhl, C., Münstedt, H. Rheological behavior of blends from a linear and a long-chain branched polypropylene. *J. Rheol.* (2005) 49, pp. 1059–1079
- [183] Torres, E., Li, S.-W., Costeux, S., Dealy, J.M. Branching structure and strain hardening of branched metallocene polyethylenes. *J. Rheol.* (2015) 59, pp. 1151–1172
- [184] Malmberg, A., Gabriel, C., Steffl, T., Münstedt, H., Löfgren, B. Long-chain branching in metallocene-catalyzed polyethylenes investigated by low oscillatory shear and uniaxial extensional rheometry. *Macromol.* (2002) 35, pp. 1038–1048

- [185] Kurzbeck, C., Oster, F., Münstedt, H., Nguyen, T.Q., Gensler, R. Rheological properties of two polypropylenes with different molecular structure. *J. Rheol.* (1999) 43, pp. 359–374
- [186] Hingmann, R., Marcinke, B.L. Shear and elongational flow properties of polypropylene melts. *J. Rheol.* (1994) 38, pp. 573–587
- [187] Kasehagen, L.J., Macosko, C.W. Non-linear shear and extensional rheology of long-chain randomly branched polybutadiene. *J. Rheol.* (1998) 42, pp. 1303–1327
- [188] Laun, H.M., Münstedt, H. Elongational behavior of a low-density polyethylene melt. *Rheol. Acta* (1978) 17, pp. 415–425
- [189] Gabriel, C., Münstedt, H. Strain hardening of various polyolefins in uniaxial elongational flow. *J. Rheol.* (2003) 47, pp. 619–630
- [190] Rasmussen, H.K., Nielsen, J.K., Bach, A., Hassager, O. Viscosity overshoot in the start-up of uniaxial elongation of low density polyethylene melts. *J. Rheol.* (2005) 49, pp. 369–381
- [191] Burghelea, T.I., Zdeněk, S., Münstedt, H. On the “viscosity overshoot” during the uniaxial extension of a low density polyethylene. *J. Non-Newtonian Fluid Mech.* (2011) 166, pp. 1198–1209
- [192] Alvarez, N.J., Marín, J.M.R., Huang, Q., Michelsen, M.L., Hassager, O. Creep measurements confirm steady flow after stress maximum in extension of branched polymer melts. *Phys. Rev. Lett.* (2013) 110, 168301, pp. 1–4
- [193] Meissner, J. Dehnungsverhalten von polyäthylen-Schmelzen. *Rheol. Acta* (1971) 10, pp. 230–242
- [194] Laun, H.M., Münstedt, H. Comparison of elongational behavior of a polyethylene melt at constant stress and constant strain rate. *Rheol. Acta* (1976) 15, pp. 517–524
- [195] Meissner, J., Hostettler, J. A new elongational rheometer for polymer melts and other highly viscoelastic liquids. *Rheol. Acta* (1994) 33, pp. 1–21
- [196] Barroso, V.C., Covas, H.A., Maia, J.M. Sources of error and other difficulties in extensional rheometry. *Rheol. Acta* (2002) 41, pp. 154–161
- [197] Schweizer, T. The uniaxial elongational rheometer RME – Six years of experience. *Rheol. Acta* (2000) 39, pp. 428–443
- [198] Schulze, J.S., Lodge, T.P., Macosko, C.W., Hepperle, J., Münstedt, H., Bastian, H., Ferri, D., Groves, D.J., Kim, Y.H., Lyon, M., Schweizer, T., Virkler, T., Wassner, E., Zoetelief, W. A comparison of extensional viscosity measurements from various RME rheometers. *Rheol. Acta* (2001) 40, pp. 457–466
- [199] Münstedt, H. New universal extensional rheometer for polymer melts. Measurements on a polystyrene sample. *J. Rheol.* (1979) 223, pp. 421–436
- [200] Sentmanat, M.L. Miniature universal testing platform from extensional melt rheology to solid-state deformation behavior. *Rheol. Acta* (2004) 43, pp. 657–669
- [201] Sentmanat, M., Wang, B.N., McKinley, G.H. Measuring the transient extensional Rheology of polyethylene melts using the SER universal testing platform. *J. Rheol.* (2005) 49, pp. 585–606

- [202] Sentmanat, M., Wang, B.N., McKinley, G.H. Measuring the transient extensional rheology of polyethylene melts using the SER universal testing platform. *J. Rheol.* (2005) 49, pp. 585–606
- [203] Aho, J., Rolón-Garrido, V.H., Syrjälä, S., Wagner, M.H. Measurement technique and data analysis of extensional viscosity for polymer melts by Sentmanat extensional rheometer (SER). *Rheol. Acta* (2010) 49, pp. 359–370
- [204] Lin, P., Wang, S.-Q. Nonisothermal condition in melt extension experiments. *J. Rheol.* (2015) 59, pp. 1329–1334
- [205] Stadler, F.J., Nishioka, A., Stange, J., Koyama, K., Münstedt, H. Comparison of elongational behavior of various polyolefins in uniaxial and equibiaxial flows. *Rheol. Acta* (2007) 46, pp. 1003–1012
- [206] Stadler, F.J., Kaschta, J., Münstedt, H., Becker, F., Buback, M. Influence of molar mass distribution and long-chain branching on strain hardening of low density polyethylene. *Rheol. Acta* (2009) 48, pp. 479–490
- [207] V. Tirtatmadja and T. Sridhar, A filament stretching device for measurement of extensional viscosity. *J. Rheol.* (1993) 37 pp. 1081–1102
- [208] Anna, S.L., McKinley, G.H., Nguyen, D.A., Sridhar, T., Muller, S.J., James, D.F., Huang, J. An interlaboratory comparison of measurements from filament-stretching rheometers using common test fluids. *J. Rheol.* (2001) 45, pp. 83–114
- [209] McKinley, G.H., Sridhar, T. Filament-stretching rheometry of complex fluids. *Annu. Rev. Fluid Mech.* (2002) 34, pp. 375–415
- [210] Bach, A., Almdal, K., Hassager, O., Rasmussen, H.K. Elongational viscosity of narrow molar mass distribution polystyrene. *Macromol.* (2003) 36, pp. 5174–5179
- [211] Bach, A., Rasmussen, H.K., Hassager, O. Extensional viscosity for polymer melts measured in the filament stretching rheometer. *J. Rheol.* (2003) 47, pp. 429–441
- [212] Nielsen, J.K., Rasmussen, H.K., Hassager, O., McKinley, G.H. Elongational viscosity of monodisperse bidisperse polystyrene melts. *J. Rheol.* (2006) 50, pp. 453–476
- [213] Nielsen, J.K., Hassager, O., Rasmussen, H.K., McKinley, G.H. Observing the chain stretch transition in a highly entangled polyisoprene melt using transient extensional rheometry. *J. Rheol.* (2009) 53, pp. 1327–1346
- [214] Rajagopalan, D. Computational analysis of techniques to determine extensional viscosity from entrance flows. *Rheol. Acta* (2000) 39, pp. 138–151
- [215] Kim, S., Dealy, J.M. Design of an orifice die to measure entrance pressure drop. *J. Rheol.* (2001) 45, pp. 1413–1419
- [216] Cogswell, F.N. Converging flow of polymer melts in extrusion dies. *Polym. Eng. Sci.* (1972) 47, pp. 64–73
- [217] Revenu, P., Guillet, J., Carrot, C., Arsac, A. Validation of Cogswell's convergent flow analysis. *J. Appl. Polym. Sci.* (1996) 62, pp. 1783–1792
- [218] Zatloukal, M., Vlček, J., Tzoganakis, C., Sáha, P. Improvement in techniques for the determination of extensional rheological data from entrance flows: Computational and experimental analysis. *J. Non-Newtonian Fluid Mech.* (2002) 107, pp. 13–37

- [219] Genieser, L.H., Brown, R.A., Armstrong, R.C. Comparison of measured centerline stress and velocity fields with predictions of viscoelastic constitutive models. *J. Rheol.* (2003) 47, pp. 1331–1350
- [220] Laun, H.M., Schuch, H. Transient elongational viscosities and drawability of polymer melts. *J. Rheol.* (1989) 33, pp. 119–175
- [221] Meissner, J. Deformationsverhalten der Kunststoffe im flüssigen und im festen Zustand. *Kunststoffe* (1971) 61, pp. 576–582
- [222] Rauschenberger, V., Laun, H.M. A recursive model for Rheotens tests. *J. Rheol.* (1997) 41, pp. 719–737
- [223] Schneider, C., Schwetz, M., Münstedt, H., Kaschta, J.K. The axial velocity distribution of a polyethylene strand during extrusion: Simulation and comparison with experiments. *Mech. Time-Depend. Mater.* (2004) 8, pp. 215–224
- [224] Wagner, M.H., Bastian, H., Bernnat, A., Kurzbeck, S., Chai, C.K. Determination of elongational viscosity of polymer melts by RME and Rheotens experiments. *Rheol. Acta* (2002) 41, pp. 316–326
- [225] Kompani, M., Venerus, D.C. Equibiaxial extensional flow of polymer melts via lubricated squeezing flow. I. Experimental analysis. *Rheol. Acta* (2000) 39, pp. 444–451
- [226] Venerus, D.C., Kompani, M., Bernstein, B. Equibiaxial extensional flow of polymer melts via lubricated squeezing flow. Part 2: Flow modeling. *Rheol. Acta* (2000) 39, pp. 574–582
- [227] Venerus, D.C., Shiu, T.-Y., Kashyap, T. Continuous lubricated squeezing flow: A novel technique for equibiaxial elongational viscosity measurements on polymer melts. *J. Rheol.* (2010) 54, pp. 1083–1095
- [228] Mick, R.M., Shiu, T.-Y., Venerus, D.C. Equibiaxial Elongational Viscosity Measurements of Commercial Polymer Melts. *Polym. Eng. Sci.* (2015) 55, pp. 1013–1017

11

Tube Models for Non-linear Viscoelasticity of Linear and Branched Polymers

■ 11.1 Introduction

This chapter presents tube-based theories of nonlinear rheology. In principle, a successful theory for the nonlinear rheology of polymer melts must incorporate all the effects described in Chapters 6 to 9 for linear rheology, as well as the relaxation and flow phenomena peculiar to the nonlinear regime described in Chapter 10. The difficulty of the task of developing theories for nonlinear rheology is such that no completely general molecular theory is available at present. Some of the difficulty arises because there are multiple ways to generalize the conceptual picture of the tube to nonlinear flow and large deformations, and so many (reasonable) guesses have been made as to the correct mechanisms to include; there is not always sufficient experimental evidence to decide between competing concepts. Thus, nonlinear rheological theories are either largely phenomenological or are restricted to special cases, such as linear polymers, monodisperse star or H polymers, or “pom-pom” polymers. Even for these restricted cases, the theories are usually only semi-quantitative, or are only appropriate for certain types of flow. In Section 11.2, we briefly describe two nonlinear relaxation mechanisms that it is broadly agreed should be included in rheological constitutive equations, namely chain retraction and convective constraint release (which were also described in Section 10.2). In Section 11.3, we consider the case of monodisperse linear polymers, discussing a number of constitutive models and their application to experimental data. The nonlinear rheology of bidisperse and polydisperse linear polymers will be considered in Section 11.4. Theories for branched polymers are discussed in Sections 11.5 and 11.6. Since our interests in this book are in relating molecular properties to polymer rheology, we will not discuss phenomenological models, which are in any case described thoroughly in other books [1–5]. Throughout this chapter, we will restrict our attention to the tube model, and discuss primarily models for which the nonlinear properties can be related to molecular parameters.

To incorporate nonlinear rheological effects into the tube model, one must introduce the effects of large deformations on molecular configurations, some of which

are summarized in Section 10.2. These effects include *large orientation* of tube segments and the chain segments they contain, *retraction* of those chain segments within the tube, and finally *convective constraint release* caused by flow-induced displacement of chains relative to each other, and consequent rearrangement of entanglements between chains. In addition to these, some modern theories consider that the localizing constraint of the tube is affected by chain deformation. This has been expressed in terms of *changes in tube diameter* or as a *tube pressure*. Following large deformation and flow, it is possible also that strong *disentanglement* of chains occurs. A further difficulty is the strong likelihood that each of these mechanisms (if and when they occur) is coupled to each of the other mechanisms. It is not possible within this chapter to cover all these mechanisms and the developments associated with them exhaustively: we instead take the approach of presenting an illustrative selection of models.

For a perfect “step” deformation, it is assumed that the molecules move and deform *affinely*, that is, the molecular deformation is the same as the macroscopic deformation. Departures from affine behavior occur after completion of the step strain, as chains relax their configurations. Some of these relaxation processes are the same ones that produce linear viscoelastic phenomena, while others only occur in the nonlinear regime.

■ 11.2 Relaxation Processes Unique to the Nonlinear Regime

11.2.1 Retraction

Within the tube model, a form of relaxation that is unique to the nonlinear regime is *retraction* within the tube, illustrated in Fig. 11.1. Following a step deformation, each chain deforms affinely, and so the tube which confines a given chain must necessarily also be deformed. For the purposes of illustration, we make two assumptions: (1) the *path* of the tube defined by the entanglements, following the chain, is also deformed affinely, and (2) the *diameter* of the tube (or the degree of perpendicular confinement of the chain) remains unchanged. The latter might be partially justified—perhaps incorrectly—by claiming that the density of entanglements is not changed in a volume-conserving deformation. It turns out that affine deformation of the tube path will always, on average, lead to an increase in tube length (some tube sections are compressed while others are stretched, but the average is always to increase the tube length). This deformation induces a large tension on the test and matrix chains. The test chain can relieve some of this tension rather quickly by

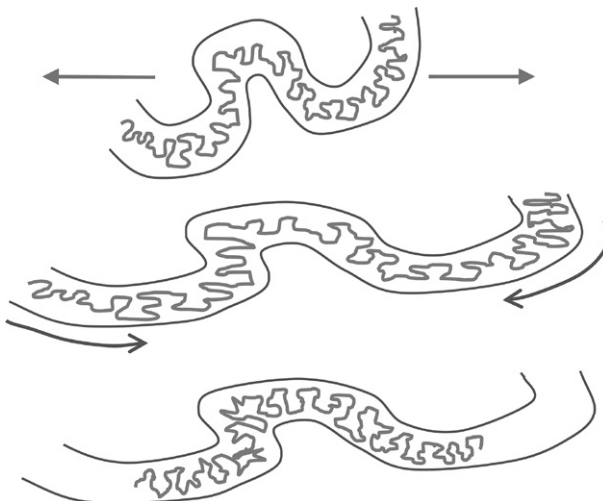


Figure 11.1 Illustration of affine deformation and retraction of a chain in a tube. Top: when the melt is deformed, but the chains and tubes are also deformed. Middle: on average this results in an increase in the contour length of the tube, so that chains are stretched along the tube axis with higher tension than their equilibrium. Bottom: the chain then retracts along the tube axis to return to its original contour length. Since this process does not involve crossing entanglements, it is relatively fast.

crinkling up within the deformed tube. This crinkling, or retraction, is rapid because it does not require the test chain to escape the tube; i.e., it requires only a Rouse-like motion, but not reptation. The retraction stops when the contour path occupied by the retracted chain equals the equilibrium length of the primitive path (and if the tube diameter is unchanged by the deformation, then the equilibrium length is also not changed). The retraction process differs from primitive path fluctuations (discussed in Section 6.4.2) in that the latter occur as fluctuations about the equilibrium length of the primitive path, while retraction occurs when the primitive path is *longer* than the equilibrium value. For a linear polymer, the longest relaxation time governing the retraction process, which is called the *retraction time or stretch relaxation time* τ_s , is expected to be roughly equal to the Rouse reorientation time for the whole chain, since the whole chain must retract, but the chain does not need to escape any entanglements to retract completely. We therefore expect τ_s to be proportional to the square of the molecular weight of the polymer, and therefore to be much smaller than the reptation time, which scales as $M^{3.4}$. From Eq. 6.3, we obtain the Rouse reorientation time (τ_r):

$$\tau_s = \tau_r = \frac{b^2 N^2 \zeta_0}{3 \pi^2 k T} = Z^2 \tau_e \quad (11.1)$$

with ζ_0 given by ζ for a melt, and we have used Eqs. 6.22 and 6.23 to replace the number of monomers $N \equiv M/M_0$ per chain with the number of tube segments per chain $Z \equiv M/M_e^G$. However, the time τ_k required to attain time-strain superposability through the retraction process after a step-strain experiment can be an order of magnitude larger than predicted by this equation [6–8], and resolving this disparity between τ_k and the theoretical value of τ_s remains an active area of research.

11.2.2 Convective Constraint Release

In our discussion of constraint release in the linear viscoelastic regime, Section 6.4.4 and Chapter 7, we noted that constraint release occurs when the matrix chains relax by the same mechanisms as the test chains, thereby releasing constraints on the test chains. Since the test chains can relax by both reptation and primitive path fluctuations, constraint release occurs when the matrix chains relax by these mechanisms. In the nonlinear regime, a new relaxation process for the test chain appears, that of chain retraction, discussed above. Since the matrix chains also undergo chain retraction, this too must lead to constraint release. Because steady state implies that the chains, on average, are no longer stretching at all, in steady-state flow retraction must occur at a rate high enough to completely cancel out the affine chain stretching produced by the flow, and this must produce constraint release at a rate dictated by the rate of flow. Another way to think of this is that the flow *convects* the matrix chains past the test chain, and so releases the constraints imposed by the matrix chains on the test chain at a rate proportional to the flow rate; see Fig. 10.4. Hence, Marrucci [9], who first clearly recognized the importance of this phenomenon and began to model it successfully, called this nonlinear process *convective constraint release*, or CCR. (The earliest seeds of the idea go back at least to Graessley in 1965 [10], who recognized that the convection of matrix chains in a flow field would release entanglements.)

In fact, the “CCR” process is a broad term that might include several different types of local tube reorganization driven by flow. In addition to the removal of entanglements by flow, there are several mechanisms via which entanglements could be replaced at the same rate (e.g., as initially noninteracting chains are brought together by flow, or through removal of intervening entanglements: some candidate mechanisms are discussed by Ianniruberto and Marrucci [11]). For thermal constraint release in the linear regime, the removal and addition of entanglements must necessarily be in balance, so that the overall degree of entanglement remains constant. This gives rise to a model for constraint release in which the tube diameter is constant and tube motion is treated as a Rouse-like process, as discussed above in Section 7.3.

Some treatments of CCR (e.g., [12, 13]) explicitly model the Rouse-like motion, and most constitutive models with CCR implicitly assume a fixed tube diameter. However, in nonlinear, nonequilibrium flow, it may not necessarily be the case that lost entanglements are fully replaced. Recent computer simulations of polymers in strong flow have found such a loss of entanglements [14], and such effects have been incorporated in constitutive models [15, 16]. Therefore, it is important to distinguish between (i) tube reorganization or reorientation, and (ii) actual entanglement loss as two distinct and separate effects of CCR.

The earliest tube models included only the simplest nonlinearities, that is, convective constraint release was neglected (since its importance was not clearly recognized), and the retraction was assumed to occur so fast relative to the rate of flow that the chains were assumed to remain unstretched. The linear relaxation processes of constraint release and primitive path fluctuations were also ignored, so that the models contained only one linear relaxation mechanism, namely reptation, and only the nonlinearity associated with large orientation of tube segments, but no stretch. Subsequent models added the omitted relaxation phenomena, one at a time, incorporating first chain stretch and then tube reorientation due to CCR. In what follows we present important constitutive models that included these two effects, starting with models for monodisperse linear polymers.

■ 11.3 Monodisperse Linear Polymers

11.3.1 No Chain Stretch: The Doi-Edwards Equation

Doi and Edwards noted that since $\tau_s \equiv \tau_r$ is expected to be much smaller than the reptation time τ_d , then for flows that are fast compared to the rate of reptation $1/\tau_d$, but slow compared to the rate of retraction $1/\tau_s$, one can assume that the chains remain completely retracted during flow; i.e., there is no chain stretch. Under this assumption, Doi and Edwards, in a seminal series of papers [17–20], derived the famous constitutive equation that bears their name. The Doi-Edwards (DE) constitutive equation, introduced in Section 10.3.2, is written as:

$$\sigma = \int_{-\infty}^t dt' m(t-t') \mathbf{Q}[E(t,t')] \quad (11.2)$$

where $\mathbf{Q}[E(t,t')]$ is the “Doi-Edwards tensor” representing the change in orientation of a tube segment given a deformation represented by inverse deformation gradient E (see Appendix B) between time t and t' . The *memory function* $m(t-t')$ is given by (see Eq. 10.13)

$$m(t-t') = \sum_{i=1}^{\infty} \frac{G_i}{\tau_i} \exp[-(t-t')/\tau_i] \quad (11.3)$$

This memory function contains the same distribution of relaxation times as the linear viscoelastic theory of reptation. Thus, from Eq. 6.31, we have

$$G_i = \frac{8}{\pi^2} \frac{G_N^0}{i^2}; \quad \tau_i = \frac{\tau_d}{i^2} \quad i \text{ odd} \quad (11.4)$$

Since, for reptation, this relaxation spectrum is dominated by the longest relaxation time, we can, with reasonable accuracy, simplify Eq. 11.2 to

$$\sigma = G_N^0 \int_{-\infty}^t \frac{dt'}{\tau_d} \exp[-(t-t')/\tau_d] Q[E(t,t')] \quad (11.5)$$

Here G_N^0 is the plateau modulus discussed in Sections 5.7, 5.8, and 6.3.2. The nonlinear aspects of the Doi-Edwards theory, including the effects of retraction, are contained in the nonlinear strain measure $Q[E(t,t')]$. A highly accurate approximation for this strain measure due to Currie [21] is:

$$Q \approx \left(\frac{5}{J-1} \right) B - \left[\frac{5}{(J-1)(I_2 + 13/4)^{1/2}} \right] C \quad (11.6)$$

where

$$J \equiv I_1 + 2(I_2 + 13/4)^{1/2} \quad (11.7)$$

and $I_1 \equiv \text{tr}(B)$ and $I_2 \equiv \text{tr}(C)$ are the strain invariants defined in Eqs. 10.9 and 10.10. B and C are the Finger tensor and Cauchy tensor respectively, defined in Appendix B. This simplest version of the Doi-Edwards theory invokes the “independent alignment approximation,” in which the portion of polymer in each tube segment is assumed to orient independently of the others.

The DE equation was the first detailed molecular theory for the rheology of polymer melts and since its introduction has been the basis for almost all theories for the dynamics and rheology of entangled polymers. The predictions of the DE equation have been explored in detail in many publications (for reviews, see [1, 4, 22, 23]). Summing up these reviews, we can say that while the DE equation inspired all that followed and does capture some aspects of the rheology of melts, even for the simplest case of monodisperse linear polymers it is not a realistic, quantitative theory except in a few special types of deformation.

One type of deformation for which the Doi-Edwards theory does make apparently accurate predictions is the step shear strain, where it correctly predicts the strain

softening observed at long times after the step. Thus, Eq. 11.5 gives the following formula for the shear stress σ :

$$\sigma = \gamma h(\gamma) G_N^0 \exp(-t / \tau_d) \quad (11.8)$$

where the damping function $h(\gamma)$, first mentioned in Section 10.2.2, describes the degree of strain softening of the melt. A prediction of $h(\gamma)$ can be obtained from the DE tensor $\mathbf{Q}[\mathbf{E}(t, t')]$ given by Eq. 11.6. This predicted damping function is compared to that obtained experimentally for an entangled polystyrene solution in Fig. 11.2. A similar plot for melts was given in Fig. 10.6. In fact, this excellent prediction of the damping function may be fortuitous: inclusion of additional mechanisms, such as CCR, has a tendency to make such predictions worse!

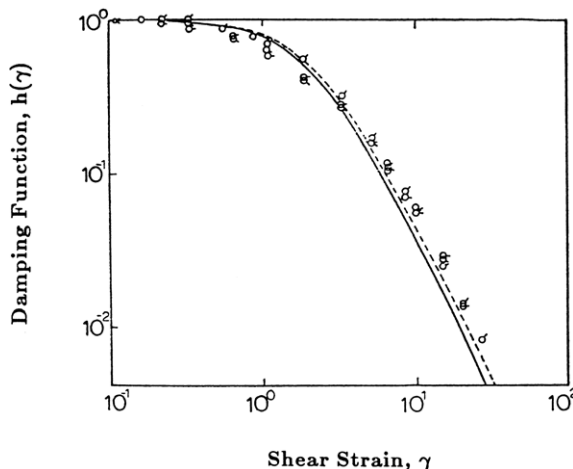


Figure 11.2 Damping function $h(\gamma)$ obtained from step-shear experiments on an entangled 20% solution of polystyrene of molecular weight $1.8 \cdot 10^6$ in chlorinated diphenyl (symbols) (data of Fukuda et al. [24]) compared to the predictions of the Doi-Edwards theory with (solid line) without (dashed line) the independent alignment approximation. From Doi and Edwards [18].

The biggest apparent failing of the DE equation is in steady-state shearing flow where it predicts excessive shear thinning. So severe is the shear thinning in the Doi-Edwards theory, that the shear stress (which is the viscosity times the shear rate) passes through a maximum as the shear rate increases, and at high shear rate, it decreases with increasing shear rate, as shown in Fig. 11.3. This is because at high flow rates, tube segments and chains are aligned in the direction of flow, while some residual component of the alignment in the flow gradient direction is required to produce a shear stress. Hence, the shear stress maximum is obtained when there is a balance between orientation due to flow and stress relaxation, i.e., both occurring at a rate of $1/\tau_d$. This maximum in shear stress makes the DE equation numerically

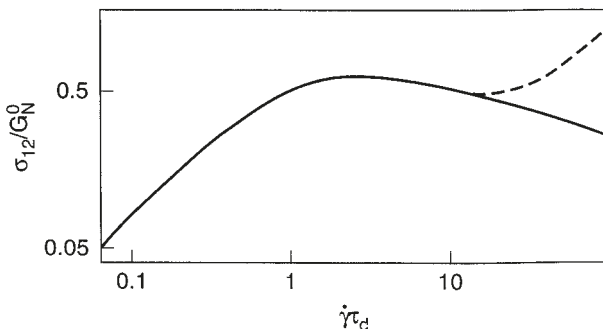


Figure 11.3 Dimensionless shear stress versus dimensionless shear rate (Weissenberg number) defined as $\dot{\gamma}\tau_d$ as predicted by the Doi-Edwards theory, Eq. 11.2 (solid line). The dashed line adds a speculated contribution from Rouse modes. From Doi and Edwards [20].

unstable in simulations of shearing flows, leading to so-called *constitutive instabilities* that are manifested as *shear banding*, which is a stratification of the shear rate in simple shearing flow. Such anomalous behavior was not observed experimentally until relatively recently, when it has been reported for highly entangled polymer melts and solutions; see Section 11.3.7. In extensional flows, the DE theory predicts extension thinning, rather than the extension thickening often seen in experimental extensional flows, sometimes even for linear polymers. Other failings of the DE theory include its incorrect prediction of the dependence of the zero-shear viscosity on polydispersity.

As we will see below, these deficiencies are caused by the assumption that the retraction process is infinitely fast and by the neglect of constraint release processes, especially of convective constraint release, discussed below. Lesser difficulties result from its neglect of primitive path fluctuations. Neglect of the finite rate of retraction and of convective constraint release limit the validity of the DE theory to either long times after step strains or to slow flows, that is flows with velocity gradients below about $1/\tau_d$. To extend the validity of the DE theory up to moderate strain rates, which we here define as rates ranging from $1/\tau_d$ to $1/\tau_s$ or so, convective constraint release must be accounted for. To describe fast flows, which we here define as flows with strain rates above $1/\tau_s$, the finite rate of retraction must be included. We will show how these processes can be included in the theory in Sections 11.3.2 and 11.3.3 below. We will discuss inclusion of the finite retraction rate first (in Section 11.3.2), even though its role only becomes evident in the fast-flow regime, while convective constraint release, which is discussed in Section 11.3.3, already exerts its influence in the intermediate flow regime. For those interested in learning more about the original DE theory, thorough discussions can be found elsewhere [1, 2, 22], and so we will pursue this topic no further here.

11.3.2 Chain Stretch: The Doi-Edwards-Marrucci-Grizzuti (DEMG) Theory

The assumption that the retraction process is infinitely fast was removed by Marrucci and Grizzuti [25]. The resulting improved theory, called the DEMG (Doi-Edwards-Marrucci-Grizzuti) model, allows “chain stretch,” in that the primitive path of the chain is no longer held fixed but can become longer than its equilibrium value. The full DEMG theory is rather complex [26], since it includes a diffusion equation involving the tube contour variable that must be solved numerically. However, a simplified version of this theory that neglects variations along the tube coordinate was developed by Pearson et al. [27]. We will refer to this, and other models that omit the tube coordinate, as “toy” models. Thus, the model of Pearson et al. is a toy version of the DEMG model. In toy models, reptation is described by only a single, longest, relaxation time. Thus, Eq. 11.5 can be considered a toy version of the Doi-Edwards equation.

More recently, “differential” versions of the theory have been developed [28, 29], which express the evolution of the tube orientation using a differential equation, rather than memory integral of the form of Eqs. 11.2 and 11.5. Though it may be argued that the integral formalism initiated by Doi and Edwards is a more faithful representation of the evolution of tube orientation with strain, differential models capture the main features of the constitutive behavior, and are easier to handle numerically (and therefore more amenable to flow computation). For the remainder of this chapter we will focus only on differential models, but note that there is often a memory integral equivalent to the equations we present. The differential “toy” version of the DEMG model is [28, 29]:

$$\overset{\nabla}{S} = -2(\kappa : S)S - \frac{1}{\lambda^2 \tau_d} \left(S - \frac{\delta}{3} \right) \quad (11.9)$$

$$\frac{d\lambda}{dt} = \lambda(\kappa : S) - \frac{k_s(\lambda)}{\tau_s}(\lambda - 1) \quad (11.10)$$

$$\sigma = 3 G_N^0 k_s(\lambda) \lambda^2 S \quad (11.11)$$

Equation 11.9 describes the evolution of the dimensionless orientation tensor S . This orientation tensor describes the average orientation of tube segments in three-dimensional space. In this equation, the symbol ∇ above the orientation tensor S is the “upper convected derivative,” which is defined for an arbitrary tensor X as

$$\overset{\nabla}{X} \equiv \frac{\partial}{\partial t} X - \kappa \cdot X - X \cdot \kappa^T \quad (11.12)$$

The tensor κ is the transpose of the velocity gradient tensor (see Appendix B). The first term on the right hand side of Eq. 11.9 is a geometrical factor that ensures that the flow terms in the upper convected derivative do not lead to “stretching” of the orientation tensor, i.e., they ensure the trace of the tensor S remains at a value of 1. The second term represents relaxation of orientation, where δ is the unit tensor. The factor of λ^2 multiplying the orientation relaxation time τ_d is introduced here to avoid shear thickening, which can otherwise occur in such differential models at high flow rates (see, for example, [30]). A similar factor appears below in Eq. 11.20.

Equation 11.9 captures much of the behavior predicted by the integral DE equation, Eq. 11.2, except that it predicts a zero second normal stress difference, rather than the value predicted by the regular DE model, Eq. 11.2, which is $-2/7$ times the first normal stress difference at low shear rates.

The Doi-Edwards theory predicts that the stress tensor σ equals the plateau modulus G_N^0 times the tube orientation tensor S . However, when chain stretching occurs (which is neglected by the DE theory but included in the DEMG theory), the stress is amplified relative to the DE theory; see Eq. 11.11. The degree of amplification is the square of the chain stretch λ , which is the length of the primitive path relative to equilibrium. In the Doi-Edwards theory, which includes no chain stretch, we have $\lambda = 1$. In the DEMG theory, where there is chain stretch, λ is governed by a new equation, the stretch Eq. 11.10. In this equation, the first term on the right side $\lambda \kappa : S$ describes affine stretching of the primitive path in the flow. The second term on the right side describes the retraction of the chain in the tube, and hence the shrinkage of the primitive path. The term $\lambda - 1$ guarantees that this shrinkage stops when the chain stretch reaches unity, which corresponds to equilibrium.

The rate of shrinkage is controlled by the retraction time τ_s given, according to the tube model, by Eq. 11.1. That is, the model prediction is that the retraction time should be the Rouse reorientation time τ_r (the same as the longest timescale for primitive path fluctuations; see Section 6.4.3). This second relaxation time governing chain retraction or stretch is shorter than the relaxation time τ_d governing chain orientation. These two time constants divide the range of shear rates into three regimes: the slow regime where $\dot{\gamma} < 1/\tau_d$, the intermediate regime in which $1/\tau_d < \dot{\gamma} < 1/\tau_s$, and the fast regime where $\dot{\gamma} > 1/\tau_s$. A similar partition of rates applies to extensional flow, and we will say more about these three regimes in what follows. Here we note that, theoretically, τ_s (equal to the Rouse reorientation time) should scale with the second power of molecular weight, while the reptation time τ_d scales roughly with the 3.4 power. This scaling of the Rouse reorientation time seems to be roughly consistent with available stress overshoot data in transient start-up of shearing (see Figs. 11.5 and 11.7) and with the onset of extension thickening in extensional flow of polymer solutions (Fig. 11.8). However, in the step-strain experiments of Archer and coworkers [6, 7, 31] and Osaki and coworkers [8] the retraction process seems

to come to completion only at a time τ_k that is much longer than the theoretical value of τ_s , and only becomes much less than the reptation time τ_d for highly entangled melts. At present there is no explanation of this discrepancy.

The coefficient $k_s(\lambda)$ in Eqs. 11.10 and 11.11 describes the nonlinearity of the spring. For a Hookean, infinitely extensible chain, there is no nonlinearity, and $k_s(\lambda) = 1$. In the original DEMG theory, Hookean springs were assumed, but this assumption must be corrected, especially for extensional flow for which Hookean springs give unbounded extensional viscosities at high extension rates. For real chains, $k_s(\lambda)$ should be given by the inverse Langevin function, a good approximation to which is the Padé approximation [32], normalized so that $k_s(\lambda)$ goes to unity when there is no stretch ($\lambda = 1$):

$$k_s = \frac{(3\lambda_{\max}^2 - \lambda^2)/(3\lambda_{\max}^2 - 1)}{(\lambda_{\max}^2 - \lambda^2)/(3\lambda_{\max}^2 - 1)} \quad (11.13)$$

Here $\lambda_{\max} = L_{\max}/L_{\text{eq}}$, and L_{\max} , the maximum length to which a tube segment can be stretched, is given by $L_{\max} = 0.82 l_0 N_e$, where l_0 is the backbone bond length (1.54 Å for a carbon-carbon bond), and N_e is the number of backbone bonds in an entanglement spacing or tube segment. The factor of 0.82 is due to the zig-zag conformation of a fully extended carbon backbone. L_{eq} , the equilibrium length of a tube segment, equals $\sqrt{C_\infty N_e l_0^2}$, where C_∞ is the characteristic ratio of the polymer (Section 2.1.2). The value of C_∞ is normally in the range of 5–10 [33], and is 9.6 for polystyrene [34]. Thus, λ_{\max} is given by $0.82 \sqrt{N_e/C_\infty}$, which has a value of around five for polystyrene. For monodisperse melts, in general, λ_{\max} is not very large, but can be larger than 10 for entangled solutions or in polydisperse melts where long chains are diluted by faster relaxing short chains, since N_e is inversely proportional to the polymer concentration.

Once S and λ have been obtained by solving Eqs. 11.9 and 11.10, and $k_s(\lambda)$ from Eq. 11.13, the stress tensor σ can be obtained from Eq. 11.11. Fortunately, the set of Eqs. 11.9 through 11.13, which defines the toy version of the DEMG theory, is nearly identical in its predictions to the full DEMG model. The DEMG model, in full or toy form, improves some aspects of the Doi-Edwards equation but not others.

In fast shearing flows, with shear rates greater than $1/\tau_s$, the DEMG theory shows overshoots in both shear stress σ and first normal stress difference N_1 as functions of time after start-up of steady shearing [26], in agreement with experiments (as will be presented in Section 11.3.5). These overshoots in both σ and N_1 are an improvement over DE theory, which shows only the overshoot in σ and not the one in N_1 .

However, the DEMG theory does *not* improve on the DE equation in one most important respect: the DEMG theory does not remove the extreme shear thinning

of the Doi-Edwards model at steady state. This may seem surprising; the DEMG model allows for chain stretch, which should, in general, lead to larger stresses at high strain rates, and therefore potentially less shear thinning, than does the DE model. Indeed, it is the presence of the chain stretch that allows the DEMG equation to predict an overshoot in N_1 , as is observed in experiments. The reason the DEMG theory fails to predict higher stresses *at steady state* in shear is that in shear flow it is the off-diagonal component of the tube orientation tensor that couples to the velocity gradient $\boldsymbol{\kappa}$. Thus, the product $\boldsymbol{\kappa} : \mathbf{S}$ in Eq. 11.10 reduces to just $\dot{\gamma} S_{12}$, where 1 indicates the flow direction, 2 is the gradient direction, and the velocity gradient tensor $\boldsymbol{\kappa}$ has only one non-zero component, which is the shear rate $\dot{\gamma}$. Now as a tube segment is rotated towards the flow direction by the vorticity of the shearing flow, S_{12} decreases, ever more so as $\dot{\gamma}$ increases, and hence the product $\boldsymbol{\kappa} : \mathbf{S} = \dot{\gamma} S_{12}$ in Eq. 11.10 is never able to get very large at steady state. Thus the retraction term (the last term) in Eq. 11.10 is always able to compete with the stretching term, at any shear rate, and this keeps the chain stretch λ from staying very large when steady state is reached. In a sense, the rotation of the tube causes the shear flow to “lose its grip” on the chain, and hence the chain retracts in the tube. The *temporary* stretching of the chain, which occurs before retraction, leads to large overshoots in shear stress and first normal stress difference, but this stretch is not sustained at steady state. Hence, the steady-state rheology of the DEMG theory in shear is much the same as that of the DE theory. In particular, the DEMG theory inherits from the DE theory the maximum in steady-state shear stress as a function of shear rate shown in Fig. 11.3.

In uniaxial extensional flow, on the other hand, the product $\boldsymbol{\kappa} : \mathbf{S}$ reduces to $\dot{\epsilon}(S_{11} - S_{22})$. Since rotation of tube segments into the flow direction in extensional flow leads to a monotonic increase in $(S_{11} - S_{22})$, the product $\boldsymbol{\kappa} : \mathbf{S} = \dot{\epsilon}(S_{11} - S_{22})$ grows with extension rate $\dot{\epsilon}$. Thus, large chain stretch *can* be sustained at steady state in the DEMG theory, which is an improvement over the DE theory, which shows only extension thinning at high extension rates. Thus, for fast extensional flows, the DEMG theory predicts *extension thickening*, as shown in Fig. 11.4. (When the finite extensibility of the chains is accounted for, the thickening regime gives way to a plateau viscosity at the highest extension rates, not shown in Fig. 11.4.) Note in Fig. 11.4 that between the low-strain-rate region where the extensional viscosity is constant and the high-extension-rate regime where there is extension thickening, there is an intermediate regime where extension thinning is predicted. This intermediate regime occurs at extension rates between $1/\tau_d$ and $1/\tau_s$, where the flow is fast enough to orient tube segments, but not fast enough to stretch them. In the intermediate regime, stress due to tube orientation is saturated, but stress due to tube stretching is absent, and so the extensional stress is nearly constant as a function of extension rate. Therefore, the viscosity (which is the stress divided by

the extension rate) decreases with increasing extension rate in this regime. Since τ_d is predicted to scale with the third power of molecular weight M , while τ_s scales only with the second power, it follows that as molecular weight increases, the width of the intermediate regime should increase as well, and so this regime should be quite wide for high-molecular-weight, monodisperse polymers. As we shall see (in Fig. 11.8), these three regimes (low-rate plateau, intermediate-rate extension thinning, and high-rate extension thickening) can all be observed in experimental extensional-flow data for nearly monodisperse, entangled polymer solutions, thus confirming this prediction of the DEMG theory.

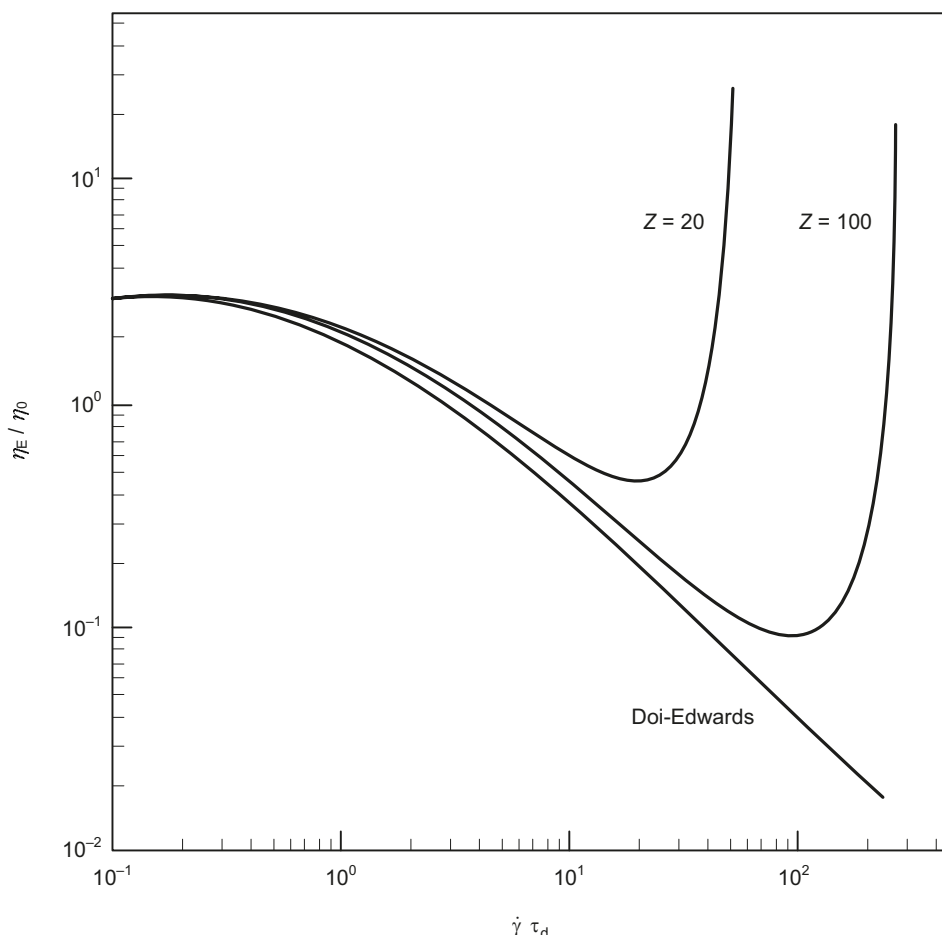


Figure 11.4 Predictions of the DEMG theory for η_E/η_0 as a function of Weissenberg number, for $Z = 20$ and 100 entanglements per chain. The chain is taken to be infinitely extensible, i.e., $k_s(\lambda)=1$. The prediction of the Doi-Edwards model is also shown. From Marrucci and Grizzuti [25].

The three regimes (slow flow, intermediate flow, and fast flow) should also exist in shear, but the DEMG theory fails to predict the correct behavior in the third, fast-flow, regime, because the rotation of tube segments in the flow prevents chain stretch from occurring. The DEMG theory, like the Doi-Edwards theory, also predicts excessive shear thinning in the intermediate regime, where chain stretching is absent. Thus, in addition to chain stretching, some other mechanism is missing from the DE theory, a mechanism that acts not only at high shear rates but also at intermediate rates, between $1/\tau_d$ and $1/\tau_s$. This missing mechanism is *convective constraint release*.

11.3.3 Convective Constraint Release (CCR) and the GLaMM Model

Convective constraint release, discussed in Section 11.2.2, was first clearly recognized and modeled in a simple manner by Marrucci [9]. After this pioneering work, various efforts have been made to develop full constitutive equations whose predictions can be compared quantitatively to experimental data in both steady and transient flows. For this, it seems imperative to incorporate effects of both chain stretch and CCR. Such models have been proposed by Mead, Larson, and Doi [35]; Graham, Likhtman, Milner, and McLeish [12, 13]; Fang, Kröger, and Öttinger [36]; and Marrucci and Ianniruberto [37–39], among others. Here, after presenting Marrucci’s basic idea of CCR, we discuss the more microscopically detailed Graham-Likhtman-and-Milner-McLeish (GLaMM) theory [13], which is widely considered the state-of-the-art tube model for linear polymers. In Section 11.3.4, we present constitutive equations that are simpler, and easier to use in multi-dimensional flow simulations, than the GLaMM equations. Detailed comparisons of theory with rheological data for linear polymers are presented in Sections 11.3.5 and 11.3.6.

Marrucci [9] suggested that when the shear rate $\dot{\gamma}$ exceeds the inverse reptation time $1/\tau_d$, polymer molecules are convected away from each other faster than they can relax by reptation. As a result, entanglement constraints are destroyed at a rate comparable to $\dot{\gamma}$, rather than at the rate of reptation $1/\tau_d$. Marrucci therefore proposed that the overall rate of relaxation of entanglements, which can be characterized by the inverse of an overall relaxation time τ , be given by

$$\frac{1}{\tau} = \frac{1}{\tau_d} + \beta \dot{\gamma} \quad (11.14)$$

where β is a constant of order unity. When this formula is generalized to flows other than shear, it becomes

$$\frac{1}{\tau} = \frac{1}{\tau_d} + \beta \boldsymbol{\kappa} : \mathbf{S} \quad (11.15)$$

where the contraction $\kappa : \mathbf{S}$ is the trace of the tensor product of the velocity gradient κ and the orientation tensor \mathbf{S} . When this expression for the relaxation time is used instead of the bare reptation time τ_d in an approximate version of the DE tube model, the major defect of the DE equation, namely the decrease in shear stress with increasing shear rate $\dot{\gamma}$ at $\dot{\gamma}$ greater than $1/\tau_d$, disappears, and instead the shear stress remains on a plateau at $\dot{\gamma}$ above $1/\tau_d$ [9]. The physical reason for this is that the relaxation of tube orientation due to flow permits a component of orientation in the flow gradient direction, which is then sufficient to produce shear stress and (at higher flow rates) chain stretching.

While Marrucci's suggestion of CCR fixed the apparent deficiency of excessive shear thinning in the Doi-Edwards model, and indicated the physical reason why this thinning was avoided in practice, it did not attempt a microscopic description of the detailed chain dynamics for a chain under flow. Most "toy" models for CCR share this feature with Marrucci's original model, and (as we will see in the next section) merely use the CCR mechanism as a justification for modifying the orientation relaxation time, in a similar manner to Eq. 11.15.

It is, however, possible to do better than this. Likhtman et al. [12] presented a more microscopic theory of convective constraint release that describes explicitly the constraint-release Rouse motion of the tube (see Section 7.3) that occurs as a result of either reptative or convective constraint release. In doing this they explicitly assumed that when constraints are "released" that they are also dynamically replaced by other chains, so that a constraint release event may be described by a local "hop" of the tube, which remains at essentially a constant tube diameter. Graham et al. [13] extended this to include chain stretch in a theory that has become known as the "GLaMM" model (after the authors, "Graham-Likhtman-and-Milner-McLeish"). In order to describe relaxation from reptation and stretch relaxation (i.e., due to chain motion along the tube) and constraint release Rouse motion (from local hopping of the tube), they found it necessary to use more general dynamical variables than simply the local tube orientation and stretch. Instead, they obtained a differential dynamical equation for the quantity $f(s, s') = \langle \partial\mathbf{R}/\partial s \, \partial\mathbf{R}/\partial s' \rangle$ that represents the correlation in orientation and stretch between tube segments at two different locations s and s' along the tube contour. Solution of their equations requires numerically incrementing $f(s, s')$ over the two-dimensional space defined when both coordinates s and s' are varied over the length of the tube. When $s = s'$, the quantity $f(s, s')$ contains all the information about the local orientation and stretch required to obtain the stress.

Rather than simply assuming (as Marrucci did in his original proposal) that the rate of CCR is proportional to the flow rate, Graham et al. note that the process that actually leads to a release of constraints is the *retraction* of chain ends through the entanglement mesh, caused by stretch relaxation. They, therefore, calculated the rate of convective constraint release self-consistently from the rate of chain retraction.

This allows for transients in the rate of constraint release during start-up flows: the rate of constraint release builds as the chains stretch in fast flows. Their Rouse “hopping rate” was then set by the rate of constraint release multiplied by a parameter c_v , which is essentially the number of Rouse hops taken by the test chain per tube segment vacated by a matrix chain. This parameter is analogous to the parameter β in the Marrucci formulation of CCR in Eq. 11.15 (which was given the symbol c in the original Marrucci paper [9]).

As noted earlier, the inclusion of CCR in the equations for chain orientation leads to a substantial improvement over the Doi-Edwards and DEMG theories, especially in removing, or greatly reducing, the maximum in shear stress as a function of shear rate. The CCR mechanism, as included in the GLaMM theory and in the earlier theory of Marrucci [9], permits tube segments to disorient somewhat even in intermediate and fast flows, for which $\dot{\gamma} > 1/\tau_d$. This increases the component f_{12} of the tensor $f(s, s')$, leading to a larger shear stress σ than in the absence of CCR. In addition, in fast flows at shear rates comparable to or greater than $1/\tau_s$, the increase in f_{12} leads to an increase in the rate of chain stretch, so that at steady state the chain stretch becomes greater than would be the case without the CCR term. CCR increases chain stretch because the less oriented tube segments can be “gripped” more effectively by the flow. The result, at shear rates comparable to or greater than $1/\tau_s$, is an increase in both the steady-state shear and first normal stress difference. Because of its complexity, and in particular the numerical expense of the two-dimensional space swept out by s and s' , the theory of Graham et al. [13] is not very suitable for application to complex flows, even for a monodisperse polymer. However, its most important predictions are captured in a highly simplified toy version of this model, which we present below.

11.3.4 Toy Models Containing CCR and Chain Stretch

11.3.4.1 “Rolie-Poly” Model for CCR

Likhtman, Graham, and McLeish [40, 41] reduced the microscopic theory of Graham et al. [13] to a simplified, one-mode differential toy model, commonly known as the “Rolie-Poly” model (ROuse LInear Entangled POLYmers). In the absence of chain stretch, this may be written in a simple form for tube orientation:

$$\overset{\nabla}{S} = -2(\kappa : S)S - \left(\frac{1}{\tau_d} + 2\beta \kappa : S \right) \left(S - \frac{\delta}{3} \right) \quad (11.16)$$

and the stress is obtained from Eq. 11.11 with the chain stretch set to $\lambda = 1$. This equation is exactly equivalent to Eq. 11.9 for the orientation in the DEMG model, except that a CCR relaxation rate $2\beta \kappa : S$ has been added, so that the total relaxation

rate is practically identical to Marrucci's original proposal [9] given in Eq. 11.15. β is a constant that is proportional to the parameter c_v of the GLaMM model. This gives a plateau in shear stress at both intermediate and high shear rates.

When chain stretch is added [41], the Rolie-Poly model equation becomes:

$$\frac{\nabla}{\tau} = -\frac{2(\lambda-1)}{\lambda \tau_s} \tau - \left(\frac{1}{\tau_d} + 2\beta \frac{(\lambda-1)}{\tau_s} \lambda^{\delta-1} \right) (\tau - \delta) \quad (11.17)$$

where the stretch, λ is obtained from:

$$\lambda = \sqrt{\frac{\text{tr } \tau}{3}} \quad (11.18)$$

and the stress is proportional to the tensor τ :

$$\sigma = G_N^0 \tau \quad (11.19)$$

Equation 11.17 combines both the orientation relaxation and stretch relaxation processes, with separate relaxation times τ_d and τ_s , in a single, compact, equation. Though it is usual to solve the model in the form of Eq. 11.17, it is instructive to separate the equation out into orientation and stretch components, so that $\tau = 3 \lambda^2 S$, giving:

$$\frac{\nabla}{S} = -2(\kappa : S) S - \frac{1}{\lambda^2} \left(\frac{1}{\tau_d} + 2\beta \frac{(\lambda-1)}{\tau_s} \lambda^{\delta-1} \right) \left(S - \frac{\delta}{3} \right) \quad (11.20)$$

$$\frac{d\lambda}{dt} = \lambda(\kappa : S) - \frac{1}{\tau_s}(\lambda-1) - \left(\frac{1}{\tau_d} + 2\beta \frac{(\lambda-1)}{\tau_s} \lambda^{\delta-1} \right) \frac{(\lambda^2-1)}{2\lambda} \quad (11.21)$$

The orientation equation Eq. 11.20 is almost identical to the nonstretching equation Eq. 11.16, but the constraint release relaxation rate is now proportional to the rate of stretch relaxation $(\lambda-1)/\tau_s$. This respects the physical situation that release of constraints is caused by the *retraction* of chain ends through the entanglement mesh, which is caused by stretch relaxation. The stretch equation Eq. 11.21 may be compared to Eq. 11.10: it contains a (usually negligible) contribution from the orientation relaxation time, but also a contribution from CCR, reflecting the fact that constraint release relaxes both orientation and stretch. A similar relaxation term for chain stretch is present in the model proposed by Mead, Larson, and Doi [35].

The Rolie-Poly model gives qualitatively correct predictions in all three regimes: slow flow ($\dot{\gamma} \leq 1/\tau_d$), intermediate flow ($1/\tau_d \leq \dot{\gamma} \leq 1/\tau_s$), and fast flow ($\dot{\gamma} \geq 1/\tau_s$). The parameter β controls the level of CCR and the exponent δ controls the effect of chain stretching on the rate of CCR. (Note that the symbol δ is here a scalar exponent, and

is not the unit tensor δ .) A negative value of δ leads to suppression of CCR when the chain is stretched and therefore to larger overshoots in shear stress and first normal stress difference during start-up of steady shear. Likhtman and Graham [41] set $\delta = -1/2$ and $\beta = 0.5$, the latter corresponding roughly to $c_v = 0.05$. These choices of the two parameters β and δ make the simplified theory match more exactly the predictions of the full theory. The theory is also readily extended to multiple modes, merely by assigning a new equation to each new relaxation mode. The constants G_N^0 and $\tau_{d,i}$ for each mode i are obtained by fits to linear viscoelastic data. Often, only one stretch relaxation time $\tau_{s,1}$ for the first (longest) mode needs to be assigned, since the higher modes have stretch times fast enough to be assumed instantaneous; for these modes, Eq. 11.17 reduces to Eq. 11.16. The predictions of the multi-mode version of this model for start-up of steady shear will later be compared to experimental data for an entangled polybutadiene solution (in Fig. 11.7).

It is possible to modify the Rolie-Poly model to include finite extensibility, simply by increasing both the stress σ and rate of retraction $(\lambda - 1)/\tau_s$ by the factor $k_s(\lambda)$ introduced in Eq. 11.13.

11.3.4.2 Differential Model of Ianniruberto and Marrucci

All of the above differential equations suffer the defect that even under slow-flow conditions the second normal stress difference is zero. This defect is eliminated in a CCR constitutive equation of Ianniruberto and Marrucci [37], referred to as the “double constraint release with chain stretch” (DCR-CS) model:

$$\tau = \frac{1}{2(1/\tau_d + |\boldsymbol{\kappa} : \mathbf{S}|)} + \tau_s \quad (11.22)$$

$$\nabla^2 S^2 + 2S^2(\boldsymbol{\kappa} : \mathbf{S}) + \frac{2}{\tau} S \left(\mathbf{S} - \frac{1}{3}\boldsymbol{\delta} \right) = 0 \quad (11.23)$$

$$\frac{d\lambda}{dt} = \lambda \boldsymbol{\kappa} : \mathbf{S} - \frac{1}{\tau_s} [k'_s(\lambda) \lambda - 1] \quad (11.24)$$

$$\sigma = G_N^0 k'_s(\lambda) \lambda^2 S \quad (11.25)$$

$$k'_s = \frac{\lambda_{\max} - 1}{\lambda_{\max} - \lambda} \quad (11.26)$$

Equations 11.22 to 11.25 are the counterparts to Eqs. 11.9 to 11.11 of the DEMG theory, or of Eqs. 11.19 to 11.21 of the Rolie-Poly model. The most significant difference between these equations is the form of the orientation equation, Eq 11.23.

This may be compared to Eqs. 11.10 and 11.20, which are simple differential equations for orientation, with the drawback that they lead to a zero second normal stress difference in simple shear. However, in Eq. 11.23 of the Ianniruberto and Marrucci model, the use of the square of the orientation tensor leads to a ratio of N_2/N_1 of -0.25 at low shear rates, which is close to the values typically observed in experiments on entangled solutions and melts [42, 43].

Other differences are more minor. In Eq. 11.22, the CCR term is just $|\kappa : S|$, similar to the CCR term in the Rolie-Poly theory without chain stretch, as given in Eq 11.16. In contrast, the stretching versions of the Rolie-Poly model (Eqs. 11.17 and 11.20) contain a CCR term proportional to the rate of stretch relaxation $(\lambda - 1)/\tau_s$, which gives transients in the CCR rate during start-up of fast flows. The expression Eq. 11.22 for the orientation relaxation time contains not only the reptation time τ_d and the rate of convective constraint release $|\kappa : S|$, but also the stretch time τ_s . This guarantees that even for velocity gradients greater than $1/\tau_s$, the rate of orientation relaxation remains bounded by $1/\tau_s$. This effectively switches off the CCR effect for fast flows.

Finally, Eq. 11.24 is a stretch equation, similar to Eq. 11.21 in the Rolie-Poly theory, except that there is no CCR term in Eq. 11.24. Ianniruberto and Marrucci argued that even when constraints on the chain are released rapidly, the chain as a whole cannot respond on a time scale faster than the retraction time τ_s of the chain, which is already included in Eq. 11.24. Note that the nonlinearity of the spring constant used in Eq. 11.24 is given by $K'_s(\lambda) = (\lambda_{\max} - 1)/(\lambda_{\max} - \lambda)$ in Eq. 11.26, which is somewhat different from, but qualitatively similar to, that used in Eq. 11.13. The DCR-CS model has been compared favorably to an extensive set of extensional flow data for concentrated polystyrene solutions by Bhattacharjee et al. [44].

However Bhattacharjee et al. [44] and Wapperom et al. [45] showed that the DCR-CS model anomalously predicts shear thickening in steady shear flows. This defect has been corrected by Marrucci and Ianniruberto [38, 39], by using a tensor A that includes both chain orientation and stretch, in a similar manner to the Rolie-Poly equation (Eq. 11.17).

We have, here, presented two “toy” models which capture elements of the constitutive behavior of linear polymers with chain stretch and CCR included. As noted earlier, several other toy models are also available. The Rolie-Poly model is derived from a more microscopic model, and contains the particular physics that constraint release rate is proportional to the rate of retraction $(\lambda - 1)/\tau_s$, and that CCR relaxes both stretch and orientation. Yet, this model has a zero second normal stress difference. The DCR-CS model does have a suitable second normal stress difference, but the constraint release rate is not obtained from the retraction rate, CCR does not relax chain stretch, and it suffers the possibility of shear thickening. There appears, then, to remain scope for developments which combine all the favorable elements of the above models.

11.3.5 Comparison of Theory with Data for Monodisperse Linear Polymers: Shearing Flows

The predictions of tube models that include CCR, such as the Mead, Larson, and Doi model [35], and the models of Likhtman et al. [12, 13, 40, 41] and of Ianniruberto and Marrucci [11, 37–39], discussed above, have been compared to experimental data on start-up of shear flow for entangled monodisperse polymer solutions and melts. For steady-state shear and extensional flow of solutions, and shear on melts, these comparisons show roughly similar levels of agreement, although only the theory of Ianniruberto and Marrucci can predict a non-zero second normal stress difference. We will further discuss extensional flow of melts and solutions below, in Section 11.3.6.

To compare the predictions of any of these equations to experimental data, the model parameters must be assigned. These parameters are the plateau modulus G_N^0 , the reptation time τ_d , and the stretch time τ_s . The GLaMM model [13] (Section 11.3.3 above) also contains the CCR parameter c_v corresponding to the parameter β in the toy Rolie-Poly version. Obviously, G_N^0 , τ_d , and τ_s depend not only on the type of polymer, but also on the solvent and the polymer concentration in solution. (τ_d and τ_s also depend on the molecular weight.) As in the case of melts, we expect that for solutions there should only be two fundamental parameters, namely the plateau modulus G_N^0 and the monomeric friction coefficient ζ . The other parameters should depend on these via equations given in Chapter 6.

Ideally, these parameters should be fixed by comparison with linear viscoelastic data, before making predictions in the nonlinear regime. In this context, an advantage of the GLaMM model [13] is that it is parameterized so as to give similar predictions to the detailed Likhtman-McLeish theory [46] for monodisperse linear polymers, in the linear viscoelastic regime. The Likhtman-McLeish theory has three main fitting parameters: the plateau modulus G_N^0 , the entanglement molecular weight M_e^G , and the entanglement time τ_e (see Section 6.3). The first two of these should (in principle) be related to each other via Eq. 6.21, though they are often treated as separate fitting parameters, with Eq. 6.21 enforced only approximately, in treating real viscoelastic data. The entanglement time τ_e encodes the monomer friction coefficient via Eq. 6.23. A fourth parameter c_v in both the Likhtman-McLeish and GLaMM theories, which sets the amount of constraint release, is usually fixed at a value of 0.1. Having fitted these, all other parameters are predicted from this base set of parameters. For example, the stretch relaxation time τ_s is predicted to equal the Rouse reorientation time of the polymer, so $\tau_s = Z^2 \tau_e$ where Z is the number of entanglements per molecule, i.e., the molecular weight is $M = Z M_e^G$. So, the nonlinear rheology is then predicted using the GLaMM model without further parameter adjustment.

The procedure outlined above, which was to obtain the fundamental tube-theory parameters from fitting a theoretical model to linear viscoelastic data, is certainly

the most ideal approach. However, even in this case it should be remembered that the obtained parameters depend to some extent on both the quality of the available data, and on the choice of theoretical model. Fitting with different theoretical models will result in different parameters. It is therefore a good idea if the models used for the linear and nonlinear viscoelastic data are mutually consistent.

When using toy models, such as Rolie-Poly or the DCR-CS models of Section 11.3 above, then typically the plateau modulus G_N^0 and reptation time τ_d are still fitted to linear viscoelastic data (often these toy models are used in a multi-mode framework, and fitted using a spectrum of moduli and relaxation times [41, 47]). There still remains to estimate the stretch relaxation time τ_s . This may be achieved by using Eq. 6.39 or 6.41 to estimate the effect of primitive path fluctuations (PPF) on the reptation time and then to use $\tau_s = \tau_{d,true}/3Z$ where $\tau_{d,true}$ is the “true” reptation time in the absence of PPF. A similar method was proposed by Pattamaprom and Larson [48]. Perhaps more commonly, τ_s is simply treated as a fitting parameter to match nonlinear viscoelastic data, with a check on whether the fitted value is reasonable.

Historically, nonlinear viscoelastic models for linear polymers have mostly been verified by comparison to data taken for entangled polymer solutions, which are easier to measure than melts due to lower torques in the rheometer and a lower tendency towards instabilities (see Section 10.8 above). A number of comparisons with polymer solution data are presented in the original GLaMM model paper [13]. More recently, data for polymer melts have become available, both in shear and in extension (see Section 11.3.6 below for a fuller discussion of extensional data). Auhl et al. [49] presented start-up shear data for polyisoprene melts spanning a wide range of molecular weights and degrees of entanglement, making use of time-temperature superposition to increase the effective range of applied shear rates. Using the Likhtman-McLeish theory [46], they obtained the plateau modulus G_N^0 , the entanglement molecular weight M_e^G , and the entanglement time τ_e consistently for the whole range of molecular weights. Then, without any further adjustment of parameters, they compared their transient shear data against predictions of the GLaMM model [13].

Figure 11.5 shows both data and theoretical predictions for three molecular weights, corresponding to $Z = 7.0, 19.7$, and 46.9 entanglements per molecule. The data and theory are within reasonable agreement given experimental error, especially at the higher molecular weights. Several regimes of shear rate $\dot{\gamma}$ are observed. For $\dot{\gamma} < 1/\tau_d$ the transient shear stress growth coefficient follows the linear viscoelastic envelope. However, for $\dot{\gamma} > 1/\tau_d$ (i.e., for orientation Weissenberg numbers greater than one), shear thinning is observed, and the shear stress passes through a weak maximum before settling to its steady-state value. This maximum is caused when the polymers are oriented between the flow direction and flow gradient direction, a configuration which is favorable for increased shear stress. At later times, polymers are flattened out in the flow direction, giving a lower shear stress.

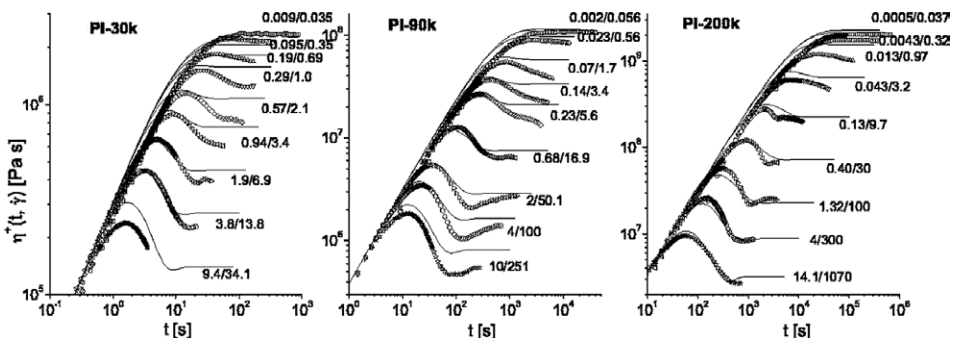


Figure 11.5 Transient shear stress growth coefficient as a function of time t at different strain-rates for three PI melts of molecular weights 33.6 kg/mol (PI-30 K), 94.9 kg/mol (PI-90 k), and 225.9 kg/mol (PI-200 K) corresponding to $Z = 7.0$, 19.7, and 46.9 entanglements per molecule respectively. Data are shown at a reference temperature of -35°C , along with the predictions of the GLaMM model [13]. The numbers next to each curve correspond to Weissenberg numbers with respect to the stretch and orientation relaxation times. From Auhl et al. [49].

On further increasing the shear rate to $\dot{\gamma} > 1/\tau_s$ (i.e., for stretch Weissenberg numbers above one) the transient shear stress passes through a stronger overshoot, occurring at a larger strain, before settling to its steady-state stress. This large maximum is caused by chains stretching while they are oriented by the flow.

Figure 11.6 shows the steady-state stress (normalized by the plateau modulus) as a function of flow rate (normalized by the orientation relaxation time) for the same set of polyisoprenes together with some of lower molecular weight. Also shown are predictions from the GLaMM model. Here, the shear thinning is obvious and, for the highest molecular weights, the shear stress approaches a plateau as shear rate is increased beyond $\dot{\gamma} = 1/\tau_d$. This plateau is more obvious in the model than in the data, but in neither case does the slope become negative. In the model, this is because the CCR is sufficiently active to avoid the catastrophic shear thinning that would certainly lead to shear banding instabilities. If the amount of CCR is reduced in the model (by decreasing the parameter c_v) then the GLaMM model, like the Doi-Edwards model in Section 11.3.1, predicts catastrophic shear thinning. For a further discussion of shear banding, see Section 11.3.7.

The model also predicts an increase in steady shear stress at yet higher rates such that $\dot{\gamma} > 1/\tau_s$. Although the data agree with the model in predicting the increase in transient shear stress overshoots in the stretching regime, there is no evidence in the data of a corresponding increase in steady shear stress.

Toy models can also be used successfully to model shear data of linear entangled polymers. Figure 11.7 shows both transient shear stress and first normal stress growth coefficients for a 7% solution of polybutadiene with molecular weight 813 kg/mol [41].

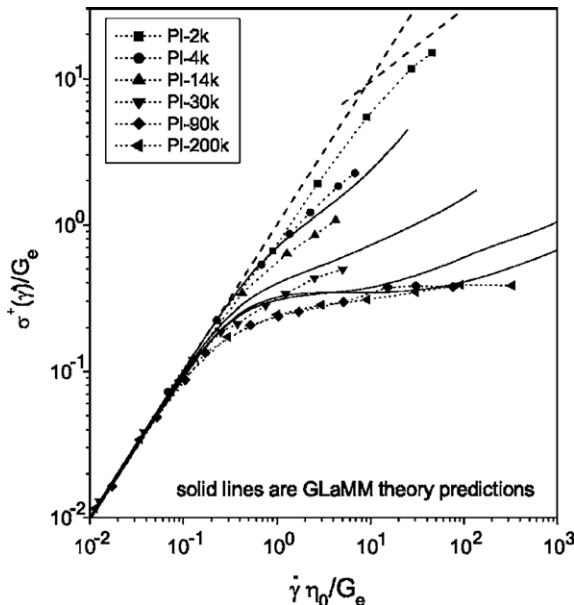


Figure 11.6 The steady-state stress (normalized by the plateau modulus) as a function of flow rate (normalized by the orientation relaxation time) for the same polyisoprene melts as in Fig. 11.5, and some of lower molecular weight, together with predictions using the GLaMM model [13]. From Auhl et al. [49]

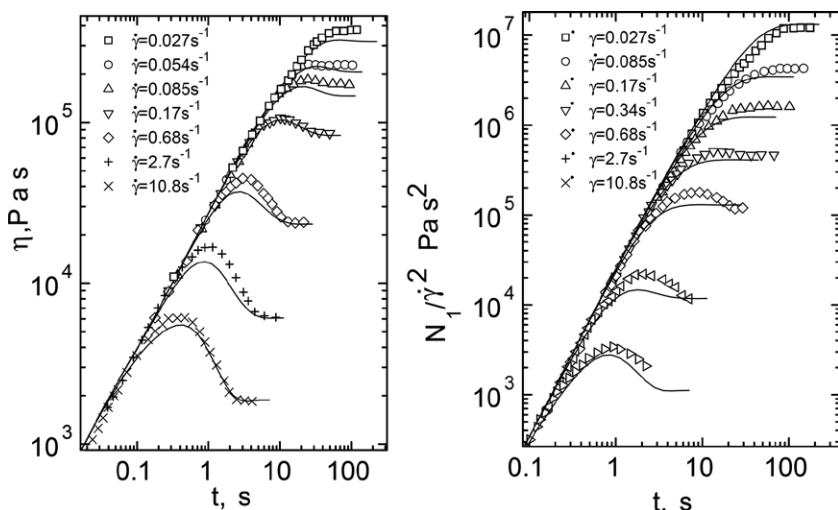


Figure 11.7 Predictions of shear stress and first normal stress growth coefficients by the Rolie-Poly model of Likhtman and Graham [41] for a 7% solution of polybutadiene with molecular weight 813 kg/mol. From Likhtman and Graham [41]

The data is fit using a multi-mode version of the Rolie-Poly model, first by matching the experimental linear viscoelastic spectrum with a discrete set of modes (see Section 4.4 for a description of this procedure), and then by assigning non-zero stretch relaxation times to the two slowest modes only (all others are calculated using the nonstretching model of Eq. 11.16). Thus, τ_s is treated here as a fitting parameter to match nonlinear viscoelastic data. According to [41], τ_s is found to be the correct order of magnitude but not exactly at the expected value. Curiously, the CCR parameter β is set to zero in this data fit, so that the model resembles quite closely the DEMG model without CCR. Catastrophic shear thinning is avoided in this case by the wide distribution of relaxation times in the linear viscoelastic spectrum, most likely due to sample polydispersity. These issues are most likely due to the “toy” nature of the model—the actual values of the fitted parameters should not be expected to have physically exact values. Instead, toy models are more suited to data fitting, with the purpose of using the model in computations for more complex flows.

Thus nonlinear constitutive equations that describe reptation, time-dependent chain retraction, and constraint release by reptation and chain retraction, are in promisingly good agreement with nonlinear data in shear flows of monodisperse entangled polymer solutions and melts.

11.3.6 Extensional Flows of Melts and Solutions of Linear Polymers

In steady-state uniaxial extensional flows, all the chain-stretching models described above from Sections 11.3.2 to 11.3.4 predict three regions of flow; see Fig. 11.4. For monodisperse polymers, these regions are defined by the extension rate $\dot{\varepsilon}$ relative to the two relaxation times τ_d and τ_s . For $\dot{\varepsilon} < 1/\tau_d$, the extension rate is too low to significantly affect the chain’s configuration, and the flow is in the linear viscoelastic region. In this slow-flow regime, the steady-state uniaxial extensional viscosity η_E is equal to three times the zero-shear viscosity $3\eta_0$. (Likewise, for start-up flows in the slow-flow regime, the tensile growth coefficient $\eta_E^+(t)$ is equal to three times the linear stress growth coefficient $\eta^+(t)$.) At higher extension rates, such that $1/\tau_d < \dot{\varepsilon} < 1/\tau_s$, the flow is fast enough to orient the primitive path of a molecule, but not to stretch it. Hence, in this intermediate regime, the tensile growth coefficient is predicted to be extension thinning; that is, $\eta_E^+(t, \dot{\varepsilon})$ drops below the linear viscoelastic envelope defined by $3\eta^+(t)$ at long times. For fast extension rates, $\dot{\varepsilon} > 1/\tau_s$, the extensional flow is able to stretch the polymer molecules; i.e., the molecular stretch λ begins to rise above unity.

By comparison, in a shearing flow, molecular orientation makes $\kappa : S$ in Eqs. 11.10, 11.21, or 11.24 smaller at higher strain rates, so that the driving term for chain stretch, $\lambda \kappa : S$, is modest even when λ is large. CCR increases $\kappa : S$ somewhat, but in

a shear flow, chain stretch grows only gradually with shear rate even at high strain rates. But in an extensional flow $\kappa : S$ is large at high extension rates; hence, growth of λ makes the driving term $\lambda \kappa : S$ ever larger as the stretch λ increases. Thus, extensional flow is prone to runaway chain stretch at strain rates above a critical value around $\dot{\epsilon} = 1/\tau_s$. Of course, the chain stretch is limited by the maximum extensibility of the polymer chain, set by the function $k_s(\lambda)$; see Section 11.3.2 and Eq. 11.13. The region where chain stretch saturates may be considered a fourth flow region.

Figure 11.8 shows predictions of steady-state extensional viscosity using DEMG theory (Section 11.3.2) and a CCR model due to Mead, Larson, and Doi (the “MLD model”) [35]. Both predict reasonably well the extensional viscosities of polystyrene solutions. These data were obtained using the *filament stretching rheometer* developed by Sridhar and coworkers [50] (see Section 10.10.2), which is able to access high strains in extensional flows for polymer solutions. The parameters of the theories were estimated from linear viscoelasticity and molecular theory, using the methods discussed in Section 11.3.5 [47, 51]. The data show the predicted three regions of extensional viscosity. This observation of the three flow regimes, and especially of the extension thinning in the intermediate flow regime, is a strong confirmation of the basic tube model and of the existence of two time scales τ_d and τ_s , controlling tube orientation and stretch respectively.

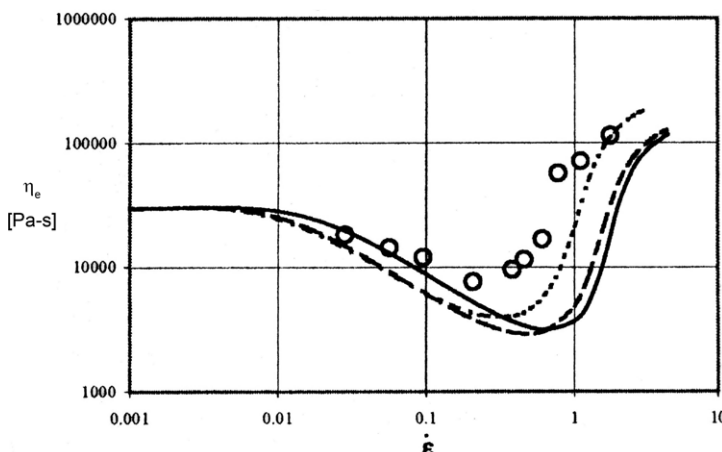


Figure 11.8 Comparison of the predictions of the DEMG model (solid line) and Mead-Larson-Doi model [35] (dashed and dotted lines) to experimental data (symbols) for the uniaxial extensional viscosity $\eta_E(\dot{\epsilon})$ versus extension rate $\dot{\epsilon}$. The data are for a 6% solution of 10.2 million molecular weight polystyrene in diethyl phthalate at 21 °C. The parameters used in the MLD and DEMG theories are $G_N^0 = 294$ Pa for both models; $\tau_d = 21$ s, and $\tau_s = 0.51$ s for the DEMG theory, and $\tau_d = 83.4$ s, and $\tau_s = 1.08$ s for the “Milner-McLeish” method of obtaining the time constants for the Mead-Larson-Doi model (dashed line), and $\tau_d = 123$ s, and $\tau_s = 1.58$ s for the “Doi-Kuzuu” method (dotted line). From Bhattacharjee et al. [47].

Note that in Fig. 11.8, the MLD and DEMG theories give qualitatively similar predictions in extensional flow for monodisperse polymers. This shows that CCR has only a minor effect on chain dynamics in extensional flow, which lacks the subtle coupling of stretch and orientation present in flows with vorticity, such as shear. While chain orientation effects are not difficult to capture (even without CCR!) in molecular models, the chain stretch effects are evidently difficult to model accurately, as shown by the rather imperfect agreement between theory and experiment in Fig. 11.8. Predictions of the GLaMM model in both start-up of steady extension and start-up of steady shear for entangled polystyrene solutions can be found in Graham et al. [13]; see Fig. 11.9. The agreement between the theory and the experiments is

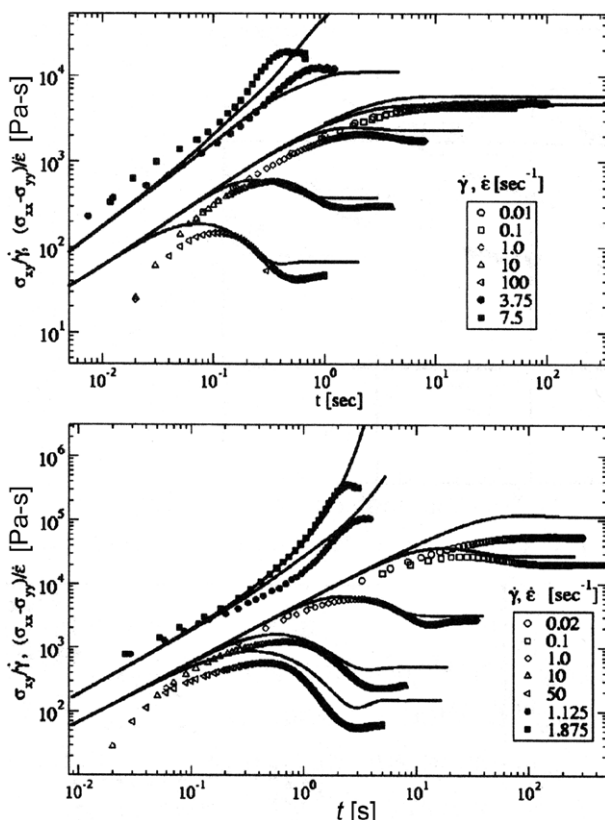


Figure 11.9 Comparison of predictions of shear and extensional stress growth coefficients $\eta^+(t, \dot{\gamma})$ and $\eta_E^+(t, \dot{\epsilon})$ according to the GLaMM model [13] with experimental data for 7% solutions in tricresyl phosphate at 40 °C of nearly monodisperse polystyrenes of molecular weights (a) 2.89 million and (b) 8.42 million at the rates shown. The parameters of $\tau_e = 1.911 \cdot 10^{-3}$ s, $M_e^G = 270,000$, and $G_e = (5/4) G_N^0 = 8075$ Pa are obtained from linear viscoelastic measurements and $c_v = 0.1$ sets the rate of constraint release. The Rouse reorientation time is set to be $\tau_r = Z^2 \tau_e$. From Graham et al. [13].

reasonably good, except at high strains in extensional flow, where agreement fails because of the lack of inclusion of finite extensibility (i.e., non-Hookean chains) in the GLaMM model.

In general, recent models that include CCR effects as well as chain stretch are usually in at least semi-quantitative agreement with experimental shear and extensional data for entangled polymer solutions. Quantitative agreement is not always attained, however, and accurate modeling of chain stretch is still elusive.

There is, however, substantial evidence of discrepancies between measured extensional data for entangled polymer melts and solutions. It has only been relatively recent that extensional viscosities and transient extensional stress growth coefficients have been reliably measured for polymer melts. Hassager and coworkers [52] have shown that the filament stretching rheometer of Sridhar and coworkers can be used for melts as well as solutions, and by carefully measuring and controlling the time-dependent filament diameter, they have obtained plateau stresses at high strains that allow steady-state extensional viscosities to be determined for molten polymers. Their data for two nearly monodisperse polystyrene melts having molecular weights of 200,000 and 390,000 contain something of a surprise. These data are presented in Fig. 11.10 and seem to show only the first two regions of flow, not the third region of thickening predicted by theory and exhibited by the entangled solutions, discussed above. Furthermore, the extension thinning region shows a weaker thinning exponent than the -1 exponent expected from theory. (The same can be said for the data for polymer solutions in Fig. 11.8.) These melts, especially the one of higher molecular weight, ought to be sufficiently well entangled for the theory to apply. Hence, the qualitative divergence of these data from the predictions of the tube model was both unexpected, and disturbing. An initial explanation of these data by

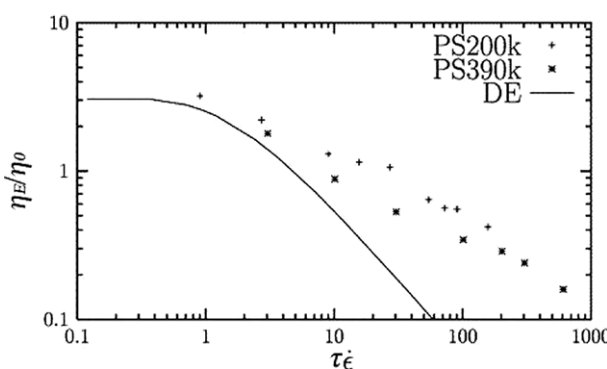


Figure 11.10 Steady-state uniaxial extensional viscosity normalized by the zero shear viscosity versus Weissenberg number $Wi = \tau \dot{\epsilon}$ for nearly monodisperse polystyrene melts with molecular weights of 200,000 (+) and 390,000 (*), where τ is roughly the reptation time. The line is the prediction of the Doi-Edwards theory. From Bach et al. [52].

Marrucci and Ianniruberto [53] suggested that extensional flow modified the “tube pressure” experienced by chains, changing the tube diameter: this predicted the observed scaling of steady stress with strain rate. However, this explanation failed to account for the apparent lack of a chain stretching regime, and it did not account for the difference between polymer solutions and melts. Their explanation has since been largely replaced by a more likely proposal, which is that the significant chain orientation produced by the strong extensional flow gives rise to a reduction in the effective friction coefficient ζ [28, 54–58].

A more recent set of data from the Hassager group, shown in Figs. 11.11 and 11.12, illustrates this point. Figure 11.11 shows extensional rheology data from a polystyrene melt of molecular weight 285 kg/mol together with data from a solution of polystyrene with molecular weight 545 kg/mol in oligomeric polystyrene of molecular weight 2 kg/mol. The solution was designed so that it had the same number of entanglements per polymer as the 285 kg/mol melt, as evidenced by an identical shape of linear viscoelastic spectrum [55]. The data in Fig. 11.11 are presented on a normalized scale, with the stress normalized by the plateau modulus of each liquid, and all times and flow rates normalized by a characteristic timescale. Hence, the data from the polystyrene melt, and the polystyrene solution, can be directly compared.

It is clear that the two sets of data share many features. At low extension rates, both sets follow the linear viscoelastic curve. At higher extension rates, such that $1/\tau_d < \dot{\epsilon} < 1/\tau_s$, there is evidence of extension thinning, because flow is fast enough to orient the primitive path of a molecule, but not to stretch it. At higher flow rates still, such that $\dot{\epsilon} > 1/\tau_s$, chains begin to stretch, and this is indicated by a departure of the transient stress growth coefficient above the linear viscoelastic envelope, i.e., extension hardening. Crucially, both the data for the melt and for the solution exhibit this transition, so there is a chain-stretching regime in both, visible in the transient data. The initial departure from the linear viscoelastic envelope is identical for both the melt and the solution. However, the final level of steady-state stress obtained is different and the polystyrene melt consistently reaches a lower level of steady-state stress than the corresponding solution on this normalized stress scale. The result is that the steady-state extensional viscosity for the melt, as a function of extension rate, continues to decrease beyond $\dot{\epsilon} > 1/\tau_s$, so that there is no obvious onset of chain stretching in the steady-state data (similar to Fig. 11.10). The steady-state data for the solution do, however, exhibit a transition for $\dot{\epsilon} > 1/\tau_s$.

Moreover, as the data in Fig. 11.12 demonstrate, the strength of the transition in the steady-state data depends upon the dilution of the solution [56]. This figure shows normalized steady-state extensional viscosities for a series of solutions of different molecular weight polystyrenes, diluted to different extents so as to obtain the same number of entanglements per molecule. Whilst the extensional viscosity of the melt continues to decrease as the chain-stretch transition is passed, the data for all

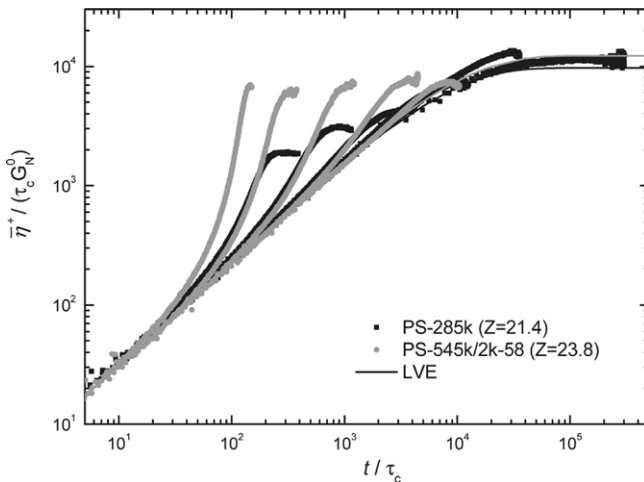


Figure 11.11 Transient extensional stress growth coefficient at 130 °C for polystyrene melt (285 kg/mol) and a solution of 58% polystyrene (545 kg/mol) in styrene oligomer (2 kg/mol), with the same number of entanglements per polymer as the 285 kg/mol melt. Stresses are normalized by the plateau modulus; flow rates and times normalized by a characteristic timescale. Actual flow rates are, for the melt: 0.03, 0.01, 0.003, 0.001, 0.0003, and 0.00003 s⁻¹ and for the solution: 0.45, 0.23, 0.076, 0.023, and 0.0076 s⁻¹. From Huang et al. [55].

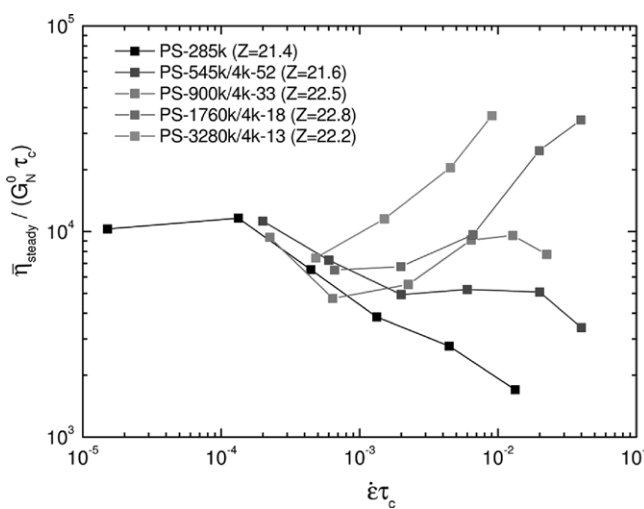


Figure 11.12 Normalized steady-state viscosity as a function of normalized stretch rate for a series of polystyrene solutions of increasing molecular weight, and correspondingly increasing dilution in oligomeric polystyrene (4 kg/mol) so as to achieve identical number of entanglements per molecule. From Huang et al. [56].

solutions show an upturn in extensional viscosity through the stretch transition, the strength of the upturn increasing with greater dilution. This means that an upward departure from the linear viscoelastic envelope in the transient stress data is a better indicator of the onset of chain stretch than the steady-state data, especially for polymer melts.

In conclusion, the data from Figs. 11.11 and 11.12 demonstrate a breakdown of universality for polymeric liquids in strong extension. Polystyrene solutions and melts with the same number of entanglements per chain exhibit many similar properties: an identical shape of linear viscoelastic spectrum, identical behavior in nonlinear shear [57], identical behavior in nonstretching extensional flows, and identical departure from the linear viscoelastic envelope when chains stretch for $\dot{\epsilon} > 1/\tau_s$. However, the steady-state stress is not universal, and this indicates that an extra parameter beyond the plateau modulus G_N^0 , the entanglement molecular weight M_e^G , and the entanglement time τ_e is required. As noted above, the growing consensus is that this nonuniversal behavior results from a reduction in the effective friction coefficient ζ with increasing monomer orientation, the friction reduction being less important for solutions than for melts. It is likely that different monomer chemistries will exhibit different degrees of friction reduction. A number of theoretical models [28, 54, 57, 58] have illustrated the effects of friction reduction in extensional flow.

11.3.7 Constitutive Instabilities and Slip

We noted in Section 11.3.1 that the prediction of a maximum in steady-state shear stress as a function of shear rate was considered a basic failure of the Doi-Edwards constitutive equation. Such a prediction implies that the same shear stress is produced by more than one shear rate. In such a situation, a uniform shearing flow at shear rates near or above the inverse of the reptation time τ_d would become unstable to a so-called constitutive instability, leading to spontaneous formation of inhomogeneities in the rate of shearing, possibly stratified into shear bands parallel to the shearing surfaces, with shear rate varying from one band to the next [59, 60]. The simplest form these bands might take would be a “fast” band with high shear rate above $1/\tau_d$ sliding parallel to a slow band with low shear rate below $1/\tau_d$. This “shear banding” phenomenon was considered to be unobserved for polymeric liquids until the last ten years or so. Since then, there have been reports, largely from the group of Shi-Qing Wang using particle tracking methods, of shear banding and related phenomena in well-entangled polymer solutions. Observations include banding in steady shear, transient banding during start-up shear [61, 62], and a quasi-elastic yielding during relaxation following steady shear [63]. These observations have been controversial, partly due to the molecular interpretation offered by Shi-Qing Wang, and partly because of disputes concerning experimental protocol and whether the

effects are due to edge instabilities. For example, an eminent group of rheologists attempted but failed to repeat some of the experiments; yet their apparent failure may have been due to sample mischaracterization [64–66]. There is a pressing need for independent confirmation (or not) of the observations. What seems certain, whether or not the observations are confirmed as true shear banding, is that observation of these phenomena requires precisely controlled conditions including the use of highly monodisperse and well-entangled polymers (tens of entanglements per molecule, at least).

For the purposes of this chapter we may note, simply, that such observations are wholly in keeping with the tube model as set out so far in this chapter. As just noted, the Doi-Edwards model introduced in Section 11.3.1 actually predicts the non-monotonic flow curve associated with such shear banding phenomena, even when modified to include chain stretch (in Section 11.3.2). Convective constraint release (CCR) was introduced into the model (Section 11.3.3 onwards) largely because no one had at the time observed shear banding, so this was viewed as a failure of the model that required correction.

It now seems possible that the effects of CCR may not be so strong: a slightly smaller value of the (*a priori* unknown) CCR parameter c_v in the GLaMM model, or the corresponding parameter β in the toy Rolie-Poly version, produces a non-monotonic flow curve for highly monodisperse, well-entangled polymeric liquids, but retains a monotonic curve in other cases. Using the Rolie-Poly model as a candidate (but simple) constitutive model that can be used in simulations of nonuniform flow, predictions have been made of both steady state and transient shear banding [67]. There are indications, in fact, that transient shear banding should occur to some extent in any material that undergoes a stress overshoot during start-up shear, the instability occurring when stress decreases with increased shear strain [68]. It is also possible, using the Rolie-Poly model, to predict the observed quasi-elastic yielding during relaxation following steady shear [69–71].

A related phenomenon, observed for highly entangled melts, is “wall slip” in which the bulk melt slides either along the wall or, more likely, along a thin layer of chains adsorbed to the wall. This may be distinguished from the shear banding just described: in shear banding, the fast shear band is, in principle of macroscopic dimensions, much greater than a few molecules, while in wall slip, the fast shear is confined to microscopic dimensions close to the wall. In a cone-and-plate and circular or plane Couette flow, high levels of slip near, if not at the wall, have been observed directly using particle-imaging and other techniques [72–74].

These anomalies in steady shear flow or start-up of steady shearing flow are usually seen or are most pronounced in especially highly entangled polymers, ones for which the molecular weight is roughly 50 times higher than the entanglement molecular weight M_e . Wall slip gives rise, for example, to sudden increases in flow

rate as pressure or stress is gradually increased. This is seen especially in flows through capillaries, where the sudden increase in flow rate is called “spurt” [75, 76]. Doi and Edwards, in their original series of papers, suggested that spurt might be a manifestation of the shear banding instability inherent in their original constitutive model [20], but this proposal has been largely discounted. Instead, it is most likely that spurt is due to wall-slip, i.e., from microscopic molecular behavior close to the wall. For polybutadiene melts, Park et al. [77] found there was an effective maximum in shear stress at the wall as a function of slip velocity: while this is in some ways analogous to the maximum in shear stress as a function of shear rate in the Doi-Edwards model, it instead leads to local wall slip as opposed to shear banding in the bulk of the material. This topic, however, is too complex to be discussed in more detail here.

11.3.8 Entanglement Stripping and Chain Tumbling

In the preceding sections, we focused on the mechanisms of nonlinear flow which have dominated discussion of the rheology of linear polymer chains: reptation, tube orientation, chain stretch, and CCR. However, more recently other flow mechanisms have begun to receive attention. One such mechanism is “entanglement stripping.” The slip-link simulations described in Section 6.5 have also been applied in nonlinear flows, and a common observation is that the number of slip-links per chain in the simulation decrease in strong nonlinear flows [78].

The mechanism giving rise to the reduction is clear: when chains retract, then the chain ends pass through slip-links and these slip-links are deleted, i.e., “stripped off” the chains. If no measures are taken to reintroduce slip-links at the same rate then the number of slip-links per chain is, naturally, reduced. The exact details of this depend sensitively on the assumed dynamics of slip-link deletion and reformation in the algorithm—in this context many assumptions are possible and the choice appears somewhat arbitrary. However, to prevent reduction in the number of slip-links requires an explicit change to the algorithm for slip-link dynamics beyond what is assumed in linear rheology and so most slip-link algorithms predict this reduction in slip-link number.

The “entanglement stripping” observed in slip-link simulations might be dismissed as a curiosity, and simply a feature of that type of model, but recent molecular dynamics and dissipative particle dynamics simulations of strong shear of linear polymer melts by Khomami and coworkers [14, 79, 80] produced similar observations. They employed one of the entanglement detection algorithms detailed in Section 6.3.6 to identify the number of entanglements per chain in the strongly deformed chain configurations in nonlinear flow. It appears that the number of entanglements identified by such methods does decrease at high flow rates.

It is possible to incorporate such effects into tube-based models, where the reduction in entanglement number can be interpreted as a flow-induced increase in tube diameter and entanglement molecular weight. Ianniruberto and Marrucci have developed such a model for linear polymers [15, 16]. However, it is possible that the effects of entanglement stripping might be more significant for branched polymer melts: Hawke et al. [30] have proposed that such stripping is responsible for overshoots in stress observed for highly branched resins (see Section 11.5.2.4).

In addition to entanglement stripping, Khomami and coworkers [14, 79, 80] also observed that (i) in strong flows, the distribution of chain end-to-end vectors becomes strongly non-Gaussian, and that (ii) chains undergo a “tumbling” rotational motion similar to what is observed for unentangled polymers. Both observations are potentially significant, the first because most nonlinear tube models invoke “closure approximations” in order to obtain useable constitutive equations (see, e.g., the derivation of the GLaMM model [13] where the approximations are explicitly written). These closure approximations depend on assumptions about the chain configurational distribution, which might not be appropriate if the distribution is non-Gaussian. The tumbling motion may also give rise to additional relaxation mechanisms which are not explicitly invoked in the majority of tube models (though reference [57] contains a first attempt to include this mechanism).

While existing constitutive equations based on tube models give a good representation of much of the observed response to nonlinear flow, there remain details of the chain motion which are not captured by these models. It remains to be seen whether these details give significant changes to the viscoelastic response.

11.3.9 Processing Flows

While improvements to the tube model are still required, tube models with CCR are now accurate enough to be used in numerical simulations of complex flows, at least for linear polymers without spikes or other unusual features in the molecular weight distribution. A dramatic example was provided by the McLeish team, who showed that the GLaMM model of Graham et al. and the related Rolie-Poly model can be used not only to predict the linear and nonlinear rheology of a nearly monodisperse polystyrene melt, but also to predict accurately both the birefringence and neutron scattering patterns in the same melt in flow through a contraction [81–83]. Without CCR, the tube model predicts that the steady-state shear stress exhibits a maximum at a Weissenberg number near unity, which renders it completely unsuitable for simulations of processing flows. As a result, in the past, most nonlinear constitutive equations used in polymer processing simulations have not been derived from the tube model. Now that CCR models have largely fixed the problem of the stress maximum there is the potential of using molecular-based tube models in such simulations.

However, while progress has been made in predicting complex flows of polymers under idealized conditions, as indicated by the examples just given, there remain challenges in applying this work to industrial processing flows: major barriers are the heterogeneity of commercial polymers, the often high processing rates, the complexity of the flow geometries, and issues such as wall-slip.

■ 11.4 Polydisperse Linear Polymers

The models described in Section 11.3 are intended to capture the physics of flow for monodisperse linear polymers. Industrial resins, however, are polydisperse, often containing a broad range of molecular weights. There is thus considerable interest in generalizing the above constitutive laws to mixtures of multiple molecular weights. One option, used frequently, is simply to use multi-mode versions of toy models, such as those presented in Sections 11.3.3 and 11.3.4, as a means to describe measured experimental data and characterize the viscoelastic response of a given resin. In this mode of operation, the linear experimental viscoelastic response of a given material would first be modeled by decomposition into a set of modes (i.e., a discrete relaxation spectrum, see Section 4.4). Then a “toy” model constitutive equation (e.g., Eqs. 11.17 to 11.19 for the Rolie-Poly model) would be assigned to each linear viscoelastic mode. For each mode, nonlinear parameters, such as the stretch relaxation time, are established by fitting the model to experimental nonlinear viscoelastic data in shear and extension. Typically, only the slowest modes would require a non-zero stretch relaxation time, while faster modes are described by “nonstretching” versions of the constitutive model. This approach forgoes any attempt to predict constitutive behavior from the molecular weight distribution, but is instead a data-fitting exercise. The hope is that the toy model used captures enough of the necessary physics so that, after the model is matched to a limited set of nonlinear viscoelastic data, it then becomes predictive of the response of the material to more general deformations. Hence, a nonlinear model with parameters fixed in this way can be used, for example, in flow computations for flow in complex geometries, as seen for example in Hassell et al. [84].

However, we saw in Chapter 7 that polydispersity can give rise to complex physics even in the linear viscoelastic regime, when relaxation of short chains gives rise to constraint release on longer chains. The result was a competition and interplay between different relaxation mechanisms for the longer chains: reptation, primitive path fluctuations, and constraint-release (CR) Rouse motion. For a mixture of just two chain lengths, the eventual relaxation pathway depended on the relative rates of these processes, as determined by the molecular weights and concentrations of

the different components. The following discussion relies on some of the concepts introduced in Chapter 7, since it is to be expected that similar complexity is present in the nonlinear viscoelastic response of polydisperse materials.

A striking illustration of this complexity was provided by Auhl et al. [85]. They presented extensional rheology data for a series of polyisoprene blends in which long chains (483 kg/mol) were diluted with much shorter, but still entangled, chains (33.6 kg/mol). These blends were carefully designed to obey two specific criteria:

1. The timescale for the subsection of chain between two long chain entanglements to relax by local CR-Rouse motion ($\tau_{\text{CR,loc}}$, as defined in Section 7.3.2) must be significantly faster than the flow timescales of interest. This criterion ensures that the *thin tube*, representing entanglements on long chains from short chains, is locally equilibrated with respect to the *fat tube*, representing entanglements between long chains (see Section 7.3.3).
2. Constraint release motion, however, must not be so fast that “tube reptation” along the fat tube is faster than chain reptation along the thin tube (see Section 7.3.3 and Eqs. 7.6 and 7.7). This criterion ensures that chain transport along its length—both for reptation and stretch relaxation—is most rapidly achieved by chain motion along the tortuous path of the thin tube, rather than along the smoother path of the fat tube.

The extensional rheology data, shown in Fig. 11.13, contain a rather surprising result. The data for the pure 483 kg/mol polyisoprene exhibit extension hardening at flow rates above 10 s^{-1} , which is to be expected, given an anticipated Rouse reorientation time of around 0.13 s. However, as the long chains are progressively diluted by the short, faster chains, the flow rate at which the onset of extension hardening is observed becomes progressively *slower*, to the extent that at a dilution of 4% the extension hardening is observed at flow rates as small as 2 s^{-1} , and even 0.5 s^{-1} . The effective stretch relaxation time of the long chains is, counterintuitively, becoming larger (slower) as the long chains are diluted with short ones!

This surprising result may be understood in terms of the two specific design criteria listed above for this series of melts. The first criterion ensures that the thin tube is locally equilibrated in the fat tube. This ensures that the fat tube sets the relevant scale for the stress from long chains in the melt, and is the appropriate scale for evaluating tube orientation and stretch relaxation. If the chain is stretched in the fat tube, by an amount λ_{fat} , then (as shown by Auhl et al. [85]) the thin tube rapidly equilibrates, by constraint release, so that the stretch in the thin tube is obtained from:

$$\lambda_{\text{thin}}^2 = \phi \lambda_{\text{fat}}^2 + 1 - \phi \quad (11.27)$$

where ϕ is the fraction of slow constraints (roughly equal to the long chain fraction). In the limit of small stretch, this can be approximated as:

$$\lambda_{\text{thin}} - 1 = \phi (\lambda_{\text{fat}} - 1) \quad (11.28)$$

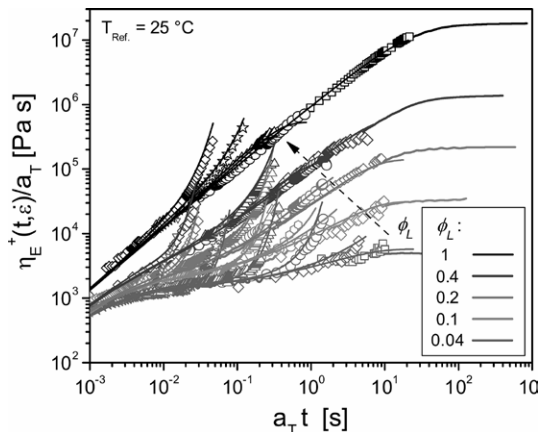


Figure 11.13 Transient elongational stress growth coefficient for a series of polyisoprene blends of 480 kg/mol polymers diluted in 33.6 kg/mol polymers at concentrations of 100%, 40%, 20%, 10%, and 4% of the longest polymer from top to bottom. Data taken at different temperatures are shifted by time-temperature superposition to a reference of 25 °C. Effective flow rates are: 0.1, 1, 10, 100 s⁻¹ (100% data); 0.12, 1.2, 10, 100 s⁻¹ (40% data); 0.1, 1.24, 9.9, 102 s⁻¹ (20% data); 0.1, 1, 2, 9.85 s⁻¹ (10% data); 0.1, 0.5, 2, 9.81, 46.7, 224 s⁻¹ (4% data). Also shown are fits to the data using multi-mode Rolie-Poly equations. From Auhl et al. [85].

At the same time, the second criterion above ensures that stretch relaxation (which requires motion of the chain along its length) is most rapidly achieved by motion along the thin tube. Hence the rate of stretch relaxation in the fat tube is driven by the stretch in the thin tube, and is, for small stretch:

$$\frac{d\lambda_{\text{fat}}}{dt} = -\frac{1}{\tau_r} (\lambda_{\text{thin}} - 1) = -\frac{\phi}{\tau_r} (\lambda_{\text{fat}} - 1) \quad (11.29)$$

where we have used Eq. 11.28 to relate the thin tube and fat tube stretch. Hence, the natural timescale for stretch relaxation is $\tau_{s,\text{eff}} = \tau_r/\phi$, which matches the experimental observation that the stretch relaxation time increases with dilution.

In practice, what happens is that at the same time stretch is relaxed via chain motion along the thin tube, constraint release from the short chains *adds* stretch, so as to maintain the equilibrium implied by Eqs. 11.27 and 11.28. It is the balance between these two effects that results in the enhanced stretch relaxation time.

Note that violation of either of these two criteria leads to a reduction in the enhanced stretch relaxation time. If constraint release from the short chains is too slow, then the first criterion is violated. The thin tube does not locally equilibrate inside the fat tube, and the effective dilution is reduced so that the relevant length scale for stretch and orientation becomes closer to the thin tube. In this case, the effective stretch

relaxation time returns towards the Rouse reorientation time τ_r . On the other hand, if constraint release from the short chains is too fast, violating the second criterion, then tube reptation (motion along the fat tube by CR) begins to compete with motion along the thin tube. This speeds up the stretch relaxation, until (at extremely fast CR rates) stretch relaxation occurs via free Rouse motion along the fat tube, again at the Rouse reorientation time τ_r . So, if the short chains are too short, or too long, the interesting effect observed by Auhl et al. [85] may be expected to disappear.

In a polydisperse melt, a wide range of chain lengths will be present, and one may anticipate that a multiplicity of effects occur, with some chains too short, some chains too long, and some just right to produce the enhancement in stretch relaxation time. There is some evidence that such effects do occur in polydisperse melts, with both Münstedt [86] and Minegeshi et al. [87] observing extension hardening at surprisingly low rates, for both unimodal and bimodal polydisperse polystyrene melts.

Read et al. [88] produced a very detailed constitutive model for binary polymer melts, which was effectively a development of the GLaMM model, including reptation, constraint release, and primitive path fluctuations. The enhanced stretch relaxation time identified above emerged naturally within this model. They successfully described nonlinear viscoelastic data from both Auhl et al. [85] and from Nielsen et al. [89]. A toy model equivalent of this work has not yet been published, nor has this model been generalized to polydisperse systems. Mishler and Mead [90, 91] have recently published a constitutive model for polydisperse melts in which the enhanced stretch relaxation time is explicitly imposed (rather than emerging naturally from the theory). They were then able to use the model to describe, successfully, the data from Minegeshi et al. [87].

■ 11.5 Polymers with Long-Chain Branching

For a linear chain or an arm on a branched polymer, there is at least one free end, and retraction occurs rapidly, with a time constant controlled by the Rouse reorientation time of the chain. Therefore, for the simplest type of branched polymer, the star, we do not expect the nonlinear properties to be qualitatively different from those of linear polymers. This, indeed, appears to be the case. In step-shearing deformations, the “damping function” of star polymers [92–94] has been found to be nearly identical to that of linear polymers (shown in Fig. 11.2). Likewise, in steady uniaxial extensional flow, the curve of extensional viscosity or stress versus extension rate for stars is similar to that of linear polymers. Both the star and linear polymers show three regions of extensional flow: a linear dependence of extensional stress on extension rate in the slow-flow region, a plateau in stress (i.e., thinning

of extensional viscosity) in the intermediate-flow region, and a stress upturn, or thickening, in the fast-flow region.

Figure 11.14 reveals two main differences between the extensional rheology of stars and that of linear polymers. First, for stars, extension thickening occurs at a Weissenberg number $Wi_s \equiv \dot{\varepsilon} \tau_s$ based on the arm Rouse reorientation time $\tau_s = \tau_r = \tau_e Z_a^2$ of around 0.1, where Z_a is the number of entanglements in an arm. For linear polymers, thickening starts at around $\dot{\varepsilon} \tau_s = 1$. This difference is partly explained because the linear chain can retract from two ends, while the star arm can retract from only one; therefore, the star arm should retract one fourth as fast as a linear molecule of the same molecular weight. This is because the retraction or stretch time $\tau_{s,S}$ of a star arm is given by $\tau_{s,S} = 4 \tau_e Z_a^2 = 4 \tau_{s,L}$, where $\tau_{s,L} = \tau_e Z^2$ is the stretch time of a linear chain with the same number of entanglements $Z = Z_a$ as the star arm. There may also be an effect similar to what is observed in binary blends of linear polymers, as discussed above in Section 11.4. Constraint release from the rapidly relaxing arm ends may operate in a similar manner to constraint release from the short chains in a binary blend, giving a similar enhancement of the effective stretch relaxation time. Apart from these quantitative differences, Fig. 11.14 shows that the extensional rheology of star polymers (with only one branch point) is qualitatively similar to that of linear polymers [95, 96].

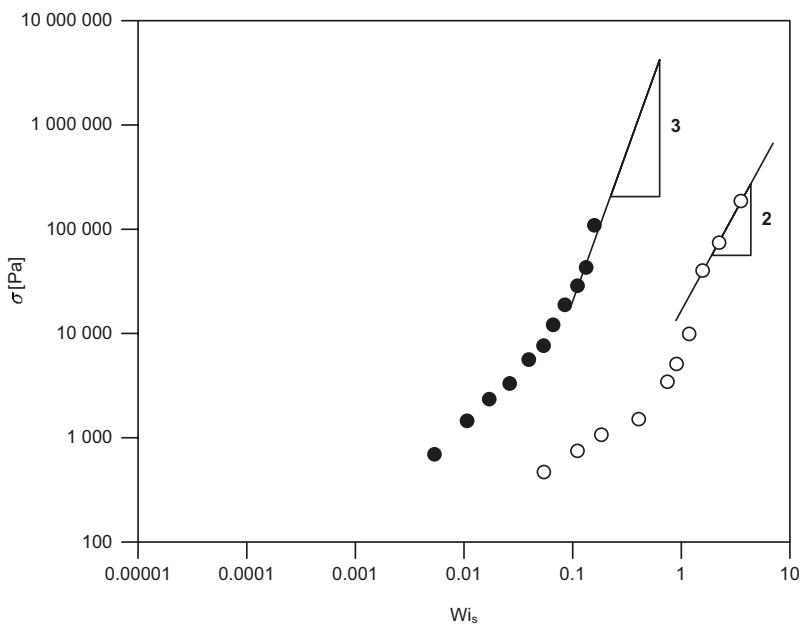


Figure 11.14 Steady-state extensional stress versus Weissenberg number Wi_s (based on the Rouse reorientation time τ_s) for solutions of various linear (open symbols) and star (filled symbols) polystyrene entangled solutions. From Bhattacharjee et al. [97]; see also ref. [95].

However, for a polymer with more than one branch point, such as an H polymer or a comb, there is a “backbone” portion of the molecule with no free ends that lies between two or more branch points. Without free ends, retraction of the backbone is severely impeded. As a result, the nonlinear properties of polymer molecules with more than one branch point are expected to be very different from those of linear or star polymers. This expectation is supported by experimental data for low-density polyethylenes, which are known to contain multiple long-chain branching, as discussed in Section 10.9.8. Figure 11.15, for example, shows the uniaxial extensional stress growth coefficient for several polymer melts. The polystyrene melt, PS I, and the high-density polyethylene melt, HDPE I, both of which lack long-chain branching (LCB), show little strain hardening. However, the low-density polyethylenes LDPE III and IUPAC A show pronounced strain hardening. It is evidently LCB, rather than molecular weight or viscosity, that is responsible for the differences in

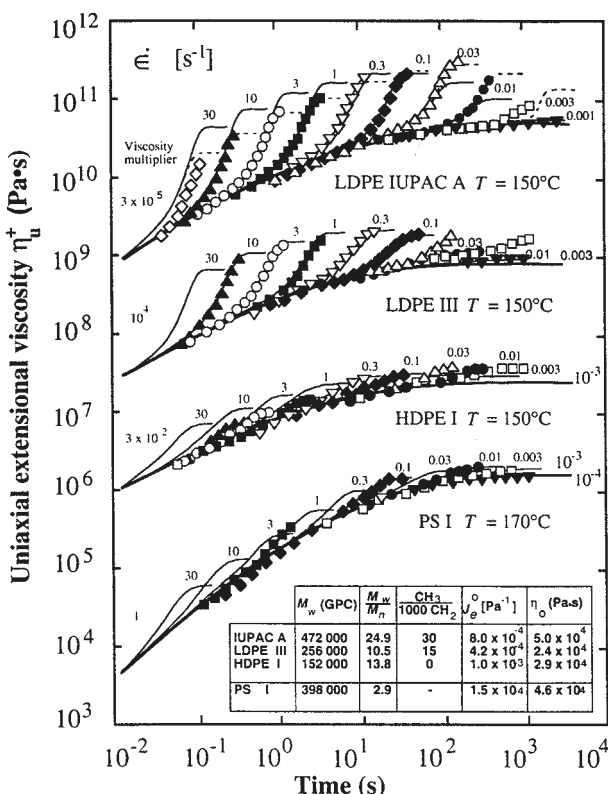


Figure 11.15 Stress growth coefficient $\eta_E^+(t, \dot{\epsilon})$ as a function of time at the extension rates $\dot{\epsilon}$ shown. Data are for an unbranched polystyrene (PS I), a high-density polyethylene without long side branches (HDPE I), and two low-density polyethylenes with long side branches (LDPE III and IUPAC A). Curves shifted to avoid overlap. From Laun [96].

strain hardening among these melts, since PS I, which lacks strain hardening, has a higher molecular weight and a larger zero-shear viscosity than LDPE III, which shows strain hardening.

Strain hardening in extensional flow is of practical importance, since it signals that molecular bonds are becoming highly oriented, and thus the modulus and strength of a fiber drawn in a strain-hardening melt will be higher than in one that is not. In addition, strain hardening in extension-dominated processing flows typically makes the processing operation less prone to instabilities [98–102]. Thus, long-chain-branched polyethylenes, such as LDPE, that are well known for their strain hardening, are also sometimes easier to process than linear polymers.

The relationship between branching and strain hardening is not always as clear as it appears in Fig. 11.15. Melts, such as high-density polyethylene or even polystyrene that nominally lack long-chain branching, sometimes show fairly pronounced strain hardening; see Fig. 11.16 (top) for example. The strain hardening in this high-density polyethylene melt might be due to a small high-molecular-weight spike or tail in the molecular weight distribution (i.e., a polydispersity effect as discussed in Section 11.4), or it might be due to a low level of long-chain branching that can sometimes be present in polyethylenes that are thought to be free of LCB. Although polydispersity can evidently produce some strain hardening, LCB is more effective in producing pronounced strain hardening.

For example, Fig. 11.16 (bottom) shows the extreme strain hardening that is induced in a polypropylene melt by introducing long-chain branches through exposure to an electron beam. Polypropylene melts that are free of long branches are normally almost entirely lacking in strain hardening. Similarly, Kasehagen and Macosko [103] have observed that chemical cross linking induces pronounced strain hardening during uniaxial extension of polybutadiene, which is normally not strain hardening. A similar result was obtained by Auhl et al. [104], who cross-linked polypropylene by electron-beam radiation. Torres et al. [105] studied the HDB series of branched metallocene polyethylenes discussed in Section 3.9.2 (and listed in Table 3.1) showing that the degree of strain hardening increased with branching content. They were able to link this to the increased fraction of comb-like and tree-like molecules in the resins.

An interesting observation is that long-chain-branched polymer melts sometimes show an overshoot in extensional stress during start-up of steady elongation. For many years the only report of such a phenomenon was that of Meissner and coworkers [107], but it has also been seen by Hassager's group using a filament-stretching rheometer [30, 108–110]. We will discuss this effect and its possible causes in more detail below, in Sections 11.5.2.4 and 11.5.3.

Interestingly, the extreme strain hardening observed in extensional flows of long-chain-branched polymers is not accompanied by any significant change in the

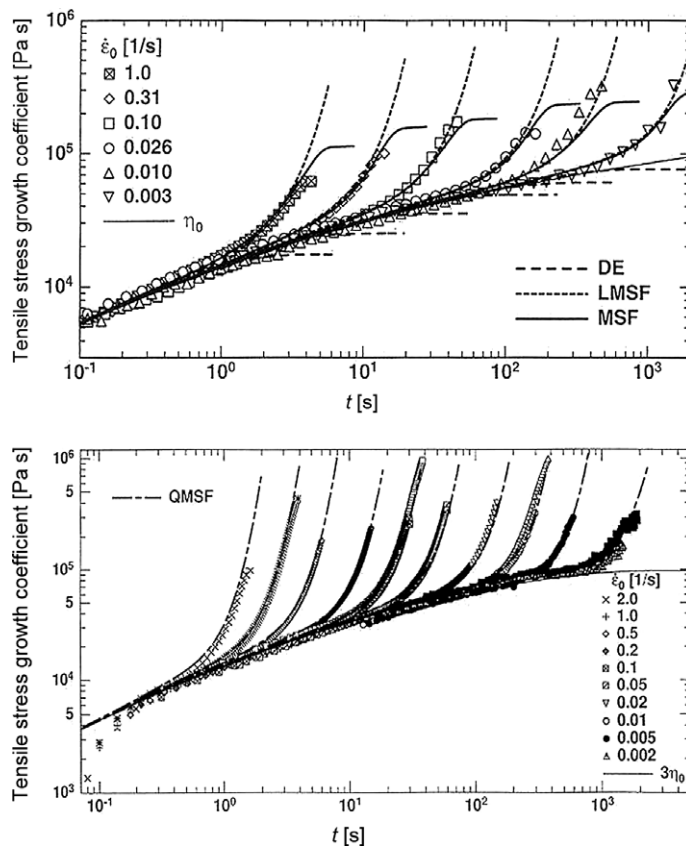


Figure 11.16 Stress growth coefficient $\eta_E^+(t, \dot{\varepsilon})$ after start-up of steady extension at the extension rates $\dot{\varepsilon}_0$ shown for (top) an HDPE (HDPE I) with $M_w = 104,000$ and $M_n = 18,900$ at $150^\circ C$, and (bottom) a polypropylene (PP 2) with $M_w = 586,600$ and $M_n = 61,750$ at $180^\circ C$, into which long-chain branches were introduced by electron-beam radiation. The lines are predictions of the Doi-Edwards theories and phenomenological constitutive equations of Wagner et al. From Wagner et al. [106].

steady-state shear properties, in particular the shear thinning, relative to linear polymers. Figure 11.17, for example, shows that the steep, thickening properties of LDPE in extensional flows contrast markedly with the pronounced thinning behavior observed in shearing flows. The thickening behavior in uniaxial extension is also observed in other extensional flows, in particular planar extension [111]. (For a definition of planar extensional flow, see Section 10.9.) The need to predict both the thickening behavior in uniaxial and planar extension, and at the same time, the thinning behavior in shear, is a major challenge in the development of molecularly based constitutive equations for branched polymer melts [112, 113]. In what follows, we discuss tube models that are able to meet this challenge, at least qualitatively.

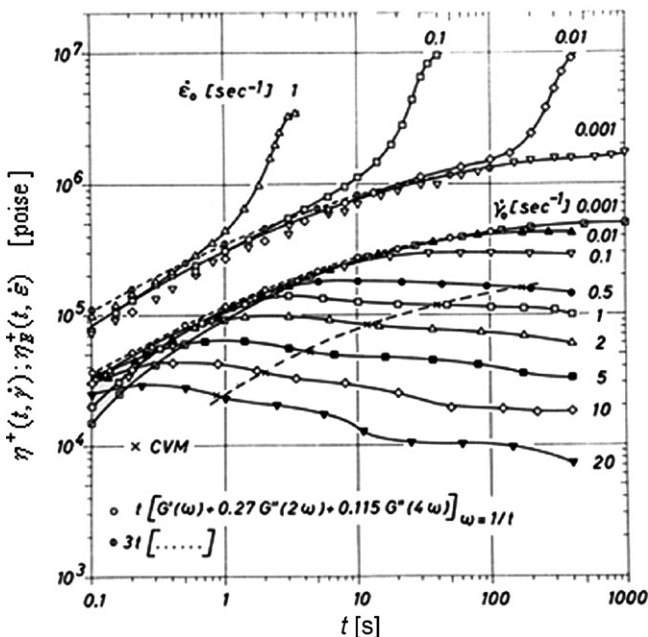


Figure 11.17 Uniaxial extensional stress growth coefficient $\eta_E^+(t, \dot{\varepsilon})$ (upper data sets) and shear stress growth coefficient $\eta(t, \dot{\gamma})$ (lower data sets) as functions of time after start-up of steady uniaxial extension at various extension rates $\dot{\varepsilon}$ and after start-up of steady shear at various shear rates $\dot{\gamma}$ for LDPE—IUPAC A at 150 °C; From Meissner [114].

11.5.1 The Pom-Pom Model

McLeish and Larson [113] developed a nonlinear viscoelastic theory for an idealized branched polymer with multiple branches but only two branch points. This molecular structure, called the *pom-pom*, is a generalization of the H polymer in that each of the two branch points of the pom-pom is permitted to have an arbitrary number of branches, q ; see Fig. 9.4. In its simplest form, the pom-pom model contains two basic time constants: the backbone reptation time τ_b , and the backbone stretch time τ_s . McLeish and Larson [113] provide equations for deriving these two times, and the arm relaxation time τ_a from the molecular structure of an idealized pom-pom molecule. However, since the pom-pom model is more commonly used as a multi-mode model to fit experimental data (see Section 11.5.3 below) the relaxation times of the pom-pom model are usually treated as fitting parameters.

We expect that $\tau_s < \tau_b$. If the strain rate is greater than $1/\tau_b$ but less than $1/\tau_s$, the backbones will become oriented by the flow, but not stretched. If, however, the strain rate is greater than $1/\tau_s$, the backbone can be stretched by the flow.

The equations of the original pom-pom model were given in both integral and an approximate differential form [113]. The differential form is the one more commonly used in flow computations, and is:

$$\dot{\mathbf{A}} - \boldsymbol{\kappa} \cdot \mathbf{A} - \mathbf{A} \cdot \boldsymbol{\kappa}^T = -\frac{1}{\tau_b} (\mathbf{A} - \boldsymbol{\delta}) \quad (11.30)$$

$$\mathbf{S} = \frac{\mathbf{A}}{\text{tr}(\mathbf{A})} \quad (11.31)$$

$$\dot{\lambda} = \lambda \boldsymbol{\kappa} : \mathbf{S} - \frac{1}{\tau_s} (\lambda - 1) \quad \text{for } \lambda < q \quad (11.32)$$

$$\sigma = 3 G \lambda^2 \mathbf{S} \quad (11.33)$$

Equations 11.30 and 11.31 give the differential equation for the orientation tensor \mathbf{S} via the auxiliary tensor \mathbf{A} . These are easy to solve and give almost the same result as the integral model, except that the differential approximation predicts a zero second normal stress difference in shearing flows. Hawke et al. [30] recently noted a drawback with Eqs. 11.30 and 11.31 which becomes apparent when studying stress relaxation after steady extensional flow. In such cases the trace of the auxiliary tensor \mathbf{A} grows very large, resulting in an unphysical increase in the effective orientation relaxation time for the tensor \mathbf{S} . Hawke et al. [30] propose that the orientation equation should be replaced by an equation equivalent to Eq. 11.9 for the DEMG model, i.e.

$$\overset{\nabla}{\mathbf{S}} = -2 (\boldsymbol{\kappa} : \mathbf{S}) \mathbf{S} - \frac{1}{\lambda^2 \tau_b} \left(\mathbf{S} - \frac{\boldsymbol{\delta}}{3} \right) \quad (11.34)$$

This modification removes the unphysical increase in relaxation time, and illustrates the strong similarity between the pom-pom model and the Doi-Edwards or DEMG theory. We note that McLeish and Larson [113] considered an equation very similar to Eq. 11.34, but rejected it because of unphysical shear thickening at high flow rates. As discussed above in Section 11.3.2, the factor of λ^2 multiplying the orientation relaxation time τ_b avoids this shear thickening.

Equation 11.32 is the stretch equation. It is also similar to its counterpart in the DEMG theory; see Eq. 11.10. The main difference in the theory for the pom-pom is that the stretch λ is limited to be equal to or less than q , the number of arms on each end of the backbone. If the stretch attains the value q , then the chain tension along the backbone tube equals the sum of the tensions in the pom-pom arms. At this point it becomes possible for *branch point withdrawal* to occur, i.e., for the arms to be pulled into the backbone tube. Therefore, q is the maximum value that the backbone stretch can obtain. In the terminology of the pom-pom model, q is called

the priority; for a more general definition of the priority see Section 11.6.1. Since the backbone stretch cannot exceed the value q , we have dropped the nonlinear spring force coefficient $k_s(\lambda)$ (present in Eq. 11.10) from Eq. 11.32.

Finally, Eq. 11.33 is the equation for the stress tensor σ . In general the modulus G for the model does not equal the plateau modulus, G_N^0 , because the pom-pom backbones are diluted by the faster relaxing arms, and (in general) by other chains. The original model [113] included an additional contribution from portions of arms pulled into the backbone tube, but this can usually be neglected and is omitted in the most common multi-mode application of the model (Section 11.5.3 below). The above equations for the pom-pom model also neglect the effects of convective constraint release (CCR). For long-chain branched polymers, CCR has so far been considered only for the relatively simple case of star polymers [115].

Figure 11.18 shows the predicted extensional and shear stress growth coefficients after start-up of uniaxial extensional flow and shear flow for the pom-pom model. Notice that at each extension rate, the viscosity increases with time to a plateau value, which at low extension rates, $\dot{\varepsilon} < 1/\tau_b$, is three times the zero-shear viscosity. At higher extension rates, $1/\tau_b < \dot{\varepsilon} < 1/\tau_s$, chain orientation occurs, but no chain stretch. Hence, in this intermediate regime, extension thinning occurs, and the viscosity lies below the linear viscoelastic limit (although only slightly below it in Fig. 11.18).

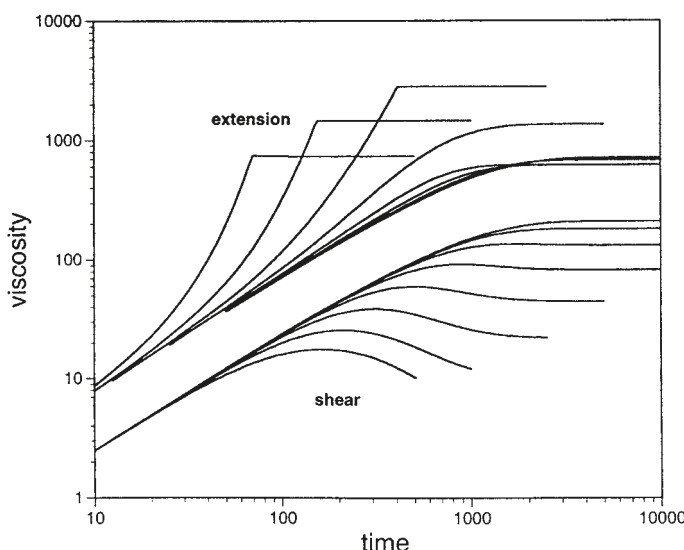


Figure 11.18 Stress growth coefficients in extension $\eta_E^+(t, \dot{\varepsilon})$ and in shear $\eta(t, \dot{\gamma})$ as functions of time at various strain rates as predicted by the pom-pom model with $q = 5$ branches per branch point. When made dimensionless using the backbone relaxation time, these rates, $\dot{\varepsilon} \tau_b(0)$ or $\dot{\gamma} \tau_b(0)$, are 0.27, 0.54, 1.1, 2.25, 4.5, 9, 18, and 36. From McLeish and Larson [113].

At still higher strain rates, $\dot{\epsilon} > 1/\tau_s$, strain hardening and extension thickening occur due to chain stretching, and the viscosity rises above the linear viscoelastic limit. Figure 11.18 shows that the pom-pom model predicts both thickening in extension and thinning in shear. Notice that these predictions in Fig. 11.18 are qualitatively similar to the experimental data for LDPE in Fig. 11.17.

In the pom-pom model, for $\dot{\epsilon} > 1/\tau_s$, the plateau value of the uniaxial stress growth coefficient, which is the extensional viscosity, is dictated by the inequality in Eq. 11.32. This inequality has no counterpart in the DEMG theory, where chain stretching at $\dot{\epsilon} > 1/\tau_s$ is only halted when the chains become fully extended. In the pom-pom model, however, once a backbone becomes stretched enough that the stretch λ reaches the value q (the number of arms on each end of the backbone), the tension in the backbone is high enough to pull the arms into the tube of the backbone. This keeps the backbone stretch from exceeding the value q . Thus, the greater the number of arms, q , the greater the degree of stretch possible before the arms are pulled into the backbone tube, and the greater the tension that the backbone can support. Hence, as q increases, there is an increase in the degree of strain hardening attained; see Fig. 11.19.

Notice in Fig. 11.18 that as the dimensionless strain rate $\dot{\epsilon} \tau_s$ increases above unity, the viscosity plateau decreases. This is because the stress has reached a saturation value set by the backbone tension required to pull the arms into the backbone tube.

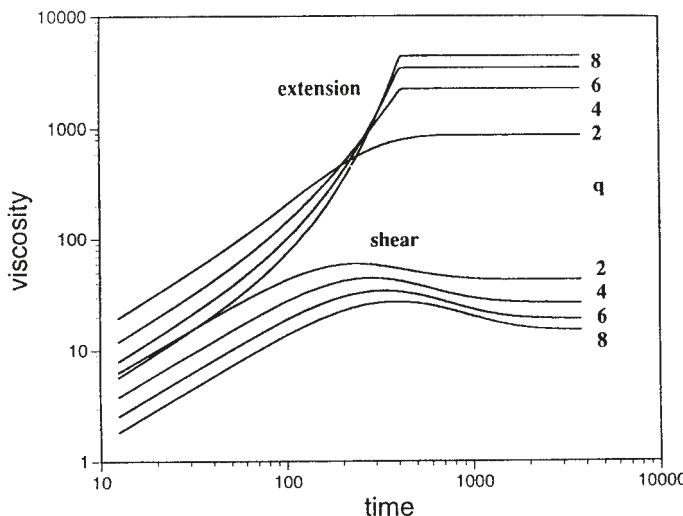


Figure 11.19 Stress growth coefficients in extension $\eta_E^+(t, \dot{\epsilon})$ and shear $\eta^+(t, \dot{\gamma})$ as functions of time after start-up of steady flow for pom-pom molecules with various numbers of arms q per branch point. The stress at early times gets lower with increasing number of arms because these computations assume dilution of the modulus G as arm number increases. From McLeish and Larson [113].

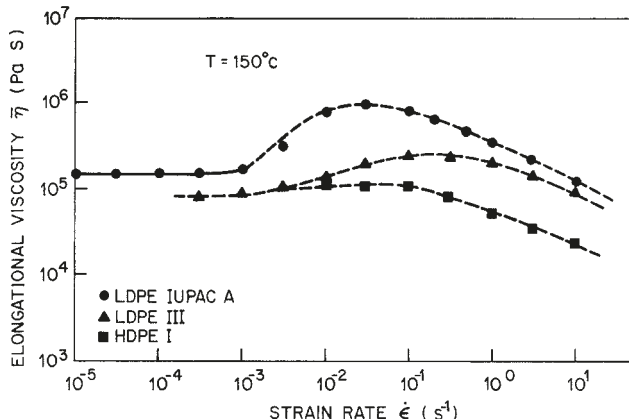


Figure 11.20 Extensional viscosity $\eta_E^+(\dot{\epsilon})$ for three polyethylene melts at 150 °C. The squares are for a high-density polyethylene (HDPE I: $M_w = 152,000$ and $M_w/M_n = 13.8$) that is believed to lack long-chain branching, while the other two samples (LDPE III: $M_w = 256,000$ and $M_w/M_n = 10.5$, and LDPE IUPAC A: $M_w = 472,000$ and $M_w/M_n = 24.9$) contain long-chain branches. From Laun [96].

Thus, as the strain rate is increased beyond this point, since the stress is constant, the steady-state viscosity decreases, since the viscosity is stress divided by strain rate. A local maximum in the extensional viscosity as a function of strain rate is indeed commonly observed for long-chain-branched polyethylenes; see Fig. 11.20.

An additional experimental indication that arms can be pulled into the backbone tube is shown in the shear damping function plotted in Fig. 11.21 for H polymers [116]. This damping function shows that the H polymer is less strain softening than linear polymers up to a strain of about 4 ($\log(\text{strain}) = 0.6$); above this strain, the damping function of the H polymer bends over and follows a curve similar to that of linear polymers. Similar data for pom-pom molecules have been reported by Archer and Juliani [117]. This suggests that at strains below the critical one, the backbone stretches, but that above a critical strain of around 4, the backbone ceases to stretch any further, because rather than stretch, the backbone pulls the arms into the backbone tube. (For star molecules, as noted earlier, the damping function is virtually identical to that of a linear molecule over the whole range of strain [92, 93].) Nevertheless, these experiments are tricky to do and the results may not be absolutely conclusive.

Thus, one of the differences between the predictions of the pom-pom model and the DEMG model for linear molecules is the inequality in Eq. 11.32. In steady uniaxial extension, this criterion produces a saturation value of the stress and a local *maximum* in the extensional viscosity, while in the DEMG model, the stress has no saturation value. (If finite extensibility is included in the DEMG model, then there is a saturation in viscosity, but no viscosity maximum.) Experimental data of McLeish

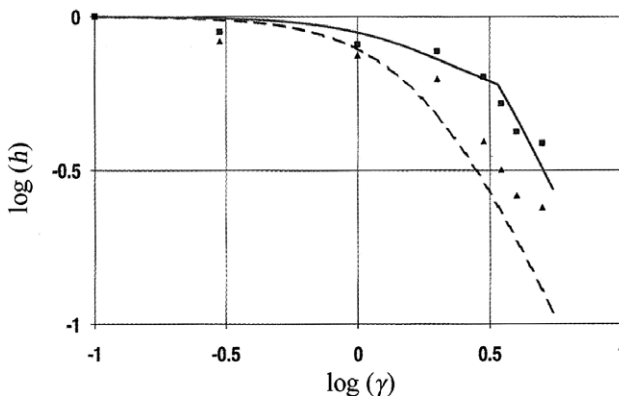


Figure 11.21 The damping function at early time ($1s \ll \tau_s$; squares) and at late time ($673s \gg \tau_s$; triangles) obtained from step shear experiments for a polyisoprene H polymer with arm and backbone molecular weights of $M_a = 20,000$; $M_b = 111,000$. The solid line is the prediction of the theory of McLeish et al. [116] for the early-time damping function, while the dashed line is the prediction of that theory for the late-time damping function; the latter equals the Doi-Edwards damping function for linear polymers. From McLeish et al. [116].

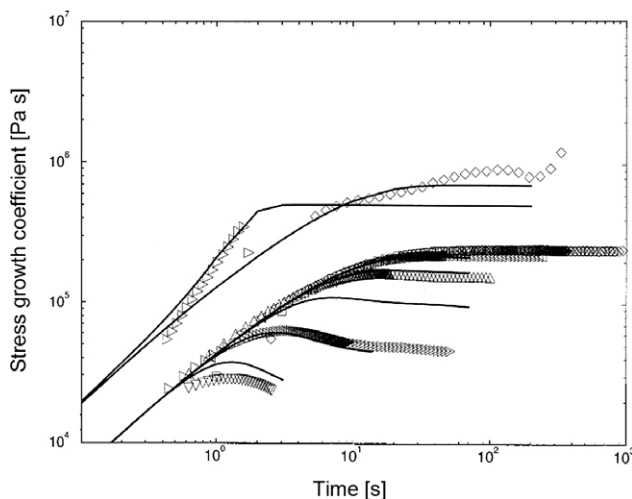


Figure 11.22 Comparison of theory (lines) and experiment (symbols) for stress growth coefficients in start-up of steady shear (lower curves) and start-up of steady extension (upper curves) for a polyisoprene H polymer with $M_a = 20,000$; $M_b = 111,000$. The extension rates are 0.03 and 1 s^{-1} , while the shear rates are $0.01, 0.03, 0.1, 0.3, 1$, and 3 s^{-1} . From McLeish et al. [116].

et al. [116] for a melt of polyisoprene H-molecules indicate the predicted decrease in extensional viscosity at high extension rate; see Fig. 11.22. Figure 11.22 also compares the predictions of a refined version of the pom-pom model by McLeish et al. [116] with these data for start-up of steady uniaxial extension as well as data

for start-up of steady shear. The theory shows good agreement with these data, although some adjustments had to be made to parameter values based on the linear viscoelastic data for this H polymer. Again, such experiments are difficult for model polymers which often have stronger instabilities and greater tendency to rupture under strain.

Although the pom-pom equations and DEMG models are very similar in structure, a practical difference between linear and branched polymers of similar molecular weight is the values of the relaxation times. For linear polymers, the stretch relaxation time τ_s is proportional to the square of the molecular weight of the molecule, while for branched polymers, τ_s depends exponentially on the molecular weight of the arms. This means that it is much easier to obtain a long stretch relaxation time for a long-chain-branched polymer with multiple branch points per molecule than for a linear polymer of the same chemical type and same overall molecular weight. The lack of chain stretch for many linear melts is manifested in extensional flow studies by the relatively modest strain hardening observed, for example in the data for polystyrene and HDPE in Figs. 11.15 and 11.16. We noted, however, in Section 11.4 that even a small amount of high-molecular-weight polymer that is able to stretch in a processing flow can confer strain hardening on a melt (see Fig. 11.13) and therefore aid in processing. The relative advantages of using long chain branching versus high-molecular-weight tails in the molecular weight distribution to control polymer processing behavior seem not to have been very thoroughly explored, at least in the published literature.

11.5.2 Revisions to the Pom-Pom Model

While the pom-pom model presented in the last section makes qualitatively correct predictions of the nonlinear rheology of branched polymer melts, it has quantitative deficiencies that have been addressed. Some important revisions of the pom-pom model are described below.

11.5.2.1 Drag-Strain Coupling

Blackwell et al. [118] noted that the pom-pom equations predict an abrupt cessation of backbone stretching when the stretch λ reaches the value q , the number of arms on each end of the backbone (Eq. 11.32). This abrupt transition produces sudden changes in the slopes of curves of the extensional stress growth coefficient versus time that are not found in experimental data. This problem is fixed by including a smoothing term in Eq. 11.32, such as:

$$\dot{\lambda} = \lambda \boldsymbol{\kappa} : \mathbf{S} - \frac{1}{\tau_s} (\lambda - 1) e^{\nu^*(\lambda-1)} \quad (11.35)$$

where the exponential term accelerates relaxation of stretch when the stretch λ becomes large, thus smoothing the approach to maximum stretch. This term can be justified by considering in more detail the drag on the branch point, and how its effective value depends on the stretch in the backbone [118]. It has been found that setting $\nu^* = 2/(q-1)$ gives smooth fits to experimental data. Sometimes the inclusion of drag strain coupling is accompanied by dropping the condition $\lambda \leq q$, as is done in the “extended pom-pom” model described in Verbeeten et al. [119], and in Section 11.5.2.3 below. This avoids some computational difficulties which arise in complex flow simulations when strictly enforcing the $\lambda \leq q$ condition.

11.5.2.2 Correction for Reversing Flows

For highly nonlinear flows in which the stretch becomes saturated at the maximum value q , and then a reversal occurs in the direction of deformation, the backbone stretch λ predicted by the pom-pom equations can become less than unity. In this case, Lee et al. [120] argue that relaxation of the shortened tube back to its equilibrium length will create new, randomly oriented tube segments for the backbone, and therefore accelerate the orientational relaxation of the backbone. Lee et al. accounted for this by replacing the time constant τ_b in the pom-pom equations by a modified backbone reorientation time given by

$$\frac{1}{\tau_b^*} = \begin{cases} \frac{1}{\tau_b} & \text{for } 1 \leq \lambda \leq q \\ \frac{1}{\tau_b} + \frac{\dot{\lambda}}{\lambda} - \boldsymbol{\kappa} : \boldsymbol{S} & \text{for } \lambda < 1 \end{cases} \quad (11.36)$$

11.5.2.3 Second Normal Stress Difference and Other Corrections: The Extended Pom-Pom Model

Verbeeten et al. [119], noting that the pom-pom model predicts a zero second normal stress difference and suffers discontinuities in some stress predictions, as well as other problems associated with the differential form, suggested the following revised pom-pom equation set, which they call the “extended pom-pom model”:

$$\nabla \boldsymbol{\Sigma} + 2 \boldsymbol{\kappa} : \boldsymbol{S} + \frac{1}{\tau_b \lambda^2} \left[3 \alpha \lambda^4 \boldsymbol{S} \cdot \boldsymbol{S} + (1 - \alpha - 3 \lambda^4) \boldsymbol{S} : \boldsymbol{S} \right] \boldsymbol{S} - \frac{(1-\alpha)}{3} \boldsymbol{\delta} = 0 \quad (11.37)$$

$$\dot{\lambda} = \lambda \boldsymbol{\kappa} : \boldsymbol{S} - \frac{1}{\tau_s} (\lambda - 1), \quad \tau_s = \tau_{s,0} e^{-\nu^*(\lambda-1)}, \quad \nu = \frac{2}{q} \quad (11.38)$$

$$\boldsymbol{\sigma} = G_N^0 (3 \lambda^2 \boldsymbol{S} - \boldsymbol{\delta}) \quad (11.39)$$

The constant α , when non-zero, introduces a non-zero second normal stress difference. Verbeeten et al. have also shown how to combine all three of the above equations into a single equation for the stress tensor.

11.5.2.4 Stress Overshoots, Accelerated Relaxation, and Entanglement Stripping

As noted above, long-chain-branched polymer melts sometimes show an overshoot in extensional stress during start-up of steady elongation, as has been seen by Hassager's group using a filament-stretching rheometer [30, 108–110]. This group also examined stress relaxation after steady flow both before and after the stress overshoot, finding that melts taken past the overshoot exhibited a greatly accelerated rate of stress relaxation. Neither of these features are anticipated in the original pom-pom model. An *ad hoc* modification to the pom-pom model was proposed by Hoyle et al. [110] by increasing the rate of stretch relaxation with orientation and flow. However, since this extra relaxation is switched off when the flow stops it cannot describe the accelerated stretch relaxation.

A possible explanation of the phenomenon has recently been proposed by Hawke et al. [30], who note that entanglement stripping, i.e., the reduction in number of entanglements in strong flow described above in Section 11.3.8 for linear melts, has the potential for very strong effects in branched polymer melts. This is because (i) entanglement stripping would have a sudden onset at the point of branch point withdrawal, and (ii) it could lead to enormous acceleration of relaxation rates, due to the exponential dependence of relaxation times on entanglement number in branched polymers.

Based on this insight, Hawke et al. [30] proposed a modified version of the pom-pom model, introducing an extra dynamical variable to account for the reduction in the number of entanglements following branch point withdrawal, resulting in both a decrease in the stress level and exponential acceleration of relaxation rates. They were able to use this model to describe the data of Hassager and co-workers, reproducing both the stress overshoots and stress relaxation after steady flow, as shown in Fig. 11.24 below.

While this proposal of entanglement stripping in branched polymers appears to be a candidate explanation (both qualitatively and in quantitative modeling) for the observations of the Hassager group, the mechanism cannot easily be confirmed using experiments on industrial melts: it remains still to be tested either by simulation, or by independent experiments on model polymers.

11.5.3 Empirical Multi-Mode Pom-Pom Equations for Commercial Melts

The branching structure of commercial branched polymer melts is vastly more complex than that of a simple pom-pom, and so the pom-pom model described above is unable to make quantitative predictions of the rheology of such melts. Inkson et al. [121], however, have shown that a phenomenological multi-mode version of the pom-pom equations is able to fit both the nonlinear transient extensional and shear rheology of IUPAC A, a commercial LDPE with long-chain branching. Multiple modes are introduced by writing the stress tensor as the sum of a series of partial stresses:

$$\boldsymbol{\sigma} = \sum_i \boldsymbol{\sigma}_i \quad (11.40)$$

where each $\boldsymbol{\sigma}_i$ is the contribution to the stress from a single mode. The stress from mode i is obtained by solving a set of pom-pom equations for that mode. That is, for mode i , we write down a set of equations analogous to Eqs. 11.30 through 11.32 (or the equivalent equations after modifications introduced in the previous section) but with the parameters τ_b , τ_s , and q subscripted with mode index i , and with the orientation tensor \mathbf{S} , tensor A , and stretch λ subscripted as well:

$$\dot{\mathbf{A}}_i - \boldsymbol{\kappa} \cdot \mathbf{A}_i - \mathbf{A}_i \cdot \boldsymbol{\kappa}^T = -\frac{1}{\tau_{b,i}} (\mathbf{A}_i - \boldsymbol{\delta}) \quad (11.41)$$

$$\mathbf{S}_i = \frac{\mathbf{A}_i}{\text{tr}(\mathbf{A}_i)} \quad (11.42)$$

$$\dot{\lambda}_i = \lambda_i \boldsymbol{\kappa} : \mathbf{S}_i - \frac{1}{\tau_{s,i}} (\lambda_i - 1) e^{\nu^*(\lambda_i - 1)} \quad (11.43)$$

$$\boldsymbol{\sigma}_i = G_i \lambda_i^2(t) \mathbf{S}_i \quad (11.44)$$

In the above, we have used the differential approximation for the tensor \mathbf{S}_i , and have used the “drag-strain coupling” correction of Blackwell et al., so that the backbone relaxation times $\tau_{b,i}$ are constants. We have discussed the use of multi-mode equations earlier, for example to account for the effect of polydispersity in Section 11.4 where each mode could be considered to account for a different component of the molecular weight distribution. However, in the multi-mode pom-pom equation, as applied to commercial polymer melts, each “mode” does not necessarily correspond to a component of the molecular weight distribution, but to a “mode” of backbone relaxation. For example, for a “comb”-type polymer containing many long side branches, portions of the backbone near the interior are very slow to relax, and can be very highly stretched, since there are many arms on each side of the backbone that can help sustain very high tension. These parts of the molecule ought to be characterized by high values of the parameters $\tau_{b,i}$ and $\tau_{s,i}$ as well as a high value

of q_i . On the other hand, portions near the end of the backbone can relax faster, and hence are characterized by smaller values of $\tau_{b,i}$ and $\tau_{s,i}$ and, in addition, these backbone portions cannot sustain a high level of stretch, since this part of the backbone can relieve its tension by drawing in the few arms on the side nearest the end of the backbone; hence such backbone segments are characterized by small values of q_i . Accounting for the contribution of each portion of the backbone to the stress by using a separate mode for each cannot be done with absolute rigor for commercial branched polymers, both because of the complexity of the molecular weight and branching distributions for these melts and because of uncertainties about the branching distributions of commercial polymers. We will describe some attempts to make such predictions below, in Section 11.6.2. In the present section we are considering instead fits to commercial nonlinear data which can be made by empirically adjusting the parameters of the multi-mode pom-pom model [121, 122].

For each mode of the model, there are four fitting parameters: $\tau_{b,i}$, $\tau_{s,i}$, q_i , and G_i . The two parameter sets $\{\tau_{b,i}\}$ and $\{G_i\}$ control the linear viscoelastic properties of the melt (e.g., G' and G''), and all the $\tau_{b,i}$ and G_i values can therefore be obtained empirically by fitting the experimental linear viscoelastic data for a given melt—see Section 4.4 for a description of this procedure. The remaining two parameter sets $\{\tau_{s,i}\}$ and $\{q_i\}$ are nonlinear parameters that were obtained by Inkson et al. for IUPAC A by fitting the data for the stress growth coefficient in start-up of uniaxial extensional flow for multiple extension rates. This method not only gives an excellent fit to the extensional data (see Fig. 11.23 (top)) but the predictions for shear stress in start-up of steady shear flow (using the same parameters determined in extensional flow) are in good agreement with the shear data even though these data were not used in the fitting procedure; see Fig. 11.23 (bottom). Doerpinghaus and Baird [123] showed that not only can the multi-mode pom-pom model describe extensional and shear data for LDPE, but it can also describe similar data for sparsely branched metallocene-catalyzed polyethylenes. Furthermore, they showed that the ratio $\tau_{b,i}/\tau_{s,i}$ obtained by fitting extensional data decreases with increasing branching, as expected, since for a given polymer molecular weight, more highly branched molecules will have a smaller innermost backbone segment, and hence a smaller ratio $\tau_{b,i}/\tau_{s,i}$.

Thus the parameters obtained by this method of fitting seem to reflect to some extent the branching characteristics of commercial polymers, although the fitted values of q_i obtained for lightly branched polymers seem too high to be realistic [123].

Following the same multi-mode strategy, but using their pom-pom model modified for stress overshoots (see above, Section 11.5.2.4), Hawke et al. [30] were able to fit a rich dataset for a commercial LDPE, obtained from the filament stretching rheometer, as shown in Fig. 11.24. These data include overshoots in stress during steady elongational flow. They also include substantial acceleration in stress relaxation upon flow cessation, when the material is taken beyond the stress overshoot.

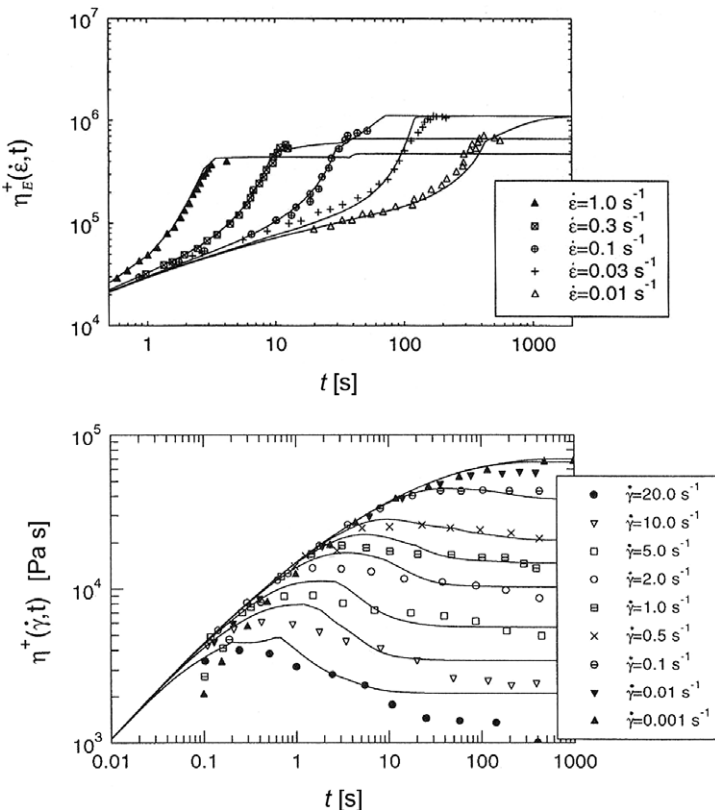


Figure 11.23 Top: Extensional stress growth coefficient data $\eta_E^+(t, \dot{\varepsilon})$ of IUPAC-A LDPE (Laun and Münstedt [124]) fitted to a nine-mode pom-pom model by adjustment of the values of $\tau_{s,i}$ and q_i . Bottom: Shear stress growth coefficient for the same melt, with predictions of the same nine-mode model with the same parameter values. From Inkson et al. [121].

This acceleration is sufficient to produce a “crossover” in the stress relaxation curves, whereby a melt stretched for longer (beyond the stress overshoot) relaxes stress sooner than an identical melt in which the stress relaxation was initiated earlier. As can be seen in Fig. 11.24, by treating the parameters in their model as fitting parameters, Hawke et al. were able to obtain a reasonable quantitative match to the data, and certainly a qualitative reproduction of the main features of the response during both flow and relaxation.

Evidently it is not a good idea to draw firm conclusions about the fitted values of parameters in a multi-mode model. But the main reason for fitting the multi-mode pom-pom model to extensional data for commercial branched polymers is not to characterize the branching characteristics of the melt, but rather to obtain a constitutive equation that can be used in numerical simulations of viscoelastic flows

of commercial polymers. Various versions of the pom-pom model do, in fact, give remarkably good predictions of the important features of multi-dimensional flows of branched polymers, including die entry and exit flows, flow past cylinders, and other flows similar to those that occur in polymer processing [110, 120, 125, 126]. Hoyle et al. [110] were able to show that stress overshoots obtained in the filament stretching rheometer, similar to those in Fig. 11.24, could be associated with the observation of a characteristic cusp shape in the birefringence pattern in a cross-slot flow. Thus, while *a priori*, molecular-level predictions of the nonlinear rheology of commercial branched polymers are still in their infancy, practical constitutive equations that include the effects of long-chain branching seem to be available.

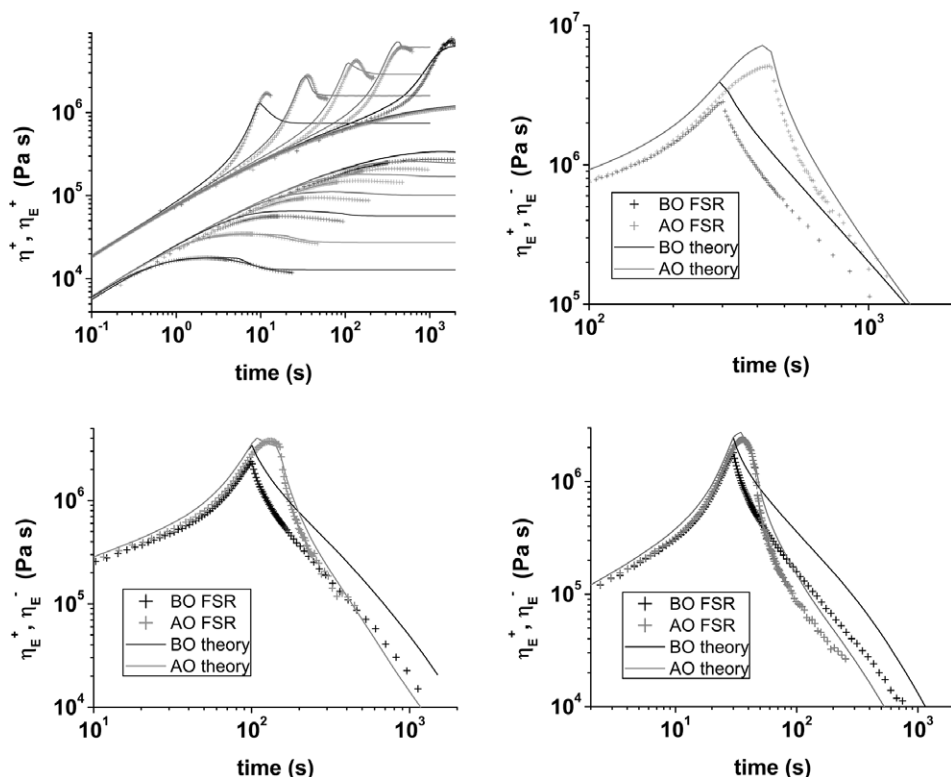


Figure 11.24 Comparison of a multi-mode version of the model of Hawke et al. [30] (lines) with the FSR data (symbols) for extension and shear data, for the LDPE DOW 150 R sample ($M_w = 242 \text{ kg/mol}$, $M_n = 22 \text{ kg/mol}$). Top left: steady shear (rates of $0.003, 0.01, 0.03, 0.1, 0.3, 1, 3 \text{ s}^{-1}$) and steady extension (rates of $0.003, 0.01, 0.03, 0.1, 0.3 \text{ s}^{-1}$). Top right: Relaxation following extensional flow at rate 0.01 s^{-1} . Bottom left: Relaxation following extensional flow at rate 0.03 s^{-1} . Bottom right: Relaxation following extensional flow at rate 0.1 s^{-1} . Data is shown for relaxation both before the overshoot (BO) and after the overshoot (AO). For each rate, the flow has been stopped at Hencky strains of 3 and 4.5 for the BO and AO case, respectively. From Hawke et al. [30].

Finally, we note that if one abandons any effort to model the time constants of the polymer, and simply uses the experimental linear viscoelastic data directly as input, there are nonlinear constitutive equations that can be used to predict the nonlinear rheology of linear and long-chain branched melts. For example, it is possible to use the discrete relaxation spectrum obtained from fitting to experimental data to define the memory function in an integral equation such as Eq. 10.6 or Eq. 10.11. The equations of Wagner and coworkers [127] are notable examples which have been successfully used to model nonlinear rheology of long chain branched polymer melts.

■ 11.6 Towards Prediction of Nonlinear Viscoelasticity from Molecular Parameters

While model polymers have proved a useful tool in understanding much of the physics of entangled polymer rheology, industrial resins are far from being model polymers—they are typically polydisperse both in strand length and branching topology. Attempts to understand the viscoelasticity of such resins from a fundamental, molecular, viewpoint, need to undertake two significant tasks, as indicated in a recent review [128]: (i) determining, as accurately as possible, the distribution of branched molecular shapes and molecular weights, and (ii) inferring the viscoelastic response from the molecular shapes, based on the concepts learnt from model polymers. Neither task is straightforward: the current state of the art, as described below, is that we have only an approximate understanding of each. Nevertheless, even with this limited understanding it appears possible to make predictions that are in reasonable agreement with viscoelastic data. We focus here on methods for predicting rheology, rather than the molecular distribution, which was the subject of Chapter 3.

11.6.1 Seniority and Priority

One might hope to capture the essential features of branched polymer relaxation in an approximate way, expecting that averaging over the extreme dispersity of most resins will mask inaccuracies in the approximate approach. To describe linear rheology, the main feature of branched polymer relaxation, as described in Chapter 9 and especially Section 9.2.1, is that branched polymers relax from the outside segments first. To capture this feature, Rubinstein et al. [129] introduced a quantity which they called *seniority*, initially as a means of describing relaxation of entangled polymers close to the classical gel point. The *seniority* of a chain segment within a given

branched molecule may be evaluated by counting the number of strands (inclusive of the current strand) to the furthest free end in each chain direction. The seniority is then the smaller of the two values obtained. A branched polymer chain, decorated with the seniority values of the strands, is shown in Fig. 11.25. The idea is that the outermost chain strands have seniority 1, and relax first. The next strands inwards have seniority 2, and relax next, and so on. Thus, it is anticipated that an approximate mapping from seniority to relaxation time of the chain strand may be possible, so that a description of the distribution of strand seniorities in the molecule allows prediction of the relaxation time distribution. Such a mapping would be exact for a regular structure such as a Cayley tree, but can only be approximate where there is polydispersity of strand length and branching structure. The seniority statistic has now, largely, been superseded by more accurate computational methods for evaluating the linear viscoelasticity of polydisperse branched resins, as described in Section 9.5.

For modeling nonlinear flow, the concept of *priority* introduced in Section 11.5.1 above for pom-pom molecules can be generalized to general branched structures in order to calculate the maximum stretch of a given chain strand (which determines the limit of extensional stress). This was first done by Bick and McLeish [130] for the classical gelation ensemble, and used to calculate the damping function for a melt of such polymers. Since each free end carries a strand tension of 1, and this tension is propagated through the branch points towards the interior of the molecule, the priority of a given strand is obtained by counting the number of free ends attached in each chain direction, and then taking the smaller of the two values. When the stretch of a given chain strand becomes larger than its *priority*, then the tension in that strand becomes larger than the maximum possible total tension from all the strands outside it, so the branch point at one end is able to withdraw into the tube. This is analogous to the branch point withdrawal process in the pom-pom model. Hence, the stretch in that strand cannot become larger than its priority. A branched polymer chain, decorated with the priority values of the strands, is shown in Fig. 11.25.

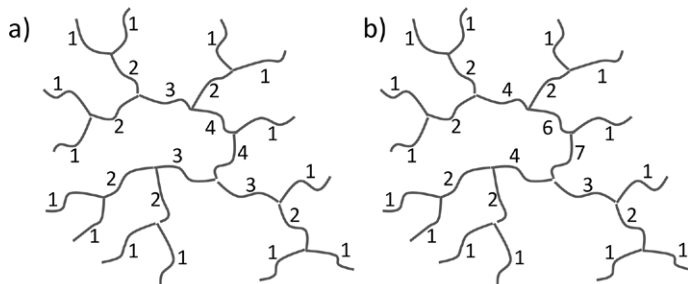


Figure 11.25 (a) Schematic branched polymer decorated with the “seniority” values of the polymer strands. (b) The same polymer decorated with the “priority” values. From Read [128].

The advantages of the seniority and priority measures are that they are simple to calculate for a given polymer molecule. It is also, in some instances, possible to obtain the statistical distribution for these quantities analytically, or via mathematical recursion relations. This was the approach taken in the original papers defining seniority [129] and priority [130] and also (based on the statistical treatment described in Section 3.9.2) in metallocene systems [131, 132].

Read and McLeish [131] identified a potential problem with the priority statistic: some sections of the molecules may relax much faster than the current flow timescale, and so are unable to transfer chain tension from the outside of the molecule towards the inside. Thus the maximum stretch (the “priority”) of a given segment should depend on the flow rate, and the priority as defined above gives an absolute maximum value of the stretch, applicable only at high flow rates. Read and McLeish suggested that, at lower flow rates, any chain sections relaxing faster than the flow timescale should be effectively “snipped” from the molecules when evaluating the priorities; the “snipped” priority values were typically much smaller. More recently, Read and co-workers [133, 134] have proposed an alternative scheme in which stretch relaxation times of different chain segments are used to determine whether they are able to transfer chain tension from the outside of a molecule towards the inside.

Read and McLeish [131] made the first, and perhaps only, attempt to use the seniority and priority statistics to make predictions of the nonlinear rheology for industrial polymer resins. Taking the statistical distribution of molecular shapes from constrained geometry metallocene catalysts (see Section 3.9.2) they predicted the joint statistical distribution of seniority and priority. They derived an approximate correspondence between seniority and relaxation time, and then (ambitiously) mapped their derived seniority and priority distribution onto a set of pom-pom modes, so making predictions of extensional viscosity as a function of their model parameters. No direct comparisons with experimental data were attempted, since the scheme was evidently far too approximate. Nevertheless, this work represented the first attempt at using tube theory to predict general nonlinear flow behavior on the basis of a quantitative description of branching structure for a class of industrial polymer resins, and pointed forward to the more recent work described in the next section.

11.6.2 Computational Prediction of Nonlinear Rheology for Polydisperse Branched Polymers

In Section 9.5 we described several computational algorithms, designed to predict the linear viscoelastic response of polydisperse branched polymers and industrial resins. A natural next step is the ambitious task of constructing computational schemes for prediction of nonlinear rheology. In principle, coupled tube-model equations, similar

to those derived by Blackwell et al. for the ideal Cayley tree architecture [135] (but most likely more complex), should be solved for every chain strand within a representative molecular distribution. Such an algorithm may be possible to construct, but no one has done it yet.

A simpler, and much more approximate, possibility was considered by Read et al. [133, 134]. Recognizing that the multi-mode pom-pom model is very successful at matching the rheology of branched polymers (once the nonlinear parameters have been determined by data-fitting to extensional rheology data, as described above in Section 11.5.3), they attempted to predict a numerical ensemble of pom-pom modes based upon the solution of the linear rheology within their BoB algorithm [136] (Section 9.5).

We recall, from Section 9.5, that the BoB algorithm (like all such computational schemes) operates by storing a representative set of polymer molecules in computer memory, and then solving tube model equations to determine the relaxation time of each chain strand within the stored polymer ensemble. The proposed method for nonlinear rheology prediction was to split the predicted linear relaxation spectrum into a set of Maxwell modes with different relaxation times, and then in turn to split each Maxwell mode into a distribution of pom-pom modes based upon the chain segments predicted to be relaxing stress at that timescale. Typically this resulted in thousands of pom-pom modes, due to the large dispersity in types of segment relaxing at a given time. For consistency with the linear rheology predictions, stress relaxation was noted to have two separate contributions, each with a corresponding set of pom-pom modes: stress relaxation by entanglement escape of strands, and stress relaxation by release of constraints on neighboring strands.

As indicated in Sections 11.5.1 and 11.5.3, a single pom-pom mode requires two nonlinear parameters: a stretch relaxation time and a maximum stretch (the *priority*, as described in Section 11.6.1 above). These two parameters must be determined for each strand in the numerical mixture of polymers stored in the computer. Read et al. found that there was sufficient information within the BoB algorithm to achieve this. The stretch relaxation time could straightforwardly be determined from one of the internal solution variables, related to updating the retraction potential as side arms relax [134].

The *priority* could be obtained based on the branched topological structure of the stored molecules. The priority of any chosen segment was proposed to depend on the applied flow rate and was calculated by propagating chain tension onto that segment from its connected free ends, i.e., tension is propagated from the outside of the molecule inwards. Here, Read et al. noted that only segments which stretch in the flow are capable of transferring tension: segments which do not stretch cannot transfer tension inwards from the chain ends. Since a segment can only stretch if the flow rate exceeds the inverse of its stretch relaxation time this gives a plausi-

ble criterion to decide which chain ends are counted when determining segment priorities (maximum stretch) at a given flow rate. More importantly, this criterion could be cast as a computational algorithm and automatically implemented for a large number of molecules. In general, the priority of a given segment is expected to increase with increasing flow rate, since more and more segments are able to stretch and transfer chain tension inwards.

Read et al. used their method to study a series of tubular reactor LDPE resins, characterized according to molecular weight distribution, and radius of gyration contraction factor (g-factor) as a function of elution volume in the gel permeation chromatogram. This latter quantity is a measure of branching density, because more highly branched molecules have smaller radius of gyration. The linear rheology of the resins was also measured, and for three of the resins the transient stress coefficient was measured in nonlinear shear and extension. The goal of the study was to use simulated molecular topologies to predict the rheology.

Read et al. did not have access to detailed reactor parameters or design with which to predict the shapes and sizes of the highly branched LDPE molecules. In any case, definitive prediction the molecular distribution remains a challenging topic for polymer reaction engineers [128]. Instead, Read et al. chose a simpler, more approximate approach. Recognizing that an ideal tubular reactor is equivalent to a batch reaction, they made use of a simple Monte Carlo scheme [137] to predict a representative set of molecular topologies, using a superposition of two, or three, batch reactions. Possible justifications for this approach include the fact that a tubular reactor is rarely an ideal batch reaction; there is a boundary layer which takes more time to travel through the tube, and there are usually multiple injection points for reagents. In the absence of detailed information about the industrial reactors, it was felt (or perhaps hoped) that using a superposition of batch modes (constrained by molecular weight distribution and g-factor) might give a reasonable representation of the mixture of molecules in the resins. There is scope for using a more detailed and accurate reactor model in conjunction with their methodology for predicting nonlinear rheology.

Read et al. found that, having matched the molecular weight and g-factor distribution of the resins, and using the same rheological parameters for all resins (entanglement time, entanglement molecular weight, plateau modulus), their BoB algorithm was able to make a reasonably close prediction of the linear rheology. So, for example, the terminal viscosity of each resin was predicted to within roughly a factor of two, accurate enough to rank the resins in order of increasing viscosity. Small adjustments to the reaction parameters (whilst maintaining the fit of the molecular weight and g-factor distribution) allowed the linear rheology of the resins to be accurately matched (see Fig. 11.26). In truth, it would be wholly unreasonable to expect a more accurate prediction than this. The relaxation time of chains in a branched polymer

melt depends exponentially on arm molecular weight, so even a small error in molecular shape, or in tube model parameters, can have large effects on the predicted linear viscoelasticity. In this sense, the rheology is far more sensitive than either molecular weight or g-factor to the molecular parameters.

Having matched the linear rheology, there were no further free parameters to adjust in their model, and so Read et al. used their approximate scheme (outlined above) to predict with reasonable accuracy the transient viscosity of the resins in start-up shear and extension, as illustrated in Fig. 11.26. The nonlinear rheology predictions in Fig. 11.26 are slightly different from the original article [133] due to a small error in the original code, as described in a follow-up paper [134]. Predictions were also made for a high-density polyethylene melt made using a constrained geometry metallocene catalyst [134], successfully capturing the fact that extension hardening was much smaller than for the LDPEs, but also underestimating the extent of the extension hardening.

Of course, these predictions were not perfect: for example, whilst the onset of extension hardening was well predicted, the final stress under extension was typically underestimated, especially at lower extension rates. This discrepancy could be blamed on a number of factors, such as incomplete knowledge of the molecular topology. There are also indications that their scheme for predicting flow-dependent priority—which was designed for the case of extreme polydispersity—fails to capture the maximum stretch in more regular, ideal polymer structures. A recent study of the comb topology [138] indicated that coupling between different sections of the backbone leads to a collective behavior which increases the maximum stretch across the whole backbone. Such coupling is not considered in the scheme of Read et al. and may be present in more irregular structures.

So, it should be wholly apparent that there are approximations made at each level of the scheme of Read et al. They used an approximate scheme for predicting molecular shapes, a now-debated methodology for prediction of linear rheology (see Sections 9.5 and 9.6) and an approximate parameter mapping onto a multi-mode pom-pom constitutive model. All this being noted, their predictions are (perhaps surprisingly) reasonable, though not perfect. In this sense, the work of Read et al. might simply provide a pragmatic and practical method for prediction of nonlinear rheology from reactor variables; it is an ambitious pointer as to what may be possible, rather than the final word on the topic.

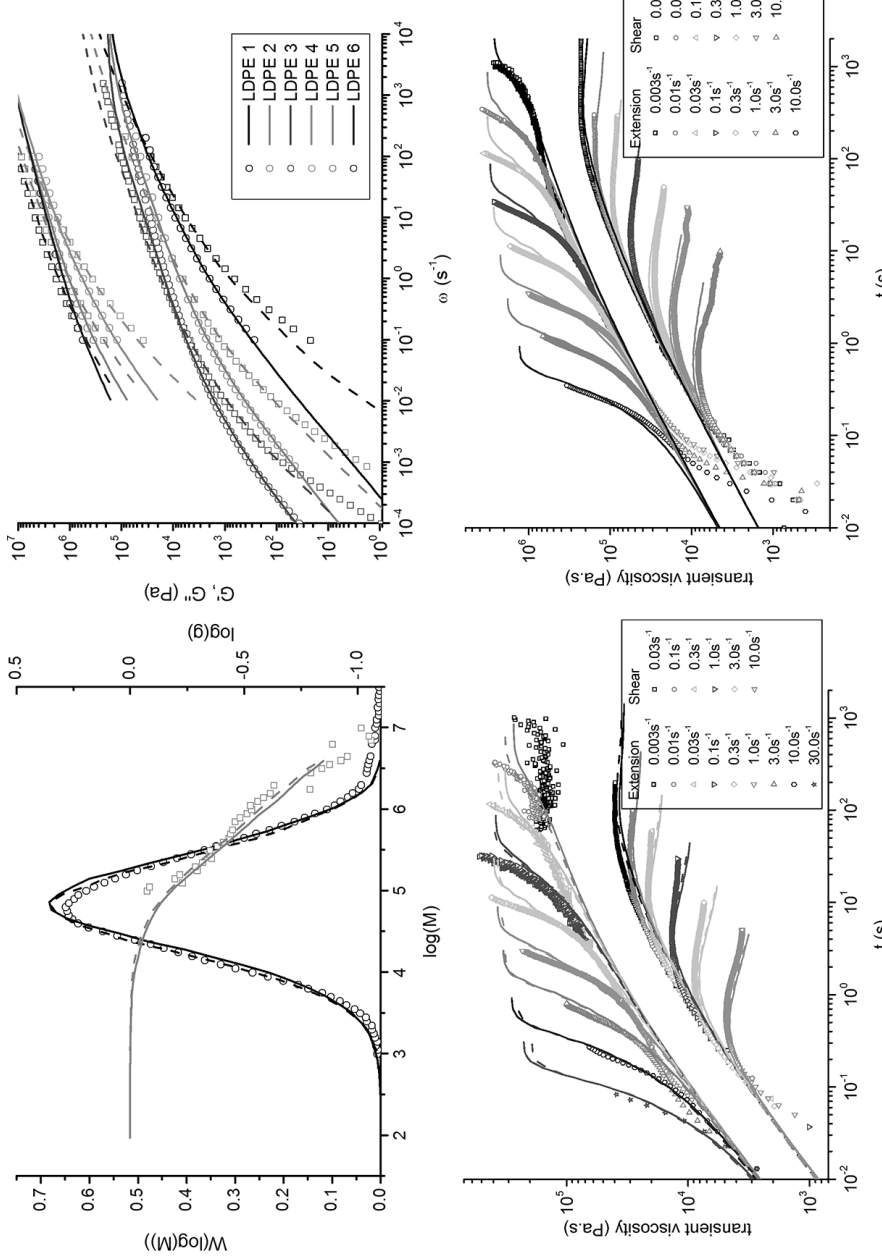


Figure 11.26 Top left: Matching the molecular weight distribution and radius of gyration g -factor for a tubular LDPE (LDPE2). Dashed and solid lines represent two different fits. Top right: Predictions of linear rheology for a series of six tubular LDPEs (using identical rheological parameters). Predictions of nonlinear rheology (start-up shear and extension at different rates) for [bottom left] LDPE2 and [bottom right] LDPE3. Data and theoretical predictions from ref. [133]. Nonlinear predictions corrected as described in ref. [134]. From Read et al. [128, 133].

■ 11.7 Summary

Nonlinear viscoelastic phenomena in the rheology of polymer melts and entangled solutions include shear thinning in shearing flows and extension thinning and thickening in extensional flows. “Thinning” means that the viscosity or stress growth coefficient falls below its low-strain-rate value, while “thickening,” or “strain hardening” means the reverse. For polymer melts, thinning is ubiquitous in shearing flows, while in extension either thinning or thickening can be obtained, depending on the extension rate and the molecular characteristics of the polymer, particularly the molecular weight distribution and most especially the presence of long-chain branches. The thinning or thickening characteristics of polymer melts are extremely important factors in the “processability” of a polymer, that is, the ease with which it is shaped into a useful product. Shear thinning is usually desirable since it implies faster flows and lower pressure drops in extrusion or injection molding than would be the case for a polymer with the same zero-shear viscosity but no shear thinning. In extension-dominated processing flows, such as fiber spinning or film blowing, extension thickening is usually desired, since it generally leads to more stable processing conditions and higher molecular orientation, and therefore stronger product, at least in the stretch direction.

Within the tube model, the behavior in the nonlinear regime is controlled by orientation and stretching of tube segments, which, in turn, are controlled by the reptation time $\tau_{d,i}$ and the stretch time $\tau_{s,i}$, where $\tau_{d,i}$ for each component i of the polydisperse melt is always as large or larger than the corresponding $\tau_{s,i}$ for that component. When the shear or extensional strain rate ($\dot{\gamma}$ or $\dot{\epsilon}$) exceeds $1/\tau_{d,i}$, tube segments for component i become highly oriented, and this contributes to thinning in either shear or extensional flow. When the extension rate exceeds $1/\tau_{s,i}$, the tube segments can stretch, leading to extension thickening or extensional strain hardening. Thus, for extensional flow, as the extension rate increases, one expects that for polymers without long side branches extension thinning will occur first, followed by extension thickening. This behavior (thinning followed by thickening) has been observed for both solutions and melts of linear polymers. However, the extent of extension thickening, and the increase of steady-state stress, appears not to be universal between polymer melts and solutions. This may be due to orientation induced changes in the effective monomeric friction. In shear flow, even at shear rates that lie above $1/\tau_{s,i}$ for many or all of the components of the melt, shear thickening is not observed, because shear flow rotates tube segments into orientations that resist stretching, even for shear rates high compared to $1/\tau_{s,i}$.

The simplest nonlinear tube model is the classical Doi-Edwards (DE) constitutive equation for linear polymers, which accounts for reptation and affine rotation of tube

segments. The Doi-Edwards equation predicts thinning in both shear and extension, because it accounts for orientation of tube segments, but it is unable to predict extension thickening because it neglects the stretching of tube segments. Inclusion of tube stretch leads to the Doi-Edwards-Marrucci-Grizzuti (DEMG) equation, which predicts extension thickening in fast extensional flows, and improves upon the predictions of the DE equation in transient shear. However, both the Doi-Edwards and DEMG models show excessive shear thinning at steady state in shearing flow, because both models neglect convective constraint release (CCR), which is the release of constraints caused by the sweeping away of the chains that define the tube enclosing a given “test” molecule. Convective constraint release, proposed by Marrucci and coworkers, is included in the Graham-Likhtman-and-McLeish-Milner (GLaMM), the Rolie-Poly, the Ianniruberto-Marrucci, and other tube models, and these models show a level of shear thinning that matches experimental data. The models also readily incorporate constraint release due to reptation and primitive path fluctuations. With these details included, they provide good agreement with transient stress data from start-up of both steady shear and extension. They also hold the possibility of capturing at least some of the flow instabilities, such as shear banding, that have been reported for polymeric liquids.

Predictions for polydisperse linear polymers must account for the complex interplay between constraint release from fast relaxing short polymers and both stretch and orientation relaxation of the longer chains that dominate the stress response. In the extreme case of a “binary” melt of long and short polymers, it has been shown both by experiments and theoretical modeling that this can lead to an enhancement in the stretch relaxation time of the long chains, so that extension thickening is observed at lower than expected rates. Incorporating such effects into a general model for polydisperse linear polymers remains an ongoing task.

The tube concept has also been used to develop theories for the nonlinear viscoelastic properties of branched polymers. Polymers with more than one branch point contain one or more backbone portions bounded by branch points at each end. Such backbone strands relax with great difficulty, and so are easy to stretch in flow fields that are at least partially extensional. The highly stretched backbones enhance the stress, leading to strain hardening in extensional flows, although in steady simple shear flows, branched polymers can be more shear thinning than ordinary linear polymers. Qualitatively, the effect of multiple branch points on the nonlinear rheology can be accounted for by the pom-pom model, which describes backbone orientation and stretch for monodisperse polymers that contains two branch points with multiple arms at each branch point. The pom-pom model gives estimates for both the backbone orientation time and backbone stretch time and predicts that the level of strain hardening is controlled by the number q of branches per branch point (the *priority*).

The pom-pom theory is relatively simple and has been applied with success to the prediction of experimental nonlinear shear and extensional stresses in flows of monodisperse H polymers. With appropriate modifications, the pom-pom model can capture second normal stress differences, and overshoots in stress during extension. The pom-pom model has been extended to a multi-mode form whose predictions can be fitted to data for commercial branched polymers by *ad hoc* adjustment of the model parameters. While the resulting multi-mode model is phenomenological, it does give very good fits to extensional and shear rheological data for commercial polymers, once the parameters are established using rheological data. More importantly, it has proven successful in predicting stresses in complex multidimensional flows like those that occur in polymer processing.

More recently, an attempt has been made to predict the nonlinear viscoelastic response of industrial resins from the distribution of their branched polymer structures. This has built on apparently successful computational algorithms for prediction of the linear viscoelasticity (Section 9.5) and has attempted a mapping from such algorithms onto a multi-mode pom-pom ensemble. Such methods contain many approximations. Often the distribution of branched structures is not accurately known (especially for commercial low-density polyethylenes). The method assumes decoupling between the different pom-pom modes, whereas in real polymers different segments are coupled together. Further, the physics of maximum stretch in branched polymers has not yet been fully established, so that there may be inaccuracies in assignment of parameter values to the pom-pom modes.

Given all these uncertainties, the predictions appear to be surprisingly good. This approximate methodology, or something like it, may turn out to be of practical use despite its limitations. Development of more precise theories for the nonlinear rheological properties of model polymers, such as pom-pom and comb-like branched polymers [138], and for mixtures of such molecules with linear and star polymers (thus addressing constraint release), may provide the necessary insights to allow improvement of the present methodology.

No doubt, there will continue to be rapid progress in the coming years in the development of theories for the nonlinear rheology of linear and long-chain-branched polymers.

■ References

- [1] Larson, R.G. *Constitutive Equations for Polymer Melts and Solutions* (1988) Butterworths, London
- [2] Larson, R.G. *The Structure and Rheology of Complex Fluids* (1999) Oxford University Press
- [3] Bird, R.B., Armstrong, R.C., Hassager, O. *Dynamics of Polymeric Liquids*. Vol. 1, 2nd ed. (1987) Wiley, New York
- [4] Tanner, R.I. *Engineering Rheology* (1985) Oxford University Press, New York
- [5] Dealy, J.M., Wang, J. *Melt Rheology and its Applications in the Plastics Industry* (2013) Springer, Dordrecht
- [6] Archer, L.A. Separability criteria for entangled polymer liquids. *J. Rheol.* (1999) 43, pp. 1555–1571
- [7] Sanchez-Reyes, J., Archer, L.A. Step shear dynamics of entangled polymer liquids. *Macromol.* (2002) 35, pp. 5194–5202
- [8] Inoue, T., Uematsu, T., Yamashita, Y., Osaki, K. Significance of the longest Rouse relaxation time in the stress relaxation process at large deformation of entangled polymer solutions. *Macromol.* (2002) 35, pp. 4718–4724
- [9] Marrucci, G. Dynamics of entanglements: A nonlinear model consistent with the Cox-Merz rule. *J. Non-Newtonian Fluid Mech.* (1996) 62, pp. 279–289
- [10] Graessley, W.W. Molecular entanglement theory of flow behavior in amorphous polymers. *J. Chem. Phys.* (1965) 43, pp. 2696–2703
- [11] Ianniruberto, G., Marrucci, G. Convective orientational renewal in entangled polymers. *J. Non-Newtonian Fluid Mech.* (2000) 95, pp. 363–374
- [12] Likhtman, A.E., Milner, S.T., McLeish, T.C.B. Microscopic theory for the fast flow of polymer melts. *Phys. Rev. Lett.* (2000) 85, pp. 4550–4553
- [13] Graham, R.S., Likhtman, A.E., Milner, S.T., McLeish, T.C.B. Microscopic theory of linear, entangled polymer chains under rapid deformation including chain stretch and convective constraint release. *J. Rheol.* (2003) 47, pp. 1171–1200
- [14] Sefiddashti, M.H.N., Edwards, B.J., Khomami, B. Individual chain dynamics of a polyethylene melt undergoing steady shear flow. *J. Rheol.* (2015) 59, pp. 119–153
- [15] Ianniruberto, G., Marrucci, G. Convective constraint release (CCR) revisited. *J. Rheol.* (2014) 58, pp. 89–102
- [16] Ianniruberto, G. Quantitative appraisal of a new CCR model for entangled linear polymers. *J. Rheol.* (2015) 59, pp. 211–235
- [17] Doi, M., Edwards, S.F. Dynamics of concentrated polymer systems. Part 1—brownian motion in the equilibrium state. *J. Chem. Soc., Faraday Trans. 2* (1978) 74, pp. 1789–1801
- [18] Doi, M., Edwards, S.F. Dynamics of concentrated polymer systems. Part 2—Molecular motion under flow. *J. Chem. Soc., Faraday Trans. 2* (1978) 74, pp. 1802–1817

- [19] Doi, M., Edwards, S.F. Dynamics of concentrated polymer systems. Part 3—Rheological properties. *J. Chem. Soc., Faraday Trans. 2* (1978) 74, pp. 1818–1832
- [20] Doi, M., Edwards, S.F. Dynamics of concentrated polymer systems. Part 4—Rheological properties. *J. Chem. Soc., Faraday Trans. 2* (1979) 75, pp. 38–54
- [21] Currie, P.K. Calculations on the Doi-Edwards model for concentrated polymers systems. *Proc. 8th Int. Congr. Rheol.* Naples, Italy (1980) 1, pp. 357–362
- [22] Doi, M., Edwards, S.F. *The Theory of Polymer Dynamics* (1986) Clarendon, Oxford
- [23] Lodge, T.P., Rotstein, N.A., Prager, S. Dynamics of entangled polymer liquids: Do linear chains reptate? *Adv. Chem. Phys.* (1990) 79, pp. 1–132
- [24] Fukuda, M., Osaki, K., Kurata, M. Nonlinear viscoelasticity of polystyrene solutions. 1. Strain-dependent relaxation modulus. *J. Polym. Sci., Polym. Phys. Ed.* (1975) 13, pp. 1563–1576
- [25] Marrucci, G., Grizzuti, N. Fast flows of concentrated polymers: Predictions of the tube model of chain stretching. *Gazz. Chim. Ital.* (1988) 118, pp. 179–185
- [26] Pearson, D.S., Herbolzheimer, E., Grizzuti, N., Marrucci, G. Transient behavior of entangled polymers at high shear rates. *J. Polym. Sci., Part B: Polym. Phys.* (1991) 29, pp. 1589–1597
- [27] Pearson, D.S., Kiss, A.D., Fetter, L.J., Doi, M. Flow-induced birefringence of concentrated polyisoprene solutions. *J. Rheol.* (1989) 33, pp. 517–535
- [28] Desai, P.S., Larson, R.G. Constitutive model that shows extension thickening for entangled solutions and extension thinning for melts. *J. Rheol.* (2014) 58, pp. 255–279
- [29] Larson, R.G., Desai, P.S. Modeling the rheology of polymer melts and solutions. *Annu. Rev. Fluid Mech.* (2014) 47, pp. 47–65
- [30] Hawke, L.G.D., Huang, Q., Hassager, O., Read, D.J. Modifying the pom-pom model for extensional viscosity overshoots. *J. Rheol.* (2015) 59, pp. 995–1017
- [31] Islam, M.T., Sanchez-Reyes, J., Archer, L.A. Nonlinear rheology of highly entangled polymer liquids: Step shear damping function. *J. Rheol.* (2001) 45, pp. 61–82
- [32] Cohen, A. A Padé approximant to the inverse Langevin function. *Rheol. Acta* (1991) 30, pp. 270–273
- [33] Flory, P.J. *Statistical Mechanics of Chain Molecules* (1969) John Wiley & Sons Inc., New York
- [34] Fetter, L.J., Lohse, D.J., Richter, D., Witten, T.A., Zirkel, A. Connection between polymer molecular weight, density, chain dimensions, and melt viscoelastic properties. *Macromol.* (1994) 27, pp. 4639–4647
- [35] Mead, D.W., Larson, R.G., Doi, M. A molecular theory for fast flows of entangled polymers. *Macromol.* (1998) 31, pp. 7895–7914
- [36] Fang, J., Kröger, M., Öttinger, H.C. A thermodynamically admissible reptation model for fast flows of entangled polymers. II. Model predictions for shear and extensional flows. *J. Rheol.* (2000) 44, pp. 1293–1317
- [37] Ianniruberto, G., Marrucci, G. A simple constitutive equation for entangled polymers with chain stretch. *J. Rheol.* (2001) 45, pp. 1305–1318

- [38] Marrucci, G., Ianniruberto, G. A note added to “Predictions of rheometric and complex flows of entangled linear polymers using the double convection-reptation model with chain stretch. *J. Rheol.* (2003) 47, pp. 267–268
- [39] Marrucci, G., Ianniruberto, G. Flow-induced orientation and stretching of entangled polymers. *Philos. Trans. R. Soc., A* (2003) 361, pp. 677–688
- [40] Likhtman, A.E., Graham, R.S., McLeish, T.C.B. How to get simple constitutive equations for polymer melts from molecular theory. *Proc. 6th Eur. Congr. Rheol.* (2002) pp. 259–260
- [41] Likhtman, A.E., Graham, R.S. Simple constitutive equation for linear polymer melts derived from molecular theory: Rolie-poly equation. *J. Non-Newtonian Fluid Mech.* (2003) 114, pp. 1–12
- [42] Magda, J.J., Lee, C.-S., Muller, S.J., Larson, R.G. Rheology, flow instabilities, and shear-induced diffusion in polystyrene solutions. *Macromol.* (1993) 26, pp. 1696–1706
- [43] Brown, E.F., Burghardt, W.R. First and second normal stress difference relaxation in reversing double-step strain flows. *J. Rheol.* (1996) 40, pp. 37–54
- [44] Bhattacharjee, P.K., Nguyen, D.A., McKinley, G.H., Sridhar, T. Extensional stress growth and stress relaxation in entangled polymer solutions. *J. Rheol.* (2003) 47, pp. 269–290
- [45] Wapperom, P., Keunings, R., Ianniruberto, G. Prediction of rheometrical and complex flows of entangled linear polymers using the double-convection-reptation model with chain stretch. *J. Rheol.* (2003) 47, pp. 247–265
- [46] Likhtman, A.E., McLeish, T.C.B. Quantitative theory for linear dynamics of linear entangled polymers. *Macromol.* (2002) 35, pp. 6332–6343
- [47] Bhattacharjee, P.K., Oberhauser, J., McKinley, G.H., Leal, L.G., Sridhar, T. Extensional rheometry of entangled solutions. *Macromol.* (2002) 35, pp. 10131–10148
- [48] Pattamaprom, C., Larson, R.G. Constraint release effects in monodisperse and bidisperse polystyrenes in fast transient shear flows. *Macromol.* (2001) 34, pp. 5229–5237
- [49] Auhl, D., Ramirez, J., Likhtman, A.E., Chambon, P., Fernyhough, C. Linear and nonlinear shear flow behavior of monodisperse polyisoprene melts with a large range of molecular weights. *J. Rheol.* (2008) 52, pp. 801–835
- [50] Tirtaatmadja, V., Sridhar, T. A filament stretching device for measurement of extensional viscosity. *J. Rheol.* (1993) 37, pp. 1081–1102
- [51] Ye, X., Larson, R.G., Pattamaprom, C., Sridhar, T. Extensional properties of monodisperse and bidisperse polystyrene solutions. *J. Rheol.* (2003) 47, pp. 443–468
- [52] Bach, A., Almdal, K., Hassager, O., Rasmussen, H.K. Elongational Viscosity of narrow molar mass distribution polystyrene. *Macromol.* (2003) 36, pp. 5174–5179
- [53] Marrucci, G., Ianniruberto, G. Interchain pressure effect in extensional flows of entangled polymer melts. *Macromol.* (2004) 37, pp. 3934–3942
- [54] Yaoita, T., Isaki, T., Masubuchi, Y., Watanabe, H., Ianniruberto, G., Marrucci, G. Primitive chain network simulation of elongational flows of entangled linear chains: Stretch/orientation-induced reduction of monomeric friction. *Macromol.* (2012) 45, pp. 2773–2782

- [55] Huang, Q., Mednova, O., Rasmussen, H.K., Alvarez, N.J., Skov, A.L., Almdal, K., Hassager, O. Concentrated polymer solutions are different from melts: Role of entanglement molecular weight. *Macromol.* (2013) 46, pp. 5026–5035
- [56] Huang, Q., Hengeller, L., Alvarez, N.J., Hassager, O. Bridging the gap between polymer melts and solutions in extensional rheology. *Macromol.* (2015) 48, pp. 4158–4163
- [57] Costanzo, S., Huang, Q., Ianniruberto, G., Marrucci, G., Hassager, O., Vlassopoulos, D. Shear and extensional rheology of polystyrene melts and solutions with the same number of entanglements. *Macromol.* (2016) 49, pp. 3925–3935
- [58] Ianniruberto, G. Extensional flows of solutions of entangled polymers confirm reduction of friction coefficient. *Macromol.* (2015) 48, pp. 6306–6312
- [59] Cates, M.E., McLeish, T.C.B., Marrucci, G. The rheology of entangled polymers at very high shear rates. *Europhys. Lett.* (1993) 21, pp. 451–456
- [60] Fielding, S.M., Olmsted, P.D. Kinetics of the shear banding instability in startup flows. *Phys. Rev. E* (2003) 68, article no. 036313
- [61] Ravindranath, S., Wang, S.-Q., Olechnowicz, M., Quirk, R.P. Banding in simple steady shear of entangled polymer solutions. *Macromol.* (2008) 41, pp. 2663–2670
- [62] Wang, S.-Q., Ravindranath, S., Boukany, P.E. Homogeneous shear, wall slip, and shear banding of entangled polymeric liquids in simple-shear rheometry: A roadmap of nonlinear rheology. *Macromol.* (2011) 44, pp. 183–190
- [63] Boukany, P.E., Wang, S.-Q., Wang, X. Step shear of entangled linear polymer melts: New experimental evidence for elastic yielding. *Macromol.* (2009) 42, pp. 6261–6269
- [64] Li, Y., Hu, M., McKenna, G.B., Dimitriou, C.J., McKinley, G.H., Mick, R.M., Venerus, D.C., Archer, L.A. Flow field visualization of entangled polybutadiene solutions under nonlinear viscoelastic flow conditions. *J. Rheol.* (2013) 57, pp. 1411–1428
- [65] Wang, S.Q., Liu, G., Cheng, S., Boukany, P.E., Wang, Y., Li, X. Letter to the editor: Sufficiently entangled polymers do show shear strain localization at high enough Weissenberg numbers. *J. Rheol.* (2014) 58, pp. 1059–1069
- [66] Li, Y., Hu, M., McKenna, G.B., Dimitriou, C.J., McKinley, G.H., Mick, R.M., Venerus, D.C., Archer, L.A. Response to: Sufficiently entangled polymers do show shear strain localization at high enough Weissenberg numbers. *J. Rheol.* (2014) 58, pp. 1071–1082
- [67] Adams, J.M., Fielding, S.M., Olmsted, P.D. Transient shear banding in entangled polymers: A study using the Rolie-Poly model. *J. Rheol.* (2011) 55, pp. 1007–1032
- [68] Moorcroft, R.L., Fielding, S.M. Criteria for Shear banding in time-dependent flows of complex fluids. *Phys. Rev. Lett.* (2013) 110, 086001
- [69] Agimelen, O.S., Olmsted, P.D. Apparent fracture in polymeric fluids under step shear. *Phys. Rev. Lett.* (2013) 110, 204503
- [70] Einaga, Y., Osaki, K., Kurata, M., Kimura, S., Tamura, M. Stress relaxation of polymer solutions under large strain. *Polym. J.* (1971) 2, pp. 550–552
- [71] Marrucci, G., Grizzuti, N. The free-energy function of the Doi-Edwards theory—analysis of the instabilities in stress-relaxation. *J. Rheol.* (1983) 27, pp. 433–450

- [72] Archer, L.A., Larson, R.G., Chen, Y.-L. Direct measurements of slip in sheared polymer solutions. *J. Fluid Mech.* (1995) 301, pp. 133–151
- [73] Migler, K.B., Hervet, H., Leger, L. Slip transition of a polymer melt under shear-stress. *Phys. Rev. Lett.* (1993) 70, pp. 287–290
- [74] Archer, L.A. Wall slip: Measurement and modeling issues. Chapter 4 of *Polymer Processing Instabilities* Hatzikiriakos, S.G., Migler, K.B. (Eds.) (2005) Marcel Dekker, New York
- [75] McLeish, T.C.B., Ball, R.C. A Molecular approach to the spurt effect in polymer melt flow. *J. Polym. Sci., Part B: Polym. Phys.* (1986) 24, pp. 1735–1745
- [76] Vinogradov, G.V., Malkin, A.Y., Yankovskii, Y.G., Borisenkova, E.K., Yarlykov, B.V., Berezhnaya, G.V. Viscoelastic properties and flow of narrow distribution polybutadienes and polyisoprenes. *J. Polym. Sci., Part A-2* (1972) 10, pp. 1061–1084
- [77] Park, H.E., Lim, S.T., Smillo, F., Dealy, J.M., Wall slip and spurt flow of polybutadiene. *J. Rheol.* (2008) 52, pp. 1201–1239
- [78] Doi, M., Takimoto J.-I. Molecular modelling of entanglement. *Philos. Trans. R. Soc., A* (2003) 361, pp. 641–652
- [79] Mohagheghi, I., Khomami, B. Elucidating the flow-microstructure coupling in the entangled polymer melts. Part I: Single chain dynamics in shear flow. *J. Rheol.* (2016) 60, pp. 849–859
- [80] Mohagheghi, I., Khomami, B. Elucidating the flow-microstructure coupling in entangled polymer melts. Part II: Single chain dynamics in shear flow. *J. Rheol.* (2016) 60, pp. 861–872
- [81] Bent, J., Hutchings, L.R., Richards, R.W., Gough, T., Spares, R., Coates, P.D., Grillo, I., Harlen, O.G., Read, D.J., Graham, R.S., Likhtman, A.E., Groves, D.J., Nicholson, T.M., McLeish, T.C.B. Neutron-mapping polymer flow: Scattering, flow-visualization and molecular theory. *Science* (2003) 301, pp. 1691–1695
- [82] Graham, R.S., Bent, J., Hutchings, L.R., Richards, R.W., Groves, D.J., Embrey, J., Nicholson, T.M., McLeish, T.C.B., Likhtman, A.E., Harlen, O.G., Read, D.J., Gough, T., Spares, R., Coates, P.D., Grillo, I. Measuring and predicting the dynamics of linear monodisperse entangled polymers in rapid flow through an abrupt contraction. A small angle neutron scattering study. *Macromol.* (2006) 39, pp. 2700–2709
- [83] Collis, M.W., Lele, A.K., Mackley, M.R., Graham, R.S., Groves, D.J., Likhtman, A.E., Nicholson, T.M., Harlen, O.G., McLeish, T.C.B., Hutchings, L.R., Fernyough, C.M., Young, R.N., Constriction flows of monodisperse linear entangled polymers: Multiscale modeling and flow visualization. *J. Rheol.* (2005) 49, pp. 501–522
- [84] Hassell, D.G., Lord, T.D., Scelsi, L., Klein, D.H., Auhl, D., Harlen, O.G., McLeish, T.C.B., Mackley, M.R. The effect of boundary curvature on the stress response of linear and branched polyethylenes in a contraction-expansion flow. *Rheol. Acta* (2011) 50 pp. 675–689
- [85] Auhl, D., Chambon, P., McLeish, T.C.B., Read, D.J. Elongational flow of blends of long and short polymers: Effective stretch relaxation time *Phys. Rev. Lett.* (2009) 103, 136001

- [86] Münstedt, H. Dependence of the elongational behavior of polystyrene melts on molecular weight and molecular weight distribution. *J. Rheol.* (1980) 24, pp. 847–867
- [87] Minegishi, A., Nishioka, A., Takahashi, T., Masubuchi, Y., Takimoto, J., Koyama, K. Uniaxial elongational viscosity of polystyrene/a small amount of UHMW-PS blends. *Rheol. Acta* (2001) 40, pp. 329–338
- [88] Read, D.J., Jagannathan, K., Sukumaran S.K., Auhl, D. A full-chain constitutive model for bidisperse blends of linear polymers *J. Rheol.* (2012) 56 pp. 823–873
- [89] Nielsen, J.K., Rasmussen, H.K., Hassager, O., McKinley, G.H. Elongational viscosity of monodisperse and bidisperse polystyrene melts. *J. Rheol.* (2006) 50, pp. 453–476
- [90] Mishler, S.D., Mead, D.W. Application of the MLD “toy” model to extensional flows of broadly polydisperse linear polymers: Part I—Model development *J. Non-Newtonian Fluid Mech.* (2013) 197, pp. 61–79
- [91] Mishler, S.D., Mead, D.W. Application of the MLD “toy” model to extensional flows of broadly polydisperse linear polymers: Part II. Comparison with experimental data. *J. Non-Newtonian Fluid Mech.* (2013) 197, pp. 80–90
- [92] Watanabe, H. Viscoelasticity and dynamics of entangled polymers, *Prog. Polym. Sci.* (1999) 24, pp. 1253–1403
- [93] Osaki, K., Takatori, E., Kurata, M., Watanabe, H., Yoshida, H., Kotaka, T. Viscoelastic properties of solutions of star-branched polystyrenes. *Macromol.* (1990) 23, pp. 4392–4396
- [94] Pearson, D.S. Recent Advances in the molecular aspects of polymer viscoelasticity. *Rubber Chem. Technol.* (1987) 60, pp. 439–496
- [95] Ye, X., Sridhar, T. Extensional properties of three-arm polystyrene solutions. *Macromol.* (2001) 34, pp. 8270–8277
- [96] Laun, H.M. Stresses and recoverable strains of stretched polymer melts and their prediction by means of a single-integral constitutive equation. *Proc. 8th Int. Congr. Rheol.* Naples, Italy (1980) Vol. 2, pp. 419–424
- [97] Bhattacharjee, P.K., Ye, X., Sridhar, T. Effect of molecular architecture on extensional flow of polymeric fluids. *Proc. 2nd Inter. Symp. Appl. Rheology* (2003) Seoul, Korea
- [98] McKinley, G.H., Hassager, O. The Considère condition and rapid stretching of linear and branched polymer melts. *J. Rheol.* (1999) 43, pp. 1195–1212
- [99] Larson, R.G. Instabilities in viscoelastic flows. *Rheol. Acta* (1992) 31, pp. 213–263
- [100] Fisher, R.J., Denn, M.M. A theory of isothermal melt spinning and draw resonance. *AICHE J.* (1976) 22, pp. 236–246
- [101] Petrie, C.J.S., Denn, M.M. Instabilities in polymer processing. *AICHE J.* (1976) 22, pp. 209–236
- [102] Fielding, S.M. Criterion for extensional necking instability in polymeric fluids. *Phys. Rev. Lett.* (2011) 107, 258301
- [103] Kasehagen, L.J., Macosko, C.M. Nonlinear shear and extensional rheology of long-chain randomly branched polybutadiene. *J. Rheol.* (1998) 42, pp. 1303–1327

- [104] Auhl, D., Stange, J., Münstedt, H., Krause, B., Voigt, D., Lederer, A., Lappan, U., Lunkwitz, K. Long-chain branched polypropylenes by electron beam irradiation and their rheological properties. *Macromol.* (2004) 37, pp. 9465–9472
- [105] Torres, E., Li, S.-W., Costeux, S., Dealy, J.M. Branching structure and strain hardening of branched metallocene polyethylenes. *J. Rheol.* (2015) 59, pp. 1151–1172
- [106] Wagner, M.H., Bastian, H., Hachmann, P., Meissner, J., Kurzbeck, S., Münstedt, H., Langouche, F. The strain-hardening behaviour of linear and long-chain-branched polyolefin melts in extensional flows. *Rheol. Acta* (2000) 39, pp. 97–109
- [107] Wagner, M.H., Raible, T., Meissner, J. Tensile stress overshoot in uniaxial extension of a LDPE melt. *Rheol. Acta* (1979) 18, pp. 427–428
- [108] Rasmussen, H.K., Nielsen, J.K., Bach, A., Hassager, O. Viscosity overshoot in the start-up of uni-axial elongation of LDPE melts. *J. Rheol.* (2005) 49, pp. 369–381
- [109] Huang, Q., Rasmussen, H.K., Skov, A.L., Hassager, O. Stress relaxation and reversed flow of low-density polyethylene melts following uniaxial extension. *J. Rheol.* (2012) 56, pp. 1535–1554
- [110] Hoyle, D.M., Huang, Q., Auhl, D., Hassell, D., Rasmussen, H.K., Skov, A.L., Harlen, O.G., Hassager, O., McLeish, T.C.B. Transient overshoot extensional rheology of long-chain branched polyethylenes: Experimental and numerical comparisons between filament stretching and cross-slot flow. *J. Rheol.* (2013) 57, pp. 293–313
- [111] Laun, H.M., Schuch, H. Transient elongational viscosities and drawability of polymer melts. *J. Rheol.* (1989) 33, pp. 119–175
- [112] Samurkas, T., Larson, R.G., Dealy, J.M. Strong extensional and shearing flows of a branched polyethylene. *J. Rheol.* (1989) 33, pp. 559–578
- [113] McLeish, T.C.B., Larson, R.G. Molecular constitutive equations for a class of branched polymers: The pom-pom polymer. *J. Rheol.* (1998) 42, pp. 81–110
- [114] Meissner, J.M. Modification of the Weissenberg rheogoniometer for measurements of transient rheological properties of molten polyethylene under shear, comparison with tensile data. *J. App. Polym. Sci.* (1972) 16, pp. 2877–2899
- [115] Tezel, A.K., Leal, L.G., McLeish, T.C.B. Rheo-optical evidence of CCR in an entangled four-arm star. *Macromol.* (2005) 38, pp. 1451–1455
- [116] McLeish, T.C.B., Allgaier, J., Bick, D.K., Bishko, G., Biswas, P., Blackwell, R., Blottière, B., Clarke, N., Gibbs, B., Groves, D.J., Hakiki, A., Heenan, R.K., Johnson, J.M., Kant, R., Read, D.J., Young, R.N. Dynamics of entangled H-polymers: Theory, rheology, and neutron-scattering. *Macromol.* (1999) 32, pp. 6734–6758
- [117] Archer, L.A., Juliani. Linear and nonlinear viscoelasticity of entangled multiarm (pom-pom) polymer liquids. *Macromol.* (2004) 37, pp. 1076–1088
- [118] Blackwell, R.J., McLeish, T.C.B., Harlen, O.G. Molecular drag-strain coupling in branched polymer melts. *J. Rheol.* (2000) 44, pp. 121–136
- [119] Verbeeten, W.M.H., Peters, G.W.M., Baaijens, F.P.T. Differential constitutive equations for polymer melts: The extended pom-pom model. *J. Rheol.* (2001) 45, pp. 823–845

- [120] Lee, K., Mackley, M.R., McLeish, T.C.B., Nicholson, T.M. The experimental observation and numerical simulation of transient ‘stress fangs’ within flowing molten polyethylene. *J. Rheol.* (2001) 45, pp. 1261–1277
- [121] Inkson, N.J., McLeish, T.C.B., Harlen, O.G., Groves, D.J. Predicting low density polyethylene melt Rheology in elongational and shear flows with “pom-pom” constitutive equations. *J. Rheol.* (1999) 43, pp. 873–896
- [122] Rutgers, R.P.G., Clemeur, N., Muke, S., Debbaut, B. Polyethylene flow prediction with a differential multi-mode pom-pom model. *Korea-Australia Rheol. J.* (2002) 14, pp. 25–32
- [123] Doerpinghaus, P.J., Baird, D.G. Assessing the branching architecture of sparsely branched metallocene-catalyzed polyethylenes using the pompom constitutive model. *Macromol.* (2002) 35, pp. 10087–10095
- [124] Laun, H.M., Münstedt, H.M. Elongational behavior of a low density polyethylene melt II. Transient behavior in constant stretching rate and tensile creep experiments—comparison with shear rate—temperature dependence of the elongational properties. *Rheol. Acta* (1979) 18, pp. 492–504
- [125] Bishko, G.B., Harlen, O.G., McLeish, T.C.B., Nicholson, T.M. Numerical simulation of the transient flow of branched polymer melts through a planar contraction using the pom-pom model. *J. Non-Newtonian Fluid Mech.* (1999) 82, pp. 255–273
- [126] Verbeeten, W.M.H., Peters, G.W.M., Baaijens, F.P.T. Viscoelastic analysis of complex polymer melt flows using the EXtended pom-pom model. *J. Non-Newtonian Fluid Mech.* (2002) 108, pp. 301–326
- [127] Wagner, M.H., Yamaguchi, M., Takahashi, M. Quantitative assessment of strain hardening of low-density polyethylene melts by the molecular stress function model. *J. Rheol.* (2003) 47, pp. 779–793
- [128] Read, D.J. From reactor to rheology in industrial polymers. *J. Polym. Sci., Part B: Polym. Phys.* (2015) 53, pp. 123–141
- [129] Rubinstein, M., Zurek, S., McLeish, T.C.B., Ball, R.C. Relaxation of entangled polymers at the classical gel point. *J. Phys. (Paris)* (1990) 51, pp. 757–775
- [130] Bick, D.K., McLeish, T.C.B. Topological contributions to nonlinear elasticity in branched polymers. *Phys. Rev. Lett.* (1996) 76, pp. 2587–2590
- [131] Read, D.J., McLeish, T.C.B. Molecular rheology and statistics of long chain branched metallocene-catalyzed polyolefins. *Macromol.* (2000) 34, pp. 1928–1945
- [132] Read, D.J., Soares, J.B.P. Derivation of the distributions of long chain branching, molecular weight, seniority, and priority for polyolefins made with two metallocene catalysts. *Macromol.* (2003) 36, pp. 10037–10051
- [133] Read, D.J., Auhl, D., Das, C., den Doelder, J., Kapnistos, M., Vittorias, I., McLeish, T.C.B. Linking models of polymerization and dynamics to predict branched polymer structure and flow. *Science* (2011) 333, pp. 1871–1874
- [134] Das, C., Read, D.J., Auhl, D., Kapnistos, M., den Doelder, J., Vittorias, I., McLeish, T.C.B. Numerical prediction of nonlinear rheology of branched polymer melts. *J. Rheol.* (2014) 58, pp. 737–757

- [135] Blackwell, R.J., Harlen, O.G., McLeish, T.C.B. Theoretical linear and nonlinear rheology of symmetric treelike polymer melts. *Macromol.* (2001) 34, pp. 2579–2596
- [136] Das, C., Inkson, N.J., Read, D.J., Kelmanson, M.A., McLeish, T.C.B. Computational linear rheology of general branch-on-branch polymers. *J. Rheol.* (2006) 50, pp. 207–234
- [137] Tobita, H. Simultaneous long-chain branching and random scission: I. Monte Carlo simulation. *J. Polym. Sci. Part B* (2001) 39, pp. 391–403
- [138] Lentzakis, H., Das, C., Vlassopoulos, D., Read, D.J. Pom-pom-like constitutive equations for comb polymers. *J. Rheol.* (2014) 58, pp. 1855–1875

12

State of the Art and Challenges for the Future

In this brief chapter, we give a birds-eye view of the topics we have covered and end with our impression of where the field of polymer rheology and characterization is going, or should go, to achieve its full impact on the advancement of polymer physics and the development, production, and processing of commercial polymers.

■ 12.1 State of the Art

We started this book by introducing quantities that are needed to describe the size and branching structure of a polymer molecule, principally the mean square end-to-end distance and the mean square radius of gyration $\langle R_g^2 \rangle$. The freely-jointed chain model, together with random flight calculations, gives the distribution of molecular sizes. A useful analytical approximation of this distribution is the Gaussian distribution. The characteristic ratio C_∞ describes the compactness of the coil and is smaller for more flexible molecules. For branched molecules, a branching factor g , defined as $\langle R_g^2 \rangle_B / \langle R_g^2 \rangle_L$, describes the effect of branching on the size of a molecule, and equations for its calculation have been derived for many well-defined branching structures. Dilute solutions are used in most analytical techniques. In order to use equations based on a random-flight coil size distribution, a combination of solvent and temperature called the theta condition must be used so that the effect of excluded volume is essentially eliminated. Otherwise, correlations must be used that account for swelling of the coil above its random-flight dimensions.

The most primitive measure of the breadth of a molecular weight distribution (MWD) is the polydispersity index PI, which is defined as M_w/M_n , the ratio of the weight average to the number average molecular weight. Model or “ideal” polymers for research can have PI values very close to 1, while commercial materials have rather broad distributions ranging from 2.0 to 30 or even higher. The value of PI obviously does not describe the MWD in detail. A number of equations, some empirical and

some based on polymerization models, have been developed to express the entire MWD analytically for special cases.

Aspects of molecular structure other than MWD include tacticity, chemical composition distribution (in copolymers), and branching structure. Techniques used to obtain information about molecular size include intrinsic viscosity, osmometry, and light scattering. The intrinsic viscosity is often used to determine the size of polymer molecules. For linear, monodisperse polymers, calibration constants are available for many solvent-temperature pairs that lead directly to the molecular weight. For polydisperse systems, this gives the “viscosity average” molecular weight, which is between M_n and M_w but closer to M_w . For branched molecules this yields a branching factor g' that is related to g by empirical equations for certain branching structures. Light scattering is a more elaborate measurement but gives the absolute molecular weight without the need of calibration or a model. Low-angle laser light scattering (LALLS) gives the weight-average molecular weight, while multi-angle light scattering (MALLS) also gives the mean square radius of gyration.

Gel permeation chromatography (GPC) separates heterogeneous samples into fractions having narrow distributions of molecular size. For linear molecules, this implies separation by molecular weight. If the column is calibrated with monodisperse samples, measuring only the differential refractive index (DRI) gives the molecular weight distribution. If such samples are not available, universal calibration using samples of another polymer, together with a differential viscosity (DV) detector, allows the determination of MWD. The situation is much more complicated in the case of branched polymers, since molecules of the same size may have different structures and molecular weights. If a MALLS detector is used along with DRI and DV detectors, it is possible to determine the relative amount, size, and radius of gyration of each fraction. If some information about the branching structure is available, these data can be interpreted in terms of distributions of branches among the molecules. This “triple-detector” technique is now widely used for the characterization of branched commercial polymers. As in the case of most advanced techniques, considerable care and skill are required to obtain reliable data.

A more recent development is temperature gradient interactive chromatography (TGIC), which reveals comonomer incorporation, and has been used to reveal that model branched polymers made by means of anionic polymerization contain byproducts and are thus somewhat heterogeneous.

Our ability to determine molecular structure using analytical or rheological methods is greatly enhanced if we know how the sample was made. General information, such as the type of catalyst and reactor used, are helpful, and if sufficient information is available to model the polymerization reaction, it may be possible to predict the detailed structure of the product. Using anionic or living free-radical polymerization, it is possible to make research samples having fairly well controlled and homogeneous

molecular structure. Commercial polymers range from LDPE, which has a structure so complex that it is virtually unknowable in detail, to metallocene polyolefins that can have predictable molecular weights and long-chain branching distributions.

For commercial polymers, rheological data are very useful for the characterization of molecular structure. Among the linear viscoelastic properties, the zero-shear viscosity and the storage and loss moduli are the most used. The former has a remarkably simple and universal relationship with M_w for linear polymers, and deviations from this usually indicate the presence of long-chain branches. The storage and loss moduli can be used to infer the relaxation spectrum, which provides information about the MWD of linear samples and the branching structure of branched systems. A key feature of storage modulus data for linear polymers is the plateau modulus G_N^0 , which is used to define the molecular weight between entanglements, M_e . (Two definitions of this quantity are in common use, so care is required in using published data.) The determination of G_N^0 from data, as well as the prediction of M_e using molecular theories, continue to be somewhat problematic, leading to considerable variation in published values for a given polymer.

The complexity seen in the rheological properties of a branched polymer reflects the complexity of its molecular structure. Theory provides reliable predictions of the zero-shear viscosity for well-defined branching structures and for some randomly branched systems, and empirical correlations have been proposed that relate the branching level to η_0 . The structure of low-density polyethylene is so complex that it defies precise characterization.

In general, it appears that low levels of entangled long-chain branches increase η_0 above that of a linear melt of the same molecular weight, while higher levels of branching lead to a reduction in the viscosity. However, this generalization is not to be interpreted as a rule, because temperature and molecular weight affect the relationship between η_0 and branching level.

Important developments in rheological characterization during the past decade include the rapid growth in the use of nonlinear viscoelastic properties, particularly those determined using large-amplitude oscillatory shear (LAOS) and extensional flow. The filament-stretching rheometer has made it possible to increase the maximum strain achievable and has revealed that a maximum in the extensional stress-growth coefficient does not always correspond to a steady state.

The Rouse model for a dilute solution, which involves only a single molecular parameter, the monomeric friction coefficient, is able to predict linear viscoelastic properties, including the longest relaxation time, called the Rouse time τ_R , which plays a key role in all that follows (in Chapter 6 we took care to distinguish the Rouse stress relaxation time from the Rouse reorientation time). Bueche's modification allows the Rouse model to describe the behavior of unentangled melts.

The presence of entanglements in high-molecular-weight melts dramatically complicates the modeling of rheological behavior. We focus mainly on mean-field “tube” models, but we note also recent advances in computational modeling: both molecular dynamics simulations and slip-link models now yield physical insight into entangled polymer dynamics and are proving to be useful predictive tools for some elements of macroscopic behavior. In the “tube” models, entanglements are dealt with by thinking of a given molecule imprisoned in a tube, whose walls are made up of those segments of all the surrounding molecules that are closest to it. In response to a sudden macroscopic strain, the only possible response on timescales less than a nanosecond is that of a glass that can only deform by the bending of chemical bonds, which generates a very large stress. At very short but non-zero times (i.e., microseconds to milliseconds), however, Brownian motion allows some relaxation of the stress by motions of segments of the molecule within its tube that are described by the Rouse-Bueche model. In a well-entangled, monodisperse, linear melt, further relaxation must await the escape of the molecule from the constraints of the tube, and this can only occur by slithering or “reptation.” This is a much slower process than that required for motions within the tube and gives rise to the plateau in plots of $G(t)$ and $G'(\omega)$ and two peaks in those of $G''(\omega)$ and the relaxation spectrum $H(\tau)$.

In a polydisperse system, the situation is complicated by the fact that those “entanglements” arising from nearby segments of the shorter molecules are able to reptate away relatively quickly, leading to a gradual release of the constraint imposed by the tube. A simple, semi-empirical method for dealing with this is “double reptation,” which provides useful predictions when the polydispersity index is within certain limits. More sophisticated approaches to the problem of polydispersity are presented in Chapter 7. In these more sophisticated models, constraint release is modeled either as “constraint release Rouse motion,” which is a higher-order Rouse process on the scale of the reptation of the shorter chains or by “dynamic dilution”, which is an effective widening of the tube caused by partial loss of entanglement due again to motion of short chains or rapidly relaxing entanglements. In double reptation both the chain of interest and the shorter surrounding chains are assumed to make equal contributions to the overall relaxation process, whereas in the more sophisticated model constraint release operates at a different rate.

Our understanding of how the MWD of a linear polymer is reflected in its rheological behavior is now sufficiently advanced that it is possible to use rheological data to infer the MWD except when it is very narrow or very broad. The earliest methods made use of the viscosity data and required no assumption regarding the shape of the distribution. More recent methods are based on the tube model. If reptation is the only relaxation method taken into account, use of the double-reptation scheme to account for constraint release makes it possible to infer the MWD from storage

modulus data, but the omission of other relaxation mechanisms limits the applicability of this method. The most elaborate methods take into account all possible relaxation mechanisms, but their use requires the assumption of an equation to describe the distribution. For reliable results, the data must be very accurate and precise.

New phenomena that arise when the strain is neither very slow nor very small include a dependence of viscosity on shear rate and of the relaxation modulus on strain, non-zero normal stress differences in shear, and strain hardening in extensional flows. The dependence of the relaxation modulus on strain is described phenomenologically by the damping function. And within the tube model, this is interpreted as the effect of retraction following chain stretch. Chain stretch also plays a key role in strain hardening and extension thickening in stretching flows. Meanwhile, the dependence of viscosity on shear rate is deemed to result from “convective constraint release,” which results from a sweeping away of entanglements by the shear flow. The nonlinear property that has been found to be most sensitive to molecular structure is the tensile stress growth coefficient $\eta_E^+(t, \dot{\epsilon})$. This material function is particularly sensitive to the presence of molecules that have more than one branch point. For the characterization of branched systems, this property is a valuable complement to linear viscoelastic data. While it has proven difficult to develop an instrument that can be used routinely to obtain reliable data, a new device, the Sentmanat Extensional Rheometer (SER), has shown promising results and a commercial version of the filament stretching rheometer is now available.

■ 12.2 Progress and Remaining Challenges

Considering the current rate of progress in our ability to model polymerization processes and rheological behavior, it seems reasonable to expect that in the not-to-distant future, it will be possible to do the following:

1. Predict the detailed structure of many polymers given the monomer(s), catalyst system and reaction conditions used to prepare it.
2. Given its structure, predict the rheological behavior of a polymer using molecular models.
3. Invert the above process to use rheology to determine polymer structure, or to confirm the predictions of structure that were made based on Step 1 above.
4. Using numerical flow simulations, predict the detailed behavior of a polymer during processing based on predicted rheological properties.

The description of the state-of-the-art presented in this book provides a basis for evaluating how close we are to achieving these goals and for identifying the remaining challenges.

1. The modeling of laboratory polymerization processes, described in Chapter 3, particularly catalyst reactivities and specificities, is at an advanced stage, but many industrial polymerization processes are very difficult to simulate because of inhomogeneities in temperature, composition, and flow rate, variations in operating conditions, catalyst aging, and other complexities. While industrial catalyst formulations and catalyst modeling abilities are proprietary, it seems clear that the ability to predict reactor performance, including nuances due to temperature variations and other non-idealities, will continue to evolve. Predictions of polymer structure based on reactor design and operation are steadily improving and becoming ever more sophisticated.

To confirm the predictions of the reactor models and to improve specification of product molecular weight distribution, degree of branching, and other important polymer attributes described in Chapter 2, an array of modern instrumental analysis techniques are now available, and are becoming ever more powerful. Particularly noteworthy are triple-detector GPC, TGIC, and NMR, as well as GPC-MALLS, which can characterize the branching degree of fractions of polymers eluting from a GPC column. Such methods that combine separation with characterization provide information on portions of sample, separated from each other on the basis of chain size. Naively, one can take these data as a measure of average degree of long-chain branching as a function of molecular weight. While such methods provide vastly more information on the structure of a melt than is possible by characterization only of the melt as a whole, interpretation of the results is hampered by the fact that the separations are not clean, and fractionation actually occurs on the basis of both molecular weight and branching, not on molecular weight alone. Thus, the “molecular weight” against which one plots the branching fraction is really a nominal molecular weight, and the information one actually obtains is an average light-scattering coil radius as a function of a somewhat uncertain combination of molecular weight and degree of branching. We see that our ability to obtain information about polydisperse, branched systems using GPC will require a detailed model of the separation that occurs in the columns.

Thus, improved modeling of the separation process in a GPC column should remain a research priority. From a melt composition of known or specified molecular weight and branching distribution, one would like to be able to predict the GPC-MALLS curve of branching index g versus apparent molecular weight. Success in this prediction for a given, known, melt structure would validate the model, and set the stage for creating a process for “inverting” the model, so that the GPC-MALLS curve for an unknown polymer could be inverted to obtain a

characterization of the average branching structure, molecular weight, and molecular weight distribution of each fraction. Even if model inversion should prove difficult, the existence of a validated separation model would at least allow one to use GPC-MALLS to confirm that the melt structure predicted from a reactor model is indeed consistent with the data obtained from GPC-MALLS. Priority should therefore be given to developing models of separation in a GPC column and to testing and validating the GPC-MALLS method using well defined melts that contain pre-constituted mixtures of monodisperse, and polydisperse linear, star, and/or H or comb polymers. Evaluating the performance of GPC-MALLS experiments on such model melt mixtures would go a long way towards establishing the strengths and limitations of GPC-MALLS and related methods.

2. The tube-based theories described in Chapters 6, 7, and 9 are now sufficiently advanced that automatic prediction of the linear viscoelasticity for polydisperse linear and/or branched polymers is now a reality. For linear molecules, the relaxation processes that must be included in a quantitatively accurate tube model are reptation, primitive path fluctuations, constraint release expressed as either constraint release Rouse motion or dynamic tube dilution, and high-frequency Rouse modes. For branched polymers, additional processes which must be considered include deep primitive path fluctuations and branch-point hopping. Reasonably accurate ways of including all of these phenomena have now been incorporated into several rheological theories, to the extent that (as described in Chapter 9) computational algorithms are now freely available which permit prediction of linear viscoelasticity for arbitrary mixtures of long chain branched polymers, including the broad distribution of topologies present in industrial resins. For each polymer chemical type, only a few parameters need to be obtained by fitting rheological data for simple monodisperse melts; these parameters are the plateau modulus G_N^0 , the molecular weight between entanglements M_e , and the equilibration time τ_e . Methods are also now being developed which allow the first two of these parameters to be extracted from molecular dynamics simulations.

Of course, automation of the prediction of linear viscoelasticity does not guarantee the accuracy of the method. We noted in Chapter 9 that the different computational algorithms make different assumptions about the mathematical treatment of the tube model, and so end up describing the same experimental data by using different tube model parameters, which is not very satisfactory. There is an extent to which these algorithms are “trained up” on existing sets of rheology data on certain model polymers, and are then able to make successful predictions for data on similar systems. More recently, sets of data have become available (e.g., on blends of stars with linear polymers) which push the algorithms to the limit of—and beyond!—their predictive powers. This reveals that, while such algorithms are useful codifications of our existing theoretical treatment of polymer relaxation

using the tube model, and can often be used to make accurate predictions for both model and industrial polymers, there remains more to learn. It may yet be that some of the existing theoretical framework will need discarding or reworking. In particular, areas for continued investigation include (i) the interaction between constraint release mechanisms and along-tube motion such as reptation and primitive path fluctuations, (ii) addressing the multidimensional nature of the first passage time problem of branched polymer relaxation, and (iii) further investigation into branch point hopping following side arm relaxation in the presence of constraint release.

For the first two of these, help may be available from slip-link models, which include constraint release self-consistently and which are often successful in their treatment of those polymer mixtures that give the tube-based algorithms difficulty. However, it seems that slip-link models also need to make assumptions in their treatment of branch point motion, and so understanding this may require more detailed simulation methods such as molecular dynamics simulations.

Whilst prediction of linear viscoelasticity is relatively mature, prediction of non-linear viscoelasticity is less so. As we discussed in Chapter 11, quite detailed models exist for monodisperse and bidisperse linear polymers (though even these may yet need refining based on recent observations from molecular simulations). For polydisperse mixtures, and branched polymers, our predictive capability is less well advanced, and development of a full theoretical treatment at the same level of detail would seem to be computationally intractable. On the other hand, toy constitutive models exist which can, in their multimode form, successfully fit non-linear viscoelastic data. So far, as noted in Chapter 11, one attempt has been made at a parameter mapping from a computational algorithm for linear rheology onto a toy non-linear constitutive model. Whilst not giving perfect prediction, the results of this exercise were sufficiently accurate to suggest further work of this kind is worth pursuing. Such work should be informed by further experiments, and theoretical development, on model polymer systems (e.g., combs) where more detailed theoretical treatment might be possible.

3. As described in Chapters 4 and 5, we are now able to measure linear viscoelastic properties of interest with good accuracy, assuming due care is taken in operating the equipment. The measurement of the zero-shear viscosity still poses problems for materials with broad MWDs or complex branching structures, and the development of a method to make such measurements remains a challenging enterprise, as does a method to characterize very small samples of material. From such linear viscoelastic measurements, one would like to be able to infer molecular structure (i.e., molecular weight distribution and long-chain branching distribution) or at least determine whether or not the structure inferred from the reactor model is the correct one. The ability to use rheology analytically to determine molecular

weight and especially long-chain branching distribution is needed, even if the characterization methods described in paragraph 1 above are made as reliable as possible. This is because melt rheology is much more sensitive to melt structure than any other property. It is therefore a major achievement of rheological theory, that it is now possible to make reasonably reliable determinations of the MWD of linear polymers using linear viscoelastic shear data, except in the case of very narrow or very broad distributions. This accomplishment was greatly facilitated by advances in rheological theory involving the tube model that was introduced in Chapter 6, explained in more detail in Chapter 7, and used to infer molecular weight distributions in Chapter 8.

A far greater challenge is to determine long-chain branching structure from the linear viscoelastic properties of the melt. As noted above, advanced tools now exist to compute the *forward problem*, i.e., the prediction of rheology given knowledge of branching structure. However the *inverse problem*, i.e., calculation of long chain branching structure and molecular size given only knowledge of the viscoelastic properties, is ill defined and does not have a unique solution. There can be distributions of branch length, number of branches per molecule, as well as location of branches along the backbone, and hyperbranched structures, i.e., branching on branching. As a result, for a given set of viscoelastic data, there are many possible structures, and distributions of structures, that have practically identical linear viscoelastic properties. So, the viscoelastic data on its own cannot be used to determine the branching structure.

A more sensible approach is to combine rheology with the information available from other methods, such as melt characterization with GPC, or GPC-MALLS. In particular, catalyst or reactor modeling provides constraints on the likely statistical distribution of polymer size and shape: instead of exploring an infinite variety of possible branching structures, one can instead examine distributions parameterized by a small number of variables, which can be treated as fitting parameters for the available experimental information. Using such an approach, one should in principle be able to gather enough information to specify to some degree the extent and type of long chain branching. At the least, one could use these models to check whether the branching structure inferred from the reactor model is consistent with the measured linear viscoelasticity. One could also fractionate the sample, and measure the rheology on individual fractions to obtain rheological fingerprints of narrower molecular weight slices of the whole melt, on which one has also performed GPC or intrinsic viscosity characterization. Finally, one could blend the melt at different volume fractions with a well characterized linear or star polymer and measure the linear rheology of all the blends. Since the branching structure of the original melt strongly affects the melt rheology, a wealth of information about the branching structure is in principle available from

these (potentially very large) sets of rheological data at various concentrations and molecular weights of blended linear or star polymer.

Realizing this depends, however, on having accurate models for the linear rheology of commercial branched polymers, and we noted above that there remains work to be done to improve the accuracy of existing methods. It also depends on the accuracy and reliability of catalyst or reactor modeling employed. Nevertheless, there are now multiple examples of this kind of approach in the literature, and we discussed some of these in Chapters 9 and 11. For some types of polymerization, such as for lightly branched single-site metallocene polyethylenes, the branching mechanism appears well understood and, under carefully-controlled reaction conditions, the type of branching distribution can be accurately predicted. For such resins, the prediction of linear rheology also appears to be successful, and so we can have confidence in the inferred long chain branching distribution. On the other hand, the complex structure of LDPE, and its variability from one type to another, means that we are unlikely to obtain a wholly accurate description of the detailed molecular structure of this important commercial polymer. Nevertheless, reactor modeling does provide indications of the kind of polymer structures that may be expected. In this case, as noted in Chapter 11, we must accept that we have only an approximate description of the molecular structure, and an approximate method to predict rheology, but we should also recognize that such approximate tools can still provide useful assistance in understanding and developing the material.

4. The final step is to predict the processing behavior of linear and long-chain branched polymers, based on knowledge of their molecular structures. The ability to do so would open the door to the rational design of polymer reaction chemistry to achieve desired processing characteristics. Achieving this goal will continue to require the development of powerful numerical methods capable of solving the complex nonlinear rheological constitutive equations along with the momentum, mass, and energy balances to determine the stress, flow, and temperature fields that arise in processing operations such as film blowing, fiber spinning, blow molding, and injection molding. In addition, rheological constitutive equations must be developed that can describe accurately the stresses generated by the flow and temperature histories generated in these processing operations. While the development of numerical methods for solving polymer processing flows is outside of the scope of this book, Chapter 10 introduces the measurable nonlinear rheological properties that are used to test nonlinear constitutive equations and describes the key nonlinear phenomena that must be captured by a successful constitutive equation. Chapter 11 describes constitutive equations based on the tube model and describes their successes and failures in describing nonlinear rheological behavior. In general, the task of developing constitutive models that

are not only based on accurate and detailed descriptions of molecular relaxation processes, but also applicable to commercial melts, is challenging in the extreme, especially for polymers with long branches. Detailed, realistic constitutive equations have been derived only for the simplest cases, i.e., monodisperse and bidisperse linear polymers. There has been success in using these theories for the nonlinear rheology of simple melts of linear chains to predict accurately the birefringence patterns in complex flows. However, for melts with long-chain branching, complex flow computations have only been performed using constitutive models with parameters obtained by fitting to linear and nonlinear rheological data. Whilst such an approach is still useful, it lacks a strong connection to molecular structure. A major goal for the future is therefore the continued development of constitutive equations for branched melts whose parameters are based, solely or primarily, on structural information such as the molecular weight distribution and long-chain branching distributions.

In summary, accomplishing all four of the tasks set out in Chapter 1 and recapitulated above remains some distance in future. However, the rate of progress on all fronts continues to be promising. Furthermore, even partial success in these goals will provide experimental and theoretical tools that will be of considerable value in the design of commercially useful polymer melts. We hope that this book has provided a fair summary of this progress and a stimulus to continued developments in the field.

Appendix A: Structural and Rheological Parameters for Several Polymers

These figures are extracted from an extensive tabulation published as:

Fetters, L.J., Lohse, D.J., Colby, R.H. Chain dimensions and entanglement spacings. In *Physical Properties of Polymers Handbook*, 2nd ed. (2005) Mark, J.E., Ed. Springer-Verlag, New York, Berlin.

The sources of all data shown are noted in the Handbook article.

Polymer	T	ρ	G_N^0	$\langle R^2 \rangle_0 / M$	C_∞	p	M_e g/mol	$M_C \times 10^{-3}$ g/mol	a
	K	g/cm ⁻³	MPa	Å ² /mol g ⁻¹		Å	Eq. 5.20		Å
PE	413	0.785	2.6	1.25	7.38	1.69	1040		36.0
PE	443	0.768		1.21		1.79	980	3480	
<i>a</i> -PP	298	0.852	0.48	0.678	6.00	2.88	4390		19.0
<i>a</i> -PP	463	0.765	0.42	0.678	6.00	3.20	7010		68.9
<i>i</i> -PP	463	0.765	0.43	0.694	6.15	3.12	6850		69.0
<i>s</i> -PP	463	0.766	1.35	1.03	9.12	2.10	2180		47.4
PIB	298	0.918	0.34	0.570	6.73	3.18	6690	13100	61.7
<i>cis</i> -PI	298	0.910	0.58	0.679	5.20	2.69	3890		51.4
<i>cis</i> -PBd	298	0.900	0.76	0.758	4.61	2.44	2930	8200	47.1
PBd-30	298	0.894	0.98	0.813	5.67	2.28	2260	5600	42.9
<i>a</i> -PMMA	413	1.13	0.31	0.390	8.22	3.77	12500	29500 ¹	69.9
<i>a</i> -PS	413	0.969	0.20	0.437		3.92	16600	33000 ²	85.2
<i>i</i> -PS	413	0.969	0.19	0.420		4.08	17500		85.7
<i>a</i> -PVA	333	1.08	0.35	0.490		3.14	8540	24500 ³	64.7
PDMS	298	0.970	0.20	0.422		4.06	12000	24500	71.2

1. 490 K

2. 183 K

3. 428 K

Polymers Listed

PE	Polyethylene
<i>a</i> -PP	atactic polypropylene
<i>i</i> -PP	isotactic polypropylene
<i>s</i> -PP	syndiotactic polypropylene
PIB	polyisobutylene
<i>cis</i> -PI	<i>cis</i> -polyisoprene
<i>cis</i> -PBd	1,4-polybutadiene, 96% <i>cis</i> content
PBd-30	polybutadiene with 30% vinyl content
<i>a</i> -PMMA	atactic poly(methyl methacrylate)
<i>a</i> -PS	atactic polystyrene
<i>i</i> -PS	isotactic polystyrene
<i>a</i> -PVA	atactic poly(vinyl acetate)
PDMS	poly(dimethylsiloxane)

Appendix B: Some Tensors Useful in Rheology

Velocity Gradient

The velocity gradient is simply $\text{grad } \vec{v}$ or $\nabla \vec{v}$, for which the components are given by:

$$[\nabla \vec{v}]_{ij} = \frac{\partial v_j}{\partial x_i}$$

In Chapter 11, we use the transpose of this, which we call $\boldsymbol{\kappa}$, the components of which are:

$$\kappa_{ij} \equiv \nabla \vec{v}_{ij}^T = \frac{\partial v_i}{\partial x_j}$$

Rate of Deformation

The rate of deformation tensor is

$$\dot{\gamma} = \nabla \vec{v} + \nabla \vec{v}^T = \boldsymbol{\kappa}^T + \boldsymbol{\kappa}$$

And its components are:

$$\dot{\gamma}_{ij} = \kappa_{ij} + \kappa_{ji}$$

This is obviously a symmetric tensor

Displacement Functions

Before defining finite measures of strain that can be used in writing constitutive equations, it is necessary to describe the deformation of a fluid element in quantitative terms. This is done by first describing the position of each fluid element as a function of time and then looking for a way to describe deformation by comparing the motion of neighboring fluid particles. We keep track of a fluid particle by first giving it a label that differentiates it from all other particles. This is done by specifying its position vector \vec{x} at some reference time t_0 . Then the position of this particle at some other time, t_1 , is given unambiguously by the displacement function $\vec{x}[t_1, \vec{x}(t_0)]$. To illustrate the use of this function, consider the case of the

simple shear deformation shown in Fig. 10.5. The shear strain γ is a function of time, with $\gamma(0) = 0$. The origin for the coordinate system is on the lower, stationary plate. Since we will be considering only the particle shown, for the moment, we need not mention its label in our equations.

The distance moved by the particle during the time interval from t_0 to t_1 is $[x_1(t_1) - x_1(t_0)]$, and the shear strain that occurs during this time interval is:

$$\gamma(t_2) - \gamma(t_1) = \frac{x_1(t_1) - x_1(t_0)}{x_2(t_0)}$$

The components of the displacement function, in terms of the shear strain, are:

$$x_1(t_1) = x_1(t_0) + x_2(t_0)[\gamma(t_1) - \gamma(t_0)]$$

$$x_2(t_1) = x_2(t_0)$$

$$x_3(t_1) = x_3(t_0)$$

It will also prove useful to us later to work out the displacement functions for simple (uniaxial) extension. Our convention for describing simple (uniaxial) extension will be that x_1 is the stretch direction. If we take the plane $x_1 = 0$ to represent a fixed end of a sample, then the distances of a fluid particle from this plane at times t_1 and t_2 are related to the Hencky strain ε at these two times by:

$$\ln\left[\frac{x_1(t_1)}{x_1(t_0)}\right] = \varepsilon(t_1) - \varepsilon(t_0)$$

And the displacement functions are:

$$x_1(t_1) = x_1(t_0) \exp[\varepsilon(t_1) - \varepsilon(t_0)]$$

$$x_2(t_1) = x_2(t_0) \exp\{(-1/2)[\varepsilon(t_1) - \varepsilon(t_0)]\}$$

$$x_3(t_1) = x_3(t_0) \exp\{(-1/2)[\varepsilon(t_1) - \varepsilon(t_0)]\}$$

Displacement Gradient Tensor

To describe deformation, we will examine the relative displacement of two neighboring fluid particles. At time t_0 , these particles are separated by the vector $d\vec{x}(t_0)$ and at time t_1 by the vector $d\vec{x}(t_1)$. A quantity that provides complete information about the relative displacement of any two such particles in a very small volume of the fluid is the displacement gradient tensor F whose components are given by:

$$F_{ij}(t_0, t_1) = \frac{\partial x_i(t_1)}{\partial x_j(t_0)}$$

Another tensor that relates the two vectors is the inverse of the displacement gradient tensor, which is often represented as E . Its components are:

$$E_{ij}(t_0, t_1) \equiv F_{ij}^{-1}(t_0, t_1) = \frac{\partial x_i(t_0)}{\partial x_j(t_1)}$$

This tensor can be used to determine $d\bar{x}(t_1)$, given $d\bar{x}(t_0)$, as follows:

$$dx_i(t_1) = F_{i1}(t_0, t_1) dx_1(t_0) + F_{i2}(t_0, t_1) dx_2(t_0) + F_{i3}(t_0, t_1) dx_3(t_0)$$

And the inverse displacement gradient tensor can be used to calculate $d\bar{x}(t_1)$ given $d\bar{x}(t_2)$.

It will be useful for us later to know the components of F and F^{-1} for simple shear and simple (uniaxial) extension. For simple shear these are shown below:

$$F(t_0, t_1) = \begin{bmatrix} 1 & [\gamma(t_1) - \gamma(t_0)] & 0 \\ 0 & 1 & 0 \\ 0 & 0 & 1 \end{bmatrix}$$

$$E(t_0, t_1) = \begin{bmatrix} 1 & [\gamma(t_0) - \gamma(t_1)] & 0 \\ 0 & 1 & 0 \\ 0 & 0 & 1 \end{bmatrix}$$

And for simple (uniaxial) extension:

$$F_{ij}(t_0, t_1) = \begin{bmatrix} e^{[\varepsilon(t_1) - \varepsilon(t_0)]} & 0 & 0 \\ 0 & e^{\{(-1/2)[\varepsilon(t_1) - \varepsilon(t_0)]\}} & 0 \\ 0 & 0 & e^{\{(-1/2)[\varepsilon(t_1) - \varepsilon(t_0)]\}} \end{bmatrix}$$

$$E_{ij}(t_0, t_1) = \begin{bmatrix} e^{[\varepsilon(t_0) - \varepsilon(t_1)]} & 0 & 0 \\ 0 & e^{\{(-1/2)[\varepsilon(t_0) - \varepsilon(t_1)]\}} & 0 \\ 0 & 0 & e^{\{(-1/2)[\varepsilon(t_0) - \varepsilon(t_1)]\}} \end{bmatrix}$$

The Cauchy Tensor and the Finger Tensor

It may seem that the displacement gradient tensor would be useful to describe deformation, but this is not the case. It is easy to demonstrate this by reference to motions of a fluid element that do not involve deformation. First, we consider simple translation, i.e., the fluid element simply moves from one place to another,

keeping its shape and not rotating. The vector connecting two particles inside this element will be unaltered by the translation, and the displacement gradient tensor will thus reduce to the unit tensor, indicating that nothing of interest has happened. This looks promising. However, if we consider simple rotation of a fluid element, the displacement gradient tensor does not reduce to the unit tensor and is a function of the amount of rotation, and of time if the rotation is occurring continuously.

Two tensors that do not suffer from this deficiency and can be used to describe large deformations are the Cauchy tensor, C , and the Finger tensor B , whose components can be represented in terms of those of the displacement gradient tensor and its inverse.

$$C_{ij}(t_0, t_1) = F_{1i} F_{1j} + F_{2i} F_{2j} + F_{3i} F_{3j}$$

$$B_{ij}(t_0, t_1) = E_{i1} E_{j1} + E_{i2} E_{j2} + E_{i3} E_{j3}$$

We are now in a position to write the components of these two tensors for the special cases of simple shear and simple extension. For simple shear we have:

$$C_{ij}(t_0, t_1) = \begin{bmatrix} 1 & [\gamma(t_1) - \gamma(t_0)] & 0 \\ [\gamma(t_1) - \gamma(t_0)] & \left\{ 1 + [\gamma(t_1) - \gamma(t_0)]^2 \right\} & 0 \\ 0 & 0 & 1 \end{bmatrix}$$

$$B_{ij}(t_0, t_1) = \begin{bmatrix} \left\{ 1 + [\gamma(t_0) - \gamma(t_1)]^2 \right\} & [\gamma(t_0) - \gamma(t_1)] & 0 \\ [\gamma(t_0) - \gamma(t_1)] & 1 & 0 \\ 0 & 0 & 1 \end{bmatrix}$$

And for simple extension:

$$C_{ij}(t_0, t_1) = \begin{bmatrix} e^{2[\varepsilon(t_1) - \varepsilon(t_0)]} & 0 & 0 \\ 0 & e^{-[\varepsilon(t_1) - \varepsilon(t_0)]} & 0 \\ 0 & 0 & e^{-[\varepsilon(t_1) - \varepsilon(t_0)]} \end{bmatrix}$$

$$B_{ij}(t_0, t_1) = \begin{bmatrix} e^{2[\varepsilon(t_0) - \varepsilon(t_1)]} & 0 & 0 \\ 0 & e^{-[\varepsilon(t_0) - \varepsilon(t_1)]} & 0 \\ 0 & 0 & e^{-[\varepsilon(t_0) - \varepsilon(t_1)]} \end{bmatrix}$$

We note that these are *relative tensors* that describe the configuration (shape and volume) of a material element at a given time t_1 relative to its configuration at some reference time t_0 . Thus, they are measures of the amount of deformation that has occurred in a material element between times t_0 and t_1 . The material is said to be in its “reference state” at the reference time $t = t_0$. For a cured rubber, there is a unique configuration of a material element that it will always return to when the extra stress is zero, and a time when the element was in this configuration is an obvious choice for the reference time. For a melt, there is no such unique, unstrained state, so some other reference time must be selected. In a laboratory experiment in which a sample of a melt is initially in a fixed, stress-free configuration, the time at which the deformation begins is an obvious reference time. For example, for a step strain experiment, the relaxation modulus $G(t)$ is measured as a function of the time from the instant of the initial strain ($t = 0$). Thus it is convenient to let the reference time be $t_0 = 0$.

However, in general, as time passes, the configuration at any given time in the past will have less and less relevance to the present state of stress in the sample, which is reflected in the fact that $G(t - t_0 = \infty) = 0$. This is because, unlike an elastic rubber, a melt has a *fading memory*, i.e., the effect of past strain on the present stress fades with time, eventually to zero, in a manner described by the relaxation modulus. Thus, for purposes of writing a general description of linear viscoelastic behavior, i.e., a constitutive equation, the only time during the strain history that is unique and continues to be relevant as time passes is the current time t , i.e., the time at which the stress is to be evaluated. Thus, this is the reference time used in Chapter 10 to describe large strains, i.e. $t_0 = t$. And deformations of a fluid element occurring at previous times, t' , are measured relative to its configuration at the reference time t .

Nomenclature

a	exponent in MHS equation	Eq. 2.89
a	tube diameter	Eq. 6.22
$a_T(T)$	shift factor for time or strain rate	Eq. 4.54
b	statistical segment length	Eq. 2.11
b_f	length of freely jointed segment	Section 2.1.2.1
b_K	Kuhn length	Eq. 2.15
b_n	effective random walk step	Eq. 2.10
$b_T(T)$	shift factor for stress	Eq. 4.60
B	empirical constant	Eq. 2.31
B	Finger tensor	Appendix B
C	Cauchy tensor	Appendix B
c	concentration (g/cm^3)	
C	constant in BSF equation	Eq. 2.88
C	constant in equation for G^* in transition region	Eqs. 6.18, 10.29
C_∞	characteristic ratio	Eq. 2.6
D_s^0	steady-state extensional creep compliance	Eq. 10.94
$D(t, \sigma_E)$	extensional creep compliance	Eq. 10.93
De	Deborah number	Eq. 10.41
DRI	Dow rheology index	Eq. 10.62
f	number of arms at a branch point	
g	branching factor based on radius of gyration	Eq. 2.16
g'	branching factor based on intrinsic viscosity	Eq. 2.99
g'_{SCB}	short-chain branching factor based on intrinsic viscosity	Eq. 2.109
g_i	relaxation strength in discrete spectrum	Eq. 4.15

$G(t)$	relaxation modulus in linear viscoelasticity	Eq. 4.1
$G(t,\gamma)$	relaxation modulus in nonlinear viscoelasticity	Eq. 10.1
G_N^0	plateau modulus	Sections 5.3.1, 6.3.2
$G^*(\omega)$	complex modulus	Eq. 4.36
$G'(\omega)$	storage modulus	Eq. 4.35a
$G''(\omega)$	loss modulus	Eq. 4.35b
$h(t)$	damping function for shear	Eq. 10.1
$H[\ln \tau]$	relaxation spectrum function	Eq. 4.18
I_1	first invariant of the finger tensor	Eq. 10.9
I_2	second invariant of the finger tensor	Eq. 10.10
j	number of bonds per monomer unit	Eq. 2.7
J	a function of I_1 and I_2	Eq. 11.7
$J(t)$	creep compliance in linear viscoelasticity	Eq. 4.20
J_r	recoverable compliance	Eq. 4.25
J_s^0	steady-state compliance	Eq. 4.21
J_N^0	plateau compliance	Eq. 4.22
k	Boltzmann's constant	
k	parameter of Schulz-Zimm distribution	Eq. 2.59
k	constant in power law for viscosity	Eq. 10.56
K_{geom}	sine of one half the bond angle	Eq. 2.5
K_m	constant in MHS equation	Eq. 2.76
K_θ	constant for solution in its theta state	Eq. 2.86
l	bond length	Eq. 2.5
lp	probability of adding a monomer	Eq. 3.4
L	extended (contour) length of molecule (R_{\max})	Eq. 2.14
$L[\ln \tau]$	retardation spectrum	Eq. 4.29
$L(t)$	length of specimen in extensional flow test	Eq. 10.85
L_p	persistence length	Eq. 2.12
$m(s)$	memory function	Eq. 10.5
M	molecular weight* (See note at end of Nomenclature)	
M_a	arm molecular weight	Eq. 5.44
m_b	average MW per backbone bond	Eq. 5.14

M_b	backbone molecular weight	
M_c	critical molecular weight for viscosity	Eqs. 5.1, 5.2
M'_c	critical molecular weight for compliance	Eqs. 5.7, 5.8
M_e	molecular weight between entanglements (Ferry)	Eq. 5.20
M_e^G	molecular weight between entanglements (Graessley)	Eq. 5.21
M_n	number average molecular weight	Eq. 2.37
M_0	monomer molecular weight	
M_v	viscosity average molecular weight	Eq. 2.42
M_w	weight average molecular weight	Eq. 2.38
M_z	z-average molecular weight	Eq. 2.40
n	number of backbone bonds	Eq. 2.6
n	exponent in power-law model for viscosity	Eq. 10.56
$n(M)$	number fraction of molecules	Section 2.2.1
n_i	number of molecules having molecular weight M_i	Eq. 2.34
N	degree of polymerization	
N_1	first normal stress difference	Eq. 10.29
N_1^+	first normal stress growth coefficient	Eq. 10.49
N_2	second normal stress difference	Eq. 10.30
N_a	Avogadro's number	
N_K	number of Kuhn length segments in freely jointed chain	Eq. 2.15
N_f	number of freely jointed segments	Eq. 2.1
n_w	weight average number of branch points per molecule	Eq. 2.21
p	extent of reaction (in Section 2.2.4 only)	Eq. 2.56
p	packing length	Eq. 5.28
pp	probability of propagation	Eq. 3.4
p^*	9.2 Å	Eq. 5.34
P	degree of polymerization ($P = N$)	Fig. 3.1 only
P_n	number average degree of polymerization	Eq. 3.2 only
$P_{CR}(t)$	constraint release volume fraction	Section 7.4.1, Eq. 7.10
$P(t)$	unrelaxed fraction of melt	Eqs. 6.29, 7.10
PI	polydispersity index $\equiv M_w/M_n$	Eq. 2.39

ΔP	pressure drop for flow through a capillary	Eq. 2.119
Q	volumetric flow rate in capillary rheometer	Eq. 2.119
$Q_0(\omega)$	intrinsic nonlinearity (zero-strain nonlinearity)	Eq. 10.52
$\boldsymbol{Q}[\boldsymbol{E}(t,t')]$	Doi-Edwards tensor	Eqs. 10.14, 11.6
r	degree of polymerization (in Section 2.2.4 only)	Eq. 2.53
R	end-to-end distance (vector of polymer molecule)	Section 2.1.2.1
R	universal gas constant	
$\langle R^2 \rangle_0$	mean square end-to-end distance of unperturbed molecule	Eq. 2.1
$\langle R_g^2 \rangle_0$	mean square radius of gyration of unperturbed molecule	Eq. 2.2
s	time elapsing between t' and t , i.e., $t - t'$	
SR	stress ratio	
SR/2	recoverable shear	
\boldsymbol{S}	tube orientation tensor	Eq. 11.9
t	in constitutive equations, time at which stress is given	
t'	a time prior to time t at which the stress is evaluated	Eq. 4.3
t_0	time at which material is in its reference state	Eq. 10.3
t_i	time constant in discrete spectrum	Eq. 4.15
T	temperature	
T_0	reference temperature	Section 4.5.1
V_h	hydrodynamic volume	Eq. 2.82
Wi	Weissenberg number (governs level of nonlinearity)	Eq. 10.42
z	expansion parameter (dimensionless excluded volume)	Eq. 2.29
z	tube co-ordinate	Eq. 6.37
Z	number of entanglements per molecule $Z = M/M_e^G$	Eq. 6.33
Z_a	number of entanglements in an arm ($Z_a = M_a/M_e^G$)	Eq. 9.2
Z_b	number of entanglements in the backbone	Eq. 9.21

Greek letters

α	swelling coefficient (expansion parameter)	Eq. 2.27
α	exponent in relationship for zero-shear viscosity	Eqs. 5.2 and 5.4
α	dilution exponent	Sections 7.3.3, 9.3.2; Eqs. 9.28, 9.29
α	parameter in model for $\xi(\tau)$	Eq. 7.12
β	average number of branch points per molecule	Eq. 3.3
β	pressure coefficient in Barus equation	Eq. 4.66
β	exponent in generalization of double reptation mixing rule	Eq. 8.42
γ	shear strain; strain amplitude in step shear	Eq. 4.1
γ_∞	recoverable strain (ultimate recoil); strain recovered at release of stress in steady shear	Section 10.7.2
$\dot{\gamma}$	shear rate	
$\dot{\gamma}_A$	apparent wall shear rate in capillary rheometer	Eq. 10.82
$\dot{\gamma}$	rate of deformation tensor	Appendix B
$\Gamma(x)$	gamma function	
Γ	branching <i>enhancement</i> factor	Eq. 5.42
δ	loss angle	Eq. 4.35
δ	unit tensor	
ε	exponent relating g to g'	Eq. 2.102
ε	Hencky strain	Eq. 4.6
ε_b	biaxial strain	Eq. 10.96
ε_r	recoverable strain (extensional flow)	Section 10.10.1
$\dot{\varepsilon}$	Hencky strain rate	Eq. 10.84
ζ	monomeric friction coefficient in melt	Eq. 6.4
ζ_0	monomeric friction coefficient, unperturbed molecule	Eq. 6.2
η_0	zero-shear viscosity	Eq. 4.10
$\eta(\dot{\gamma})$	shear-rate dependent viscosity	Section 10.7.1
$\eta^+(t)$	shear stress growth coefficient in linear viscoelasticity	Eq. 4.8
$\eta^+(t, \dot{\gamma})$	shear stress growth coefficient—nonlinear viscoelasticity	Eq. 10.47
$\eta_E^+(t, \dot{\varepsilon})$	tensile stress growth coefficient	Eq. 10.87
$\eta_E(\dot{\varepsilon})$	extensional viscosity	Eq. 10.90
η^*	complex viscosity	Eq. 4.37

$[\eta]$	intrinsic viscosity	Eq. 2.75
$[\eta]_\theta$	intrinsic viscosity under theta conditions	Eq. 2.84
η_s	viscosity of solvent	Section 2.5.1
η_{red}	reduced viscosity	Section 2.5.1
η_{inh}	inherent viscosity	Section 2.5.1
Θ_0	cone angle of rotational rheometer fixture	Eq. 10.77
κ	velocity gradient tensor defined in Appendix B	Eq. 11.9
λ	time constant characterizing non-Newtonian viscosity	Eqs. 10.57, 10.58
λ	average number of branch points per 1000 carbon atoms	Eq. 2.74
λ	chain stretch	Section 11.3.1, Eq. 11.9
ν_e	density of network strands	Eq. 5.18
π	osmotic pressure (in Section 2.6.1 only)	Eq. 2.112
ρ	density	
ρ_0	density at reference temperature	
σ	parameter of Gaussian distribution	Eq. 2.3
σ	shear stress in a simple shear deformation	
σ_o	stress amplitude in oscillatory shear	Eq. 4.33
σ_A	apparent wall shear stress in capillary rheometer	Eq. 10.81
σ_E	net tensile stress ($\sigma_{zz} - \sigma_{rr}$)	Section 10.10.1
σ_{ij}	component of stress tensor (linear viscoelasticity)	Eq. 4.4
τ	independent relaxation time variable in expressions for relaxation modulus	
τ_1	longest relaxation time; equal to τ_R in Rouse model	
τ_a	arm relaxation time	
τ_b	backbone relaxation time	
τ_d	reptation (disengagement) time	Eqs. 6.31, 6.34
τ_e	equilibration time	Eq. 6.23
τ_r	Rouse reorientation relaxation time (= stretch relax. time)	Eqs. 6.3, 6.11
τ_R	Rouse stress relaxation time	Eqs. 6.3, 6.11
τ_1	longest relaxation time from terminal- zone data or discrete spectrum	
τ_k	time after which relaxation modulus curves superpose	Fig. 10.3

τ_s	Retraction or stretch relaxation time (= Rouse reorientation time)	Eq. 11.1
ϕ	polymer volume concentration	
Φ	constant for a given polymer in dilute solution	Eq. 2.84
χ	polymer orientation angle	Eq. 10.69
$\Psi(t, \gamma)$	normal stress relaxation ratio	Eq. 10.37
$\Psi_1(t, \gamma)$	first normal stress relaxation coefficient	Eq. 10.36
$\Psi_1^+(t, \dot{\gamma})$	first normal stress growth coefficient	Eq. 10.38
$\Psi_{1,0}$	limiting zero-shear-rate value of $\Psi_1(\dot{\gamma})$	Eq. 10.66
$\Psi_1(\dot{\gamma})$	first normal stress diff. coefficient in steady shear	Eq. 10.63
$\Psi_2(\dot{\gamma})$	second normal stress diff coefficient in steady shear	Eq. 10.64
$\Psi(t, \gamma)$	normal stress relaxation ratio	Eq. 10.37

- * The International Union of Pure and Applied Chemistry (IUPAC) recommends the term *molar mass* (MM), which has SI units of g mol^{-1} . But *molecular weight* (MW) is widely used, and the American Chemical Society accepts both terms. However, MW is a dimensionless ratio that depends on the acceleration of gravity and is numerically very close to MM (g/mol), and one cannot change its units. The number often called “molecular weight (kg/mol)” is actually $\text{MW}/1000$ (no units). This number can also be called molar mass (kg/mol).

Author Index

A

Abbasi, M. 400, 401
Acharya, M. 429
Adams, C. H. 127
Adams, J. M. 491
Aerts, J. 39
Afshar-Taromi, F. 84
Agarwal, P. K. 48, 126
Aguilar, M. 187
Ahirwal, D. 137
Ahmad, N. 164
Ahmadi, M. 344
Ahn, K. H. 398
Aho, J. 440
Albers, I. 84
Alcoutlabi, M. 417
Allal, A. 203, 230, 280, 296, 301
Allen, C. R. G. 125
Allgaier, J. 50, 74, 187, 321, 506
Almdal, K. 429, 431, 487, 488
Alobaidi, F. 90
Alt, F. P. 92
Altuntas, E. 50, 54
Alvarez, N. J. 429, 437, 488
Ambler, M. R. 39
Anantawaraskul, S. 69
Anderssen, R. S. 129, 298
Andreev, M. 246, 356
Ankiewicz, N. S. 129
Anna, S. L. 440
Annis, B. K. 29, 70

Ansari, M. 151
Arabi, H. 344
Archer, L. A. 73, 176, 179, 277, 359, 385,
387, 388, 411, 418, 464, 470, 491, 506
Arens, L. 400, 401
Arman, J. 140, 161, 235
Armstrong, R. C. 5, 404, 442, 461
Arnett, R. L. 285
Arriola, D. J. 90
Arsac, A. 442
Attalah, P. 76
Attané, P. 405
Auhl, D. 70, 89, 182, 237, 263, 270,
271, 312, 347, 358, 401, 430, 432,
481, 494, 500, 517
Auriemma, F. 91, 164
Avgeropoulos, A. 14, 75
Awati, K. M. 420
Axelson, D. E. 78

B

Baaijens, F. P. T. 509, 514
Bach, A. 429, 437, 441, 487, 500,
509, 514
Bacova, P. 334, 346
Baek, S. G. 417
Baier, M. C. 89
Bailly, C. 162, 181, 230, 234, 247,
301, 332, 344, 356
Baird, D. G. 512
Balke, S. T. 90

- Ball, R. C. 174, 275, 316, 319, 492, 515
Ballard, D. G. H. 78
Baltas, A. 79
Bandrup, J. 10
Barroso, V. C. 401, 438
Baschnagel, J. 148
Bastiaansen, C. 79, 409
Bastian, H. 387, 438, 443, 501
Bates, F. S. 29, 70
Bathauer, M. 84
Bauer, B. J. 50
Baumann, H. 16
Baumgaertal, A. 54, 128, 295, 322
Beaucage, G. 89
Becker, F. 440
Bednarick, J. 140
Beigzadeh, D. 48, 85, 86, 87, 88, 89
Benallal, A. 230, 299
Benham, E. 80
Bent, J. 127, 493
Bercea, M. 406
Berezhnaya, G. V. 492
Bernnat, A. 443
Bernstein, B. 443
Berry, G. C. 43, 148, 200, 405
Bersted, B. H. 291
Berthold, J. 92
Bertin, D. 75
Berzin, F. 90
Bessho, N. 389
Betso, S. R. 404
Bhattacharjee, P. K. 429, 430, 479,
 481, 498
Bick, D. K. 321, 506, 516
Binder, K. 148
Bird, R. B. 5, 374, 461
Bisbee, W. 221, 222
Bishko, G. 321, 506, 514
Biswas, P. 321, 506
Blackwell, R. J. 508, 518, 321, 506
Blotti re, B. 321
Bochmann, M. 29
B hm, L. L. 92, 125, 246
Boisson, H. 83
Boode, J. W. 431
Booij, H. C. 422
Borisenkova, E. K. 492
Borsig, E. 81
Boukany, P. E. 490, 491
Bowles, W. A. 310
Boyd, R. H. 8, 9
Brands, A. M. G. 39
Brant, P. 40, 164, 168, 171, 181
Braunschweig, H. 84
Breitling, F. M. 84
Brereton, M. G. 127
Brochard, F. 167
Broedersz, C. P. 399
Brookhart, M. 81
Brown, E. F. 387, 390, 419, 479, 491
Brown, R. A. 442
Brown, R. 50
Br ll, R. 54, 49
Buback, M. 440
Bueche, F. 173, 203
Buijtenhuijs, A. 91
Burghardt, W. R. 387, 390, 391, 419, 479
Burghlea, T. I. 437
Butcher, A. F. 397
Butera, R. 167
Butler, T. I. 408
Buzzo, D. M. A. 70
Byutner, O. 170
- C**
- Caldwell, K. 50
Canich, J. M. 84
Cao, J. 223, 318
Carnahan, E. M. 90
Carreau, P. J. 404
Carrot, C. 230, 301, 442
Cates, M. E. 490

- Chaffin, K. A. 29, 70
 Chai, C. K. 443
 Chakrabarti, A. 81
 Chambon, P. 181, 271, 430, 481, 495
 Champouret, Y. 81
 Chang, H. K. 74, 348
 Chang, T. 44, 50, 74, 345, 347, 348,
 357, 432
 Chappa, V. 246
 Charleux, B. 75
 Charpenier, P. A. 85
 Cheatham, M. 50
 Chen, X. 312, 340, 348
 Chen, Y. L. 415, 491
 Chen, Y.-C. 164
 Chen, Z. 81
 Cheng, S. 491
 Cheng, T. 66
 Cheng, Z. 75
 Chiang, H. H. 404
 Chiang, R. 26
 Cho, D. 54, 74
 Chopi, H. 50, 74
 Christiansen, E. B. 417
 Chu, K.-J. 83
 Chum, P. S. 85
 Clarke, N. 321, 506
 Clasen, C. 31
 Clegg, D. W. 123
 Clemeur, N. 512
 Cluett, W. R. 90
 Coates, P. D. 493
 Cocchini, F. 297
 Cogswell, F. N. 442
 Cohen, A. A. 471
 Cohen, R. E. 5, 14, 132, 150, 163,
 167, 187, 211, 234, 260, 266, 277,
 308, 319, 322, 404
 Cole, K. S. 139
 Cole, R. H. 139, 299
 Collis, M. W. 493
 Collyer, T. A. 123
 Cong, R. 50, 53
 Coppola, S. 396
 Costanzo, S. 490
 Costeux, S. 69, 85-89, 91, 136, 171,
 182, 312, 410, 433, 500
 Coto, B. 49
 Cotts, P. M. 43
 Covas, H. A. 438
 Covezzi, M. 92
 Cox, W. P. 421
 Cramail, H. 83
 Crawley, R. L. 394
 Crosby, B. J. 187
 Cross, M. M. 404
 Cudré-Mauroux, N. 292
 Cuijpers, J. 81
 Currie, P. K. 466
 Cziep, M. A. 137, 400, 401
- D**
- D'Agnillo, L. 47
 Daniels, D. R. 135, 187, 321
 Daoud, M. 260
 Daoust, D. 74
 Das, C. 70, 89, 312, 334, 349, 347,
 352, 432, 517-519
 Daugulis, O. P. 81
 Davidson, D. W. 299
 Davies, A. R. 129
 de Gennes, P. G. 224, 260, 293
 de Groot, A. W. 49, 50, 54
 De Luca, D. 70
 de Pablo, J. J. 246
 De Rosa, C. 91, 164
 De Rosa, M. E. 322
 Dealy, J. M. 4, 38, 48, 50, 51, 74,
 89-91, 108, 127, 129, 132, 151, 171,
 181, 182, 186, 292, 339, 348, 397,
 410, 417, 418, 420, 421, 425, 433,
 442, 461, 500, 501

- Debbaut, B. 512
Decker, M. N. 410
Dedmezian, A. H. 51
Dees, M. 420
Deffieux, A. 181
deGennes, P. G. 167
deGroot, A. W. 38, 48, 51, 89, 151, 171, 182, 185, 187, 425
Dekmezian, A. H. 90
Demarmels, A. A. 379
Demirors, M. 185
den Doelder, J. 89, 312, 432, 517
Denberg, M. 431
Denn, M. M. 124, 500
Derail, C. 230, 299
des Cloizeaux, J. 232, 334, 237, 295
Desai, P. S. 469
Dev, D. 81
Devoux, J. 74
DeVries, K. L. 412
Di Girolamo, R. 91, 164
Dick, G. K. 413
Dimitriou, C. J. 491, 512
Doi, M. 5, 11, 15, 198, 208, 227, 241, 270, 317, 318, 354, 355, 396, 411, 465, 466, 469, 474, 492
Dolle, V. 54
Dong, Z. 76
Driva, P. 432
Drott, E. E. 49
Duever, T. A. 85
DuPrez, F. 71
- E**
- Ebner, K. 90
Ebrahimi, N. G. 384
Echeverría, I. 119
Eckstein, A. 29, 298
Edwards, S. F. 11, 15, 16, 167, 168, 198, 241, 318, 386, 396, 412, 465, 466
Efstratiadis, V. 72, 175, 178
- Egersdörfer, L. 430
Einaga, Y. 491
Elberli, B. 404
Ellis, M. 414
Embery, J. 493
Endere, H.-F. 92
English, A. D. 293, 293
Everaers, R. 219, 221, 230, 278
Ewen, B. 167
Ewoldt, R. H. 399, 401, 402
- F**
- Fadeev, A. Y. 49
Famini, Z. 399
Fan, W. 29, 70
Fanconi, B. M. 50
Fang, J. 474
Farago, B. 167
Fasano, A. 92
Fernández, M. 425
Fernyhough, C. M. 321, 493
Ferri, D. 93, 438
Ferry, J. D. 4, 11, 105, 114, 162, 201, 266, 293, 324
Fetters, L. J. 14, 16, 35, 75, 76, 137, 150, 163, 164, 167, 169-171, 175, 178, 186, 203, 211, 277, 281, 282, 322, 325, 326, 327, 333, 432, 469, 471
Fiedlerova, A. 81
Fielding, S. M. 426, 490, 491, 500
Finger, F. L. 310, 500
Fixman, M. 35
Florea, D. 399
Flory, A. 415
Flory, P. J. 14, 15, 22, 33, 35, 471
Ford, E. A. 82
Forsman, W. C. 167
Foteinopoulou, K. 219
Fox, T. G. 33, 35, 148, 200
Frattini, P. L. 419

Friedman, E. M. 27
Friedrich, C. 29, 137
Friedrich, Ch. 160, 297, 298
Frischknecht, A. L. 332
Froelich, D. 150, 151
Fuchs, K. 160
Fujiki, T. J. 79, 408
Fukada, M. 391, 467
Fuller, G. G. 418, 419
Furukawa, Y. 66
Fytas, G. 178

G

Gabriel, C. 84, 126, 151, 158, 159, 184, 286, 311, 346, 431, 434, 436
Galiatsatos, V. 89
Gallez, X. A. 74
Gao, P. 81
Garbella, R. W. 417
Garcia-Franco, C. A. 14, 75, 89, 137, 140, 164, 168, 171, 175, 181, 186, 187, 326, 327, 407, 422
Garritano, R. 414
Gell, C. B. 72, 175, 178
Gendron, R. 421
Genieser, L. H. 442
Gensler, R. 434
Ghosh, P. 81
Giacomin, A. J. 400, 417
Gibbs, B. 321, 506
Giddings, J. 50
Gigmes, D. 75
Gilbert, P. H. 400
Ginsburg, A. 54
Gleissle, W. 415
Gloor, W. E. 24, 25
Godard, P. 74
Gogos, C. G. 409
Gold, L. 71
Goseki, R. 73
Gotsis, A. D. 91, 493

Gough, T. 493
Graessley, W. W. 5, 7, 14, 40, 72-75, 135, 140, 150, 151, 161, 163, 164, 166, 169, 173, 174, 178, 179, 203, 214, 241, 261, 270, 282-285, 295, 300, 302, 322, 326, 327, 372, 373, 394, 405, 464
Graham, R. S. 465, 475-477, 480, 493
Greco, F. 245, 246, 278, 318, 358
Green, P. F. 261
Grest, G. S. 219, 221, 230, 278
Grillo, I. 493
Grizzuti, N. 164, 469, 491
Groves, D. J. 187, 321, 438, 493, 506, 512
Gruver, J. T. 175, 176
Guillaneuf, Y. 75
Guillet, J. 230, 301, 442
Gupta, S. 245
Guttman, C. M. 50
Guzmán, J. D. 297

H

Hachmann, P. 428, 501
Hadjichristidis, N. 14, 16, 30, 35, 50, 72-75, 137, 169, 175, 181, 186, 203, 247, 325-327, 345, 348, 356, 396, 423
Hadjichristidis, N. 71
Hagaman, E. W. 70
Hagenaars, A. 234, 237, 301
Hager, B. L. 405
Hakiki, A. 321, 342, 506
Halasa, A. F. 157, 162, 270, 277
Hall, R. 357
Halley, P. J. 124
Ham, J. S. 173, 176
Hamashima, N. 38, 48
Hamielec, A. E. 85
Hanot, A.-S. 420
Hanson, D. E. 79, 408

- Hanson, S. 83
Haraman, E. W. 29
Harlen, O. G. 401, 493, 494, 500, 512, 514, 518
Harmandaris, V. A. 148
Hassager, O. 5, 374, 426, 429-432, 437, 441, 442, 461, 487, 488, 490, 493, 497, 500
Hassell, D. G. 494, 500
Hatzikiriakos, S. G. 151, 418, 420, 421, 432
Havriliak, S. 140
Hawke, L. G. D. 470, 493
Hawkins, R. J. 187, 442
Hay, G. 420
Hazlitt, L. 50
He, C. 89, 91, 127, 187
He, J. S. 230
He, J. 162, 164
Heck, M. 400, 401
Heenan, R. K. 321, 506
Helfand, E. 174, 270, 317
Hengeller, L. 488
Hepperle, J. 432, 438
Herbolzheimer, E. 469
Hermans, N. 420
Hervet, H. 491
Heurtefeu, B. 83
Heymans, N. 167
Hieber, C. A. 40
Hingmann, R. 435
Hirao, A. 71, 73, 432
Hlatky, G. G. 83
Hoefsloot, C. J. 79
Hogt, A. H. 91
Honerkamp, J. 129, 132, 296-298
Hosoi, A. E. 402
Hostettler, J. 417, 438
Houli, S. 73, 181
Houwink, R. 31
Hoy, R. S. 219
Hoyle, D. M. 347, 401, 450
Hsiao, B. S. 48
Hsiao, T.-L. 164
Hsu, W. L. 157, 162, 270
Hu, M. 491
Hu, W. 51, 90
Hua, C. C. 245
Huang, C.-L. 164
Huang, J. S. 167
Huang, J. 440
Huang, Q. 357, 429, 437, 470, 488, 490, 493, 500
Hunt, B. J. 42
Hustad, P. D. 90
Hutcheson, S. A. 417
Hutchings, L. R. 127, 345, 493
Hutton, J. F. 415
Hyun, K. 398, 400
- I**
- Ianniruberto, G. 245, 246, 278, 318, 358, 405, 427, 464, 465, 474-479, 488, 490
Iatrou, H. 14, 73, 74, 181, 345
Iedema, P. D. 79
Im, K. 50, 74, 348
Immergut, E. H. 10
Inagaki, H. 41
Inkson, N. J. 89, 312, 512, 518
Inoue, T. 170, 208, 261, 262, 355, 385, 394, 464, 488
Isawa, J. 181
Ishida, S. 127, 261, 262
Ishizone, T. 73
Islam, M. T. 388, 411, 470
Isomura, T. 394
Iwama, M. 34, 36
- J**
- Jagannathan, K. 221, 237, 263, 270, 358, 497

- James, D. F. 440
 Janeschitz-Kriegl, H. 231
 Janigova, I. 81
 Janzen, J. 187, 308, 314
 Jeberien, H. E. 415
 Jing, Z. 164
 Johnson, J. M. 321, 506
 Jones, T. D. 29, 70
 Juliani 359, 506
- K**
- Kaerigama, K. 181
 Kahvand, H. 390, 391
 Kaivez, A. 74
 Kaji, E. 90
 Kalika, D. S. 124
 Kalogerakis, N. 418, 419
 Kamada, K. 32, 34, 36
 Kaminsky, W. 80, 83, 84
 Kang, B.-G. 357
 Kant, R. 187, 321, 506
 Kao, C. I. 85, 408
 Kapnistos, M. 70, 84, 89, 132, 135,
 312, 345, 352, 432, 517
 Karimkhani, V. 84
 Karjala, T. (See also *Plumley*) 185
 Karol, F. J. 92
 Kaschta, J. K. 84, 126, 135, 159, 431,
 440, 443
 Kasehagen, L. J. 182, 388, 435, 500
 Kashyap, T. 443
 Kataoka, T. 405
 Katzarova, M. 357
 Kazakevich, Y. V. 49
 Keblinski, P. 150
 Keddie, D. J. 75
 Kelmanson, M. A. 89, 312, 352, 518
 Kempf, M. 137
 Keßner, U. 135
 Keunings, R. 162, 230, 234, 237, 301,
 322, 344, 479
- Khaliullin, R. N. 245, 247
 Khomami, B. 465, 492
 Kikukawa, S. 91
 Kilb, R. W. 38, 47
 Kim, D.-M. 79
 Kim, M.-H. 29
 Kim, Man-Ho 70
 Kim, P. 50, 74, 345
 Kim, S. 42
 Kim, Y. H. 438
 Kimani, S. M. 347
 Kimura, S. 491
 Kiparissides, C. 79, 352
 Kirkwood, K. M. 396
 Kirste, R. G. 17
 Kiss, A. D. 175, 178, 325, 415, 469
 Kissin, Y. V. 91
 Kitagawa, K. 212
 Klein, C. O. 398
 Klein, D. H. 494
 Klein, J. 260
 Klein, P. G. 127
 Kleinova, A. 81
 Knight, G. W. 85, 404, 408
 Knight, J. R. 182
 Knox, J. R. 163
 Ko, C. 50
 Kocen, R. 247
 Koenig, J. L. 29
 Kojimoto, T. M. 389
 Kokko, E. 84, 184
 Kolodka, E. 85
 Kompani, M. 443
 Koppi, K. A. 93
 Koran, F. 418
 Kotaka, T. 41, 178, 256, 257, 388, 497
 Kouloumasis, D. 247, 356
 Koyama, K. 91, 440, 497
 Kraft, M. 126
 Krallis, A. 79
 Kramer, E. J. 261, 333

- Krasheninnikov, V. G. 91
Kratz, R. F. 126
Kraus, G. 174, 176
Krause, B. 182, 310, 500
Kreer, T. 148
Krejsa, M. R. 51
Kremer, K. 219, 221, 278
Krishnamoorti, R. 169, 203
Kröger, M. 148, 219, 474
Krömer, H. 49, 78, 91
Kruse, W. A. 17
Kuhlman, R. L. 90
Kuhn, R. 11, 49, 78, 91
Kulicke, W. M. 31, 415
Kulkarni, A. S. 89
Kumar, S. K. 150
Kumazawa, K. 127
Kunamaneni, S. 70
Kurata, M. 34, 36, 371, 388, 389, 391, 467, 491, 497
Kurelec, L. 81, 430, 434, 501
Kuzuu, N. Y. 317
Kwang, S. C. 398
Kwang, U. K. 38
- L**
Labaig, J. J. 140
Lafuente, P. 186, 425
Lai, S. Y. 182, 404, 408
Langeloth, M. 246
Langouche, F. 501
Lanver, U. 49
Lappan, U. 182, 310, 500
Larson, R. G. 5, 73, 166, 187, 203, 219, 327, 230, 235-237, 245, 261, 270, 280, 283, 284, 312, 314, 318, 321, 322, 324, 327, 329, 340, 348, 354, 355, 357, 374, 386, 387, 389, 410-412, 414-416, 461, 469, 474, 479, 481, 485, 491, 500, 501, 502, 504
Laun, H. M. 128, 327, 389, 410, 414, 418, 420, 425, 435, 438, 442, 443, 498, 500, 513
Lazar, M. 81
Leal, L. G. 135, 166, 280, 322, 396, 430, 481, 501, 504
Leblanc, J. L. 2
Leblans, P. J. R. 79, 409, 422
Lecacheux, D. 13
Lechner, M. D. 49
Lederer, A. 182, 310, 415, 500
Lee, C. S. 412, 415, 479
Lee, H. C. 50
Lee, H. 50, 74, 277, 345, 347, 348, 432, 509
Lee, M. H. 50, 74, 348
Lee, S. 357
Lee, W. 50, 74
Leed, S. J. 398
Lefay, C. 75
Leger, L. 491
Leino, C. R. 83
Lele, A. K. 493
Lemstra, P. J. 81
Lentzakis, H. 129, 334, 346, 432, 519
Léonardi, F. 230, 296, 301
Lesec, J. 13
Levine, A. J. 327
Levy, G. C. 78
Li, H. 75, 76
Li, S.-W. 32, 50, 74, 89, 90, 182, 348, 433, 500
Li, Y. 491
Li, X. 491
Likhtman, A. E. 166, 181, 219, 221-223, 229, 243, 247, 277, 280, 300, 318, 322, 356, 465, 475, 480, 481, 493
Lilge, D. 184
Lim, S. T. 418, 492
Lin, P. 440

- Lindner, J. S. 16, 35
 Link, G. 126
 Lippits, D. 81
 Liu, C. Y. 162, 164, 230
 Liu, G. 491
 Liu, L. 48
 Liu, Y. 292
 Lodge, A. S. 377, 389, 438
 Lodge, C. E. 438
 Lodge, T. P. 285, 418, 466
 Löfgren, B. 84, 184, 434
 Lohse, D. J. 14, 75, 137, 150, 163, 164, 167-171, 181, 186, 203, 211, 277, 322, 326, 327, 345, 421, 432, 471
 Lomollini, P. 93
 Lord, T. D. 494
 Lunkwitz, K. 182, 310, 500
 Lusignan, C. P. 187
 Lynch, D. T. 82
 Lyon, M. K. 75, 137, 186, 326, 327, 438
 Lyons, J. W. 49, 54
- M**
 Machado, J. 322
 Mackay, M. E. 124, 413, 420
 Mackley, M. R. 81, 493, 494, 509
 Macko, T. 49, 54
 Macosko, C. W. 4, 123, 182, 388, 399, 435, 438, 500
 Magda, J. J. 412, 415, 417, 438, 479
 Maia, J. M. 438
 Maier, R.-D. 29, 298
 Majesté, J.-C. 203, 230, 280, 301
 Makuuchi, K. 91
 Malik, M. I. 44, 50, 52
 Malik, T. M. 140
 Malkin, A. Ya. 291, 492
 Malmberg, A. 84, 433, 434
 Mandelkern, L. 78
 Mangnus, M. 185, 187, 420
 Man-Ho, K. 29
 Marchand, J. M. G. 90
 Marczinke, B. L. 435
 Maric, M. 50, 74, 348
 Marin, G. 140, 161, 163, 203, 230, 235, 196, 280, 296, 299-301, 322, 409
 Marín, J. M. R. 437
 Maring, D. 398
 Mark, H. 31
 Marrucci, G. 245, 246, 275, 278, 358, 373, 405, 464, 465, 469, 474, 478, 488, 490, 491
 Marth, M. 297, 298
 Martínez-Salazar, J. 151, 187
 Masse, M. 322
 Masubuchi, Y. 245, 246, 278, 318, 358, 396, 488, 497
 Masuda, T. 212, 383
 Matsumiya, Y. 127, 237, 262, 262, 270, 355, 346, 358
 Matyjaszewski, K. 75
 Mavrantzas, V. G. 148, 223
 Mavridis, H. 187, 302, 407
 Mayer, J. W. 261
 Mayo, N. 53
 Mays, J. 50, 348, 357
 Mays, J. W. 16, 30, 35, 74, 76, 412
 McDaniel, M. 80
 McFaddin, D. 89
 McGrory, W. J. 293
 McKenna, G. B. 134, 166, 280, 322, 398, 415, 417, 491
 McKinley, G. H. 166, 280, 322, 398, 399, 401, 402, 426, 430, 439, 440, 442, 479, 481, 497, 500
 McLeish, T. C. B. 70, 73, 85, 86, 89, 127, 166, 174, 187, 198, 227, 229, 243, 263, 271, 275, 277, 280, 300, 312, 316, 318, 319, 321, 322, 332, 342, 352, 388, 401, 430, 432, 465, 475, 476, 480, 490, 492-495, 500-502, 504, 506, 508, 512, 514-518

- McMillan, F. M. 66
Mead, D. W. 90, 140, 237, 282, 294, 295, 298, 474, 497
Mecking, S. 89
Mednova, O. 488
Meerveld, J. A. 205
Mehta, A. 48
Mei, G. 92
Meijer, H. E. H. 150, 164
Meijerink, N. L. J. 39
Meimaroglou, D. 79, 352
Meira, G. R. 38
Meissner, J. 91, 126, 389, 403, 417, 428, 438, 440, 500, 501
Mendelson, R. A. 14, 37, 49, 75, 186, 310, 326, 327
Menezes, E. V. 322, 385, 394
Merger, D. 400
Merrick-Mack, J. 89
Merz, E. H. 421
Mesgar, M. 81
Meunier, D. M. 54
Mewis, J. 2, 414
Mhetar, V. R. 418
Michelsen, M. L. 437
Mick, R. M. 443, 491
Migler, K. B. 491
Mihsara, S. 79, 408
Miller, M. D. 49, 50, 54
Miller, M. J. 417
Miller, W. R. 126
Mills, P. J. 261
Milner, S. T. 75, 127, 150, 167, 169, 186, 221-223, 273, 277, 318, 321, 327, 332, 422, 432, 465, 475, 480
Minegishi, A. 497
Mirabella, F. M. 82
Miros, A. 181
Mishler, S. D. 497
Moad, G. 75
Mohagheghi, I. 492
Moldenaers, P. 414
Monge, Ph. 140, 161, 235, 300
Monrabal, B. 50, 52-54
Montfort, J.-P. 140, 161, 203, 230, 235, 280, 299, 300
Moocroft, R. L. 491
Moreno, A. J. 334, 346
Morrison, F. A. 4, 387
Morse, D. C. 246
Mortensen, K. 429
Mott, P. H. 385
Muchtar, Z. 181
Mourey, T. H. 187
Mueller, S. J. 325
Muke, S. 512
Mühlaupt, R. 29, 137
Muliawan, E. B. 432
Müller, A. H. E. 75
Müller, G. 46
Müller, K.-H. F. 83
Muller, M. 148
Müller, M. 246
Muller, R. 150, 151
Muller, S. J. 412, 440, 479
Müller-Plathe, F. 246
Munoz-Escalona, A. 186, 425
Münstedt, H. 2, 4, 84, 126, 135, 151, 158, 159, 182, 184, 286, 288, 310, 346, 411, 425, 430-438, 440, 443, 497, 500, 501, 513
- N**
- Nagao, M. 127
Nair, D. M. 245
Nakano, Y. 181
Nam, J. G. 398
Namba, S. 181
Narimissa, E. 380
Navard, P. 407
Neergaard, J. 245
Negami, S. 140

Neithamer, D. R. 84
 Nekoomanesh, M. 344
 Newberrys, M. 399
 Ng, T. S. K. 399
 Ngai, K. L. 131, 175
 Nguyen, D. A. 429, 430, 440, 479
 Nguyen, T. Q. 434
 Nicholson, T. M. 493, 514
 Nicol, E. 349
 Nicolai, T. 349
 Nicolas, J. 75
 Nielsen, J. K. 135, 430, 431, 437, 442, 497, 500
 Nikopoulou, A. 50, 74, 345, 348, 396
 Nishioka, A. 440, 497
 Nishizawa, K. 371
 Nixon, A. 421
 Nobile, M. R. 297
 Nordmeier, E. 49
 Nuel, L. 124

O

Oberhauser, J. P. 430, 481
 Ohta, S. 391
 Okamoto, K. 181
 Okano, M. 421
 Olechnowicz, M. 490
 Olmsted, P. D. 490, 491
 Olson, D. J. 391
 Onogi, S. 212
 Orbey, H. 129
 Orfanou, K. 345
 Ortín, A. 53
 Ortseifer, M. 398
 Osaki, K. 170, 208, 356, 371, 385, 388, 391, 394, 464, 467, 491, 497
 Oster, F. 434
 Otegui, J. 151
 Öttinger, H. C. 34, 148, 394, 417, 419, 474

P

Pabeledinskas, A. 90
 Padmanabhan, S. 81
 Pakula, T. 178
 Palmen, J. 137, 422
 Palmstrom, C. J. 261
 Pandey, A. 81
 Paraskeva, S. 14, 75
 Park, H. E. 50, 74, 90, 132, 348, 418, 492
 Park, S. J. 50, 237, 261, 270, 279, 312, 321, 324, 326, 329
 Park, W.-S. 394
 Park, Y. 420
 Parrott, A. 50
 Pasch, H. 44, 49-51, 52
 Pastor, D. 187
 Patel, S. S. 415
 Pathak, J. 50, 74, 345
 Pattamaprom, C. 203, 230, 235, 236, 283, 284, 301, 302, 314, 327, 386, 481, 485
 Pearson, D. S. 76, 226, 270, 175, 178, 282, 317, 325, 395, 401, 469, 497
 Peebles, L. H. 2 2, 27
 Peiti, C. 406
 Pell, R. J. 54
 Penlidis, A. 47
 Peon, J. 187
 Pérez, O. 80
 Perny, S. 50, 74
 Peters, B. L. 246
 Peters, G. W. M. 150, 399, 509, 514
 Petrie, C. J. S. 500
 Phan-Thien, N. 399
 Phillips, P. J. 8, 9
 Piel, C. 84
 Pierrard, J. M. 405
 Pilyugina, E. 356
 Pipkin, A. C. 399
 Pispas, S. 30

- Pitsikalis, M. 14, 30, 72, 75, 175, 178, 345
Pladis, P. 79, 352
Plazek, D. J. 119, 126, 131, 133-135, 155, 159, 397
Plumley (Kajala), T. A. 404, 408
Poitou, A. 409
Pollard, R. 297
Ponmurugan, M. 222, 223
Porter, R. S. 415
Poulos, Y. 14, 75
Prager, S. 466
Priddy, D. B. 93
Provencher, S. W. 295
Prud'homme, R. E. 140
Pryke, A. 187, 332
Pütz, M. 278
Pyckhout-Hintzen, W. 429
- Q**
Qin, J. 221-223
Quack, G. F. 175, 178, 325
Quirk, R. P. 490
Quivoron, C. 13
- R**
Rachapudy, H. 50, 74, 75, 126, 173, 283, 284, 285, 326, 327, 348
Rai, P. 36
Raible, T. 500
Rajagopalan, D. 442
Raju, V. R. 73, 75, 163, 173, 283-285, 322, 326, 327
Ramachandran, R. 89
Ramírez, J. 148, 481
Ramírez-Hernández, A. 246
Ramos, J. 151
Ran, S. 48
Randall, J. C. 51
Rasmussen, H. K. 429-431, 437, 441, 442, 487, 488, 497, 500
Rastogi, S. 81, 150, 164
Ratkanthwar, K. 396
Rätzsch, M. 91
Rauschenberger, V. 443
Ravindranath, S. 490
Read, D. J. 70, 85, 86, 89, 221, 237, 247, 263, 270, 271, 282, 291, 312, 321, 334, 346, 347, 349, 352, 358, 430, 432, 470, 493, 495, 497, 506, 515, 517-519
Redwine, O. D. 38, 48, 51, 89, 90, 151, 171, 182, 425
Reilly, P. M. 41
Reimers, M. 418
Reinheimer, P. 398
Reisch, M. S. 283
Revenu, P. 442
Richards, R. W. 70, 127, 493
Richter, D. 134, 163, 164, 167-171, 203, 277, 322, 471
Rides, M. 125
Ries, M. E. 127
Rishina, L. A. 91
Rizzato, E. 75
Robertson, C. G. 89, 187, 397, 407, 418
Rochefort, W. E. 73, 173, 401
Rodukai, M. 79
Rohlfing, D. C. 151, 314
Rojas, G. 76
Roland, C. M. 175, 385, 397
Rólón-Garrido, V. H. 380, 400, 440
Romero, L. 53
Roovers, J. 73, 135, 174, 176, 178, 179, 181, 322, 325
Rosen, S. L. 36
Roths, T. 298
Rotstein, N. A. 466
Rouse, P. E., Jr. 34, 131
Rouse, R. 200
Roy, A. 54

- Roy, D. 397
 Rubinstein, M. 5, 14, 132, 167, 234,
 260, 277, 319, 322, 515
 Rubio, P. 387
 Ruff, C. J. 14, 51, 75, 90
 Ruiz de Ballesteros, O. 91
 Rulhoff, S. 84
 Rutgers, R. P. G. 512
- S**
- Sáha, P. 442
 Saito, M. 32, 34, 36
 Saito, S. 47
 Saitoh, J. 91
 Sakurada, I. 31
 Samurkas, T. 417, 501
 Sanchez-Reyes, J. 385, 387, 411, 464,
 470
 Sancho-Tello, J. 53
 Santamaria, A. 80, 186, 425
 Sarma, K. R. 81
 Sassamannshausen, J. 29
 Scamporrino, E. 50
 Scelsi, L. 494
 Schaeffer, J. 380
 Schappacher, M. 181
 Schausberger, A. 231, 295
 Schieber, J. D. 245-247, 297, 356, 357
 Schimpf, M. E. 50
 Schindlauer, G. 231
 Schlund, B. 82
 Schmidheiny, W. 417
 Schneider, C. 443
 Schoffeleers, H. M. 39
 Scholte, G. 39
 Scholten, J. 17
 Schrepp, W. 50
 Schubert, U. S. 50
 Schuch, H. 327, 442, 501
 Schulz, D. N. 14, 75
 Schulz, G. V. 22-24, 27
 Schulz, M. D. 76
 Schulze, J. S. 438
 Schümmer, P. 420
 Schwarzl, F. R. 4, 126, 132
 Schweizer, T. 394, 416, 417, 438, 443
 Sen, S. 150
 Sentmanat, M. L. 439
 Seo, Y. 38
 Seppälä, J. 84, 184
 Seymour, R. B. 66
 Shahinur Rahman, M. 348
 Shanbhag, S. 89, 129, 245, 282, 318,
 354, 355
 Sharma, S. 81
 Shaw, M. T. 292, 404
 Shchetnikava, V. 237, 270
 Shiromoto, S. 358
 Shiu, T.-Y. 443
 Shivokhin, M. E. 247, 356, 357
 Shroff, A. R. 187, 314, 407
 Shroff, R. 302
 Shroff, R. N. 187
 Shull, K. R. 333
 Simionescu, B. 406
 Simpson, D. M. 84
 Singh, P. 15
 Sinn, H. H. 80
 Sioula, S. 14, 75
 Sirivat, A. 302
 Sivasubramanian, A. 219, 278
 Skov, A. L. 488, 500
 Slee, J. D. 291
 Slot, J. J. M. 352
 Small, P. A. 12, 38, 48
 Smillo, F. 418, 492
 Smith, G. C. 163
 Smith, G. D. 170
 Smith, G. G. 73, 75, 173
 Snijkers, F. 50, 74, 345, 348, 396
 Soares, J. B. P. 47, 69, 80, 83, 85, 517
 Sokal, A. D. 14

- Somani, R. H. 48
Sommer, C. 46
Soya, K. 90
Spares, R. 493
Sperber, O. 83
Spiess, H. W. 398
Sridhar, T. 166, 280, 322, 429, 430,
 440, 479, 481, 485, 498
Srinivas, S. 89, 181, 187, 407
Stadler, F. J. 84, 129, 151, 440
Strange, J. 182, 310, 433, 440, 500
Staverman, A. J. 132
Steeman, P. A. M. 352
Steffl, T. 84, 433, 434
Stenger, M. 125
Stephaenne, V. 181
Stephanou, P. S. 223
Stéphenne, V. 234, 237, 301
Stevens, G. W. 182
Stevens, J. C. 84
Stevens, J. 182
Stewart, C. W. 418
Stöckli, M. 416
Stockmayer, W. H. 12, 13, 35, 38, 173
Stratton, R. A. 397
Striegel, A. M. 51
Struglinski, M. J. 151, 161, 178, 322
Suarez, I. 49
Suhm, J. 29
Sukhadia, A. M. 151
Sukumaran, S. K. 219, 237, 245, 263,
 270, 278, 497
Sun, C. 164
Sun, T. 14, 40, 75
Suzuki, H. 41
Svaneborg, C. 219, 230, 278
Syrjälä, S. 440
- T**
Tackx, P. 49
Tacx, J. C. J. F. 49
Tadashi, I. 127
Takahashi, M. 181, 383, 515
Takahashi, T. 497
Takahashi, M. 79, 181, 388
Takatori, E. 388, 497
Takayama, S. 78
Takeh, A. 89, 129
Takimoto, J. 354, 355, 497
Takimoto, J.-I. 245, 492
Tamura, M. 491
Tanaka, T. 91
Tanner, R. I. 399, 461
Tao, H. 285
Taylor, G. I. 426
Teishev, A. Ye. 291
Tezel, A. K. 501, 504
Tezuka, Y. 71
Thaens, W. 420
Thang, S. H. 75
Theodorou, D. N. 148, 219
Thimm, W. 297, 298
Thomas, C. P. 285
Tiemersma-Thoone, G. 422
Tirtaatmadja, V. 440, 485
Tobita, H. 38, 47, 48, 79, 352, 519
Todd, D. 409
Togawa, Y. 358
Toporowski, P. M. 73
Torres, E. 89, 182, 433, 500
Toyama, K. 245
Trathnigg, B. 44
Treat, T. A. 293, 293
Trinkle, S. 137
Tripp, B. C. 415
Tsai, J.-C. 164
Tsang, W. K. W. 397
Tsarevsky, N. V. 75
Tschoegl, N. W. 105, 114
Tsenoglou, C. J. 187
Tsenoglou, C. 91, 232, 295
Tsukahara, Y. 181

Tsunashima, Y. 34, 36

Tsutsubuchi, M. 358

Tuminello, W. H. 231, 292, 293, 299

Tung, L. H. 25

Turrell, G. 405

Tzoganakis, C. 442

Tzoumanekas, C. 219

U

Ueda, S. J. 405

Uematsu, T. 170, 208, 385, 464

Uhl, C. 433

Uneyama, T. 246

Urakawa, O. 127, 257, 383

Usami, T. 78

Utracki, L. A. 82, 421

V

Van Damme, F. A. 49, 54

van den Brule, B. H. A. A. 124

van der Hoff, B. M. E. 41

Van Dyke, T. J. 203, 301, 327

van Egmond, J. W. 419

van Gurp, M. 137

van Kempen, T. H. S. 399

van Meerveld, J. 148, 394, 417

Van Puyvelde, P. 420

van Ruiten, J. 431

van Ruymbeke, E. 50, 74, 162, 234,

237, 270, 301, 332, 344, 345, 348,

352, 356, 430, 432

Varshney, S. K. 73, 176, 179, 388

Vaughan, G. A. 84

Vaultier, F. 83

Vega, J. F. 14, 80, 151, 150, 164, 186,

187, 425

Velis, G. 14, 75

Venerus, D. C. 357, 387, 390, 391,

419, 443, 491

Venkatraman, S. 421

Ver Strate, G. 282

Verbeeten, W. M. H. 509, 514

Vergnes, B. 90

Vermant, J. 414

Vinogradov, G. V. 492

Viovy, J. L. 167, 260, 300

Virkler, T. 438

Vitalini, D. 50

Vittorias, I. 79, 89, 312, 432, 517

Vitus, F. J. 175, 178, 325

Vlassopoulos, D. 50, 73, 74, 135, 148, 181, 332, 334-346, 348, 396, 432, 490, 519

Vlček, J. 442

Voigt, D. 182, 310, 500

von Burchard, W. 34

von Meerwall, E. D. 282, 285

Vrentas, C. M. 389

W

Wagener, K. B. 76

Wagner, M. H. 378-380, 387, 400, 500, 515

Wagner, N. J. 2

Wallace, W. E. 50

Walter, P. 137

Wang, B. N. 439

Wang, C. 164

Wang, J. 4, 90, 108, 185, 270, 461

Wang, S. 157, 162

Wang, S. Q. 157, 162, 440, 490, 491

Wang, X. 490

Wang, Y. 49, 491

Wang, Z. 318, 340

Wang, Z.-G. 167

Wanke, S. E. 82

Want, W.-J. 85

Wapperom, P. 479

Wardhaugh, L. T. 170

Warren, S. 397

Wasserman, S. H. 151, 241, 295, 296

Wassner, E. 438

- Watanabe, H. 127, 129, 178, 198, 237, 256, 257, 261, 262, 270, 319, 355, 356, 358, 388, 396, 432, 488, 497
- Waymouth, R. 26, 70
- Weese, J. 129, 132, 160, 296
- Wei, L. 164
- Weng, W. 48, 51, 90
- Wenzel, T. T. 90
- Wesslau, W. 25
- White, J. L. 90
- White, P. S. 81
- Wignall, G. D. 29, 70
- Wilhelm, M. 137, 398, 400, 401
- Williams, M. C. 170
- Willner, L. 134
- Wilson, J. R. 182
- Wilson, R. H. 187
- Wimmer, M. 81
- Wingstrand, S. L. 429
- Winniford, L. 49, 54
- Winter, H. H. 91, 128, 181, 295, 322
- Witten, T. A. 163, 164, 167, 170, 277, 322, 471
- Wolkowicz, R. I. 167
- Wong, C.-P. 405
- Wood-Adams, P. M. 38, 48, 51, 69, 85-89, 91, 127, 136, 151, 167, 171, 181, 182, 186, 187, 292, 339, 410, 425
- Wool, R. P. 167
- Worch, J. 89
- Worthoff, R. H. 420
- Wozumi 90
- Wright, P. J. 14, 75
- Wu, S. 162, 163, 167, 293
- Wulkow, M. 79
- Wyss, H. M. 399
- X**
- Xenidou, M. 14, 75, 137, 186, 326, 327, 432
- Xu, J. 410
- Xu, W. 75
- Y**
- Yaghini, N. 79
- Yamaguchi, M. 79, 388, 409, 515
- Yamakawa, H. 15
- Yamashita, Y. 170, 208, 385, 464
- Yamazaki, M. 256
- Yang, L. 48
- Yankovskii, Y. G. 492
- Yaoita, T. 358, 488
- Yarlykov, B. V. 492
- Yasuda, K. Y. 404
- Yau, W. 50, 185
- Ye, X. 485, 498
- Ye, Z. 76, 90, 171
- Yoshida, H. 178, 256, 388, 497
- Yoshii, F. 91
- Young, R. N. 187, 321, 332, 342, 493, 506
- Younghouse, L. B. 76
- Yu, J. 164
- Z**
- Zang, Y. H. 150, 151
- Zatloukal, M. 442
- Zdeněk, S. 437
- Zeevenhoven, B. L. F. 91
- Zhang, M. 82
- Zhang, Z. 75
- Zhou, Q. 219, 282, 318
- Zhou, Z. 50
- Zhu, J. 75, 318
- Zhu, S. H. 419
- Zhu, S. 85, 90, 171
- Zhu, X. 75
- Zhu, Y. 49
- Zifferer, G. 16
- Zimm, B. H. 12, 13
- Ziogas, M. 41

- Zippelius, A. 246
Zirkel, A. 163, 164, 167, 169, 170,
203, 277, 322, 471
- Zorn, R. 134
Zuideveld, M. A. 89
Zurek, S. 515

Subject Index

A

- Activation energy for flow 131, 327
- Addition polymers 68
- Affine deformation (Stretching) 216, 370, 371, 378, 383, 462–464
- Anionic polymerization 2, 18, 35, 50
- Apparent extensional viscosity 442
- Apparent wall shear rate, in capillary rheometer 419, 421
- Apparent wall shear stress, in capillary rheometer 419
- Apparent viscosity 421
- Arrhenius temperature dependence 130, 279, 280

B

- Backbone relaxation, in branched polymers 336, 338, 504, 511
- Barus equation, for pressure effect 136
- Biaxial extension (Equibiaxial extension)
 - Description of 426
 - Rheometers for 446
 - Sensitivity to molecular structure 435
- Bivariate characterization 54
- BoB model for branched polymers
 - Linear viscoelasticity 340–361
 - Non-linear viscoelasticity 518, 519
- Boltzmann superposition principle 105–108, 115, 375
- Tensorial form of 375

Bottle brush molecules 92, 181

Branch point motion 332–334, 336, 358–360, 542

Branching (see *Branching factors, Long-chain branching, Short-chain branching*)

Branching factors

- For short-chain branches 39, 40
- Intrinsic viscosity, definition of based on 37
- Radius of gyration, definition of based on 12, 37, 38
- Randomly branched polymers, value of for 13
- Star polymers, value of for 12, 56
- Zero-shear viscosity, as basis for definition of 200

Branching frequency, in copolymers 48

Breathing modes (see *Primitive path fluctuations*)

Brownian motion 152, 154, 156, 199

BSF equation (Correction for non-theta state) 52

Bueche–Ferry law 208, 213

C

Capillary rheometers (see *Rheometers, capillary and slit*)

Carreau equation, for viscosity 404

Carreau–Yasuda equation, for viscosity 404

Cauchy strain tensor 377–380, 549

- Cayley tree 29, 70, 339, 345, 347, 514, 518
- Cessation of elongational flow
 - (see *Stress relaxation after extensional flow*)
- Cessation of steady shear – stress relaxation following (see *Stress relaxation after cessation of steady shear*)
- Chain growth polymerization 67, 68
- Chain orientation – role of in nonlinear viscoelasticity 395, 470, 476, 479, 486, 488, 504
- Chain scission 45, 91
- Chain-shrinking methods (for entanglement detection) 219
- Chain stretch, in tube model
 - (see also *Retraction*) 469–473
- DEMG model of 469
- Pom-pom molecule, used for 502–509
- Rouse-Poly theory, role of in 476
- Chain growth polymerization 67
- Chain tumbling 493
- Characteristic ratio
 - Definition of equation 10
 - Values of, for several polymers 457
- Chemical composition distribution (CCD)
 - (see also *Copolymers*) 52, 87
- Chirality, detection of by NMR 51
- Chromium oxide catalysts 80, 92
- Cole-Cole plots 139, 140
- Comb molecules 13, 173
 - (see also *Bottle brush molecules*)
- Backbone relaxation in 336
- Branching factor g' for below 38
- Chromatography, separation in 48
- Dynamic dilution in 330, 340
- Metallocene polymers, in 182, 352, 433
- Nonlinear viscoelastic behavior of 432
- Relaxation mechanisms for 316
- Synthesis of 70
- Time-marching algorithm for 344, 345
- Tube model prediction of behavior of 337, 342, 345
- Complex compliance 123
- Complex coordination catalysts (CCC) 80
- Complex modulus (see also *Storage and loss moduli*) 120
- Complex viscosity
 - Definition of 120
 - Molecular weight determination, use of to determine 291, 292
 - Plots of 171
- Complexity, thermorheological
 - (see *Time-temperature superposition*)
- Computational rheology predictions 345–353, 517–521 (see also *BoB model*, *Hierarchical model*, *Pom-pom polymers*, *Slip-link model*, *Time-marching algorithm*)
- Compliance (see *Creep compliance*, *Recoverable compliance*, *Steady-state compliance*, *Extensional creep compliance*)
- Compliance, of rheometers 389, 414, 417
- Concertina modes (see *Primitive path fluctuations*)
- Condensation polymers 67, 76
- Considère criterion, validity for stability of extension 426
- Constitutive equations 374
 - (see also *Rubberlike liquid*)
- Continuum mechanics, models based on 377
- Differential 381 (see also *Tube models*, *equations based on below*)
- Doi-Edwards (see *Doi-Edwards constitutive equation*)
- Integral 377 (see also *Doi-Edwards constitutive equation*)

- Tube models, equations based on 465–493, 497–515
 - Constitutive instabilities 490
 - Constrained geometry catalysts 84–89, 350–353 (see also *Metallocene catalysts*)
 - Constrained recoil (see *Creep recovery*)
 - Constraint release (see *Constraint release Rouse relaxation, Convective constraint release, Double reptation, Dual constraint, Tube dilation*)
 - Constraint release Rouse relaxation 259, 475
 - Tube dilation theories, in 272–276, 328, 341
 - Contour length (see *Primitive path*)
 - Contour length fluctuations (CLF) (see *Primitive path fluctuations*)
 - Contour length relaxation (see *Retraction*)
 - Controlled rheology, grades of polypropylene 90
 - Convective constraint release (CCR) 373, 405, 464, 474, 476
 - Copolymers
 - Ethylene – α -olefin, synthesis of 9, 69
 - Extensional strain hardening in 430, 433
 - Linear rheological behavior of 170
 - Long-chain branches in 84, 407
 - Corotational derivative 381
 - Cox-Merz rule
 - Origin 421
 - Prediction of, using tube model 422
 - Creep compliance 114–119 (see also *Steady-state compliance*)
 - Extensional flow, defined for 426
 - Typical polymers, behavior of 158
 - Creep recovery (Constrained recoil) 117
 - CReTA algorithm (see *Chain shrinking methods*)
 - Critical molecular weights
 - Entanglement effect on creep compliance, value of for 160, 167
 - Entanglement effect on viscosity, value of for branched polymers 173
 - Entanglement effect on viscosity, value of for linear polymers 148, 167, 209
 - Cross equation, for viscosity
 - Description equation 404
 - Extrapolation, use of for 405
 - Long-chain branching, effect of on viscosity, use of to describe 408
 - Metallocene polyethylenes, used to fit data for 404
 - Crosslinking, of polyethylene 81, 84
 - Crossover modulus 164
 - CRYSTAF (Crystallization analysis fractionation) 53
- ## D
- Damping function 370
 - Behavior of for molten polymers 384
 - Chain retraction, relationship to 370
 - Constitutive equations, role of in 379
 - Doi-Edwards prediction of 383, 384, 467
 - Equations for 386
 - Independent alignment (IA) 384
 - Molecular structure, effect of on 388
 - Molecular weight, effect of on 384
 - Polydispersity, effect of on 387
 - DCR-CS model 478
 - Deborah number 392, 393, 398
 - Degree of polymerization 71
 - DEM-G model (see *Doi-Edwards-Marrucci-Grizzuti model, Chain stretch*)
 - Dendrimers 30
 - Dielectric properties 355
 - Differential scanning calorimeter 52
 - Dimensionless groups (see *Deborah number, Weissenberg number*)

- Discrete relaxation spectrum 113
 Disengagement time (Reptation time) 225, 281–283
 Doi-Edwards constitutive equation
 – Description of 379, 380, 465
 – Differential version of 469
 Doi-Edwards-Marrucci-Grizzuti (DEMG model) 469
 Doi-Edwards (strain) tensor 380, 409, 466
 Double reptation 231
 – Bidisperse melts, predictions of for 233
 – Limitations of 256
 – Molecular weight distribution, use of to determine 94
 – Monodisperse melts, predictions for 232
 – Polydisperse melts, predictions for 239
 Double-step strain 391
 Dow rheology index (DRI), for branched metallocene polyethylenes 408
 Drag-strain coupling, in tube models for nonlinear viscoelasticity 508
 DSC (see *Differential scanning calorimeter*)
 Dual constraint model 230, 234, 236, 313, 325
 Dynamic dilution (see *Tube dilation, Hierarchical and Bob models*)
- E**
 Edge fracture, in rotational rheometers 394, 415, 416
 Electron-beam radiation, effect of on rheology 182, 183, 310, 434
 Elongational flow (see *Extensional flow*)
 End-to-end distance, mean square 8, 10, 14, 15
 Entanglement molecular weight (see *Molecular weight between entanglements, Critical molecular weight*)
- Entanglements
 – Description of 208
 – Evidence of 209
 – Identification in computer simulation 218
 – Loss of, in non-linear deformations 464, 465, 474, 492, 510
 Entanglement stripping 492, 510
 Equibiaxial extension (see *Biaxial extension*)
 Equilibration time τ_e 218
 Equilibrium compliance, of crosslinked polymer 115, 158
 Equilibrium modulus, of crosslinked polymer 107, 110, 154, 155, 165
 Equivalent freely-jointed 8, 11
 Excluded volume 14
 Expansion parameter, for non-theta solvent 15
 Extension thickening and thinning 427
 Extensional creep compliance (Tensile creep compliance) 426, 431
 Extensional flow, uniaxial (see also *Biaxial extension, Planar extension*)
 – Branched metallocene polyethylene, behavior of 433
 – Definition of 423
 – DEMG theory prediction of 485
 – Experimental methods for 438–443
 – GLaMM model prediction of 486
 – LDPE, behavior of 425, 434–437
 – Linear low-density polyethylene, behavior of 425, 430, 431
 – Linear, monodisperse melts, behavior of 429, 484
 – Long-chain branching in model polymers, effect of on 497
 – Long-chain branching, random, effect of 434, 515
 – Polydispersity, effect of 494–496
 – Rheometers for 438

- Solutions and melts, comparison of behavior of 429, 484–489
 - Start-up of 423, 424
 - Stress overshoot in 436, 437, 512, 513
 - Tube model prediction of 484–490, 496, 507, 513, 514, 521
 - Typical melts, behavior of in 422–436
- Extensional rheometers (see *Uniaxial extensional flow, experimental methods for*)
- Extensional viscosity
(see also *Extensional flow, uniaxial*)
- Behavior, types of 427
 - Definition of 424
 - LDPE, behavior of for 424–436
 - LLDPE, behavior of for 430, 431
 - Linear polymers, behavior of for 484–490
 - Long-chain branching, effect of on 425, 434–436, 497–508
 - Low strain rate limiting behavior of 424, 425
 - Measurement of 437–443
 - Normalization of (see *Trotton ratio*)
 - Tube model prediction of 484–490, 504–506, 484–490, 496, 513, 514, 521
- Extra stress (Viscous stress) 109, 376
- F**
- Fading memory 108
- Field flow fractionation 50
- Filament stretching rheometer, for uniaxial extension 440, 441
- Film production, polyethylenes for 82
- Finger strain tensor 377, 466, 549
 - Affine deformations, use of to describe 378
 - Rubberlike liquid, use of in 377
 - Scalar invariants of 379, 466
- First normal stress difference
(see *Normal stress differences*)
- Flexibility, of chain 69, 167
- Force rebalance transducer 125, 414
- Free-draining molecule 34
- Freely-jointed chain 7, 8
- Free-radical polymerization 78
- Friction coefficient (see *Monomeric friction coefficient*)
- G**
- Gas-phase polymerization (see *Reactors, industrial*)
- Gaussian chain (Random coil) 8–12
- Gaussian size distribution 9
- Gel permeation chromatography (GPC)
 - Branched polymers 47
 - Interactive chromatography 49
 - LDPE, use for 48
 - Linear polymer, used for 44
- Generalized Maxwell model (see *Discrete relaxation spectrum*)
- Ghost chain (see *Phantom chain*)
- GLaMM model 474–476
- Glass transition temperature 131
- Glassy behavior 106, 152, 159, 165
- GPC (see *Gel permeation chromatography*)
- Graham-Likhtman and Milner-McLeish model (see *GLaMM model*)
- H**
- H polymers
 - Extensional flow behavior of 507
 - Linear viscoelastic behavior of 176, 349, 350
 - Metallocene polymers, content of in 182
 - Nonlinear stress relaxation of 388
 - Stress growth of in shear and extension 507

- Tube models for nonlinear viscoelasticity of 507
- HDPE (see *High-density polyethylene*)
- Hencky strain rate 423, 424
- Hierarchical model for branched polymers 340
- High-density polyethylene (HDPE)
 - Branching in 80
 - Extensional flow behavior of 429
 - Manufacture of 79
 - Plateau modulus of 163
- HPLC (High-pressure liquid chromatography) (see *Gel permeation chromatography*)
- Hydrodynamic volume 33, 37, 38, 45
- Hyperbranched polymers 30, 39

- I**
- Independent alignment (IA) assumption, in DE theory 383, 466, 467
- Inherent viscosity 11, 40
- Interactive chromatography (see *Gel permeation chromatography*)
- Interrupted shear 396
- Intrinsic viscosity 31–40
- Isotropic stress field 375

- K**
- K-BKZ constitutive equation 379, 383
- Kremer-Grest model 219
- Kuhn length 11

- L**
- Large- and medium-amplitude oscillatory shear 398–402
 - Chain stretch, generation of by 401
- LDPE (see *low-density polyethylene*)
- Likhtman-McLeish model, for linear viscoelasticity 228, 229
- Likhtman-Milner-McLeish model, for nonlinear viscoelasticity 470, 480
- Light scattering 42, 43
- Linear low density polyethylene (LLDPE)
 - (see also *Metallocene polymers, Copolymers*)
- Extensional flow behavior of 430, 431
- Structure and synthesis of 81, 82
- Living free-radical polymerization 75
- LLDPE (see *Linear low density polyethylene*)
- Lodge rubberlike liquid (see *Rubber-like liquid model*)
- Lodge-Meissner rule 389–391
- Long-chain branching (LCB)
 - 186–189, 309, 407, 408, 433, 497
 - (see also *Star polymers, Comb polymers, Cayley trees*)
- Detection of using rheology 434, 435
- Dilution, use of to determine 488
- Extensional flow, effect of on 431–437
- High-density polyethylene, LCB in 429
- Index for (see *Dow rheology index*)
- Linear viscoelastic behavior, effect of on 159, 172–185
- Metallocene polyethylenes 84–89, 182, 433
- Multiple branching, tube models for 330–338
- Polydisperse, molecular models for 339
- Tube models for randomly branched polymers 345–353
- Viscosity curve, effect of on 407–409
- Zero-shear viscosity, effect of on 184, 185
- Longest Rouse relaxation time (see *Rouse relaxation times*)
- Loss angle 163
- Loss modulus (see *Storage and loss moduli*)
- Low-density polyethylene (LDPE)
 - Branching structure of 70, 78
 - Extensional deformation, behavior of in 425, 435–437, 499, 519–521

- GPC used to study 48, 49
 - Invention of 78
 - Linear behavior of 184, 185
 - Manufacture of 91
 - Pom-pom model used for 70, 505, 506, 511–514, 519–521
 - Recoverable compliance of 158, 159
 - Thermorheological complexity of 135
 - Viscosity of 403
 - Zero-shear viscosity of 184, 185
- Lower-convected derivative 381

M

- Macromonomers 74, 84, 86, 88, 181
- MALDI-TOF (see *Mass spectrometry*)
- Mark-Houwink-Sakurada equation
(see *MHS equation*)
- Marrucci model, for nonlinear viscoelasticity 474
- Mass spectrometry 50
- Master curve (see *Time-temperature superposition*)
- Maxwell element 110
- Maxwell model for relaxation modulus (see *Discrete relaxation modulus*)
- Mean path methods (for entanglement detection) 221–224
- Medium-amplitude oscillatory shear (see *Large-amplitude oscillatory shear*)
- Melt strength test 409, 442
- Membrane osmometry 41
- Metallocene catalysts 83
(see also *Constrained-geometry catalysts, Post-metallocene catalysts*)
- Metallocene polyolefins
 - Copolymers of 83, 84, 89, 171
 - Creep compliance of 158
 - Extensional strain hardening in 433, 434
 - Linear rheological behavior of 171
 - Long chain branching in 84–89, 433

- Strain hardening in extensional flow of 433
 - Zero-shear viscosity of 151
- MHS equation (Mark, Houwink, Sakurada equation) 31, 32
- Milner-McLeish theory
 - Linear polymers 227, 230, 322
 - Monodisperse stars 322–327
 - Star-linear blends 357
- Molecular dynamics simulations 277
 - Entanglements and tubes, detection of using 218–223
 - For non-linear deformations 492, 493
- Molecular stress function model 380
- Molecular weight between entanglements M_e (see also *Plateau modulus*)
 - Definitions of 165–170, 213
 - Determination of 167, 170
 - Molecular structure, effects of on 164
 - Polyethylene, values for 163
 - Prediction of, from a theory 167–170, 220
 - Solution concentration, effect of on 167
 - Values of, for several polymers 278, 547
- Molecular weight distribution
 - Averages of 18–20
 - Effect of on zero-shear viscosity 150–152
 - Equations for 20–26
 - Rheology, use of to determine 291–303
- Monodisperse polymers
 - Molecular weight distribution of 17
 - Polyethylene-like polymers for research 72, 73
 - Polypropylene 90
- Monomeric friction coefficient
 - Dependence on temperature 203
 - (see also *Volger-Fulcher equation*)
- Dilute solutions, of 200

- Melts, of 203
- Values of, for several melts 278

N

- NMR (see *Nuclear magnetic resonance*)
- Normal stress differences
 - Definitions of 389
 - Low shear rate limiting behavior of 390
 - Measurement of 413, 414, 416, 417
 - Relaxation of 406
 - Rubberlike liquid prediction of 389
 - Steady shear behavior of in
(see *Viscometric functions*)
- Normal stress growth coefficients 394
- Normal stress ratio (β, Ψ) 379, 412
(see also *Stress ratio*)
- Normal stress relaxation ratio 390
- Nuclear magnetic resonance 51
 - Short-chain branches, use of to measure 40, 48

O

- Occupied volume 168
- Orientation, of chain
(see *Chain orientation*)
- Orientation angle 419
- Orientation tensor 469
- Oscillatory shear, small amplitude 120
(see also *Storage and loss moduli, Large-amplitude oscillatory shear*) 120
 - Experimental methods for 132

P

- Packing length
 - Definition of 169
 - Values of, for several polymers 547
- Packing model 167, 169 (see also *Packing length and Pervaded volume*)
- Persistence length 11
- Pervaded volume, of a molecule 168
- Phantom chain 14

- Pipkin diagram 399
- Planar extension 423
- Plateau compliance 115
- Plateau modulus (see also *Molecular weight between entanglements*)
 - Branching, effect on 164
 - Definition of 107, 211
 - Determination of 162, 163
 - Polyethylene, values for 163
 - Tacticity, effect of on 164
 - Values for several polymers 278, 547
- Poly(methyl methacrylate) (PMMA) 67, 160
- Poly(vinyl acetate)
 - Retardation spectrum of 159
 - Storage and loss modulus of 156
 - Time-temperature superposition of data for 156
- Polybutadiene
 - And chain flexibility 69
 - Hydrogenation of, to simulate monodisperse polyethylene 72
 - Synthesis of 73
- Polydispersity index
 - Definition of 19
 - Determination of, based on rheological data 302
- Polyethylene (see also *High-density, Low-density, Linear low density, Ultra-high molecular weight, Film production*)
 - Plateau modulus and M_e of 163
 - Monodisperse samples for research 75
- Polypropylene
 - Controlled rheology grades of 90
 - Crosslinking of 435
 - CRYSTAF, use of for 52
 - High-melt strength 90
 - Long-chain branching in 90, 435, 436
 - Tacticity in 28
 - Polymerization of 90

- Visbreaking of 90
- Polystyrene
 - Branching in 93
 - Damping function of 384, 387
 - Normal stress differences of 389, 390, 395
 - Reactors for 93
 - Stress relaxation of, nonlinear 371
 - Tacticity of, effect of on plateau modulus of 164
- Polyvinyl chloride (PVC) 77
- Pom-pom polymers 70
 - Damping function of 388
 - Extensional behavior predicted by 504–507
 - LDPE, use of to model behavior of 75, 432, 511–515, 518
 - Multi-mode model for 511–515
 - Shear modification, modelling of 409
 - Tube models for nonlinear viscoelasticity of 502–510
- Post-metallocene catalysts 89, 90
- Pressure, effect of on rheological properties (see *Time-pressure superposition*)
- Primitive path (Contour length),
definition of 214–224
- Primitive path analysis
(see *Chain shrinking methods*)
- Primitive path fluctuations (PPF)
226–231, 273–275
 - Deep 227, 275
 - Definition of 217
- Priority (Topological characteristic of branched polymers) 515
- Processing of melts 78, 493
- R**
- Rabinowich correction, in capillary rheometry 420
- Radius of gyration 9
- Random coil (see *Gaussian chain*)
- Random walk 8
- Random walk step, effective 214
- Reactors, industrial 76–92
 - Continuous stirred tank (CSTR) 76
 - Emulsion 77, 93
 - Gas-phase 77, 82–84, 92
 - LDPE, effect of type on damping function 388
 - Pipe-loop 92
 - Polyethylenes, for making 91
 - Polystyrene, for making 93
 - Slurry 77, 83, 92
 - Solution 77, 83, 93
 - Suspension 93
 - Tubular, for LDPE 76, 78, 79
- Recoverable compliance 117, 158, 159
- Recoverable shear strain 411
(see also *Ultimate recoil*)
- Recoverable strain in extension 427
- Relaxation modulus
 - Chain retraction, role of in 370, 371
 - Linear viscoelasticity 105, 107
 - Maxwell model for 110, 111, 113
(see also *Discrete relaxation modulus*)
 - Time-strain separability in 372, 378, 384 (see also *Damping function*)
 - Wall slip, effect of on measurement of 387
- Relaxation spectra
 - Continuous 114
 - Discrete 113
- Reptation 224–227
- Reptation time (see *Disengagement time*)
- Retardation spectrum
 - Continuous 118, 158, 159
 - Discrete 462
- Retraction of chain in tube (Contour length relaxation) 370–372, 462–517
- Reversing flow 391
- Rheological equations of state
(see *Constitutive equations*)

- Rheometers, capillary and slit 419, 420
Rheometers, extensional (see *Extensional flow, experimental methods for*)
Rheometers, rotational
 - Bearings for 126
 - Errors, sources of in 415, 416
 - Linear viscoelasticity, for 123–125
 - Nonlinear viscoelasticity, for 413–417
 - Normal stress differences, use to measure 416, 417
Rheometers, sliding plate 417, 418
Rheotens tester (see *Melt strength test*)
Rolie-Poly model 476–479, 483, 491, 496
Rouse-Bueche model for unentangled melts 148, 160, 199–208
Rouse model for unentangled polymer solutions 200
Rouse motions, longitudinal 242
Rouse reorientation relaxation time 202, 218, 385, 386
Rouse spectrum (Relaxation in tube) 242–244
Rouse stress relaxation time 202, 204, 429
Rubberlike liquid model 377, 378, 380
- S**
Scalar invariants, of a tensor 378, 379, 466
Second-order fluid 409
Seniority (Topological characteristic of branched polymers) 515
Sentmanat extensional rheometer (SER) 439, 440
Shear banding 468, 482, 490–492
Shear modification 79
Shear stress growth and decay functions 109, 393–397
Shear stress transducer 417, 418
- Shift factors (see *Time-temperature superposition, Time-pressure superposition*)
Short-chain branching (see *Copolymers, α -olefin – ethylene*)
Short chain matrix 263–265
Simple fluid model and normal stress differences 409
Single-site catalysts 82–89
(see also *Metallocene catalysts*)
Size exclusion chromatography (SEC)
(see *Gel permeation chromatography*)
Sliding plate rheometer 417, 418
Slip (see *Wall slip*)
Slip-link models 244–248
 - Branched polymers 353–357, 278
 - Branchpoint hopping in 358–360
 - Non-linear viscoelasticity 492
Spurt effect, in capillary rheometers 418, 420
Star polymers
 - Asymmetric 72, 175
 - Bidisperse, modelling of 327
 - Damping function of 388
 - Deep primitive path fluctuations in 317, 318
 - Dynamic dilution, used to model 319–322
 - Extensional flow behavior of 431, 432, 497, 498
 - Linear polymers, blends with 328–330, 354–358
 - Metallocene polymers, in 84, 86, 433
 - Milner-McLeish theory for (see *Milner-McLeish theory*)
 - Normal stress ratio of 412
 - Shear stress growth and decay of 393–397
 - Slip-link models for 354–358
 - Symmetric, viscoelastic behavior of 173–178

- Symmetric, tube models for 317–322
 - Synthesis of 73–76
 - Tube models for 311, 314–330, 349–358
 - Viscosity of 407, 412
- Start-up of steady shear (Stress growth) 393–397, 478–483, 507, 512
- Statistical segment length 11
- Steady-state compliance 115
- Monodisperse polymers, behavior of 160
 - Polydispersity, effect of on 161
- Step polymerization 67
- Stirred-tank reactor, CSTR (see *Reactors, industrial*)
- Stoke's law and Stoke's radius 34
- Storage and loss moduli 120–122
 - Long-chain branching, effect of on 155–157, 172, 307–359
 - Measurement of 123–125
 - Molecular weight, effect of on 157
- Strain hardening in extension 378, 425–427, 445, 486–490, 495–502, 504, 505, 513, 514, 521
- Strain softening in extension 425
- Strain tensors
 - Finite strain 377–380, 549–553 (see also *Cauchy tensor* and *Finger tensor*)
 - Infinitesimal strain 375
- Stress growth in steady shear 109, 393–397
- Stress growth in uniaxial extension 109, 393–397
- Stress-optic law 418, 419
- Stress ratio (SR) 389, 390
- Stress relaxation, after step shear strain (see *Relaxation modulus*)
- Stress relaxation after cessation of extensional flow 503, 510, 513, 514
- Stress relaxation after cessation of steady shear 503, 510, 513, 514
- Stress relaxation modulus (see *Relaxation modulus*)
- Stretch time 502, 522, 523, 532
- Swelling coefficient (see *Expansion parameter*)
- T**
- Tacticity
- Definition of 28, 29
 - In polypropylene 28, 29, 90, 164
 - In polystyrene 164
- Temperature gradient interactive chromatography (TGIC) 49, 50, 74, 348, 536
- Temperature rising elution fractionation (TREF) 52
- Tensile creep compliance (see *Extensional creep compliance*)
- Tensile extension (see *Extensional flow, uniaxial*)
- Tensile stress growth coefficient 42
- Tensile stress, net 438
- Terminal zone 106
- Thermal-flow fractionation 50
- Thermoplastic elastomers 90
- Thermorheological behavior (see *Time-temperature superposition*)
- Theta solvent (see *Theta state*)
- Theta state 14–16
- Theta temperature (see *Theta state*)
- Time-marching algorithm 344, 345
- Time-pressure superposition 136
- Time-strain separability 372, 378
- Time-temperature superposition (see also *Complexity*) 130–136
- Toy models, for nonlinear viscoelasticity 469, 476–479, 502–511
- Transducers (see *Force rebalance transducer*, *Shear stress transducer*)

- Transition zone 106
- TREF (see *Temperature rising elution fractionation*)
- Trouton ratio 424
- Tube coordinate 227, 228, 243, 317–321, 330, 331, 340
- Tube diameter
- Definition of 214–217
 - Values of for several polymers 278, 547
- Tube dilation (Dynamic dilution) 127, 274–278, 319–331
- Tube models
- Branched polymers, use of for modeling of 307
 - For linear viscoelasticity 208–248
 - For nonlinear viscoelasticity 461–533
 - Parameters for 218–244, 278, 547
 - Rheological behavior, qualitative interpretation of, in terms of 197, 208–214
- Tube reptation 266
- Tube segment 215, 226, 244, 261
- U**
- Ultimate recoil 411
- (see also *Recoverable shear*)
- Ultrahigh molecular weight polyethylene (UHMWPE) 81
- Ultimate recoil (Recoverable strain) 411
- UNIPOL process 92
- Unperturbed chain 8
- Upper convected derivative 381, 469
- Upper convected Maxwell model 378
- V**
- Van Gurp-Palmen plot 136–138
- Viovy diagram 267, 268
- Visbreaking (see *Polypropylene*)
- Viscometric functions (see also *Viscosity, Normal stress differences*)
- Definitions of 389, 396
 - Effects of IA assumption on 390
- Viscosity (see also *Zero-shear viscosity, Extensional viscosity*)
- Effect of shear rate on 402–405 (see also *Tube model description of*)
 - Pressure dependence of 136
 - Tube model description of 405, 406, 467
- Viscous stress (see *Extra stress*)
- Voigt model 118
- Volger-Fulcher equation 203
- W**
- Wagner's equation (Wagner's model) 379, 394, 411, 412
- Wall slip
- Rheometers, occurrence in 418
 - Step strain, effect of on data 387, 390, 415, 491, 492
- Weissenberg number 393, 398, 401
- WLF temperature dependence 130, 131
- Z**
- Z algorithm (see *Chain shrinking methods*)
- Zero-shear viscosity
- Branching, effect of on 181–187
 - Critical weight for entanglement for 148
 - Definition of 109
 - Limiting value of at very high molecular weights 170
 - Measurement of, problems in 151, 156
 - Molecular weight, effect of on 148–150
 - Molecular weight distribution, effect of on 150–152
 - Monomeric friction coefficient, use of to determine 277
 - Polyethylene 183
 - Polypropylene, effect of branching 183
 - Rouse time, relationship with 204, 386
 - Stars and combs 173
- Ziegler-Natta catalysts 81, 82, 92

Dealy · Read · Larson

Structure and Rheology of Molten Polymers

Recent advances in polymer science have made it possible to relate quantitatively molecular structure to rheological behavior. At the same time, new methods of synthesis and characterization allow the preparation and structural verification of samples having a range of branched polymeric structures. This book unites this knowledge to enable production of polymers with prescribed processability and end-product properties.

Methods of polymer synthesis and characterization are described, starting from fundamentals. The foundations of linear viscoelasticity are introduced, and then the linear behavior of entangled polymers is described in detail. This is followed by a discussion of the molecular modeling of linear behavior. Tube models for both linear and branched polymers are presented. The final two chapters deal with nonlinear rheological behavior and tube models to describe nonlinearity.

In this second edition, each chapter has been significantly rewritten to account for recent advances in experimental methods and theoretical modeling. It includes new and updated material on developments in polymer synthesis and characterization, computational algorithms for linear and nonlinear rheology prediction, measurement of nonlinear viscoelasticity, entanglement detection algorithms in molecular dynamics, nonlinear constitutive equations, and instabilities.

Contents:

- Structure of Polymers
- Polymerization Reactions and Processes
- Linear Viscoelasticity - Fundamentals
- Linear Viscoelasticity - Behavior of Molten Polymers
- Tube Models for Linear Polymers - Fundamentals
- Tube Models for Linear Polymers - Advanced Topics
- Determination of Molecular Weight Distribution Using Rheology
- Tube Models for Branched Polymers
- Nonlinear Viscoelasticity
- Tube Models for Nonlinear Viscoelasticity of Linear and Branched Polymers

HANSER

www.hanserpublications.com

Hanser Publications

ISBN 978-1-56990-611-8



9 781569 906118